Alma Mater Studiorum – Università di Bologna

DOTTORATO DI RICERCA IN

Ingegneria Civile, Chimica, Ambientale e dei Materiali

Ciclo XXIX

Settore Concorsuale di afferenza: 08/B3

Settore Scientifico disciplinare: ICAR/09

TITOLO TESI

Monitoring and Real Field Data for understanding the Structural Behaviour and Health of Historical Buildings

Presentata da: Simonetta Baraccani

Coordinatore Dottorato   **Relatore**

Luca Vittuari   **Tomaso Trombetti**

                                               Correlatori
                                               Matthew J. DeJong
                                               Giada Gasparini

Esame finale anno 2017

Contents

Chapter 13   187

**13   Cathedral of Modena: the seismic analyses of structural elements via Discrete Element
Methods   187**

Abstract

The monumental historic buildings are an important part of cultural heritage, which have to be preserved for future generations in order to transmit their history, culture and art, having also to meet the practical test of utility and a suitable safety level. These buildings, for their history and complexity, are very different from ordinary structures and the application of the methods commonly used in civil engineering for the analysis of the structural behaviour not always seem to be appropriate for historical masonry monuments of unique features. Therefore, it clearly appears the need of a reliable estimation of the actual level of safety in order to plan effective interventions. In the knowledge process of the historical buildings, a fundamental contribution is played by the Structural Health Monitoring (SHM) whose aim is to evaluate the evolution of the structural health through a continuous real-time monitoring by means small removable sensors. In recent years, several historical monuments have been equipped with monitoring systems, but no standardized procedure for systematic interpretation of the data acquired by static SHM is yet available. The main purpose of the current research work is to introduce an approach for a standardized analysis of the data recorded by a static Structural Health Monitoring system installed in an historical building. The identification of a stationary or evolutionary "condition" has been evaluated through the introduction of specific tools, referred to as reference quantities, which can be interpreted as descriptors of the recorded data. This approach is intended as a contribution to move forward in the systematic use of the data acquired by the monitoring system within a policy for management of cultural buildings. Indeed the systematic collection of the values (along the time) of these reference quantities, referred to as reference values, in a database allows to make interesting comparisons among similar buildings in order to produce guidelines useful for the interpretation of data acquired by static monitoring system of masonry monuments. The data acquired by the monitoring system allow also to calibrate and validate the numerical models adopted for the structural analyses of the monuments. However, to conceive a unique tool able to describe all the possible structural responses of the historical masonry monuments is complex, and most likely impossible. Quite often, more reliable results can be obtained by employing a multi-analysis method that integrates different approaches. The second purpose is to provide a summary of the studies conducted on a real monumental building, namely the Cathedral of Modena (UNESCO world heritage) aimed at its reliable structural assessment based on a multi-disciplinary multi-analysis approach (MDMA), integrating the real field data obtained by the SHM.

Sommario

Gli edifici storici monumentali rappresentano una porzione importante dell'eredità culturale, che deve quindi essere preservata nel futuro garantendone un adeguato livello di sicurezza. Questi edifici, per la loro storia e complessità, sono molto diversi dalle strutture ordinarie e l'applicazione dei metodi comunemente utilizzati nell'ingegneria civile per l'analisi del comportamento strutturale non sono generalmente in grado di coglierne tutte le peculiarità. D'altra parte, una stima affidabile del livello effettivo di sicurezza attuale di questi edifici risulta fondamentale al fine di pianificare interventi efficaci. Un notevole aiuto in questa fase è dato dall'installazione di sistemi di monitoraggio strutturale (SHM) che, grazie a dispositivi removibili e non invasivi, permette di monitorare la salute dell'edificio e capire quindi se è in una condizione stabile o se ci sono fenomeni evolutivi dei parametri sott'osservazione. Le applicazioni di sistemi di monitoraggio strutturale su edifici monumentali hanno visto una notevole crescita negli ultimi anni ma ad oggi non è presente in letteratura una procedura uniformata che permette un'interpretazione dell'ingente quantità di dati ottenibili. Il primo obiettivo della tesi è proprio quello di introdurre un approccio per l'interpretazione dei dati ottenuti dai sistemi di monitoraggio statico identificando delle quantità di riferimento, estrapolabili dai dati, che permettono di identificare la presenza di possibili evoluzioni nello stato di salute dell'edificio. Questo approccio mira a dare un contributo verso l'uso sistematico e standardizzato dei dati acquisiti dai sistemi di monitoraggio all'interno di una politica di gestione degli edifici culturali. Queste "quantità di riferimento" costituendo una nomenclatura specifica, permettono, se applicate in maniera sistematica, di fare confronti interessanti con i dati registrati su edifici simili e costituire linee guida utili per l'interpretazione dei dati acquisiti dal sistema di monitoraggio statico di monumenti in muratura. I dati ottenuti dal monitoraggio strutturale costituiscono anche un elemento fondamentale nella validazione e calibrazione dei modelli numerici adottati per l'analisi strutturale degli edifici storici. Tuttavia, l'identificazione di un unico strumento e modello in grado di descrivere tutte le peculiarità dei monumenti in muratura storica è praticamente impossibile. Risultati più affidabili possono essere ottenuti impiegando un metodo multi-analisi che integra i risultati ottenuti dall'applicazione di approcci diversi. Il secondo scopo è quello di realizzare una sintesi degli studi condotti su un vero edificio monumentale, ossia la cattedrale di Modena (patrimonio mondiale UNESCO) finalizzato alla sua valutazione strutturale affidabile basata su un multi-disciplinare approccio multi-analisi (MDMA), integrando la dati reali ottenuti dal SHM.

Acknowledgments

Chapter 1

1 Introduction

1.1 Background

Cultural heritage monuments represent inestimable values and not removable resources of most of European countries, which have to be preserved for future generations in order to transmit their history, culture, art. The correct management of cultural heritage buildings is a crucial issue: on one side, the conservative restoration requires compatible and limited intervention techniques in order to preserve the integrity of the monuments, and on the other side, this implies a profound knowledge of the structural behaviour, often difficult to understand and to predict for these complex buildings.

The most widespread construction material used, especially in Italy, for the monumental buildings is the masonry that is characterized by a quite complex mechanical behaviour due to composite nature resulting from the interaction of bricks and mortar (both characterized by significantly different behaviour under tension and compression) thus leading to specific issues to be faced when analysing and modelling these constructions . Moreover, historical monuments are built and modified during the centuries by using various construction techniques, workmanships of different expertise, with the result of a complex fabric, characterized by a high degree of uncertainties, quite far from our modern buildings. In most cases, their actual configuration and the state of conservation are not only the result of the natural degradation due to aging effects, but also the consequence of the impact of past extreme natural events (such as earthquakes, floods, groundwater changes), which may sometime have caused partial or total collapses. The inherent complexity of historical buildings (due to the articulated geometrical configuration, the use of different construction techniques, different materials, the level of the connections between orthogonal walls), together with the natural material decay and the effects of natural hazards, makes the assessment the "structural health" extremely challenging. Furthermore, all

the uncertainties due to this complexity render each monument a "unique". This means that there is no baseline directly applicable in order to obtain useful information concerning the "health" of the structure and the approach commonly used for the assessment of modern steel and concrete building (largely based on the use of computer software and well-established guidelines or codes) cannot be simply adopted for historical buildings. On the other hand such effects tend to inevitably reduce the level of safety and therefore increases the risks to future extreme events, but the monuments have also to meet the practical test of utility. Therefore, it clearly appears the need of a reliable estimation of the actual level of safety in order to plan effective interventions. In this respect, while for the case of conventional structures, a common strategy to reduce the uncertainties and therefore provide a reliable assessment of the "structural health" is based on the use of extended in situ experimental tests (destructive tests). For the case of cultural heritage sites, the authorities responsible of monuments conservations in the spite of preserving the original integrity often prohibit this strategy.

An alternative approach to reduce the uncertainties in the knowledge of historical sites should be based on the development of a multidisciplinary approach aimed at providing an "integrated knowledge" through the mutual exchanging of expertise and capabilities offered by different fields. In this interdisciplinary knowledge process a fundamental contribution is played by the Structural Health Monitoring (SHM) whose aim is to evaluate the evolution of the structural health through a continuous real-time monitoring.

Hence, the main feature of Structural Health Monitoring strategy for monuments is to be geared towards a long-term evaluation of what is 'normal' structural performance or 'health'. In this regard several studies available in the scientific literature, in fact, reported the main information obtained through structural health monitoring. However, such information are not so easy to compare given that a no unique approach is used for data analysis and interpretation.

Similarly, the assessment methods commonly used for the analyses of the "structural health" and for the evaluations of the effects of extreme events, consisting in the developments of single computer-based model and numerical simulations, do not always appear as appropriate for the case of historical monuments. Generally, only one model of the whole building is not able to capture all the structural peculiarities.

1.2 Objective

As the previous section mentioned, the first fundamental step for preservation of historical monuments is the deep knowledge of the building. The historical monuments have to be considered, hence, as a real model of themselves to be observed, studied and controlled. A fundamental contribute in the knowledge process of the monuments is given by the implementation of a real-time monitoring systems, that allow a long-term evaluation of the structural health and the identification of damage and degradation phenomena. In recent years, several historical monuments have been equipped with static and dynamic

monitoring systems. Even though several studies were focused on the interpretation of the data acquired by dynamic monitoring, no standardized procedure for systematic and easy data interpretation of data are yet available. Due to the fact that measurements are made during long-term periods, the recorded data contain a very large amount of information, whose interpretation is not straightforward. Consequently, the choice of the methods to process the vast heap of information and provide useful and simple measures of a structure's health status appears crucial.

The main purpose of the current research work is to introduce an approach for a standardized analysis of the data recorded by a static Structural Health Monitoring system installed in an historical building.

The identification of a stationary or evolutionary "condition" has been evaluated through the introduction of specific tools, referred to as reference quantities, which can be interpreted as descriptors of the recorded data. Such descriptors could be used as the roots for the establishment of a standardized procedure for data analysis and interpretation. Indeed the systematic collection of the specific values (along the time) of these reference quantities, referred to as reference values, in a database could allow to make interesting comparisons among similar buildings in order to produce guidelines useful for other researchers or even practitioners approaching to the monitoring of monumental buildings.

The second purpose is to provide a summary of the studies conducted on a real monumental building, namely the Cathedral of Modena (UNESO world heritage) aimed at its reliable structural assessment based on a multi-disciplinary multi-analysis approach (MDMA), integrating the real field data obtained by the SHM.

1.3   Outline of Thesis

The approach taken to achieve the aforementioned objectives is as follows. The thesis is subdivided in two main parts.

Part One is related to the Structural Health Monitoring (SHM)

This part is composed of Chapter 2, which provides the state-of-the-art on the main strategies, methods and applications of the SHM strategy for the civil structures. In Chapter 3, the primary objective of the thesis is presented: an approach for a standardized analysis of the data recorded by a static SHM system installed in an historical building. This approach, introducing appropriate descriptors able to characterize the main features of the data acquired by the monitoring, allows to identify if the phenomena under observation through the SHM system are in a stable condition or not. Chapter 4 illustrates the removal signal irregularities procedure and an overview of the signal analyses that could be used in the interpretation of the data acquired by static monitoring systems. Chapter 5, 6 and 7 present the application of the procedure proposed for the interpretation of the data obtained from the static monitoring system, on three case studies: the Asinelli tower, the Garisenda tower and the Cathedral of

Modena, respectively. The large amount of data recorded by the monitoring systems installed on the three monuments are analysed using the approach proposed in § 2.3. The signal frequency analyses on the recorded data is also carried out and the results obtained compared with those obtained making use of the approach proposed. The main results obtained from the analyses are presented in these chapters, while the systematic calculation of the descriptors are presented in the Appendix A, B and C. Chapter 8 provides reference values, extrapolated to the descriptors obtained through the analyses of the three monuments, which may be guidelines useful for the interpretation of data acquired by static monitoring system of other masonry monuments.

Part Two is focused on the reliable structural assessment of the monumental buildings.

This part is composed of Chapter 9, which first provides an overview of the main methods applicable to the study of masonry historical buildings. Then, in the same chapter a possible approach for the reliable assessment of the structural "health" of historical monuments based on a multi-disciplinary multi-analysis approach (MDMA) integrating the real field data obtained by the SHM is presented. The MDMA approach is grounded on the experience obtained during an almost decade of studies on the Cathedral of Modena, developed within of a Scientific Research Committee, with the purpose of identifying its potential structural vulnerabilities and criticalities. The integrated knowledge of a monument is the first step to develop consistent structural analyses and, thus, to understand correctly its structural health. The knowledge process obtained for the Modena Cathedral through the mutual exchange of expertise and capabilities of different disciplines is presented in Chapter 10. Chapter 11 provides the main results of different structural analyses, based on the information obtained from the integrated knowledge, in order to identify the main static and seismic vulnerabilities of the Cathedral. The structural behaviour of the Cathedral has been investigated through simple limit schematizations and Finite Element models of increasing complexity. Due to the complexity of the monument and the relevant influence of different factors (such as construction phases, soil properties, existing cracks, interaction with the Tower, as highlighted from the integrated knowledge), instead of a unique 3D FE model in which all factors are simultaneously taken into account, several specific 3D FE models have been performed to separately investigate, the effects of each single factor. Chapter 12 presents the main results obtained from the study of the local collapse mechanisms of the main substructures of the Cathedral. In addition, the results, in terms of stress and deformation, of the most damaged vaults, after the 2012 Emilia Romagna earthquake, obtained through analyses on 3D Finite element models are provided. Chapter 13 treats the most vulnerable cross section of the Cathedral of Modena (characterized by different soil stiffness at the base and absence of tie-rods) through a Discrete Element (DE) modelling in order to evaluate the interactions between the vaults and the longitudinal walls under seismic loads. First, the modelling criteria using Discrete Element Method and a possible calibration of the springs at the base of the walls in order to take into account of the interaction soil-foundation- structure are presented. A sensitivity analysis is also conducted on a simple buttressed vault in order to evaluate the

different influence on the structural response due to the modelling parameters. Then both static and dynamic analyses are performed on the DEM model of the cross section and the results are compared with the crack patterns as observed before and after the 2012 Emilia Earthquake. The structural response of the DEM model has been also compared with the response of corresponding FE models. The results obtained from the different structural analysis approaches are compared in order to identify the preliminary limitations and reliability of these methods when applied to the structural assessment of masonry historical buildings. Chapter 14 summarizes this research work and discusses possible future researches.

Part I

STRUCTURAL HEALTH MONITORING

Chapter 2

2 Structural Health Monitoring: state of the art

2.1 Introduction

The process of implementing a damage detection strategy for aerospace, civil and mechanical engineering infrastructure is referred to as *Structural Health Monitoring (SHM)* (Sohn et al. 2003). This process, based on the continuous monitoring of the behaviour of critical parts, allows to provide a prognosis of the actual state (evolution of damage, residual life, etc.). SHM in civil engineering is a relatively new phenomenon. For this reason, it is very important to develop methods and models adapted for the needs in civil engineering applications.

This Chapter presents a state-of-the-art on the main strategies, methods and applications of the SHM strategy for the civil structures.

2.2 Structural Health Monitoring for civil structures

The main objective of a monitoring system installed in a civil structure is the evaluation of its "structural health". A SHM strategy requires a continuum monitoring of the structures through an assembly of sophisticated electronic devices with the purpose of detecting the presence of potential structural criticalities and/or incoming damages. The word "damage", when used with reference to buildings, describes situations that can influence their present or future behaviour in an adverse way (Sohn et al. 2003). The evolution of a structural damage can be slow as it typically happens when temperature, fatigue, corrosion, subsidence phenomena are involved but it can also sudden accelerate when extreme events such as earthquakes, hurricanes and explosions happen.

SHM systems may prove invaluable to evaluate the level of structural damage shortly after an earthquake. The damage caused by an earthquake are not always immediately obvious and recognizable by visual inspection, but sometime damage hidden within a structure. The monitoring can provide useful information of what and where damage may have occurred, but also whether immediate action is necessary to guarantee the safety of the people. The rapid reuse of buildings for production activities can significantly reduce the economic damage caused by earthquakes, as well as that of public buildings can significantly reduce the social problems. Figure 2-1shows the organization of a typical SHM system.
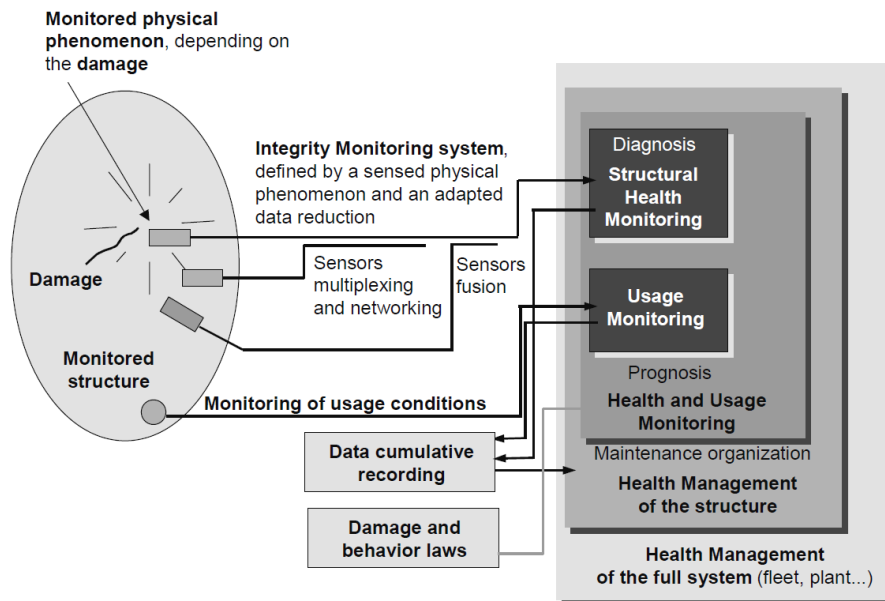
Figure 2-1- Example of SHM system (Balageas et al. 2006)

Generally, in the civil engineering the SHM is used in the following cases:

- structures subject to long-term movement or degradation of materials,
- modifications to an existing structure,
- monitoring of structures affected by external works,
- monitoring during demolition,
- feedback loop to improve future design based on experience,
- fatigue assessment,
- novel systems of construction,
- assessment of post-earthquake structural integrity,
- decline in construction and growth in maintenance needs, and
- the move towards performance-based design philosophy.

To the considerable cost of the SHM sensors, these system are generally applied to relevant construction, such as large dams, bridges, gas/oil production installations and cultural heritage buildings (Brownjohn 2007).

An advanced SHMS is composed by:

- measurement devices (sensors): sensors are installed directly on the structural elements, they measure physical parameters and transfer the information as a digital or analogy signal.
- cables / radio waves: means for transmitting the signals from the sensors to the acquisition units.
- A/D converters, signal conditioners, filters: electronic devices transforming the analog signals to digital information. Signal amplifiers and Conditioners are used to amplify very small ambient signals, thus enabling a reliable evaluation.
- data acquisition unit: a data-logger that receives all the signals measured by the sensors. This is accompanied by an industrial PC equipped with large hard disks since large amounts of measuring data have to be processed.
- data processing software: specifically designed software capable of data management and remote control of the system.
- internet router Network: connection enabling data transfer to end users.

2.2.1 Structural Health Monitoring in Cultural Heritage buildings

The SHM has a very important role in the diagnostic process of cultural heritage buildings, for which generally, the identification of the structural behaviour is affected by many uncertainties. In the last decade, the number of SHM system designed and implemented on historic structures increased considerably. SHM perfectly meets principles and guidelines of Italian and European seismic codes concerning the historical buildings, which require the preservation of the structural architectural integrity, promoting removable, non-invasive and compatible solutions in the knowledge process, restoration and strengthening. The importance of monitoring in Cultural Heritage is also stress in the Italian Guidelines, which indicate the monitoring as the main tool for informed conservation of the historical buildings (Guidelines for Evaluation and Mitigation of Seismic Risk to Cultural Heritage 2011)

A SHM system installed on historical buildings allows to identify, locate and classify type and severity of damages induce by external actions or degradation phenomena and to assess their effect on the structural performance, by means small removable sensors. The most common damage phenomena that can occur on the historical buildings are due to displacements and inclinations of portion of the structure, cracks, foundation displacements and settlements, vibration induced by traffic loads and corrosion (Figure 2-2Figure 2-1).

SHM system applied to historical monuments can be considered a knowledge-based assessment tool, which monitoring for a suitable span of time, leads to the following key findings:

- assessment of structural vulnerabilities, through the correlation between environmental actions (temperature, wind, earthquake, new forces applied to the structure, foundations settlements, changes of the boundary conditions) and the structural response (crack width, movement and tilt of the support structures, differential movements of the foundation structure, etc.);
- study of the long-term behaviour ;
- definition of a procedure to verify promptly abnormal behaviour or exceeded warning level;
- control the damage states of buildings in a post-seismic scenario.
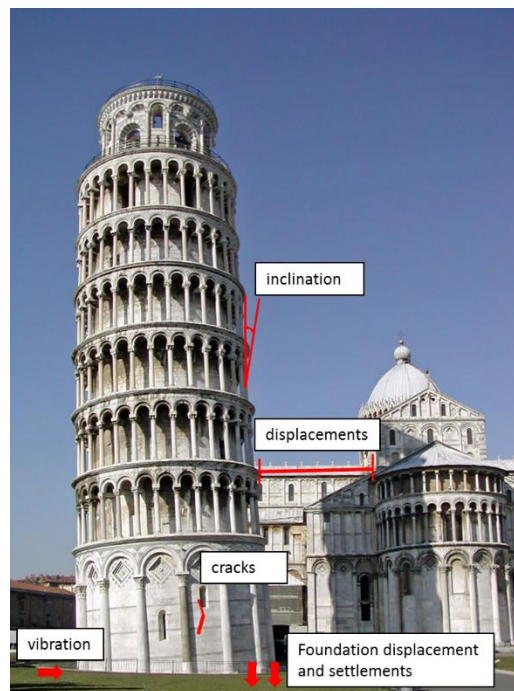
Figure 2-2: The typical damage phenomena that can occur on the historical buildings are shown as example for the Pisa Tower in Italy

SHM can be divided into several different categories depending on the time schedule (duration and frequency of the measurements), phenomenon to be observed, and the techniques/instruments used. Figure 2-3 displays a classification of the monitoring techniques for civil buildings.
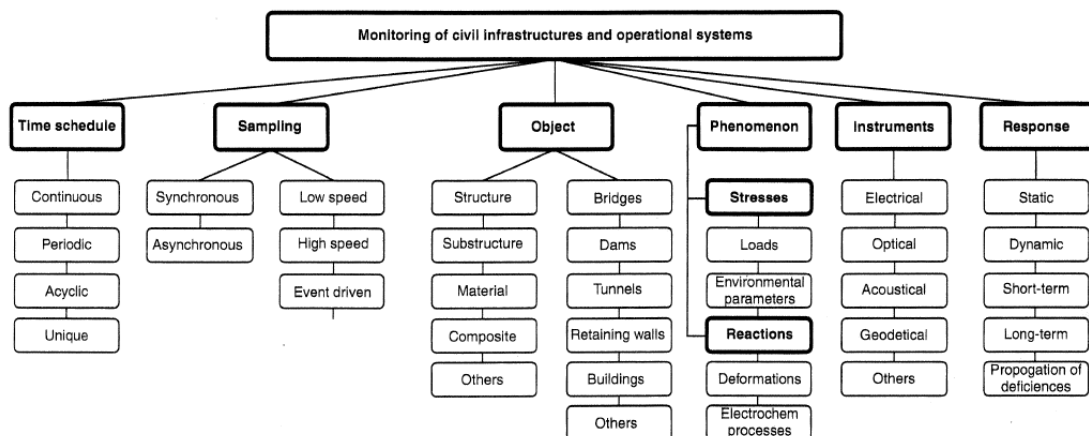
Figure 2-3-Classification of monitoring techniques in civil buildings (Bergmeister & U. Santa 2001)

2.2.2 Time schedule

The time strategy describes the duration and frequency of the measurements. The duration dependent is characterized as:

- short-term,
- long-term,
- periodic, continuous, and triggered monitoring.

The frequency of the measurements are defined as:

- periodic: measurements at pre-defined intervals,
- continuous: permanent automatic measurements, for example every hour.

The selected strategy depends on the phenomena to be observed.

2.2.2.1 Long-term monitoring

The monitoring of a structure is considered to be long term when the monitoring is carried out permanent over a period of years-to-decades. Recent advances in sensor technology, data acquisition, computer power, communication systems and data now makes it possible to construct this type of system. Continuous monitoring should only be considered if the changes in loading are slow, such as gradual temperature changes, or if the loads are not predictable, e.g. natural hazards such as floods, hurricanes or earthquakes. In addition if a structure is affected by slow degradation processes and the methods to prevent this are limited or should be postponed as long as possible. This is the case for monitoring of

historical structures and monuments where the aesthetics can not be changed. For such structures, the only way to find the state of the health is to use non-destructive tests since no material can be removed and tested to evaluate the material properties.

The first step is to reflect on all possible ways the construction might respond to externally induced impacts and to choose which quantities to measure, where to measure them, and to select adequate instruments to do so.

2.2.2.2 Short-term Monitoring

Short term monitoring can be used if the state of the structure is to be examined at a specific point in time. This is a typical measure if an inspection shows a deficiency or damage in the structure and the safety is questioned. Short-term monitoring gives more information than a visual inspection since the structural safety can be controlled. These types of monitoring are often used to evaluate a change. Examples are: changed of traffic loads, change of the structural system, strengthening of a structure, etc. If several periodic monitoring measures are repeated frequently over an extended period it will be defined as periodic continuous monitoring..

2.2.2.3 Continuous or triggered monitoring

In long-term monitoring operations the collection of data can be continuous or periodic. Frequent periodic monitoring is when data is collected at regular time intervals. Triggered periodic monitoring is when data collection is initiated or triggered by a specific event, e.g. when a measured parameter exceeds a threshold. The sampling interval for each data collection depends on the dynamic nature of the studied phenomena, see also load dependency. Typical application for frequent periodic monitoring is when the loads are static and the monitored phenomenon changes gradually for example if the yearly temperature effect of a dam should be monitored. A typical application for triggered monitoring is measurements of trains passing a bridge. Here, the interesting samples are only when the train is on the bridge. Continuous monitoring is used when rapid changes due to stochastic events are expected. Mostly, these types of data streams are processed to decrease the amount of data collected.

2.2.3 Phenomenon to be observed and sensors

Based on the phenomenon to be observed, the quantities to be monitored significantly change as well as the features of the instruments needed. An estimation of the magnitudes of changes in the quantities to be measured, allow to definition of the range, resolution, accuracy and sensitivity of the instrument (Bergmeister & U. Santa 2001). The prevalent phenomena to be observed concerning the civil structures are:

- Mechanical: displacement, inclination, rotations, deformation ...
- Physical: material temperature, humidity,...
- Chemical: pH, chlorine, sulfate,...
- Environmental: air temperature, humidity, solar irradiation, wind,...
- Actions: vehicle loads, forces,...

The response obtained from the monitoring of the different phenomena listed can be subdivided on:

- Static: measurement of slowly varying parameters
- Dynamic: measurement of vibrations and other dynamic responses

2.2.3.1 Static SHM monitoring

Measurements of phenomena such as cracks opening, inclination, settlements, corrosion and phenomena caused by environmental properties, for example temperature, humidity, wind, are most of the time quasi-static since they vary slowly over the time. Generally, to monitor these quantities is enough to measure the peak values over a longer time depending on the speed of actions that create the phenomenon. This is defined as static monitoring.

2.2.3.2 Dynamic SHM monitoring

Measurements of phenomenon such as fatigue or induced by ambient vibration vary fast over the time. Dynamic monitoring is performed with a much higher sampling rate compared to static monitoring in order to obtain the structural behaviour from dynamic loads.

2.2.4 Sensor technology

The typology of sensors used in the civil monitoring is extensive and growing. Different applications with various techniques, like electrical, optical, acoustical, geodetical etc are available. For the past few decades, some of the more common used sensors are inclinometers, deformeters, distanziometer, load cells, accelerometers, etc...These sensors have proven to be highly robust, reliable, repeatable and accurate in a variety of applications. Following are some details on some the sensors mentioned:

- Inclinometers – measure horizontal and vertical angular inclination to very high levels of precision, and output the data in analogue or digital form. In SHM applications, inclinometers are employed to monitor movement over time of bridges, buildings and other large structures.
- Accelerometers – measure acceleration and deceleration of dynamic systems. Low 'g' range accelerometers are used within SHM to monitor accelerations induced into bridges and other structures to check design calculations and long-term critical safety.

- Load cells – transducers used to convert a force into an electrical signal and offer measurement of tension, compression and shear forces. Load cells are available in many physical shapes and forms to suit particular applications and types of loading. The majority of today's designs employ precision strain gauges as the primary sensing element, whether foil or semiconductor, and feature low deflection and high frequency response characteristics. SHM applications for load cells include bridge lifting/weighing, vehicle/crane load monitoring, and earthquake force monitoring.

Recently, a significant number of innovative techniques and sensors for civil engineering purposes have been developed through the evolution of fibre optic sensors, lasers etc. together with the effective wireless transmission data and analyse the vast volumes being stored. Table 2-1 shows some examples of suitable sensors to monitor specific phenomenon of civil structures.

Table 2-1- Suitable sensors to monitor specific phenomenon of civil structures.

Phenomenon	Sensor Types	Response
Crack opening	Defometers LVDT (Linear Variable Differential Transformer)	Static
Displacements	Laser GPS LVDT	Static or Dynamic
Inclinations	Inclinometers	Static
Strain	Extensometers Fibre optic	
Foundation displacements and settlements	Piezometers LVDT	Static
Whether condition	Thermometer	Static
Vibration	Accelerometers	Dynamic
Corrosion	Scanning sensors	Static

2.3   Conclusions

The important role of the implementation of SHM systems on the historical monuments is highlighted in this chapter. A SHM system installed on historical buildings allows to identify, locate and classify type and severity of damages induced by external actions or degradation phenomena and to assess their effect on the structural performance, by means small removable sensors. Moreover, SHM systems may prove invaluable to evaluate the level of structural damage shortly after an earthquake. It was also highlighted that several devices are currently available for structural monitoring, making more difficult the developing of standardized procedure for the interpretation of these data.

Chapter 3

3   Static Structural Health Monitoring: interpretation of the data acquired by the monitoring of monumental buildings

3.1   Introduction

The Static Structural Health Monitoring (SSHM) system typically acquired 2 to 4 data per hour and is generally used to monitor the evolutions of the "state or conditions" of the monument. The recorded raw data need to be analyzed in order to gather some useful information on the evolution of the condition of the building under observation. A stationary condition reasonably suggests that the structure is in a safe condition, whilst a non-stationary response (especially in the cases where a clear trend is observed in the data) may indicates a significant evolution of the state of damage, which may preclude the structural safety of the monument.

The identification of a stationary or evolutionary "condition" may appear simple in theory, while, in actual practice, it proved to be quite cumbersome, given that the recorded signals are significantly affected by a number of external factor (climate changes and anthropic effects) which render the identification of a potential damage evolution not so straightforward (Sohn 2007).

A brief overview of the methods present in literature for the interpretation of the data acquired by static monitoring will be presented in this chapter. In addition, an approach for the critical interpretation of the data acquired by the static monitoring of historical buildings will be presented. This approach, introducing appropriate descriptors able to characterize the main features of the data acquired by the monitoring, allows to identify the evolution of the state of the monuments.

3.2   Literature review

In the last years, several studies were focused on the interpretation of the data acquire by dynamic monitoring system of historical buildings (Beskhyroun et al. 2011), (Robert-Nicoud et al. 2005), (Anastasi et al. 2009), (Magalhães et al. 2016), (Tyagunov & Petryna 2016), (Ivorra & Pallarés 2006). In recent years, several structures, and in particular historical monuments, have been equipped with permanent static monitoring systems, able to record the response in terms of displacements and strains over very long periods of time and, theoretically, for the entire life of the structure. Despite the number of applications, a procedure aimed at interpreting the data and at providing a means for detecting and localizing the insurgence of damage and the safety of the structure level from the measurements is still lacking. Due to the fact that measurements are not made during special purpose short-term experiments, but during long-term day-to-day operation, the data contain a very large amount of information, the meaning of which is not always clear. As a consequence, the main problem of a continuous static long-term monitoring system is not the acquisition of the data, but rather the choice of the methods to process the vast heap of information and provide useful and simple measures of a structure's health status (Lanata & Grosso 2006).

In the 2000 Grosso et all.(Grosso et al. 2000) have presented an interpretation of the data acquired by the monitoring system composed by more than 60 SOFO fibre optic long-base sensors along the east quay wall of the San Giorgio pier. To carry out interpretation of the measurements and correlation with the mechanical behaviour of the structure, a computer method, named SPADS, has been used. According to this algorithm, the structure is subdivided into macro-elements, each one containing several cells in which the sensors are installed. From the data of each campaign, an average curvature is computed for every cell, both in the vertical and in the horizontal planes. Among the various environmental sources causing long-period displacement of the wall, it has been found that temperature is playing the most important role. However, the concepts of macro-elements and this algorithm can be useful to transform sensor strain data into curvatures but it is not a procedure applicable to all the devices installed on historical monuments. Omenzetter et al., in 2004, have focused their attention to the identification of abrupt, anomalous and potentially onerous events in the time histories of static, hourly sampled strains recorded by a multi-sensor SHM system installed in a major bridge structure and operating continuously for a long time. Statistical analysis of wavelet coefficient time series is conducted to detect outliers, i.e. data that significantly protrude from the remainder (Omenzetter et al. 2004). Recently a statistical method known as proper orthogonal decomposition (POD) has been proposed as a damage detection algorithm for the continuous static monitoring of civil structures (Lanata & Grosso 2006), (Posenato et al. 2008). The POD has been used for extracting a temporal and spatial correlation between the static structural responses measured at different sensor locations. The comparison in time of extracted correlations is able to detect relative changes between adjacent sections that can indicate that damage has occurred and localize it. The method has been applied by the authors on data obtained by means of

a computer simulation of a typical bridge structure subjected to environmental loadings. However, this method require a distribution of the sensors along the elements to be monitored and it is scarcely applicable to the data acquired by the monitoring of monuments in which generally, due to their geometry complexity, the sensors are located in specific critical portions (often belonging to different sub-structures of the building with different structural behaviour).

The data acquired by the static monitoring were often used to calibrate and validate the numerical models of the structures. (Robert-Nicoud et al. 2005), (Onate et al. 2000), (Ivorra et al. 2010). In addition, several studies reported examples on the use of the static monitoring in order to understand the structural behaviour of historical monuments. For instance, Rossi et al. (Rossi & Rossi 1998) reported the results obtained from automatic monitoring system installed on the Cathedral in Mexico city in order to control the response of the supporting structures during the under excavation works. In addition, the results obtained by the static monitoring of St. Mark's Basilica in Venice have been also presented. In particular, in this study the correlation between the data recorded by the sensors (crak-gaunges, long base extensometers, inclinometers..) and the temperature is highlighted (the relative horizontal movements of pillars recorded by the extensometers are strongly correlated and out-of-phase with respect to temperature data). Masciotta et al. presented the results obtained from the monitoring of the main cracks and towers tilting of the Church of Saint Torcato (Masciotta et al. 2016). In this study a specific threshold values to establish appropriate warning levels for structural stability of the church and the correlation between the recorded data and the ambient parameters have been reported. The correlation between cracks and environmental parameters is very limited (the cracks monitored are inside the church) while a strong correlation between the oscillations of the towers and the seasonal fluctuations of the temperature is registered, (e.g. Figure 3-1).
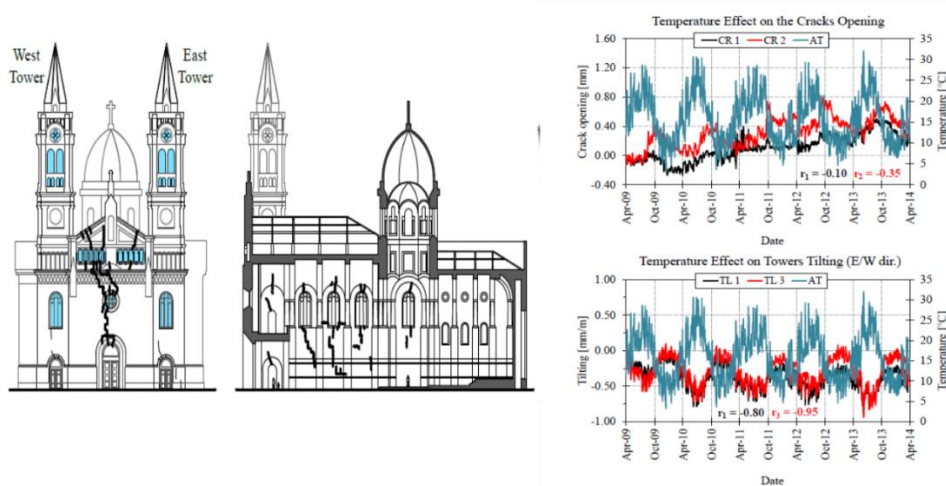

Figure 3-1: Structural damage in the church of saint Torcato and variation of cracks opening and towers tilting versus temperature (AT), (Masciotta et al. 2016)

3.3 Approach for a critical interpretation of the data acquired by a Static SHM system

SSHM systems return discrete time series which can be generally referred to as $x(t_i)$, where x represents the monitored quantity (e.g. displacement, strain, angle inclination, crack width, temperature, …) and ti represents a specific instant of time t (Brockwell & Davis 2009).Each monitored quantity is here assumed to be a function of two main factors:

$$x(t) = f[F(t), S(t)] \tag{3.1}$$

F(t) represents the (time-dependent) external forces acting on the structure, and S(t) represents the time evolution of the "state" of the structure, i.e. the condition of the structure due to its geometrical configuration, the materials mechanical properties, its boundary conditions, etc. In general, the state of the structure can be assumed stationary if it does not change significantly from year to year or not stationary if it changes with time. The variation of the state may be due to different factors such as material degradation, soil-structure interaction, etc.

The external actions F(t) on the building can be classified into three main groups (ASCE7-98 1998):

- Dead loads D(t): the permanent forces acting on a structure such as the self-weight of the structure;
- Live loads L(t): the non-permanent forces acting on the structure. In detail, these encompass the forces that depend on the weather effects, which are herein referred to as natural forces, N(t), such as wind, temperature, precipitations, etc.
- Accidental loads A(t): the forces depending on rare events, such as earthquakes, hurricanes, explosions, etc.;

Therefore, the external actions F(t) can be decomposed into:

$$F(t) = D(t) + L(t) + A(t) \tag{3.2}$$

while the state S(t) may be seen as:

$$S(t) = S(t_0) + \Delta S(t_0, t) = S_0 + \Delta S(t_0, t) \tag{3.3}$$

where S_0 is the state of the structure at time t_0 (which is assumed as known), and $\Delta S(t_0, t)$ represents the variation of the state over the time. In the case of $\Delta S(t_0, t)$ is approximately null over a certain time period, it follows that the state can be assumed as stationary (i.e. $S(t) = S(t_0)$). On the contrary, in the case of $\Delta S(t_0, t)$ differs from zero on a certain time period (on average) , it follows that the state is not stationary and some potential damage evolution is in act.

The main problem for data interpretation is that the components of the records due to the external forces are generally larger (order of magnitudes) than the components relegated to the eventual change in the

state, a direct analysis of the time-history recorded often does not allow to detect the evolution of the state. On the other hand, in the case of dead and loads are within their usual ranges, we expect that the recorded data should be characterized by predominant components due to seasonal and daily temperature excursions (assuming the temperature as the predominant external factor). In the absence of extreme events inducing accidental actions $A(t) = 0$, and assuming that the live loads are predominately due to the natural forces $L(t) = N(t)$, $F(t)$ can be expressed as the sum of the two components $D(t)$ and $N(t)$. Moreover, assuming constant dead loads, $D(t) = \overline{D}$ Equation (3.2) specifies as follows:

$$F(t) = \overline{D} + N(t) \tag{3.4}$$

Substituting Equations (3.2), (3.3) and (3.4) in Equation (3.1) leads to:

$$x(t) = f\,[\overline{D},\, N(t),\, S_0,\, \Delta S(t_0, t)] \tag{3.5}$$

For historic buildings, generally composed of massive masonry walls, the temperature is typically the external factor which mainly affects the structural response (in usual operational condition). It is here assumed that the natural forces are periodic functions with two fundamental components:

$$N(t) = N_1(t) + N_2(t) \tag{3.6}$$

N_1 has period T equal to 365 days (due to the motion of revolution of the earth around the sun) leading to the annual oscillations and a contribution N_2 with a period T equal to 1 day (due to the motion of rotation of the earth around its axis) leading to the daily oscillations. Based on all the above assumptions and considerations, the time series $x(t)$ can be decomposed into two main components:

$$x(t) = x_1(t) + x_2(t) \tag{3.7}$$

$x_1(t)$ is the periodic component of $x(t)$ depending on $N(t)$ and $\overline{D}$, while $x_2(t)$ is the component of $x(t)$ depending on the state $S(t)$.

3.3.1 Reference quantities

In the light of all the above consideration, it appears that a useful analysis of the data from a SHM system have to focus on the identification of the potential evolutionary trends of response, which typically oscillates following the daily and seasonal thermal excursions. To do that, it is first necessary to characterize these seasonal and daily effects by introducing appropriate descriptors, hereafter referred to as "reference quantities"

The collection of these "reference quantities" constitute a specific nomenclature for an interpretation of the data obtained from a structural monitoring that also allow to collect data in a systematic fashion and thus compare them with those of similar structural typologies. The systematic identification of the "reference quantities" from the recorded data allows to identify the presence of potential evolutionary trends of the monitored state by the specific sensor. In effect, the "reference quantities", extracting useful information of the data recorded in a daily and annual span of time, allow to compare these values over all the period of monitoring.

With reference to the *j*-th generic day, the quantities of interest are:

- the *Daily Amplitude* ($\delta_{day,j}$), that represents the difference between the maximum and minimum of the discrete time series recorded $x(t_i)$ in the specific j-th day

$$\delta_{day,j} = \left[max\ x(t_i) - min\ x(t_i) \right] \qquad \forall\ t_i \in \text{j-th day} \qquad (3.8)$$

- the *Mean Daily Value* ($\mu_{day,j}$), that represents the mean value of the discrete time series recorded $x(t_i)$ in the specific j-th day

$$\mu_{day,j} = \frac{1}{n_j} \sum_{i=1}^{n_j} x(t_i) \qquad\qquad \forall\ t_i \in \text{j-th day} \qquad (3.9)$$

- the *Absolute Daily Residuals of the Mean Value* ($r_{\mu day, j(k-k_0)}$), that represents the difference between the mean value, recorded in the j-th day, of the k-th year and the k_0-th year (reference year, generally corresponding to the first year of monitoring)

$$r_{\mu day, j(k-k_0)} = \mu_{\mu day, j(k)} - \mu_{\mu day, j(k_0)} \qquad (3.10)$$

- the *Progressive Daily Residuals of the Mean Value* ($rp_{\mu day, j(k+1-k)}$), that represents the difference between the mean value, recorded in the j-th day, of the $k+1$-th year and the k-th year

$$rp_{\mu day,\,j(k_{+1}-k)} = \mu_{day,\,j(k_{+1})} - \mu_{day,\,j(k)} \qquad\qquad (3.11)$$

With reference to the y-th year, the quantities of interest are:

- the *Annual Amplitude* ($\Sigma_{year,y}$), that represents the difference between the maximum and minimum of the discrete time series recorded x(t$_i$) in the specific y-th year

$$\Sigma_{year,y} = \left[max\ x(t_i) - min\ x(t_i) \right] \qquad \forall\ t_i \in \text{y-th year} \qquad (3.12)$$

- the *Mean Annual Value* ($M_{year,y}$), that represents the mean value of the discrete time series recorded x(t$_i$) in the specific y-th year

$$M_{year,y} = \frac{1}{n_y} \sum_{i=1}^{n_y} x(t_i) \qquad \forall\ ti \in \text{y-th year} \qquad (3.13)$$

- the *Absolute Annual Residuals of the Mean Value* ($r_{\mu day,\,j(k-k_0)}$), that represents the difference between the mean annual value recorded in the k-th year and the k$_0$-th year (reference year, generally corresponding to the first year of monitoring)

$$R_{Myear,(k-k_0)} = M_{year,k} - M_{year,k_0} \qquad\qquad (3.14)$$

- the *Progressive Annual Residuals of the Mean Value* ($Rp_{Myear,(k+1-k)}$), that represents the difference between the mean annual value recorded on the k$_{+1}$-th year and the k-th year

$$Rp_{Myear,(k_{+1}-k)} = M_{year,k_{+1}} - M_{year,k} \qquad\qquad (3.15)$$

In addition also sudden drops may be present in the recorded time series x(t$_i$). These sudden drops may be related either to an instrument malfunctioning, either to external factors, or to extreme events (such as earthquakes, hurricanes, …) and are here identified through the letter Δ. Table 3-1 collects the "reference quantities" defined. For the sake of clarity, in order to describe the "reference quantities" a fictitious signal is displayed in Figure 3-2 and some of its corresponding reference quantities are presented in Figure 3-3.
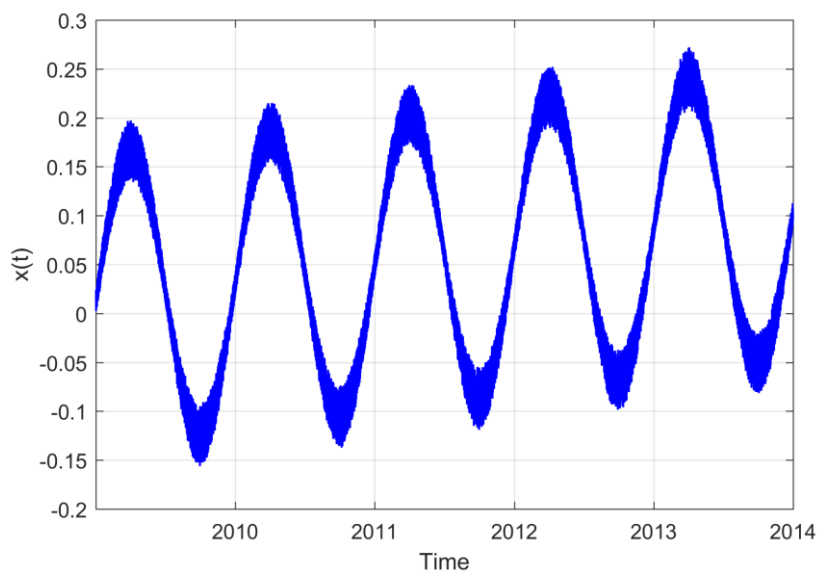
Figure 3-2- Time series x(t)
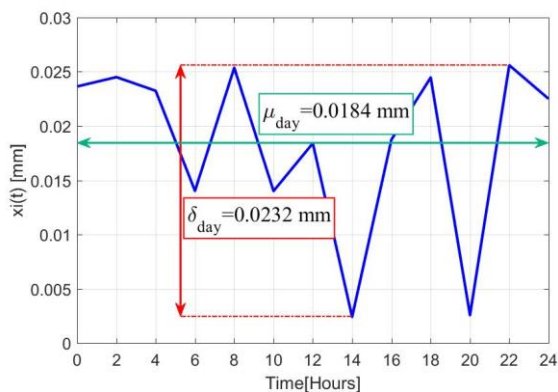
(a)
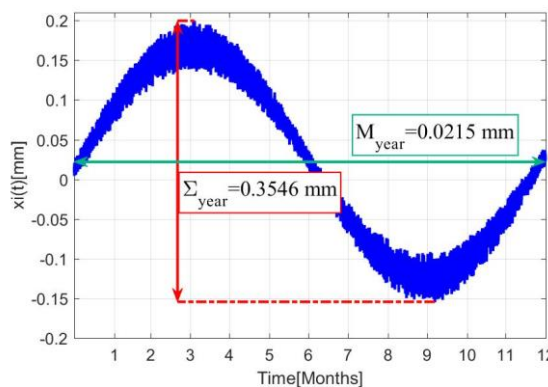
(b)
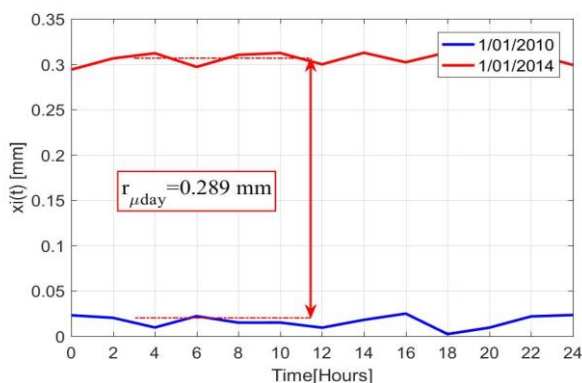
c)
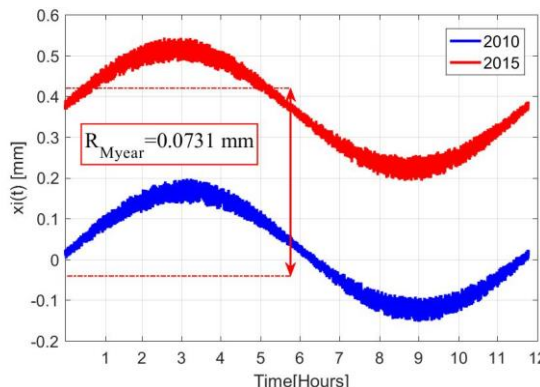
d)

Figure 3-3: Reference quantities of the fictitious signal: (a) Daily amplitude and Mean Daily Value, (b) Annual amplitude and Mean Annual Value,(c) Absolute Daily Residuals of the Mean Value and (d) Absolute Annual Residuals of the Mean Value

Table 3-1- The introduced "reference quantities" for the analysis of the recorded data.

Reference quantity	Definition	Mean value within the observation period Δt
Daily Amplitude	$\delta_{day,j} = \left[max\ x(t_i) - min\ x(t_i) \right]$ $\quad \forall\ t_i \in$ j-th day	$\overline{\delta} = \dfrac{1}{N_{\Delta t}} \sum\limits_{j=1}^{N_{\Delta t}} \delta_{day,j}$
Mean Daily Value	$\mu_{day,j} = \dfrac{1}{n_j} \sum\limits_{i=1}^{n_j} x(t_i)$ $\quad \forall\ t_i \in$ j-th day	$\overline{\mu} = \dfrac{1}{N_{\Delta t}} \sum\limits_{j=1}^{N_{\Delta t}} \mu_{day,j}$
Absolute Daily Residuals of the Mean Value	$r_{\mu day,j(k-k_0)} = \mu_{\mu day,j(k)} - \mu_{\mu day,j(k_0)}$	$\overline{r_{\mu}} = \dfrac{1}{N_{\Delta t}} \sum\limits_{j=1}^{N_{\Delta t}} r_{\mu day,j(k-k_0)}$
Progressive Daily Residuals of the Mean Value	$rp_{\mu day,j(k_{+1}-k)} = \mu_{day,j(k_{+1})} - \mu_{day,j(k)}$	$\overline{rp_{\mu}} = \dfrac{1}{N_{\Delta t}} \sum\limits_{j=1}^{N_{\Delta t}} rp_{\mu day,j(k_{+1}-k)}$
Annual Amplitude	$\Sigma_{year,y} = \left[max\ x(t_i) - min\ x(t_i) \right]$ $\quad \forall\ t_i \in$ y-th year	$\overline{\Sigma} = \dfrac{1}{N_{\Delta t}} \sum\limits_{y=1}^{N_{\Delta t}} \Sigma_{year,y}$
Mean Annual Value	$M_{year,y} = \dfrac{1}{n_y} \sum\limits_{i=1}^{n_y} x(t_i)$ $\quad \forall\ t_i \in$ y-th year	$\overline{M} = \dfrac{1}{N_{\Delta t}} \sum\limits_{y=1}^{N_{\Delta t}} M_{year,y}$
Absolute Annual Residuals of the Mean Value	$R_{Myear,(k-k_0)} = M_{year,k} - M_{year,k_0}$	$\overline{R_M} = \dfrac{1}{N_{\Delta t}} \sum\limits_{y=1}^{N_{\Delta t}} R_{Myear,(k-k_0),y}$
Progressive Annual Residuals of the Mean Value	$Rp_{Myear,(k_{+1}-k)} = M_{year,k_{+1}} - M_{year,k}$	$\overline{Rp_M} = \dfrac{1}{N_{\Delta t}} \sum\limits_{y=1}^{N_{\Delta t}} Rp_{Myear,(k_{+1}-k),y}$
Drop	Δ	

3.4   Conclusions

An approach for a standardized analysis of the data recorded by a Structural Health Monitoring system installed in an historical building has been presented. It has been assumed that the recorded time series may be decomposed into two fundamental components. The first one related with the natural actions and characterized, in absence of extreme events (such as explosion earthquake, hurricanes,…), by a substantial periodic behaviour. The second one related to the evolution of the state indicating possible evolution of structural damage. Once the recorded signal is depurated from the first components (the periodic one), the eventual evolution of the state of the structure can be more easily detected. The evolution of the trend has been evaluated through the definition of reference quantities as descriptors of the recorded data. The difference between the values of these parameters evaluated in a different span of time allow to identify the possible evolutionary trends of the signal, considering that the influence of the external factors is always present and it is repeated similarly year-after year. Aside the identification of the eventual evolution of the structural damage, the other main objective of these "reference" quantities is the definition of a common nomenclature for the interpretation of the data acquired by monitoring system of the monuments. These quantities could be collected in a database and used as to evaluate the records of similar buildings to have a more sound interpretation of the SMH data.

Chapter 4

4 Real data processing

4.1 Introduction

The fictitious signal showed in the previous section represent the ideal discrete time series acquired by the monitoring system. The real recorded data often present irregularities due to malfunctioning of the sensor, which must be removed before performing the processing for the interpretation of the signal. After the removal of signal irregularities and drops it is possible proceed with the signal analyses. As explained before, the main objective in the interpretation of the data acquired from the SSHM system is identify if the phenomena under observation are in a stable condition or not. The "reference quantities" introduced allow to directly identify if the recorded signal is repeated over time in a stationary condition or not. The difference between the values of these parameters evaluated in a different span of time allow to identify the possible evolutionary trends of the signal, considering that the influence of the external factors is always present and it is repeated similarly year-after year. Another possibility to estimate the trend is to develop a signal frequency analysis in order to identify and then remove the main periodicity of the signal. The signal frequency analyses applied to the static monitoring data will be introduced in this section and used to validate the approach presented in the previous chapter. As mentioned before, the temperature is typically the external factor which mainly affects the structural response of historical masonry buildings. However, a statistical analysis to evaluate the influence of the different external factors on the recorded data seems opportune and will be explain in this chapter.

4.2   Removal signal irregularities

The irregularities can lead to an interpretation of the signal not corresponding to the real behavior of the phenomenon. The sensors installed on the monumental buildings are generally located at accessible areas and thus they can be subjected to accidental impact. The movement of the device causes interruptions or drops that can change the mean value of the recorded data (Figure 4-1a). Generally a repositioning of the sensor is necessary. In this case the time series analysis have to consider the two parts (before and after the repositioning) separately. The time series can present other drops, such as spikes that do not change the mean value, related to the sensibility of the devices to the external factors (rain, snow...) or extreme events (earthquakes). Figure 4-2a shows the data recorded by a sensor very sensible to the weather conditions. It is clear that without the removal of the drops is impossible understand the trend recorded by the signal (Figure 4-2b). It is of fundamental importance identify the nature of each drops recorded in order to remove the spike corresponding to incorrect recorded data and focus the attention on the data recorded during an earthquake. This analysis consist on the identification of each drops recorded and in a critical comparison with the information collected concerning to the earthquakes occurred close to the monument (Figure 4-3). Then the incorrect data (not significant for the analysis but due to incorrect recording by the device) are removed from the time series through a specific filter (Figure 4-2b).

(a)   (b)
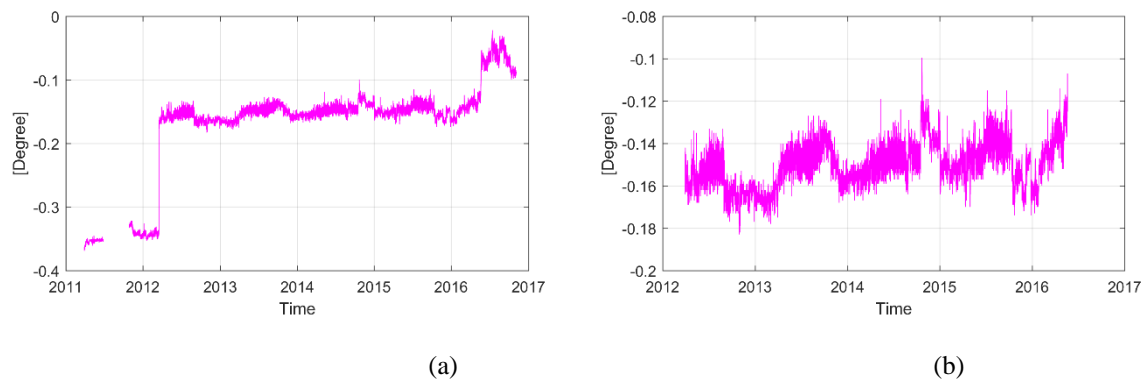
Figure 4-1: (a) Signal as recorded by the sensor, (b) Removal of signal irregularities

(a)   (b)
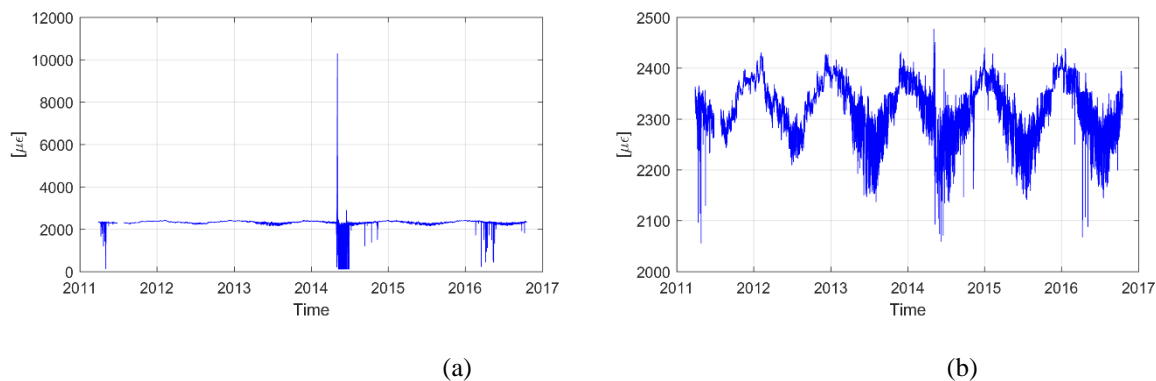
Figure 4-2: (a) Signal as recorded by a sensor very sensible to the weather conditions, (b) Removal of signal irregularities
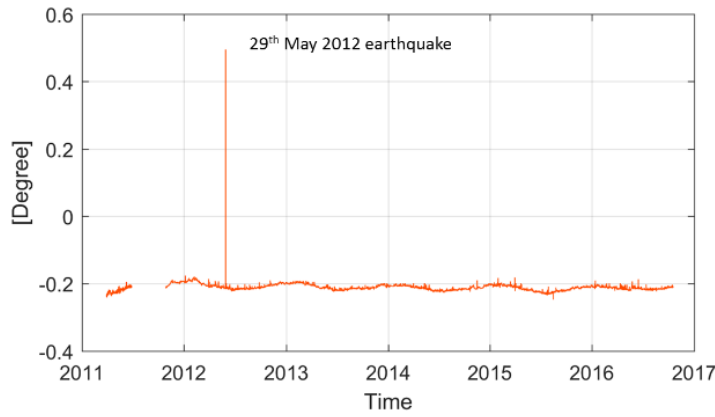
Figure 4-3: Drop recorded by the sensor during the 2012 Emilia earthquake

4.3   Signal analyses

The recorded data for a random physical phenomenon may be thought of as one physical realization of a stochastic process. Stochastic process are subdivided in stationary or non stationary. The stochastic process is defined weakly stationary when the mean value (first moment) and the autocorrelation function (joint moment) defined in Equations 4.1 and 4.2 do not vary as time varies. In particular, the mean value is a constant and the autocorrelation function is dependent only on the time displacement τ .

$$\mu_x(t_1) = \lim_{N \to \infty} \frac{1}{N} \sum_{k=1}^{N} x_k(t_1)$$

(4.1)

$$R_{xx}(t_1, t_1 + \tau) = \lim_{N \to \infty} \frac{1}{N} \sum_{k=1}^{N} x_k(t_1) x_k(t_1 + \tau)$$

(4.2)

If the Equations 4.1 and 4.2 vary as time varies, the stochastic process is said to be non-stationary (Julius S. Benedat 2000).

For the special case where all possible moments and joint moments are time invariant, the random processes is said to be strongly stationary. Nonstationary stochastic process may be further categorized in terms of specific types of nonstationary properties. The data, whether from physical measurements or numerical modelling, most likely will have one or more of the following problems: (i) the total span is too short, (ii) the data are non-stationary, and (iii) the data represent nonlinear process. Facing such data, we have limited options to use in the analysis(Huang et al. 1998). The non-stationarity of a time series can be due to the presence of: (i) a trend; (ii)seasonality and (iii) other evolutionary effects. The signal analysis for the data acquired by the static SHM aims at the estimation of these three components. When analyzing periodic fluctuations in measured data, the most common form of data analysis is Fourier analysis, which uses the postulate that any signal can be constructed as a sum of sinusoidal functions. Fourier analysis describes the signals as the sum of sine waves, with infinite extent, with different

frequencies. Fourier analysis, for its prowess and its simplicity, has dominated the data analyses efforts since its introduction, and has been applied to all kind of data. Although the Fourier transform is valid under extremely general conditions (Titchmarsh 1948), there are some crucial restrictions of the Fourier spectral analysis: the system should be linear; and the data should be periodic or stationary; otherwise, Fourier spectral analysis may give misleading results. For lack of alternatives, however, Fourier spectral analysis is still used to process such data. In the recent years, new methods for analyzing nonlinear and nonstationary data have been developed. For instance, an alternative data analysis tool has been proposed by Norden E. Huang called the Hilbert-Huang Transform (HHT) (Barnhart 2011). The HHT technique for analyzing data consists of two components: a decomposition algorithm called empirical mode decomposition (EMD) and a spectral analysis tool called Hilbert spectral analysis. The key part of the method is the 'EMD' method. The algorithm attempts to decompose nearly any signal into a finite set of functions, whose Hilbert transforms give physical instantaneous frequency values. These functions are called intrinsic mode functions (IMFs). The algorithm utilizes an iterative sifting process which successively subtracts the local mean from a signal. The sifting process is as follows:

- Determine the local extrema (maxima, minima) of the signal.
- Connect the maxima with an interpolation function, creating an upper envelope about the signal.
- Connect the minima with an interpolation function, creating a lower envelope about the signal.
- Calculate the local mean as half the difference between the upper and lower envelopes.
- Subtract the local mean from the signal.
- Iterate on the residual.

The sifting process is repeated until the signal meets the definition of an IMF. Then, the IMF is subtracted from the original signal, and the sifting process is repeated on the remainder. This is repeated until the final residue is a monotonic function. The last extracted IMF is the lowest frequency component of the signal, better known as the trend. The sifting process is stopped when the signal meets the criteria of an IMF. The definition of an IMF was formed to ensure that the IMF signals give physical frequency values when using the Hilbert transform. The definition of an IMF, therefore, is a signal which has a zero-mean, and whose number of extrema and zero-crossings differ by at most one(Huang et al. 1998),(Mukhopadhyay & Betti 2013) . IMFs are considered monocomponent functions which do not contain riding waves. Once a signal has been fully decomposed, the signal can be written as the finite sum of the IMFs and a final residue. Appears therefore clear that this method not allow to identify separately the main components of the signal. For this reason, and only with the objective to validate the approach proposed in the previous chapter, the Fourier analyses will be applied to the recorded data by the static monitoring system. First, however, an analysis to assess which external factors influence more the structural response of the historical buildings is presented.

4.3.1 Influence of the external factors

The raw data obtained from the SHM systems should be analyzed in order to identify relationships between the recorded quantities and the external factors such as temperature, wind, humidity…. (Palermo et al. 2013). For each record y_i, with $i= 1,…..,m$, m is the number of instruments, an empirical regression model has been built using a polynomial function such as the one shown below:

$$y_i = \beta_0 + \sum_{j=1}^{n} \beta_j \left[x\right]_j + \varepsilon \tag{4.3}$$

where ε is the regression model error and x_j is the vector containing the measurements of the j-th external factor,

Equation 4.3 can be also rewritten in a compact and matrix form:

$$y_i = A\beta + \varepsilon \tag{4.4}$$

where

$A = \begin{bmatrix} 1 & x_1 & x_2 & ... & x_n \end{bmatrix}$ is a matrix collecting the vectors (time series) of the recorded external factors.

The values of parameter β of the polynomial function are evaluated using:

$$\beta = \left(A^T A\right)^{-1} A^T Y \tag{4.5}$$

The relative importance on the structural response of each external effect i is evaluated through the normalizing and centering the measured external effects on their mean value, as following

$$\tilde{x}_i = \frac{\mu_{x,i} - x_i}{\sigma_{x,i}} \tag{4.6}$$

where $\mu_{x,i}$ is the mean of the recorded data for an external effect i and $\sigma_{x,i}$ is the corresponding standard deviation. The parameter values β calculated using the normalized external effects $\tilde{x}$ constitute a vector (n x 1) called β'. The relative importance of each external effect is contained in the vector $\tilde{\beta}'$ and it has been obtained using the following equation:

$$\tilde{\beta}' = \frac{\left|\beta'\right|}{\sum_{i=1}^{n}\left|[\beta']_i\right|} \tag{4.7}$$

4.3.2 Signal frequency analysis

The main periodicity of the data recorded has been obtained through a frequency analysis of the signal using a Fourier analysis (formulated by Joseph Fourier in the early 1800s). The Fourier Transform (FT) is a mathematical technique that transforms a function of tim*e, x(t)*, to a function of frequency *X(ω)*. In effect, FT decomposes a waveform or a function into sinusoids of different frequencies, which sum to the original waveform. It identifies or distinguishes different frequency sinusoids and their respective amplitudes. Fourier transform can be expressed as x(t) → X(f) according to:

$$X(f) = \int_{-\infty}^{+\infty} x(t)e^{-j\omega t}dt \tag{4.8}$$

where ω = 2πf , and f denotes frequency in Hz

X(f) contains all the information of the original signal x(t). Further, x(t) can be obtained from X(f) by the inverse Fourier transformation:

$$x(t) = \int_{-\infty}^{+\infty} X(f)e^{j\omega t}df \tag{4.9}$$

In the case of signal obtained by monitoring system, the function x(t) is known at evenly spaced points x(nT) where T = 1/fs and fs is the sampling rate, the Discrete Fourier transform (DFT) would be given by:

$$X(f) = \sum_{n=-\infty}^{+\infty} x_n(t)e^{-j\omega T} \tag{4.10}$$

This function is periodic with period fs. The sampled function can be recovered by inverse transform:

$$x(t)\frac{1}{f_s} = \int_{-\frac{f_s}{2}}^{+\frac{f_s}{2}} X(f)e^{j\omega T}df \tag{4.11}$$

The main periodicity of the data recorded by the monitoring system can be evaluated trough the Fast Fourier transform (FFT), an efficient implementation of the discrete Fourier transform (DFT).

First, the recorded signal will be transform in a signal characterized by zero mean and unit variance as follows:

$$Y(t) = \frac{x(t) - \mu}{\sigma} \tag{4.12}$$

The FFT allows identifying the main periodicities of the signal. The periodicities that can be associated to seasonal effects will be removed with an appropriate filter. The inverse Fourier Transform of the filtered signal allows to reconstruct the signal not affected by the influence of the seasonal effects.

4.4 Conclusions

The real data acquired by the static monitoring system generally present several irregularities due to malfunctioning of the sensors, which have to be removed in order to evaluate correctly the trend recorded. In this chapter, examples of such irregularities are presented and the importance of a critical comparison between these irregularities and the information collected concerning to the extreme external factors (generally earthquakes) that occurred close to the monument were highlighted. Moreover, the main features of the data obtained from physical measurements and the available methods for their signal analyses are briefly reported. In addition, the methods that will be used for the analyses of the assessment of the influence of the external factors on the recorded data and for the signal frequency analysis in order to estimate the trend and main periodicity of the signal in the next chapters were presented.

Chapter 5

5   A case study of the Asinelli Tower

5.1   Introduction

In the 2011, a static SHM system has been installed on the Asinelli tower, a masonry leaning tower built at the end of the 12th century in order to monitor the health of the monument after the strengthening interventions that were performed between 1998 and 2008. The monitoring system will be described in this Chapter, i.e. the localization of the sensors on the tower and the type of sensors used.

The large amount of data recorded by the monitoring system has been analyzed using the approach proposed in § 3.3 in order to evaluate if the phenomena under observation are in a stable condition or not. The signal frequency analyses on the recorded data have been also carried out and the results obtained in terms of residuals (i.e. signal not affected by the seasonal effects which should be representative of the state of the building) compared with the residue obtained making use of the approach proposed. The main results obtained from the analyses are presented in this Chapter.

5.2   The Asinelli Tower

The city of Bologna preserves traces from past civilizations, especially the medieval era. During the XII and XIII centuries, a large number of towers were erected by some of the richest families (Costa 1984). Some of them still stand nowadays and the two most majestic, the Garisenda and Asinelli are the symbol of the city (Figure 5-1a). The Asinelli tower was most probably completed in 1119 reaching a height of almost 100 m thanks to the introduction of advanced construction methods for the time (Cavani 1912). During the Second World War, the Tower was used as a watchtower. It tilts toward Sud-West of 2.23 m. Its cross-section is approximately square for the whole height with a gradual decrease (almost linear) of the side width from 8.5 m at the base to 6.0 m at the top, excepting a sudden discontinuity at a height of 34 m. The external walls were built using the so-called "a sacco" technique (Figure 5-1b): two skins of brick masonry with an internal rubble and mortar fill. The fill is com-posed of irregular materials including brick fragments and irregular stones bound by aerial mortar. Common solid bricks are used for the outer skins, while the basement is realized with selenitic bricks. The total thickness of the masonry (the two skins plus the internal fill) decreases almost linearly from 3.15 m at the base to 0.45 m at the top. Three main discontinuities are present at 11.5 m, 34.0 m and56.0 m. The masonry assemblies are not regular, with variations in both the width of the bricks and the thickness of the mortar (from1.0 cm to 3.0 cm)

(a)   (b)
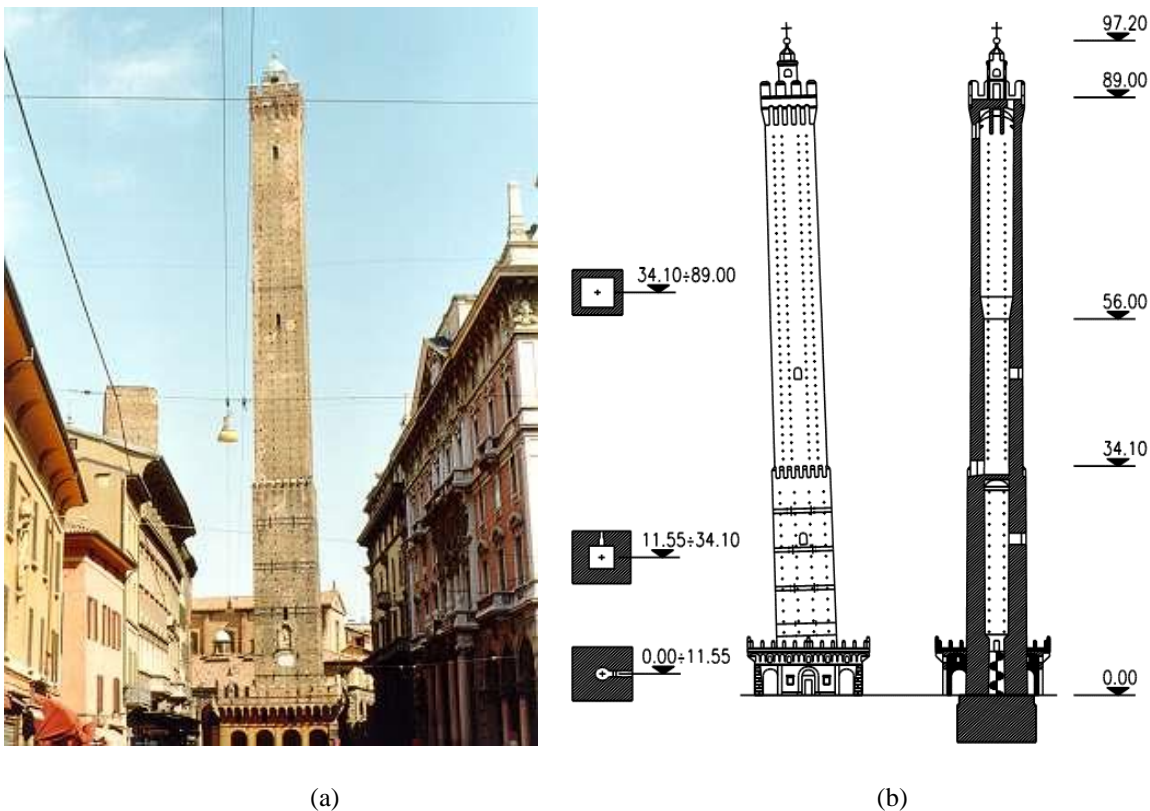
Figure 5-1- (a) The Asinelli tower of Bologna, (b) The tower elevation with the indication of the main discontinuities;

Several strengthening interventions were performed in the last decade (1998 - 2008) on the tower. The strengthening interventions were developed in two main phases:

- Phase 1: (a) masonry consolidation through substitution of the damage bricks and injection of high strength mortar (Figure 5-2a); (b) installation of steel frame in order to provide a connection between the two masonry layers (Figure 5-2b).

- Phase 2: installation of external steel ties in order to provide a lateral confinement to the masonry (Figure 5-2c).

(a)

(b)

(a)

Figure 5-2- Details of the strengthening interventions of the tower: (a) masonry consolidation: before the substitution of the damage bricks and injection of high strength mortar (left) and after (right), (b) installation of steel frame and (c) installation of external steel ties

5.3   Types and location of instruments

At the beginning of year 2011, a SHM system was installed in the Asinelli tower in order to monitor:

- the opening of the main cracks,

- the variation of the stress level of the steel ties,

- the masonry compression at critical locations,

- the variation in the inclination of the towers,

- the environmental parameters (temperature, wind direction and wind speed).

Data are acquired at time intervals of 15 minutes.

The nomenclature of the monitoring instruments used has been chosen using the following principles: the first letter indicates the name of the monument, the second and third the position of the instrument and then the last the type of instrument. The following symbols have been used:

A=Asinelli,

FN=North front, **FS**=South front, **FE**=East front, **FO**=West front (Figure 5-3),

F=long base deformeter, **D**=deformeter, **I**=inclinometer, **E**=extensometer, **L**=laser displacement sensor, **T**= thermometer, **V**=gonioanemometer sensor.
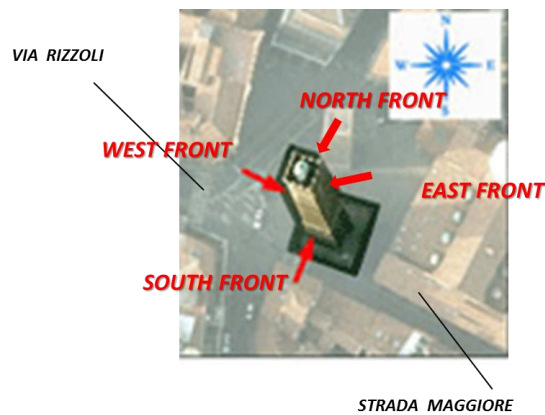
Figure 5-3: Identification of the different Fronts of the Asinelli tower

Table 5-1 summarised the typology and the position of the different instruments installed along the height of the Asinelli tower which are then displayed in Figure 5-4

Table 5-1-Typology and position of the instrument installed on the Asinelli tower

Sensor	N.	Location	Type
Long Base Deformeter	8	5 on the masonry of the West front(FO): at different level 3 on the masonry of the South front (FS): at different level.	Invar wire Deformeter
Deformeter	5	4 on cracks of the West front (FO) 1 on a crack of the East front (FE)	OG400 deformeters
Inclinometer	8	4 on the wall of the West front (FO): at different level. 4 on the wall of the South front (FS): at different level.	Dual axis inclinometer ELS-XX-V
Extensometer	6	3 on the steel ties of the West front (FO) 3 on the steel ties of the South front (FS)	Vibrating Wire Spot Weldable Strain Gauge
Laser displacement sensor	3	1 on the West front (FO) with target on Prendiparte tower 1 on the South front (FS)with target on Santa Maria della Vita dome 1 on the South (FS)front with target on a building on Santo Stefano street	Long Range Laser Displacement Sensors DLS-B
Thermometer	2	1 on the west front (FO) 1 on the South front (FS)	
Gonioanemometer sensor	1	At the top of the tower	
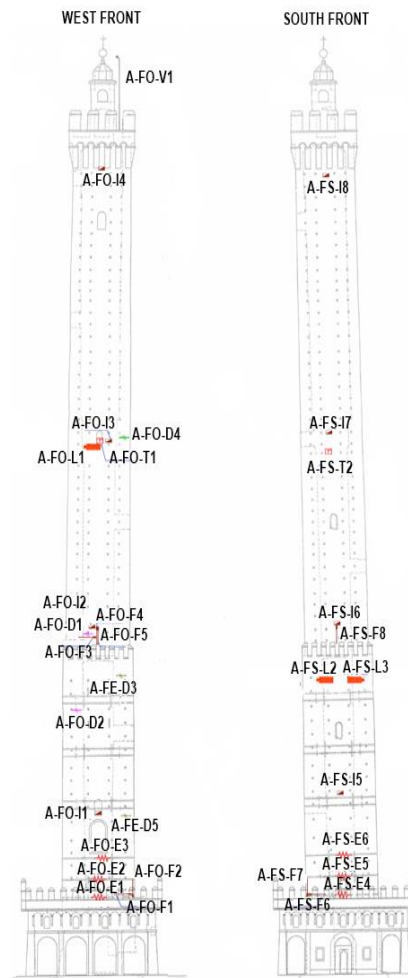
Figure 5-4: Monitoring system of Asinelli Tower

The instruments installed on the Asinelli tower are briefly described below.

Long base Deformeters: Invar wire Deformeter

Deformeters are simple devices used to monitor the crack and deformation propagation in the structure they are applied on. They are employed during structural (cracks in buildings, joints of bridges, etc.) and geotechnical monitoring (soil subject to landslide, cracks in rocks, etc.), and during monitoring operations of rotations, displacements, and deformations. There are a wide range of products suitable such as mechanical joint meters (linear, two or three-dimensional), electrical joint meters (vibrating wire and potentiometer), and wire deformeters. The long base deformeters installed on the Asinelli tower in order to monitor the stress of critical portions of masonry are Invar wire deformeters (Figure 5-5). They use an invar wire and a pre-stretching system to give a structural extension compared to electronic deformeters, so to allow the measurement of two anchor points at a distance of more than 20m. Wire Deformeters are employed during geotechnical, structural, and convergence monitoring and during operations to measure deformations on a medium or long-term basis. Automated, computerized measures can be either read in loco or stored in a local data logger to be submitted to a remote data

acquisition unit, through different transmission methods. Table 5-2 collects some technical specification of the Invar wire Deformeters.
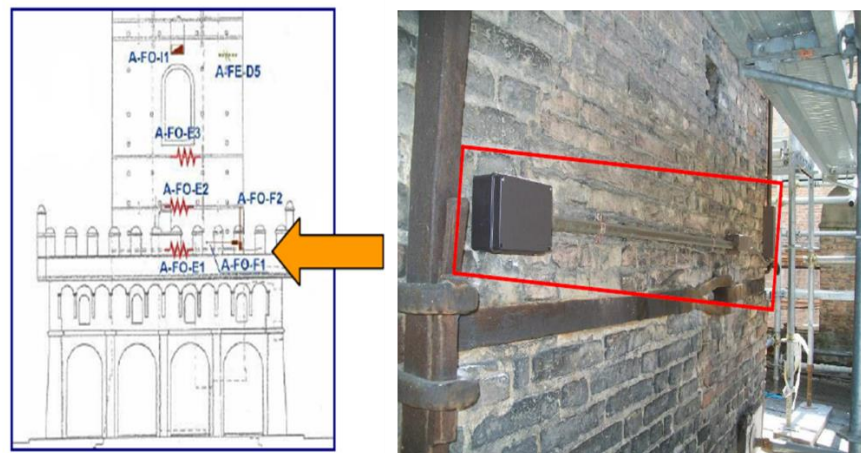
Figure 5-5- Invar wire deformeters (F1) installed on the West Front

Table 5-2-Technical specification of the Invar wire Deformeters

TECHNICAL SPECIFICATIONS	
Measurement Range	25 mm
Measuring Base	1500 mm
Precision	< 0,05 %
Accuracy	< 0,015 mm
Temperature Range	(-10/+80)°C

Deformeter: OG400

The deformeters used on the Asinelli tower to control the opening of the main cracks are OG400 defometers (Figure 5-6). They can be used in tough environments, which may even require brief immersions. The instrument allows a precise monitoring of relative movements of cracks and rocks. Installation is made easier by two M6 uniball joints, with a 6mm hole, placed at the ends of the device. The sliding bar can be extended for complex installations. Readings in mm can be obtained through a manual readout unit (OG180) or a data logger and a 4-20mA converter for potentiometers. The uniball joints at both ends of the device make the fixing easier and allow the transducer to monitor uneven and non linear movements. The high degree of protection makes the instrument reliable even in tough installations. The relatively low resistance allows the instrument to be insensitive to interferences and external electrical noise, even at medium distances. Table 5-3 collects some technical specification of OG400 Deformeters.
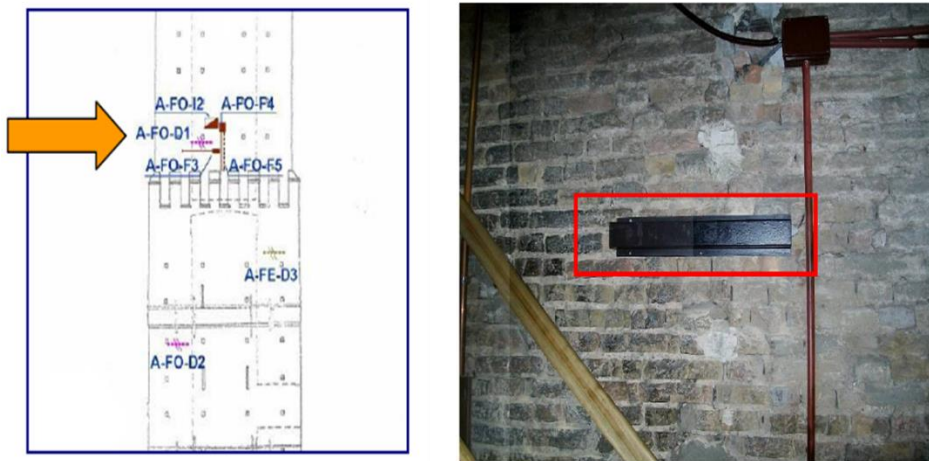
Figure 5-6- OG400 Deformeters (D1) installed on the West Front

Table 5-3- Technical specification of the OG400 Deformeters

TECHNICAL SPECIFICATIONS	
Measurement Range	300 mm
Accuracy	< 0,05 %
Measuring Base	150 mm
Diameter	15 mm
Temperature working	from -20°C to +80°C

Extensometer: Vibrating Wire Spot Weldable Strain Gauge

The extensometers installed on the Asinelli tower in order to monitor the stress on the steel ties are vibrating wire spot weldable strain extensometers (Figure 5-7). They are designed primarily to measure strains on the surface of steel structures but may also be used on other types of material. The extensometer consists of two end blocks with a tensioned steel wire between them. The end blocks are attached to stainless steel tabs, which may be attached to steel structures by spot welding, using alternative end blocks, bonded, or grouted. Precision tensioning is carried out on site using a special tensioning jig and the gauge can be set for compression, tension or at mid point. The strain gauge operates on the principle that a tensioned wire, when plucked, vibrates at its resonant frequency. The square of this frequency is proportional to the strain in the wire. Around the wire is a magnetic coil which when pulsed by a vibrating wire readout or data logger interface plucks the wire and measures the resultant resonant frequency of vibration. As the steel or other surface undergoes strain the end blocks will move relative to each other. The tension in the wire between the blocks will change

accordingly thus altering the resonant frequency of the wire. Table 5-4 collects some technical specification of Vibrating Wire Spot Weldable strain extensometers.
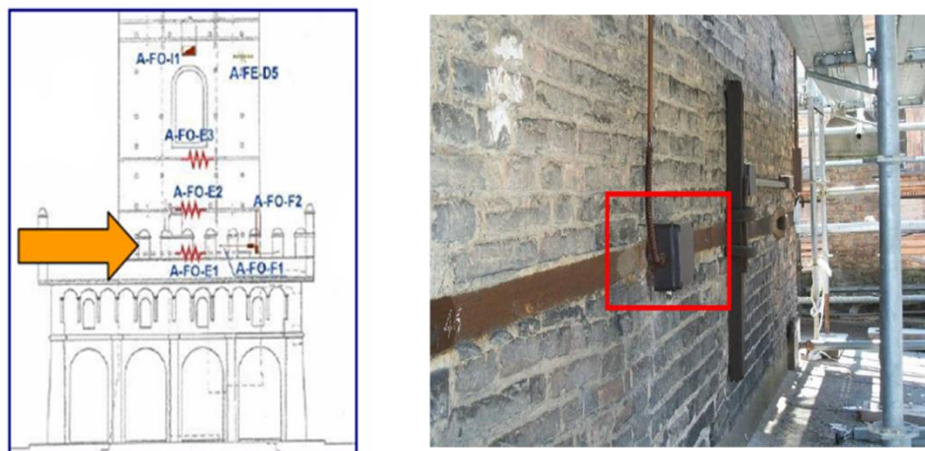
Figure 5-7- Vibrating Wire Spot Weldable strain extensometers (E1)

Table 5-4- Technical specification of the Vibrating Wire Spot Weldable strain extensometers

TECHNICAL SPECIFICATIONS	
Gauge length	50,8mm
Range	3000 µ-strain
Temperature range	(-20/+80)°C
Accuracy	0,5 % FS

Laser displacement: Long Range Laser Displacement Sensors DLS-B

The displacements of the Asinelli tower are monitored through the DLS-B Laser distance meter (Figure 5-8a). These sensors aim three fix points: Prendiparte tower, the dome of S. Maria della Vita church and a building on S. Stefano street (Figure 5-8b). These sensors are optoelectronic devices used to measure distances through a laser. Measurement is contactless, quick, easy, and extremely accurate. Measurement is contactless, quick, easy, and extremely accurate. Laser distance meters may be equipped with a tripod base to set up permanent stalls. They can be either portable or equipped with a tripod base. Measurements can be taken through a manual or automated system. Table 5-5 collects some technical specification of Long Range Laser Displacement Sensors DSL-B Series.

(a)   (b)
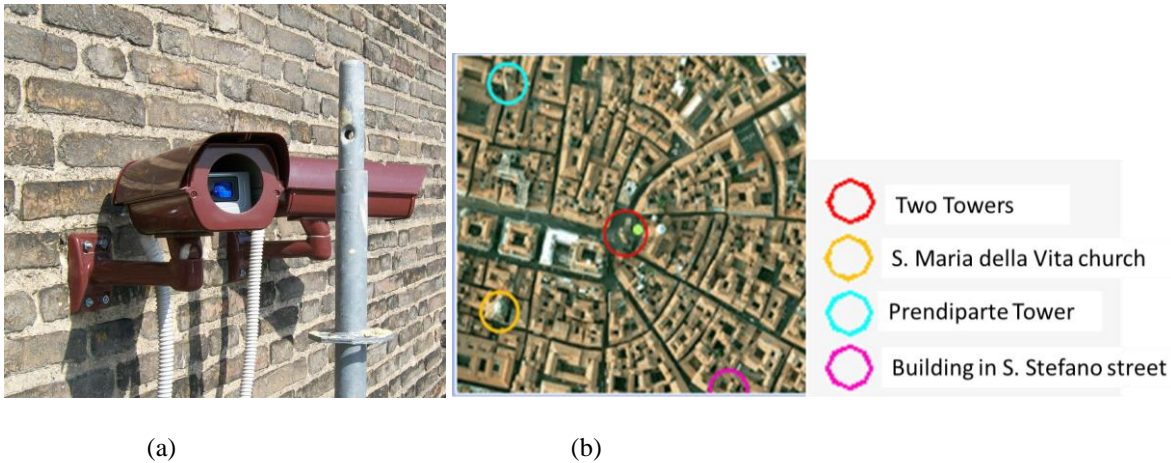
Figure 5-8- Long Range Laser Displacement Sensors DSL-B Series (L1) installed on the West Front

Table 5-5- Technical specification of the Long Range Laser Displacement Sensors DSL-B Series

TECHNICAL SPECIFICATIONS	
Accuracy	± 3 mm
Measurement range (on reflective surface)	0,05-500 m
Measurement range (on reflective surface)	0,05-65 m
Operating Temperature	(-20/+50)°C
Dimensions (h x w x l)	54x80x150 mm

Inclinometers: Dual axis inclinometer ELS-XX-V

The inclinations of the walls are monitored through the installation of a dual axis inclinometer (Model ELS-XX-V) on the height of the tower (Figure 5-9a). The x component record positive value along the South-East direction and negative value along the North-West direction. While the y component record positive value along the North-East direction and negative value along the South-West direction. These devices combine an electrolytic level sensor with a CMOS hybrid signal conditioning circuit. The level sensor contains 3 platinum contacts hermetically sealed in a cover, partially filled with a conductive fluid. When the sensor is at its zero position the electrical impedance of the fluid from the central electrode to each other electrodes is equal. When the sensor tilts the movement of the fluid determines the change of the impedance in proportion to the angle of tilt. Table 5-6 collects some technical specification of Long Range Laser Displacement Sensors DSL-B Series.
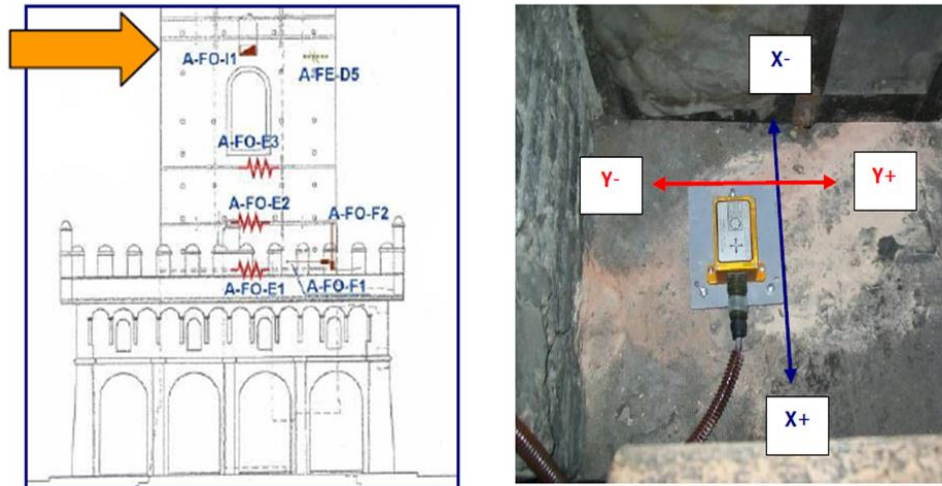
Figure 5-9- Dual axis inclinometer ELS-XX-V (I1) installed on the West Front

Table 5-6- Technical specification of the Dual axis inclinometer ELS-XX-V

TECHNICAL SPECIFICATIONS	
Measuring range	(±5/±10) °
temperature range	(-20/+70) °C
Zero temperature drift T 0-60°	< 0,2°
Temperature Sensitivity drift T 0-60°	< 0,4°
Weight	1,2 Kg

Thermometer

The temperature is recorded by means of two thermometers installed externally on the West front at 55.8 meters (T1) and internally on the South front at 57.50 meters (T2), respectively (Figure 5-10)

Figure 5-10: Thermometers installed on the Asinelli tower

Gonioanemometer: Combined Wind Sensor

The wind speed measure is recorded through a combined wind sensor, which is manufactured with materials to high reliability and duration, and permits to maintain in long time the characteristics of sensibility and precision (Figure 5-11). The sensor, installed on the top of the tower, uses a special high precision potentiometer that assures high resolution, high sensibility and a long mechanical life, with an operative angle of 360°. The mechanical body shape, permit at the sensor, to resist at high wind speed or squalls (up to 300km/h). Finally the use of materials like the anodized aluminium and the stainless steel, guarantees an optimal resistance to the corrosion due to the atmospheric agents, assuring therefore one long time duration. The sensor is equipped with electrical protections.
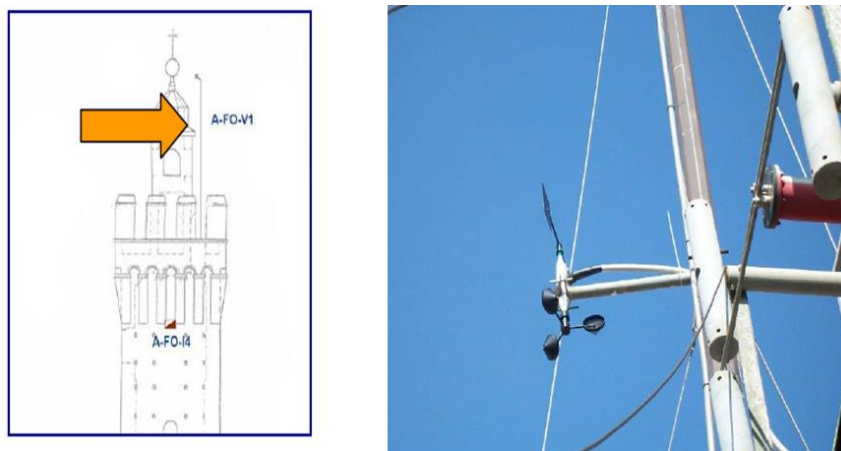
Figure 5-11: Combined Wind Sensor installed on the top of the tower

5.4 Reference quantities

The reference quantities defined in § 3.3 have been identified for all the data recorded by the monitoring system of the Asinelli tower. Appendix A.1 provides the systematic identification of these reference quantities. In the next section, the salient results, obtained from the interpretation of the static monitoring data through the proposed procedure, are illustrated.

It is noted that the laser distance meters have recorded many spike throughout the monitoring period. Their data are therefore not reliable in order to perform evaluations on the structural health of the tower.

5.4.1 Long Base Invar Deformeters

Long base Invar Deformeters A-FO-F1- A-FO-F2

Long base deformeters F1 and F2, installed at the south-west corner base of the Asinelli tower (corner under the slope), measure the horizontal and vertical masonry deformation, respectively, (displacement between two points, positive values indicates that the distance between the two extremes of the instrument is increasing). In more detail, Figure 5-12a displays the row-data, e.g. displacements versus

time over years 2011-2016. In the same graph, also the temperature variation (as recorded by the thermometer T1) is displayed. The temperature effect is significant and for these specific instruments the recorded data are out-of-phase with respect to temperature data (a high inverse correlation is evidenced). Figure 5-12b and d represents the time-history of the daily amplitude. The values of the daily amplitudes recorded during the cold season are one order of magnitude less than those recorded during the hot season. Figure 5-12c and e show the absolute daily residuals (with reference to the first year of monitoring) as evaluated for F1 and F2, respectively. These quantities allow to quantify the evolutionary trend of the signals. For F1 a cumulative trend of +0.02mm (meaning increase in tension in the horizontal direction) and for F2 a cumulative trend of -0.017 mm (meaning increase in compression in the vertical direction) has been observed in the six years.

(a)

(b)…………………………………………………..(c)

(d)………………………………………………..(e)
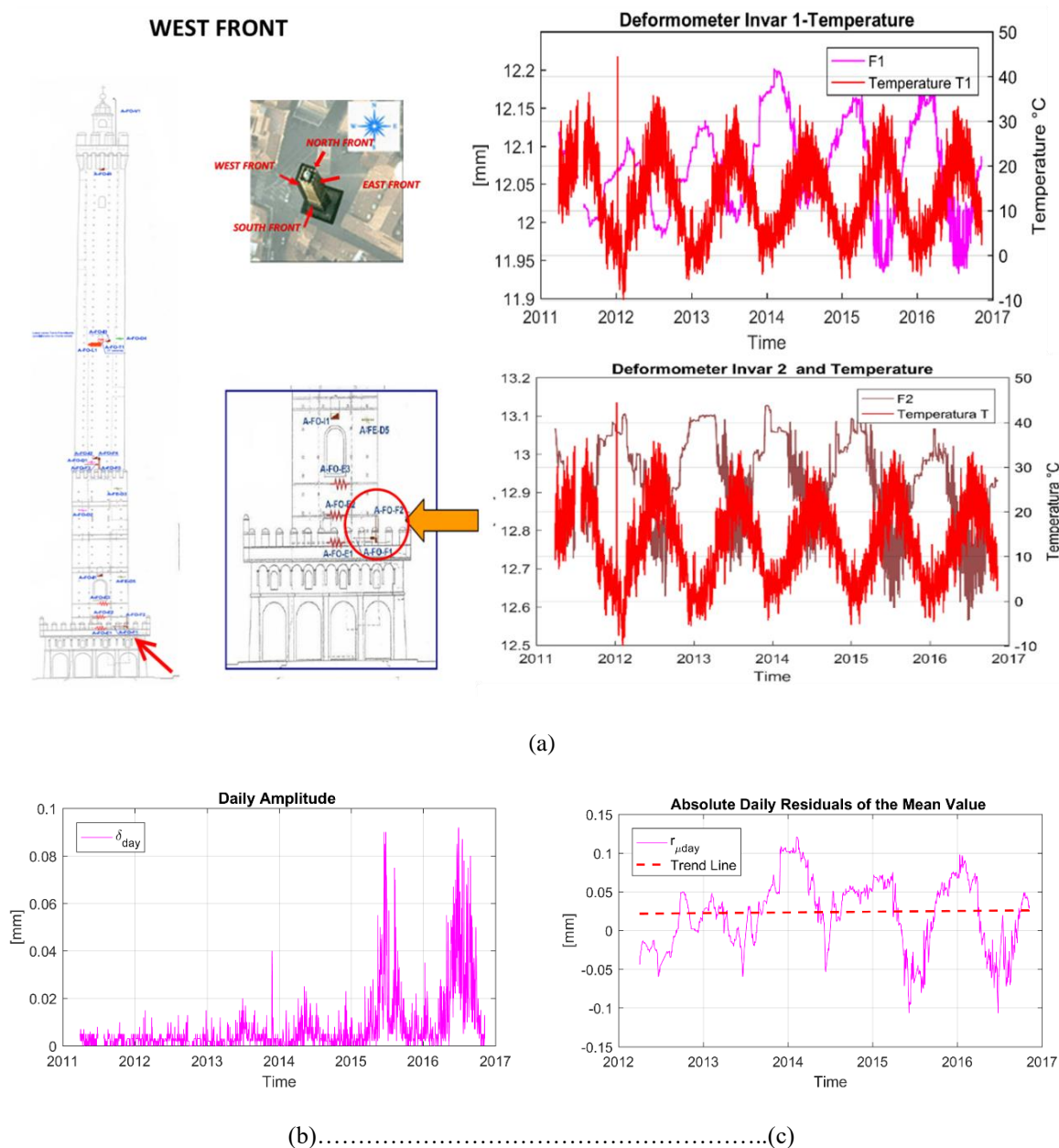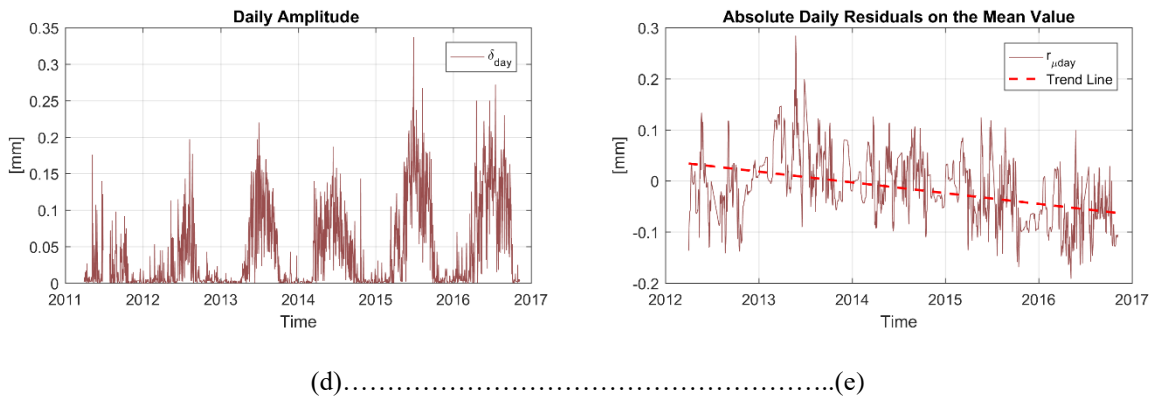
Figure 5-12: Long base Invar Deformeters A-FO-F1- A-FO-F2: (a) row-data recorded by F1 and F2 considering also the temperature variation, as recorded by the thermometer T1, (b)and (c) time-history of the "daily amplitude and absolute daily residuals evaluated for F1 and (d),(e) time-history of the "daily amplitude and absolute daily residuals evaluated for F2

Long base Invar Deformeters A-FO-F3- A-FO-F4

Long base deformeters F3 and F4, installed at the West front of the Asinelli tower (at the height of 34 m), measure the horizontal and vertical masonry deformation, respectively. Similarly, Figure 5-13a displays the row-data and the temperature variation (as recorded by the thermometer T1). The temperature effect is significant and also for these instruments the recorded data are out-of-phase with respect to temperature data. Figure 5-13b and d represents the time-history of the "daily amplitude". The values of the daily amplitudes recorded during the cold season are one order of magnitude less than those recorded during the hot season. Figure 5-13c and e show the absolute daily residuals as evaluated for F3 and F4, respectively. F3 shows a cumulative trend of -0.07 mm (meaning increase in compression in the horizontal direction) and F4 a cumulative trend of -0.002 mm (meaning increase in compression in the vertical direction) in the six years.

(a)

(b)…………………………………………………..(c)

(d)…………………………………………………..(e)
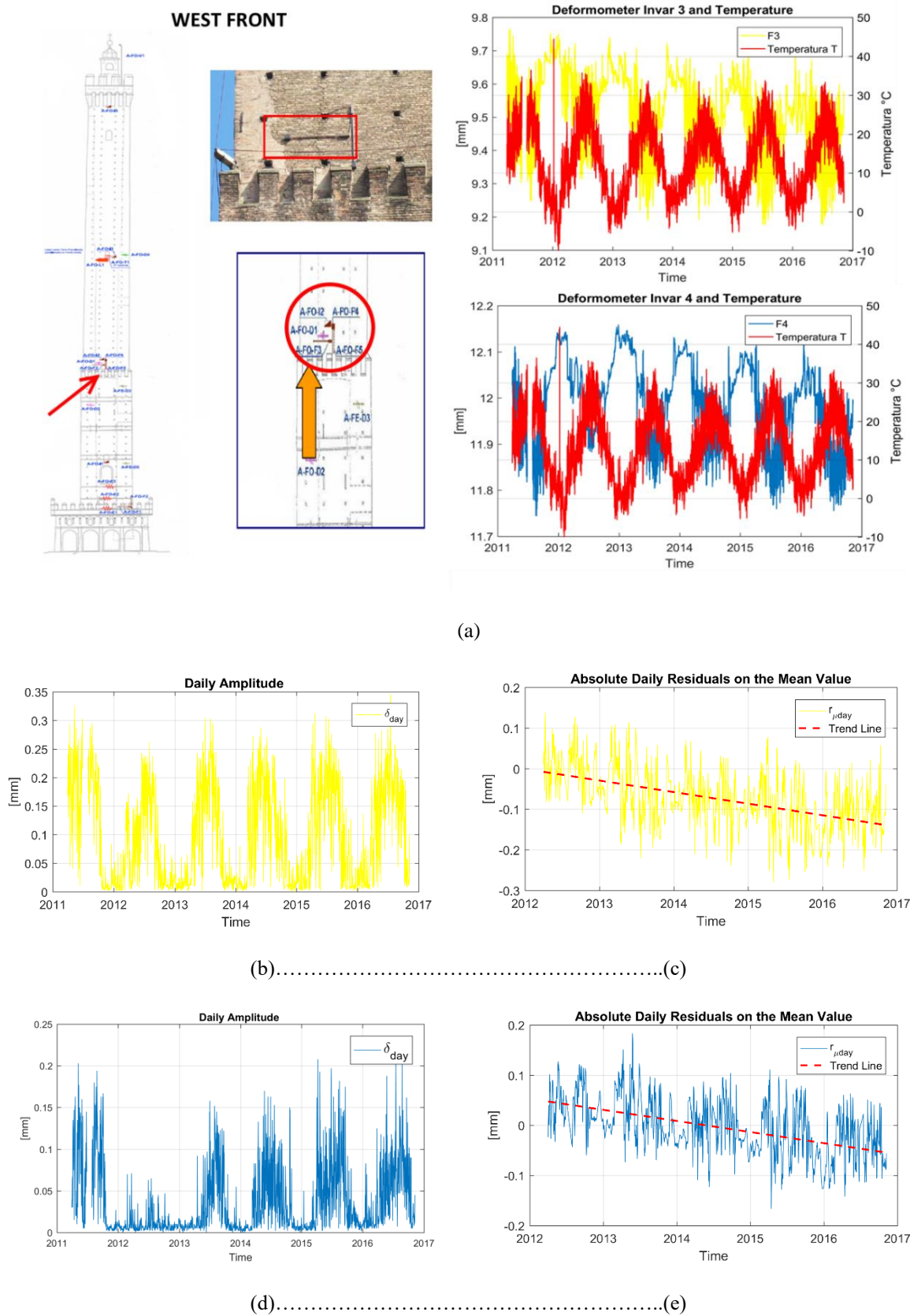
Figure 5-13: Long base Invar Deformeters A-FO-F3- A-FO-F4: (a) row-data recorded by F3 and F4 considering also the temperature variation, as recorded by the thermometer T1, (b)and (c) time-history of the "daily amplitude and absolute daily residuals evaluated for F3 and (d),(e) time-history of the "daily amplitude and absolute daily residuals evaluated for F4

Long base Invar Deformeters A-FO-F5

Long base deformeters F5, installed at the same position of F4 but inside of the Asinelli tower, measure the vertical masonry deformation. Figure 5-14 displays the row-data and the temperature variation (as recorded by the thermometer T2). The recorded data are out-of-phase with respect to temperature data. The absolute daily residuals displays a cumulative trend of +0.03 mm (meaning increase in tension in the vertical direction) in the six years.
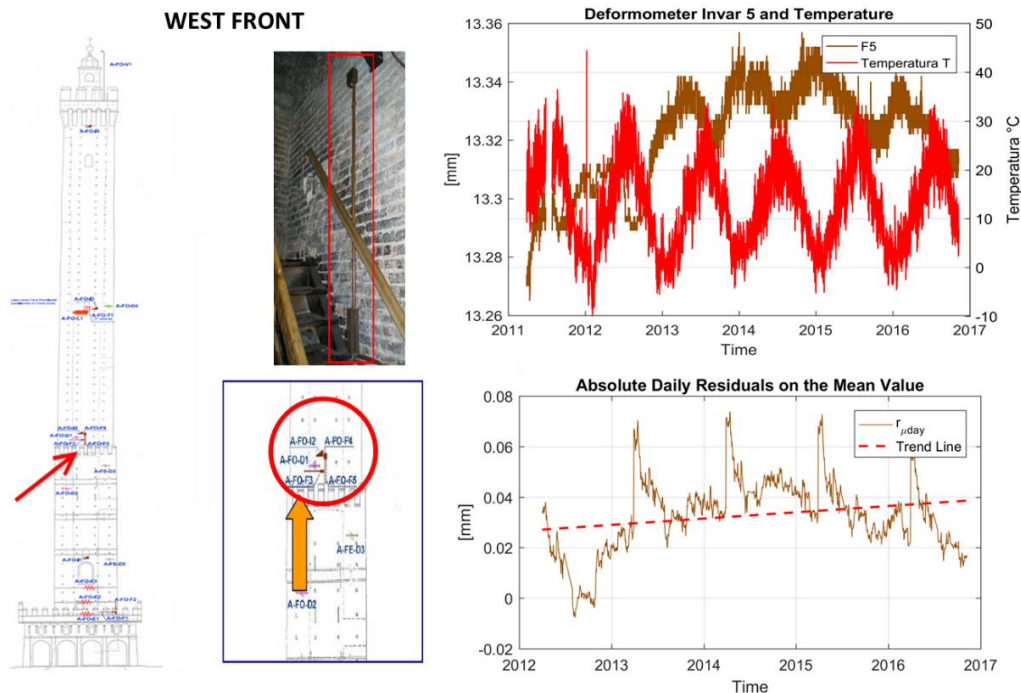
Figure 5-14: Long base Invar Deformeters A-FO-F5: row-data recorded by F5 considering also the temperature variation, as recorded by the thermometer T2, and the absolute daily residuals evaluated

Long base Invar Deformeters A-FS-F6-A-FS-F7

Long base deformeters F6 and F7, installed at the south-west corner base of the Asinelli tower (corner under the slope-South Front), measure the horizontal and vertical masonry deformation, respectively. Also in this case, Figure 5-15 a displays the row-data and the temperature variation (as recorded by the thermometer T1). F6 recorded a drop in the 21th June 2013 due to a malfunction of the instrument that influence its trend. The recorded data by F7 are out-of-phase with respect to temperature data. The values of the daily amplitudes recorded during the cold season are around one order of magnitude less than those recorded during the hot season (Figure 5-15b, d). The time history of the absolute daily residuals display for F6 a cumulative trend of -0.1 mm (meaning increase in compression in the horizontal direction) and for F7 a cumulative trend of -0.02 mm (meaning increase in compression in the vertical direction) in the six years (Figure 5-15c, e). It is noted that the high value of the residue recorded on the six years by F6 is due to the drop. Considering only the last years, the absolute daily residuals display a cumulative trend of -0.03 mm.

(a)

(b)……………………………………………………..(c)

(d)……………………………………………..(e)
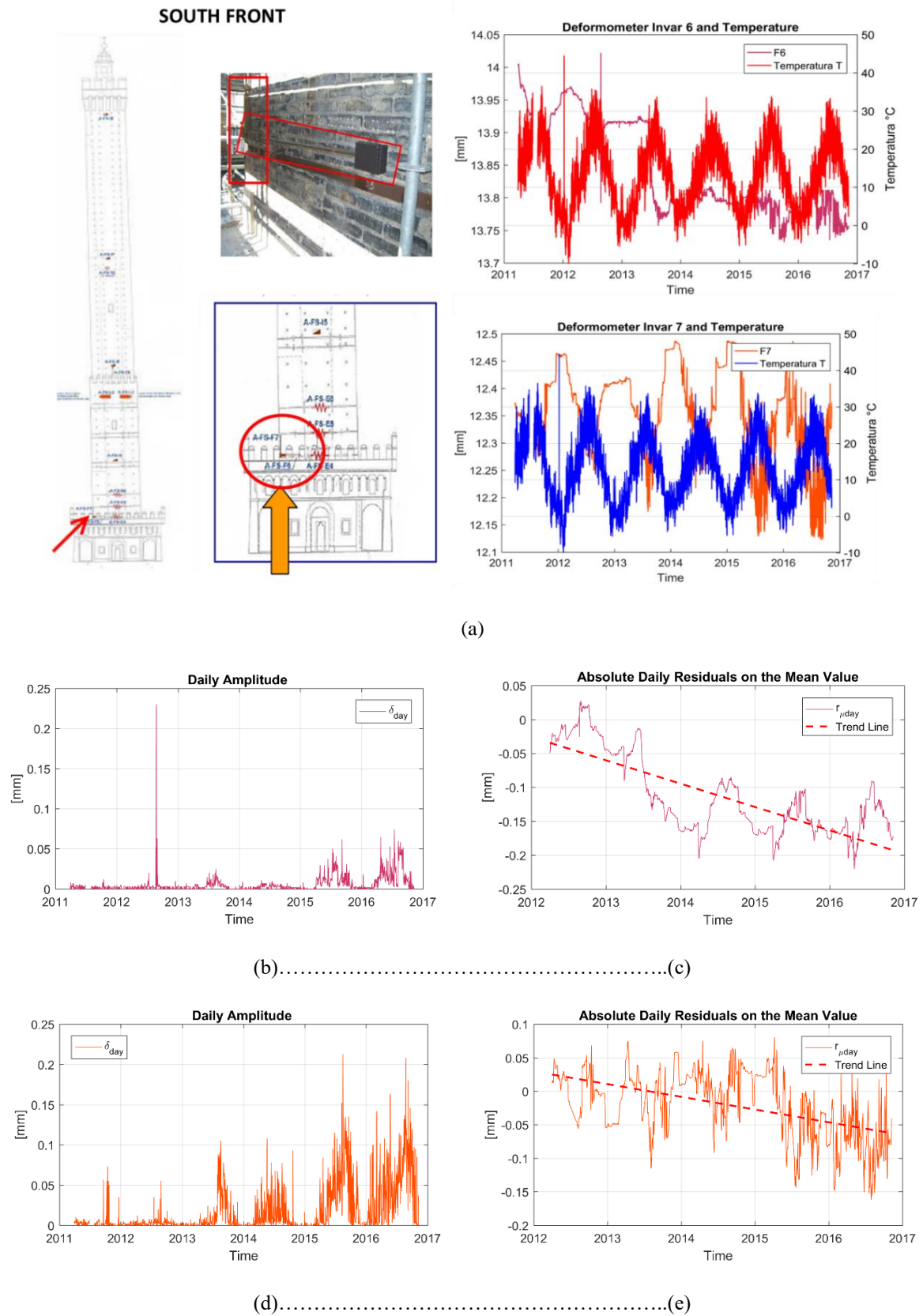
Figure 5-15: Long base Invar Deformeters A-FS-F6- A-FS-F7: (a) row-data recorded by F6 and F7 considering also the temperature variation, as recorded by the thermometer T1, (b)and (c) time-history of the "daily amplitude and absolute daily residuals evaluated for F6 and (d),(e) time-history of the "daily amplitude and absolute daily residuals evaluated for F7

Long base Invar Deformeters A-FO-F8

Long base deformeters F8, installed at the South front of the Asinelli tower (at the height of 34 m), measure the vertical masonry deformation. Figure 5-16 displays the row-data and the temperature variation (as recorded by the thermometer T1). The recorded data are out-of-phase with respect to temperature data. During the first year the sensor record anomalous data, therefore, the reference quantities were calculated starting from the 2013. The absolute daily residuals displays a cumulative trend of -0.004 mm (meaning increase in compression in the vertical direction) in the five years.
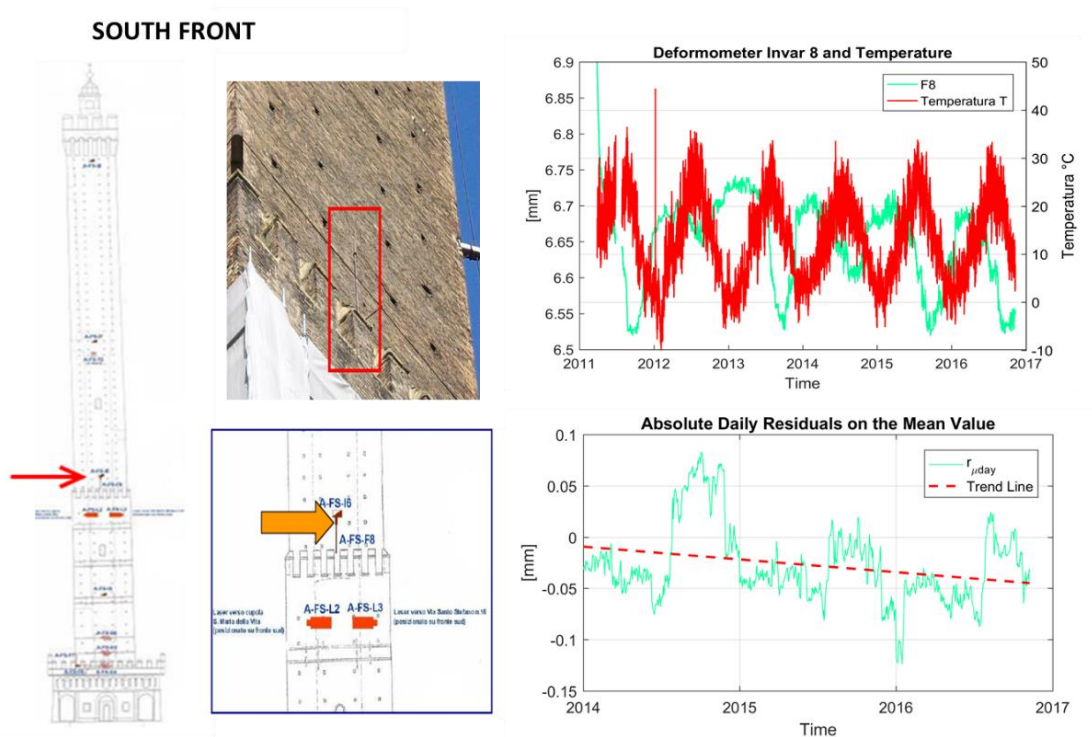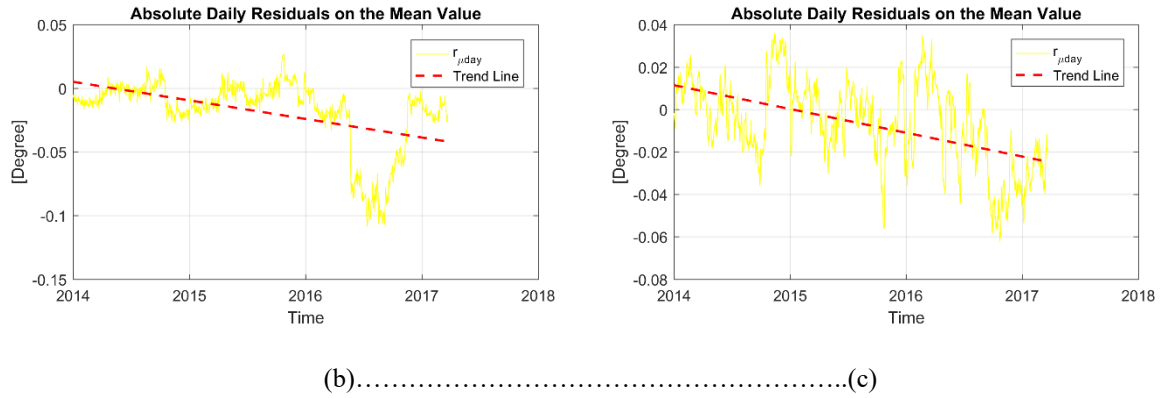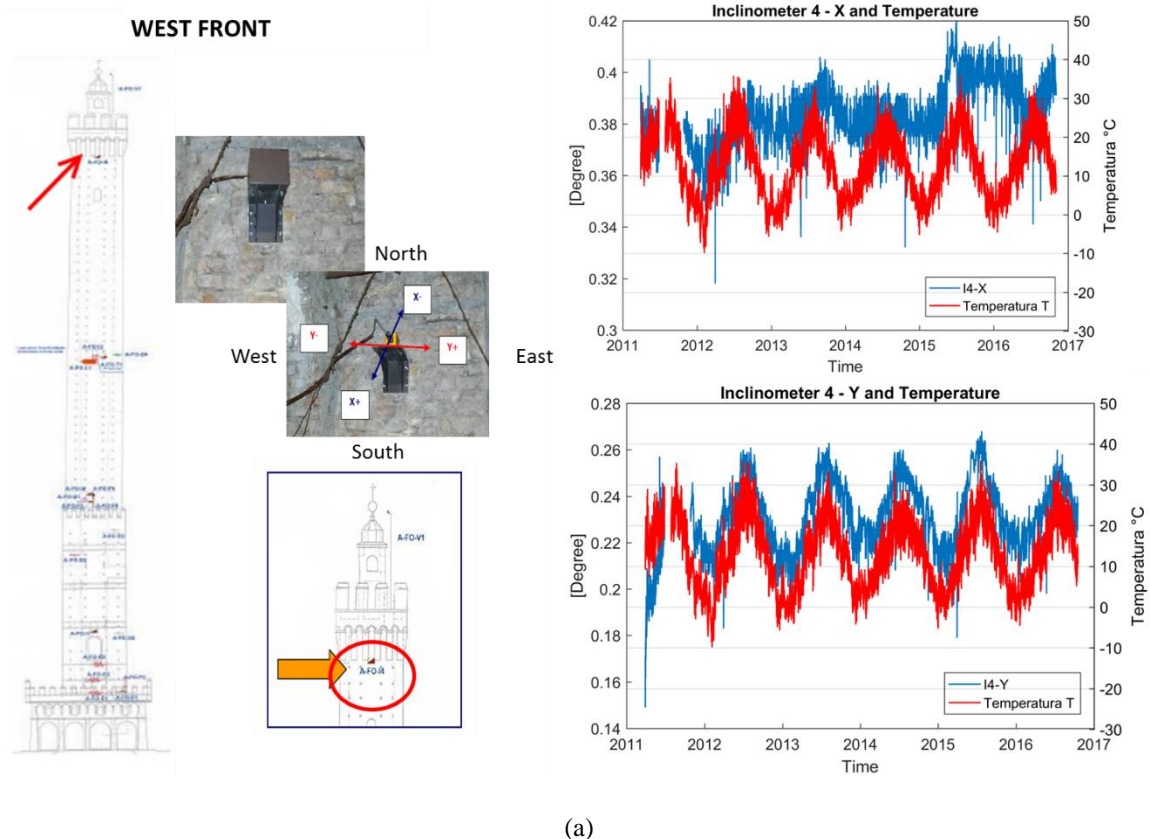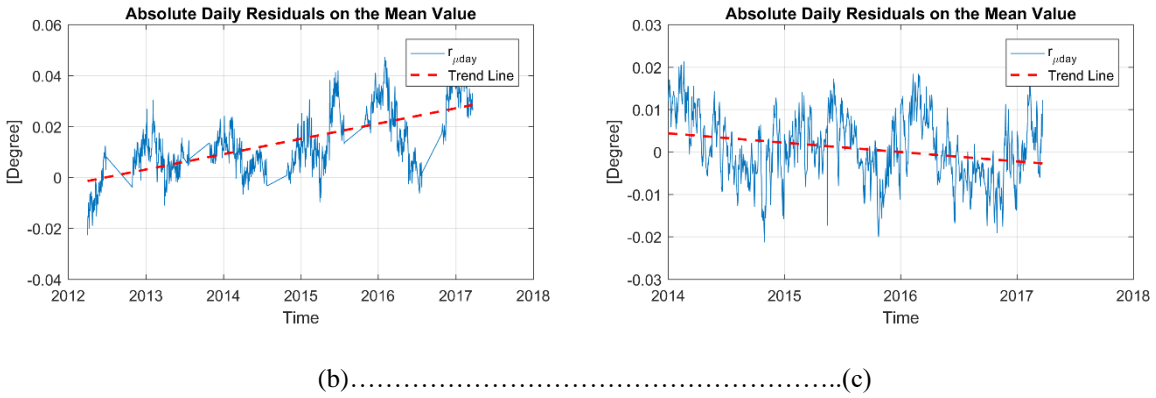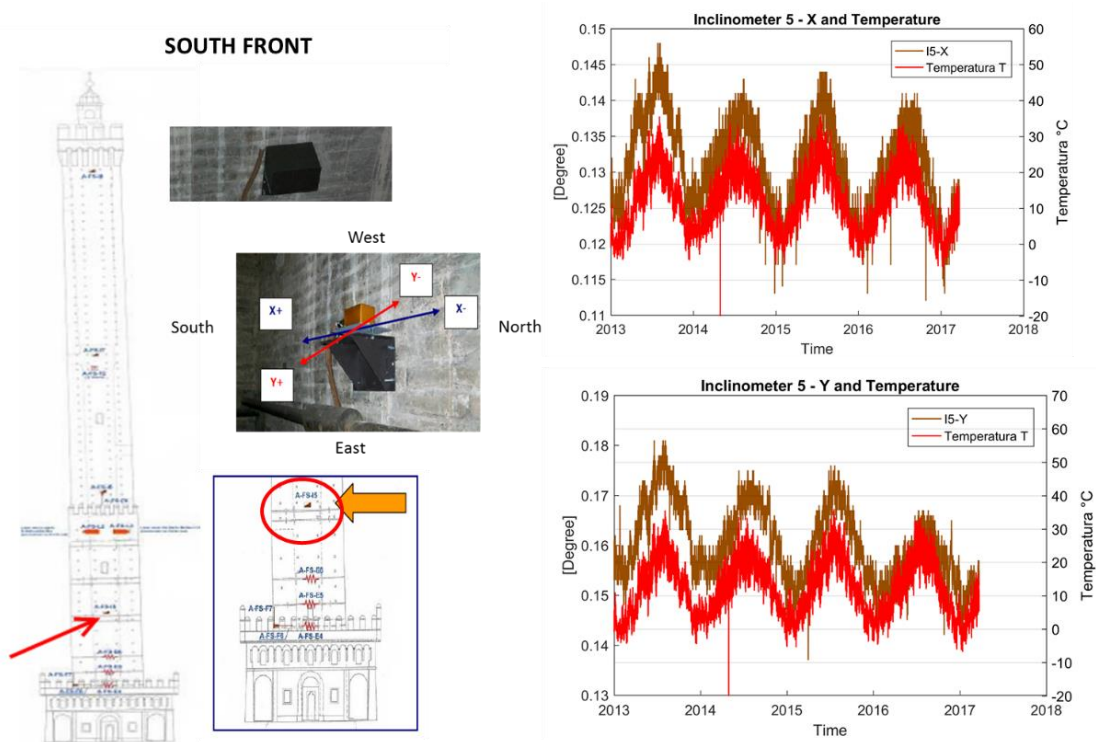

Figure 5-16: Long base Invar Deformeters A-FS-F8: row-data recorded by F8 considering also the temperature variation, as recorded by the thermometer T1, and the absolute daily residuals evaluated

In Table 5-7 the mean values over the period monitored of the reference quantities are collected for all the long base deformeters.

Table 5-7-Men values of the reface quantities over the six years of monitoring for the 8 long base deformeters

Sensor	Year	$\delta_{day,j}$ [mm]	$\text{rp}_{\mu day}$ [mm]	$\text{r}_{\mu day}$ [mm]	M_{year} [mm]	Σ_{year} [mm]	Rp_{Myear} [mm]	R_{Myear} [mm]
A-FO-F1	mean	0.008	0.003	0.022	12.067	0.182	-0.001	0.016
A-FO-F2	mean	0.040	-0.016	-0.017	12.943	0.444	-0.019	-0.016
A-FO-F3	mean	0.101	-0.025	-0.071	9.545	0.504	-0.026	-0.071
A-FO-F4	mean	0.037	-0.007	-0.002	11.997	0.354	-0.011	0.005
A-FO-F5	mean	0.007	0.006	0.032	13.321	0.042	0.006	0.033
A-FS-F6	mean	0.006	-0.031	-0.109	13.848	0.097	-0.031	-0.105
A-FS-F7	mean	0.017	-0.016	-0.019	12.352	0.283	-0.017	-0.012
A-FS-F8	mean	0.008	-0.017	-0.004	6.648	0.163	-0.005	-0.006

5.4.2 Deformeters

The deformeters D3 and D4 recorded a malfunction during the six years of monitoring and their data are not reliable. For this reason, the data recorded by these devices are not considered.

Deformeters A-FO-D1-A-FO-D2

The deformers D1 and D2 record a small movements indicating that the two monitored cracks are in a stable condition. In particular, the movements of the crack monitored by D2 are often smaller than the full scale of the sensor (Figure 5-17).
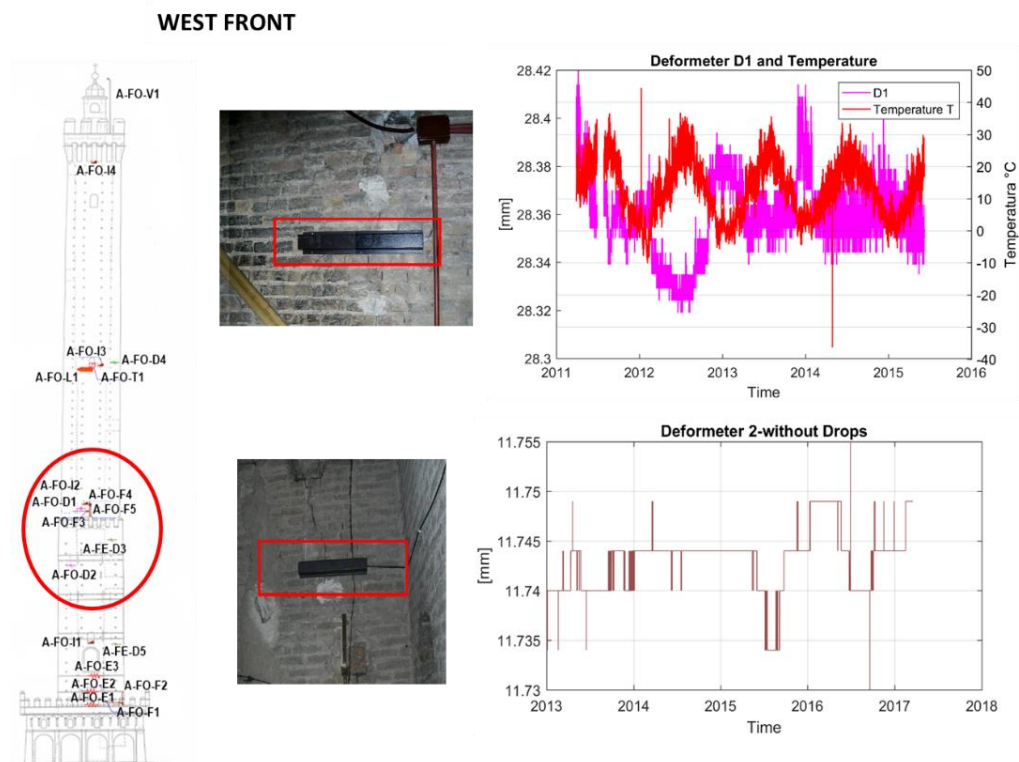
Figure 5-17: Deformeters D1 and D2 installed on two cracks located in the West front of the tower

Deformeters A-FE-D5

Deformeters D5 monitor the movements of a crack in the East front of the tower. The recorded data by D5 are out-of-phase with respect to temperature data. Also in this case, the sensor record anomalous data during the first year, therefore, the reference quantities were calculated starting from the 2013. The absolute daily residuals displays that the crack is opening of 0.003 mm in the last five years (Figure 5-18).
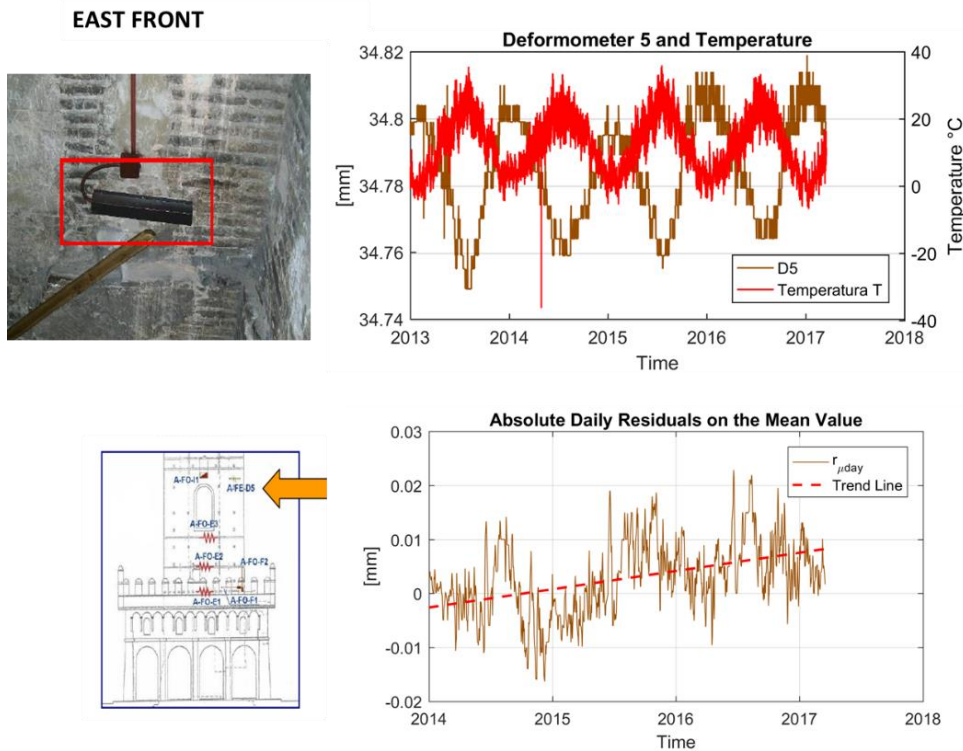
Figure 5-18: Deformeters D5 installed on crack located in the East front of the tower

In Table 5-8 the mean values over the period monitored of the reference quantities are collected for the deformeters D1, D2, D5.

Table 5-8- Men values of the reface quantities over the six years of monitoring for the deformeters

Sensor	Year	$\delta_{day,j}$ [mm]	$rp_{\mu day}$ [mm]	$r_{\mu day}$ [mm]	M_{year} [mm]	Σ_{year} [mm]	Rp_{Myear} [mm]	R_{Myear} [mm]
A-FO-D1	mean	0.0151	-0.0028	-0.0045	28.3604	0.0918	-0.0025	-0.0072
A-FO-D2	mean	0.001	0.001	0.003	28.362	0.102	-0.005	-0.010
A-FE-D5	mean	0.003	0.002	0.003	28.362	0.102	-0.005	-0.008

5.4.3 Extensometers

The general trend recorded by the extensometers is similar to that recorded by the long base deformeters: the recorded data are out-of-phase with respect to temperature data and the values of the daily amplitudes recorded during the cold season are one order of magnitude less than those recorded during the hot season. This can be related to the thermal contraction of the masonry.

Extensometers A-FO-E1- A-FO-E2- A-FO-E3

Extensomiters E1, E2 and E3, installed on the still ties in the West front at the base of the Asinelli tower, measure the stress state of the ties. In more detail, Figure 5-19a displays the row-data recorded by the extensometers with the temperature variation (as recorded by the thermometer T1). The values of the daily amplitudes recorded during the cold season are one order of magnitude less than those recorded during the hot season (Figure 5-19 b, d, f). The absolute daily residuals reveal for E1 a cumulative trend of -4με (meaning decrease in stress), for E2 a cumulative trend of -30 με, and for E3 a cumulative trend of -5 με, in the six years (Figure 5-19 c, e, g).

(a)

(b)…………………………………………………..(c)

(d)…………………………………………………..(e)

(f)…………………………………………………..(g)
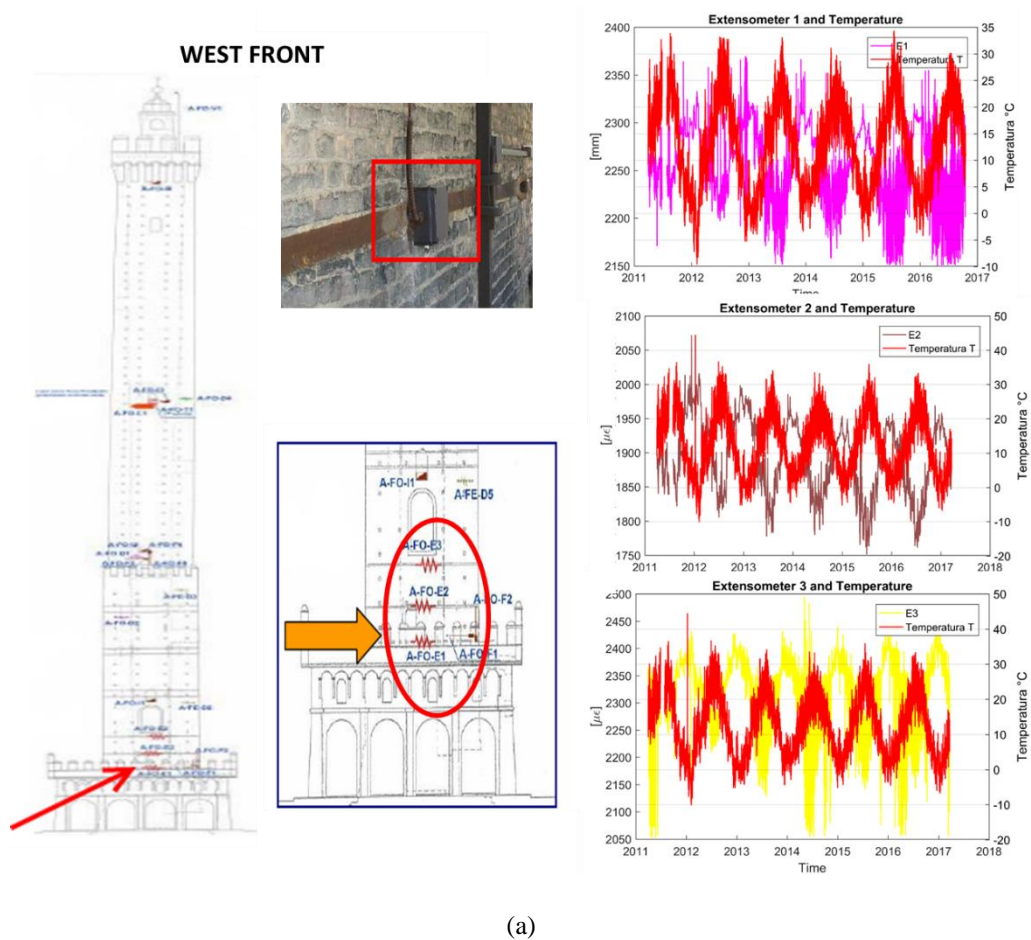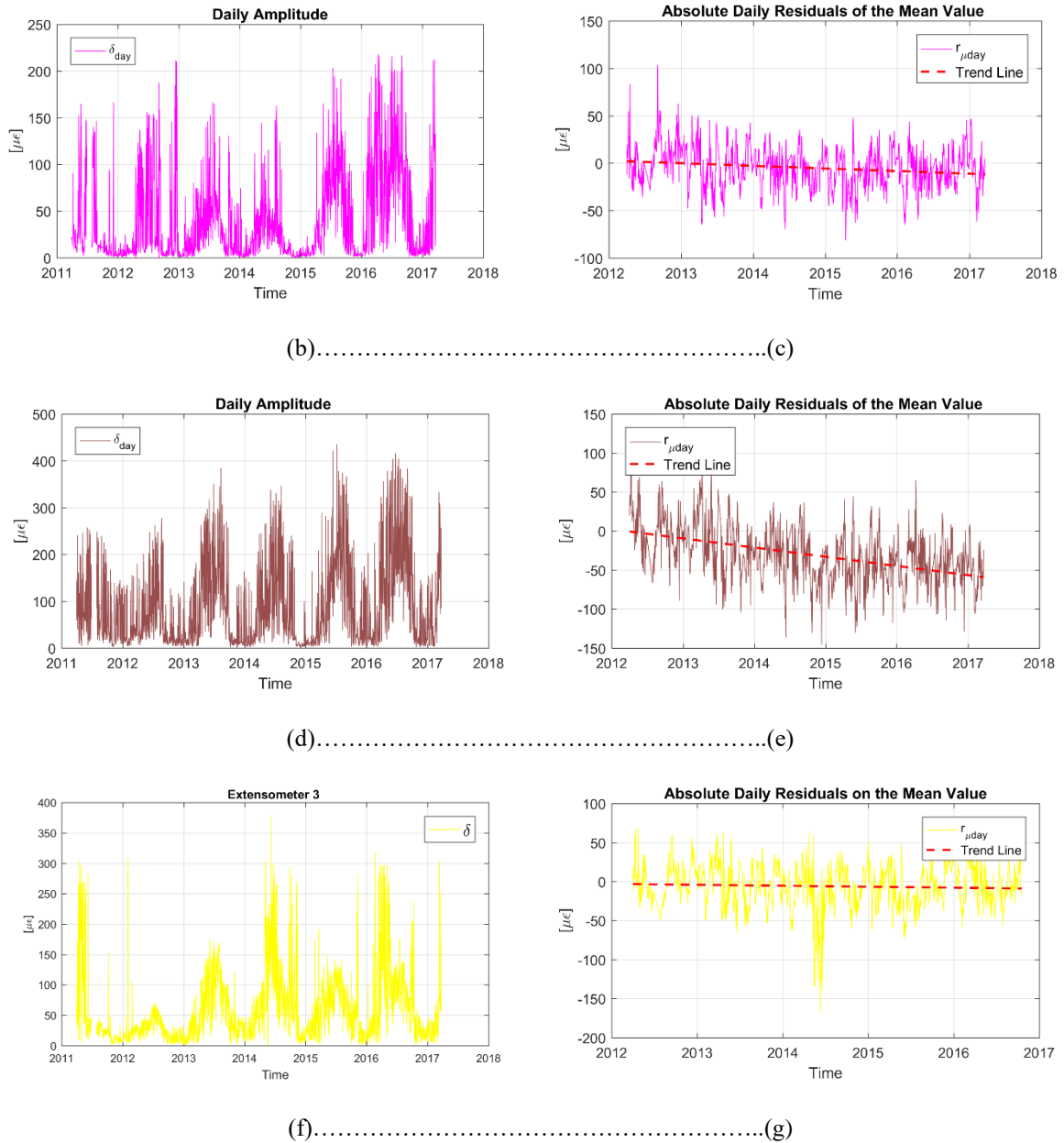
Figure 5-19: Extensometers A-FO-E1- A-FO-E2- A-FO-E3: (a) row-data recorded by E1, E2 and E3 considering also the temperature variation, as recorded by the thermometer T1, (b), (c) time-history of the "daily amplitude and absolute daily residuals evaluated for E1, (d),(e) time-history of the "daily amplitude and absolute daily residuals evaluated for E2 and (f),(g) time-history of the "daily amplitude and absolute daily residuals evaluated for E3.

Extensometers A-FS-E4- A-FS-E5- A-FS-E6

Extensomiters E4, E5 and E6, installed on the still ties in the South front at the base of the Asinelli tower, measure the stress state of the ties. In more detail, Figure 5-20a displays the row-data recorded by the extensometers with the temperature variation (as recorded by the thermometer T1). The recorded data are out-of-phase with respect to temperature data and the values of the daily amplitudes recorded during the cold season are around one order of magnitude less than those recorded during the hot season

(Figure 5-20 b, d, f). The absolute daily residuals reveal for E4 a cumulative trend of -5με (meaning decrease in stress), for E5 a cumulative trend of -14 με, and for E6 a cumulative trend of -14 με, in the six years monitored (Figure 5-20 c, e, g).

(a)

(b)………………………………………………..(c)

(d)…………………………………………………..(e)

(f)…………………………………………………..(g)
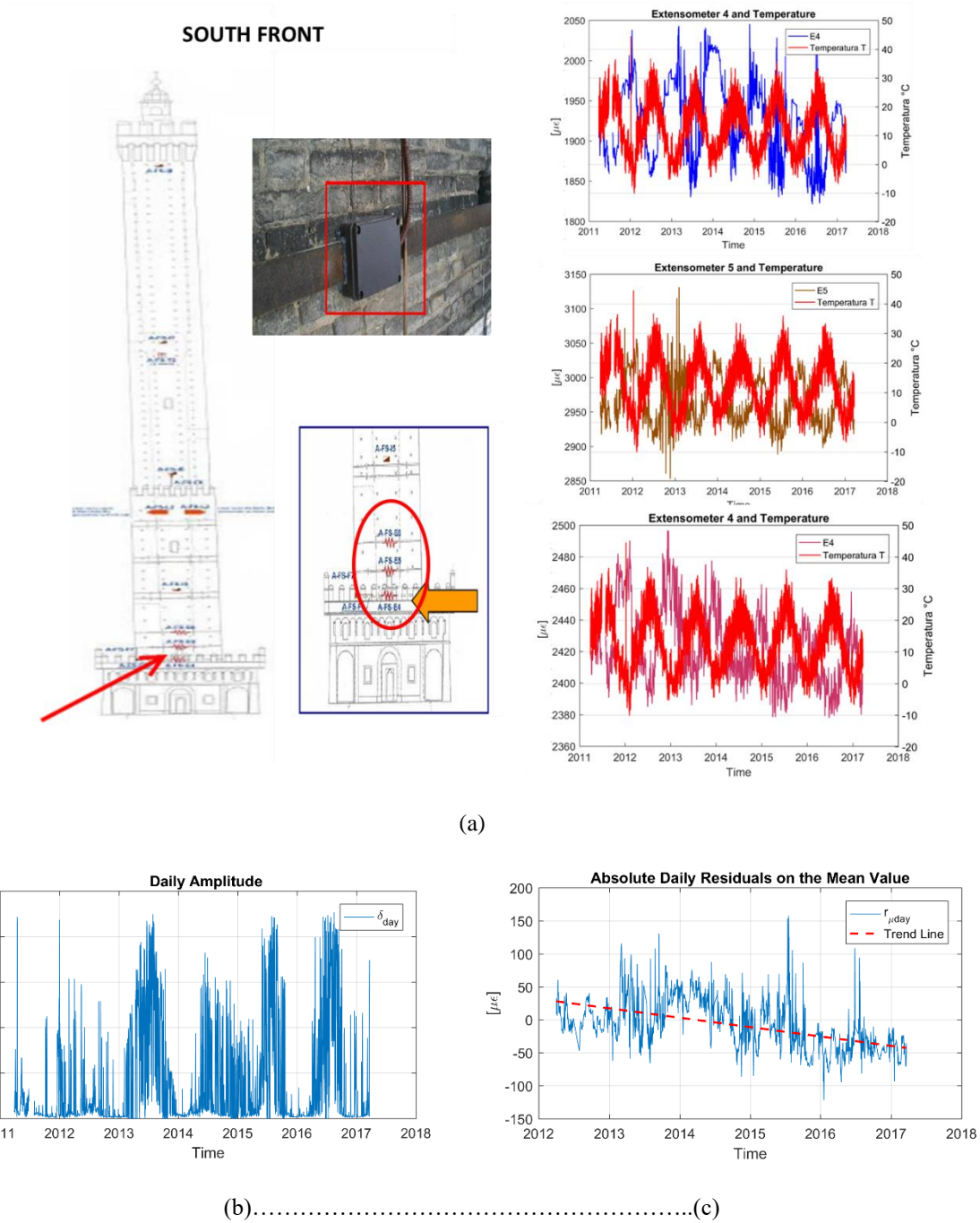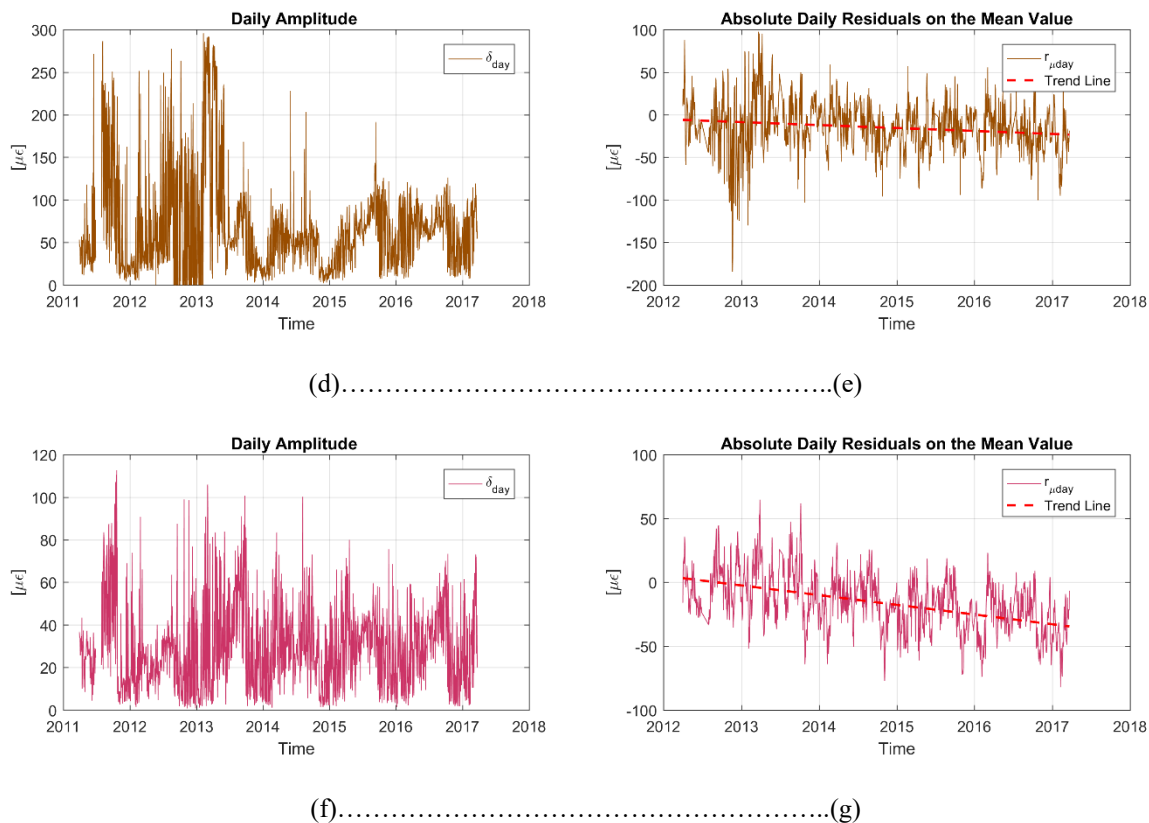
Figure 5-20: Extensometers A-FS-E4- A-FS-E5- A-FS-E6: (a) row-data recorded by E4, E5 and E6 considering also the temperature variation, as recorded by the thermometer T1, (b)and (c) time-history of the "daily amplitude and absolute daily residuals evaluated for E4, (d) and (e) time-history of the "daily amplitude and absolute daily residuals evaluated for E5 and (f) and (g) time-history of the "daily amplitude and absolute daily residuals evaluated for E6.

In Table 5-9 the mean values over the period monitored of the reference quantities are collected for all the extensometers.

Table 5-9- Men values of the reface quantities over the six years of monitoring for the extensometers

Sensor	Year	$\delta_{day,j}$ [με]	$rp_{\mu day}$ [με]	$r_{\mu day}$ [με]	M_{year} [με]	Σ_{year} [με]	Rp_{Myear} [με]	R_{Myear} [με]
A-FO-E1	mean	38.93	-0.96	-3.96	2256.89	213.17	-2.23	-4.13
A-FO-E2	mean	88.22	-8.46	-27.16	1885.19	417.68	-9.49	-24.73
A-FO-E3	mean	59.48	0.40	-5.39	2322.23	360.76	-0.80	-3.62
A-FS-E4	mean	38.73	-7.24	-5.34	1916.48	7288.12	-7.03	-1.47
A-FS-E5	mean	66.68	-5.03	-14.16	2962.70	254.58	-4.52	-10.79
A-FS-E6	mean	29.29	-5.18	-13.86	2421.53	137.48	-5.59	-13.64

5.4.4 Inclinometers

It should be noted that the inclinometers measure the inclination in the x-direction and y-direction of the wall: the x component record positive value along the South-East direction and the y component record positive value along the North-East direction. Moreover, almost all the inclinometers recorded an anomalous behaviour in the first/second year of monitoring. In this case, the reference quantities have been calculated starting from the 2013.

Inclinometer A-FO-I1

Inclinometer I1 is installed at the west front of the Asinelli tower (at the height of 17.60 m). The sensor recorded a drop in the 20th February 2013 due to a malfunction that influence its trend. Figure 5-21 a display the row-data by I1 and the temperature variation (as recorded by the thermometer T1). Figure 5-21 b and c show the absolute daily residuals as evaluated for I1 x-direction and I1 y-direction, respectively. It is noted that the high value of the residuals recorded on the six years by I1 is due to the drop recorded. Considering only the last years, the cumulative daily residuals reveal for the x component a cumulative trend of -0.009° (meaning increase in the inclination in the North-West direction) and for the y component a trend of -0.019° (meaning decrease in the inclination in the North-East direction).
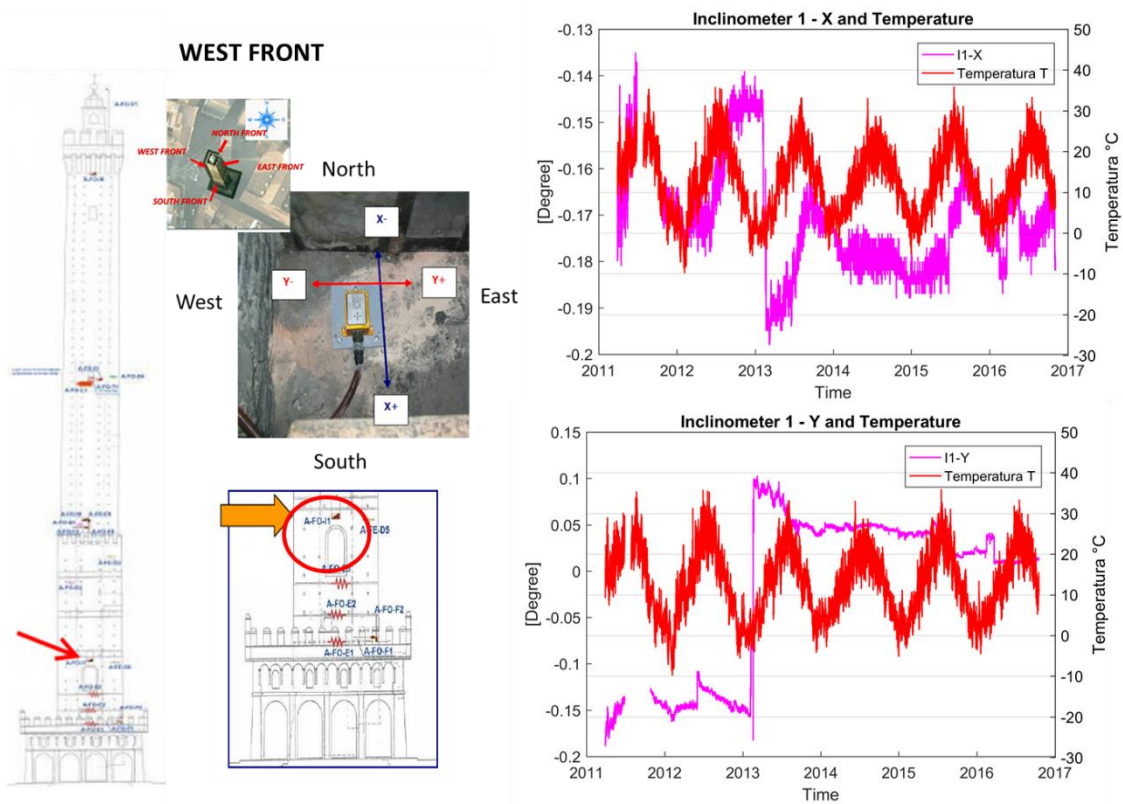
(a)
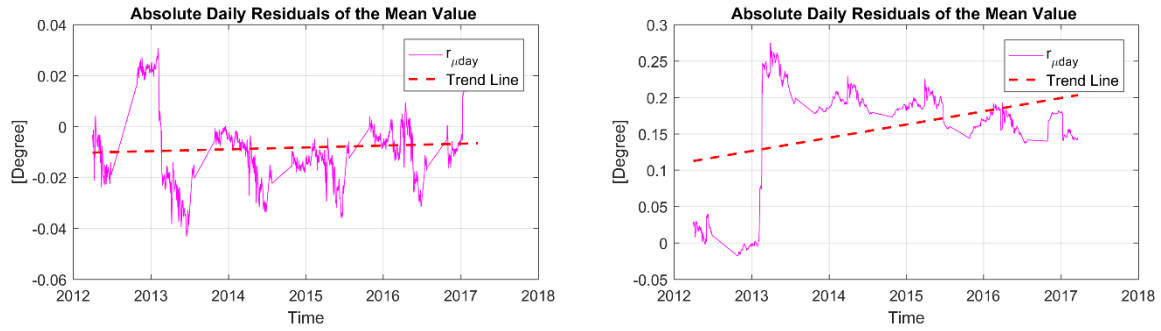
(b)…………………………………………………..(c)

Figure 5-21: Inclinometer A-FO-I1: row-data recorded by I1 considering also the temperature variation, as recorded by the thermometer T1, and (b),(c) the absolute daily residuals evaluated for both X and Y direction

Inclinometer A-FO-I2

Inclinometer I2 is installed at the West front of the Asinelli tower (at the height of 38.0 m). Figure 5-22 a display the row-data by I2 and the temperature variation (as recorded by the thermometer T1). It can be noticed that the data recorded by I2 in the y direction are in phase with respect to temperature data. The absolute daily residuals reveal for the x component a cumulative trend of -0.0001° (stable condition) and for the y component a trend of +0.007° (meaning decrease in the inclination in the South-West direction).

(a)

(b)…………………………………………………..(c)
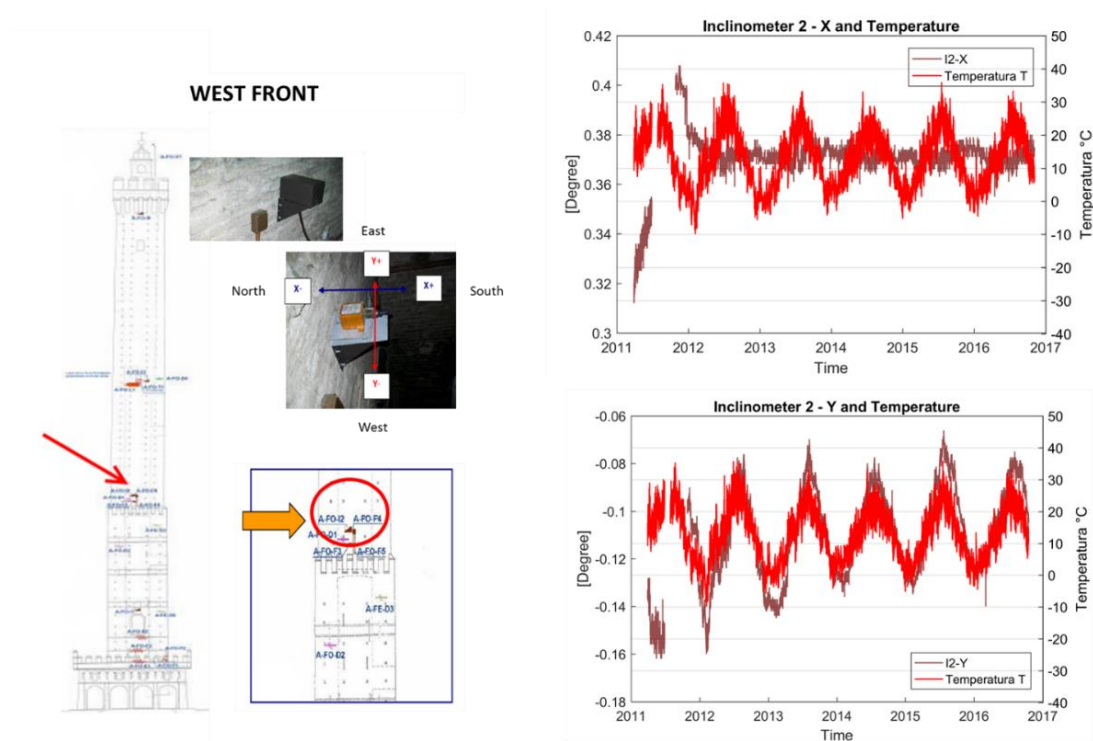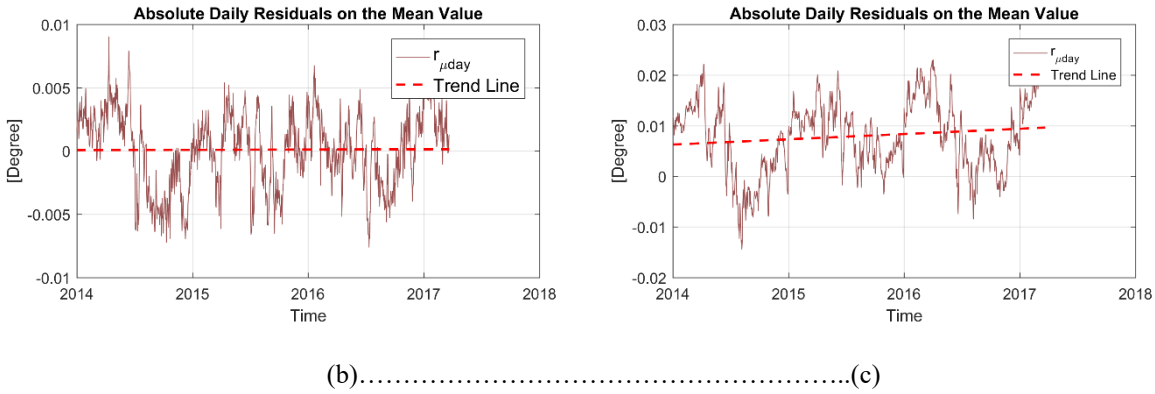
Figure 5-22: Inclinometer A-FO-I2: row-data recorded by I2 considering also the temperature variation, as recorded by the thermometer T1, and (b),(c) the absolute daily residuals evaluated for both X and Y direction

Inclinometer A-FO-I3

Inclinometer I3 is installed at the West front of the Asinelli tower (at the height of 55.8 m). The data recorded by I3 in the y-direction are in phase with respect to temperature data (Figure 5-23 a). The absolute daily residuals reveal for the x component a cumulative trend of -0.02° (increase in the inclination in the North-West direction) and for the y component a trend of -0.005° (meaning increase in the inclination in the South-West direction).

(a)

(b)…………………………………………..(c)
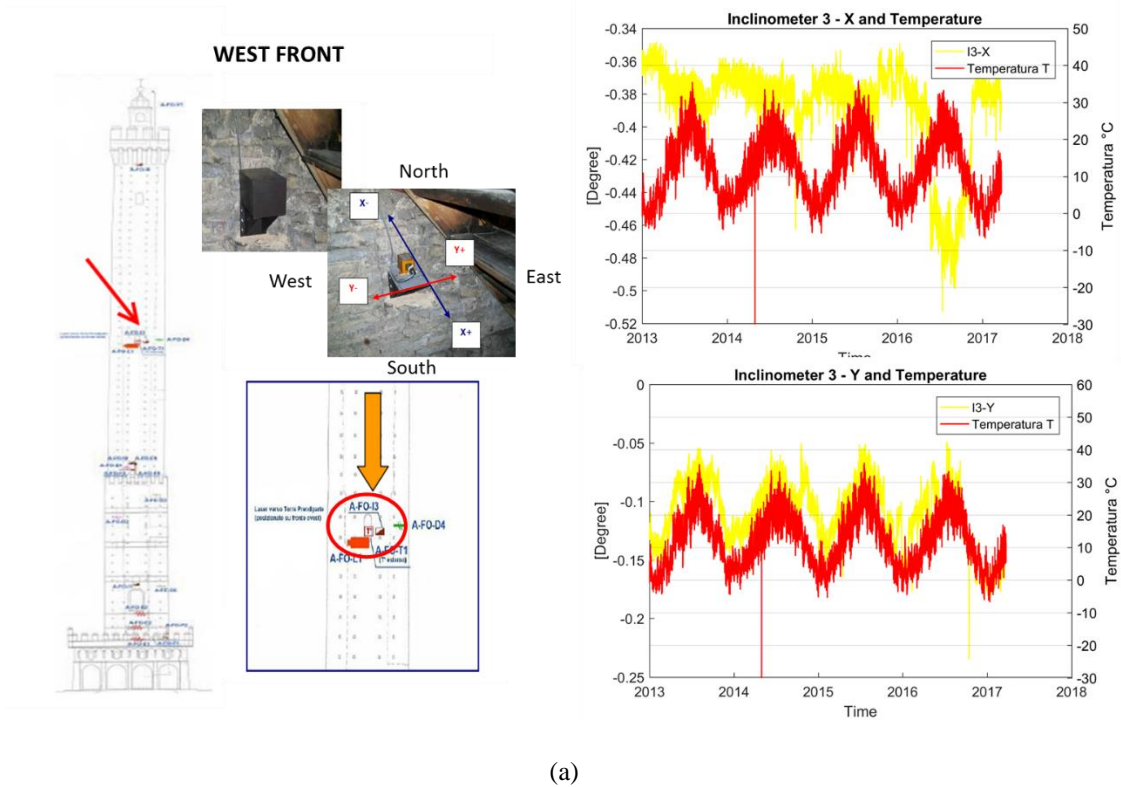
Figure 5-23: Inclinometer A-FO-I3: row-data recorded by I3 considering also the temperature variation, as recorded by the thermometer T1, and (b),(c) the absolute daily residuals evaluated for both X and Y direction

Inclinometer A-FO-I4

Inclinometer I4 is installed at the West front of the Asinelli tower (at the height of 87.5 m). The data recorded by I4 are in phase with respect to temperature data (Figure 5-24 a). The absolute daily residuals reveal for the x component a cumulative trend of +0.01° (increase in the inclination in the South-East direction) and for the y component a trend of +0.001° (meaning increase in the inclination in the North-East direction).

(a)

(b)…………………………………………………..(c)

Figure 5-24: Inclinometer A-FO-I4: row-data recorded by I4 considering also the temperature variation, as recorded by the thermometer T1, and (b),(c) the absolute daily residuals evaluated for both X and Y direction

Inclinometer A-FS-I5

Inclinometer I5 is installed at the South front of the Asinelli tower (at the height of 19.7 m). The data recorded by I5 are in phase with respect to temperature data recorded by T1 (Figure 5-25 a). The absolute daily residuals reveal for the x component a cumulative trend of -0.003° (decrease in the inclination in the South-East direction) and for the y component a trend of -0.005° (meaning decrease in the inclination in the North-East direction).

(a)

(b)………………………………………………..(c)
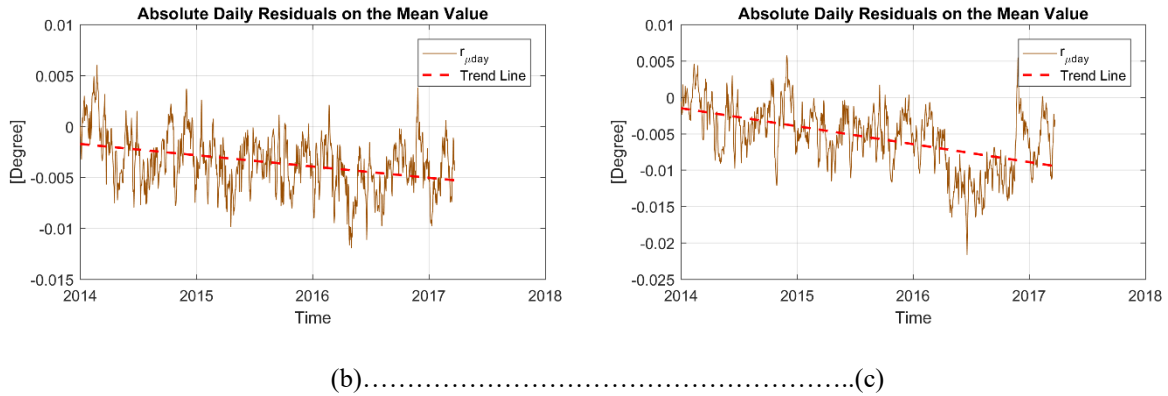
Figure 5-25: Inclinometer A-FS-I5: row-data recorded by I5 considering also the temperature variation, as recorded by the thermometer T1, and (b),(c) the absolute daily residuals evaluated for both X and Y direction

Inclinometer A-FS-I6

Inclinometer I6 is installed at the South front of the Asinelli tower (at the height of 37.2 m). The data recorded by I6 are in phase with respect to temperature data recorded by T1 (Figure 5-26 a). The absolute daily residuals reveal for the x component a cumulative trend of +0.005° (increase in the inclination in the South-East direction) and for the y component a trend of +0.01° (meaning increase in the inclination in the North-East direction).

(a)

(b)…………………………………………..(c)
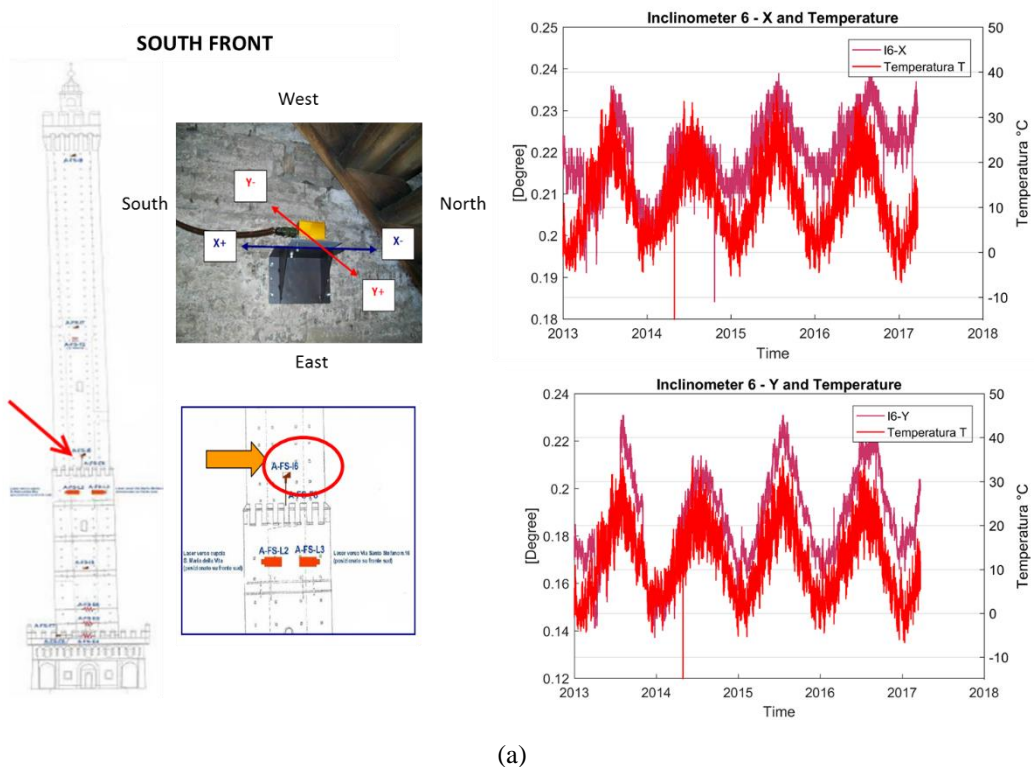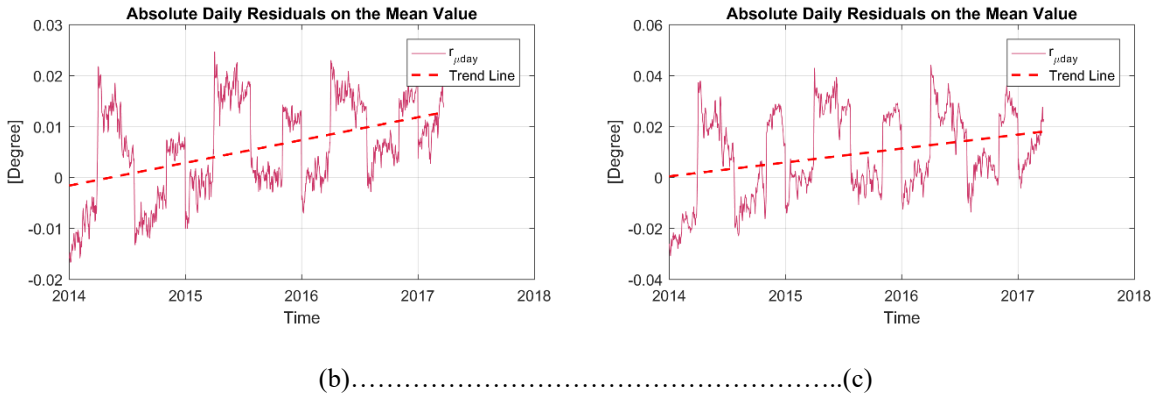
Figure 5-26: Inclinometer A-FS-I6: row-data recorded by I6 considering also the temperature variation, as recorded by the thermometer T1, and (b),(c) the absolute daily residuals evaluated for both X and Y direction

Inclinometer A-FS-I7

Inclinometer I7 is installed at the South front of the Asinelli tower (at the height of 57.50 m). The data recorded by I7 in the x-direction are in phase with respect to temperature data recorded by T1 (Figure 5-27 a). The absolute daily residuals reveal for the x component a cumulative trend of +0.01° (decrease in the inclination in the North-West direction) and for the y component a trend of +0.004° (meaning decrease in the inclination in the South-West direction).

(a)

(b)…………………………………………………..(c)
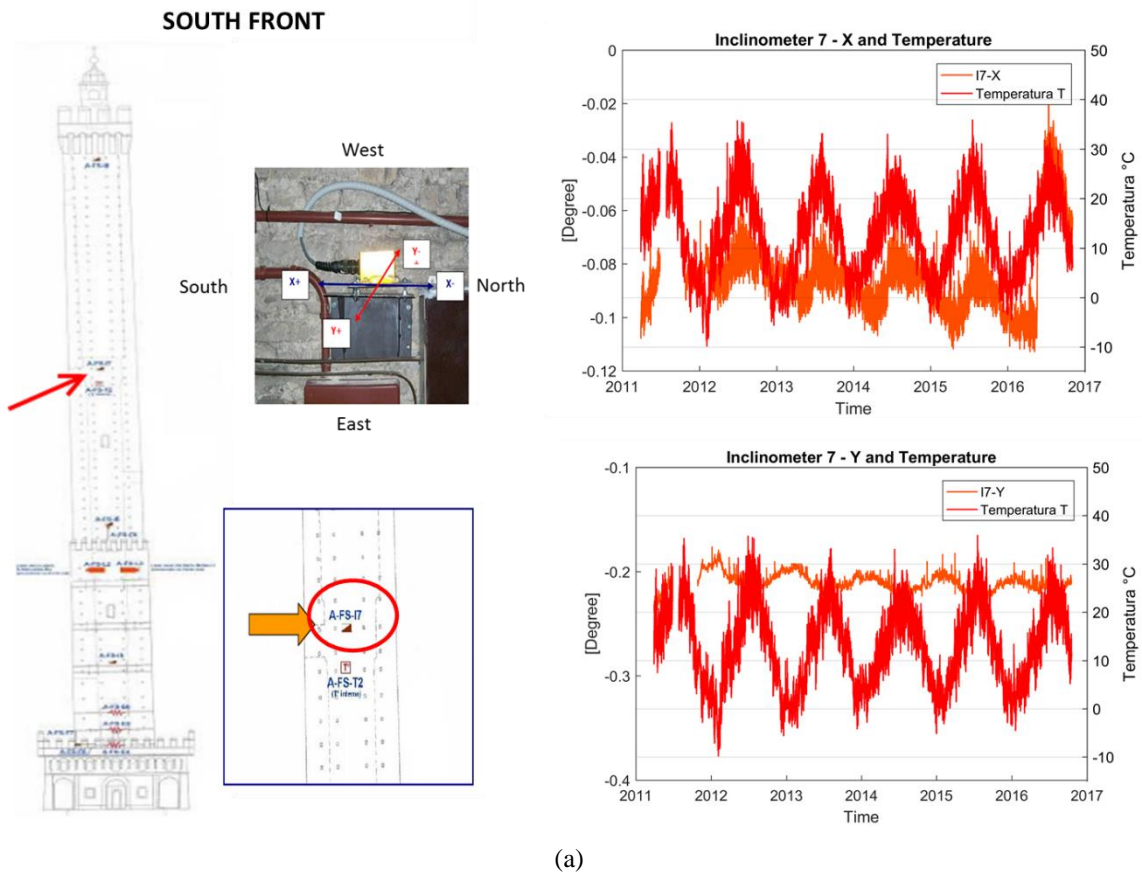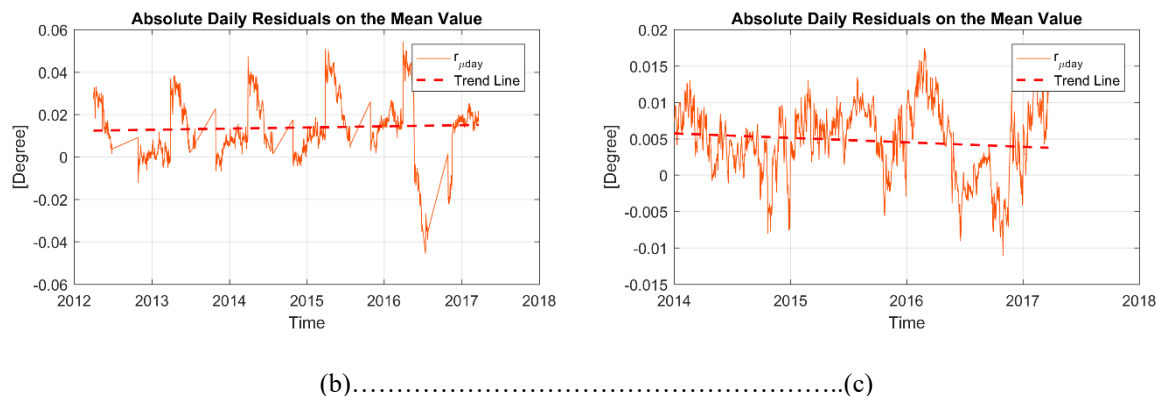
Figure 5-27: Inclinometer A-FS-I7: row-data recorded by I7 considering also the temperature variation, as recorded by the thermometer T1, and (b),(c) the absolute daily residuals evaluated for both X and Y direction

Inclinometer A-FS-I8

Inclinometer I8 is installed at the South front of the Asinelli tower (at the height of 85.0 m). The data recorded by I8 are in phase with respect to temperature data recorded by T1 (Figure 5-28 a). The absolute daily residuals reveal for the x component a cumulative trend of +0.02° (increase in the inclination in the South-East direction) and for the y component a trend of +0.01° (meaning decrease in the inclination in the North-East direction).

(a)

(b)……………………………………………..(c)
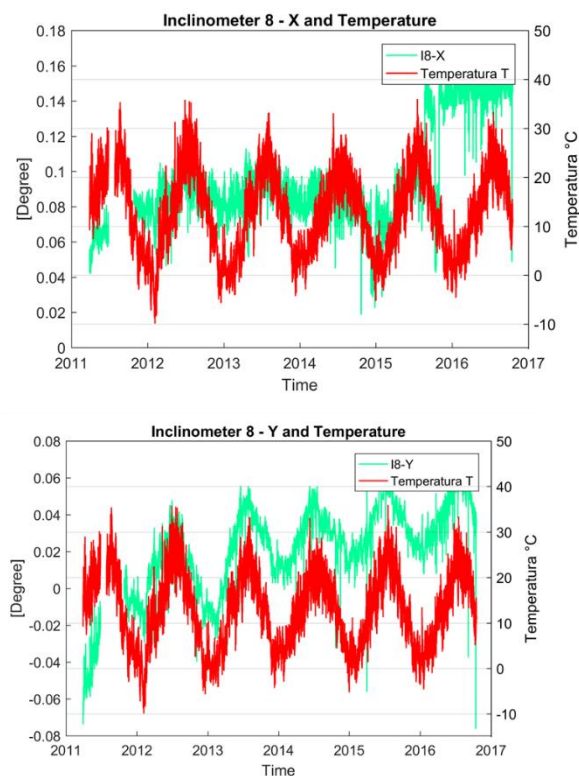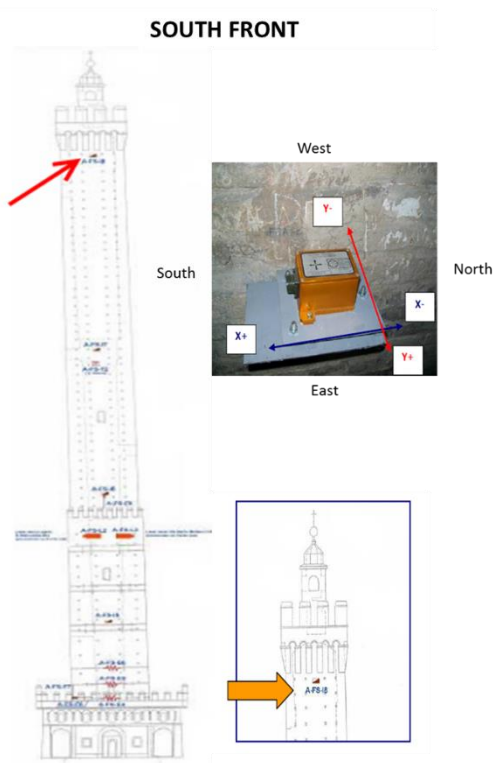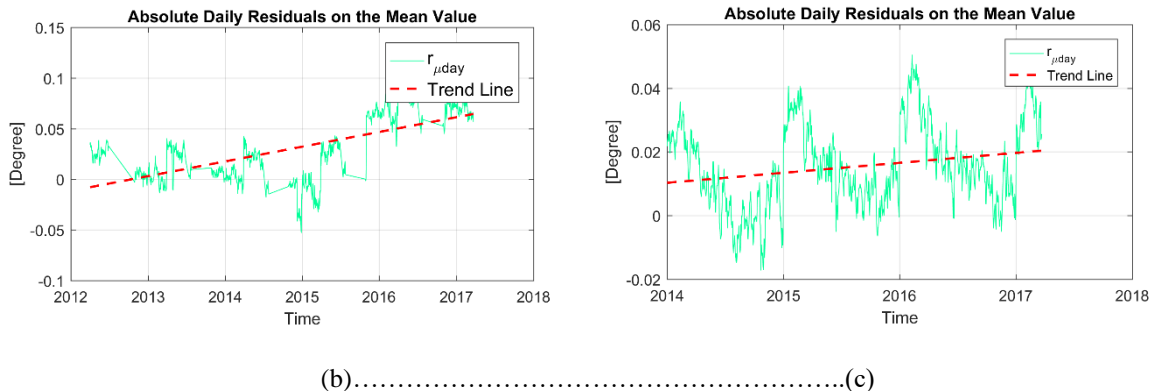
Figure 5-28: Inclinometer A-FS-I8: row-data recorded by I8 considering also the temperature variation, as recorded by the thermometer T1, and (b),(c) the absolute daily residuals evaluated for both X and Y direction

The mean values over the entire observation period of the reference quantities are collected in Table 5-10 for all the inclinometers.

Table 5-10- Men values of the reface quantities over the six years of monitoring for the inclinometers

Sensor	Year	$\delta_{day,j}$ [°]	$rp_{\mu day}$ [°]	$r_{\mu day}$ [°]	M_{year} [°]	Σ_{year} [°]	Rp_{Myear} [°]	R_{Myear} [°]
A-FO-I1-X	mean	0.0067	-0.0022	-0.0091	-0.1711	0.0437	-0.0022	-0.0102
A-FO-I1-Y	mean	0.0058	0.0334	0.1470	-0.0262	0.0882	0.0334	0.1478
A-FO-I2-X	mean	0.0064	0.0000	-0.0001	0.3716	0.0405	-0.0001	-0.0002
A-FO-I2-Y	mean	0.0057	0.0028	0.0072	-0.1060	0.0765	0.0033	0.0077
A-FO-I3-X	mean	0.0151	-0.0150	-0.0184	-0.3890	0.1029	-0.0167	-0.0202
A-FS-I3-Y	mean	0.0163	-0.0049	-0.0050	-0.1044	0.1303	-0.0044	-0.0046
A-FS-I4-X	mean	0.0168	0.0035	0.0115	0.3828	0.2045	0.0033	0.0098
A-FS-I4-Y	mean	0.0133	-0.0003	0.0007	0.2351	0.1078	0.0000	0.0010
A-FO-I5-X	mean	0.0044	-0.0015	-0.0034	0.1313	0.0288	-0.0013	-0.0032
A-FO-I5-Y	mean	0.0046	-0.0030	-0.0054	0.1608	0.0313	-0.0028	-0.0053
A-FO-I6-X	mean	0.0050	0.0030	0.0053	0.2195	0.0428	0.0032	0.0054
A-FO-I6-Y	mean	0.0058	0.0043	0.0091	0.1879	0.0775	0.0049	0.0097
A-FO-I7-X	mean	0.0123	0.0014	0.0133	-0.0722	0.1377	0.0003	0.0119
A-FS-I7-Y	mean	0.0080	0.0011	0.0045	-0.1614	0.0885	0.0011	0.0045
A-FS-I8-X	mean	0.0192	0.0156	0.0256	0.0950	0.7101	0.0157	0.0317
A-FS-I8-Y	mean	0.0130	0.0062	0.0141	0.0309	0.5978	0.0067	0.0146

5.5   Data processing

5.5.1   The influence of the external factors on the structural response

The influence of the external factors on the structural response has been investigated using the Equations 4.3-4.6. Four external factors are here considered: temperature recorded by thermometer T1, the temperature recorded by thermometer T2, and the wind in the direction x and the wind in direction y. The relative importance of each of these external factors are presented in Figure 5-29. This relationship with external factors has not been applied for the data recorded by laser displacements because large number of drops and missing data characterizes them. This study shows that the external factor which mostly influences the recorded data is the temperature. This further confirms that the validity of the approach presented.
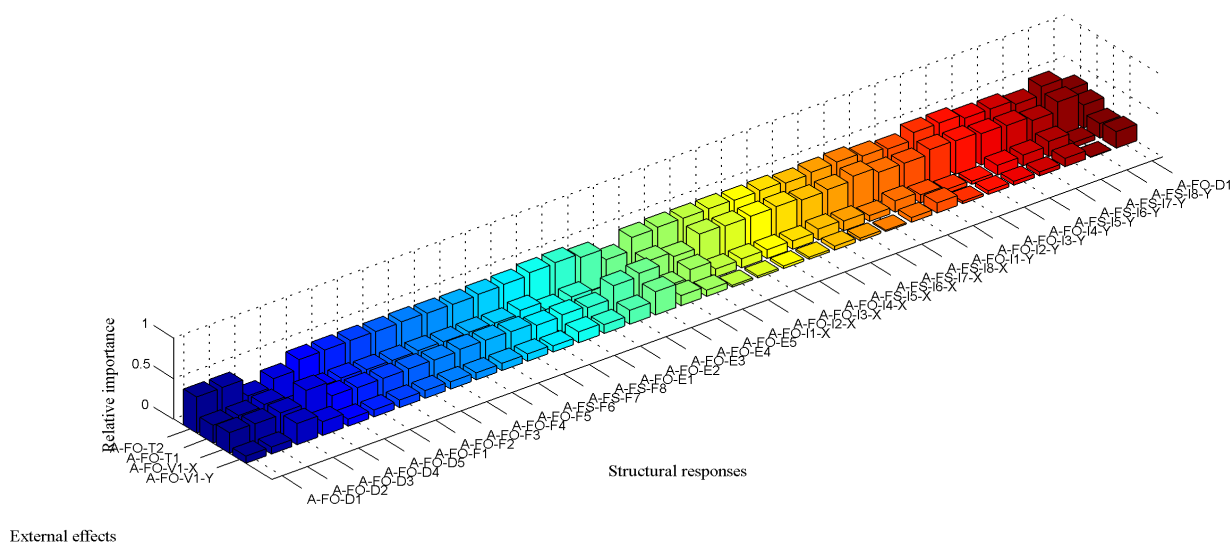
Figure 5-29: Relative importance of the external effects on the structural response of the Asinelli Tower.

5.5.2   The signal frequency analyses

Data have also been proceeded in the frequency domain in order to identify the periodical and the non-periodical components (called residue) of the signal. The time history of the residua as obtained from the frequency analysis (FFT and IFFT) is compared to the daily residua obtained from the evaluation of the reference quantities. The frequency analysis has been applied to data obtained by the instruments which have not presented malfunction, interruptions and / or many drops. For the sake of conciseness, here, the main results obtained are presented and the details of the frequency analyses for all the data investigated are provided in Appendix A.2

Long base deformeters

The long base deformeters present the predominant component of period close to T=240-270 days. The amplitude with period T=365 days appears less significant probably due to the thermal inertia of the masonry. Other important amplitudes are observed for periods equal to 120 days and 90 days. The amplitude with period T=1days does not appear significant. This fact, could be related to the characteristics of the sensors that often reach the full scale during the daily recording. Figure 5-30 a display the main components computed for the long base deformeter F1 The periodicity of the signal has been identified considering the main periodic components detected by the Fourier transform (T=270 days and T=365days),see Figure 5-30 b. The values of the residual seems to oscillate with an apparent random periodicity and its trend and variation is in good agreements with the values obtained from the time-domain analysis (Figure 5-30 c).

(a)

(b)………………………………………………..(c)
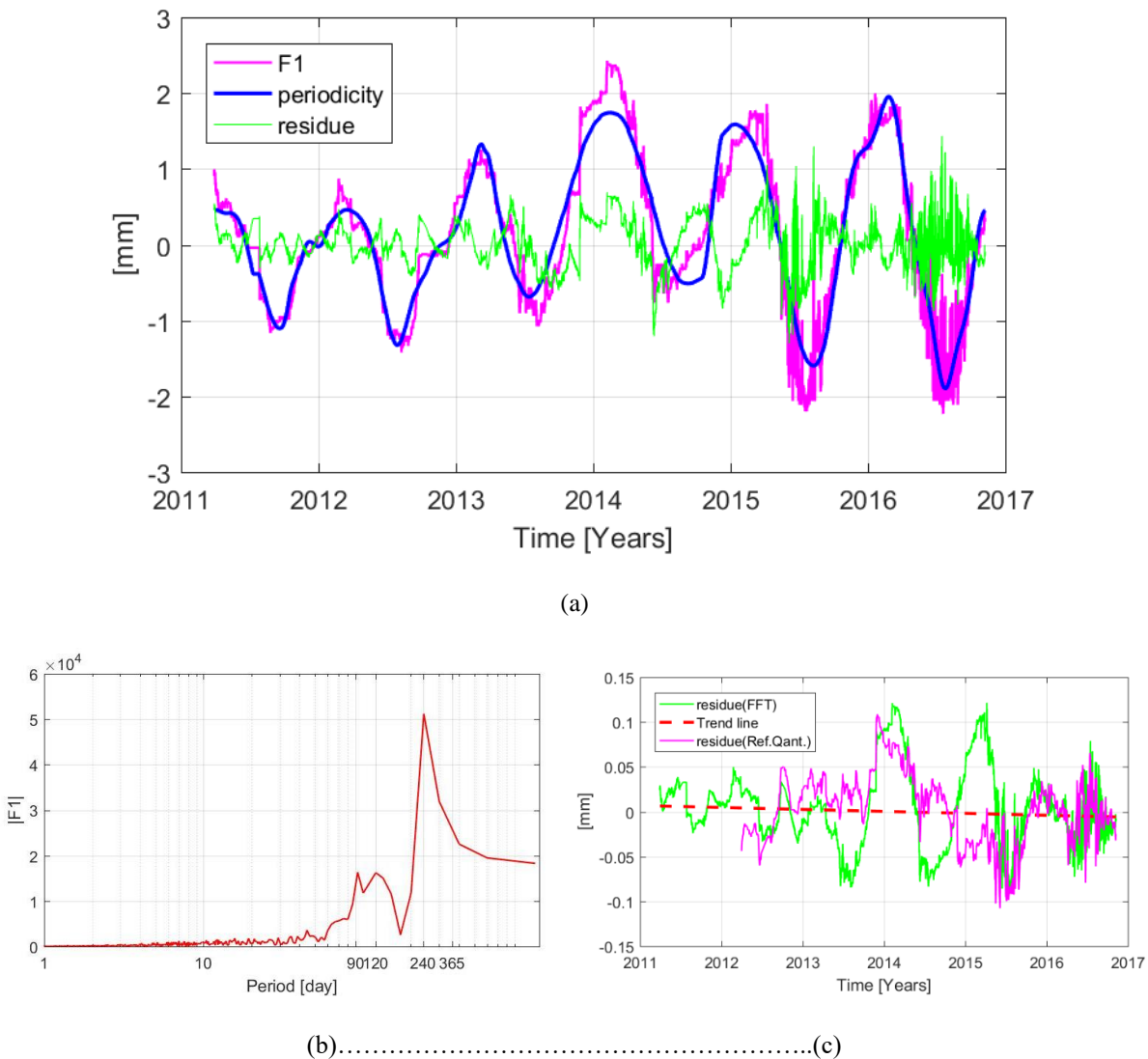
Figure 5-30: Recorded signal by the long base deformeter F1 and its main components (the periodical component and the residual), b) The Fourier Transform and c) the residue as obtained from the FFT and from the mathematical considerations (reference quantities)

Extensometers

The extensometers present the predominant components of period close to T=300-365 days. Another important amplitude is observed for period equal to 200 days. The amplitude with period T=1day does not appear significant also for the data recorded by the extensometers. Figure 5-31a display the main components evaluated for the extensometer E1. The periodicity of the signal has been identified considering the main periodic components detected by the Fourier transform (T=300 days and T=200 days), see Figure 5-31 b. The values of the residual seems to oscillate with an apparent random periodicity and its trend and variation is in good agreements with the values obtained from the time-domain analysis (Figure 5-31 c).
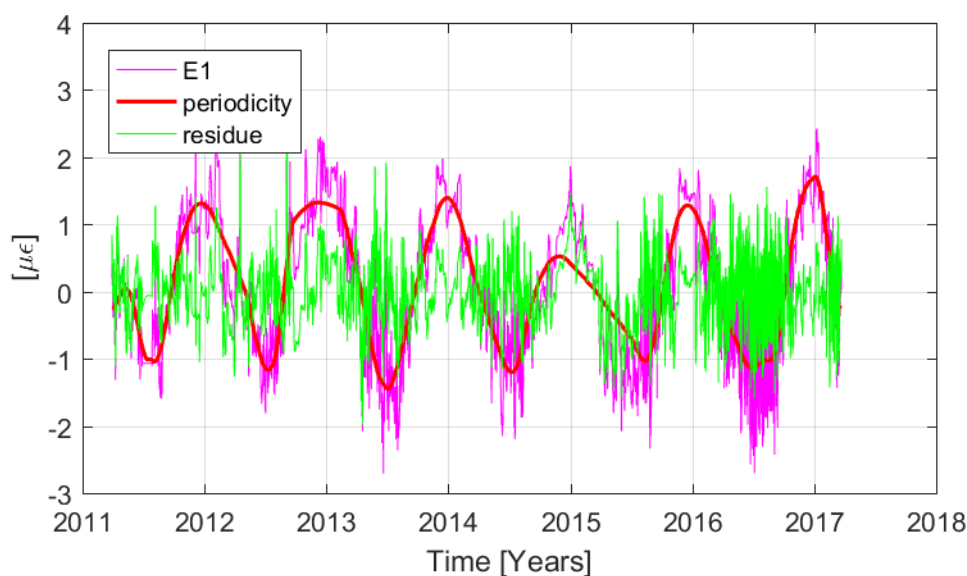
(a)
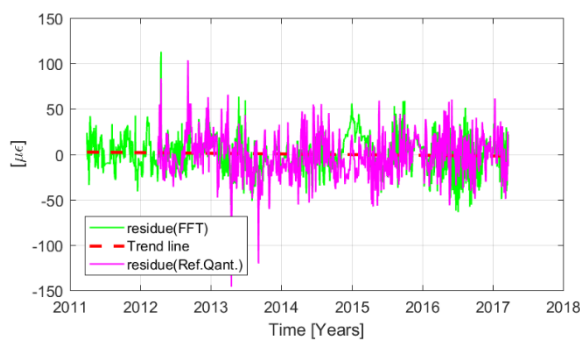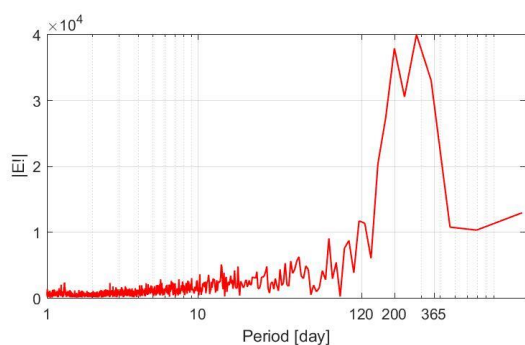
(b)……………………………………………..(c)

Figure 5-31: (a) Recorded signal by the extensometer E1 and its main components (the periodical component and the residual), (b) The Fourier Transform and (c) the residue as obtained from the FFT and from the mathematical considerations (reference quantities)

Inclinometers

The inclinometers present the predominant component of period close to T=365 days (Figure 5-32 b). The amplitude with period T=1days does not appear significant. This fact, could be related to the characteristics of the sensors that often reach the full scale during the daily recording. Figure 5-32 a display the main components computed for the inclinometer I2 in the y-direction. The trend and variation of the residue is in good agreements with the values obtained from the time-domain analysis (Figure 5-32 c).

(a)

(b)…………………………………………..(c)
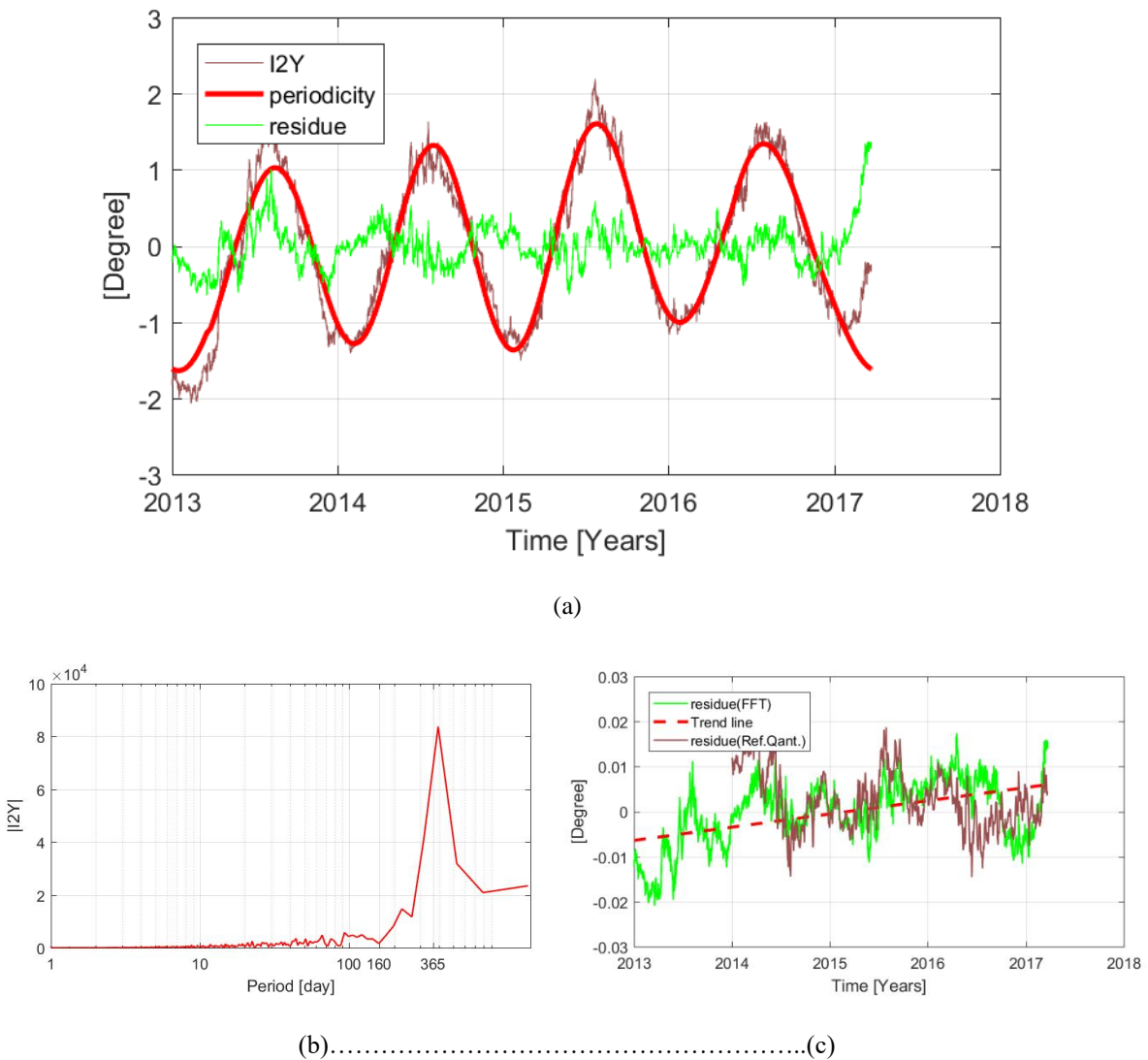
Figure 5-32: (a) Recorded signal by the inclinometer I2 and its main components (the periodical component and the residual), (b) The Fourier Transform and (c) the residue as obtained from the FFT and from the mathematical considerations (reference quantities)

5.6 Conclusions

The interpretation of the data recorded (from 2011 to 2016) by the static monitoring system installed on the Asinelli tower has been performed making use of the reference quantities presented in § 3.3. Through this investigation, the following conclusion are drawn:

- the phenomena under observation appear, in general, in a stable condition (the trend of the data over the years, even in their seasonal/annual variability, do not show specific evolutionary trend);
- the long base deformeters, which measure the horizontal and vertical masonry deformation, display a high inverse correlation with the temperature. Moreover, the values of the daily amplitudes recorded during the cold season are one order of magnitude less than those recorded during the hot season. The order of magnitude of the cumulative residues calculated on the recorded data from these devices varies between 0.002 and 0.1 mm.
- the trend recorded by the extensometers is similar to that recorded by the long base deformeters. Also in this case, the recorded data are out-of-phase with respect to temperature data and the values of the daily amplitudes recorded during the cold season are one order of magnitude less than those recorded during the hot season. These devices recorded several drops during all the monitoring period due to their sensibility to the meteorological conditions. However, the analysis of the signals after removing these irregularities shows that the steel tie on Asinelli tower recorded increases / decreases on the stress state, which remain lower than 30 $\mu\varepsilon$.
- the trend recorded by the inclinometers, which monitor the inclination of the walls of the Asinelli tower, presents, generally, a high direct correlation with the temperature data. The increase/decrease of the inclination, during the six years monitoring, remain always lower than 1 degree.

The study of the influence of the external factors on the structural response of the Asinelli tower reveals that the temperature is the factor, which mostly influences the recorded data.

In addition, the main periodicity of the recorded data have been investigated through the signal frequency analyses. The long base deformeter and the extensometer reveal the predominant component with period of T= 240-300 days (i.e. lower than the expected one with period of T=365 days). This fact could be related to the thermal inertia of the masonry walls. The periodic component of the data recorded by the inclinometers is essentially given by the harmonic with period T1=365 days. The trend and variation of the non-periodic components (residue) obtained from the FFT analyses are usually in good agreements with the values obtained from the time-domain analysis (reference quantities §3.3).

Chapter 6

6 A case study of the Garisenda Tower

6.1 Introduction

In the 2011, a static SHM system has been also installed on the Garisenda tower, a masonry leaning tower adjacent to the Asinelli tower and built in the 11th century.

In this Chapter, organized in the same way of the previous one, the monitoring system installed on the Garisenda tower will be described.

The large amount of data recorded by the monitoring system has been analyzed using the approach proposed in § 3.3 in order to evaluate if the phenomena under observation are in a stable condition or not. The signal frequency analyses on the recorded data have been also carried out and the results obtained in terms of residuals (i.e. signal not affected by the seasonal effects which should be representative of the state of the building) compared with the residue obtained from the time-domain analyses proposed. The main results obtained from the analyses are presented in this Chapter.

6.2 The Garisenda Tower

The Garisenda, the older of the "Two Tower", can be dated around the last two decades of the eleventh century (Figure 6-1a). During the construction phases, the foundation soil underwent important subsidence phenomena, which caused a visible tilt of the tower (Ceccoli et al. 2001). The tower is 48 m high and has a slope of 3.22 m towards South-East. As the Asinelli tower, the cross section of the Garisenda tower is not constant with the height: the base presents an external selenitic layer that cover the external wall for the first 3.5 m; above the selenitic base the cross section (built using the ancient "a sacco" technique) reduces with height as the common construction practice at the time of construction (Figure 6-1b). The same strengthening interventions performed on the Asinelli tower, were also carried out on the Garisenda tower.

Height=2.50 m

Height=44.0 m
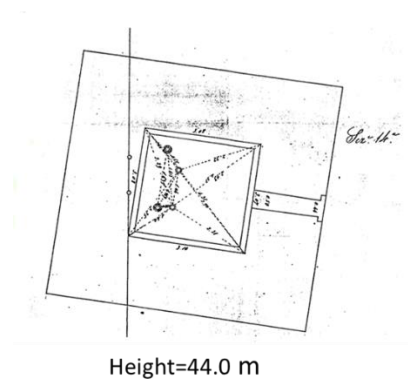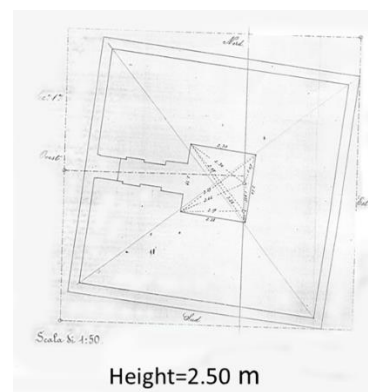
(a)   (b)

Figure 6-1: (a) The Garisenda tower of Bologna, (b) Tower cross section at two different heights

6.3 Types and location of instruments

At the beginning of year 2011, a SHM system was also installed in the Garisenda tower in order to monitor the same phenomena described in § 5.3 for the Asinelli tower.

The nomenclature of the monitoring instruments used is:

G=Garisenda,

FN=North front, **FS**=South front, **FE**=East front, **FO**=West front (Figure 6-2),

F=long base deformeter, **D**=deformeter, **I**=inclinometer, **E**=extensometer, **L**=laser displacement sensor, **T**= thermometer, **V**=gonioanemometer sensor.
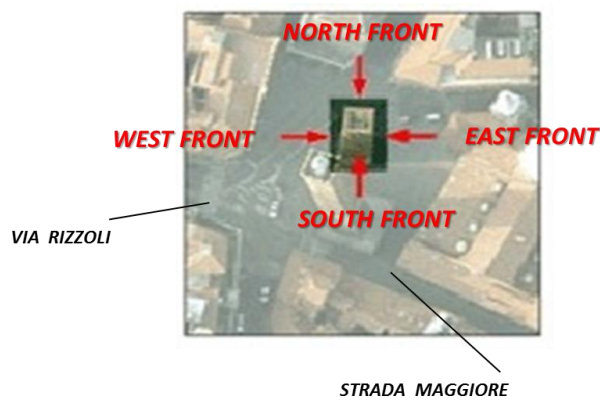
Figure 6-2: Identification of the different Fronts of the Garisenda tower

Table 6-1 summarised the typology and the position of the different instruments installed along the height of the Garisenda tower, which are then displayed in Figure 6-3.
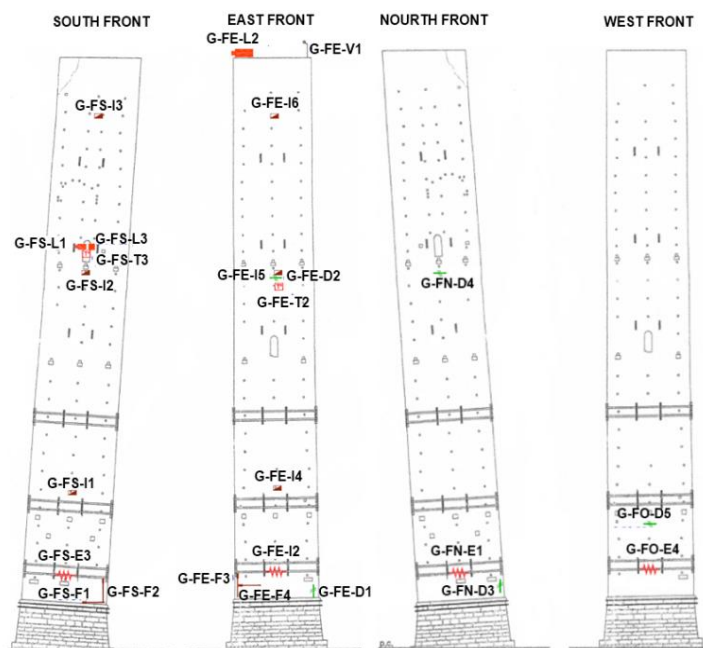
Figure 6-3: Monitoring system of GarisendaTower

Table 6-1- Typology and position of the instrument installed on the Garisenda tower

Sensor	N.	Location	Type
Long Base Deformeter	4	2 in the corner of the masonry of the South front(FS) 2in the corner of the masonry of the East front (FE)	Invar wire Deformeter
Deformeter	5	2 on cracks of the East front (FE) 2 on cracks of the North front (FN) 1 on a crack of the West front (FO)	OG400 Deformeters
Inclinometer	6	3 on the wall of the South front (FS): at different level. 3 on the wall of the East front (FS): at different level.	Dual axis inclinometer ELS-XX-V
Extensometer	4	1 on the steel ties of the North front (FN) 1 on the steel ties of the East front (FE) 1 on the steel ties of the South front (FS) 1 on the steel ties of the West front (FO)	Vibrating Wire Spot Weldable Strain Gauge
Laser displacement sensor	3	1 on the South front (FS) with on Santa Maria della Vita dome 1 on the East front (FE)with target on Prendiparte tower 1 on the South (FS)front with target on the Asinelli tower	Long Range Laser Displacement Sensors DLS-B
Thermometer	2	1 on the East front (FE) 1 on the South front (FS)	
Gonioanemometer sensor	1	At the top of the tower	

The typology of the instruments installed on the Garisenda tower are the same of those installed in the Asinelli tower and already described in §6.3. Following only the information of the three fix points pointed by the distanziometer and the landmarks for the inclination recorded by the inclinometers are reported.

Laser displacement:

These sensors aim three fix points: Prendiparte tower, the dome of S. Maria della Vita church and Asinelli tower (Figure 5-8b).

Inclinometers:

The x component record positive value along the East direction and negative value along the West direction. While the y component record positive value along the North direction and negative value along the South (Figure 6-4).
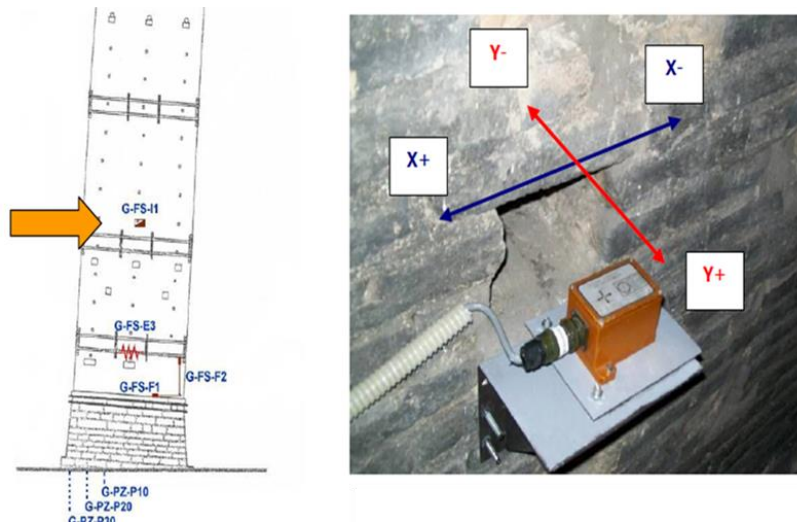
Figure 6-4: Dual axis inclinometer ELS-XX-V (I1) installed on the South Front

6.4   Reference quantities

The reference quantities defined in § 3.3 have been identified for all the data recorded by sensor of the monitoring system of the Garisenda tower. Appendix B.1 provides the systematic identification of these reference quantities. In the next section, the salient results, obtained from the interpretation of the static monitoring data through the proposed procedure, are illustrated. It is noted that the laser distance meters have recorded many drops throughout the monitoring period. Their data are therefore not reliable in order to perform evaluations on the structural health of the tower.

6.4.1 Long Base Invar Deformeters

Long base Invar Deformeters G-FS-F1- G-FS-F2

Long base deformeters F1 and F2, installed at the South-East corner base of the Garisenda tower (corner under the slope), measure the horizontal and vertical masonry deformation, respectively. In more detail, Figure 6-5 a displays the row-data recorded by the two devices. In the same graph, also the temperature variation (as recorded by the thermometer T1) is displayed. As already see for the data recorded by the long base deformeters installed on the Asinelli tower, the recorded data are out-of-phase with respect to temperature data and the values of the daily amplitudes recorded during the cold season are one order of magnitude less than those recorded during the hot season (Figure 6-5 b, d). The absolute daily residuals reveal for F1 a cumulative trend of +0.007mm (meaning increase in tension in the horizontal direction) and for F2 a cumulative trend of -0.10 mm (meaning increase in compression in the vertical direction) in the six years.

(a)

(b)……………………………………………………..(c)

(d)……………………………………………..(e)
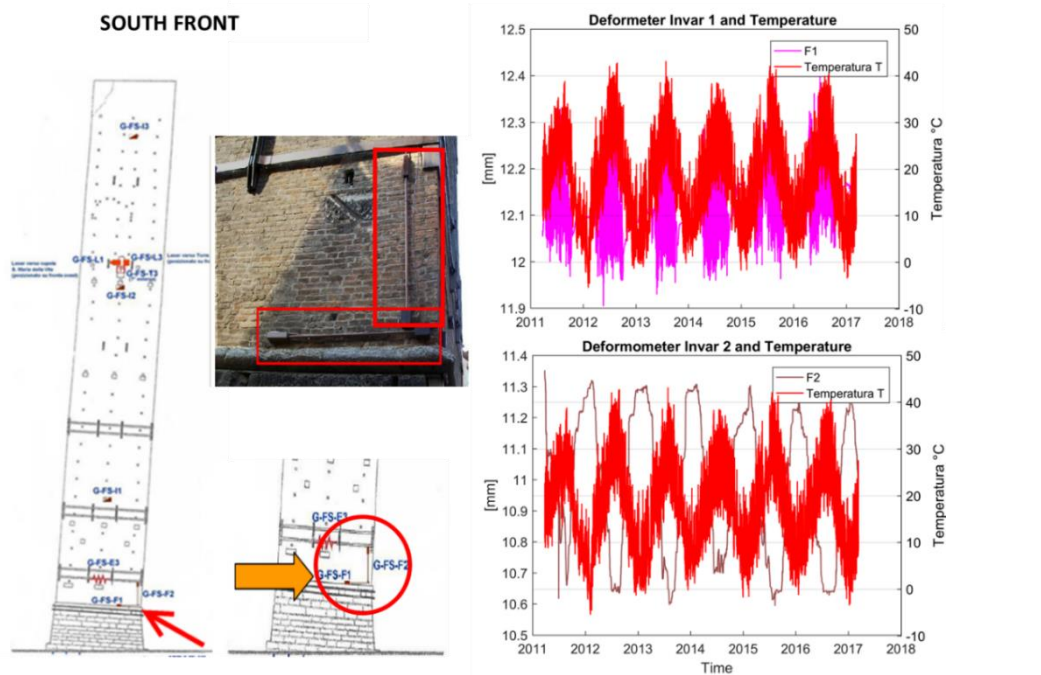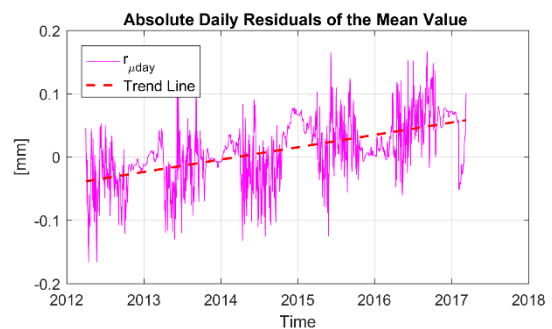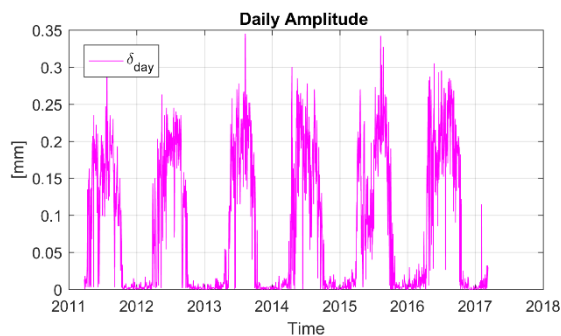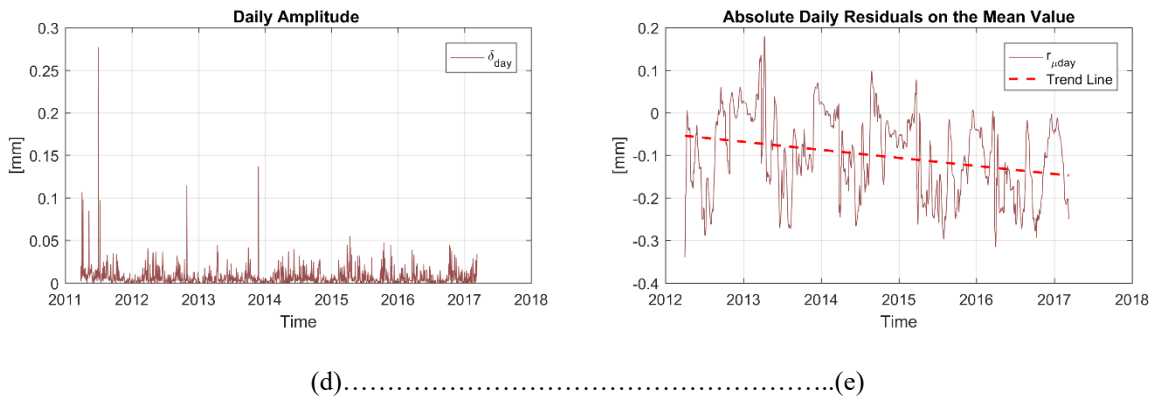
Figure 6-5: Long base Invar Deformeters G-FS-F1- G-FS-F2: (a) row-data recorded by F1 and F2 considering also the temperature variation, as recorded by the thermometer T1, (b)and (c) time-history of the "daily amplitude and absolute daily residuals evaluated for F1 and (d),(e) time-history of the "daily amplitude and absolute daily residuals evaluated for F2

Long base Invar Deformeters G-FE-F3- G-FE-F4

Long base deformeters F3 and F4, installed at the East front the Garisenda tower (corner South-East under the slope), measure the horizontal and vertical masonry deformation, respectively. In more detail, Figure 6-6 a displays the row-data and the temperature variation. The recorded data are out-of-phase with respect to temperature data and the values of the daily amplitudes recorded during the cold season are one order of magnitude less than those recorded during the hot season (Figure 6-6 b, d). The absolute daily residuals reveal for F3 a cumulative trend of -0.02mm (meaning increase in compression in the horizontal direction) and for F4 a cumulative trend of -0.06 mm (meaning increase in compression in the vertical direction) in the six years (Figure 6-6 c, d).
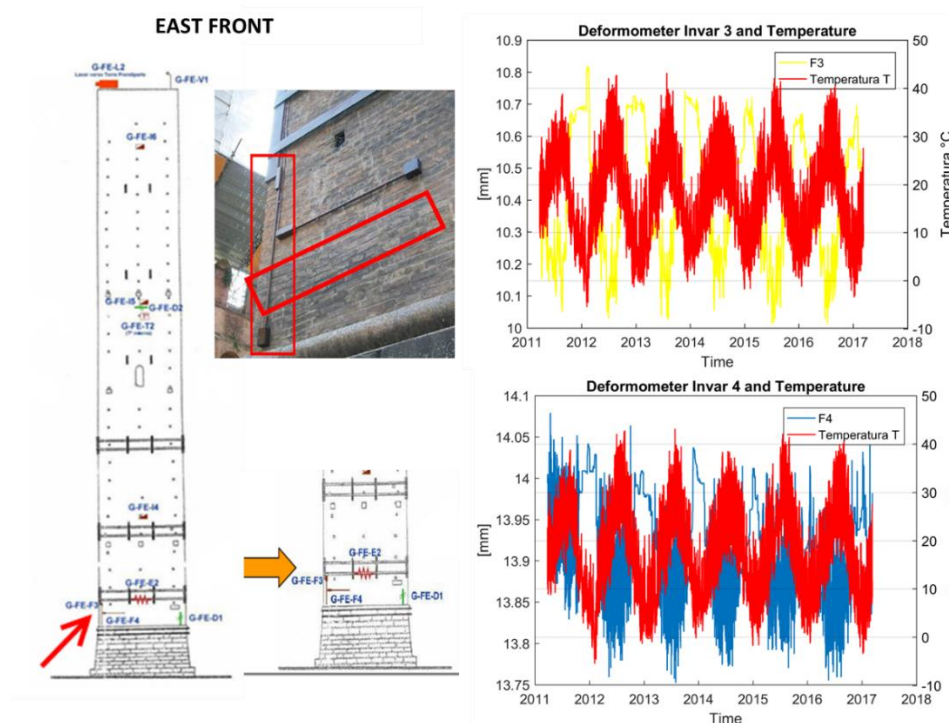
(a)
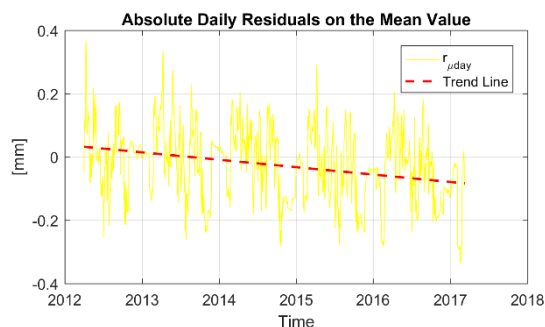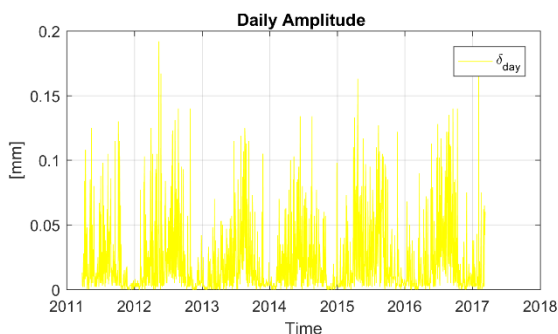
(b)…………………………………………………..(c)
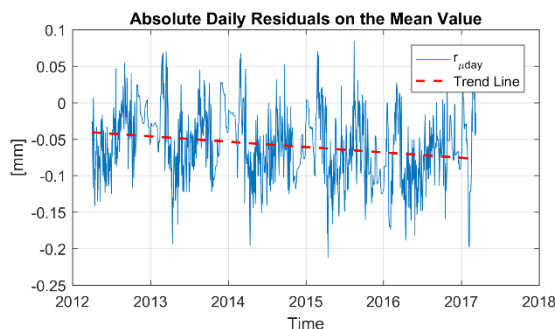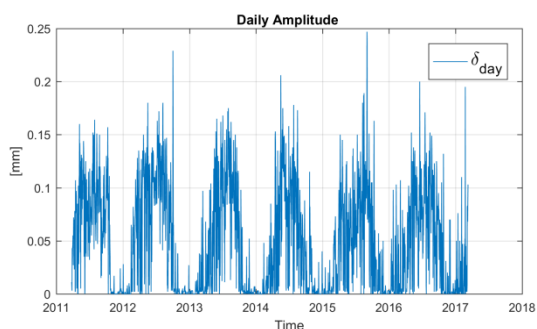
(d)…………………………………………………..(e)

Figure 6-6: Long base Invar Deformeters G-FE-F3- G-FE-F4: (a) row-data recorded by F3 and F4 considering also the temperature variation, as recorded by the thermometer T1, (b)and (c) time-history of the "daily amplitude and absolute daily residuals evaluated for F3 and (d),(e) time-history of the "daily amplitude and absolute daily residuals evaluated for F4

The mean values over the entire observation period of the reference quantities are collected in Table 6-2 for all the long base deformeters.

Table 6-2-Men values of the reface quantities over the six years of monitoring for the long base deformeters

Sensor	Year	$\delta_{day,j}$ [mm]	$rp_{\mu day}$ [mm]	$r_{\mu day}$ [mm]	M_{year} [mm]	Σ_{year} [mm]	Rp_{Myear} [mm]	R_{Myear} [mm]
G-FS-F1	mean	0.083	0.008	0.007	11.962	0.390	0.011	0.003
G-FS-F2	mean	0.007	-0.033	-0.099	10.628	0.681	-0.035	-0.072
G-FE-F3	mean	0.021	-0.010	-0.021	10.031	1.164	-0.005	0.031
G-FE-F4	mean	0.048	-0.018	-0.060	13.773	0.275	-0.017	-0.062

6.4.2 Deformeters

Deformeters G-FE-D1- G-FE-D2

Deformeters D1 and D2, installed at the East front of the Garisenda tower, measure the evolution of two cracks. Figure 6-7a displays the row-data and the temperature variation (as recorded by the thermometer T2). The recorded data are out-of-phase with respect to temperature data and the values of the daily amplitudes recorded during the cold season are around one order of magnitude less than those recorded during the hot season (Figure 6-7 b, d). The absolute daily residuals reveal for D1 a cumulative trend of +0.002mm (meaning slight opening of the crack monitored) and for D2 a cumulative trend of +0.03 mm (meaning opening of the crack monitored) in the six years.

(a)

(b)……………………………………………………..(c)

(d)……………………………………………………..(e)
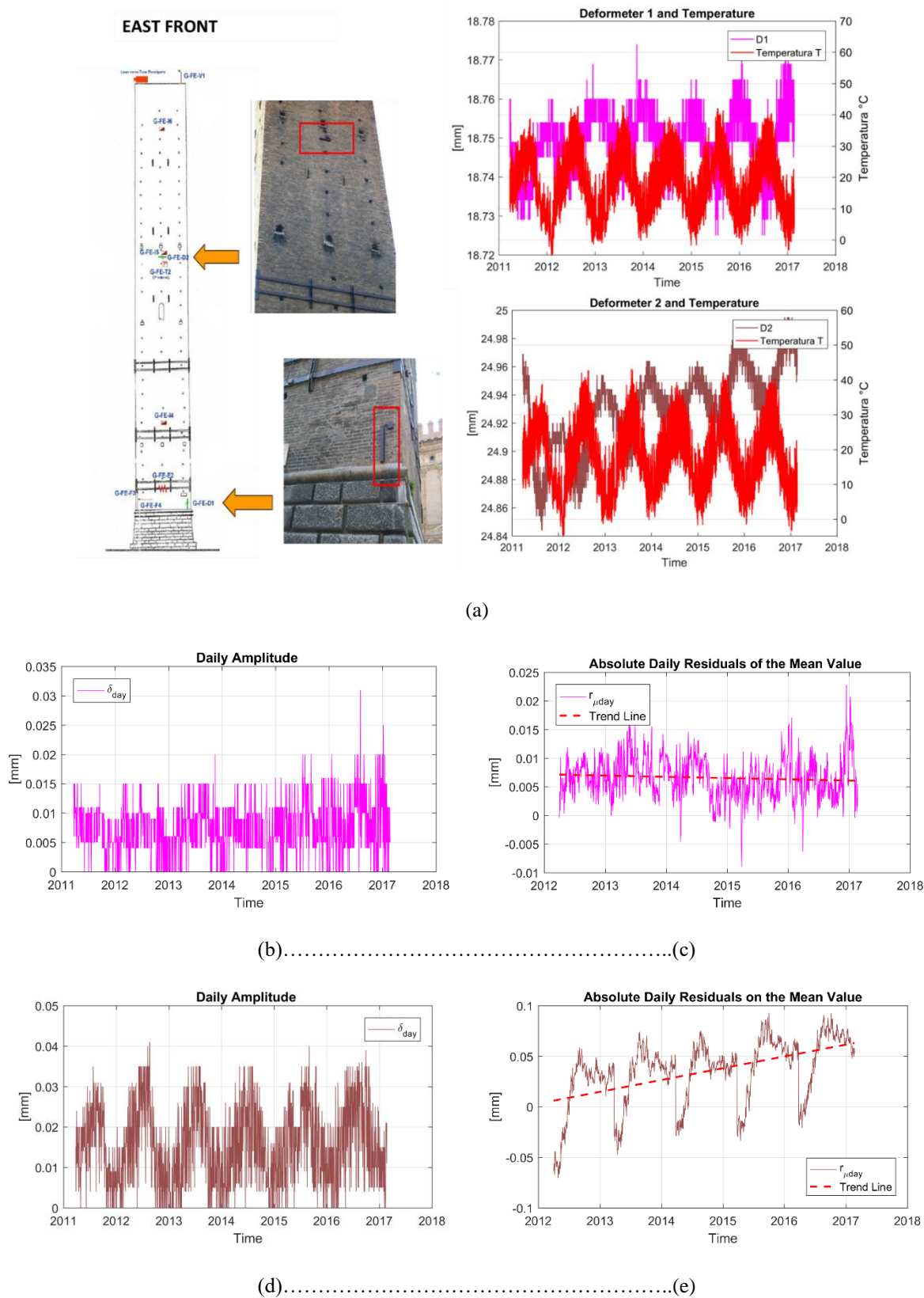
Figure 6-7:Deformeters G-FE-D1- G-FE-D2: (a) row-data recorded by D1 and D2 considering also the temperature variation, as recorded by the thermometer T1, (b) and (c) time-history of the "daily amplitude and absolute daily residuals evaluated for D1 and (d),(e) time-history of the "daily amplitude and absolute daily residuals evaluated for D2

Deformeters G-FN-D3- G-FN-D4

Deformeters D3 and D4, installed at the North front of the Garisenda tower, measure the evolution of two cracks. Figure 6-8 a displays the row-data and the temperature variation (as recorded by the thermometer T2). The recorded data are out-of-phase with respect to temperature data and the values of the daily amplitudes recorded during the cold season are around one order of magnitude less than those recorded during the hot season (Figure 6-8Figure 6-7 b, d). The absolute daily residuals reveal for D3 a cumulative trend of +0.002 mm (meaning slight opening of the crack monitored) and for D4 a cumulative trend of -0.014 mm (meaning closing of the crack monitored) in the six years.

(a)

(b)……………………………………………..(c)

(d)…………………………………………..(e)
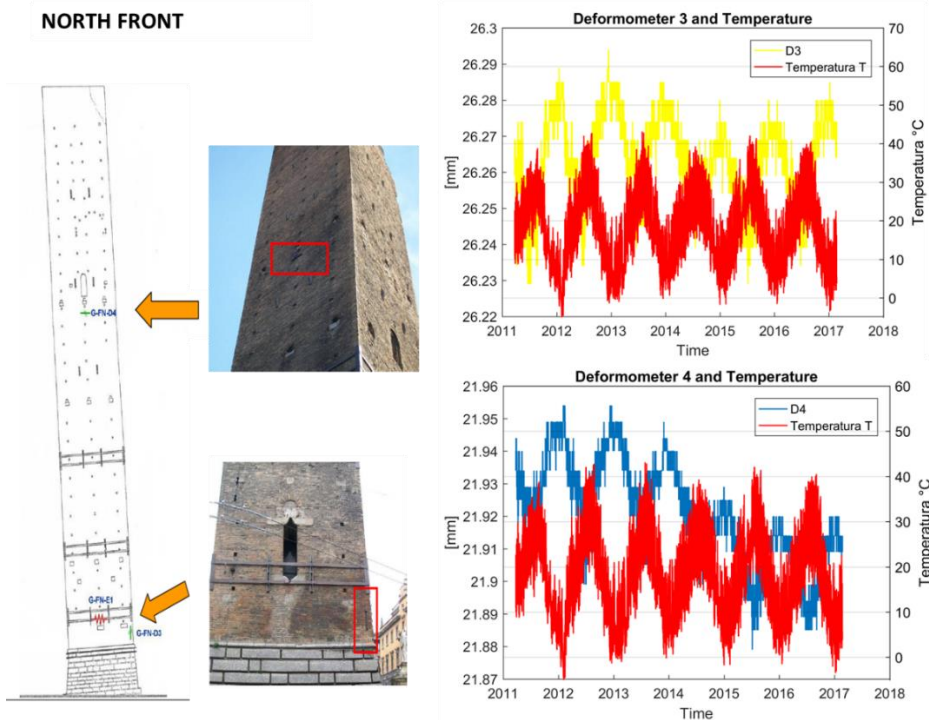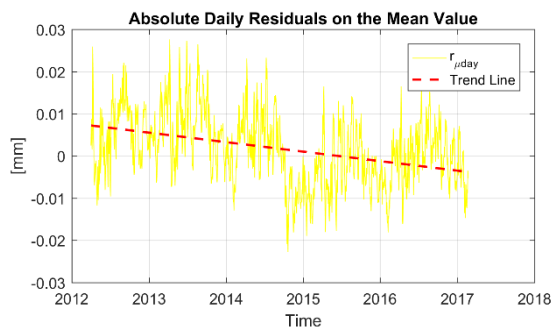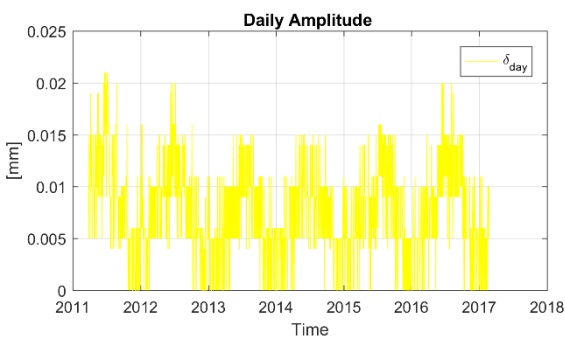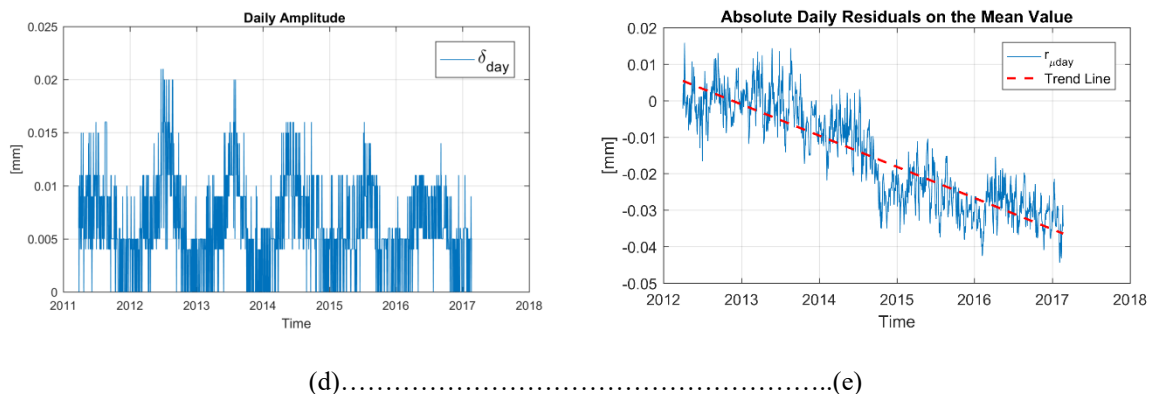
Figure 6-8: Deformeters G-FN-D3- G-FN-D4: (a) row-data recorded by D3 and D4 considering also the temperature variation, as recorded by the thermometer T2, (b) and (c) time-history of the "daily amplitude and absolute daily residuals evaluated for D3 and (d),(e) time-history of the "daily amplitude and absolute daily residuals evaluated for D4

Deformeters G-FO-D5

Deformeter D5, installed at the West front of the Garisenda tower, measure the evolution of the crack. The recorded data are out-of-phase with respect to temperature data (Figure 6-9).The absolute daily residuals reveal that the crack under observation has opened of 0.08 mm during the six years of monitoring.
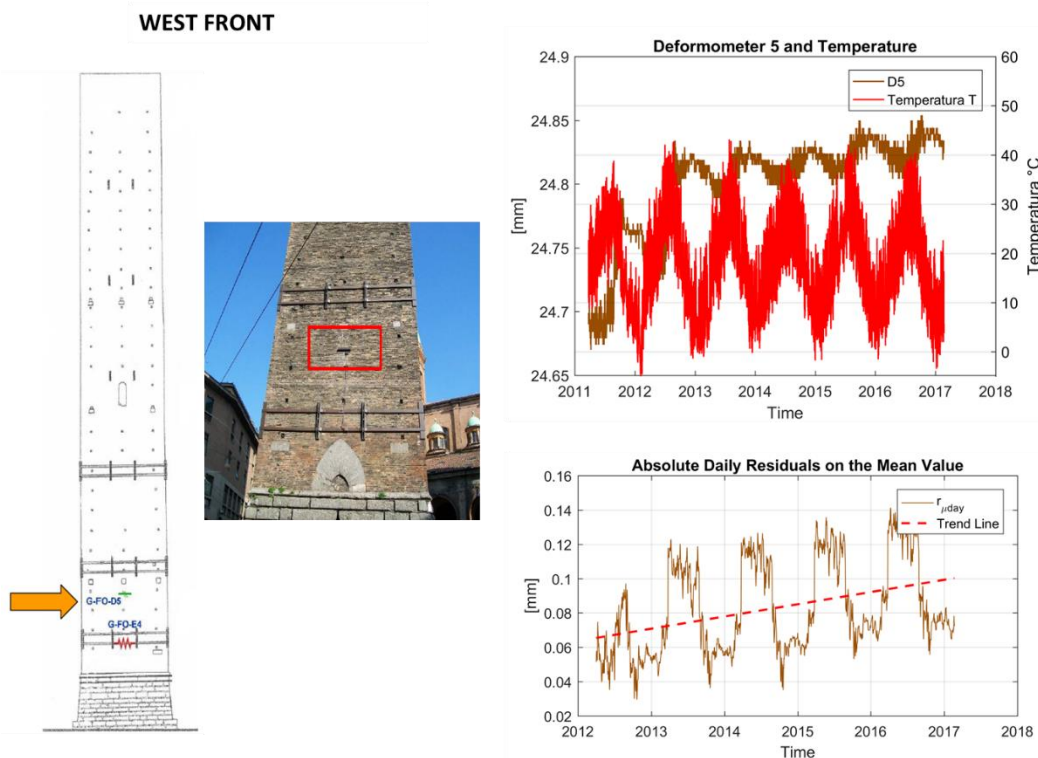
Figure 6-9: Deformeters G-FO-D5-row-data recorded considering also the temperature variation, as recorded by the thermometer T2, and absolute daily residuals

The mean values over the entire observation period of the reference quantities are collected in Table 6-3 for all the deformeters.

Table 6-3: Men values of the reface quantities over the six years of monitoring for the deformeters

Sensor	Year	$\delta_{day,j}$ [mm]	$\mathrm{rp}_{\mu day}$ [mm]	$\mathrm{r}_{\mu day}$ [mm]	M_{year} [mm]	Σ_{year} [mm]	Rp_{Myear} [mm]	R_{Myear} [mm]
G-FE-D1	mean	0.007	0.002	0.002	18.749	0.038	0.001	0.008
G-FE-D2	mean	0.016	0.011	0.033	24.932	0.092	0.010	0.033
G-FN-D3	mean	0.008	0.000	0.002	26.263	0.050	0.000	0.005
G-FN-D4	mean	0.006	-0.006	-0.014	21.922	0.045	-0.006	-0.012
G-FO-D5	mean	0.011	0.023	0.082	24.798	0.073	0.021	0.086

6.4.3 Extensometers

Extensometers G-FN-E1-G-FE-E2-G-FS-E3-G-FO-E4

Extensomiters E1, E2, E3 and E4, installed respectively on the still ties of the North, East, South, West front at the base of the Garisenda tower, measure the stress state of the ties. The data recorded by the extensometers are out-of-phase with respect to temperature data. The values of the daily amplitudes recorded during the cold season are one order of magnitude less than those recorded during the hot season (Figure 6-10 b, Figure 6-11 b, Figure 6-12 b, Figure 6-13 b). The time history of the absolute daily residuals reveal that:

-   E1 recorded a cumulative trend of -21$\mu\epsilon$ (meaning decrease in stress);
-   E2 recorded a cumulative trend of -9$\mu\epsilon$ (meaning decrease in stress).
-   E3 recorded a cumulative trend of -29$\mu\epsilon$ (meaning decrease in stress).
-   E4 recorded a cumulative trend of -16$\mu\epsilon$ (meaning decrease in stress).

Figure 6-10: Extensometer G-FN-E1: (a) row-data recorded by E1 considering also the temperature variation, as recorded by the thermometer T2, (b) time-history of the "daily amplitude and (c) absolute daily residuals evaluated for E1

Figure 6-11: Extensometer G-FE-E2: (a) row-data recorded by E2 considering also the temperature variation, as recorded by the thermometer T2, (b) time-history of the "daily amplitude and (c) absolute daily residuals evaluated for E2

Figure 6-12: Extensometer G-FS-E3: (a) row-data recorded by E3 considering also the temperature variation, as recorded by the thermometer T2, (b) time-history of the "daily amplitude and (c) absolute daily residuals evaluated for E3
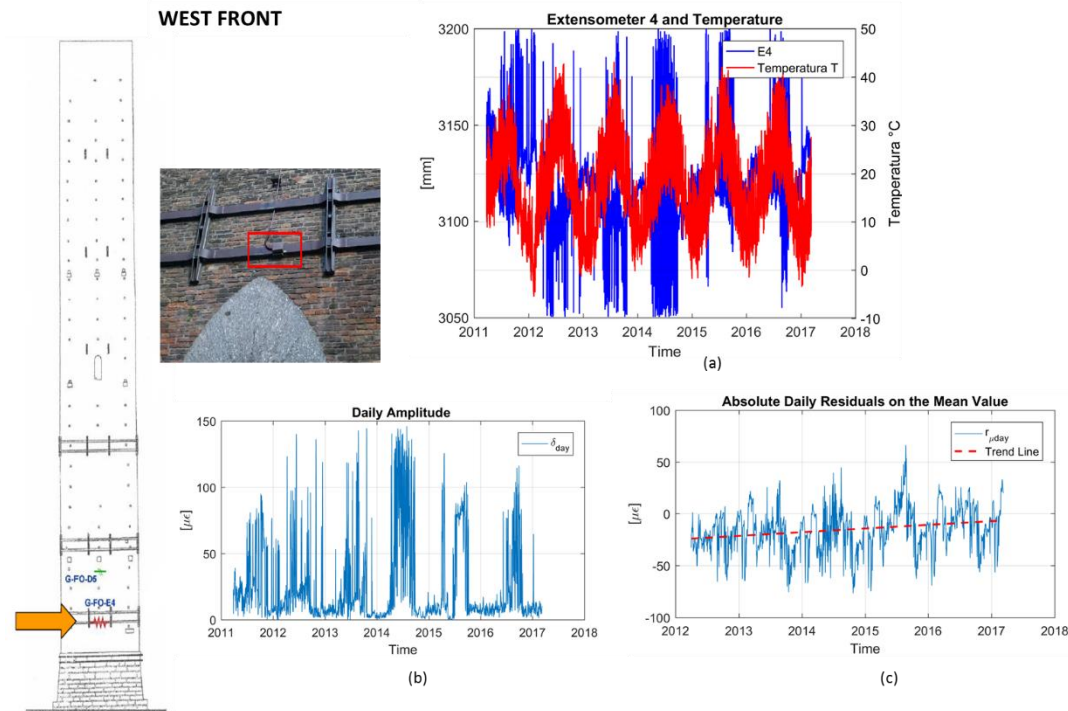
Figure 6-13: Extensometer G-FO-E4: (a) row-data recorded by E4 considering also the temperature variation, as recorded by the thermometer T2, (b) time-history of the "daily amplitude and (c) absolute daily residuals evaluated for E4

The mean values over the entire observation period of the reference quantities are collected in Table 6-4 for all the extensometers.-

Table 6-4- Men values of the reface quantities over the six years of monitoring for the extensometers

Sensor	Year	$\delta_{day,j}$ [με]	$\mathrm{rp}_{\mu day}$ [με]	$\mathrm{r}_{\mu day}$ [με]	M_{year} [με]	Σ_{year} [με]	Rp_{Myear} [με]	R_{Myear} [με]
G-FN-E1	mean	7.365	-5.302	-20.436	2682.292	66.209	-5.317	-20.420
G-FE-E2	mean	34.446	-2.720	-8.933	2137.753	107.238	-2.905	-8.351
G-FS-E3	mean	18.922	-8.124	-28.719	2592.711	91.540	-8.056	-29.844
G-FO-E4	mean	25.302	-2.699	-16.004	3115.959	139.707	-2.166	-15.984

6.4.4 Inclinometers

It should be noted that the inclinometers measure the inclination in the x-direction and y-direction of the wall: the x component record positive value along the East direction and the y component record positive value along the North direction.

Inclinometer G-FS-I1

Inclinometer I1 is installed at the South-West corner of the Garisenda tower (at the height of 13.20 m). Figure 6-14 a display the row-data by I1 and the temperature variation. It can be noticed that the data recorded by I1 are in phase with respect to temperature data. The absolute daily residuals reveal for the x component a cumulative trend of -0.004° (meaning decrease in the inclination in the West direction) and for the y component a trend of +0.012° (meaning increase in the inclination in the North direction).

(a)

(b)………………………………………………..(c)
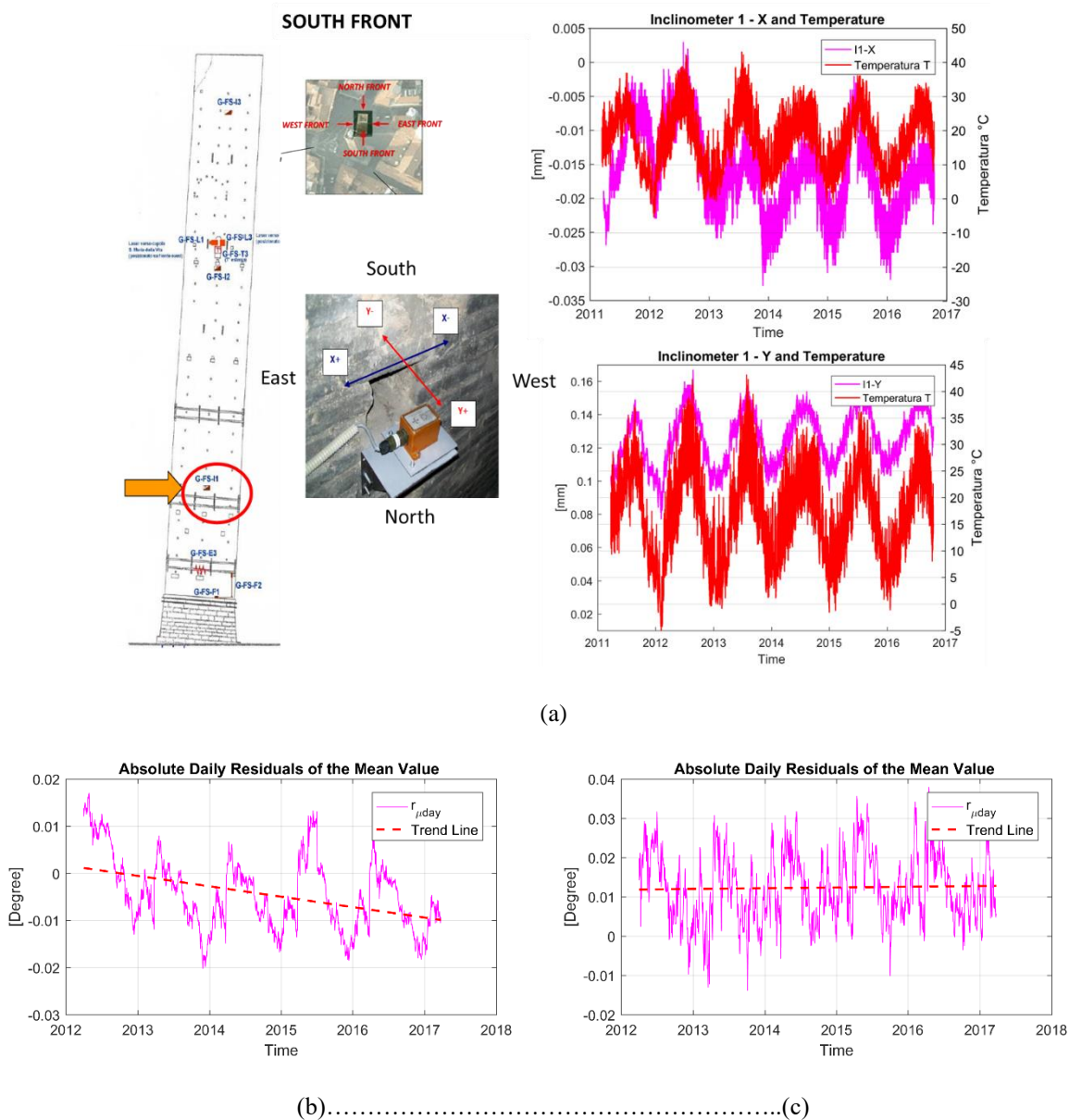
Figure 6-14: Inclinometer G-FS-I1: row-data recorded by I1 considering also the temperature variation, as recorded by the thermometer T1, and (b),(c) the absolute daily residuals evaluated for both X and Y direction

Inclinometer G-FS-I2

Inclinometer I2 is installed at the South front of the Garisenda tower (at the height of 30.65 m). Figure 6-15a display the row-data by I2 and the temperature variation. It can be noticed that also the data recorded by I2 exhibits an opposite trend with respect to the temperature. The absolute daily residuals reveal for the x component a cumulative trend of -0.006° (meaning decrease in the inclination in the East direction) and for the y component a trend of -0.006° (meaning increase in the inclination in the South direction), see Figure 6-15 b,c.

(a)

(b)……………………………………………..(c)
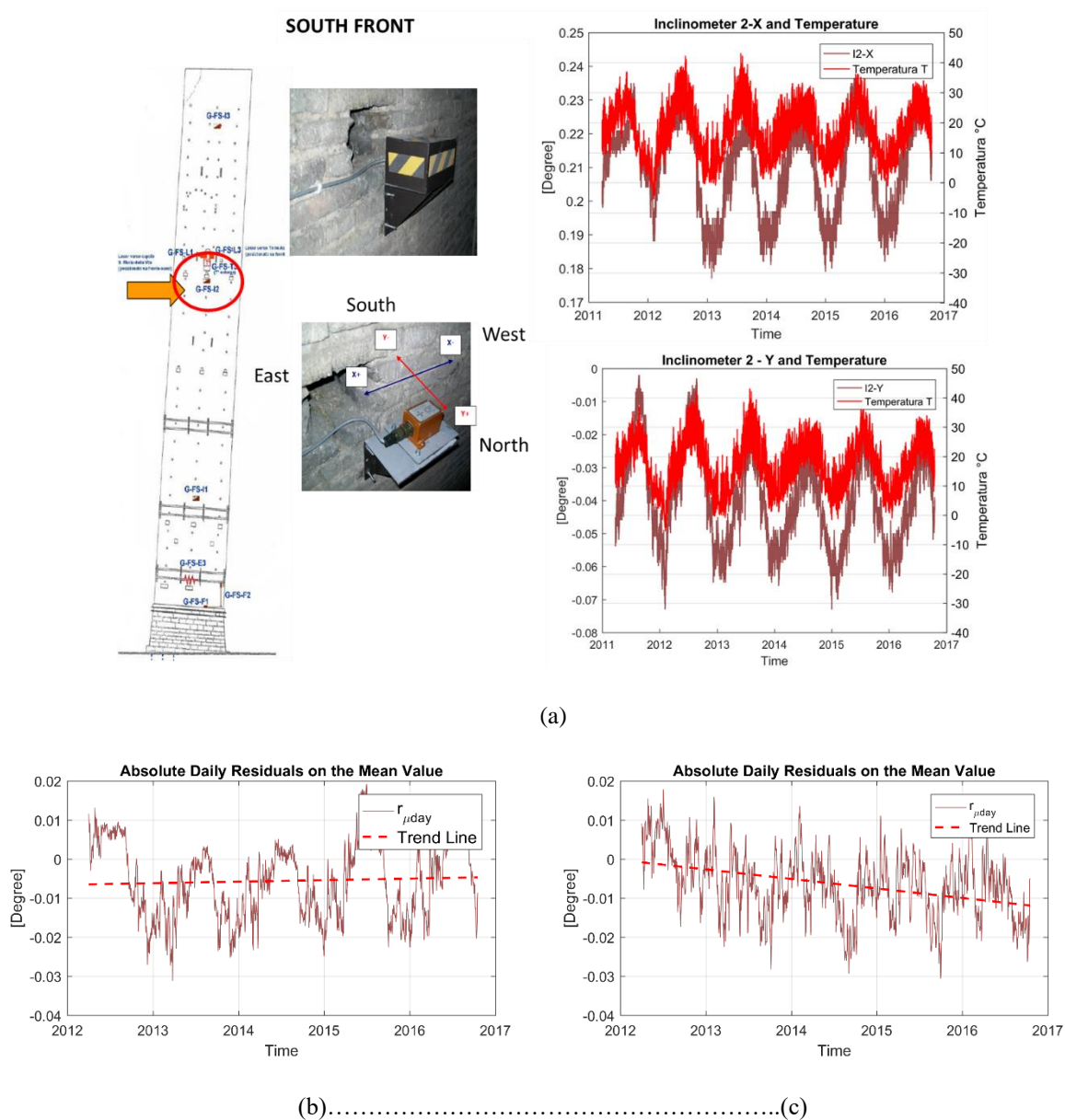
Figure 6-15: Inclinometer G-FS-I2: row-data recorded by I2 considering also the temperature variation, as recorded by the thermometer T1, and (b),(c) the absolute daily residuals evaluated for both X and Y direction

Inclinometer G-FS-I3

Inclinometer I3 is installed at the South front of the Garisenda tower (at the height of 43.30 m). Figure 6-16 a display the row-data by I3 and the temperature variation. The data recorded by I3 exhibits an opposite trend with respect to the temperature. The absolute daily residuals reveal for the x component a cumulative trend of +0.002° (meaning increase in the inclination in the East direction) and for the y component a trend of +0.014° (meaning increase in the inclination in the North direction), see Figure 6-16 b, c.

(a)

(b)……………………………………………..(c)
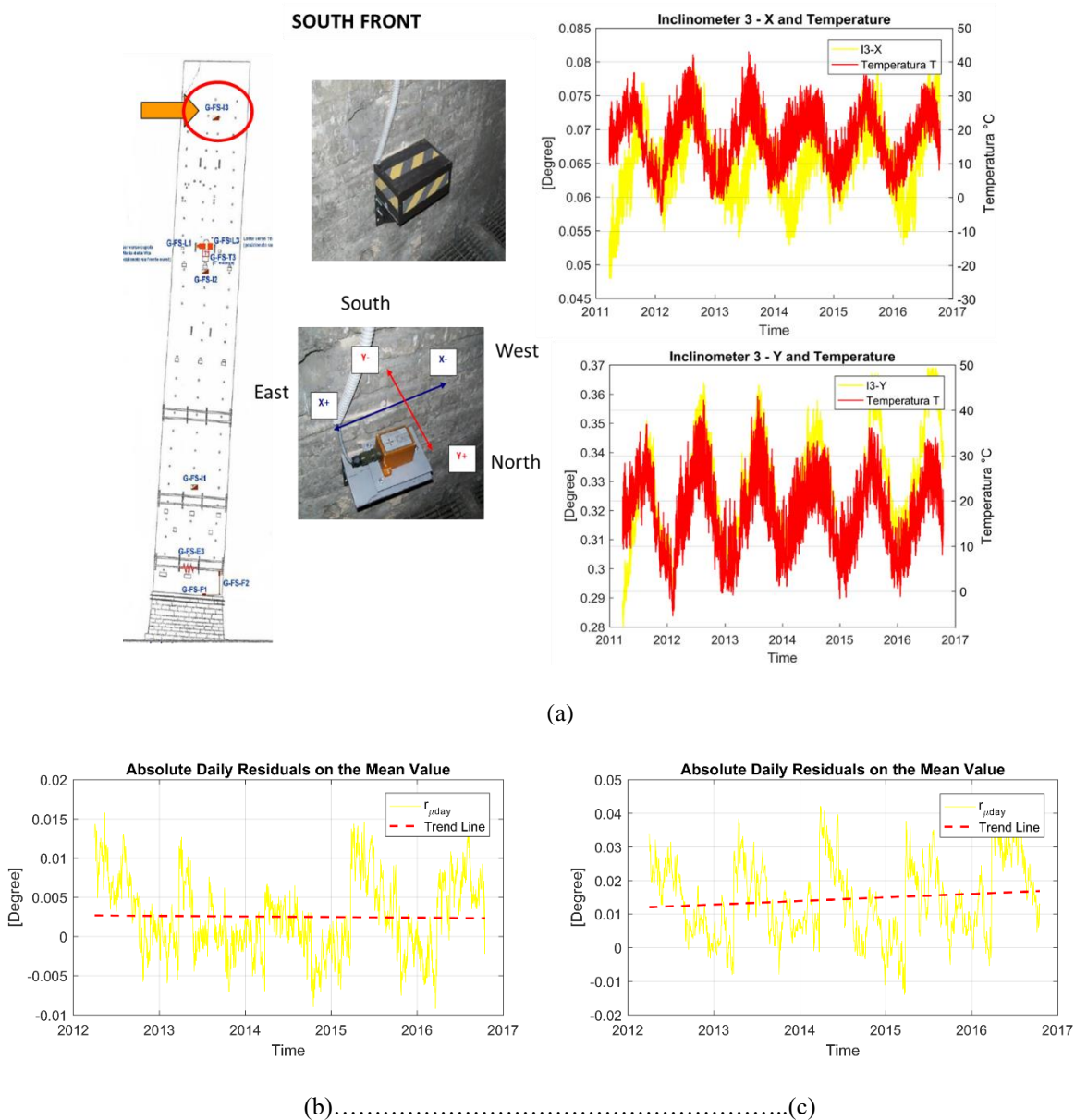
Figure 6-16: Inclinometer G-FS-I3: row-data recorded by I3 considering also the temperature variation, as recorded by the thermometer T1, and (b),(c) the absolute daily residuals evaluated for both X and Y direction

Inclinometer G-FE-I4

Inclinometer I4 is installed at the East front of the Garisenda tower (at the height of 13.20 m). Figure 6-17 a display the row-data by I4 and the temperature variation. The inclinometer I4 recorded an anomalous trend in the 2012 characterised by two drops probably due to accidental impacts. However, the data recorded are in phase with the temperature data. The absolute daily residuals reveal for the x component a cumulative trend of -0.002° (increase in the inclination in the West direction) and for the y component a trend of +0.003° (meaning increase in the inclination in the North direction), see Figure 6-17 b, c.

(a)

(b)……………………………………………………..(c)
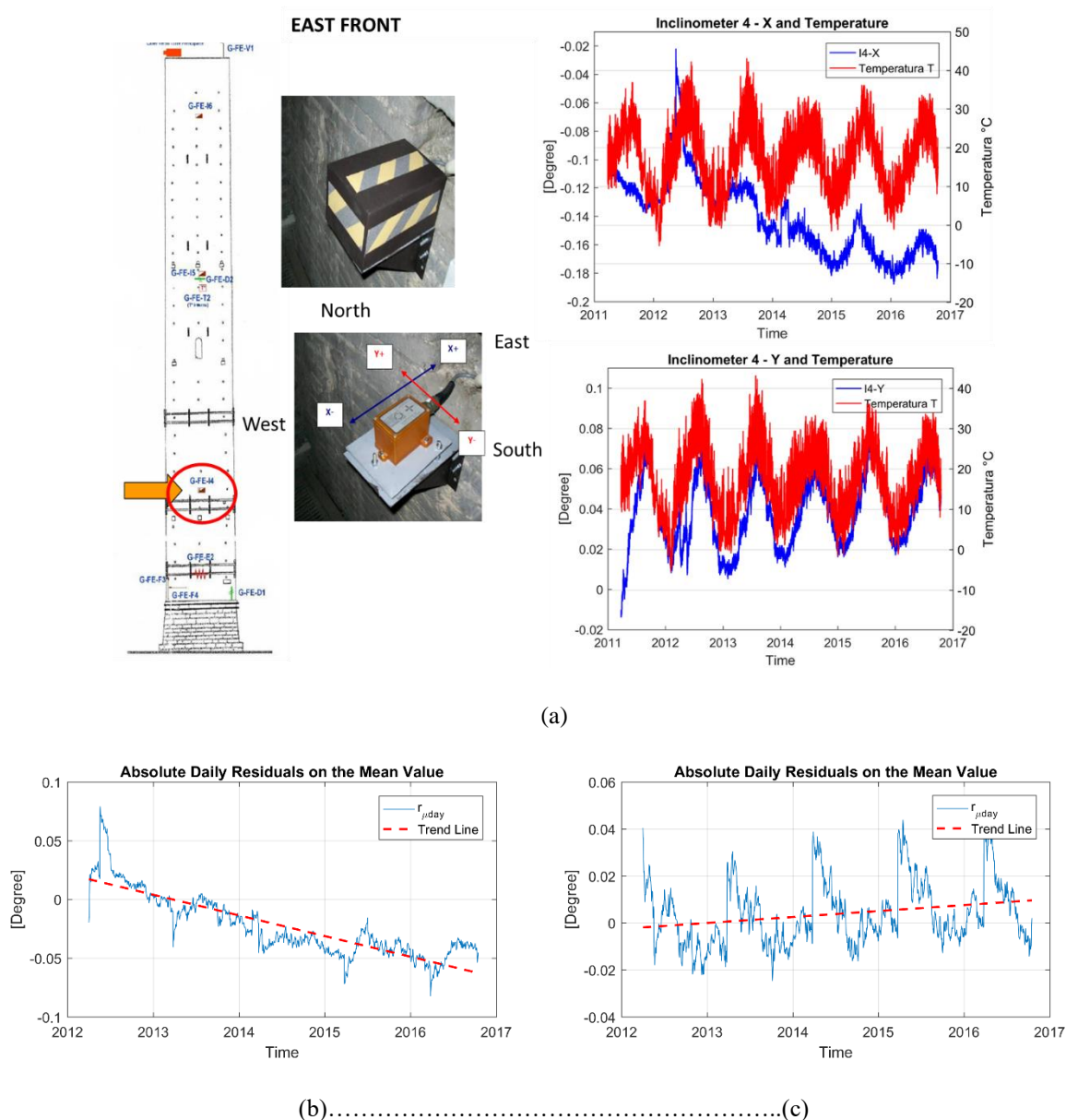
Figure 6-17: Inclinometer G-FE-I4: row-data recorded by I4 considering also the temperature variation, as recorded by the thermometer T1, and (b),(c) the absolute daily residuals evaluated for both X and Y direction

Inclinometer G-FE-I5

Inclinometer I5 is installed at the East front of the Garisenda tower (at the height of 30.65 m). Figure 6-18 a display the data recorded by I5 and the temperature variation. The data recorded are in phase with the temperature data. The absolute daily residuals reveal for the x component a cumulative trend of -0.001° (increase in the inclination in the West direction) and for the y component a trend of +0.006° (meaning increase in the inclination in the North direction), Figure 6-18 see b, c.

(a)

(b)………………………………………………..(c)
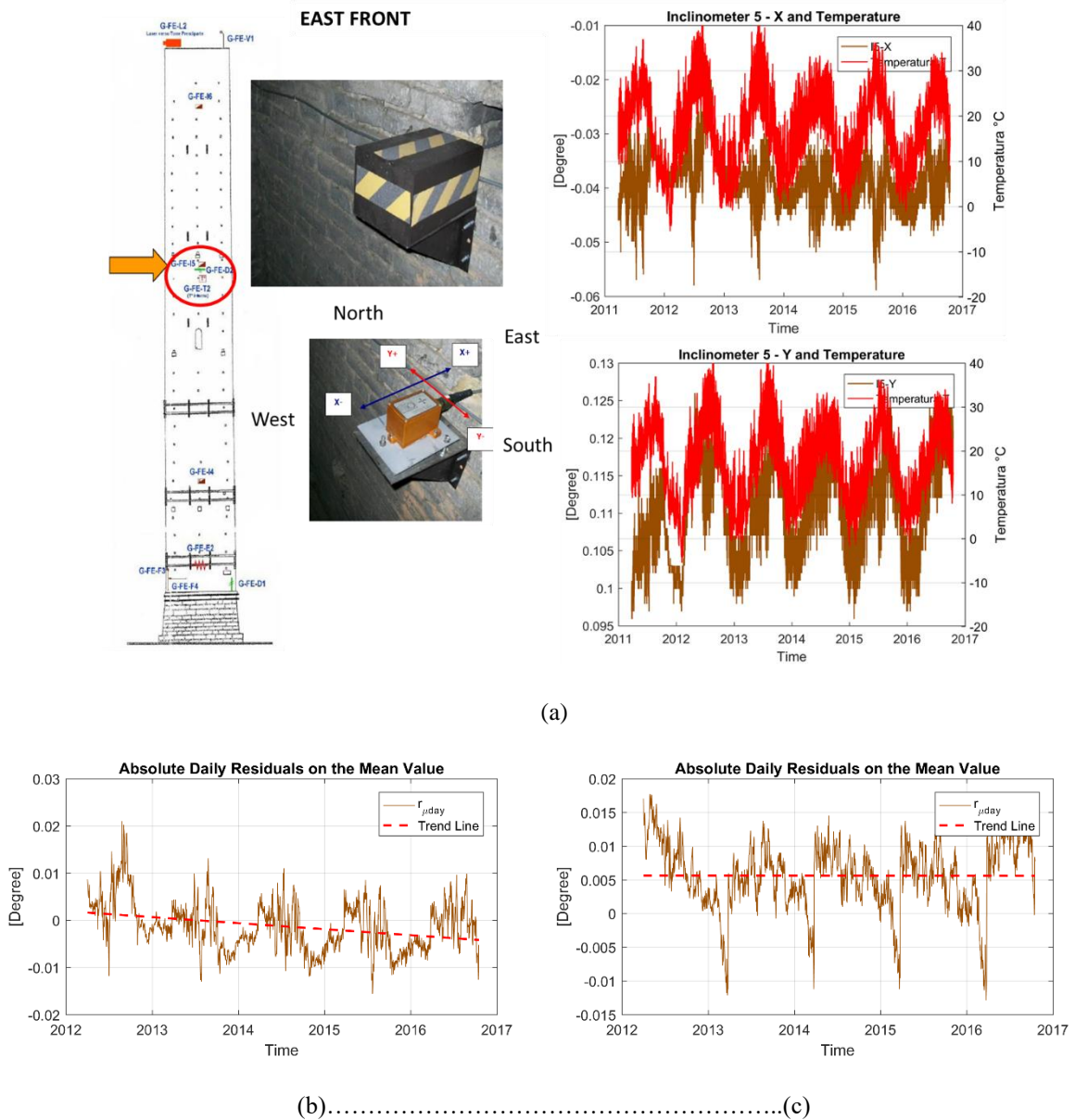
Figure 6-18: Inclinometer G-FE-I5: row-data recorded by I5 considering also the temperature variation, as recorded by the thermometer T1, and (b),(c) the absolute daily residuals evaluated for both X and Y direction

Inclinometer G-FE-I6

Inclinometer I6 is installed at the East front of the Garisenda tower (at the height of 43.30 m). Figure 6-19 a display the data recorded by I6 and the temperature variation. The data recorded are in phase with the temperature data. The absolute daily residuals reveal for the x component a cumulative trend of +0.001° (increase in the inclination in the East direction) and for the y component a trend of -0.012° (meaning decrease in the inclination in the North direction), Figure 6-19 see b, c.

(a)

(b)………………………………………………..(c)
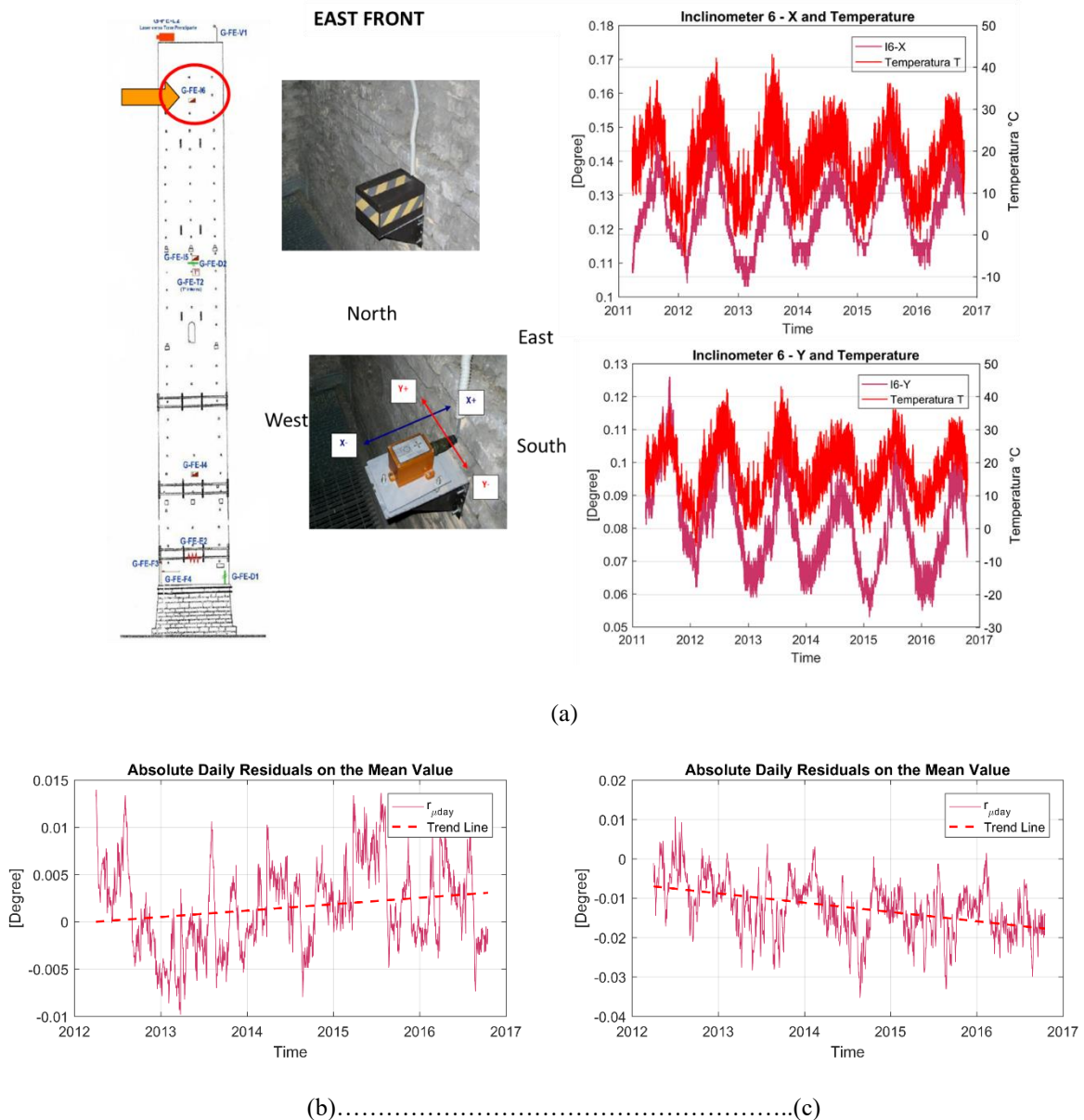
Figure 6-19: Inclinometer G-FE-I6: row-data recorded by I6 considering also the temperature variation, as recorded by the thermometer T1, and (b),(c) the absolute daily residuals evaluated for both X and Y direction

The mean values over the entire observation period of the reference quantities are collected in Table 6-5 for all the inclinometers.

Table 6-5- Men values of the reface quantities over the six years of monitoring for the extensometers

Sensor	Year	$\delta_{day,j}$ [°]	$\text{rp}_{\mu day}$ [°]	$\text{r}_{\mu day}$ [°]	M_{year} [°]	Σ_{year} [°]	Rp_{Myear} [°]	R_{Myear} [°]
A-FO-I1-X	mean	0.007	-0.001	-0.004	-0.016	0.027	-0.001	-0.005
A-FO-I1-Y	mean	0.008	0.003	0.012	0.126	0.066	0.002	0.008
A-FO-I2-X	mean	0.008	-0.001	-0.006	0.209	0.050	-0.001	-0.009
A-FO-I2-Y	mean	0.008	-0.002	-0.006	0.037	0.065	0.001	-0.001
A-FO-I3-X	mean	0.006	0.001	0.002	0.065	0.029	0.001	0.002
A-FS-I3-Y	mean	0.006	0.004	0.014	0.328	0.069	0.004	0.011
A-FS-I4-X	mean	0.007	-0.009	-0.022	-0.141	0.063	-0.010	-0.025
A-FS-I4-Y	mean	0.007	0.001	0.003	0.037	0.065	0.001	-0.001
A-FO-I5-X	mean	0.007	0.000	-0.001	-0.039	0.033	-0.0005	-0.002
A-FO-I5-Y	mean	0.008	0.002	0.006	0.111	0.030	0.001	0.005
A-FO-I6-X	mean	0.006	0.000	0.001	0.125	0.042	0.000	-0.001
A-FO-I6-Y	mean	0.008	-0.003	-0.012	0.081	0.060	-0.004	-0.016

6.5   Data processing

6.5.1   The influence of the external factors on the structural response

The influence of the external factors on the structural response has been investigated using the Equations 5.3-5.6. The considered external factors are the temperatures recorded by thermometers T1 and T2, the wind velocity and direction. For each structural response, the relative importance of each external factor is presented in Figure 6-20. Here, external effects are ordered according to their relative importance averaged over the structural responses studied. On average, most important factors are the two recorded temperatures G-FE-T2 and G-FS-T1. Wind speed and wind direction have a limited effect on the structural response.
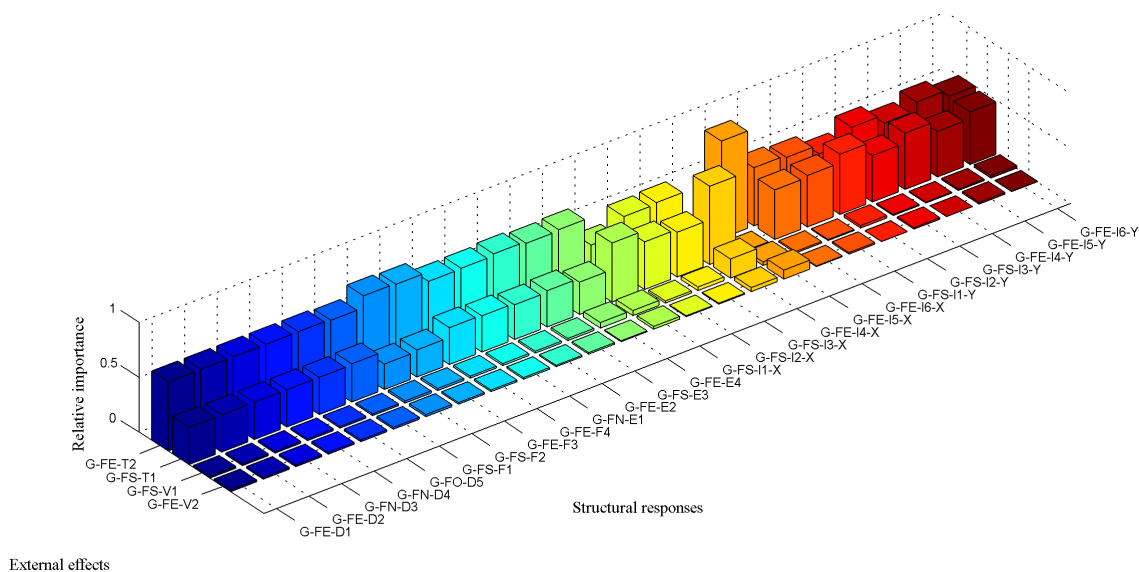
Figure 6-20: Relative importance of the external effects on the structural response of the Garisenda Tower

6.5.2 The signal frequency analyses

Data have also been proceeded in the frequency domain in order to identify the periodical and the non-periodical components (called residue) of the signal. The time history of the residua as obtained from the frequency analysis (FFT and IFFT) is compared to the daily residua obtained from the evaluation of the reference quantities. The frequency analysis has been applied to data obtained by the instruments which have not presented malfunction, interruptions and / or many drops. The main results obtained are here presented and the details of the frequency analyses for all the data investigated are provided in Appendix B.2

Long base deformeters

The long base deformeters present the predominant component of period close to T=280 days. The amplitude with period T=365 days appears less significant probably due to the thermal inertia of the masonry walls. Also in this case, the amplitude with period T=1 day does not appear significant. This fact, could be related to the characteristics of the sensors that often reach the full scale during the daily recording. Figure 6-21 a display the main components computed for the long base deformeter F2. The periodicity of the signal has been identified considering the main periodic components detected by the Fourier transform (T=280 days and T=365days), see Figure 6-21 b). The trend and variation of the residue evaluated from the FFT analyses is in good agreements with the values obtained from the time-domain analysis (Figure 6-21 c).

(a)

(b)……………………………………………..(c)
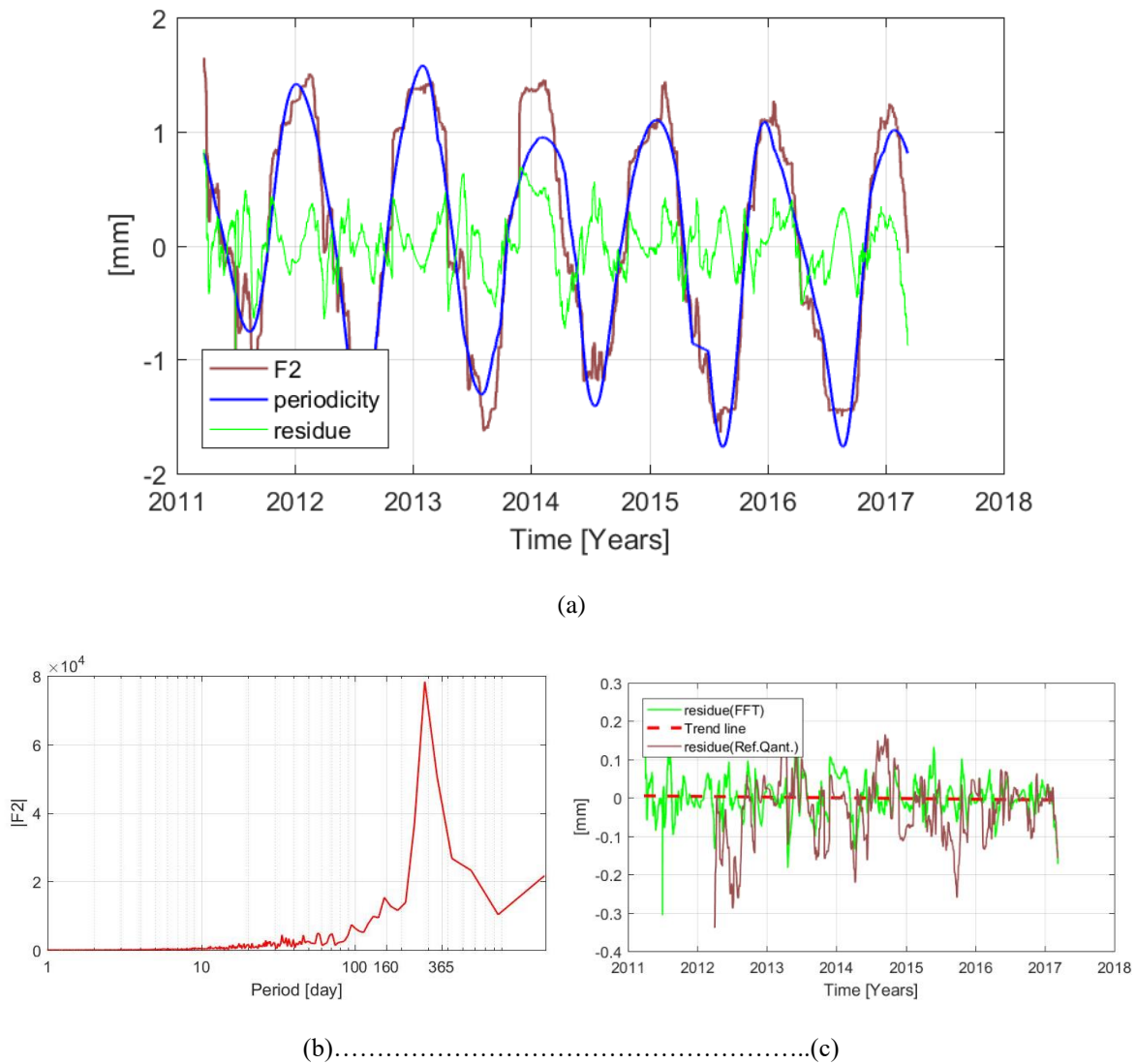
Figure 6-21(a) Recorded signal by the long base deformeter F2 and its main components (the periodical component and the residual), (b) The Fourier Transform and (c) the residue as obtained from the FFT and from the mathematical considerations (reference quantities)

Deformeters

The deformeters present the predominant component of period T=365 days. The amplitude with period T=1 day does not appear significant respect the predominant one but it is clearly recognizable. Figure 6-22 a display the main components computed for deformeter D3. The periodicity of the signal has been identified considering the main periodic components detected by the Fourier transform (T=365 days), see Figure 6-22 b). The trend and variation of the residue evaluated from the FFT analyses is in good agreements with the values obtained from the time-domain analysis (Figure 6-22 c).
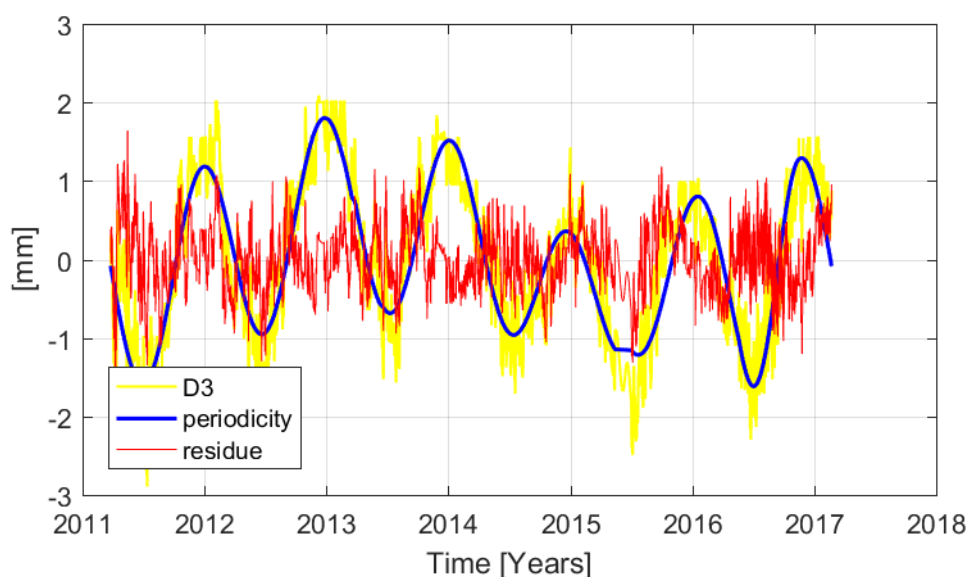
(a)
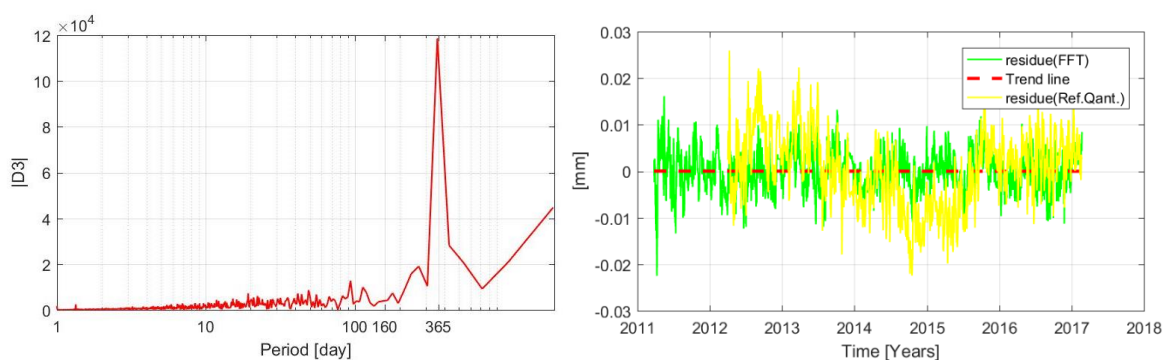
(b)……………………………………………..(c)

Figure 6-22: (a) Recorded signal by deformeter D3 and its main components (the periodical component and the residual), (b) The Fourier Transform and (c) the residue as obtained from the FFT and from the mathematical considerations (reference quantities)

Extensometers

The extensometers present the predominant component of period close to T=270-300 days. The amplitude with period T=1day does not appear significant. Figure 6-23 a display the main components evaluated for the extensometer E2. The periodicity of the signal has been identified considering the main periodic components detected by the Fourier transform (T=270 days and T=365 days), see Figure 6-23 b. The values of the residual seems to oscillate with an apparent random periodicity and its trend and variation is in good agreements with the values obtained from the time-domain analysis (Figure 6-23 c).

(a)

(b)……………………………………………..(c)
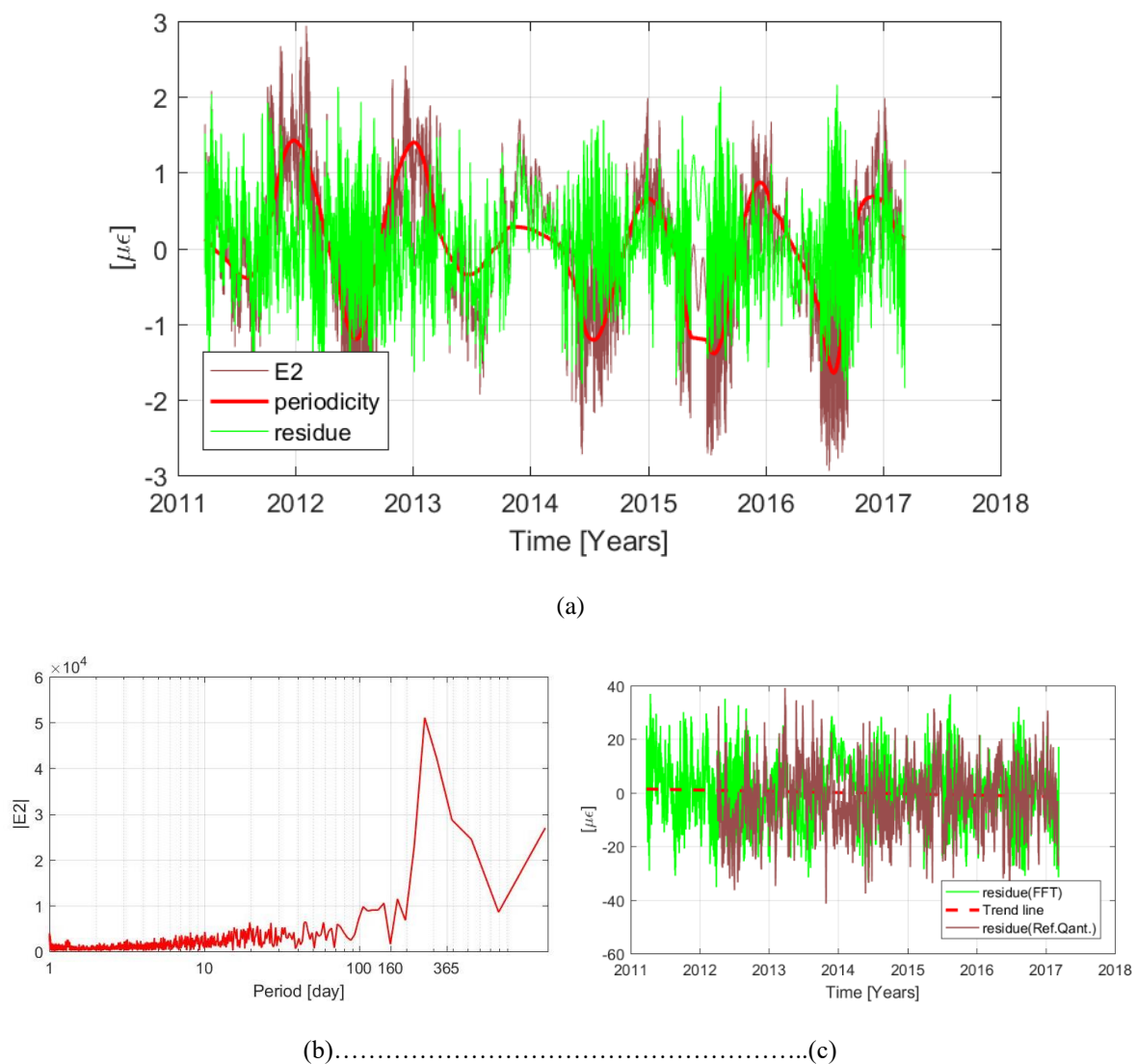
Figure 6-23: (a) Recorded signal by the extensometer E1 and its main components (the periodical component and the residual), (b) The Fourier Transform and (c) the residue as obtained from the FFT and from the mathematical considerations (reference quantities)

Inclinometers

The inclinometers present the predominant component of period T=365 days (Figure 6-24b). The amplitude with period T=1days does not appear significant. Figure 6-24 a display the main components computed for the inclinometer I2 in the x-direction. The trend and variation of the residue is in good agreements with the values obtained from the time-domain analysis (Figure 6-24 c).
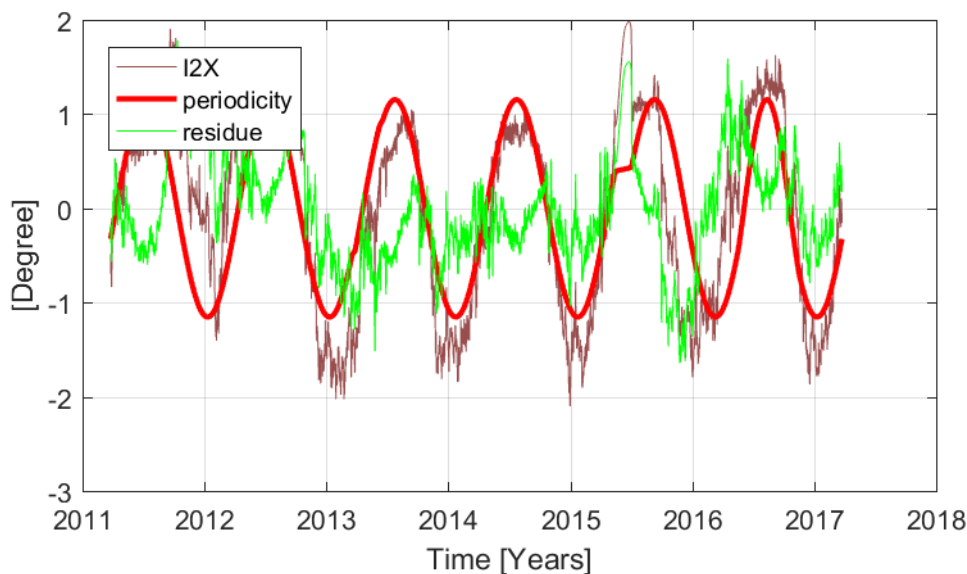
(a)
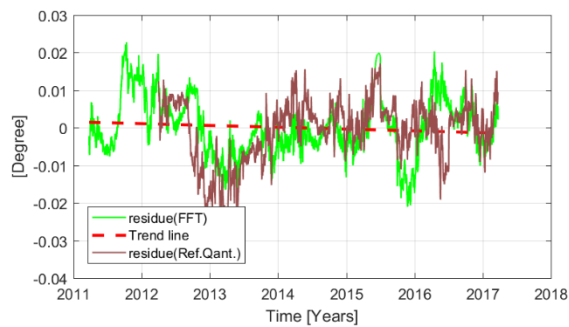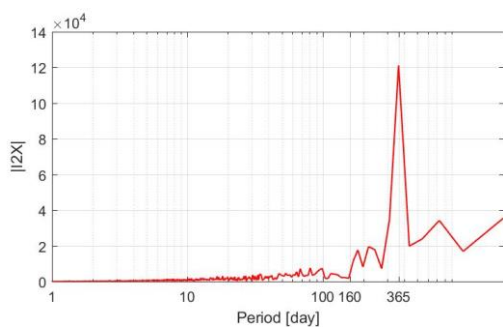
(b)……………………………………………..(c)

Figure 6-24: Recorded signal by the inclinometer I2 and its main components (the periodical component and the residual), b) The Fourier Transform and c) the residue as obtained from the FFT and from the mathematical considerations (reference quantities)

6.6   Conclusions

The interpretation of the data recorded (from 2011 to 2016) by the static monitoring system installed on the Garisenda tower has been performed making use of the reference quantities presented in § 3.3.

As we expected the data recorded by the static monitoring system of the Garisenda tower has characteristics similar to those of the data recorded on Asinelli tower. More specifically, the following conclusions are drawn:

- the phenomena under observation appear, in general, in a stable condition (the trend of the data over the years, even in their seasonal/annual variability, do not show specific evolutionary trend).

- The long base deformeters, which measure the horizontal and vertical masonry deformation, display a high inverse correlation with the temperature. Moreover, the values of the daily amplitudes recorded during the cold season are one order of magnitude less than those recorded during the hot season. The order of magnitude of the cumulative residues calculated on the recorded data from these devices varies between -0.01 and 0.01 mm.

- The deformeters, which monitor the movements of the main cracks, display a high inverse correlation with the temperature. The sensors D2 and D5 recorded an evolutionary trend, meaning that the cracks tend to open during the six years of monitoring. However, the cumulative residua are lower of 0.1 mm over the entire observation period.

- The trend recorded by the extensometers is similar to that recorded by the long base deformeters. Also in this case, the recorded data are out-of-phase with respect to temperature data and the values of the daily amplitudes recorded during the cold season are one order of magnitude less than those recorded during the hot season. The analysis of the signals after removing these irregularities shows that the steel tie on Garisenda tower recorded increases / decreases on the stress state which remain lower than 30 $\mu\varepsilon$.

- The trend recorded by the inclinometers, which monitor the inclination of the walls of the Garisenda tower, presents, generally, a high direct correlation with the temperature data. The increase/decrease of the inclination, during the six years monitoring, remain always lower than 1 degree.

The study of the influence of the external factors on the structural response of the Garisenda tower reveals that the temperature is the factor, which mostly influences the recorded data.

In addition, the main periodicity of the recorded data have been investigated through the signal frequency analyses. The long base deformeter and the extensometer reveal the predominant component with period of T= 280-300 days (i.e. lower than the expected one with period of T=365 days). This fact could be related to the thermal inertia of the masonry walls. The periodic component of the data recorded by the inclinometers and the deformeters is essentially given by the harmonic with period T1=365 days.

The trend and variation of the non-periodic components (residue) obtained from the FFT analyses are usually in good agreements with the values obtained from the time-domain analysis (reference quantities §3.3).

Chapter 7

7   A case of study of the Cathedral of Modena

7.1   Introduction

In the 2003, a static SHM system has been installed on the Cathedral of Modena, whose construction began in 1099 and finished in 1184.

In this chapter, the monitoring system installed on the Cathedral will be described.

The large amount of data recorded by the monitoring system has been analyzed using the approach proposed in § 3.3 in order to evaluate if the phenomena under observation are in a stable condition or not. The signal frequency analyses on the recorded data have been also carried out and the results obtained in terms of residuals (i.e. signal not affected by the seasonal effects which should be representative of the state of the building) compared with the residue obtained from the time-domain analyses proposed. The main results obtained from the analyses are presented in this chapter.

7.2   The Cathedral of Modena

The history and the geometry of the Cathedral of Modena will be discussed more thoroughly in § 10. A three- dimensional view of the Cathedral of Modena and the adjacent Ghirlandina Tower is display in Figure 7-1.

Figure 7-1: A three-dimensional (3D) view of the Modena Cathedral (Google Earth)

7.3 Types and location of instruments

The monitoring system allows monitoring the main cracks across the walls and vaults, the relative displacements between the cathedral and the Ghirlandina tower, the inclination of the external longitudinal walls, and the temperature. Most of the instruments were installed in 2003, while others (such as the deformeters and inclinometers) were installed at the end of 2010. Data are acquired at time intervals of 30 minutes. The following symbols have been used to indicate the type of instrument:

D=deformeter, **MGB**=biaxial joint meter, **MGT**= triaxial joint meter, **FP**=inclinometer, **T**= thermometer.

The different instruments installed on the Cathedral are displayed in Figure 7-2.
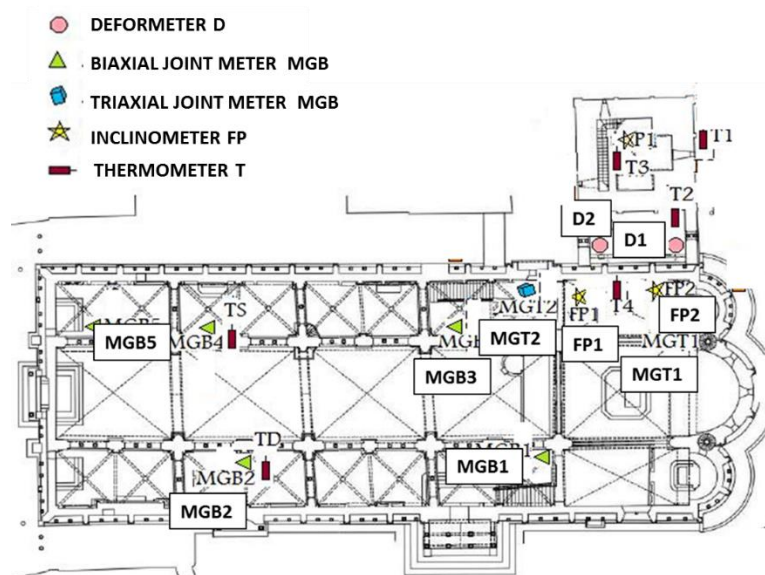
Figure 7-2: Location of the sensors.

The instruments installed on the Cathedral are briefly described below.

Invar Deformeter

The deformeters were placed on the buttresses between the Cathedral and the Ghirlandina Tower (Figure 7-3). They are designed to perform the deflection measurements of a structure of a substantial amount (in this case have an overall length of 5 meters). They consist of Invar rods having a low coefficient of thermal expansion. On the wall of the Ghirlandina tower was put the anchor support, while on the Cathedral wall is anchored to a non-contact sensor of the inductive type with 8 mm theoretical measurement range with a resolution of 0.01 mm. They are fed to a continuous voltage of 24 Vdc and the analog output signal is between 4 and 20 mA proportional to the distance between the transducer and the target. Conventionally the positive values on the graphs, which will be explained later, correspond to an estrangement between the Tower and the Cathedral, while negative values correspond to a rapprochement of the two. Table 7-1 collects some technical specification of these Invar Deformeters.
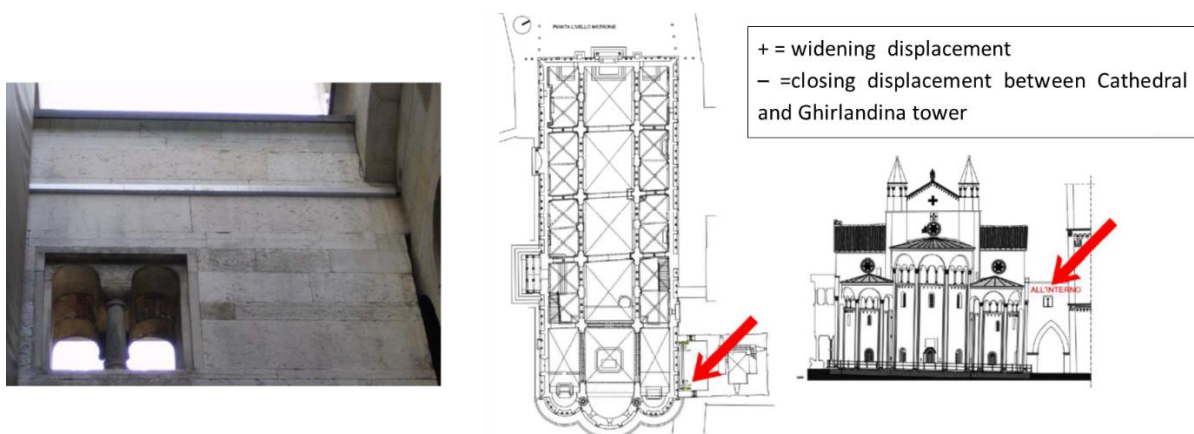
Figure 7-3: Deformeter installed on the buttress of the Cathedral (D1)

Table 7-1- Technical specification of the Invar Deformeters

TECHNICAL SPECIFICATIONS	
Full scale	8 mm
Resolution	0,4 μm
Accuracy	< 0.01mm
Dimension	5 m
Temperature Range	(-10/+80)°C

Biaxial joint meter- Triaxial joint meter

The variation in the opening of cracks in the bearing elements, due in most cases to the interaction with the ground and / or to an intrinsic degradation of materials is carried out by means of measuring instruments such as joint meters or deformeters. The joint meters are bound rigidly to the wall using anchors at the turn of the crack to be monitored. They may be biaxial, in this case the measure movements detected are in a plane (for example, a wall surface) (Figure 7-4) or triaxial if are able to detect also the displacements orthogonal to the plane (Figure 7-5). Seven main cracks of the Cathedral have been monitored through these sensors. In particular, in 2003, four biaxial joint meters were installed in the central nave and a triaxial joint meter were installed in the wall close to the two buttresses that link the Cathedral and the Tower. In December 2010, other two joint meters were installed. Table 7-2 collects some technical specification of the biaxial and triaxial joint meters.
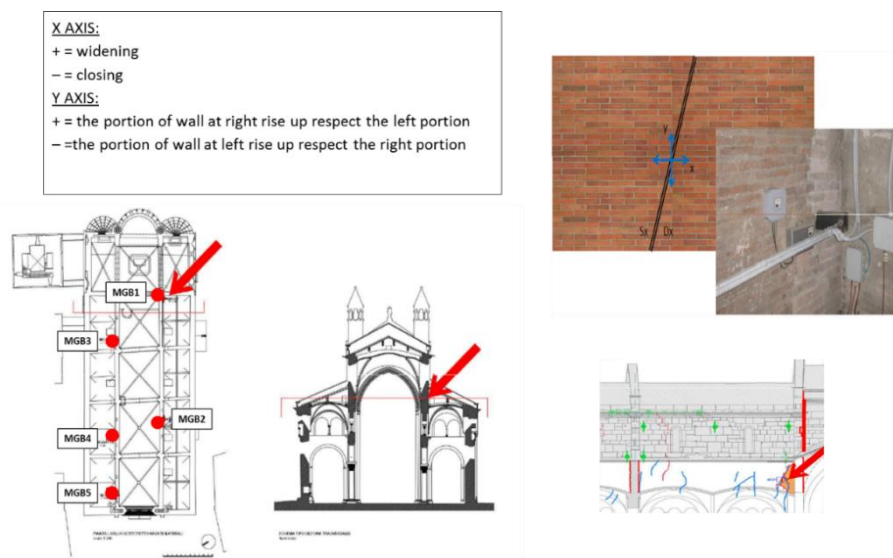
Figure 7-4: Biaxial joint meter installed in the central nave of the Cathedral (MGB1)
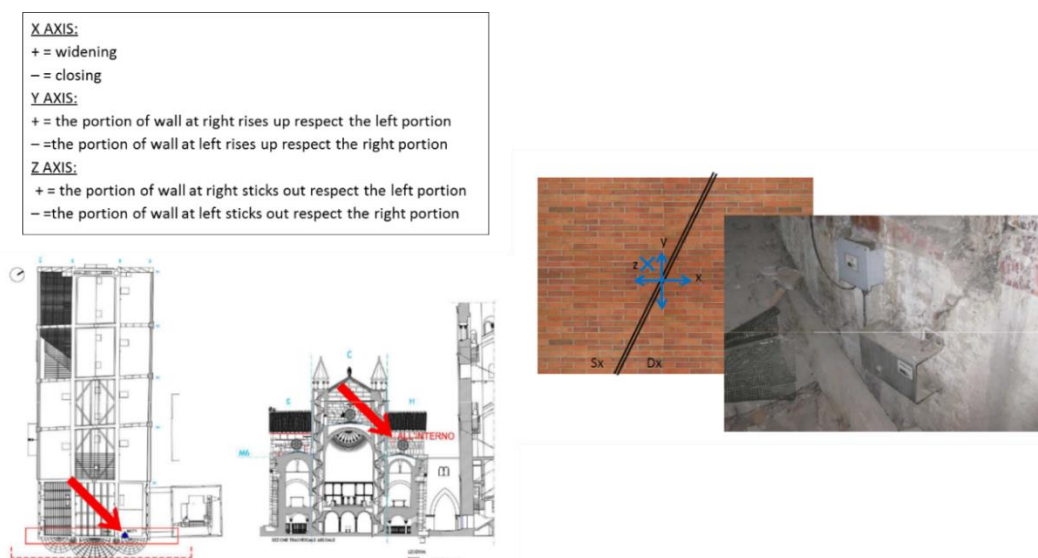
Figure 7-5: Triaxial joint meter installed in the longitudinal wall of the Cathedral (MGT1)

Table 7-2- Technical specification of the biaxial-triaxial joint meters

TECHNICAL SPECIFICATIONS	
Full scale	8 mm
Resolution	0.01 mm
Accuracy	0.01 mm
Dimension	300x 200x150 mm

Inclinometer

The inclinometers (or pendulums) installed on the cathedral are designed for the control of the stability of the buildings, and their operation is based on the principle of a plumb line (Figure 7-6). It consists of: an upper berth, to the plumb bob (consists of Invar alloy to contain the thermal expansions), and the measuring instrument (that allows to perform the automatic measurement of the plumb line portion). This data allow analysing the slope changes of the Cathedral, both periodic (due to temperature variations) and permanent ones due to real structural behaviour. Table 7-3 collects some technical specification of the inclinometers.
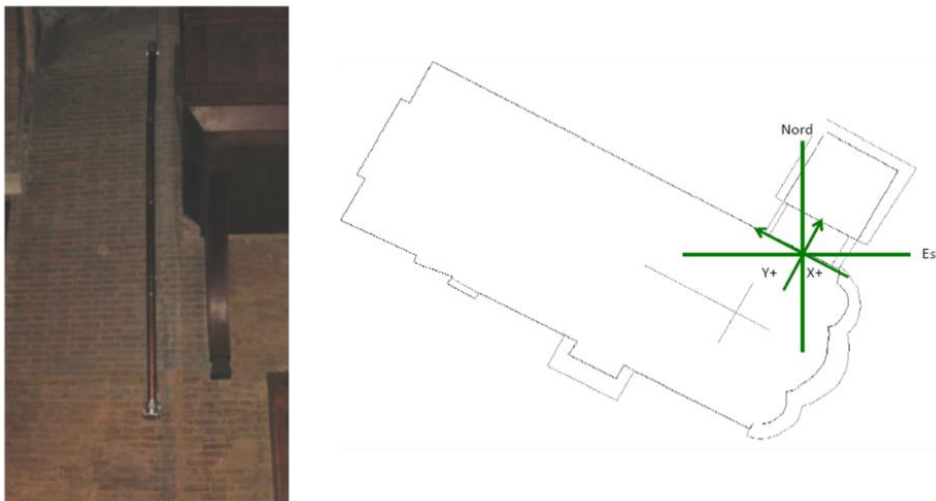
Figure 7-6: Inclinometer installed on the longitudinal wall of the cathedral (close to the buttress) FP1 and the conventional signs used.

Table 7-3- Technical specification of the inclinometers

TECHNICAL SPECIFICATIONS	
Full scale	8 mm
Resolution	0.4 μm
Accuracy	0.01 mm
Dimension	ϕ 80 mm, H=4 m

7.4 Reference quantities

The reference quantities defined in § 3.3 have been identified for all the data recorded by sensor of the monitoring system installed on the Cathedral of Modena. Appendix C.1 provides the systematic identification of these reference quantities. In the next section, the salient results, obtained from the interpretation of the static monitoring data through the proposed procedure, are illustrated.

7.4.1 Invar deformeter

The deformeters Di and D2, placed on the buttresses between the Cathedral and the Ghirlandina Tower in order to monitor the movements between the two structures, recorded significant drops during the seismic event that hit the Emilia Romagna in May 2012. In particular, the drops corresponding to the two days where the tremors of greatest intensity were recorded (20th and 29th May 2012). As mentioned above, positive values on the graph correspond to an estrangement between the Tower and the Cathedral, while negative values correspond to a rapprochement of the two.

Deformeters D1

From 1th January 2011 until 20th May 2012, D1 records a slight estrangement between the Cathedral and the tower. After the 2012 earthquake, the trend recorded by this device changes considerably. On days 20th and 29th May it has recorded two drops of $\Delta 20may = 0.53mm$ and $\Delta 29may = 0.3$ mm, respectively, that indicate an approaching of the two structures (Figure 7-7). After the seismic event, the recorded data are negative, indicating a progressive approach between Ghirlandina and Cathedral. This sensor is characterized by several missing data; therefore, the systematic identification of the reference quantities does not lead to significant results. However, it is interesting to note that the mean value of the daily amplitude, not considering the data recorded in the 2012, is around of 0.03 mm. The daily amplitudes recorded on 20th and 29th May are, thus, around 20 times more than the mean value of the daily amplitude recorded in the other years.
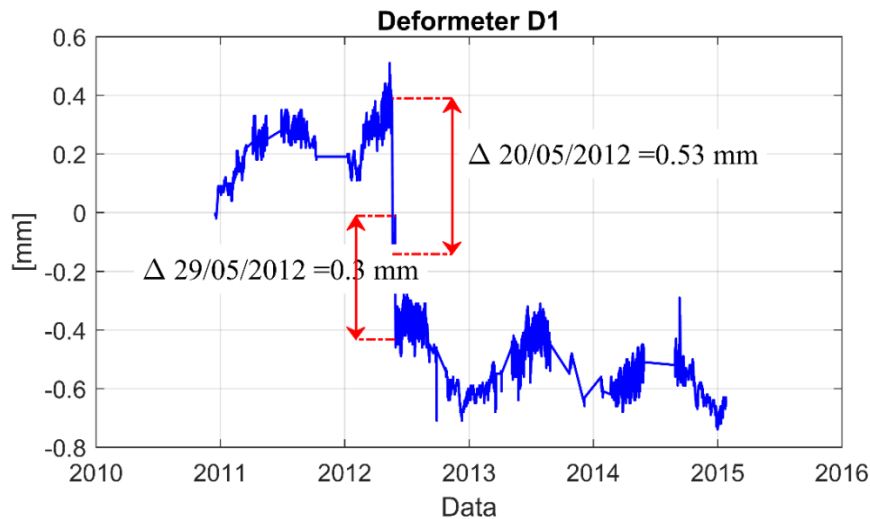
Figure 7-7: Data recorded by the deformeter D1 installed on the buttresses between the Cathedral and the Ghirlandina Tower

Deformeters D2

The deformeter D2 does not record specific anomalies during the main shocks of the 2012 Emilia earthquake. However, a drop was recorded in 27[th]August 2012 (August $\Delta 27 = 0.4$ mm). On that date it is detected a earthquake of much lower intensity compared to those of May during which the device did

not show significant changes. It excludes, therefore, that the cause of this drop is due to slight earthquake but it's probably due to interference. Before and after the drop, the device has recorded a cyclical trend. The negative values on the graph correspond to a rapprochement between the cathedral and the tower (Figure 7-8).
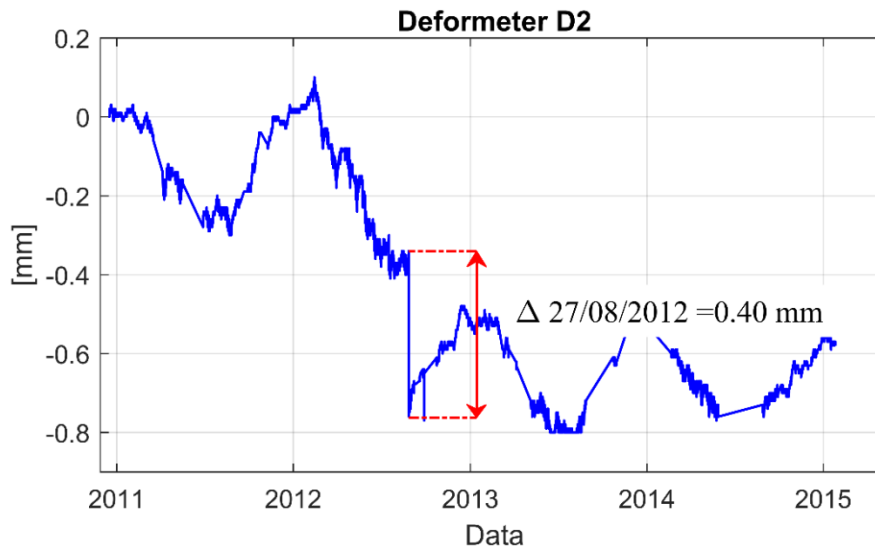
Figure 7-8: Data recorded by the deformeter D2 installed on the buttresses between the Cathedral and the Ghirlandina Tower

7.4.2 Joint meter

The biaxial joint meters MGB1, MGB2, MGB3, MGB4 and the triaxial joint meter MGT1 were installed in October 2003 while MGB5 and MGT2 was added later in 2010. It is noted that MGT2 is characterized by many missing data. For this reason its data are not reliable in order to perform evaluations on the structural health and their will not considered in the following analyses.

Biaxial joint meter MGB1

The sensor MGB1 monitors the movements of a crack located in the South aisle, apse side in correspondence with the cracks area which transversely crosses the fourth nave (see §10.3.4). The temperature effect is significant and the recorded data evidence a high direct correlation with respect to the temperature data (Figure 7-9 a). When the temperature increases, in fact, the wall tends to expand with consequent closure of the crack and, vice versa, with the decrease of the temperature, the masonry walls tends to compresses with a widening of the crack. The absolute daily residuals reveal that the crack under observation has opened of 0.02 mm and the portion of wall at right of the crack rise up of 0.03 mm respect the left portion, during all years of monitoring (Figure 7-9 b, c).
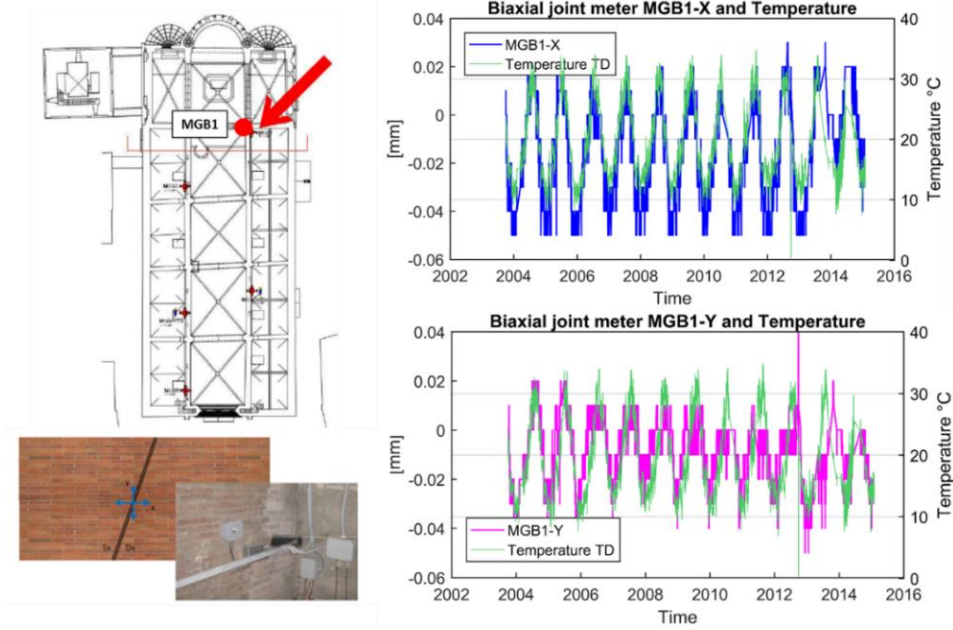
(a)
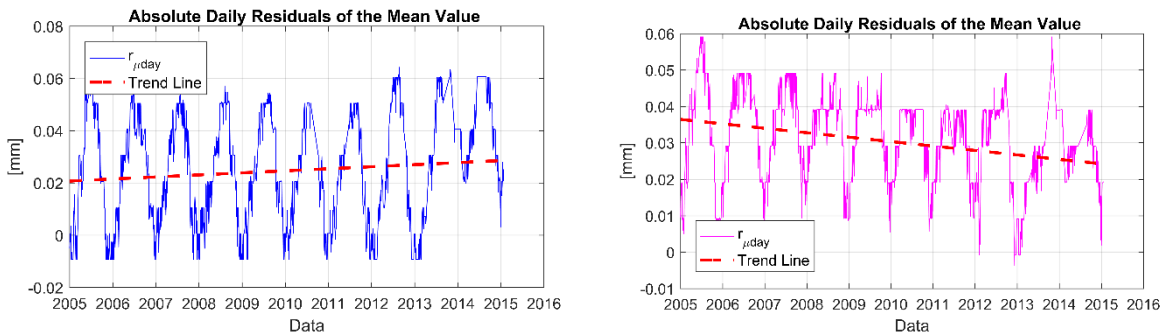
(b)………………………………………………..(c)

Figure 7-9: Biaxial joint meter MGB1: row-data recorded by MGB1 considering also the temperature variation, as recorded by the thermometer TD, and (b),(c) the absolute daily residuals evaluated for both X and Y direction

Biaxial joint meter MGB2

The sensor MGB2 monitors the movements of a crack located in the South aisle in correspondence with the cracks area, which transversely crosses the second nave (see §10.3.4). The data recorded are in phase with respect to temperature data (Figure 7-10 a). MGB2 records a cyclical trend that is repeated for all the years and, as already seen for MGB1, probably due to the correlation with the thermal variations. The trend of the daily amplitudes is, in fact, regular. Unlike what was seen for the previous device, MGB2 shows a decreasing trend over the years for both the X component that Y. This indicates that the lesion tends progressively to open up and the portion of wall at left of the crack rises up compared to the wall at the right. However, the absolute daily residuals reveal that the movements are small: a cumulative trend of -0.04 mm in both the directions is recorded (Figure 7-10 b, c).
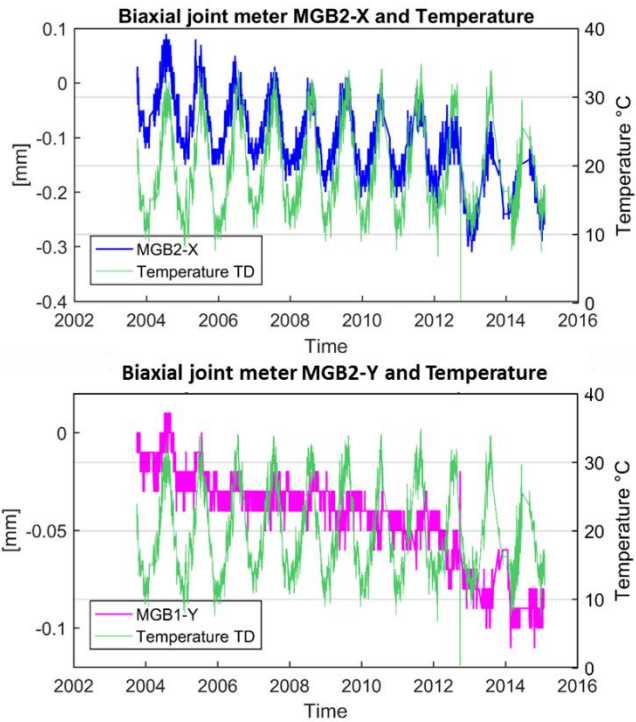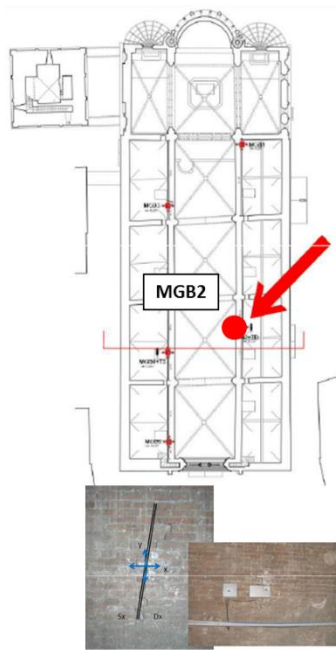
(a)
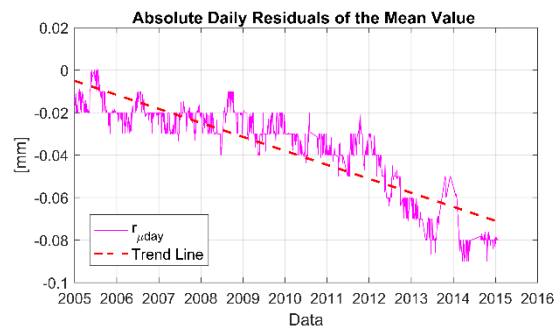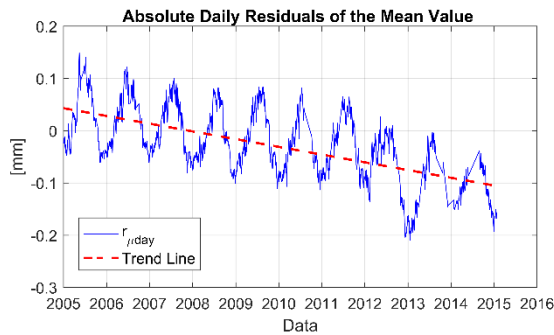
(b)……………………………………………………..(c)

Figure 7-10: Biaxial joint meter MGB2: row-data recorded by MGB2 considering also the temperature variation, as recorded by the thermometer TS, and (b),(c) the absolute daily residuals evaluated for both X and Y direction

Biaxial joint meter MGB3

The sensor MGB3 monitors the movements of a crack located in the North aisle, apse side in correspondence with the cracks area, which transversely crosses the second nave (see §10.3.4). The recorded data for the x component evidence a high direct correlation with respect to the temperature data. The data recorded for the y component appears to be out of phase with the temperature data (Figure 7-11a). The x component recorded a decreasing trend throughout the observation period, and then a gradual opening of the crack (with a cumulative trend of -0.03 mm), (Figure 7-11b). The y component, instead, recorded an increasing trend that indicates that the portion of the wall at the left of the crack rise up with respect to that of the right. Then until 2014, a decreasing trend has been recorded. The absolute daily residuals reveal for the y component a cumulative trend of +0.05mm (Figure 7-11c)

(a)

(b)…………………………………………………..(c)
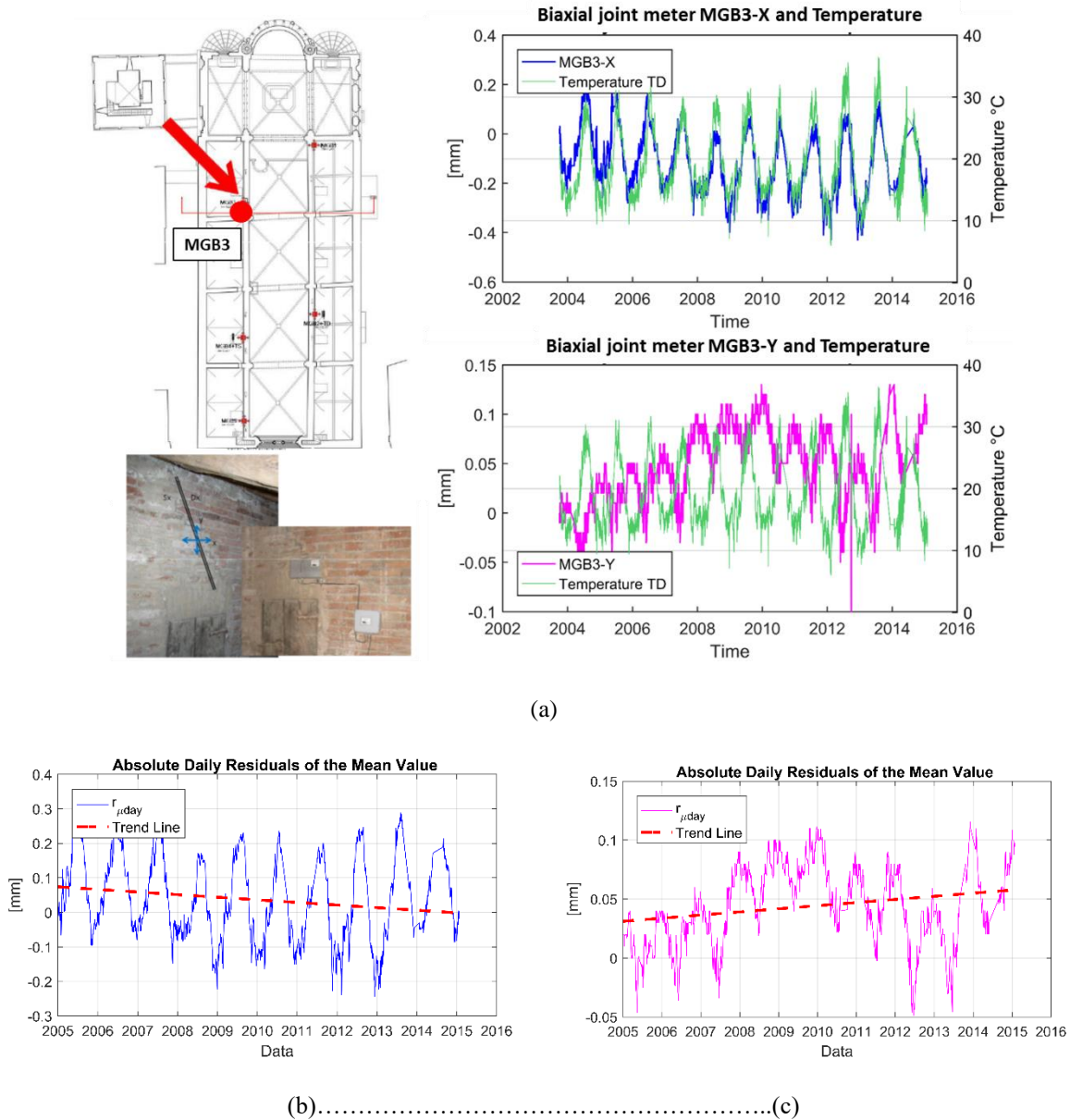
Figure 7-11: Biaxial joint meter MGB3: row-data recorded by MGB3 considering also the temperature variation, as recorded by the thermometer TS, and (b),(c) the absolute daily residuals evaluated for both X and Y direction

Biaxial joint meter MGB4

The sensor MGB4 monitors the movements of a crack located in the North aisle. The recorded data are in phase with respect to the temperature data recorded by the thermometer TS (Figure 7-12 a). The x component shows a decreasing trend, which indicates a slight opening of the crack. The absolute daily residuals reveal for the x component a cumulative trend of -0.1 mm (Figure 7-12 b). Even the y component registers a decreasing trend (the portion of wall at left of the crack tends to rise compared to the wall at the right). Moreover, three drops are recorded in 20th, 29th May and 28th September 2012, respectively of $\Delta 20May = 0.05$ mm, $\Delta 29May = 0, 08$ mm and $\Delta 28September = 0.10$ mm. The first two drops correspond with the tremors of greatest intensity of the seismic event of May 2012. The list of

earthquakes recorded in Modena does not present significant earthquakes in September. The absolute daily residuals reveal for the y component a cumulative trend of -0.13 mm (Figure 7-12 c).

(a)

(b)…………………………………………..(c)
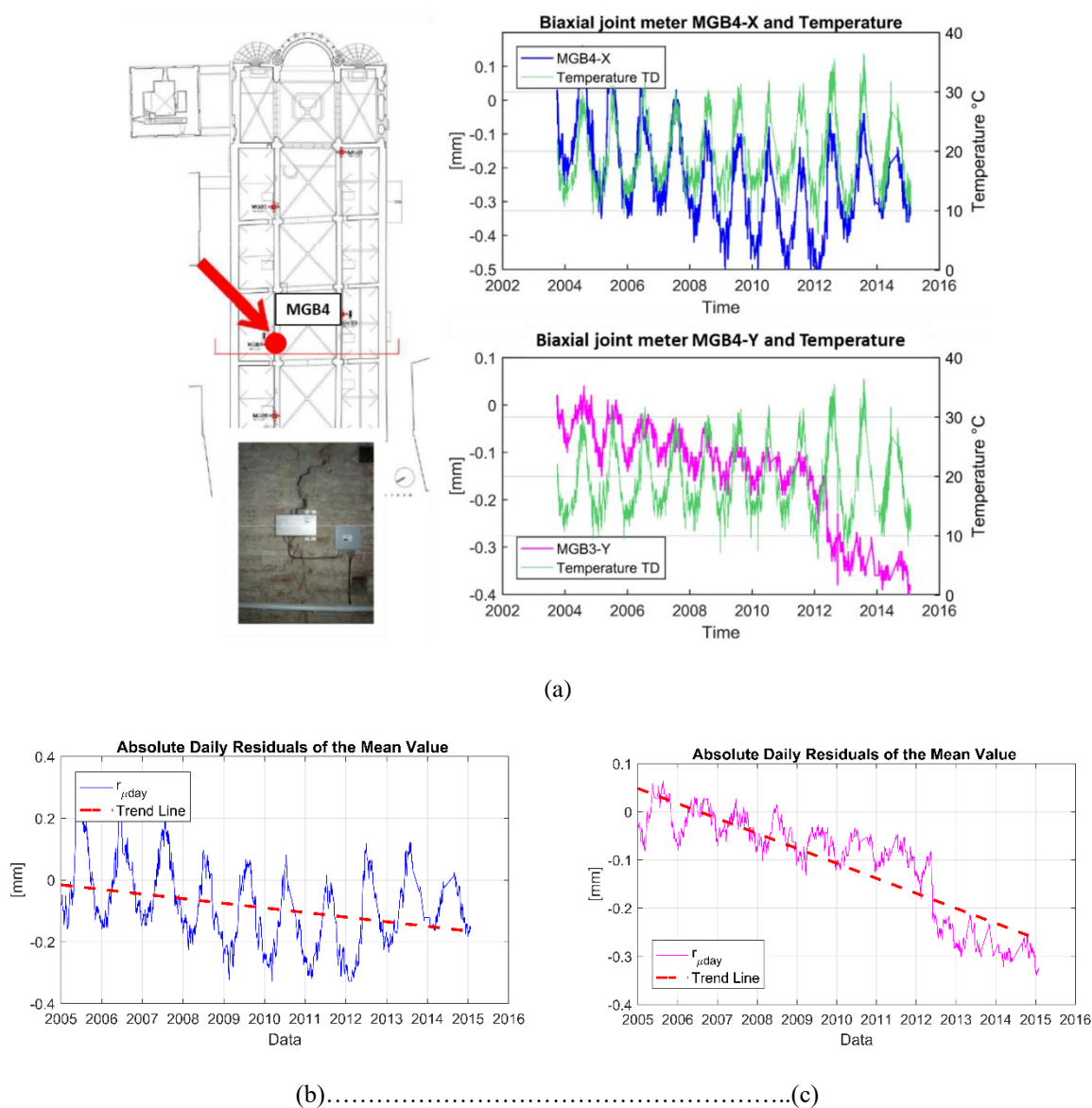
Figure 7-12: Biaxial joint meter MGB4: row-data recorded by MGB4 considering also the temperature variation, as recorded by the thermometer TS, and (b),(c) the absolute daily residuals evaluated for both X and Y direction

Biaxial joint meter MGB5

The sensor MGB5 was installed in 2010 to monitor a crack present in North aisle. The recorded data indicate that the opening of the crack (x-direction) has followed a cyclical pattern substantially due to thermal variations (Figure 7-13 a). The y component instead shows, in addition to cyclical trends relate to the temperature, two significant drops in correspondence of 20 and 29 May 2012 (Figure 7-13b). These drops indicate that seismic events in May 2012 have led to an, albeit slight, changes in the relative quota between the two walls close to the crack, with the portion of the wall to the left of the crack that is rise up of approximately 1.5 mm with respect to the right.
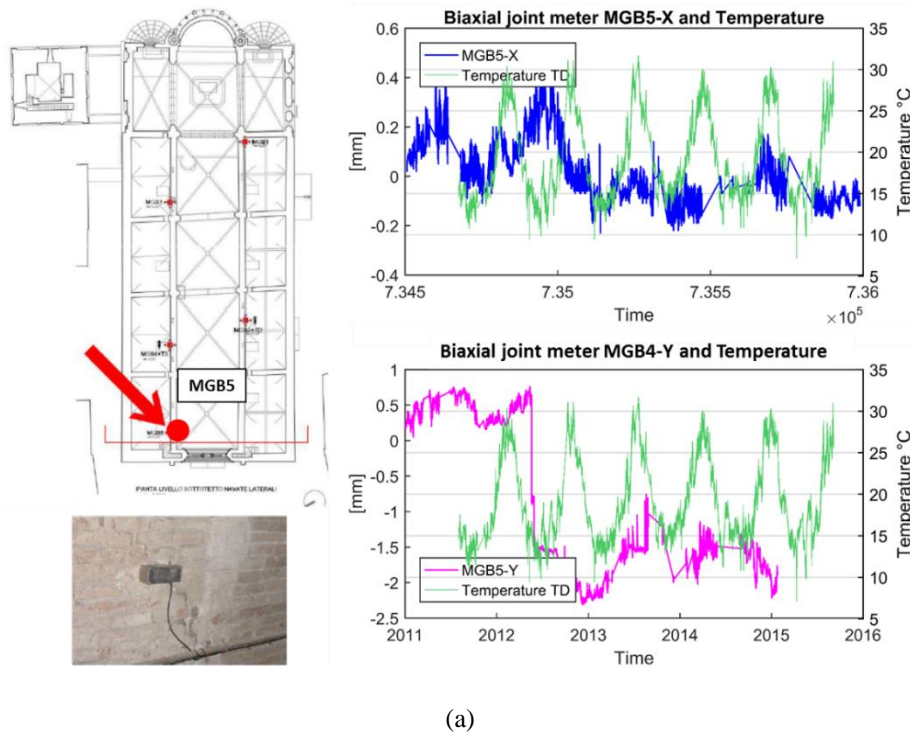
(a)
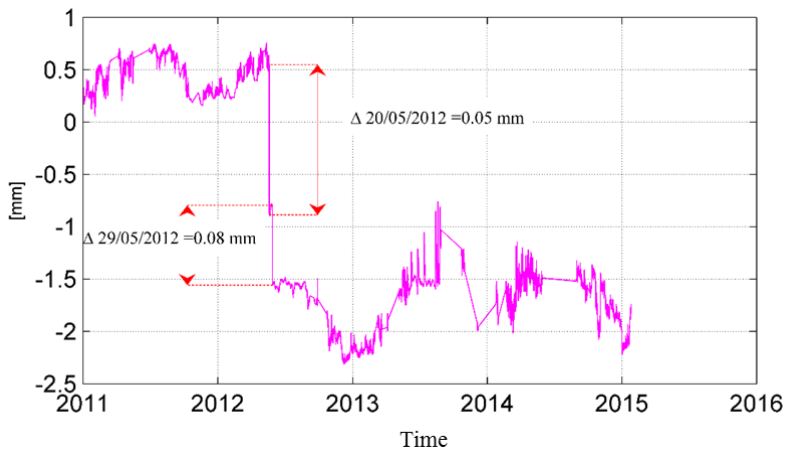
(b)

Figure 7-13: Biaxial joint meter MGB5: row-data recorded by MGB5 considering also the temperature variation, as recorded by the thermometer TS and (b) the drops recorded in the y direction during the seismic events of May 2012

Triaxial joint meter MGT1

The sensor MGT1 monitors the movements of a crack located in the transversal wall close to the apses. The recorded data are in phase with respect to the temperature data recorded by the thermometer TS (Figure 7-14 a). In the x direction, MGT1 records a cyclical trend substantially related to the effects of temperature variations. However, a slight increasing trend concentrated in the last years is recorded indicating the tendency of the crack to close over the time. The absolute daily residuals reveal a cumulative trend of -0.5 mm (Figure 7-14 b). The y component shows a decreasing trend until 2008 (the portion of the wall to the left of the crack rise up compared to that of the right). From 2008 until 2012,

the device recorded a recovery indicated by the increasing trend. During seismic events, a total drop of $\Delta = 0.13$ mm has been recorded indicating a further lifting of the left wall compared to that of the right (Figure 7-14a). The absolute daily residuals reveal a cumulative trend of -0.1 mm in the thirteen years of monitoring (Figure 7-14 c). The recordings detected in the Z direction (perpendicular to the plane) show an increasing trend, indicating, therefore, an increase in the protrusion of the right wall compared to that of the left with a cumulative residua of 0.14 mm (Figure 7-14 a, d).
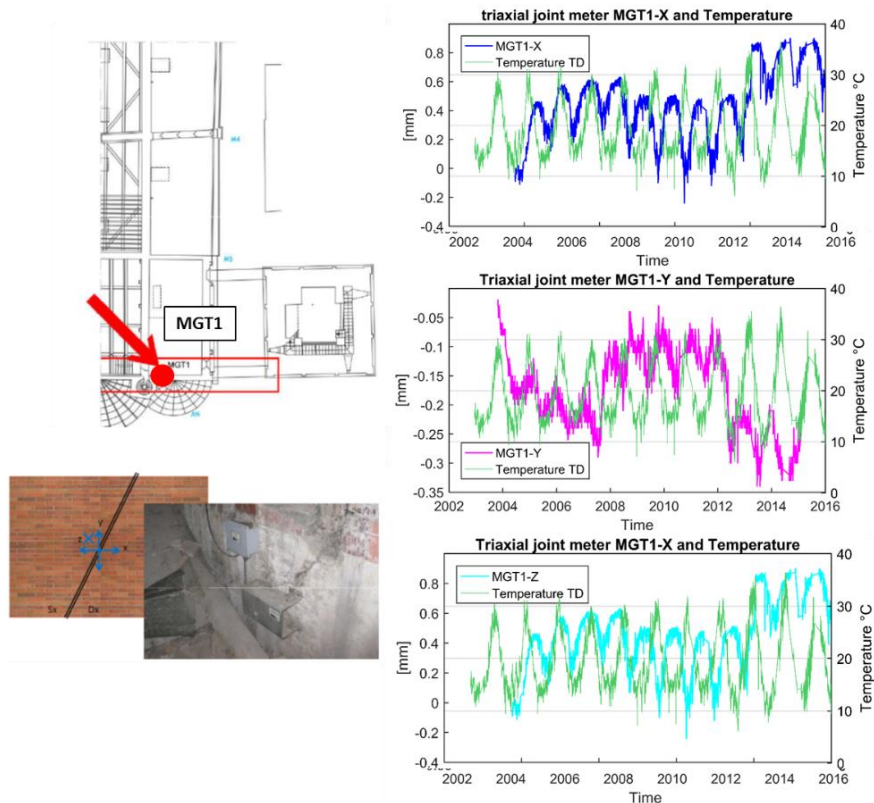
(a)
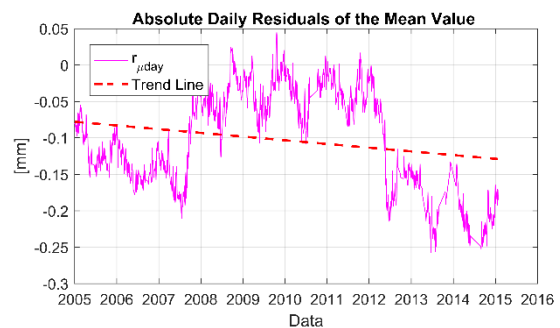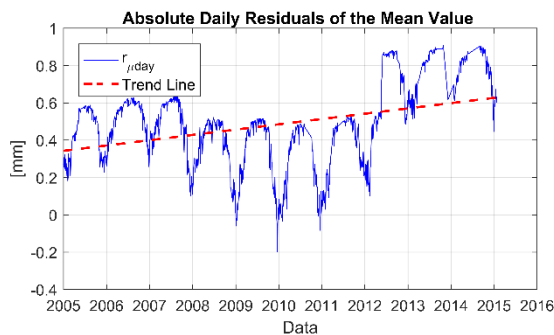
(b)…………………………………………………..(c)
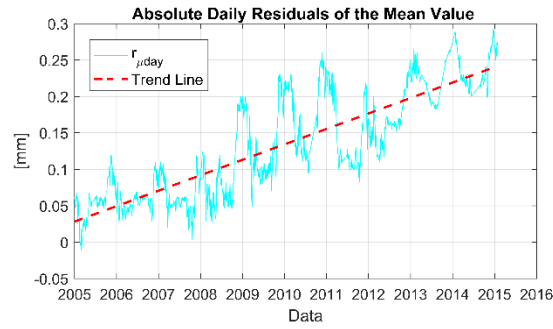
(d)

Figure 7-14: Triaxial joint meter MGT1: row-data recorded by MGT1 considering also the temperature variation, as recorded by the thermometer TS, and (b),(c), (d) the absolute daily residuals evaluated for both X , Y and Z direction

The mean values over the entire observation period of the reference quantities are collected in Table 7-4 for all the joint meters.

Table 7-4- Men values of the reface quantities over the thirteen years of monitoring for the joint meters

Sensor	Year	$\delta_{day,j}$ [mm]	$rp_{\mu day}$ [mm]	$r_{\mu day}$ [mm]	M_{year} [mm]	Σ_{year} [mm]	Rp_{Myear} [mm]	R_{Myear} [mm]
MGB1-X	mean	0.006	0.000	0.024	-0.016	0.078	0.001	0.013
MGB1-Y	mean	0.005	-0.001	0.029	-0.010	0.053	0.000	0.013
MGB2-X	mean	0.020	-0.014	-0.043	-0.124	0.200	-0.016	-0.061
MGB2-Y	mean	0.005	-0.006	-0.042	-0.049	0.038	-0.007	-0.037
MGB3-X	mean	0.022	-0.009	0.033	-0.129	0.408	-0.006	-0.005
MGB3-Y	mean	0.007	0.005	0.048	0.053	0.098	0.009	0.048
MGB4-X	mean	0.018	-0.015	-0.095	-0.250	0.376	-0.017	-0.114
MGB4-Y	mean	0.007	-0.024	-0.129	-0.174	0.108	-0.030	-0.142
MGB5-X	mean	0.059	-0.041	-0.104	0.011	0.333	-0.051	-0.198
MGB5-Y	mean	0.085	-0.457	-	-0.954	0.707	-0.239	-
MGT1-X	mean	0.035	0.035	0.501	0.462	0.536	0.050	0.484
MGT1-Y	mean	0.012	-0.008	-0.113	-0.184	0.398	-0.017	-0.140
MGT1-Z	mean	0.011	0.016	0.146	0.179	0.125	0.024	0.159

7.4.3 Inclinometer

Inclinometer FP1

The sensor FP1, located in the longitudinal wall close to the buttressed, measures the variation of the inclination of the wall. FP1 pendulum recorded a constant trend, in both the directions, up to 20 May 2012. During the 2012 earthquake, and particularly in the two days where the most significant tremors are recorded, two drops in both directions were recorded (Figure 7-15: Inclinometer FP1: row-data recorded by FP1 highlighted the drops recorded during the 2012 earthquake). The drops recorded on 20 and 29 May indicate a movement of the top of the wall of about 1.0 mm in the South-West direction, and equal to about 1.3 mm in the southeast. It is noted that in the months following the earthquake sequence have been recorded jumps probably due to interference in the instrument recording because there have been no significant seismic events on those dates. In particular, the 24th October 2014 the device records a drop that allows to recover most of the overhangs recorded during the earthquake of May 2012.
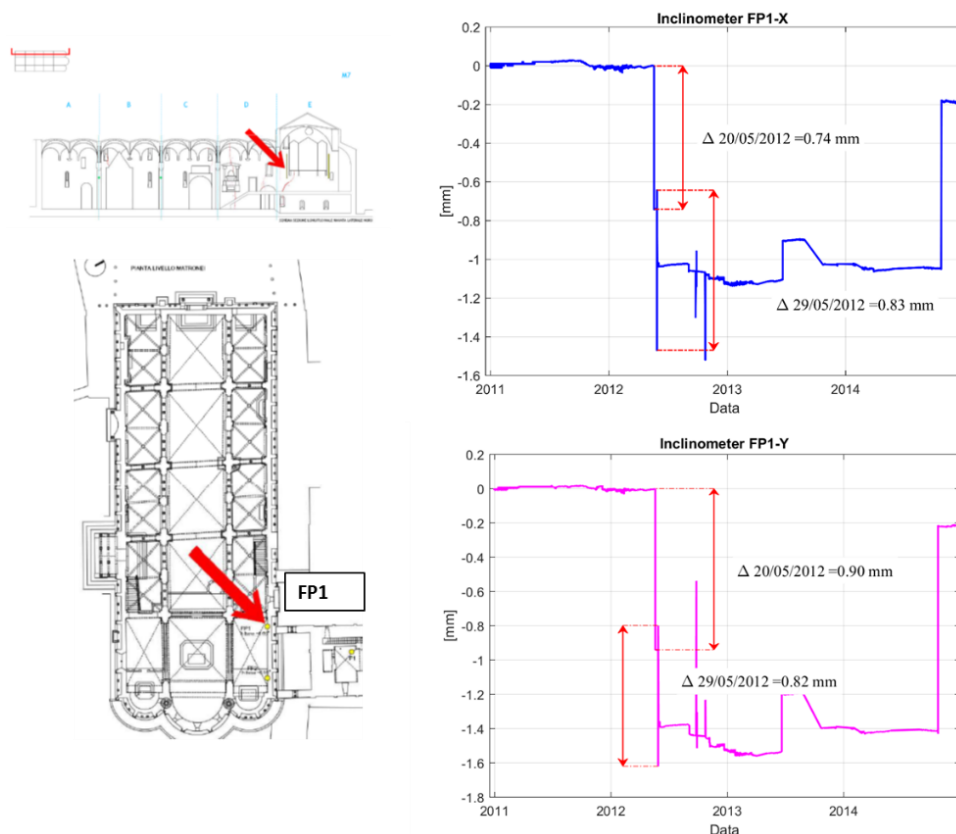
Figure 7-15: Inclinometer FP1: row-data recorded by FP1 highlighted the drops recorded during the 2012 earthquake

Inclinometer FP2

The sensor FP2 is located in the some longitudinal wall of FP1, close to the buttressed. FP2 has recorded a similar behaviour to that recorded by FP1. Before the 2012 earthquake, FP2 recorded a regular trend with very small daily amplitudes oscillations. On 20th and 29th May 2012, drops in both the directions were recorded. The drops recorded indicate movements of the top of the wall to the South-West direction (towards the inside of the Cathedral) of about 1.68 mm. On 28th September 2012 was registered another drop probably due to interference, given that it has been fully recovered on the same day, while the 21 June 2013 is recorded a drop in both the directions, indicating a further movements of the top of the wall toward the inside of the Cathedral (Figure 7-16)
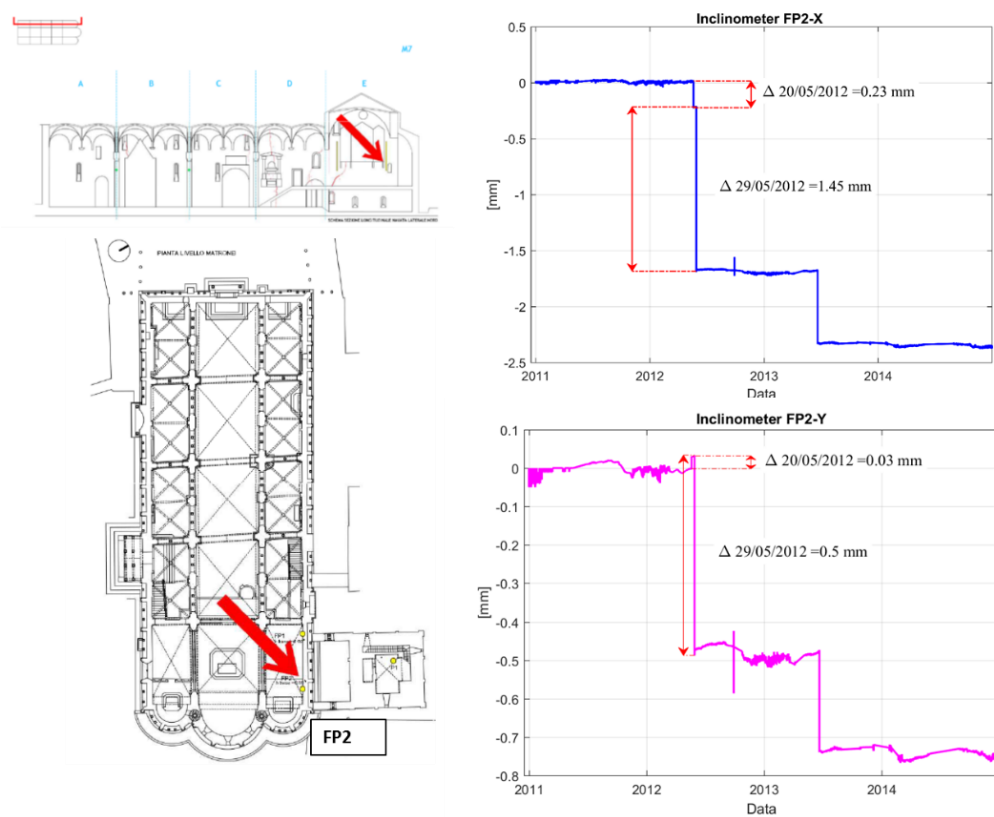
Figure 7-16: Inclinometer FP2: row-data recorded by FP2 highlighted the drops recorded during the 2012 earthquake

7.5   Data processing

The influence of the external factors on the structural response of the cathedral has been not investigated because the only external factor monitored in this case is the internal temperature.

7.5.1   The signal frequency analyses

Data have also been proceeded in the frequency domain in order to identify the periodical and the non-periodical components (called residue) of the signal. The time history of the residua as obtained from the frequency analysis (FFT and IFFT) is compared to the daily residua obtained from the evaluation of the reference quantities. The frequency analysis has been applied only to the data obtained by the joint meters have because not presented malfunction, interruptions and / or many drops. The main results obtained are here presented and the details of the frequency analyses for all the data investigated are provided in Appendix C.2

Joint meters

The joint meters present the predominant component of period close to T=360 days (Figure 7-17). Other important amplitudes are observed for periods equal to 170 days and 500 days. As already seen for the two towers, the amplitude with period T=1 day does not appear significant. The periodicity of the signal has been identified considering the main periodic components detected by the Fourier transform (T=360 days, T=170 days and T=500 days). The trend and variation of the residue evaluated from the FFT analyses is in good agreements with the values obtained from the time-domain analysis (Figure 7-17c).

(a)

(b)………………………………………………..(c)
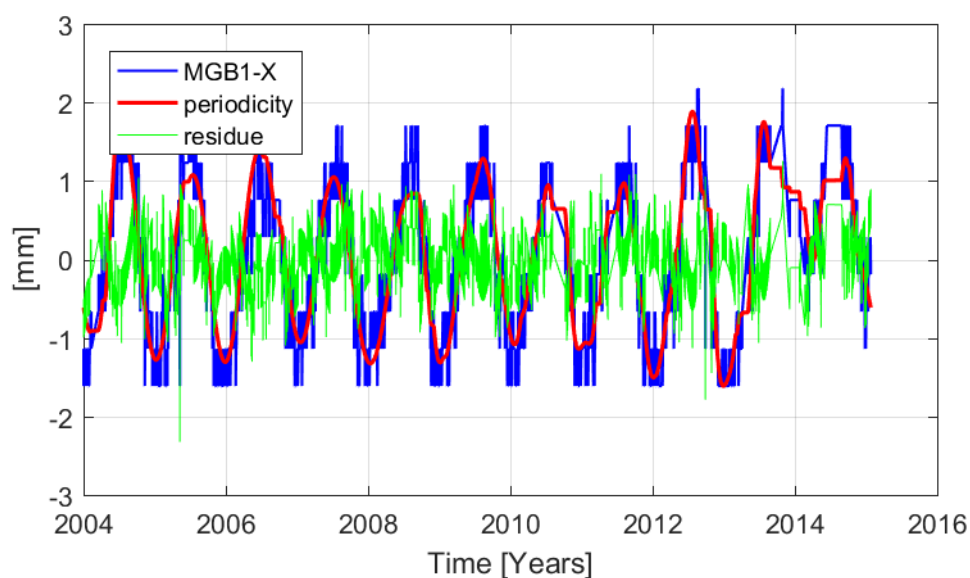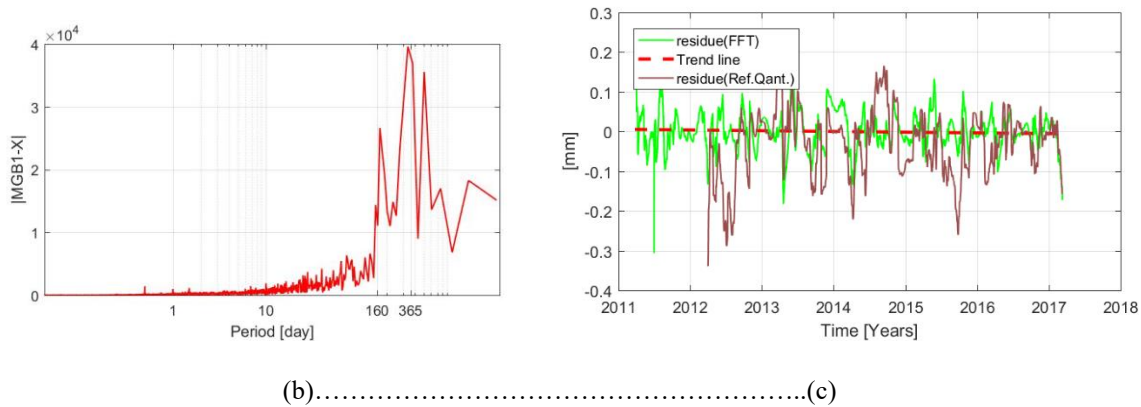
Figure 7-17: Recorded signal by the long base deformeter F2 and its main components (the periodical component and the residual), (b) The Fourier Transform and (c) the residue as obtained from the FFT and from the mathematical considerations (reference quantities)

7.6   Conclusions

The interpretation of the data recorded (from 2004 to 2015) by the static monitoring system installed on the Cathedral of Modena has been performed making use of the reference quantities presented in § 3.3.

More specifically, the following conclusions are drawn:

-   the data recorded by the devices installed on the Cathedral have allowed to control the condition of the structure after the 2012 Emilia earthquake. In particular, the analyses of the data made it possible to understand their possible evolutionary trends triggered by the seismic load.

-   The invar deformeters and the inclinometers, while not recording data continuously, have caught some movements caused by the 2012 earthquake. In more detail, the invar deformeters have recorded a rapprochement between the cathedral and the Ghirlandina tower during the earthquake. These movements are not recovered later, but the devices, after the earthquake, record again a cyclical trend meaning that the movements triggered by the earthquake are not evolving. A similar condition has been recorded by the inclinometers.

-   The joint meters, which measure the movements of some cracks, display a high direct correlation with the temperature. It should be noted that some of the joint meters record an evolutionary trend (MGB2, MGB3 and MGB4). The "evolutionary" phenomenon noted suggests the need for a precise control of the specific cracks in order to exclude dangerous amplification of the phenomenon under observation. At the moment, however, the situation appears substantially "not alarming". The order of magnitude of the cumulative residues reveals in fact small movements in the thirteen years of monitoring. Moreover, these trends showing an analogy with the main movements identified through the integrated knowledge (see § 9) and the structural analyses performed on the Cathedral (see § 10).

The main periodicity of the recorded data by the joint meters have been investigated through the signal frequency analyses and reveal the predominant component with period close to T= 365 days. Other important amplitudes are observed for periods equal to 170 days and 500 days

The trend and variation of the non-periodic components (residue) obtained from the FFT analyses are usually in good agreements with the values obtained from the time-domain analysis (reference quantities §3.3).

Chapter 8

8 Lesson learned

The systematic identification of the "reference quantities" from the data recorded by the static monitoring system of three monumental buildings has allowed to identify the presence of potential evolutionary trends of the phenomena under observation. Moreover, the collection of these "reference quantities" constitute a specific nomenclature for an interpretation of the data obtained from a static structural monitoring that also allow to collect data in a systematic fashion and thus compare them with those obtained by the static monitoring of other monuments. The collection in a database of these values could be used to have a more reliable interpretation of the SMH data recorded on similar buildings. In particular, when these reference quantities are calculated on data obtained from monitoring of several years and have not presented evolutionary trend, they may represent of "reference values" that indicate the order of magnitude of the oscillation of the phenomena under observation due to the influence of the external factors (that for masonry buildings generally is the temperature). These "reference values" can be very useful especially in the first years of monitoring of historical buildings, when is not yet possible to assess the trend of the data recorded.

The approach proposed for the critical interpretation of the data recorded by the static monitoring system has been applied to the Two Towers of Bologna and the Modena Cathedral for which the orders of magnitudes of the "reference quantities" have been identified. The mean values over the entire observation period of the reference quantities evaluated are collected in Table 8-1 for the Asinelli tower,

Table 8-2 for the Garisenda tower and Table 8-3 for the Modena Cathedral. Each value refers to a sensor typology and is obtained computing the average of all instruments of that type.

It is also noted that the residues were considered in absolute value since in this case the goal is to have the order of magnitude recorded over the years for the specific phenomenon under observation.

The comparison between the reference quantities recorded on the three monuments, even if the geometrical configuration of the Cathedral is very far from those of the towers, allowed to identify some similar trends.

Table 8-1-Reference values for each type of sensor installed on the Asinelli tower

ASINELLI TOWER-mean values over the entire observation period Δt (2011-2016)						
Sensor	$\delta_{day,j}$	$\mathrm{rp}_{\mu day}$	$\mathrm{r}_{\mu day}$	Σ_{year}	Rp_{Myear}	R_{Myear}
Long base deformeter [mm]	0.028	0.015	-0.035	0.259	0.015	0.033
Deformeter [mm]	0.008	0.002	0.004	0.099	0.004	0.008
Extensimeter [με]	53.555	4.545	11.645	276.298	4.943	9.730
Inclinometer[°] X comp.	0.007	0.005	0.011	0.04	0.005	0.012
Inclinometer[°] Y comp.	0.009	0.024	0.022	0.07	0.007	0.024

Table 8-2- Reference values for each type of sensor installed on the Garisenda tower

GARISENDA TOWER-mean values over the entire observation period Δt (2011-2016)						
Sensor	$\delta_{day,j}$	$\mathrm{rp}_{\mu day}$	$\mathrm{r}_{\mu day}$	Σ_{year}	Rp_{Myear}	R_{Myear}
Long base deformeter [mm]	0.040	0.017	0.047	0.628	0.017	0.042
Deformeter [mm]	0.010	0.008	0.027	0.080	0.008	0.029
Extensimeter [με]	21.51	4.71	18.52	263.18	101.17	4.61
Inclinometer[°] X comp.	0.007	0.002	0.006	0.041	0.002	0.007
Inclinometer[°] Y comp.	0.008	0.003	0.009	0.059	0.002	0.007

Table 8-3- Reference values for each type of sensor installed on the Modena Cathedral

MODENA CATHEDRAL-mean values over the entire observation period Δt (2004-2015)							
Sensor		$\delta_{day,j}$	$rp_{\mu day}$	$r_{\mu day}$	Σ_{year}	Rp_{Myear}	R_{Myear}
Biaxial joint meter [mm]	X comp.	0.02	0.010	0.600	0.600	0.010	0.048
	Y comp.	0.01	0.009	0.552	0.552	0.011	0.060
Triaxial joint meter [mm]	X comp.	0.035	0.035	0.501	0.536	0.050	0.484
	Y comp.	0.012	-0.008	-0.113	0.398	-0.017	-0.140
	Z comp.	0.011	0.016	0.146	0.125	0.024	0.159

The comparison between the reference quantities recorded on the three monuments, even if the geometrical configuration of the Cathedral is very far from those of the towers, allowed to identify some similar trends. In more detail, with reference to masonry and crack displacements:

-    the daily amplitude δ_{day} is of the order of magnitude of 1÷4/100;

-    the annual amplitude Σ_{year} is of the order of magnitude of 1÷6/10;

With reference to the inclination of the walls (in this case are considered only the data recorded on the Two towers):

-    the daily amplitude δ_{day} is of the order of magnitude of 7÷9/1000;

-    the annual amplitude Σ_{year} is of the order of magnitude of 4÷7/100;

It can be noted that generally the ratio $\delta_{day}/\Sigma_{year}$ is roughly equal to 1/10.

These information could be useful guidelines for the interpretation of data acquired by static monitoring system of other masonry monuments.

Part II

INTEGRATED STRUCTURAL ASSESMENT OF MONUMENTAL BUILDINGS

Chapter 9

9 An approach for the structural assessment of Monumental Buildings

9.1 Introduction

The efficient management of cultural heritage buildings is a crucial issue and the correct assessment of their safety level and conservation are of fundamental importance. In this chapter, first an overview of the main methods applicable to the study of masonry historical buildings are presented. Then, a possible approach for the reliable assessment of the structural "health" of historical monuments making use of a multi-disciplinary multi-analysis approach (MDMA) considering the building as model of itself is presented. The MDMA approach is based on the development of a multi-disciplinary research aimed at providing an "integrated knowledge" of the building through the mutual exchanging of expertise and capabilities offered by the contribution of experts in different fields. A central role in the MDMA methodology is played by the real-time monitoring of the structural health of the monument through the implementation of a Structural Health Monitoring SHM system. Then, a reliable structural analysis of the monument is carried out by a kind of multi-analysis research, which seeks at integrating the results of analyses based on different methods (according to the different aspects to be investigated). The introduced approach is grounded on the experience obtained during an almost decade of studies on the Cathedral of Modena, developed within of a Scientific Research Committee, with the purpose of identifying potential vulnerabilities and criticalities and driving the local authorities in the monument preservation. The Committee includes experts of various academic fields such as structural engineering, geotechnique, geology, restoration, architecture, history, such as firms (civil engineering firms, Structural Health Monitoring firm) and local authorities, which are in charge of the management of the monument. The mutual exchange of the information obtained from the different fields has proved to be

a fundamental operative procedure in order to identify the structural health of the monument and develop, thus, a reliable and cost effective strengthening design.

9.2 Literature review: Structural Analyses Methods

In last recent years, with the increasing interest on the conservation of historical monuments, several research were focused on the structural analyses of these complex buildings. The most widespread construction material used in Italy for the monumental buildings is the masonry. One of the greatest difficulty in the structural analyses of the monuments is to describe correctly the masonry as nonlinear and orthotropic material, generally of poor quality and with low tensile strength. Moreover, historical monuments are strongly prone to be damaged during earthquakes due to the presence of critical elements like vaulted roofing system and irregular building configuration, both in plan and elevation. Therefore, besides the problem of modelling masonry itself, any modelling technique should be able to adequately describe the geometry and morphology of the real construction, including the structural form, internal composition, connections and support conditions. An accurate description of the distribution of mass and external forces is essential for both gravity and seismic analyses (Roca et al. 2010).

The main available methods for the structural analyses of historical monuments make use of:

- Finite Element Methods (FEM): macro- or micro-modelling;
- limit analysis,
- Discrete Element Methods (DEM)

These methods will be reviewed in the next section with the purpose of evaluate their limitations and reliability. Knowing that all of these methods are appropriate to investigate specific aspects on the structural response of the historical buildings the main questions which should be asked are " How the use of these methods allow to evaluate the real structural behaviour of the monuments? "and "Is it possible to obtained a proper understanding of the historical monuments using only structural analyses?"

The approach propose in the next sections aims to answer these questions.

9.2.1 Finite Element Methods: macro-or micro modelling

Two different approaches have been developed to represent the heterogeneous masonry texture (Figure 9-1a), composed by units and joint (Lourenço 1996):

- micro-modelling: units and mortar are represented as distinct elements and the unit-mortar interface are discontinuous elements (Figure 9-1 b, c);
- macro-modelling: units and mortar are homogenized in a continuum (anisotropic or isotropic) equivalent material (Figure 9-1d).
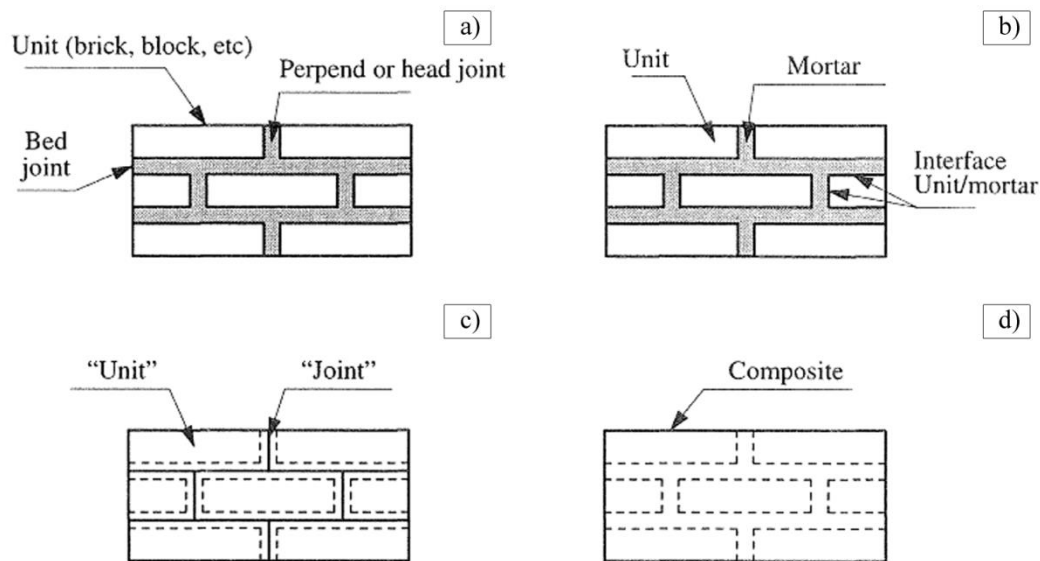
Figure 9-1: Modelling strategies for masonry structures: (a) masonry sample; (b) detailed micro-modelling; (c) simplified micro-modelling; (d) macro-modelling (Lourenço 1996).

A micro-model strategy should include all the failure mechanisms, which are cracking of joints, sliding over one head or bed joint, cracking of units and crushing of masonry. Micro modelling is suited for small structural elements with particular interest in strongly heterogeneous states of stress and strain. Several attempts to use brick-interfaces for the finite element modelling of masonry were carried out in the years (Lourenco & Rots 1996), (Rots 1997). Macro-models are applicable when the structure is composed of solid walls with sufficiently large dimensions so that the stresses across or along a macro-length will be essentially uniform. Macro modelling is probably the most popular and common approach for the analyses on large structural members or full structures. In these cases, macro modelling, which consider the material as a fictitious homogeneous orthotropic continuum may offer an adequate approach to the characterization of the structural response. However, constitutive models of the homogeneous material are difficult to be determined and non-standardized. Several studies deal with the specific constitutive formulation for the analysis of masonry structures, considering different inelastic criteria for tension and compression and different hardening/softening behaviour along each material axis (Berto et al. 2002), (Papa 2000), (Pelà et al. 2013), (Pelà et al. n.d.), (Pelà et al. 2011b). The main non-linearity besides the mechanical properties of the material can be geometrical non-linearity and constraint non-linearity. Therefore, FEM modelling can be based on linear analyses (general used to obtain some first information on the global behaviour) and more sophisticated nonlinear analysis, both in static and dynamic configurations. Elastic models can give an indication on the mechanical behaviour of the structure but they cannot follow the behaviour beyond the elastic range, while nonlinear models can be very heavy to handle and costly. For this reason, in the case of complicated structures several elastic analyses can be carried out under different hypothesis in order to obtained useful information on their structural behaviour. This methodology was applied by Macchi (Macchi et al. 2017) for the study of the leaning tower of Pisa. In a similar way, simple numerical models

based on linear elastic behaviour of materials were also used by Mola and Vitaliani (Mola & Vitaliani 1996) to analyse the St. Mark's Basilica in Venice (Figure 9-2a) and the entrance to St. Peter's Basilica in Rome (Figure 9-2b) (Macchi 2001) , while Croci analysed Colosseum in Rome (Croci 1996).
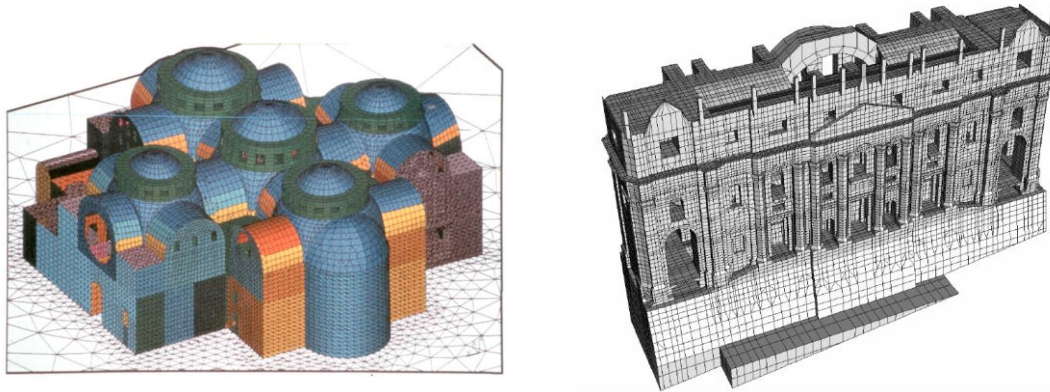
Figure 9-2: Finite linear element models: (a) St. Mark's Basilica in Venice, (b) entrance to St. Peter's Basilica in Rome

Due to the fact that masonry structures, because of very small ultimate tensile strengths, demonstrate an explicit nonlinear behaviour already at very small loads, the use of linear analysis in modelling of masonry structures is considered acceptable when the intention is to observe behaviour of a structure until appearance of the cracks, or to evaluate the places where first cracks could appear. All effects that appear in masonry structure, starting from initiation and propagation of cracks, and all the way to final collapse, can be determined by nonlinear analysis only (Smoljanović et al. 2013).

9.2.2 Limit analyses

The limit analyses, based on kinematic approach, are particular suitable for the analyses of historic churches, which generally are characterized by ineffective connections between the elements creating structurally independent parts rather than a box behaviour. Limit analysis methods are based on assumptions made by Couple in 1730 and later used by Heyman in the stone arch stability analysis (Heyman 1995): (i) masonry structures do not have a tensile strength, (i)masonry structures have an infinite strength in compression, and (ii) sliding cannot occur between joints.

In particular, these conditions enable the formulation of two theorems:

- the lower-bound theorem: the structure is safe, meaning that the collapse will not occur, if a statically admissible state of equilibrium can be found;
- the upper-bound theorem : if a kinematically admissible mechanism can be found, for which the work developed by external forces is positive or zero, the collapse will occur

The application of the upper bound theorem leads to the so-called kinematic approach (or kinematic limit analysis) for the study of masonry buildings. First, the limit analysis methods have been applied to

stone arches: if the thrust line was located inside the outline of an arch, the arch would be considered statically stabile. While, if a thrust line becomes tangent to the boundaries causing as many hinges as needed to develop a mechanism the load is the true ultimate load and the mechanism is the true ultimate mechanism (Heyman 1969), (Kooharian 1952). Later, three dimensional shape of thrust line have been study by Harvey and Maunder (Harvey & Maunder 2001) while Block et al. (Block 2005), (Block et al. 2006)developed an interactive computer analysis based on the combination of static and cinematic theorems to obtain the thrust line when treating three dimensional issues.

Limit analysis is regarded today as a powerful tool to describe the safety and collapse of structures composed by blocks (including not only arches and structures composed of arches, but also towers, façades and entire buildings). Based on the observation of real seismic failure modes of historical and traditional buildings in Italy, Giuffré and Carocci (Giuffrè 1990),(Giuffrè 1995),(Giuffrè & Carocci 1993), (Carocci 2001) proposed the use of cinematic approach, after decomposition of a structure into rigid blocks, to study the seismic vulnerability (Figure 9-3)
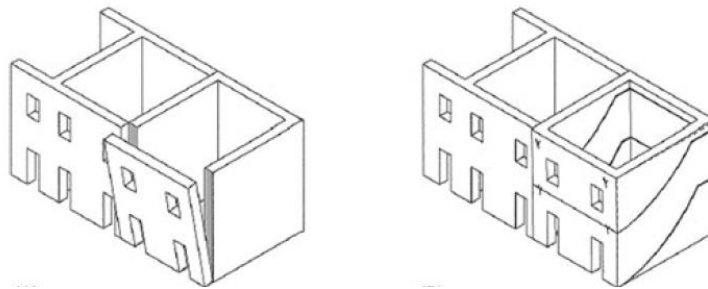
Figure 9-3: Failure modes for buildings: (a) without cross connections; (b) with cross connections(Carocci 2001)

More recently, Giuffré also attracted considerable attention with his proposal to combine block analysis with the capacity spectrum method (Fajfar 1999), (Lagomarsino 2006) to estimate seismic resistance of masonry structures. Roca (Roca et al. 2007) also suggested a method based on the static theorem for the analysis of reinforced masonry structures. Ochsendorf (Ochsendorf 2002) used the limit analysis method for the analysis of arches with deformed base, while De Luca (De Luca et al. 2004) used a finite element method combined with the limit analysis method to analyse seismic resistance of stone arches. In recent times, computer developments based on limit analysis methods have been developed [42-45] using mostly the cinematic approach. Most of these methods normally are based on the following assumptions:(i) limit load occurs with small displacements, (ii) masonry has zero tensile strength, (iii) shear behaviour in contact among blocks is perfectly plastic, (iv) hinging failure mode at a joint occurs for a compressive load independent from the rotation. Several methods have been proposed to assessment of masonry structures by limit analysis (for both in-plane or out-of plane loading) over the years, combining the aforementioned principles with modern computers and advanced numerical methods (Livesley 1978),(Ferris & Tin-Loi 2001),(Gilbert & Melbourne 1994),(Baggio & Trovalusci

1998),(Casapulla & D'Ayala 2001),(Orduña & Lourenço 2003), (Orduña & Lourenço 2005a),(Orduña & Lourenço 2005b). The kinematic limit analysis obviously does not provide a verification in terms of stresses and material strength and, thus, it can hardly be used to describe the response and predict damage for moderate or service load levels not leading to a limit condition. The limit analysis can only be used to assess the stability or safety of structures (Roca et al. 2010). Moreover, the procedure is useful to assess the value of the acceleration that a historical building actually experienced after an earthquake, using the damages mechanisms as seismic transducers, as described by Sassu et al. (Sassu et al. 2012). The Italian code obliges to use local analysis for historic churches (Norme Tecniche per le Costruzioni 2008), (Guidelines for Evaluation and Mitigation of Seismic Risk to Cultural Heritage 2011). However, limit analysis should be always considered as a complementary tool in the assessment of the seismic response of historical buildings.

9.2.3 Discrete element methods

The Discrete element method (DEM) is characterized by the modelling of the material as an assemblage of distinct blocks interacting along the boundaries. Therefore, this method, able to capture the discontinuity nature of the masonry, results particularly suitable for the study of historical buildings. The details of the formulation of the DEM will be presented in § 13.2.

DEM has been applied to study the rocking motion of block on rigid base (Dejong 2009), (DeJong & Dimitrakopoulos 2014), (Pena et al. 2007) and to model the response of several masonry structures to ground motion: arch (Lemos 1995), (Dejong 2009) (De Santis & de Felice 2012), vaults (McInerney & DeJong 2015) (Figure 9-4), out of plane mechanisms of wall (De Felice & Giannini 2001) stone bridge (Bićanić et al. 2003) and pillars and columns (Papantonopoulos et al. 2002a).
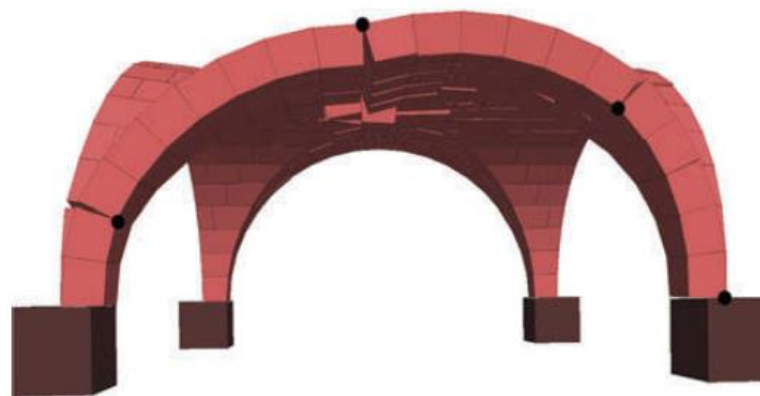
Figure 9-4: Stable groin vault exhibiting four hinges along profile(McInerney & DeJong 2015)

Bell-towers and basilicas have been also studied via DEM (Azevedo et al. 2000), (De Felice & Mauro 2010), (Figure 9-5). These studies reveal that the method is able to predict the collapse masonry structures but the definition of the appropriate modelling parameters is a difficult issue.
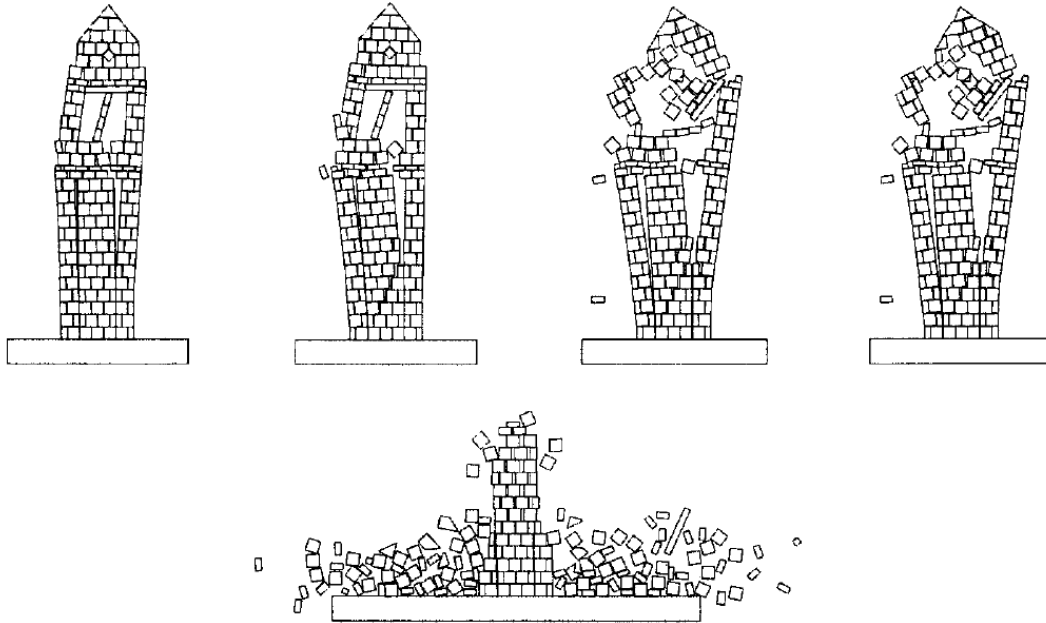
Figure 9-5: Collapse pattern for the San Giorgio in Trignano bell tower (Azevedo et al. 2000)

9.3   Multi-disciplinary multi analyses approach

Historical masonry monuments are not only works of art, but also have to meet the practical test of utility and a suitable safety level. The efficient preservation of the structural health of these unique buildings presents several challenges. From a structural point of view, historical monuments are characterized by much larger uncertainties than ordinary buildings and conventional analysis tools may fail in providing a reliable characterization of their structural behaviour. According to the principles of restoration, only with a thorough knowledge it is possible to develop a consistent structural analyses (able to represent the real structural behaviour) and conceive, thus, intervention solutions targeted at preserving the integrity of the historical monuments. The concept of integrity, often, is only interpreted as the requirement of preserving the shape and the appearance of the monument. Instead, with reference to historical monuments, the requirement of integrity is not so simple because it also implies historic integrity, by considering the changes of the monument with time, as well as material integrity that means construction techniques, materials and structural scheme. Therefore, preserving integrity requires, beside an interdisciplinary approach, the development of a holistic approach in the monuments conservation. A possible approach to reduce the uncertainties in the knowledge of historical buildings and obtain the necessary information to evaluate its structural health should be based on the development of a multi-disciplinary research aimed at providing an "integrated knowledge" through the mutual exchange of expertise and capabilities of different disciplines and a real-time monitoring of the state of the buildings (ICOMOS 2003). Moreover, as already briefly mentioned, approaches and tools commonly used in structural analysis of ordinary buildings, extensively based on numerical models, do not always seem to be appropriate for historical masonry monuments of unique features and are generally not able to provide convenient material models to describe highly nonlinear behaviour and masonry orthotropic. To conceive a unique tool valid to describe all possible structural responses of the historical masonry monuments is therefore complex, and most likely impossible. Quite often, more reliable results can be obtained by employing a multi-analysis method that integrates different approaches (from simple but more reliable limit schematizations, to more complex but, usually more sensible, finite element models, (Lourenço 2002)). Figure 9-6 display an overview of the presented Multi-Disciplinary Multi Analyses approach for a proper assessment of the structural health of historical monuments.
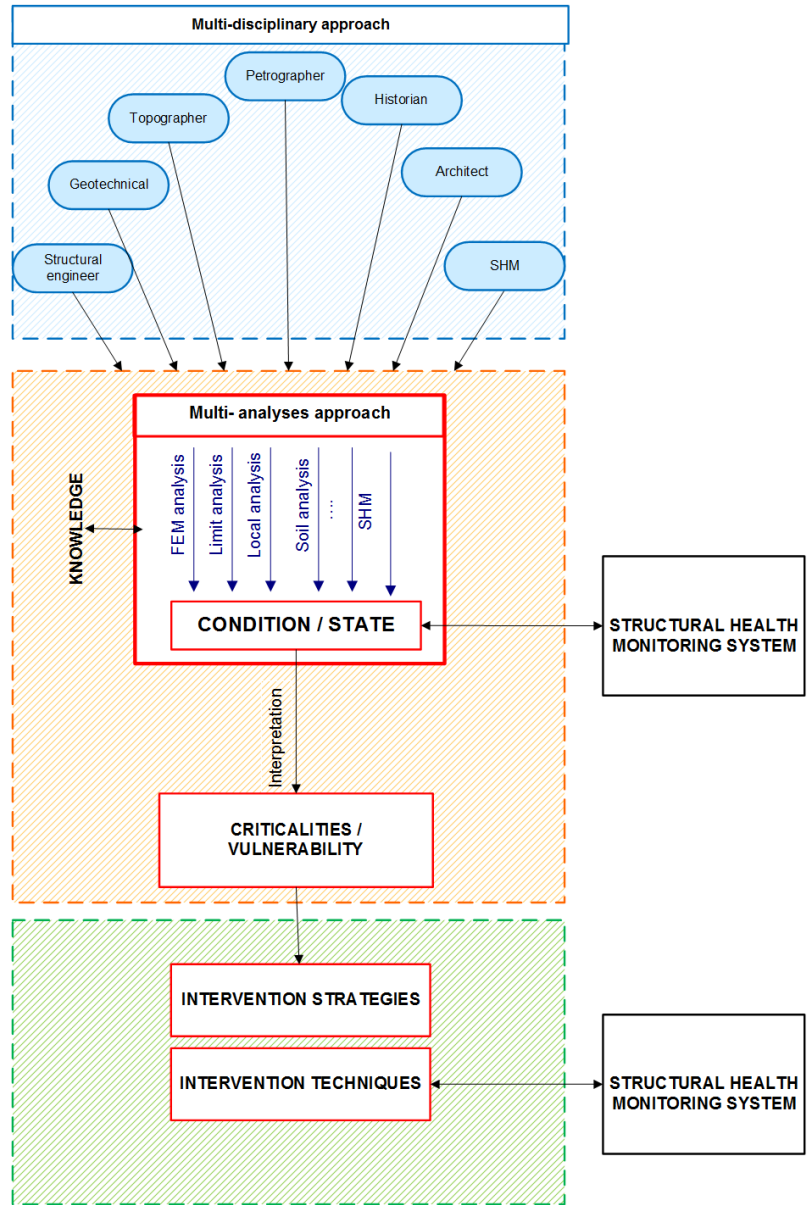
Figure 9-6: Overview of the MDMA approach

9.3.1 The Integrated Knowledge

The current standard requirements recommend an interdisciplinary approach that thanks to an investigating team that incorporates a range of skills appropriate allows discovering phenomena involving structural behaviour of the monuments. (ISCARSAH 2003), (Guidelines for Evaluation and Mitigation of Seismic Risk to Cultural Heritage 2011). A correct and complete analysis of an historical building have to be based on the historical, geometrical, material and structural knowledge of the structure in order to design structural interventions not only to guarantee safety, but also to respect the context, which surrounds them. Knowledge of the structure requires information on its conception, on its constructional techniques, on the processes of decay and damage, on changes that have been made

and finally on its present state. The following steps can usually reach this knowledge (ISCARSAH 2003):

- definition, description and understanding of the historic and cultural significance of the buildings;
- a description of the original building materials and construction techniques;
- historical research covering the entire life of the structure including both changes to its form and any previous structural interventions;
- description of the structure in its present state including identification of damage, decay and possible progressive phenomena, using appropriate types of test;
- description of the actions involved, structural behaviour and types of materials;
- implementation of a SHM system.

The purpose of the historical investigation is to understand the conception and the significance of the building, the techniques and the skills used in its construction, the subsequent changes in both the structure and its environment and any events that may have caused damage (such as past earthquakes..). Knowledge of what has occurred in the past can help to forecast future behaviour and can be a useful indication of the level of safety provided by the current state of the structure. The direct observation and the survey of the structure is essential phase in order to identify decay and damage, geometric irregularities which can be the result of previous deformations (it can indicate the junction between different building phases or alterations to the fabric) and to determining whether or not the phenomena have stabilised. The identification of the mechanical characteristics of the materials should be investigated through non-destructive tests to avoid any alterations to a structure (ISCARSAH 2003). In addition to these remarks, it must be outlined the role of the monitoring, as an essential component of the integrated studies when exploring the long-term performances. SHM system can be very useful to acquire information of possible progressive phenomena, but also during and after the implementation of strengthening intervention in order to evaluate their effectiveness. Figure 9-7 shows a schematic representation of the multi-disciplinary approach to obtain an integrated knowledge of the monuments.
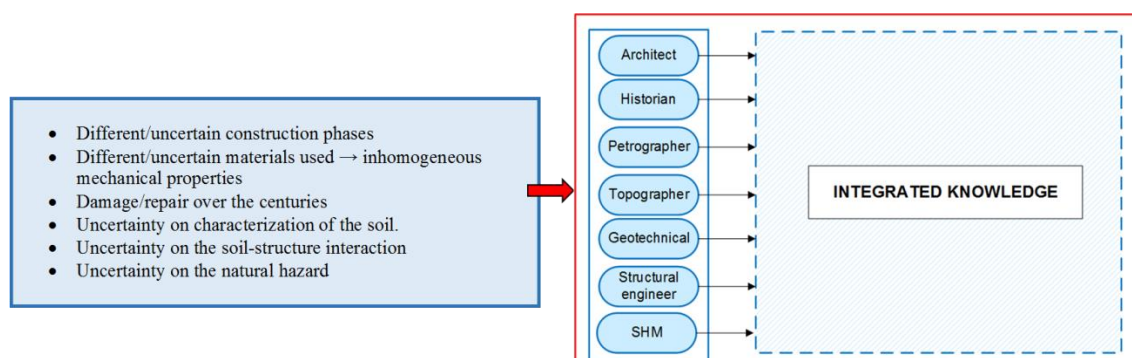
Figure 9-7: Schematic representation of the multi-disciplinary approach to obtain an integrated knowledge of the monuments

9.3.2 Multi analyses method for the assessment of the structural behaviour

The amount of data collected by the multi disciplinary approach are used to develop reliable structural analyses in order to evaluate the safety levels of the monument. The structural behaviour of a monument is usually very complex and influenced by many factors. Therefore, only one model of the whole building generally is not able to capture all the structural peculiarities. The monument should be represented by different simplified 'structural scheme', (i.e. an idealisation of the building) with different complexity and different degrees of approximation to reality. Moreover, the model used has to take into account any alterations and weakening, such as cracks, disconnections, leanings, .., whose effect may significantly influence the structural behaviour. Structural analyses of ancient masonry structures is very far from the modelling of ordinary buildings, and the most widespread tools generally based on Finite Element methods are affected by several limitations, that may be related to the material behaviour, the actual effectiveness of the connections, the effectiveness of the chains, the restraints provided by the soil. In addition, the dynamic properties of global models in terms of fundamental frequencies and modal shapes may be are very far from the real ones, provided that they are based on linear elastic analysis, whilst the masonry material is characterized by a highly non-linear response (Blasi, C., and Coïsson 2006). All these problems point to the need to develop a multiple analyses approach which integrating the potential of various methods of analyses, from simple but more robust ones, to more accurate but generally more sensible complex numerical simulations allows to assess the "structural health" of the monuments. The schematic representation of the concept of the multi analyses approach is shown in Figure 9-8.
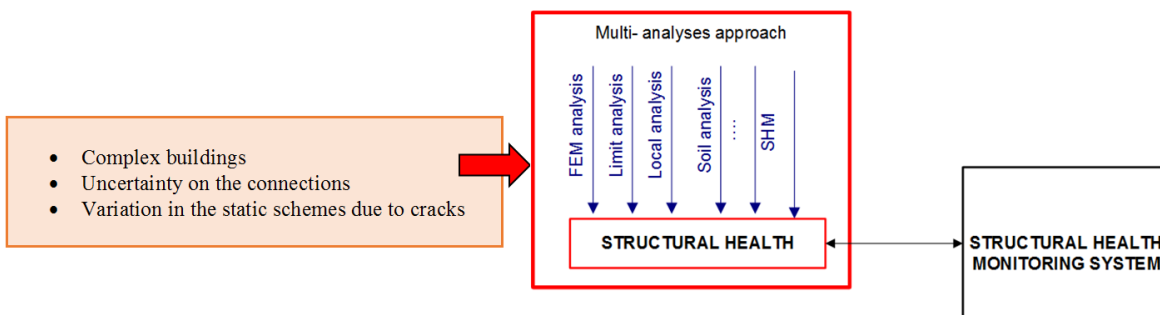
Figure 9-8: Schematic representation of the multi-analyses approach to evaluate the "structural health" of the monuments

9.4   Conclusion

An overview of the main methods applicable to the study of masonry historical buildings is presented in this chapter. Moreover, a possible approach for the reliable assessment of the structural "health" of historical monuments based on a multi-disciplinary multi-analysis approach (MDMA) considering the building as model of itself is presented. Indeed, to reduce the uncertainties in the knowledge of historical buildings and obtain the necessary information to evaluate its structural health is necessary a multi-disciplinary research aimed at providing an "integrated knowledge" through the mutual exchange of expertise and capabilities of different disciplines. The main features that should be investigated in order to obtain a proper knowledge of the historical monuments are described. The amount of data collected by the multi-disciplinary approach provide the basis to develop reliable structural analyses in order to evaluate the safety levels of the monument. In addition, the limitations of the available methods for the study of complex masonry buildings point out the need to develop a multiple analyses approach which integrating the potential of these various methods in order to assess the "structural health" of the monuments.

Chapter 10

10 Cathedral of Modena: the integrated knowledge

10.1   Introduction

The integrated knowledge process obtained for the Cathedral of Modena through the mutual exchange of expertise and capabilities of different disciplines is summarised in this chapter. In more detail, the constructional phases, the geometrical configuration, the material properties, the actual state of degradation of the Cathedral of Modena will be presented. Moreover, a seismic hazard analyses, which allow reconstructing the intensity of the earthquakes that occurred on the Cathedral in the past is presented. The knowledge of the earthquakes that hit the Cathedral in the past and its corresponding structural response can help to forecast future behaviour and can be a useful indication of the current safety level of the structure.

10.2   The Cathedral of Modena

The Cathedral of Modena and the adjacent Ghirlandina Tower are part of the UNESCO site of Piazza Grande, since 1997. The Cathedral is a masterpiece of Romanesque architecture and sculpture of northern Italy (Figure 10-1). Its construction was realized between 1099 (the date of its foundation is marked on a stone on its façade) and 1319, when the construction of the Ghirlandina was completed. Inscriptions on the façade and on the central apse celebrate respectively the sculptor Wiligelmo and the architect Lanfranco. As it will be better explained later (§10.3.1), the actual Cathedral rise up on the ruins of three previous Cathedrals (Labate 2009), the first one containing the tomb of St. Geminianus (the Modena city's patron). The in-plan geometry is approximately 25 m wide, in the transversal direction, and 66 m long, in the longitudinal direction, for an area of roughly 1650 m^2. The maximum roof height is approximately 24 m (Figure 10-2). The Cathedral has a Latin cross plant with three naves,

a false transept and the chancel (the area of the liturgical altar) in an elevated position, due to the presence of a crypt containing the corpse of the city's patron, Saint Geminianus.

(a) (b)
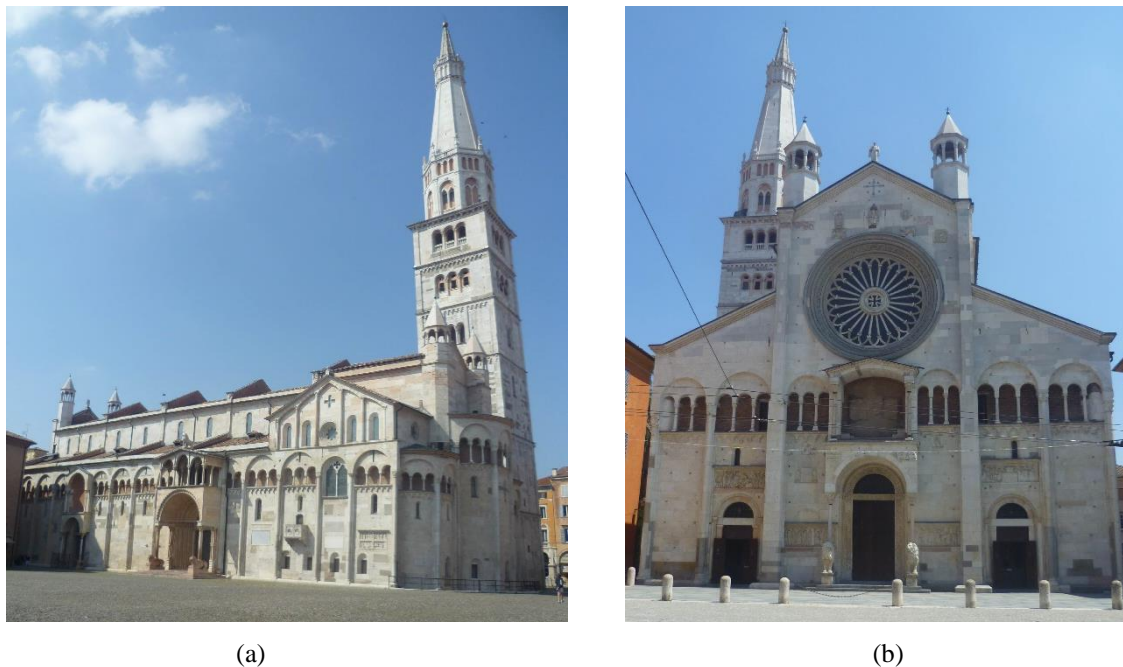
Figure 10-1: Photographs of Cathedral of Modena: (a) view of the apses and (b) view of the facade.

The structural configuration consists of heavy masonry walls, sturdy masonry and stone piers supporting the weight of impressive thin masonry vaults, added in the XV century. Both the central nave and the side aisles have four spans. The vaults of the central nave have double length span with respect to the length span of the vaults of the aisles. The maximum height of the vaults of the central nave is around 20 m, while that of the side aisles is approximately 13 m. Next to the Cathedral, there is the Ghirlandina Tower, a high tower of roughly 88 m high whose construction proceeded in parallel with that of the Cathedral up to the fourth level. The upper part of the Tower was built later, between 1261 and 1319 (Cadigliani 2009).

(b)
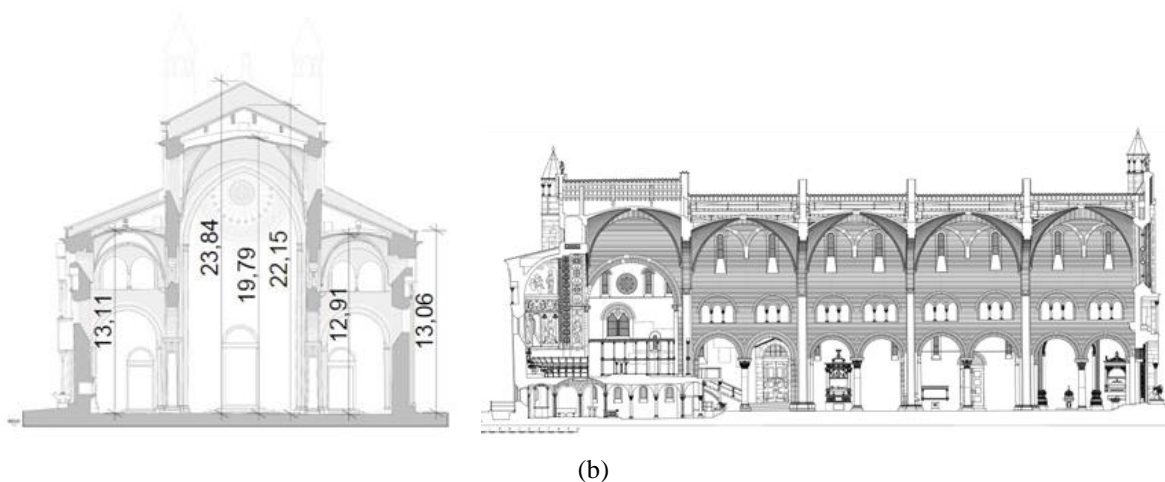
Figure 10-2: Cross-section of the Cathedral of Modena

10.3   The actual state of the Cathedral

10.3.1 The construction phases and the main interventions

The current configuration of the Cathedral is the result of various transformations and interventions that occurred on the fabric during centuries. These changes did not only affect the architecture of the Cathedral, but also influenced significantly its structural behavior. In the light of this, it is of fundamental importance to have a clear view of the most significant construction phases. Before the present Cathedral, three ones were built on the necropolis containing the tomb of St. Geminianus (the founder of the church of Modena) which is the only remaining evidence of the first one. A second Cathedral was erected in the same place around the VIII-IX century. The archaeological remains indicate that this church had a length of around 32 m and width of 18 m. The presence of polylobate piers (Bertoni 1914), discovered during past excavations, allow to suppose the existence of another Cathedral, presumably built around the XI century (Figure 10-3) (Frankl 1927).
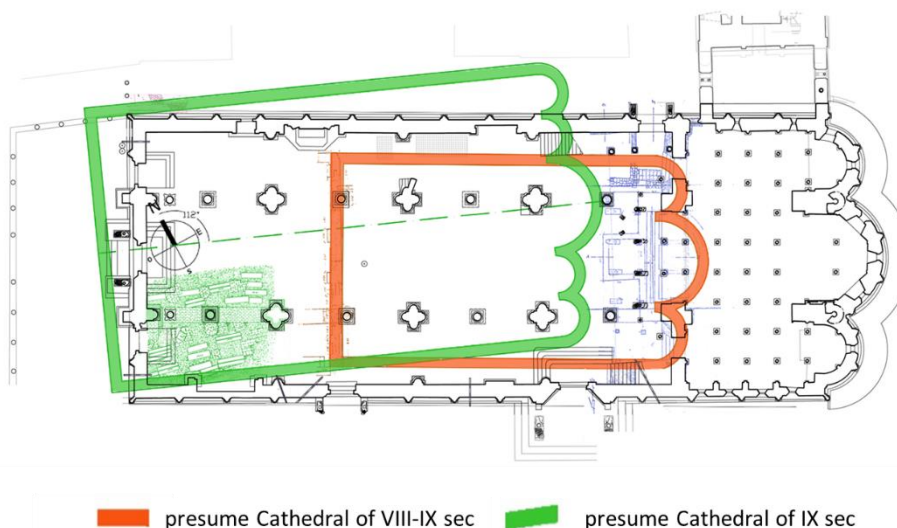
Figure 10-3: The pre-existing Cathedrals

There is an open debate about the construction phases leading to the actual fabric (Peroni 1989), (Peroni 1999), (Lomartire 1989), (Armandi 1999),(Silvestri 2013). According to the hypothesis of Porter (Porter 1917), confirmed later by other researchers, the construction began in 1099, almost in parallel, from the apses and, just few years later, from the main façade. At 1130, the complex knew the construction of the clerestory and the joining of the lateral naves where, according to Peroni (1989 and 1999) and Lomartire (1989), the initial construction was interrupted in order to maintain the portions of the pre-existing Cathedral. More recent historical studies (Silvestri 2013) suggest that the construction of the outer perimeter did not proceed in parallel from the two sides, specifically the main façade and the apses, but started from the apses (phases A) to end with the main façade (phases B), (Figure 10-4: The construction phases). In light of this alternative hypothesis, the phase C was remarked by the repair of

some damages due to early soil settlements manifested during the first two phases. This reconstruction may be further supported by the analysis of the cracking pattern. Figure 10-4 graphically represents the three construction phases according to this last hypothesis.
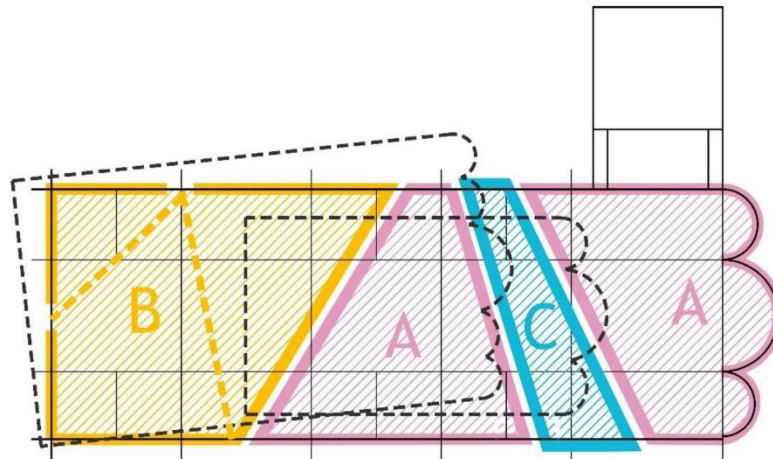
Figure 10-4: The construction phases

After the end of the construction, several interventions were carried out during the years. The elevation of the Tower in the following years caused the lowering and slight rotation of the apses due to differential soil settlements. The presbytery appeared so slanted that it was necessary to realize many reparations and reconstructions according to a new verticality and horizontality. This was one of the principal intents of the architectural renovation applied by the Campionesi masters at the Cathedral of Modena during the years 1180-1220. In the light of the studies on the construction phases, the 3D laser scanner survey was able to measure the different inclinations of the masonry walls belonging to the different phases, thus dating the successive increases of the foundation settlements along the centuries. According to several historians, the original roof system, made of timber trusses ("capriate") arranged in the transversal direction, was rebuilt after 1413. The orientation of the principal beams was changed when the vaults of the naves were constructed. Probably during this phase, the original timber beams were replaced causing deformations of the longitudinal walls. Later on, other interventions proved to be necessary after the earthquake events occurred in the 1501, 1505 1671 and 1832. The main interventions affected the vaults, the arches, the façade and the portions of walls adjacent to the Ghirlandina Tower (Dondi 1896). In the following years, additional strengthening interventions were performed, such as refilling the main cracks, repairing the roof (new wood structures connected to the masonry wall by iron chains) and connecting the walls through iron chains in the naves at different heights (Figure 10-5). At the beginning of the XX century, all the constructions built next and into the Cathedral during the years (rectory, cluster, sacristy and internal chapels) were demolished in order to restore the original Romanesque aspect. In 1975, Modena and its Cathedral were affected by the soil subsidence. During the recent years, starting from the 2006, a restoration campaign has interested the external stone facade,

until the earthquakes of the 2012 shifted the attention to the damages of the interior, principally the vaults, as it will be better explained in §11.3.4.
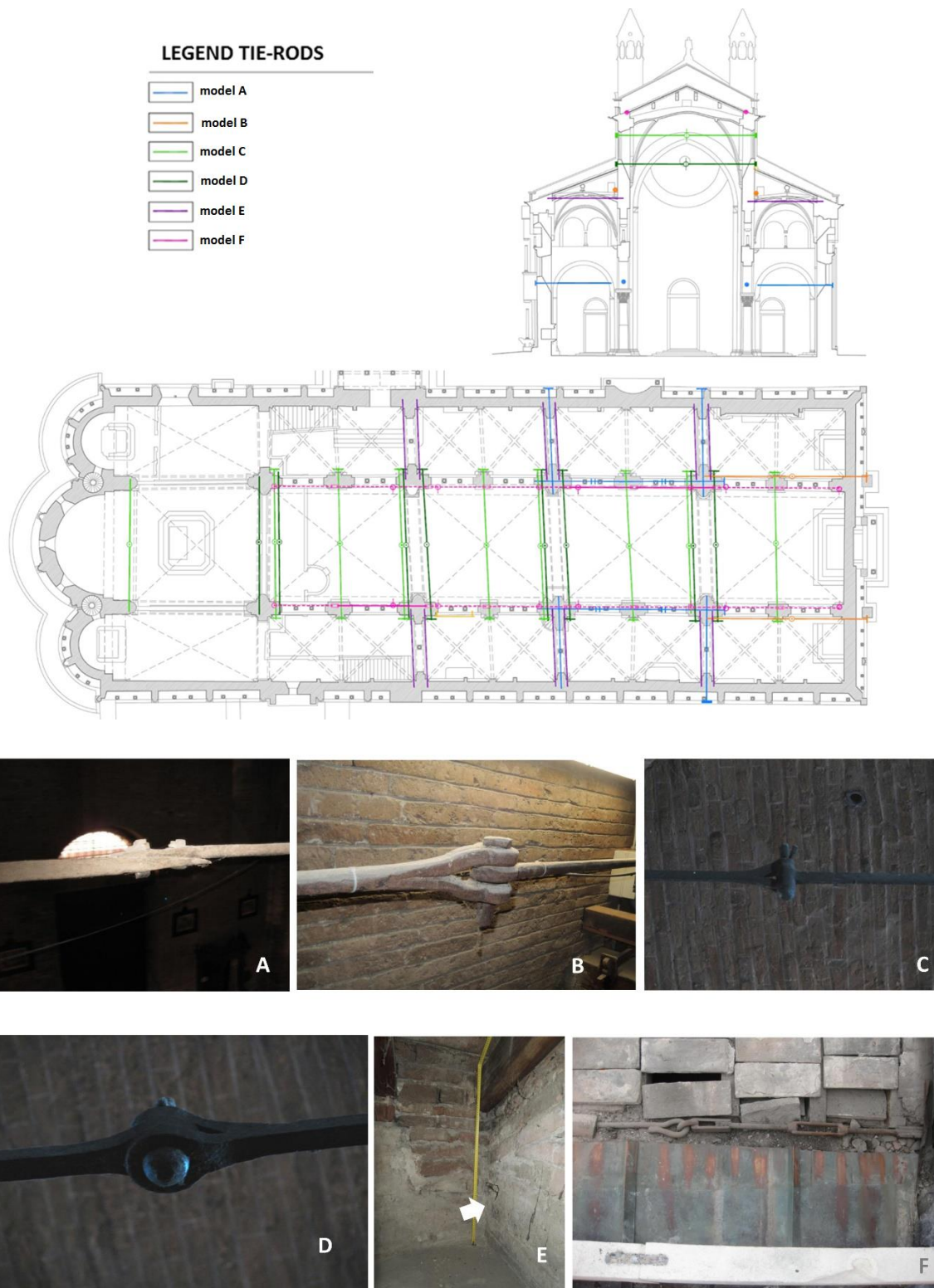
Figure 10-5: Survey of the tie-rods installed on the Cathedral during the years and respective photographers.

10.3.2 The reconstruction of the geometric configuration through laser scanner and the geotechnical investigations

A 3D laser scanner of the Cathedral was carried out to identify with accuracy walls dimensions and deviation from verticality (Castagnetti, C., E. Bertacchini, A. Capra 2011). Figure 10-6 displays the inclinations of the external wall and internal pillars as obtained from the 3D laser scanner. In general, excluding the area of the South transept, the walls are inclined towards the outside. As already clear by simple visual inspection, the overhanging increases moving closer to the Ghirlandina Tower, thus indicating a strong interaction between the Tower and the Cathedral. Notably, this interaction caused so important damages to the two masonry arches connecting the Tower with the Cathedral, at the point that they were completely reconstructed at the beginning of the last century.
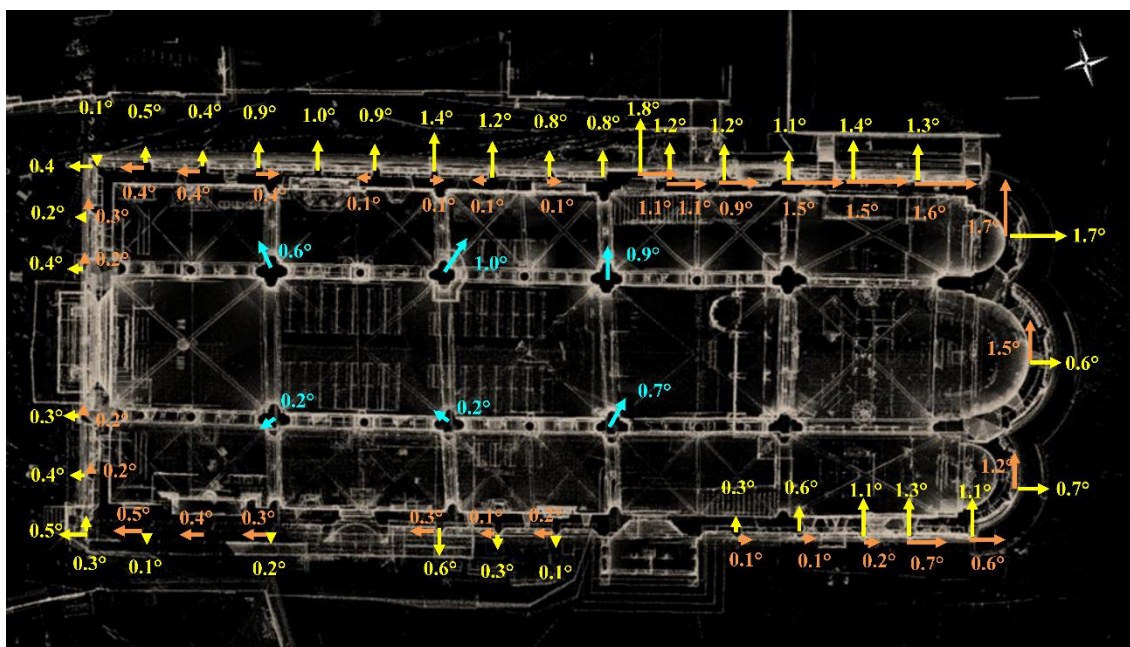
Figure 10-6: The inclinations of the external walls and internal pillars a so obtained from the 3D laser scanner.

In addition to the differential settlements induced by the interaction between the Tower and the Cathedral, also a discontinuity in the soil stiffness due to the presence of the ruins in only one portion of the plan (see Figure 10-3), could have significantly contributed to the walls deformation. Since that soil has "memory" of its previous loading history (Lancellotta 2009b), due to loading-unloading (as consequence of sequences of construction and demolitions), the soil response of these portions would be much stiffer than those parts that never experienced any previous loading-unloading. Therefore, this loading history could contribute to explain why the Cathedral suffered uneven settlements not only moving from South towards North (due to the presence of the Tower, as before explained), but also moving from East towards West. These differential settlements were also more pronounced due to the nature of the foundation soil. The soil profile were investigated up to a depth of 80 m resulting in a sequence of recently deposited alluvial horizons. The first horizon is made of medium to high-plasticity

inorganic clays with a number of millimeter-thick laminas of sands and peats. The upper portion of this horizon, which has a thickness of about 5 m to 7 m, is known as the Modena unit and it is linked to flooding events (of post-Roman era) produced by minor streams. Geological and geotechnical studies (Lancellotta 2009a),(Lancellotta 2013),(Lugli 2011) have shown events of exposition during deposition and generate layers that therefore were slightly over consolidated by desiccation. From these geotechnical investigations, also the soil mechanical properties useful for the structural analysis have been obtained. For instance, two different values of the Winkler constant may be assumed to account for the presence of a portion of more consolidated soil (see Figure 10-7).

(a)   (b)
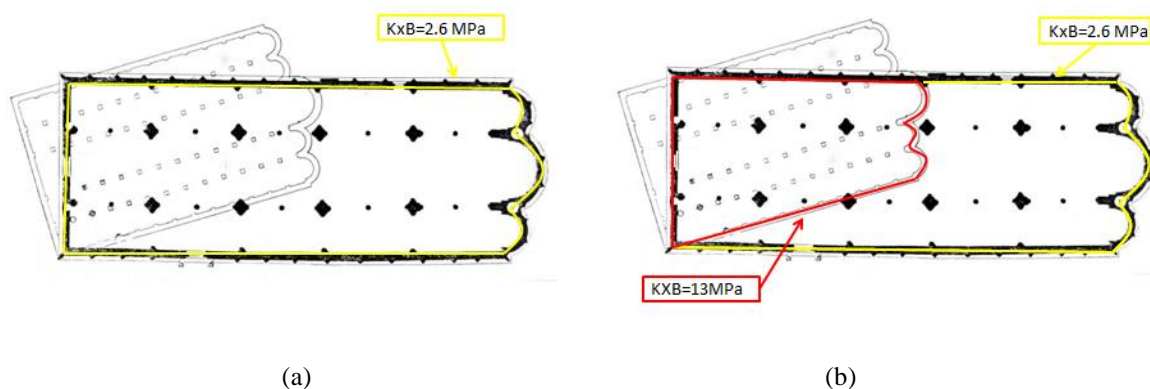
Figure 10-7: (a) Uniform distribution of Winkler's constant (W1) and (b) Non Uniform distribution of Winkler's constant (W2).

10.3.3 Material properties

It is a matter of well consolidated knowledge that the assessment of material properties of historical masonries is a rather challenging problem. Extensive destructive and non-destructive tests are typically used to evaluate material properties of ordinary existing buildings. Nonetheless, for important monuments, only limited tests are usually allowed by the local authorities in charge of the conservation of the monument. Moreover, the mechanical parameters as obtained from few non-destructive tests provide only partial and local information. This means that these few data must be critically analyzed in terms of their reliability. Therefore, experimental data have to be compared not only with values suggested by the codes or literature but as well as with values based on material models. This approach was already successfully applied to the ancient masonry "Asinelli" Tower in Bologna (Palermo et al. 2015) and has been also used in the present case. The results of video-endoscopic investigations on the facade and sonic and radar tests on the remaining walls and piers, were integrated and validated with the values suggested by the scientific literature (Tassios 1988),(Hendry 1990) or by codes (Circ. n. 617, 2009) leading to masonry and stone Young's modulus equal to E_m =1800-4000 MPa, and E_s=25000 MPa, respectively. For the timber beams, considering aging effects, the lower bounds mechanical properties have been used as suggested by the document CNR-DT 206 (Istruzioni CNR-DT 206 2007): Young's modulus E= 600 MPa, compression strength f_m=14 MPa and mean density ρ_m=350 Kg/m^3.

10.3.4 The actual state of degradation

A first detailed survey of the cracking pattern was carried out in the 2010. After the 2012 Emilia Earthquakes, the Cathedral suffered minor damages, mainly localized in the vaults. Therefore, a second survey was carried out to detect in detail the damages caused by the earthquake sequence. After this detailed survey, a strengthening intervention has been planned and the design is actually under development.

The initial crack pattern (2010) has been studied not only to monitor the state of the main cracks but also to correlate their location within the construction phases and main interventions. The analyses of past studies also helped in the classification of the cracks. In particular, the correlation between the damage and the past interventions allow to identify the probable causes and distinguish between stable cracks and still evolutionary situation. The major cracks are displayed in Figure 10-8. The main cracks are indicated in red, while grey areas indicates the zones of diffused cracks with potential high vulnerabilities. It can be noted that:

-   a large vertical crack is located in the main facade, just below the big rose window;
-   a concentration of cracks has been identified in the connection between the walls, all along the portion of the building constructed during the phase C, in the fourth span from the west;
-   another cracks concentration appears near the main facade, along a line parallel to the façade, in the second span from the west;
-   vertical cracks along the main transversal walls and arches separate the central naves from the lateral naves;

The grey areas are mainly located in the portion of the Cathedral coinciding with the location of the old Cathedrals. During the survey after the 2012 Emilia Earthquakes, new cracks appeared in the intrados of the main vaults. Moreover, an evolution of some existing cracks has been also observed (Figure 10-9).
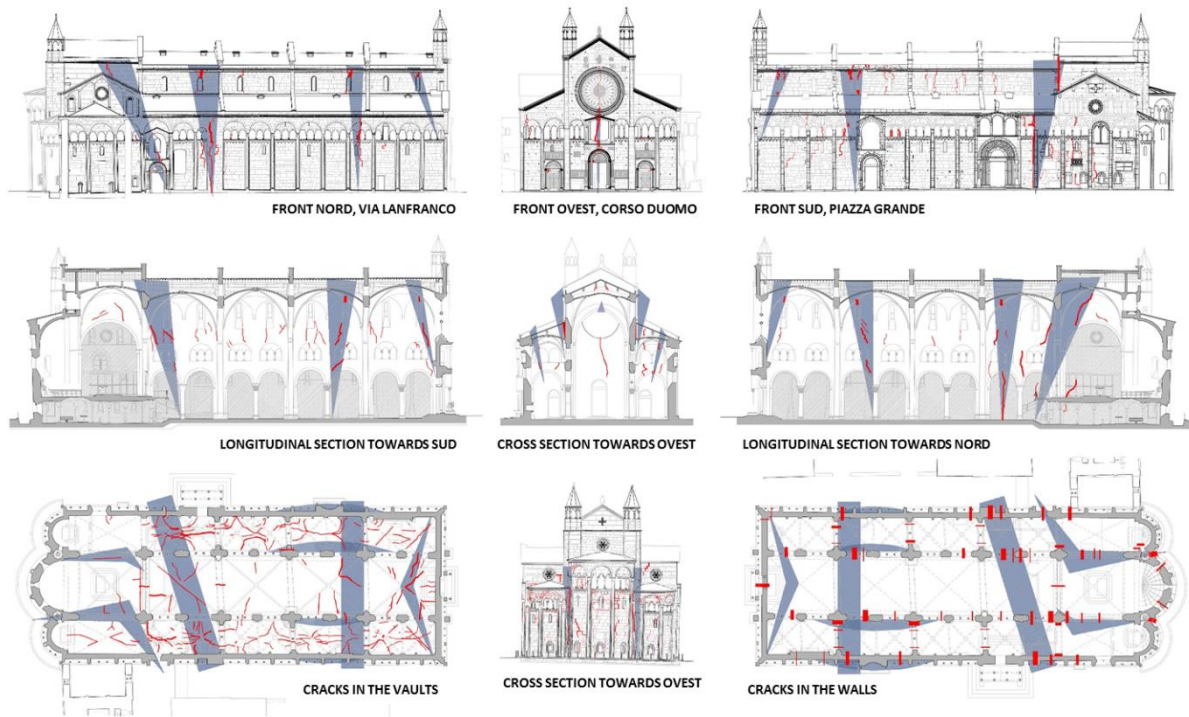
a)
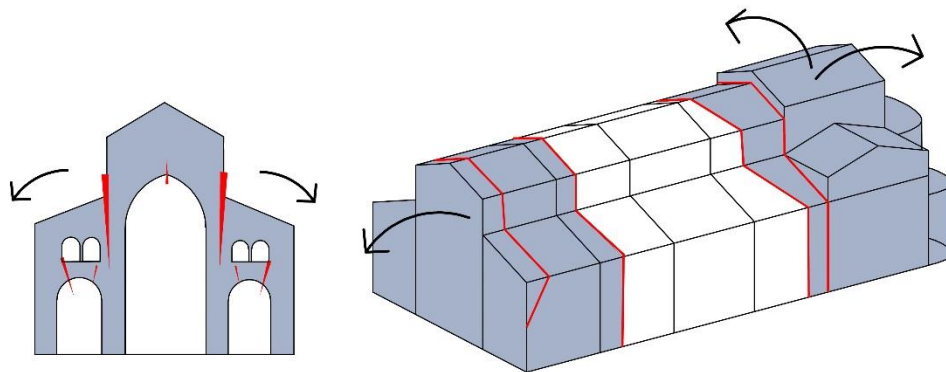
b)

Figure 10-8: (a) Crack pattern of the Cathedral of Modena and (b) main failure mechanisms of the Cathedral on the longitudinal and transverse direction

MAPS OF THE CRAKS DETECTED ON THE VAULTS-earthquakes of the 20, 29 may 2012 and 21 June 2013

20.05.2012: pga 0,04 g

— cracks reopened by the earthquake
— refilling pre-existing cracks
● material fallen to earth

29.05.2012: pga 0,04 g

— cracks reopened by the earthquake
— refilling pre-existing cracks
● material fallen to earth

21.06.2013: pga 0,02 g

— cracks reopened by the earthquake
— refilling cracks after 2012 earthquakes
● material fallen to earth

CRACKING PATTERN

a)

b)

Figure 10-9: (a) Maps of the cracks detected on the vaults after the earthquakes of the 20 and 29 May 2012 and 21 June 2013 and comparison with the crack pattern and (b) photographs on the damage caused by recent earthquakes.

10.4   Seismic Hazard analyses

The objective of the seismic hazard analysis is to compute, for a given site over a given observation time, the probability of exceeding any particular value of a specified ground motion parameter (commonly the Peak Ground Acceleration, PGA). In the case of monumental buildings, seismic hazard analysis does not allow only to predict the characteristics of possible future earthquakes, but also to obtain information on the characteristics of already occurred past earthquakes. The past seismic input

has been studied through the reconstruction and the position of the historical earthquakes that have affected the Cathedral. This analysis allows to collect information useful for the identification of the historical periods of specific cracks and failures or interventions and for the reconstruction of the history of the building. The possible future seismic input has been studied through probabilistic and deterministic seismic hazard in order to identify the most probable earthquake scenarios which can shake the site of the monuments. Typical probabilistic seismic hazard analysis (as performed according to the approach suggested by Cornell) (Cornell C.A 1968) assume that, in each point of the seismic zone area, the probability of occurrence of an earthquake is uniform. Thus, this approach is suitable for designing new buildings and for regional planning. However, it is not adequate for the identification of the seismic input to be adopted in the studies of monumental buildings, where the consequences of failure are intolerable and protection is needed against the worst that can be reasonably expected to occur. In these cases, the deterministic method is strongly recommended (Krinitzsky E.L. 1995). Two kinds of deterministic seismic hazard analyses have been performed for the site of the Cathedral of Modena:

- Historical Deterministic Seismic Hazard Analysis (HDSHA);
- Maximum Historical Earthquake Analysis (MHEA);

These analyses have been based on the following data: the ZS9 zoning (subdivision of the Italian Territory):

- the Cathedral of Modena is located in the zone 912 (http://zonesismiche.mi.ingv.it/);
- the CPTI04 earthquake catalogue (http://emidius.mi.ingv.it/CPTI04/);
- the Sabetta-Pugliese attenuation law (Sabetta & Pugliese 1987);
- the Gutenberg-Richter recurrence law (Gutenberg & Richter ,C. F. 1949).

10.4.1 Historical Deterministic Seismic Hazard Analysis (HDSHA)

HDHSA has the objective to reconstruct the intensity of historical earthquakes that have actually affected the Cathedral of Modena in the past centuries. Significant historical earthquakes have been selected from the CPTI04 earthquake catalogue, through the following criteria:

- earthquakes that occurred within 20 km from the Cathedral;
- earthquakes characterised by the greater magnitude that occurred in the ZS9 seismogenetic zones near to the site of the Cathedral;
- significant earthquakes in relation to the historical information.

Table 10-1 shows these significant earthquakes of the past and the reconstruction of their Peak Ground Accelerations, in correspondence of the site of the Cathedral, as obtained using the Sabetta-Pugliese attenuation law. Based on the five past earthquakes with epicentre in Modena (4 earthquakes with epicentre in Modena respectively in the years 1249, 1474, 1660, 1850 and the earthquake of the Appennino Modenese of 1501), it can be stated that the cathedral might have been hit by accelerations

around 0.15 g. The earthquake of 1249 was the most violent and might have rocked the Cathedral with an acceleration of approximately 0.20 g. Figure 10-10 shows the reconstruction of the median of the PGA, obtained considering the epistemic uncertainty associated to the Sabetta-Pugliese ground motion prediction model, for all earthquakes of the CPTI04 earthquake catalogue. Inspection of Figure 10-10 indicates that, looking at the past, the earthquake with acceleration between 0.15 g and 0.20 g is characterized by a return period of about 200-250 years.

Table 10-1- Reconstruction of peak Ground Acceleration (PGA) in correspondence of the site of the Cathedral of Modena for the selected earthquakes

Selection criteria	N.	Year	Location Name	Seismogenetic zone (ZS9)	R [Km] (distance)	Msp (magnitude)	PGA mode	PGA median	PGA mean value	PGA percentile 80%
Earthquakes that occurred within 20 km from the Cathedral	53	1249	**Modena**	912	0.65	4.80	0.200	0.245	0.270	0.360
	171	1474	**Modena**	912	0.12	4.61	0.170	0.211	0.232	0.310
	195	1501	Appennino	913	16.37	5.82	0.140	0.170	0.187	0.250
	279	1586	Spilamberto	913	10.86	4.53	0.070	0.083	0.091	0.120
	362	1660	**Modena**	912	0.12	4.25	0.130	0.156	0.172	0.230
	374	1671	Rubiera	912	14.26	5.23	0.100	0.117	0.129	0.170
	720	1811	Sassuolo	913	23.49	5.09	0.050	0.066	0.072	0.100
	871	1850	**Modena**	912	5.66	4.53	0.110	0.131	0.144	0.190
	984	1873	Reggiano	913	25.29	4.93	0.040	0.053	0.059	0.080
	1739	1923	Formiggine	913	15.20	5.05	0.080	0.095	0.105	0.140
	1808	1928	Carpi	912	17.83	4.54	0.040	0.054	0.059	0.080
	1859	1931	Modenese	913	15.80	4.54	0.050	0.060	0.066	0.090
	1897	1934	Vignola	913	19.38	4.06	0.030	0.033	0.037	0.060
	2237	1967	Formiggine	913	9.21	4.09	0.050	0.065	0.072	0.100
Earthquakes characterised by the greater magnitude that occurred in the ZS9 seismogenetic zones near to the site of the Cathedral	393	1688	Romagna	912	116.68	5.85	0.020	0.025	0.028	0.390
	30	1117	Veronese	906	82.03	6.49	0.050	0.062	0.068	0.090
	776	1828	Valle dello	911	209.68	5.55	0.010	0.011	0.012	0.050
	195	1501	**Appennino**	913	16.37	5.82	0.140	0.170	0.187	0.250
	278	1584	Appennino	914	147.54	5.99	0.020	0.023	0.025	0.230
	1708	1920	Garfagnana	915	88.64	6.48	0.050	0.057	0.062	0.090
	988	1873	Liguria	916	73.43	5.47	0.020	0.029	0.032	0.060
Significant earthquakes in relation to the historical information	47	1222	Basso	906	96.77	6.05	0.030	0.036	0.040	0.060
	202	1505	Bologna	913	40.57	5.41	0.040	0.050	0.055	0.080
	1499	1909	Bassa	912	85.20	5.48	0.020	0.026	0.028	0.400
	1684	1919	Mugello	915	99.06	6.18	0.030	0.040	0.043	0.060
	2509	1996	Correggio	912	30.95	5.26	0.050	0.058	0.064	0.090
		2012	Finale Emilia	912	43.42	5.90	0.060	0.071	0.078	0.110
		2012	Medolla	912	28.97	5.80	0.080	0.097	0.107	0.150
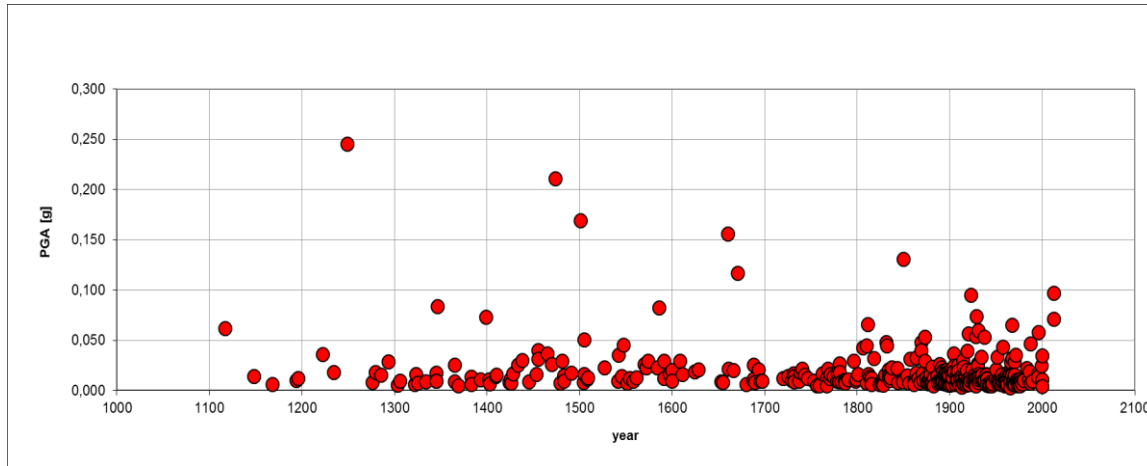
Figure 10-10: Reconstruction of the median of the PGA, obtained considering the epistemic uncertainty associated to the Sabetta-Pugliese ground motion prediction model, for all earthquakes of the CPTI04 earthquake catalogue.

10.4.2 Maximum Historical Earthquake Analysis (MHEA)

The MHEA is aimed at estimating the most violent earthquake that could occur in the future on the specific site of the Cathedral. The PGA recorded in a specific site during an earthquake depends on two factors: the magnitude and the distance between the epicentre and the site. Therefore, the worst seismic scenario for a specific site occurs with the combination of the high magnitude and null epicentre-site distance. The maximum magnitudes recorded in the past in the seismic zone (912) of the Cathedral and in the adjacent zones (913, 914, 915, 916, 911 and 906) were obtained from the earthquake catalogue. Then, it is assumed that earthquakes of such magnitudes could occur at zero distance from the Cathedral, and the intensity of the earthquake worse future is reconstructed considering the epistemic uncertainty associated to the Sabetta-Pugliese ground motion prediction model. Table 10-2 shows the list of the highest magnitudes occurred in all the considered zones and the reconstructed median, mode, mean values and 80% percentile values of the PGA variable. According to seismic activity of the two areas 912 and 913, it can be stated that a future earthquake with acceleration of about 0.50 g can occur, as shown in the Figure 10-11.

Table 10-2- Estimation, through MHEA, of the PGA that can occur in the future in the site of the Cathedral of Modena

ZS zoning	Rmin from Cathedral	Mas max	Msp max	Mode	Median	Mean value	80% percentile
912 (zone of Cathedral)	0.00	5.85	5.85	0.49	0.60	0.65	0.87
913	2.96	5.82	5.82	0.41	0.50	0.55	0.73
914	67.50	5.99	5.99	0.04	0.05	0.05	0.08
915	54.67	6.48	6.48	0.08	0.09	0.10	0.14
916	75.48	5.32	5.47	0.02	0.03	0.03	-
911	99.35	5.55	5.55	0.02	0.02	0.03	-
906	72.12	6.49	6.49	0.06	0.07	0.08	0.11

(a)   (b)
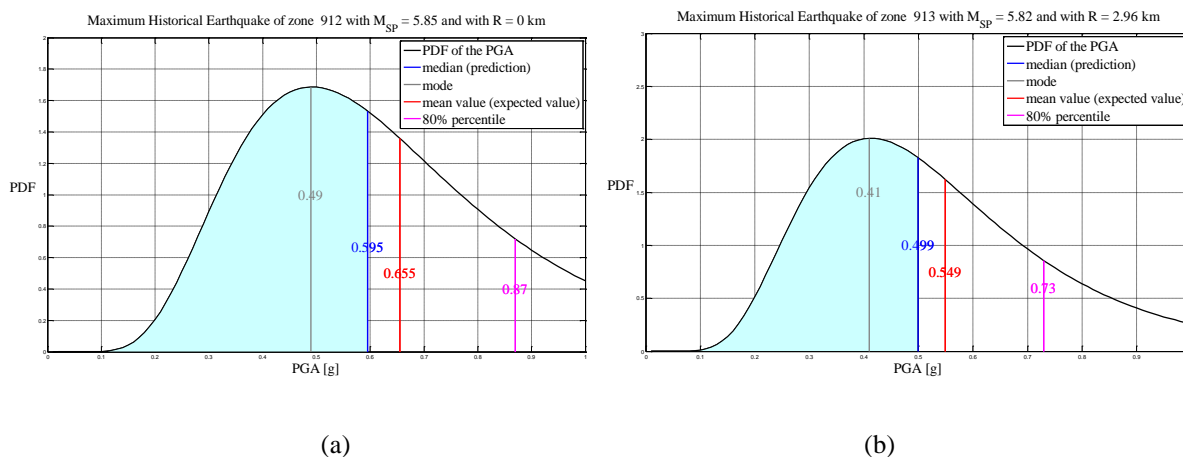
Figure 10-11: Probability density function (PDF) of the PGA in the site of the Cathedral of Modena as a result of seismic activity of zones: (a) zone 912, (b) zone 913.

10.5 The seismic input

The 20th May 2012, at 02:03:53 (UTC), Emilia Romagna region (Northern Italy) was struck by an earthquake of magnitude M=5.9 (latitude 44.890 longitude 11.230). The main shock was preceded by a M= 4.1 event on 19th May and followed on the 29th May 2012 by a 5.8Mw earthquake with epicentre 15km North West of the former event (Figure 10-12a). Several events with magnitude $4.0 \leq Ml \leq 4.5$, plus several other minor earthquakes, occurred in the same area the following days, as reported in Italian Instrumental and Parametric Data-Base (ISIDe),(Dolce et al. 2012). As reported, this earthquake sequence has caused a lot of damage / collapse in the monumental building, including the Cathedral of

Modena. The cathedral has been considered, first, as a model of itself with the purpose of understanding its intrinsic structural behaviour. For this reason, the strong motions of the main shock recorded by the station of Modena (code MDN) have been used in some of the next analyses developed on the Cathedral. The localization of the recording station MDN is reported in Figure 10-12.

(a)   (b)
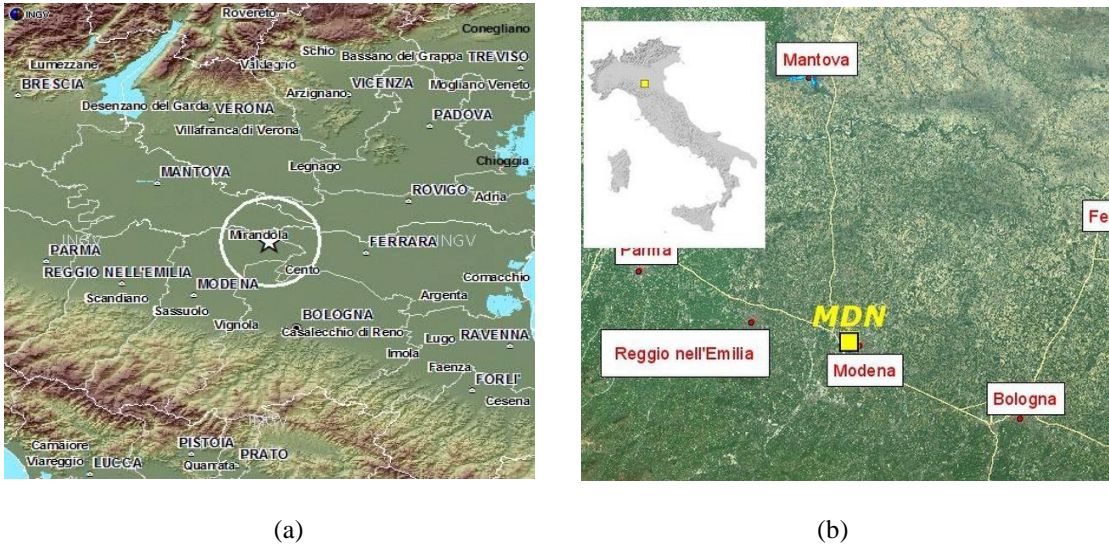
Figure 10-12(a) Location of epicentre of May 29th earthquake (INGV), (b) Localization maps of the recording station in Modena (MND)

Figure 10-13 display the acceleration as recorded by MDN station during the main shock of 20th May and used in the dynamic analyses of the Cathedral and the corresponding spectral acceleration and the spectral displacement.

(a)

(b)   (c)
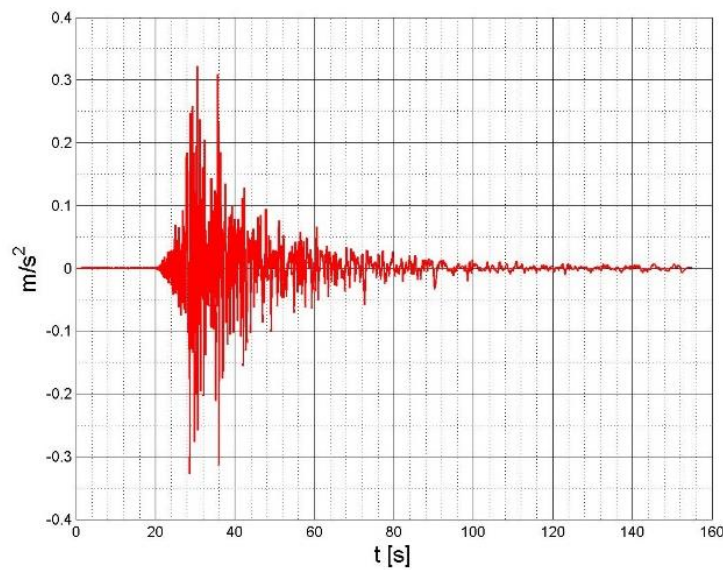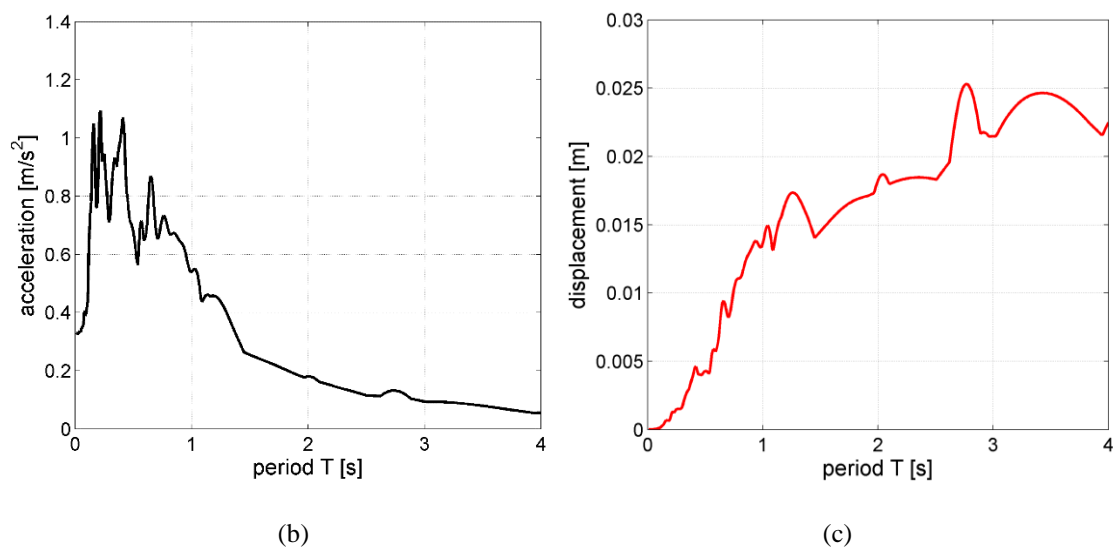
Figure 10-13: (a) The acceleration recorded by the station MDN during the main shock of 20th May 2012, (b) the corresponding spectral acceleration and (c) the corresponding spectral displacement

10.6 Conclusions

The integrated knowledge of a monument is the first step to develop consistent structural analyses and, thus, to understand correctly its structural health. The knowledge process developed for the cathedral highlighted the important role played by the following three aspects

- the presence of previous Cathedrals that gave rise to uneven settlements of the actual one, due to the influence of soil behaviour as a "material with memory";
- the construction phases; and
- the interaction with the Ghirlandina Tower.

These aspects strongly influence the structural behaviour of the cathedral and must to be considered in the structural analyses. Moreover, the seismic hazard analyses allowed reconstructing the intensity of the earthquakes that occurred on the cathedral in the past. Historical Deterministic Seismic Hazard Analysis has highlighted that four important earthquakes (peak ground acceleration around 0.15 and 0.25g) and 20 earthquakes of medium intensity (peak ground acceleration around 0.05 g e 0.10) have hit the cathedral during its life. The comparison with the historical evidence revealed that for the important earthquakes the Cathedral has reported consistent damages, which interested particularly the vaults and slender pinnacles. For earthquakes of medium-low intensity (as the 2012 earthquake) slight damages have been detected always mainly on the vaults and slender pinnacles.

Chapter 11

11 Cathedral of Modena: global structural behaviour

11.1 Introduction

The information obtained from the integrated knowledge have been used to study the global structural behaviour of the cathedral, i.e. recognize the structural elements and the actual load paths, to identify the materials properties and the appropriate restrain at the base. Different analyses (simple, but more reliable limit schematizations, and more complex, but too much sensitive to uncertainties, computer-based models) have been conducted on the global structure of the masonry fabric in order to identify the main static and seismic vulnerabilities.

11.2 The models and the simulations

The static behaviour of the cathedral has been investigated through simple limit schematizations and Finite Element models of increasing complexity (2D models, 3D models with fixed base, 3D models accounting for the soil-structure interaction). Due to the complexity of the monument and the relevant influence of different factors (such as construction phases, soil properties, existing cracks, interaction with the Tower, as highlighted in §10), instead of a unique 3D FE model in which all factors are simultaneously taken into account, several specific 3D FE models have been performed to separately investigate, the effects of each single factor. The results of the static analyses as obtained from FE models, validated through the simple static analyses performed on the substructures, have been used to interpret the cracking patterns as obtained from in situ surveys and the deformations related to changes in the geometrical configuration as obtained from the topographic surveys§10. In addition, on the 3D FE model able to better represent the static behaviour of the cathedral various seismic analyses have

been carried out in order to assess its seismic vulnerabilities. The analyses developed are summarized in Table 11-1.

Table 11-1- The different analyses developed

Model-Element	Analysis
Hand –made schematization of the roof system	Static analysis
Hand –made schematization of the main vertical elements	Static analysis
2D FEM model of the vertical elements	Static analysis
3D FEM models with different restrain at the base and load cases	Static analysis
3D FEM models	Natural frequency analysis
3D FEM models-input consistent with the SHA§10.4	Response spectrum, time history analysis
3D FEM models-input recorded during the 2012 earthquake§10.5	Time history analysis

11.3 Static analyses

11.3.1 The applied loads/actions

The effect of the gravity loads (also considering thermal effects) have been considered in the structural static analysis. The assessment of the monument against the other possible environmental loads is out of the scope of the present work. The vertical load due to snow has been estimated equal to 1.20 kN/m^2 according to the Italian building code (NTC 2008). In addition to the above described loads also the interaction between the Cathedral and the adjacent Ghirlandina Tower has been accounted for (even if, at this stage, in a rather simple way) by imposing a profile of differential vertical displacements at the base of the Cathedral, as provided by the geotechnical studies mentioned in §10.3.2. In detail, the differential displacements have been imposed in the portion closest to the Ghirlandina Tower (Figure 11-1), the vertical displacements being equal to 20 cm at corner H, 27 cm at corner G, and 30 cm at corner F. Linear variations of vertical imposed displacements have been assumed between the above mentioned points, as well as moving from the side to the center of the Cathedral.
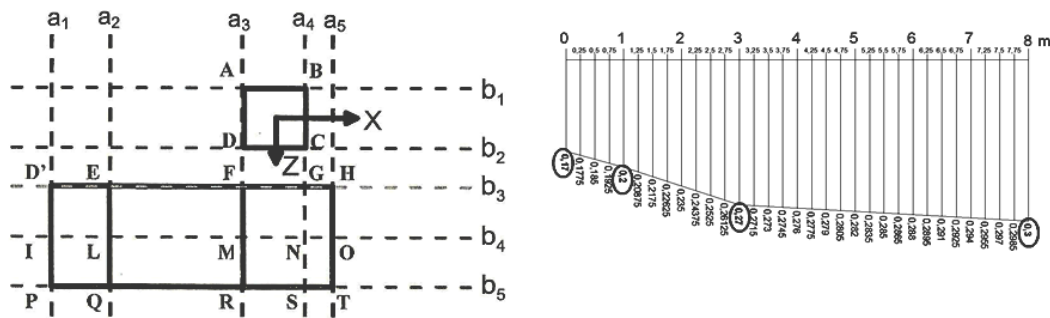
Figure 11-1: Imposed vertical differential displacements at the base due to the interaction between the Cathedral and the Ghirlandina Tower

11.3.2 Structural analysis with simple models

Simple limit schematizations have been developed for a preliminary structural analysis of the roof system and the main vertical resisting elements (i.e. walls and stone piers). Each substructure is analyzed with the purpose of obtaining the stress state of the main structural elements.

11.3.2.1 The roof system

The roof (Figure 11-2) is made of timber principal beams arranged in the longitudinal direction (indicated as Ti), which find additional supports on underlying timber beams or timber trusses - "capriate"- (indicated as ti). The roof system, transferring the gravity loads directly to the masonry walls and stone piers, is covered by thin-masonry non-structural vaults withstanding only their self-weight. It should be noted that the increment of loads (both vertical loads and thrusts) due to the presence of the vaults is negligible.

a)
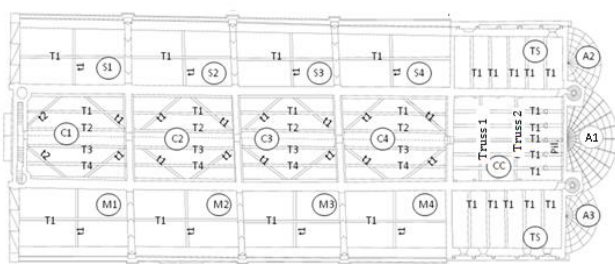
Figure 11-2: a) A 3D view of the roof system; b) Structural roof elements and c) Main beams (T_i) and trusses system (t_i)

Making use of this geometry, a simple static analysis has been performed of the roof system solely in order to evaluate the stress levels and the reactions at the base of the roof (which are then applied as loads on the masonry walls). The maximum normal stresses for the main timber beams due to self-weight only are about 5 MPa for the beams of central nave, 8 MPa for the beams in the transept, 10 MPa for the beams of the aisles. The addition of the snow load lead to an increase in the maximum stresses of about 35% leading to stresses close to the material strengths. In detail, Figure 11-3 shows the stress levels (in a color scale) of the roof beams. The stress levels in the secondary elements (trusses) are about 1 and 1.5 MPa, well below the material strengths. It is worth to note that, due to the absence of specific tests performed on the wood elements, the assumed strength is conservative.
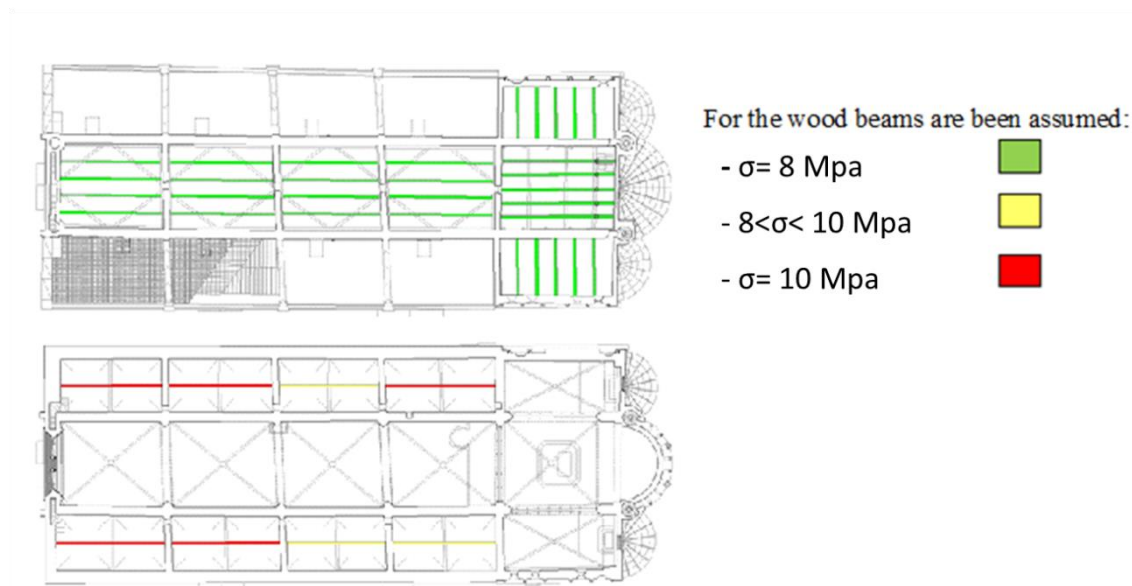
Figure 11-3: Stress level of the roof elements

11.3.2.2 The vertical resisting elements

The vertical resisting elements of the Cathedral are the masonry walls, the masonry piers and the stone columns. The masonry elements are characterised by non-uniform geometry (variations in thickness) and non-uniform mechanical properties. These discontinuities may lead to significant stress concentrations, and, in order to account for the presence of these geometrical discontinuities, in addition to homogeneous regular hand-made schematization, 2D FE models of each single wall have been also developed, assuming an ideal vertical configuration. These planar models are used to develop in-plane analysis aimed at evaluating the stress levels in the walls.

The hand-made schematizations of the single walls are used to calculate the stresses at the wall base, according to the Navier - de Saint Venant formulation, due to the self-weight, the weight of the vaults and the reactions of the roof system. In detail, the following assumptions have been made: (i) two limiting conditions: full cross-section and hollow cross-section (or "a sacco", i.e. two exterior masonry layers plus an interior layer composed of chaotic stones and filling materials; in the "a-sacco" configuration the wall inertia is equal to the inertia of the two exterior layers only); (ii) constant wall thickness equal to the average wall thickness; (iii) the presence of decorative elements has been neglected; (iv) each wall has been subdivided into homogeneous portions (i.e. same cross-section, referred to as ai, i=1,…,28) for the evaluation of the normal average stresses at the base, (iv) perfect verticality of the masonry walls. In the limiting case of full cross-section, the normal stresses due to the gravity loads are between 0.3 and 0.8 MPa for exterior walls and between 1 and 1.4 MPa for masonry piers. On the other hand, in the limiting case of hollow cross-section ("a sacco" masonry), the normal stresses due to the gravity loads double both for the external walls and the internal piers. The maximum stress at the base of the stone columns is around 3.2 MPa. The increase due to the snow load is about 2.5% of the stresses due to gravity load. These stresses levels at the walls base obtained from simple hand-made models (Figure 11-4) have then been compared with those obtained from the 2D FE models, which are reported in terms of contour maps in Figure 11-5. This comparison indicates a good agreement between the two analyses.
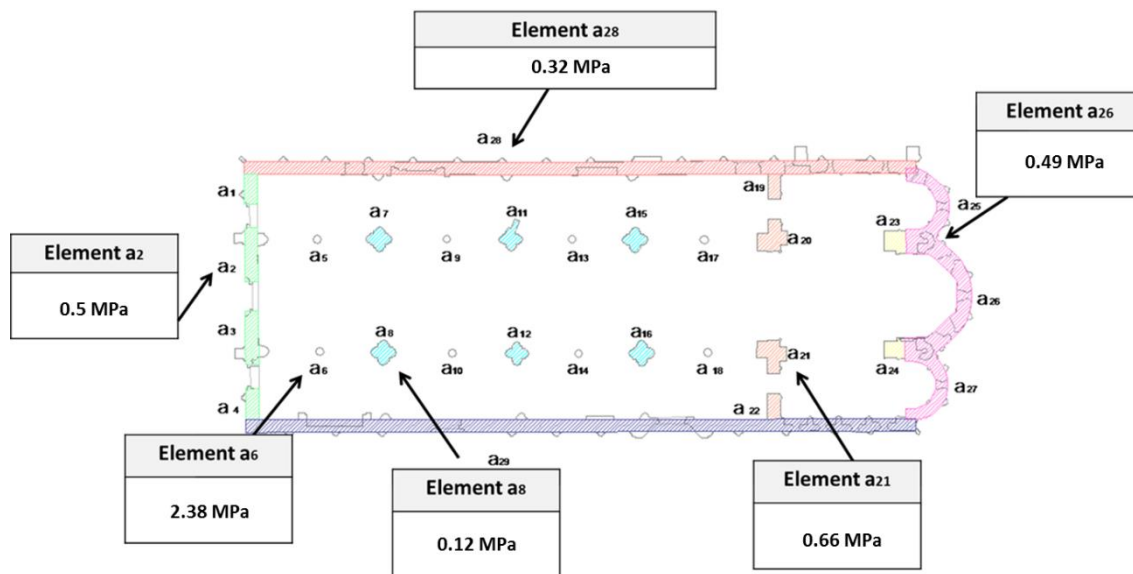
Figure 11-4: Reference values of the stress level at the base of the principal structural elements.
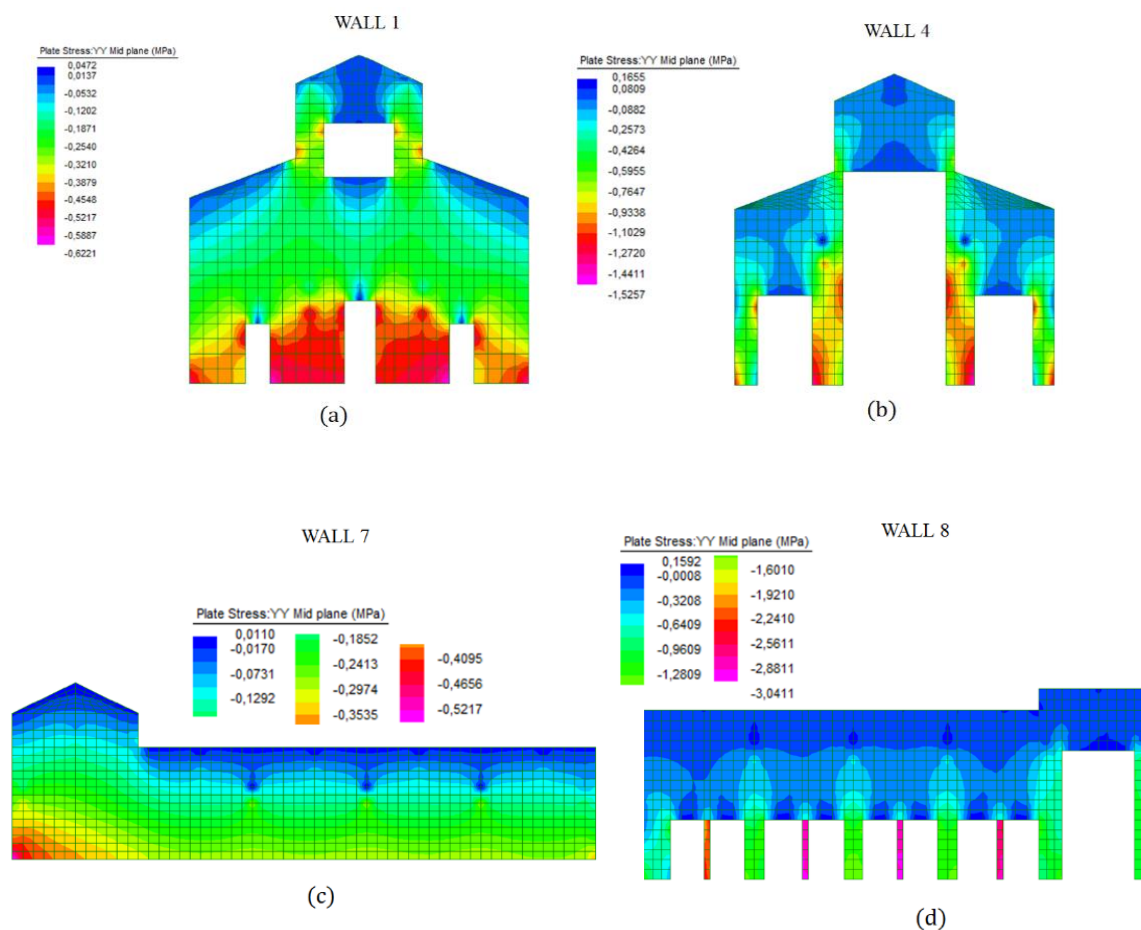
Figure 11-5: Contour maps of the normal stresses at the base of some walls obtained with two-dimensional FE models: (a) Wall 1; (b) Wall 4; (c) Wall 7; (d) Wall 8;

The 3D laser scanning showed significant inclinations of the longitudinal walls. Consequently, the walls are subjected to additional stresses due to the imperfect verticality. To account for this effect in a rather simplified way, the second order bending moments due to the eccentricity corresponding to the measured overhangs (Figure 11-6) have been included in the evaluation of the stresses. Figure 11-7 provides a schematic plan indicating the percentage increment of the normal stresses at the base of the walls and pillars due to their inclination (values are evaluated with reference to the hand-made models). The green color represents increments below 30%, the yellow color represents increments between 30% and 70%, while the red color represents increments larger than 70%. The ranges of the normal stresses at the base of the masonry walls and pillars, including also the effect of walls inclinations, are provided in the plan schematization displayed in Figure 20. Maximum stresses are around 1.5 MPa for the masonry walls and 9 MPa for the stone pillars. All values are well below material strengths.
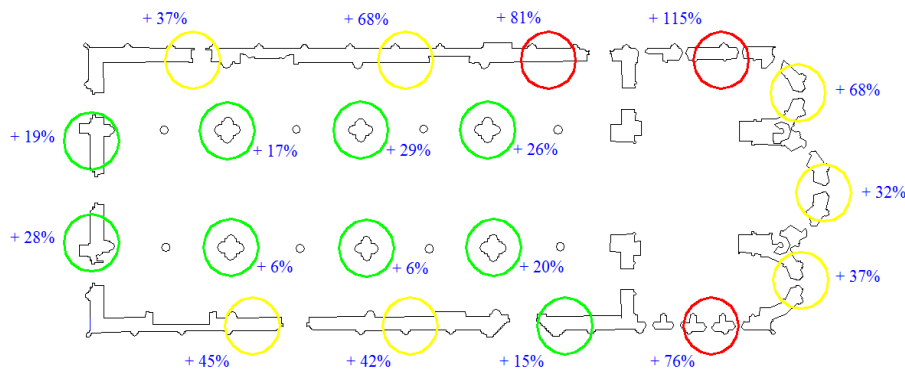
Figure 11-6: Increments of the stress at the base of the walls due to the inclination of the vertical elements.
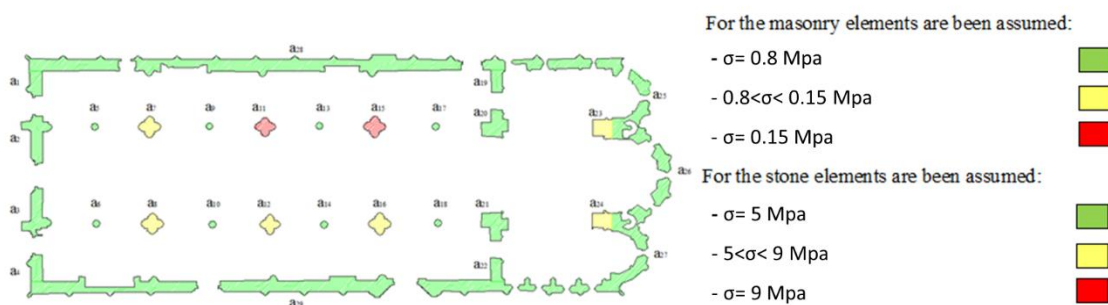
Figure 11-7: Level of stress at the base of the vertical elements including the effects of the inclinations

To simply evaluate how the presence of the arches in the transversal walls may contribute in the overall inclination of the wall, the thrusts of the arches have been calculated by assuming a simply supported arch schematization subjected to a uniform distributed load (due to the loads transmitted by the roof and the vaults). Then, the lateral forces corresponding to the calculated thrusts have been applied at the top of each corresponding wall in order to evaluate the lateral deflection, assuming a cantilever configuration and a tributary resisting wall width of 1.25 m, and thus neglecting the presence of the chains. The angle of inclination corresponding to the lateral deflection (with reference to the chord) has been compared with the measurements from the 3D laser scanning (Figure 11-8). It can be noted that

the contribution due to the thrusts, in the case of not effective chains, is significant and, in the undisturbed areas (near the façade, where the interaction with the Ghirlandina Tower is weak and the soil is more uniform) is close to the measured one. Larger discrepancies appear in the areas closer to the Ghirlandina Tower where the interaction with the Tower is more relevant or where the chains could be more effective. It has to be noted that the choice of the tributary width significantly affects the estimation of the maximum out-of-plane deformations. A tributary length of 1.00 m can be considered as a lower bound, thus leading to conservative (i.e. reasonably larger) estimations.
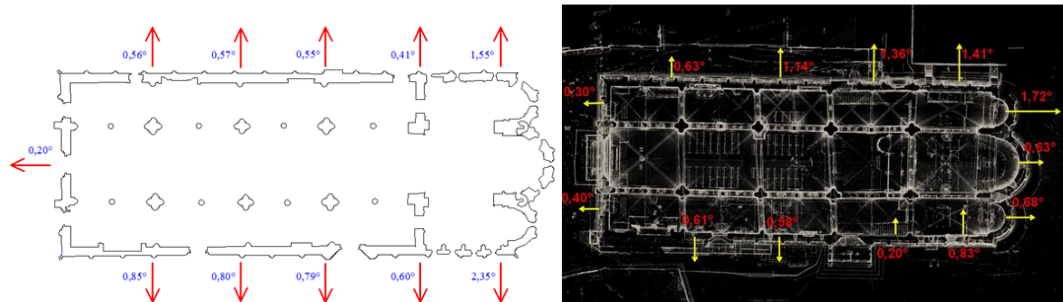
Figure 11-8: Comparison between the calculated inclinations due to only the lateral thrusts of the arches and those measured by 3D laser scanner

11.3.3 Structural analysis with 3D finite element models

Several 3D FE models have been developed to separately investigate, the effects of each single factor that could be influence the structural response of the cathedral. Once the importance of each single effect has been quantified, a unique 3D FE model has been developed in order to account for the interaction of all effects. All the models have been developed assuming: (i) homogeneous and elastic material characterized by the properties summarized §10.3.3; (ii) full cross-section masonry walls; (ii) average value of the thickness for each wall; (iii) architectural elements are not included in the model; (iv) the roof system and the vaults are not directly modeled and considered only in terms of applied vertical loads (in this respect, note that, on the contrary, the masonry arches both in the longitudinal and in transversal directions have been directly modeled). In more detail, the following types of restraints at the base have been considered to progressively investigate the soil-structure interaction:

- Fixed-base condition (F): the soil is assumed to be infinitely stiff in both vertical and horizontal directions;

- Roller-type base supports (R): the soil is assumed to be rigid in the vertical direction and with negligible lateral stiffness;

- Winkler type 1 base supports (W1): all the foundation soil is assumed to have a unique constant vertical stiffness (i.e. Winkler spring constant equal to KxB=2.6 MPa as displayed in Figure 10-7(a), with B equal to the wall thickness); the lateral stiffness is assumed to be proportional

to the applied axial load up to an horizontal displacement equal to 4 mm (i.e. a non-linear spring characterized by an elastic-perfectly plastic behavior has been assumed, as shown in Figure 11-9);

-    Winkler type 2 base supports (W2): two different vertical stiffness values are used to account for the presence of the ancient Cathedral of the XI century (i.e. Winkler spring constants equal to KxB=2.6 MPa and KxB=13 MPa as displayed in Figure 10-7(b); the same non-linear horizontal springs adopted in the W1 type supports have been used.
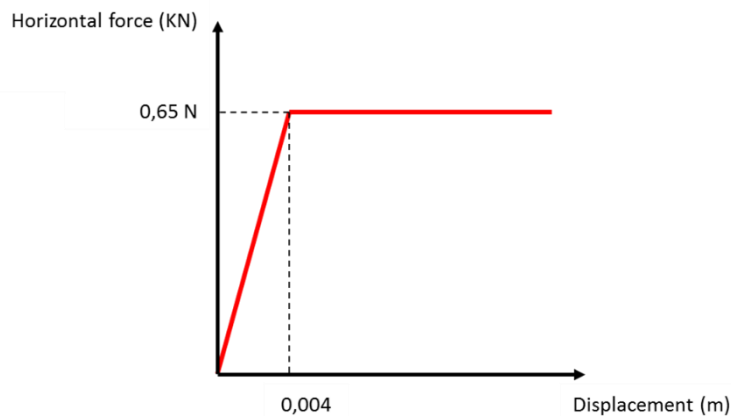
Figure 11-9: Elastic-perfectly plastic behaviour of the soil

Two geometrical configurations have been developed:

-    Undamaged configuration (UD-C);
-    Cracked configuration (C-C).

In the C-C configuration, the walls are characterized by discontinuities, which represent the main existing cracks as obtained from the in-situ inspections §10.3.4.

The response to the following single load cases have been evaluated for all models:

-    Vertical loads (V);
-    Thermal effects (T);
-    Imposed differential Displacements (D) at the base representing the interaction between the Cathedral and the Ghirlandina Tower.

As above explained, the separate analyses of each single load case and the successive combination of these elementary contributions allow a more in-depth interpretation of the possible causes of the main cracks. Table 11-2 summarizes the different models, constraints imposed at the base and the different load cases used to perform the static analyses. For instance, in order to better clarify the nomenclature introduced in Table 11-2, the response of the undamaged configuration with the fixed based condition subjected to vertical loads will be referred to as UD-C+F+V.

First, a brief overview of the most relevant aspects of the single models is presented. Then, the most relevant results of the more representative models are reported. As expected, the restraints at the base which better allow to simulate the actual behaviour of the Cathedral (i.e. to provide the most reasonable justification of the main cracks detected with the survey) is the one referred to as W2. In general, the models, which account for the initial presence of the main cracks does not lead to significant discrepancies in terms of maximum stresses. Therefore, in the following the attention will be focused on the W2 restraint and on the UD-C configuration.

Table 11-2- Summary of the specific models with a specific restrain and a specific load cases provide a specific response developed.

Model and Base Restraints	Model Response			
	Vertical loads (V)	Thermal stresses (T)	Imposed disp. (D)	Combination (C = V+T+D)
UD-C + F	UD-C + F+ V	UD-C + F +T	UD-C + F+ D	UD-C + F+ C
UD-C + R	UD-C + R +V	UD-C + R +T	UD-C + R +D	UD-C + R +C
UD-C + W1	UD-C + W1 +V	UD-C + W1 +T	UD-C + W1 +D	UD-C + W1 +C
UD-C W2	UD-C + W2 +V	UD-C + W2	UD-C + W2 +D	UD-C + W2 +C
C-C + F	C-C + F+ V	C-C + F+ T	C-C + F+ D	C-C + F+ C
C-C + R	C-C + R +V	C-C + R +T	C-C + R +D	C-C + R +C
C-C + W1	C-C + W1 +V	C-C + W1 +T	C-C + W1 +D	C-C + W1 +C
C-C W2	C-C + W2 +V	C-C + W2	C-C + W2 +D	C-C + W2 +C

The stress state for a specific longitudinal wall and transversal wall as obtained from the UD-C + W2 considering all single load cases is summarized in Figure 11-10 and Figure 11-11. It can be noted that the locations of the peaks of the tensile stresses are in good agreement with the location of the main cracks.
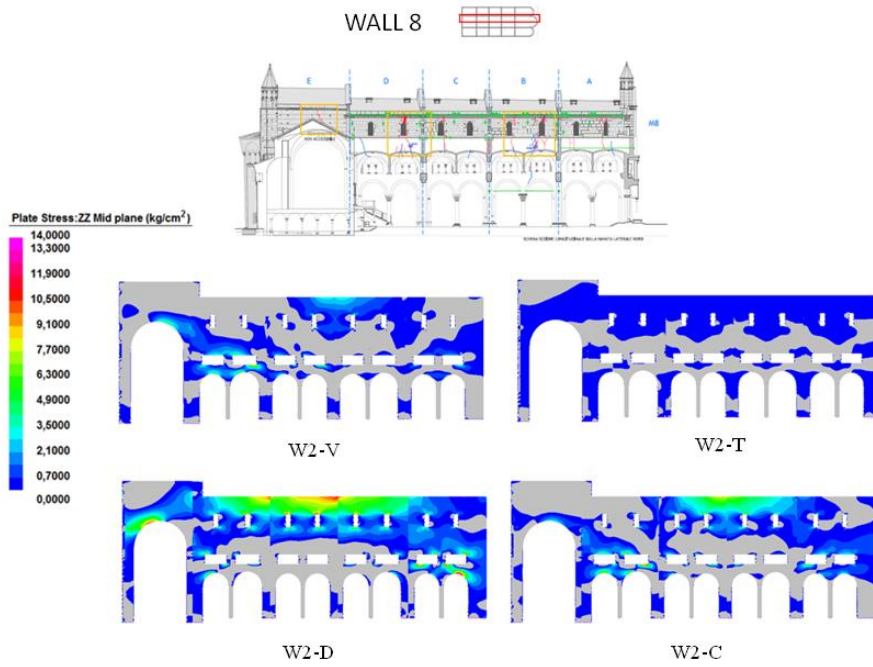
Figure 11-10: Stress of Wall 8 obtained from the W2 model with the different load cases and compared with the observed cracking patterns.
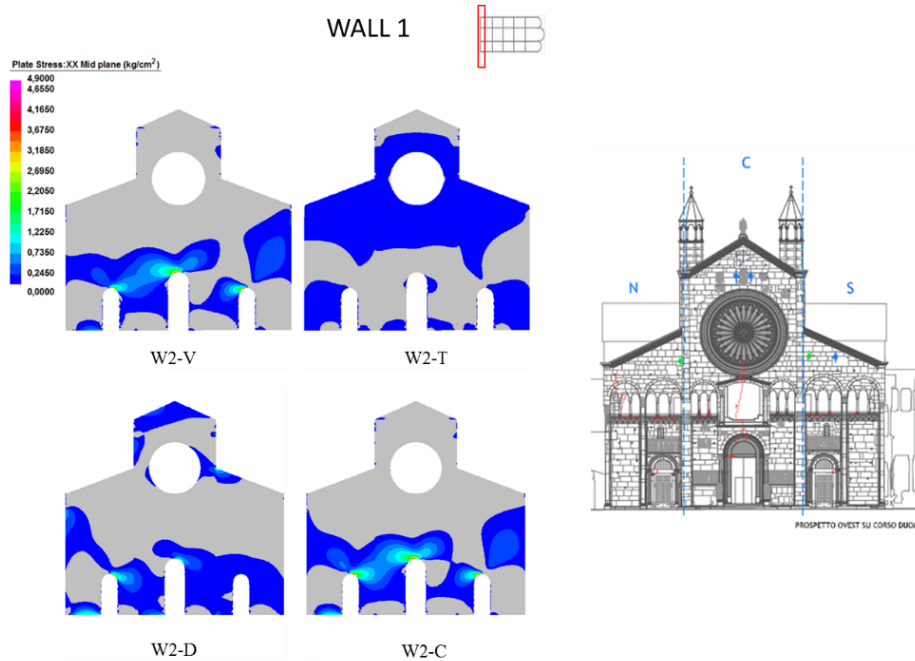
Figure 11-11: Stress of Wall 1 obtained from the W2 model with the different load cases and compared with the observed cracking patterns.

The in-plane and out-of-plane deformed shapes of a specific longitudinal wall are represented in and compared with the results of the 3D laser scanning. The deformed shapes are qualitatively consistent with the 3D laser scanning indicating that:

- the presence of the ancient ruins of the pre-existing churches reduces the vertical deformations in proximity of the facade (as indicated in Figure 11-12a);
- the interaction between the Cathedral and the Ghirlandina Tower causes significant out-of-plane displacements (Figure 11-12b) of the longitudinal walls, especially for those walls closer to the Tower.

Nonetheless, the maximum out-of-plane wall deformations leads to maximum out-of-plane inclinations of about 0.5°, thus smaller than those obtained from the 3D laser scanner and also from the simple hand calculations (see Figure 11-8). This can be explained by considering that in the FE models the entire inertia of the global wall as inserted in the whole structural context is considered. In summary, a sketch which schematically shows the main deformations is represented in Figure 11-13: (a) out-of-plane deformation of the longitudinal walls, (b) global inclination towards the Ghirlandina Tower due to differential soil settlements, which is contrasted by (c) the reactions of the masonry arches which link the Cathedral and the Tower.
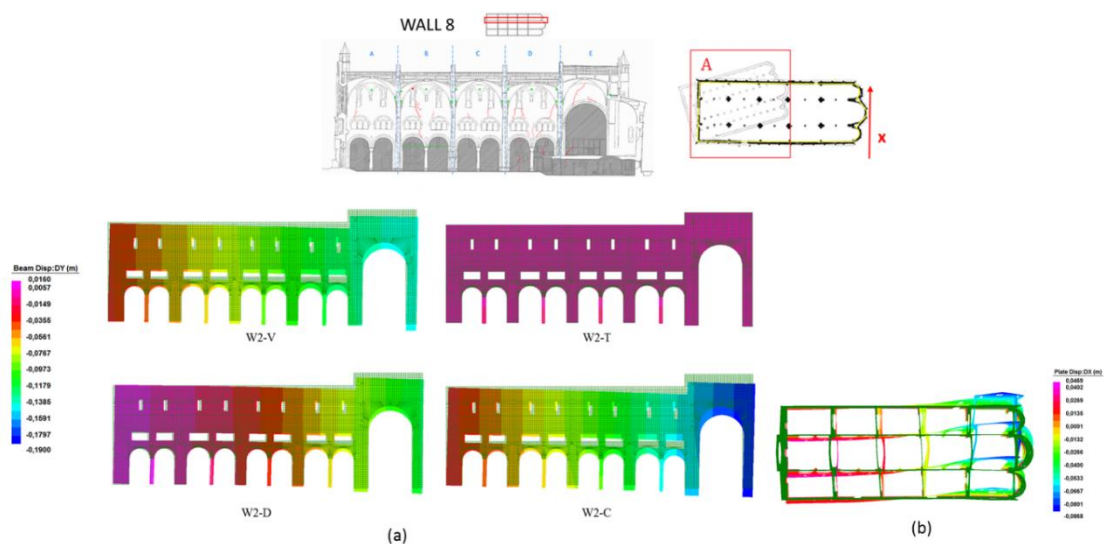
Figure 11-12: (a) in-plane deformed shape for Wall 8; (b) out-of-plane deformed shape (x direction) for all walls.

<div align="center">(a)   (b)   (c)</div>
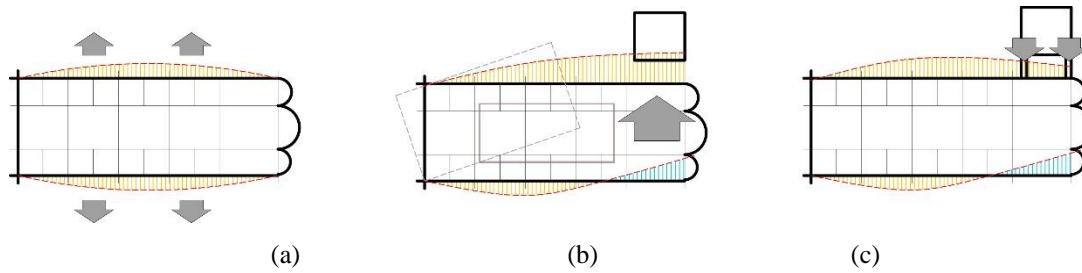
Figure 11-13: Sketch of the main global movements of the Cathedral as reconstructed by integrating the surveys with the results of the structural analyses.

11.4   Seismic Vulnerability analyses

First, the dynamic properties of the monument (natural periods and mode shapes) have been identified through a natural frequency analysis performed on the 3D finite element model which was considered the more representative of the structure, as identified in the previously section. Then, the seismic behaviour of the whole structure have been investigated considering that the seismic response of the cathedral can involve mainly two types of mechanisms:

- in-plane mechanisms and
- out-of-plane mechanisms.

Finally, time history analyses on the 3D finite element models, considering as input the acceleration recorded during the 2012 earthquake §10.5, have been developed to identify the displacements/shearing deformation at the top of the walls and piers (springings of the vaults).

11.4.1 Natural frequency analysis

Since the stress-strain constitutive of masonry structures is yet non-linear for small values of deformation, the reliability of the modes of vibration is to be taken with caution. The common design codes, such as the Italian D.M. 14/01/2008 (Norme Tecniche per le Costruzioni 2008), prescribe that the participating mass must exceed 85%; therefore, in the consecutive seismic analyses 20 mode shapes have been considered in order to satisfy this requirement. The fundamental periods are in the range of 0.25-0.35 s. Figure 11-14 shows the first five mode shapes. This analysis shows that the first mode shape is characterized by a translation in the transverse direction of the Cathedral more pronounced in the area of the heavy apses than the area of the nave and the facade. The third mode shape is characterized by a translation along the longitudinal direction.

(a)   (b)   (c)

(c)   (d)
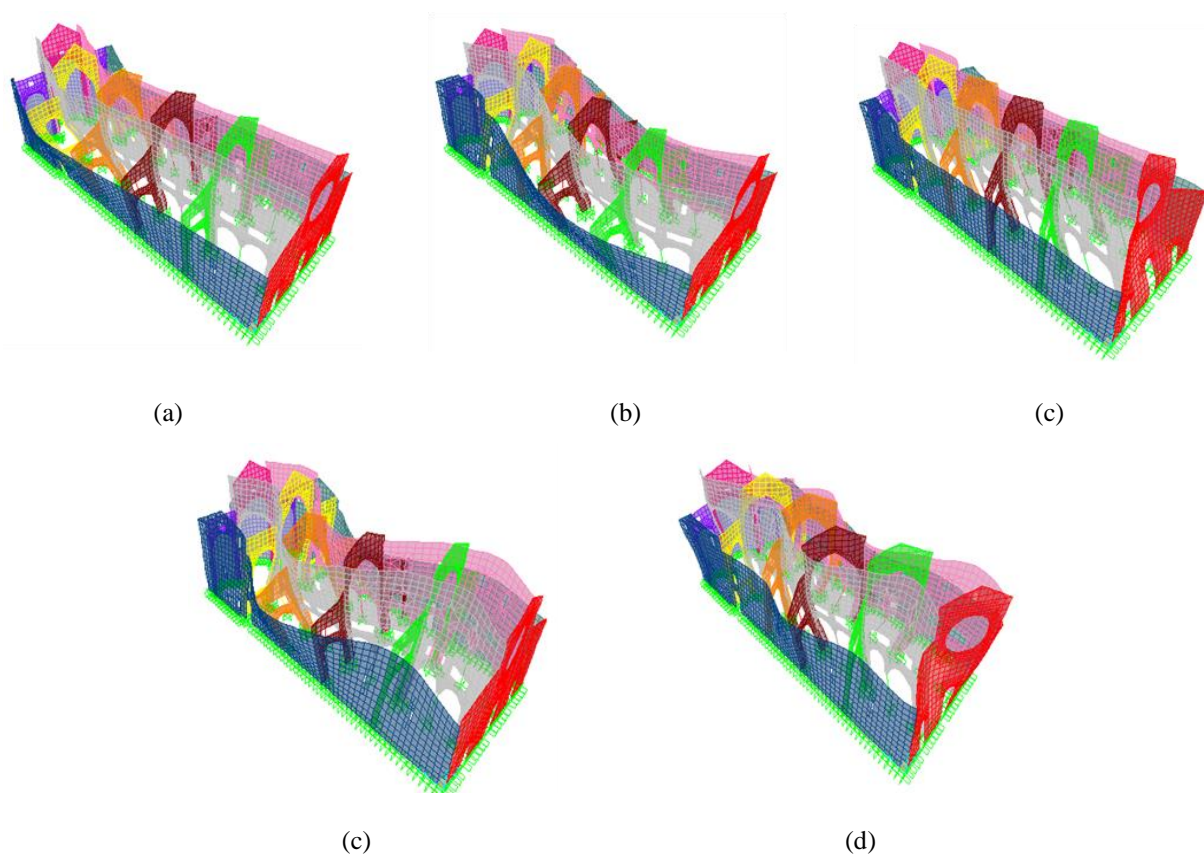
Figure 11-14 : Mode shapes; (a) T=0.35 sec ;(b) T=0,31sec;(c) T=0,28sec;(d) T=0,28sec; (e) T=0,26sec

11.4.2 Global seismic response

Response spectrum and time history analysis have been performed on the 3D finite element model (called UD-C + W2). The analysis have been devoted to the identification of the criticalities in terms of:

- in-plane mechanisms caused by high shear force (causing possible diagonal cracks or horizontal sliding);
- out-of-plane mechanisms caused by high eccentricity, defined as the ratio between the bending moment and the axial force (causing possible stress concentration at the base or overturning of the wall).

The study of the in-plane mechanisms has been conducted by evaluating the tensile stresses in the walls (diagonal cracking check) and the shear stresses at the base of the walls (sliding check). Figure 11-15 shows the comparison between the tensile stresses and the cracking patterns for the wall 1 (façade wall). In general, the results obtained from tensile stresses show a high validation with the cracking patterns. The majority of the lesions seems to be caused by the accumulation of damage over time caused by various earthquakes. The sliding check at the base is performed as follows:

$$\tau < \tau_{di} \tag{11.1}$$

where

τ is the tangential mean stress and τ_{di} is the shear strength of the masonry, as evaluated according the two diagonal cracking and (friction) sliding mechanisms:

$$\tau_{di} = \tau_{od}\sqrt{1 + \frac{\sigma_{oi}}{1,5\tau_{od}}} \tag{11.2}$$

$$\tau_{di} = \tau_{0d} + 0,4\sigma_{0i} \tag{11.3}$$

where:

τ_{od}= shear strength of the masonry (τ_{od}=1kg/cm^2);

σ_{oi}= mean compressive stress.

Figure 11-16 shows the tangential stresses calculated for wall 1 and Table 11-3 reports the values obtained for
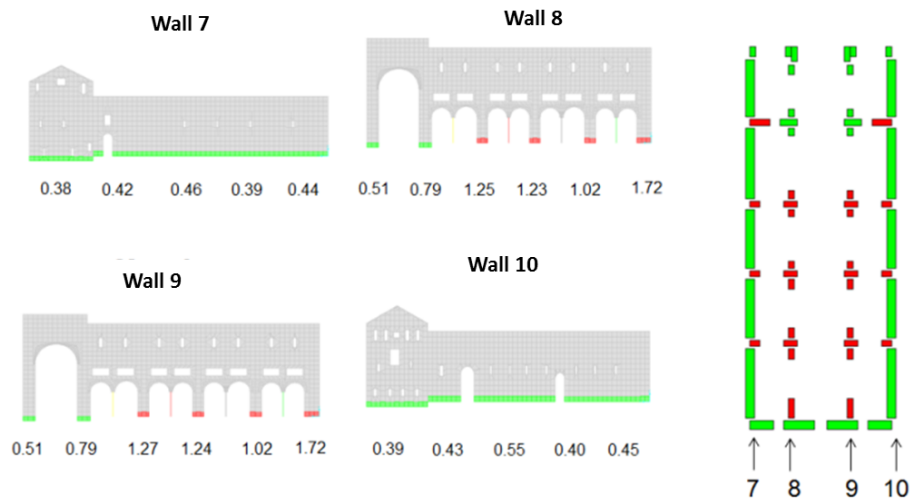
the sliding check.

(b)

Figure 11-17 summarizes the results obtained for all the walls of the cathedral and highlights that the greatest criticalities are related to the in the internal transversal walls.
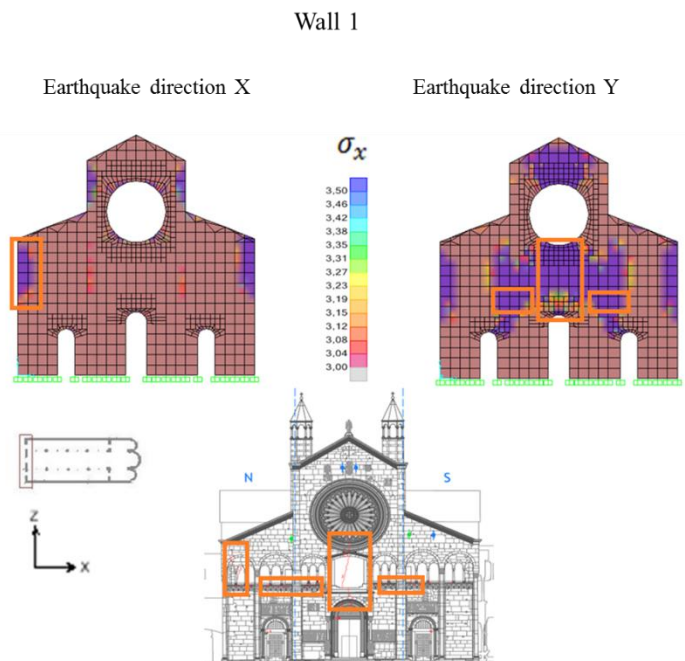
Wall 1

Figure 11-15: Comparison between tensile stresses and the cracking patterns
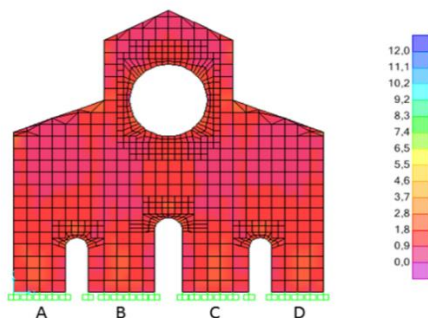
Figure 11-16: Tangential stresses

Table 11-3- Verification of the shear strength for the wall 1

	Compressive mean stress	Shear strength Eq. (12.2)	Shear strength Eq. (12.3)	Tangential mean stress (Demand)	Demand/ Capacity ratio Eq. (12.2)	Demand/ Capacity ratio Eq. (12.3)
	[Kg/cm²]	[Kg/cm²]	[Kg/cm²]	[Kg/cm²]	[]	[]
Section cut 1A	6.95	2.37	3.78	1.25	0.53	0.33
Section cut 1B	4.66	2.03	2.86	1.36	0.67	0.47
Section cut 1C	4.66	2.03	2.87	1.37	0.68	0.48
Section cut 1D	7.06	2.39	3.82	1.25	0.52	0.33
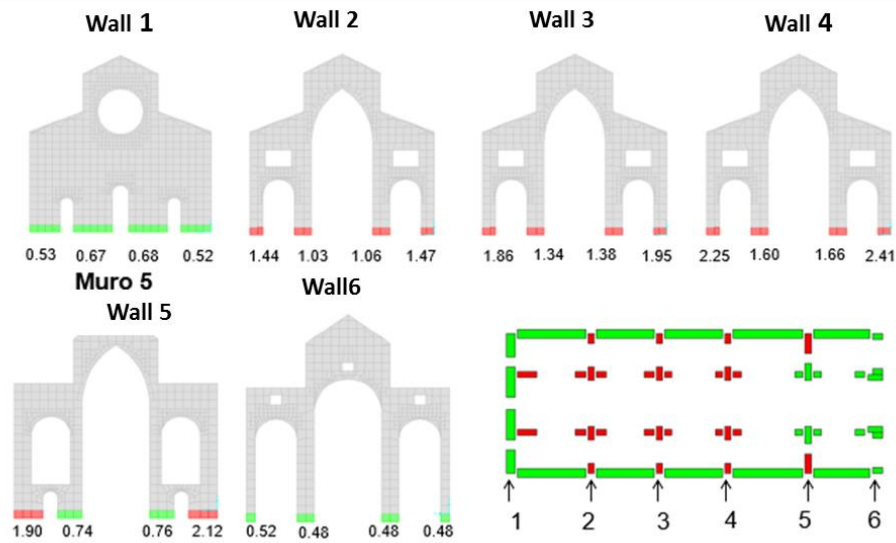
(a)
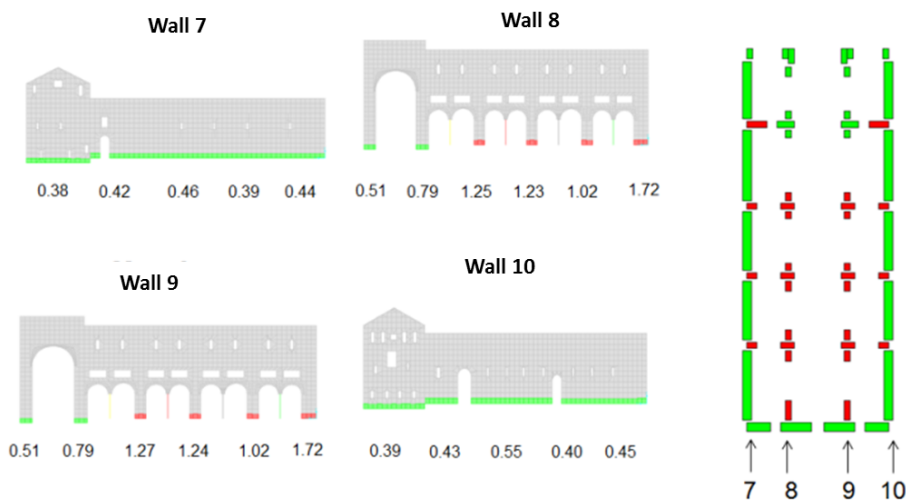
(b)

Figure 11-17: Sliding check for all the walls of the cathedral: (a) transversal walls and (b) longitudinal walls

Out-of-plane mechanisms have been identified by first evaluating the eccentricity at the base of the walls, as defined as the ratio between the bending moment and the axial force in seismic conditions, and then checking that:

- the eccentricity is below the usual reference values $s/6$ and $s/2$ (with s indicating the thickness of the wall) and

- (ii) the lateral shear stresses developed on the two vertical lateral sides of the considered wall are below some reference values (i.e. connection capacity).

In detail, the eccentricity at the base of each wall has been calculated by considering both the static loads (self weight and dead loads) and the seismic actions (that, in the case of a dynamic time-history analysis, are function of time) for each section (Figure 11-18):

$$e_{(t)} = \frac{M_{static} + M_{seismic}(t)}{N_{static} + N_{seismic}(t)} \tag{11.4}$$
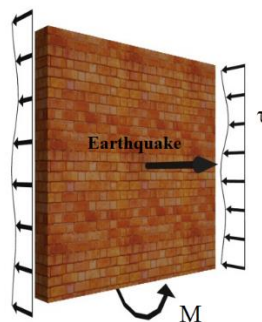
Figure 11-18: A schematic representation of a single wall with the indication of the out-of-plane seismic action, the base moment and the transversal actions due to the interaction between the orthogonal walls

The time history of the eccentricity has then been evaluated using 9 recorded accelerograms (selected from the P.E.E.R. strong motion database) consistent with the results of the seismic hazard analyses §11.4. Then the maximum absolute eccentricities have been used to check the out of plane stability of the walls. Two limit cases regarding the quality of the connection between orthogonal walls have been considered to compute the eccentricities: good connections (perfect continuity between orthogonal walls) and bad connections (partial continuity between orthogonal walls, modelled by inserting more flexible elements). Figure 11-19 a shows the time history of the eccentricity for the 1A section of the wall 1 whereas Figure 11-19 b shows the shear stresses, exchanged between the considered and the adjacent walls, obtained from the time history analysis for the wall 1. Table 11-4 shows the values of the eccentricity calculated for the various sections of the wall 1 and verify that these values are lower than s/2. Figure 11-20 provides a summary of the results obtained for all the walls of the cathedral. In can be noticed that, the study of the out of plane collapse mechanisms showed criticality in the transversal walls especially in the control sections B-C. However, the values of the shear stresses for each wall suggest that, even leading to cracked conditions at the base of the walls, the connections are able to keep the wall in a stable configuration. In two longitudinal walls, instead, the results indicate both cracked conditions at the base and values of shear stresses greater than the shear strength of the masonry in the absence of vertical loads.

(a)

Wall 1, thickness s= 145 cm

Good connection   Bad connection

(b)
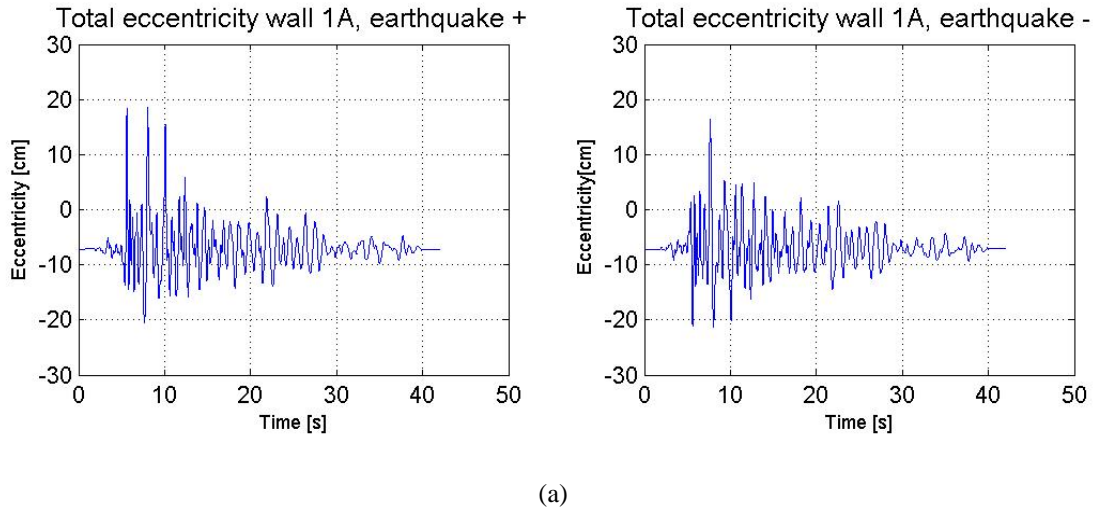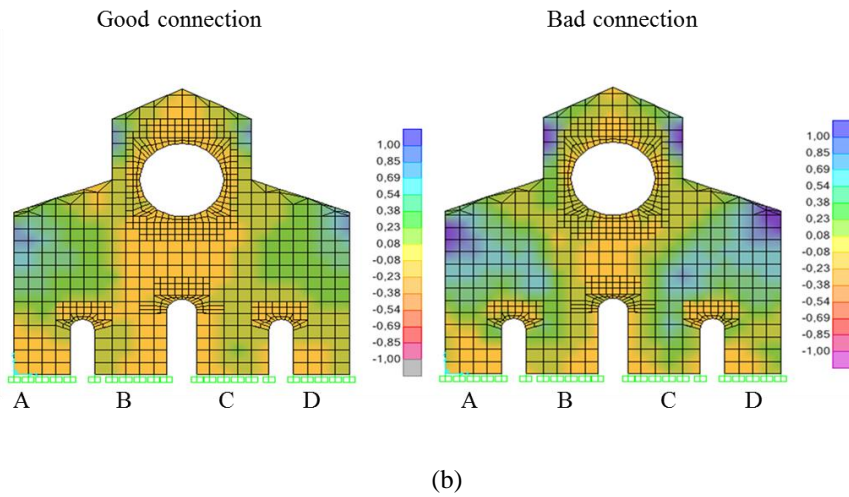
Figure 11-19: (a) The time history of the eccentricity on the 1A section (b) Tangential stresses for the wall 1

Table 11-4- Verification of the eccentricity for the wall 1

	Good connection	Bad connection		Good connection	Bad connection	Central core of inertia	s/2
	Mean + [cm]	Mean + [cm]		Mean – [cm]	Mean – [cm]	[cm]	[cm]
Section cut 1A	50,10	120,04		-26,15	-51,02	24,17	72,5
Section cut 1B	1183,40	412,82		-28,70	-99,75	24,17	72,5
Section cut 1C	1386,93	470,64		-28,60	-102,97	24,17	72,5
Section cut 1D	57,03	151,55		-26,20	-53,51	24,17	72,5
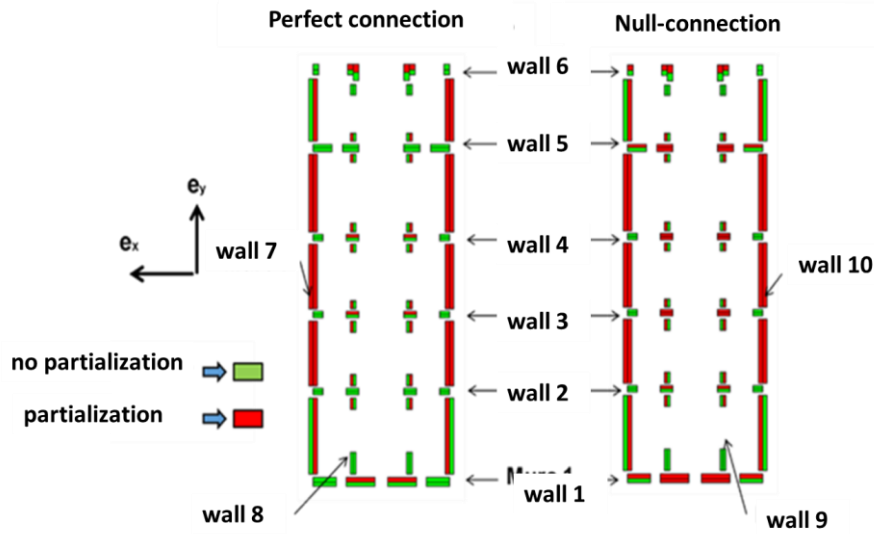
Figure 11-20: Vulnerability for the out-of-plane mechanisms in the walls

11.4.3 Time history analyses: input the main shock recorded by the station of Modena

Time history analyses on the 3D FEM model of the Cathedral, has been developed to identify the displacements/shearing deformation at the springings of the vaults (top of the walls and piers). The input considered in the analyses is the acceleration recorded by the station close to Modena (MDN) during the 2012 Emilia earthquake (with a pick ground acceleration around 0.04g). The main purpose of these analyses is the assessment of the correlation between the displacements of the springings of the vaults, due to the vibration of the underneath structures, and the damages detected. Figure 11-21 shows the nomenclature used for the vaults of the cathedral and the displacements that can interest the vaults (shearing displacement referred to VNC1 and widening referred to VNC3).Table 11-5 and Table 11-6 collect the displacements (widening and closing) and the shear displacement at the springings of the central and lateral vaults. It can be noticed that during the 2012 Emilia earthquake the springings of the vaults of the cathedral suffered shear imposed displacement lower than 1 cm and negligible widening and closing displacements.
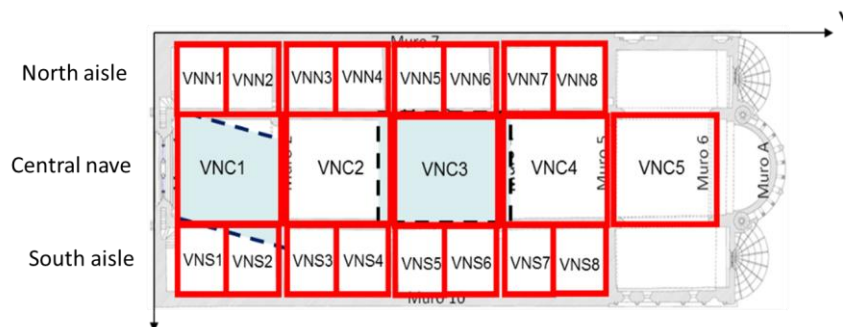
Figure 11-21: The nomenclature of the vaults of the cathedral

Table 11-5- The displacement at the springings of the central vaults as obtained from the time history analyses

Central Vault	Displacement [cm]	Shear Displacement[cm]
VNC1	0.014	0.43
VNC2	0.020	0.39
VNC3	0.03	0.39
VNC4	0.03	0.48
VNC5	0.037	0.43

Table 11-6- The displacement at the springings of the lateral vaults as obtained from the time history analyses

Lateral Vault	Displacement [cm]	Shear Displacement [cm]
VNN1-S1	0.014	0.43
VNN2-S2	0.020	0.39
VNN3-S3	0.03	0.39
VNN4-S4	0.03	0.48
VNN5-S5	0.037	0.43
VNN6-S6	0.014	0.43
VNN7-S7	0.020	0.39
VNN8-S8	0.03	0.39

The results obtained in terms of shear displacement are compared with the survey of the damage observed after the 2012 earthquakes (Figure 11-22). It can be noticed that generally the vaults mainly damaged correspond at the vaults that suffered the major shear displacement at the springings due to the vibration of the underneath walls and piers.
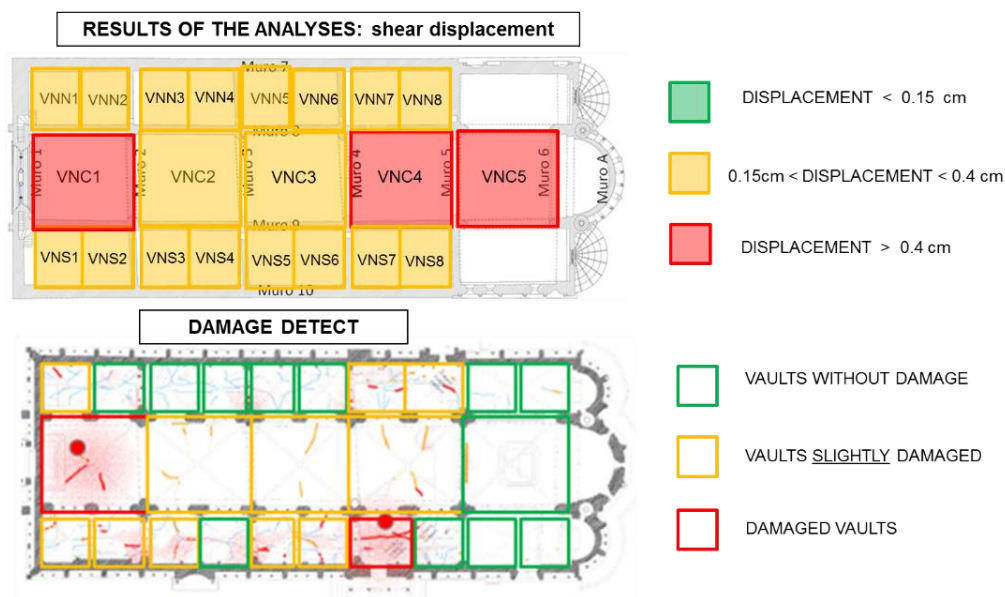
Figure 11-22: The comparison between the shear displacements and the damage detected on the vaults after the 2012 earthquahe

11.5   The main vulnerabilities and conclusions

Starting from the knowledge acquired by the multi-disciplinary approach, the structural behaviour of the Cathedral has been investigated in order to identify the more vulnerable elements of the building. The multi-analyses method which aims at integrate the results obtained by different models, (characterized by different level of accuracy according to typology of problems to be investigated) appears fundamental in order to obtain a consistent assessment of the structural behaviour of the monuments.

The results of the static analyses reveals that the different soil stiffness at the base of the cathedral strongly influence its structural behaviour. Indeed, the model, which considers the soil-structure interaction, is able to provide with more accuracy a state stress congruent with the cracks pattern detected.

Moreover, from the static analyses it can be recognized that the main vulnerabilities are:

- the tendency of the longitudinal perimeter walls to develop out-of-plane movements, as revealed by the 3D laser scanner, probably due to the unconstrained thrusts of the arches and differential settlements;
- the overall rotation movement towards the Ghirlandina Tower, caused by the strong interaction between the Cathedral and the Tower, that promotes differential soil settlements (note that the portion of the apses is significantly heavier than the other portions);
- the concentration of cracks and peaks of the tensile stresses in the portion coinciding with the location of the old Cathedrals.

The results of the seismic analyses reveal vulnerabilities of the perimeter walls with respect to out-of-plane overturning. These numerical results have been confirmed by the experimental evidences of the damages observed after the recent 2012 Emilia Romagna earthquake sequence.

Chapter 12

12 Cathedral of Modena: local structural analyses

12.1 Introduction

The seismic performances of historical masonry buildings are closely related to the behaviour of each substructure. In general, the horizontal seismic forces cause damages and/or collapses mainly in the following specific elements: large space without structural walls, arches, vaults, domes, ... , which are common in the historical churches. The analysis of the main damages suffered by Italian churches due to the recent earthquakes (L'Aquila 2009, Emilia 2012, Umbria-Marche 2016) has shown a number of common collapse mechanisms, which may involve the local response of single structural elements (Parisi et al. 2012), (Dolce et al. 2012). In particular, the information on damage location and extent, collected after these violent earthquakes, highlighted that, among all structural elements, the most vulnerable one are masonry vaults.

In this chapter, the local collapse mechanisms of the main substructures of the Cathedral have been studied. In addition, 3D Finite element models of the most damaged vaults, after the 2012 Emilia Romagna earthquake, have been developed in order to provide information on the stress and deformation state.

12.2 The models and the simulation

The local collapse mechanisms which aim at providing the value of the load that activates the failure mechanisms of each elements through kinematics models (both in-plane and out-of-plane mechanisms) have been evaluated for the single sub-elements of the cathedral. Then, the stress levels of vaults under dynamic excitation and displacement imposed at their springings have been investigated making use of 3D linear Finite element models. The analyses developed are summarized in Table 12-1.

Table 12-1- The different analyses developed

Model-Element	Analysis
Sub-elements: façade, nave, vaults, aisles…	local collapse mechanisms
3D FEM models of the vaults	Static analyses
3D FEM models of the vaults	Seismic analyses

12.3 Local collapse mechanisms

The local collapse mechanisms are strongly dependent on the construction techniques and on the connection details between orthogonal masonry walls and between the masonry walls and the possible restraining horizontal elements, such as tie-beams, well connected floors, ... The cathedral has been divided into sub-elements, i.e. structural elements characterized by an autonomous structural behaviour: the façade, the nave, the aisles, the vaults, the longitudinal perimeter walls, the columns, the transept, the triumphal arch and the apses. For each one of these sub-elements, when applicable, out-of-plane mechanisms and in-plane mechanisms have been considered. As far as the out-of-plane mechanisms are concerned, the limit analysis approach has been applied. Each sub-element is assumed to be composed by a number of stiff, incompressible and infinitely-resistant blocks, and the limit load multiplication coefficient (λ) is calculated by means of equilibrium equations. Limit load is the maximum seismic horizontal load that the structure can safely carry. In general, the limit analysis of masonry structures involves the following assumptions (Heyman 1995): (i) masonry has no tensile strength, (ii) stresses are so low that masonry has effectively an unlimited compressive strength, (iii) sliding failure does not occur. Here, only the calculations related to the evaluation of the limit load multiplication coefficient of the façade are entirely presented. The crack pattern shows lesions in the orthogonal longitudinal walls next to the facade (Figure 12-1a) that suggest a good connection between these elements. However, three different hypotheses of connections are here considered :(1) good connection between orthogonal masonry walls , (ii) bad connection (negligible connection between orthogonal masonry walls) and (III) reasonable estimation of the connection. The following mechanisms have been taken into account:

- overturning of the whole façade (Figure 12-1b and Figure 12-2– mechanism 1);
- overturning of the left portion of the façade (Figure 12-2– mechanism 2);
- overturning of the central portion of the façade (Figure 12-2– mechanism 3);
- overturning of the right portion of the façade (Figure 12-2– mechanism 4-5).

(a)   (b)
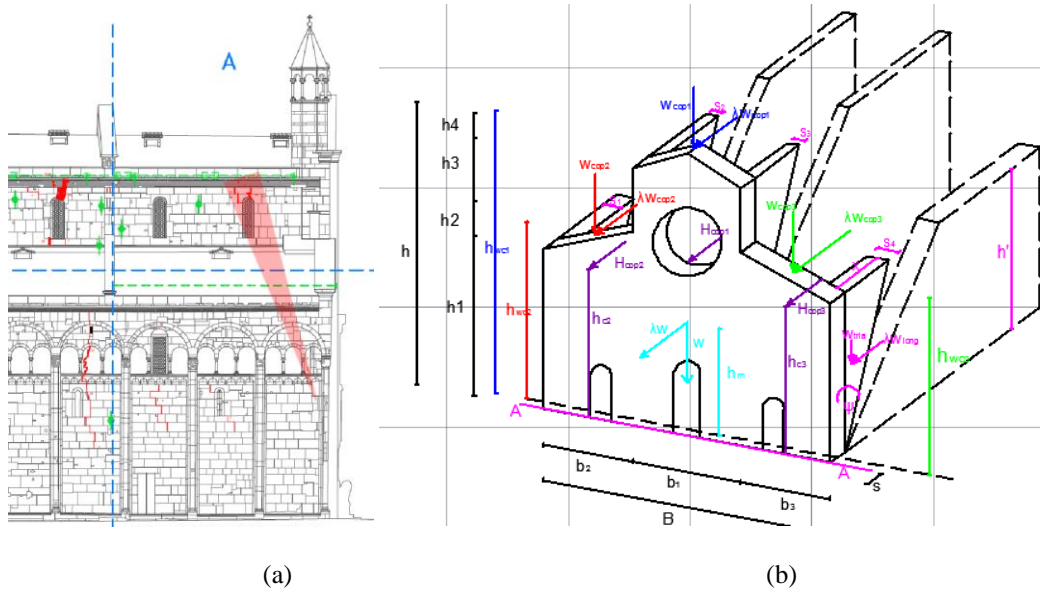
Figure 12-1: (a) Cracks in longitudinal walls of Cathedral, (b) Overturning of global facade around the base dashed straight line.

The behaviour of the wall in limit equilibrium conditions has been simulated by applying the principle of virtual works, i.e. equating the overturning moment (due to horizontal loads) and the stabilizing moment (due to self-weight):

$$M_{overturning} = M_{stabilizing}$$

$$\left[\left(\left(W - W_{holes}\right) \cdot \frac{s}{2} + W_{cop} \cdot d_c - H_{cop1} \cdot h_c + W_{tria} \cdot \left(s + \frac{1}{3}x_i\right)\right)\right] - $$
$$- \lambda \cdot \left[W_{wall} \cdot h_m - W_{holes} \cdot h_f + W_{cop1} \cdot h_{wc1} + W_{long} \cdot \left(\frac{2}{3} \cdot h_i'\right)\right] = 0 \tag{12.1}$$

The limit load corresponding to the spectral acceleration that activates the local mechanism of collapse has been obtained from Equation 12.1.

$$\lambda = \frac{\left[\left(W - W_{holes}\right) \cdot \frac{s}{2} + W_{cop1} \cdot d_{c1} + W_{cop2} \cdot d_{c2} + W_{cop3} \cdot d_{c3} - H_{cop1} \cdot h_{c1} - H_{cop2} \cdot h_{c2} - H_{cop3} \cdot h_{c3}\right]}{\left[W_{wall} \cdot h_m - W_{holes} \cdot h_f + W_{cop1} \cdot h_{wc1} + W_{cop2} \cdot h_{wc2} + W_{cop3} \cdot h_{wc3}\right]} = 0,22 \tag{12.2}$$

$$a_0 = \lambda \cdot g = 0,22g \tag{12.3}$$

Figure 12-2 shows the acceleration values that activate overturning mechanisms of the different portions of the façade for the different connection considered. These values, also considering the good connection, are higher than the acceleration reference values for the past earthquakes obtained from HDSHA §11.4.1 (0.15-0.20 g), but lower than the acceleration estimates for the possible future earthquakes obtained from MHEA §11.4.2 (0.50 g).
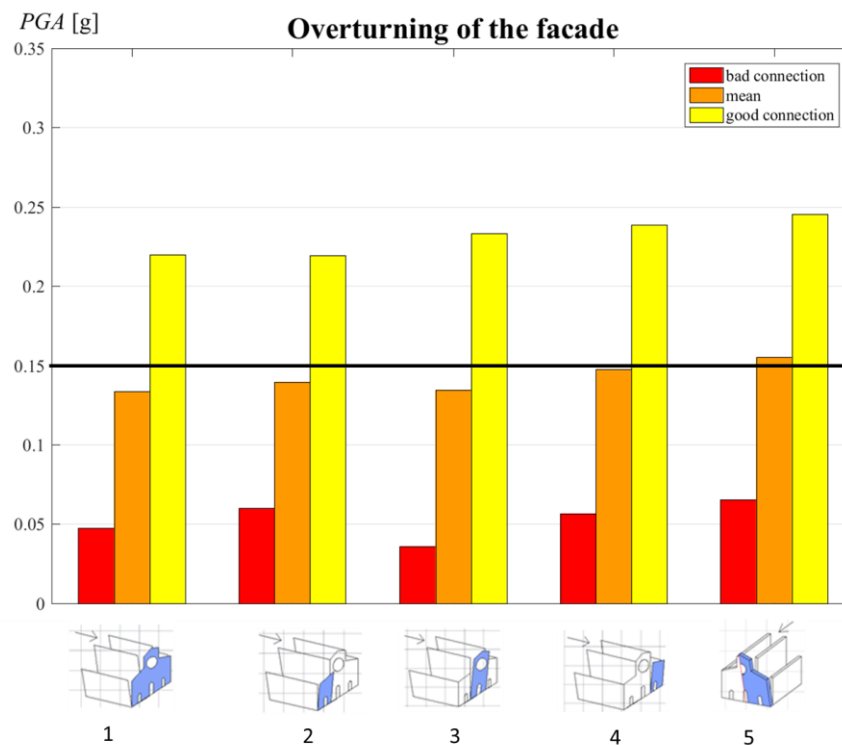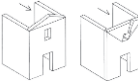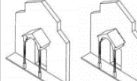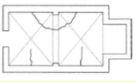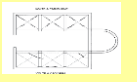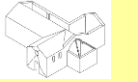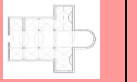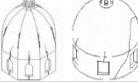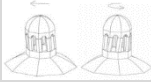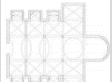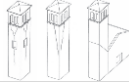
Figure 12-2: Comparison between the accelerations that activate the 4 mechanisms of collapse for the façade

The results obtained for the other substructures are summarized in Table 12-2. The acceleration that activates the failure mechanisms reported in Table 12-2 are referred to the most unfavourable condition of each elements (bad connections, more susceptible element).

In general, the study of the local mechanism of other sub-elements reveal that the main local vulnerabilities are relevant to the façade (as described above), the top façade (with trigger accelerations around 0.06 g), the cross vaults (with trigger accelerations around 0.12 g), the triumphal arch (0.07 g), the transversal response of the columns (0.14 g) and the out-of-plane behaviour of the apse walls (0.13 g).

Table 12-2-The acceleration that activates the failure mechanisms for each sub structures

1. OVERTURNING OF THE FACADE	2. OVERTURNING TOP OF THR FACADE	3. IN OLANE MECHANISMS OF THE FACADE	4. PROTHYRUM	5. TRANSVERSAL RESPONSE OF THE AULA	6. SHEAR IN THE LATERAL WALLS	7. LONGITUDINAL RESPONSE OF THE COLUMNS
0.13 g	0.06 g	0.33 g		0.17 g	0.31 g	0.14 g
8. VAULTS OF THE CENTRAL NAVE	9. VAULTS OF THE AISLES	10. OVERTURNING TRANPSET WALLS	11. SHEAR IN THE TRANSEPT	12. VAULTS OF THE TRANSEPT	13. TRIUMPHAL ARCHES	14. DOME
0.19 g	0.21 g	0.13 g	0.24 g	0.12 g	0.07 g	
15. LANTERNA	16. OVERTURNING OF THE APSE	17. SHEAR MECHANISMS ON THE APSE	18. VAULTS OF THE APSE	19. ROOF SYSTEM	20. ROOF OF THE TRANSEPT	21. ROOF OF THE APSE
	0.15 g	0.37 g	0.34 g			
22. OVERTURNING OF THE CHAPEL	23. SHEAR MECHANISMS ON THE CHAPEL	24. VAULTS OF THE CHAPEL	25. PLAN AND HEIGHT IRREGULARITIES	26. AGGETTI (PINNACLES)	27. BELL TOWER	28. CELL BELL
				0.21 g		

a < 015 g
0.15g < a <0.25 g
a > 0.25 g
Not present, or static patterns insufficiently representative of reality

12.4 The vault

The investigation of the structural behavior of the cross vaults under earthquake excitation is a fundamental issue in order to plan effective structural interventions. However, the evaluation of their seismic response is severely complex and depends on several factors, such as the three-dimensional geometry, the mechanical properties of the constituent materials and the behavior of the underneath vertical elements (lateral walls and piers) (McInerney & DeJong 2015). A vault under earthquake excitation is mainly subjected to two different phenomena (Figure 12-3):

- pseudo-static response of the vault to the relative displacements imposed at its springings, due to the horizontal movements of the underneath structures (walls and piers).
- dynamic response of the vault to the acceleration imposed at its springings due to the seismic vibration of the underneath structures (walls and piers);

(a)   (b)   (c)
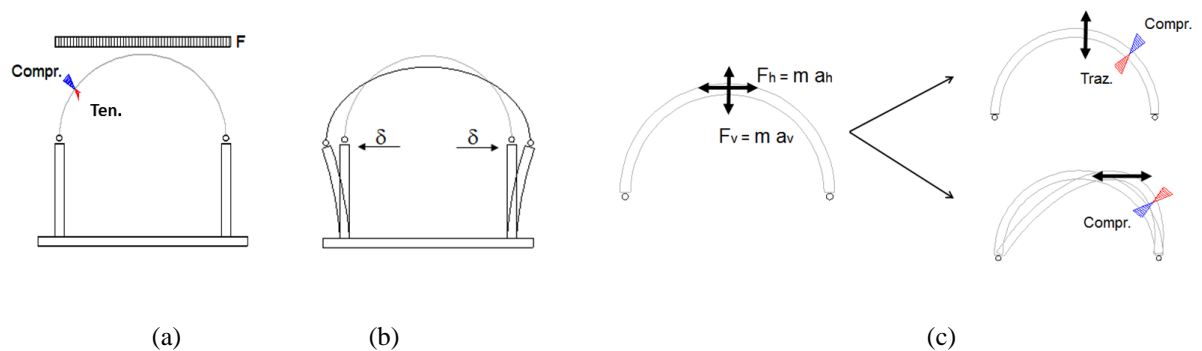
Figure 12-3: Schematization of the effects used for the assessment of the seismic response of the vaults: (a) vault undergo to vertical loads, (b) vault subject to imposed displacement at the springings and (c) vault under earthquake excitation

In this section the structural behavior of the vaults of the cathedral has been investigated. First, static analyses have been developed in order to identify the stress level due to the self-weigh and displacement imposed at their springings (as obtained in §10.4.3). Then, linear time history analyses, using the acceleration recorded by the MDN station §10.5, have been performed.

12.4.1 3D FE models of the vaults

Static and dynamic analyses have been developed on the 3D FE models of the two most damaged vaults (VNC1 and VNS7) after the 2012 earthquake of the cathedral. The FE models reproduce the actual geometry of the groin vaults, which has been determined by means of laser scanning surveys, paying particular attention to the restraining given by the support and contrast elements (Figure 12-4).The information regarding the geometry of the two vaults are reported in Table 12-3. In the FE modelling the masonry is modelled as homogeneous continuum. For this reason, the FE models are not suitable to capture the expected failure modes but may give indications on the level of stress on the vaults. High

tensile stress resulting from static and dynamic loads are assumed to indicate cracking due to material failure.
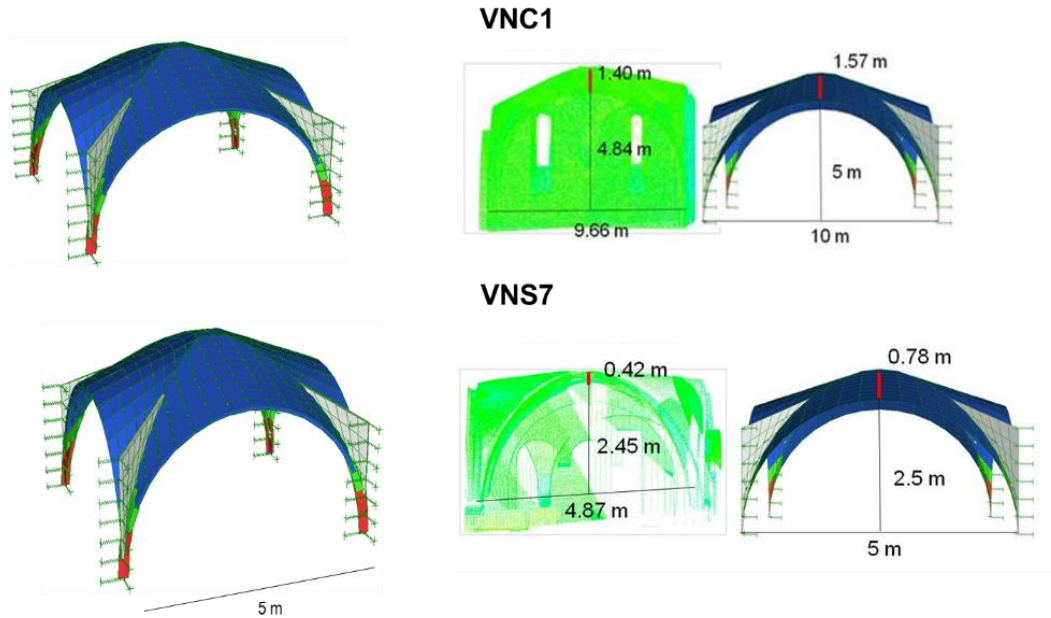
Figure 12-4: The actual geometry of the cental and lateral vaults (VNC1 and VNS7) and the corresponding 3D FE models

Table 12-3: The geometry of the central and lateral vault of the cathedral

CENTRAL VAULT (VNC1)						
Base [m]	High [m]	Area [m²]	Thickness [m]	γ [kg/m³]	Weight [KN]	E[KPa]
9.1	10.2	211	0.12	1800	7.9	4144000
LATERAL VAULT (VNS7)						
Base [m]	High [m]	Area [m²]	Thickness [m]	γ [kg/m³]	Weight [KN]	E [KPa]
5.2	5.6	70	0.12	1800	150	4144000

Static analyses considering also imposed displacements at the springings of the vaults, as obtained by the time history analyses on the global model of the cathedral, have been conducted. The increment of the level of stress (both compression and tensile stress) due to the widening and closing displacements imposed at the springings are substantially irrelevant. On the other hand, however, the shear displacements imposed causes a not negligible increment of the tensile stress at the extrados of the vaults (it can reach 2/3 kg/cm²), with particular concentrations along the diagonals. The maximum compressive stresses remain instead contained within limits compatible with the resistance of the materials characteristics (below 10 kg / cm²) (Figure 12-5 and Figure 12-6).
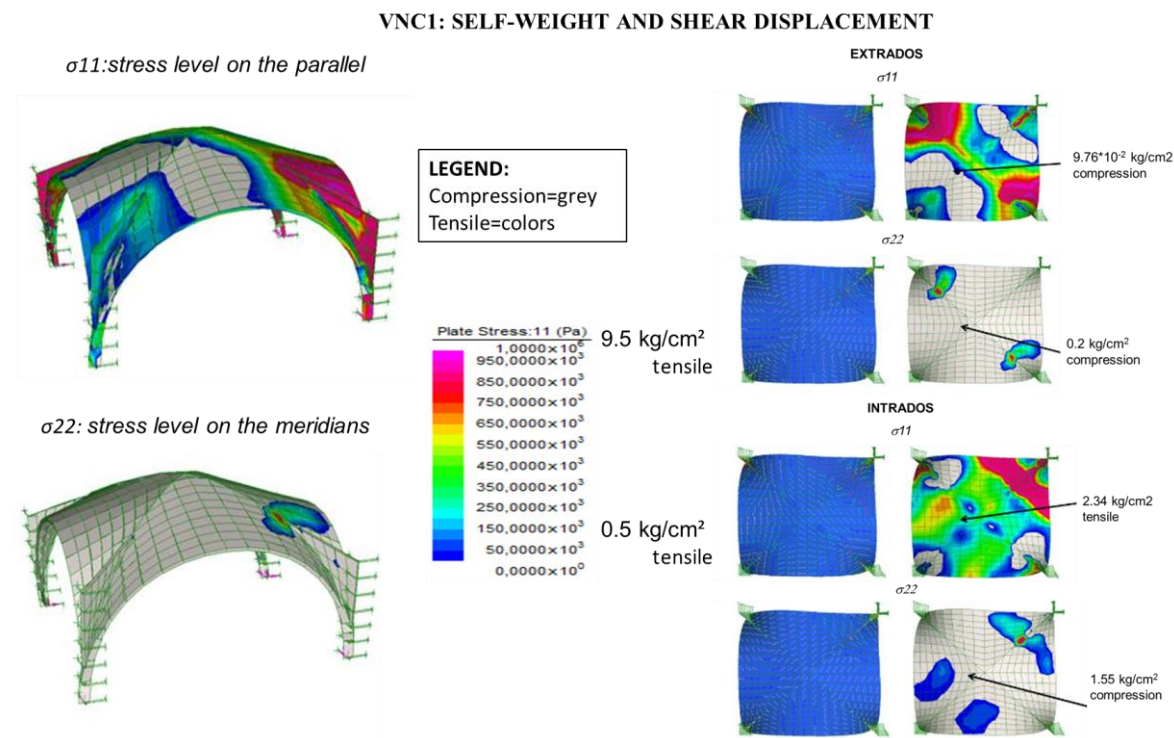
Figure 12-5:Stress levels of the vault VNC1 obtained from the static analyses considering the considering self-weight and the shear imposed displacements
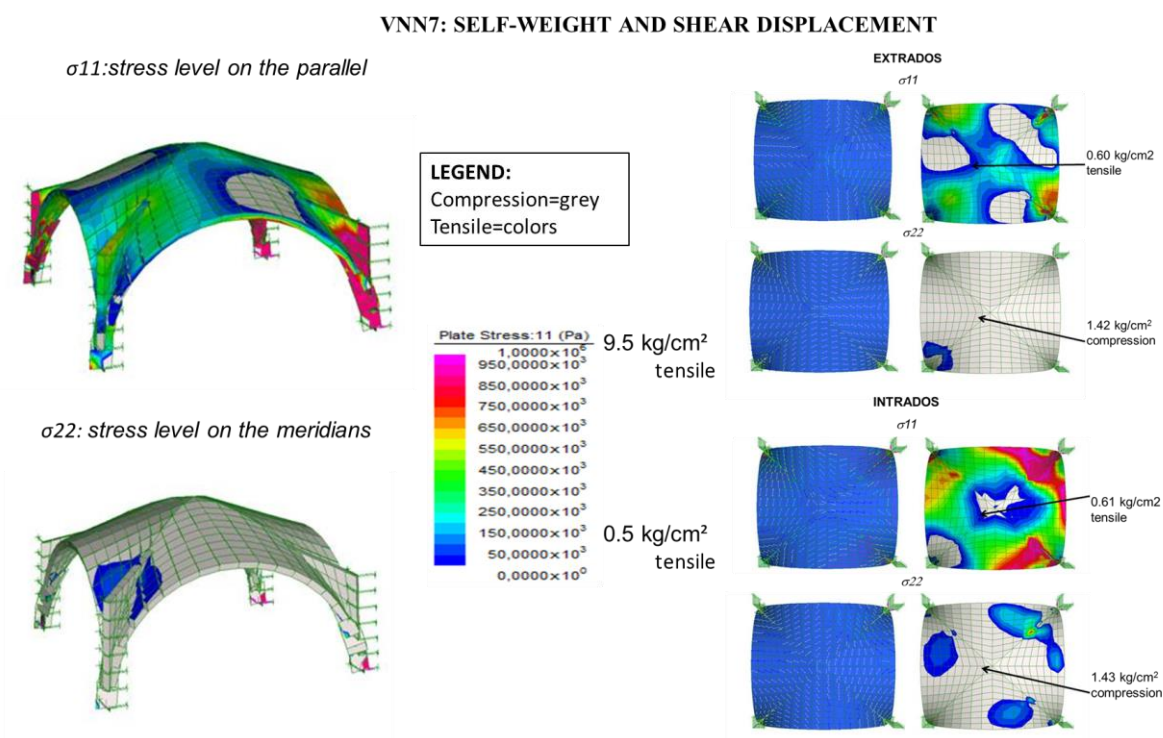
Figure 12-6: Stress levels of the vault VNN7 obtained from the static analyses considering the considering self-weight and the shear imposed displacements

Linear time history analyses on the 3D FE models of the vaults have been also developed applying as input the acceleration recorded by the station close to Modena during the 2012 earthquake. Figure 12-7 and Figure 12-8 display the stress level on the vault VNC1 and the vault VNN7 obtained from the dynamic analyses considering the self-weight and the seismic load. These analyses show that the effect of the dynamic response of the vaults is substantially comparable in terms of maximum tensile stresses to that induced by the shear displacements imposed at the springings.
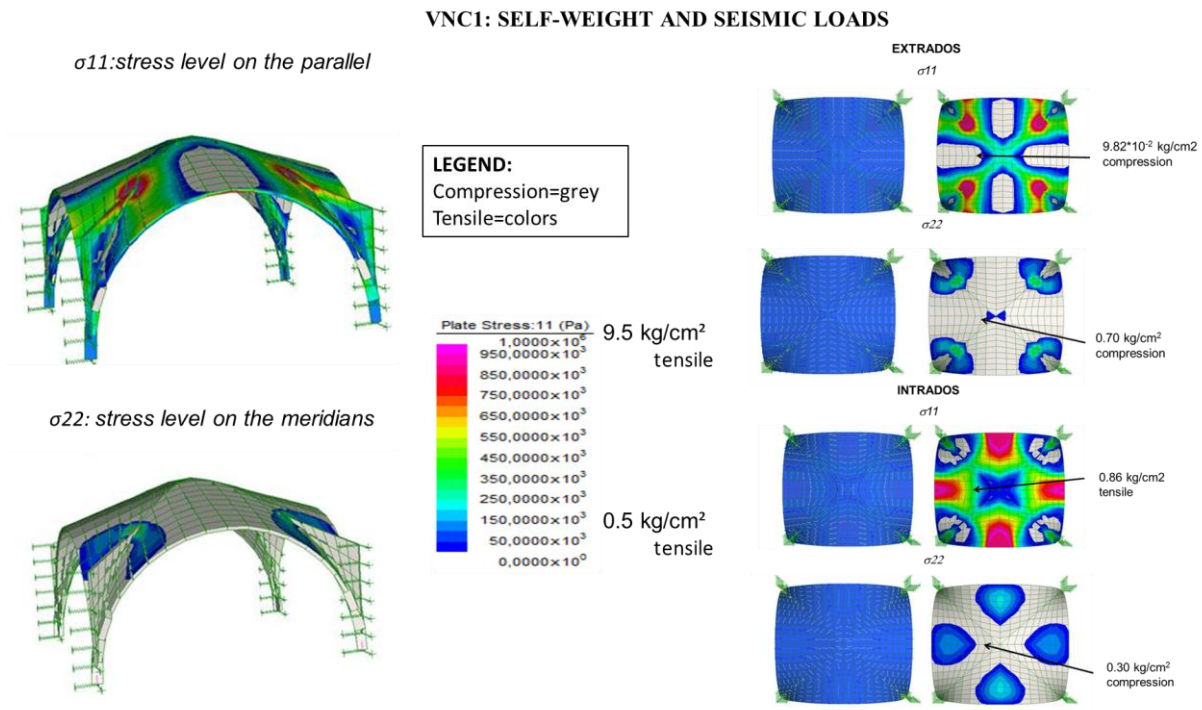
Figure 12-7: Stress levels of the vault VNC1 obtained from the dynamic analyses considering the considering self- weight and the seismic loads
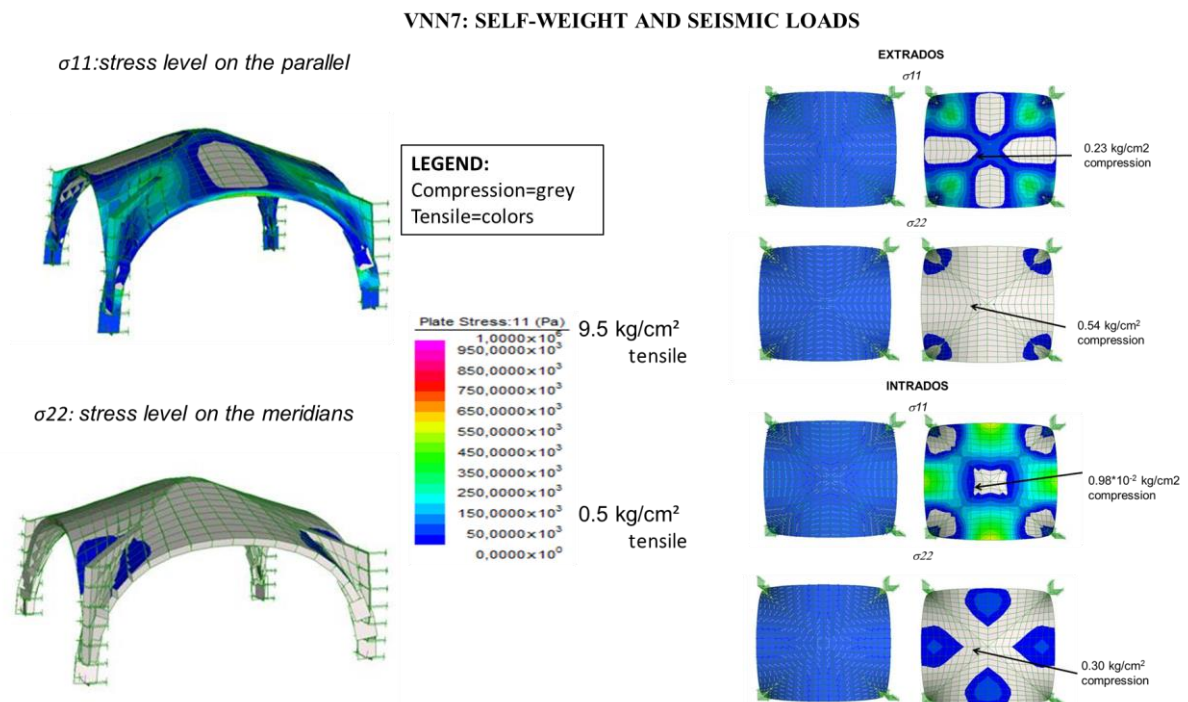
Figure 12-8: Stress levels of the vault VNN7 obtained from the dynamic analyses considering the considering self- weight and the seismic loads

12.5   Conclusions

The local collapse mechanisms allowed to identify the most vulnerable sub-structures of the cathedral of Modena. In detail, these analyses reveals that, considering a negligible connection between orthogonal masonry walls and between the masonry walls and the possible restraining horizontal elements ("bad connection") the most vulnerable elements are:

- the top of the façade: the overturning could be occur for acceleration around 0.06g;
- the triumphal arch: the collapse could be occur for acceleration around 0.07g;
- cross vaults: the collapse could be occur for acceleration around 0.12g;
- the apse walls: the out-of-plane behaviour could be occur for acceleration around 0.13g;
- the façade: the overturning could be occur for acceleration around 0.13g;
- longitudinal response of the columns: the mechanism could be occur for acceleration around 0.14g;

It is noted that, considering a good connection, the local mechanisms of collapse for the elements analysed could be activated for highest acceleration values. For this reason, it seems essential to ensure good connection between the orthogonal walls through appropriate interventions.

The static and dynamic analyses developed on the 3D model of the two most damaged vaults, after the 2012 earthquake, reveal that:

- the increment of the stress level (both compression and tensile stress) because of the widening and closing displacements imposed at the springings due to the horizontal movements of the underneath structures (walls and piers). are substantially irrelevant;
- the increment of the stress level because of the shear displacements imposed at the springings due to the horizontal movements of the underneath structures are not negligible. The increment of the tensile stress at the extrados of the vaults can reach 2/3 kg/cm^2, with particular concentrations along the diagonals. The maximum compressive stresses remain instead contained within limits compatible with the resistance of the materials characteristics (below 10 kg / cm^2);

the increment of the stress level because of the acceleration imposed at the springings due to the seismic vibration of the underneath structures (walls and piers) are substantially comparable in terms of maximum tensile stresses to that induced by the shear displacements imposed.

Chapter 13

13 Cathedral of Modena: the seismic analyses of structural elements via Discrete Element Methods

13.1 Introduction

In the previous chapters, the FEM model of the Cathedral of Modena, which considers the soil-structure interaction, has been presented. In the FE modelling the masonry is modelled as homogeneous continuum. While this procedure may give indications on the structural response of the global masonry structures, it is not suitable for the detailed stress analysis of specific portions or elements, due to the difficulty of capturing all its expected failure modes. In the light of these considerations, the most vulnerable cross section of the Cathedral of Modena has been investigated through a Discrete Element (DE) modelling.

First, the modelling criteria using Discrete Element Method and a possible calibration of the springs at the base of the walls in order to take into account of the interaction soil-foundation- structure are presented. A sensitivity analysis has been conducted on a simple buttressed vault in order to evaluate the different influence on the structural response due to the modelling parameters.

Then, both static and dynamic analyses are performed on the DEM model of the cross section of the Cathedral of Modena in order to evaluate the interactions between the vaults and the longitudinal walls and the influence of the different soil stiffness at the base. The results are compared with the crack patterns as observed before (for the static analysis) and after (for the dynamic analysis) the 2012 Emilia Earthquake. The structural response of the DEM model has been also compared with the response of corresponding FE models. The results obtained from the different structural analysis approaches have

been compared in order to identify the limitation and reliability of these methods when applied to the structural assessment of masonry historical buildings.

13.2 Modelling criteria using Discrete Element Method

Discrete element methods (DEM) were initially developed for the study of rock mechanical problems by Peter Cundall in the early 1970s (Hart, Cundall, & Lemos, 1988). Due to their capability to allow large displacements and rotation of discrete bodies these methods are particularly suitable for the analysis of the masonry structures made of massive stiff blocks and connected through mortar layers of limited thickness and pure mechanical properties in which a significant part of the deformation is due to relative motion between the blocks. The most used DEM software for both professional and research purposes are Universal Distinct Element Code (UDEC) and Three Dimensional Universal Distinct Element Code (3DEC) (Itasca, 2004). In this study, all the DEM analysis are carried out using 3DEC. 3DEC simulates the response of discontinuous bodies subjected to either static or dynamic loading. The discontinuous bodies are represented as an assemblage of discrete blocks. The joints are viewed as interfaces between distinct bodies (i.e., the discontinuity is treated as a boundary condition). It allow the detachment of the blocks and the automatically detection of new contacts during the calculation progress. The contact forces and displacements at the interfaces of a stressed assembly of blocks are found through a series of calculations, which trace the movements of the blocks. Disturbances caused by applied loads, body forces and contact forces propagate through the block system resulting in displacements of the assemblage. This is a dynamic process in which the speed of propagation of disturbance depends on the physical properties of the discrete system. Two type of blocks can be modelled by 3DEC: rigid blocks, which have six degrees of freedom (three translation and three rotational) and deformable blocks, which are subdivided internally into tetrahedral that have three translation degrees of freedom at each vertex (Itasca,2004). The assumption of rigid blocks is usually applied to structures in which the behaviour is dominated by the discontinuities and the material elastic properties may be neglected. In the present study, the masonry structures are modelled as an assemblage of rigid blocks with frictional joints. Following, the main components of DE modelling are examined.

13.2.1 Contacts blocks interaction

The representation of the interface between two blocks relies on sets of point contacts. Adjacent blocks can touch along a common edge or at discrete points where a corner meets an edge or another corner. The 3DEC program adopts two types of elementary contacts: vertex-to-face, and edge-to-edge, as shows in Table 13-1.
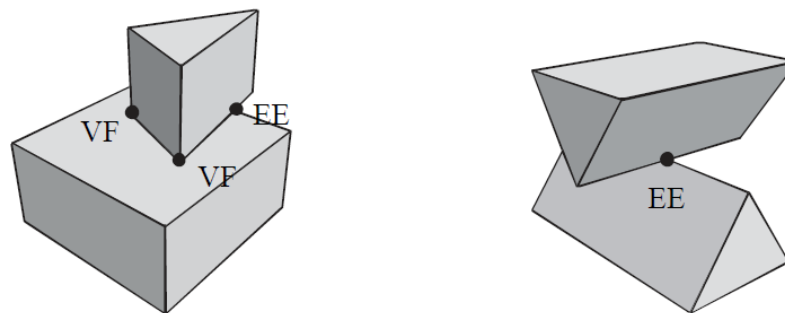
Figure 13-1: Interaction between elementary blocks vertex-to-face (VF) and edge-to-edge (EE): a) the case of face to face, and b) the case of edge to edge.

In DEM contact forces are computed using the soft contact approach, (the contact is assumed deformable). This is achieved by allowing interpenetration or overlapping of the blocks in contact. A finite normal stiffness is taken to represent the measurable stiffness that exists at a contact or joint. The contact forces are assumed to start from zero when the blocks first come in contact and increase as they interpenetrate each other. The model mechanical interaction between blocks is represented by normal and shear elastic springs that connect the blocks (interaction forces are proportional to the relative displacement between the two blocks).

Mechanical behaviour of contacts

The contact stresses are checked against the joint failure criterion to decide whether the block will slide. At each time step the new normal and shear stress, σ_n and σ_s, as a function of the joint displacement increments, old stresses and displacements, and possibly other state parameters are calculated and then compared against the strength criterion of the joint.

$$\sigma_n, \sigma_s = f(\Delta u_n, \Delta u_s, \sigma_n^0, \sigma_s^0, u_n, u_s....) \tag{13.1}$$

The basic joint constitutive model incorporated in 3DEC, and used in this study, is the generalization of the Coulomb friction law (linear elastic perfectly plastic model). In the normal direction, the stress-displacement relation is assumed to be linear and governed by the joint normal stiffness, k_n, (as shown in Eq.13.2) and zero tensile stress is generally assumed (Azevedo et al. 2000).

$$\sigma_n = k_n \cdot u_n \tag{13.2}$$

Where σ_n is the normal stress and un is the normal relative displacement between blocks. The joint normal stress is usually limited to a tensile threshold value, $\sigma_{t\max}$ (usually it is assumed to be zero). If the tensile stress is exceed the constitute equation in the normal direction becomes:

$$if\ \sigma_n < -\sigma_{t\max}\text{,then}\ \sigma_n = 0 \tag{13.3}$$

In the shear direction, the response is controlled by the shear stiffness k_s. The shear stress (Eq.13.4) is limited by a combination of cohesive and frictional strength according to the Coulomb's low (Eq. 13.5).

$$\tau_s = k_s \cdot u_s \tag{13.4}$$

$$|\tau_s| \le c + \sigma_{\max} \cdot \tan\phi = \tau_{\max} \tag{13.5}$$

Where τ_s is the shear stress and u_s is the shear relative displacement between blocks.

The joint property required in the DE modelling are, hence, the normal stiffness, k_n shear stiffness k_s, friction angle ϕ, cohesion c, and tensile strength σ_t.

13.2.2 The calculation cycle

In 3DEC, the dynamic response is performed using a time-stepping algorithm, which solves the equations of motion of the block system by an explicit finite-difference method. At each time-step, the law of motion and the constitutive equations are applied. The integration of the law of motion provides the new block positions and, therefore, the contact-displacement increments (or velocities). The contact force-displacement law is then used to obtain the new contact forces, which are to be applied to the blocks in the next time step. The size of the time step is limited by the assumption that velocities and accelerations are constant within the time-step. It is assumed that the time-step is sufficiently small, so that the disturbance cannot propagate between adjacent discrete elements during a single step (Papantonopoulos et al. 2002b). The central difference algorithm is only numerically stable if the time step Δt is less than the critical time step. An estimate of the critical time step is automatically calculated by the program using a single degree-of-freedom system analogy. The smallest block mass in the problem, m_{min}, and the largest normal or shear contact stiffness, k_{max}, are used to calculate the time step as:

$$\Delta t = frac \cdot 2 \sqrt{\frac{m_{\min}}{k_{\max}}} \tag{13.6}$$

Frac is a user-defined factor, which accounts for the fact that a block may be in contact with several blocks. A value of *frac* equal to 0.1 is usually sufficient to ensure numerical stability.

13.2.3 Damping

Mechanical damping is used in the discrete element method to solve both static (non-inertial) and dynamic problems. Discrete element method employs a mechanical damping to solve both the static (non-inertial) and dynamic problems. For these two class of problems, a different formulation of damping is used. For static analysis, an equivalent viscous damping is commonly used in the equation of motion to achieve a force equilibrium state as quickly as possible under the applied initial and boundary conditions. Damping is assumed to be velocity-proportional (the magnitude of the damping force is proportional to the velocity of the blocks) and introducing body forces that retard steady-state collapse may, in extreme cases, influence the mode of failure. In addition, the optimum proportional constant depends on the eigenvalues of the matrix, which are unknown unless a complete modal analysis is done, and velocity- proportional damping is applied equally to all nodes. In order to overcome these problems, 3DEC provides a so-called "local damping", in which the damping force on a node is proportional to the magnitude of the unbalanced force. In particular, body forces vanish for steady-state condition, the magnitude of damping constant is dimensionless and is independent of properties or boundary condition and the amount of damping varies from point to point (Itasca 2004). The "local damping" has been used in the static analyses developed.

For dynamic analysis, damping is applied in the form of Rayleigh damping:

$$\mathbf{C} = \alpha_R \mathbf{M} + \beta_R \mathbf{K} \qquad (13.7)$$

Where C, M and K are the damping, mass and stiffness matrix, respectively, α_R is the mass-proportional damping constant and β_R is the stiffness-proportional damping constant. The mass-proportional component damps the lower frequency modes of the system, which are usually associated with the movement in unison of several blocks ('sloshing'), while the stiffness-proportional component dominates the high-frequency, generally associated with inter-blocks vibration ('rattling'). Rayleigh damping can be specified by imposing a specific value of damping ratio ξ, which is dependent on the frequency as follows:

$$\xi(\omega) = \frac{1}{2} \left(\frac{\alpha_R}{\omega} + \beta_R \omega \right) \qquad (13.8)$$

Stiffness damping component increases linearly with frequency, proportional to the strain rate, while mass damping component non-linearly decreases with frequency, proportionally to the velocity. The identification of the appropriate damping is a difficult issue. The damping is necessary in order to limit

the extremely high frequency vibration, typically damp out in real material, which can cause unrealistic bouncing in numerical simulation. At the same time, over-damping the response is generally un-conservative and should be avoid (Dimitri et al. 2011). The idea is to try to evaluate the right damping for the important frequencies in the problem. In more detail, when considering the dynamic response of masonry structures the mass proportional damping should be neglected (Papantonopoulos et al. 2002b; Dejong 2009). The use of even small mass damping may artificially restrict the motion of the blocks and over- damped the response of the structure (as demonstrated in both the works through the comparison of numerical and experimental results).

13.2.4 Defining modelling parameters for the masonry structural elements of the Cathedral of Modena

Based on the consideration reported in the previous sections, the procedures adopted for the definition of the modelling parameters necessary for the study of the masonry structural elements (cross-section and vaults of the Cathedral of Modena) here analysed, are described. The masonry structure is modelled as assemblages of rigid blocks with the elasticity of all material concentrate in the joints. The tensile strength has been considered as zero. In addition, a stiffness-proportional damping is determined according to the natural frequencies of individual blocks (Dejong 2009).

Joint Stiffness

The joint stiffness, k_n and k_s are defined using the material property of the blocks as following:

$$k_n = \frac{EA}{L} \tag{13.9}$$

$$k_s = \frac{GA}{L} \tag{13.10}$$

Where E and G are the elastic and shear modulus of the masonry blocks, respectively, A is the area of the contact between the blocks, L is the length of the rigid material represented in the direction perpendicular the joint and ν is the Poisson ration of the masonry.

Critical frequency

According to the study of DeJong the single rocking block presents three different type of impact (between the block and the base): vertical translation corner impact, vertical translation edge impact and rotational impact. The natural frequency of the block related to these three impulse has been estimated considering the block always in contact with the base. In 3DEC, block contact are modelled with a spring-dashpot element at each corner-edge or corner-corner contact. Thus the single rocking block has a vertical spring with stiffness k , and a vertical damping , at each of its bottom corners (Figure 13-2).
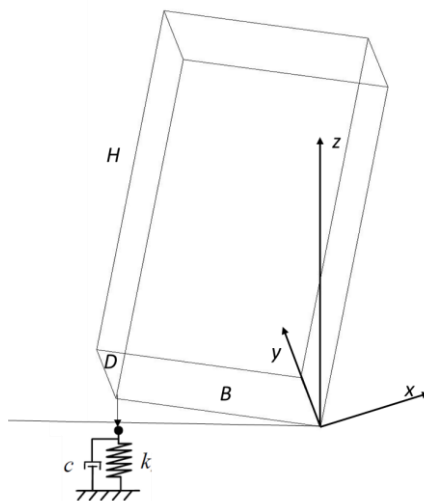
Figure 13-2: 3D single block

The natural frequency of the tree type of impacts can be evaluated as follows (Dejong 2009):

$$\text{Corner impact } \omega_c = \sqrt{\frac{k}{m}} \tag{13.11}$$

$$\text{Edge impact } \omega_e = \sqrt{\frac{2k}{m}} \tag{13.12}$$

$$\text{Rotational impact } \omega_r = \sqrt{\frac{kB^2}{J}} \tag{13.13}$$

The spring stiffness for rectangular blocks can be defined as following

$$k_i = \frac{E}{L}\left(\frac{BD}{4}\right) \tag{13.14}$$

The mass moment of inertia J, for a rectangular block, is:

$$J = \frac{m}{3}\left(B^2 + H^2\right) = \frac{\rho BHD}{3}(B^2 + H^2) \tag{13.15}$$

Thus, making use of Equations 13.11 -13.15 the impact frequencies of the system can be expressed in terms of the specific geometrical and mechanical properties of the system:

$$\text{Corner impact } \omega_c = \sqrt{\frac{EBD}{4Lm}} \tag{13.16}$$

$$\text{Edge impact } \omega_e = \sqrt{\frac{EBD}{2Hm}} \tag{13.17}$$

$$\text{Rotational impact } \omega_r = \sqrt{\frac{3EB^2}{4\rho L^2 (B^2 + L^2)}} \tag{13.18}$$

The critical damping frequency in the present study is evaluated specifying critical damping ($\xi = 100\%$) at the highest frequency of the system:

$$\text{Critical frequency } \omega_{crit} = \max(\omega_c, \omega_e, \omega_r) \tag{13.19}$$

In this way, the other frequencies will be under-damped.

Therefore, the damping at the critical impact frequency can be specified as:

$$\beta_R = \frac{2\xi}{\omega_{crit}} = \frac{\xi}{\pi f_{crit}} \tag{13.19}$$

The critical impact frequency as obtained is related to a single block. For a system of multiple blocks of approximately the same size, the critical frequency can be estimated by $\omega_{crit,m} = \omega_{crit}\sqrt{2}$ (Dejong 2009).

13.3 The modelling of masonry structural elements accounting for the soil-foundation stiffness

Generally, the DE method is used to model masonry structures considering the base as fixed by assigning a very large stiffness to the blocks, which are connected to the base. Nevertheless, as highlighted in the previous chapters the differential soil-to-foundation stiffness (in both the vertical and horizontal direction) has probably influenced the actual cracking condition of the monument. As such in the present section a specific study on the influence of the soil-to-foundation stiffness in the dynamic response as obtained through DEM simulations is carried out. In detail, a possible strategy to study the influence of the different soil stiffness at the base of the Cathedral of Modena without directly modelling the whole foundation system is based on the definition of an equivalent stiffness at the interfaces between the base of the walls and the soil, which has to be properly calibrated.

13.3.1 The equivalent stiffness

Considering the foundation as a rectangular block the interaction between the lateral soil and the foundation can be schematized through the shear stiffness k_s. (Figure 13-3 a). The soil stiffness k_s contrast the sliding and the rotation of the block. For this reason, to take into account the soil-foundation-interaction is not enough to consider only the increase of k_s, which takes account of the depth of the foundation, but we must also consider the increase of the normal stiffness (k_n) at the base due to the rotational stiffness offered by k_s. The simple calculations considered to evaluate the increment of the normal stiffness are display through the Equation 13.20-13.23.

(a)   (b)
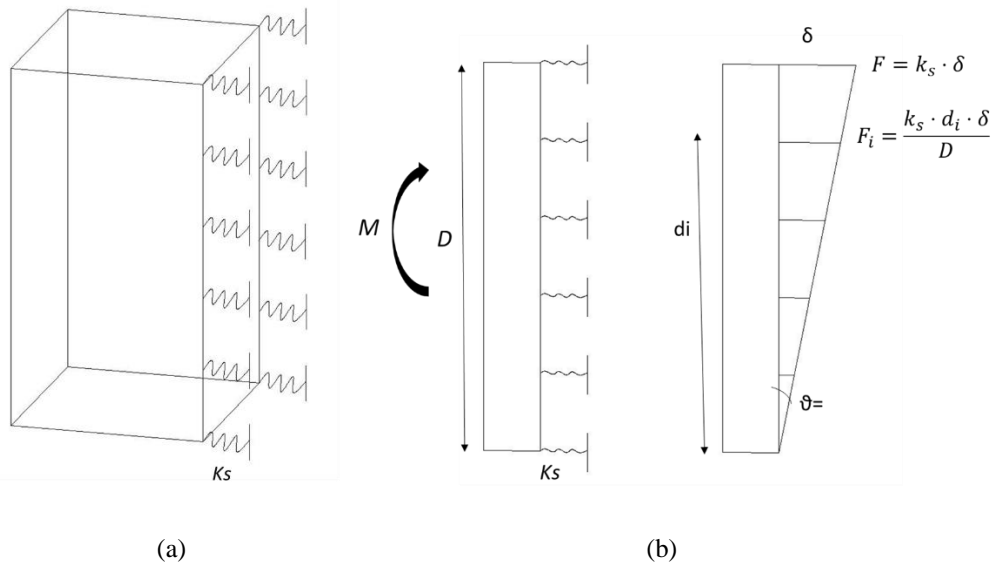
Figure 13-3: Interaction between foundation and soil

Considering the schematization of Figure 13-3 b, using a simple equilibrium equation the rotational stiffness of the block k_ϑ and the corresponding increments of the k_n are:

$$M = \sum F_i \cdot d_i = \sum \frac{k_s \cdot d_i^2 \cdot \delta}{D}$$

(13.20)

$$k_\vartheta = \frac{M}{\vartheta} = \sum \frac{k_s \cdot d_i^2 \cdot \delta}{D} \cdot \frac{D}{\delta} = \sum k_s \cdot d_i^2$$

(13.21)

$$F = \frac{M}{D} = \frac{k_\vartheta \cdot \vartheta}{D}$$

(13.22)

$$\Delta k_n = \frac{F}{\delta} = \frac{2k_\vartheta}{D^2}$$

(13.23)

$$k_{ntot} = k_n + \Delta k_n$$

(13.23)

13.3.2 Parametric study: single column with foundation

If the influence of the soil-structure interaction cannot be neglected, the normal stiffness have to be calibrate in order to obtained an equivalent stiffness able to take into account the soil-foundation-structure interaction. In order to verify if the equivalent normal stiffness introduced is able to take into account of the soil-foundation-structures a static and dynamic analyses have been conducted on a longitudinal wall (10 meters) of the Cathedral schematized trough a simple column (undergo the weight of the overlying vault and wall). First, the column without modelling the foundation (Figure 13-4a) has been analyzed considering the stiffness at the base as obtained from the geotechnical investigation (and as explained in §10.3.2). Then the structural response of the same column has been evaluated considering the equivalent stiffness at the base and the results were compared with those obtained modelling the foundation. (Figure 13-4b). The elastic modulus (E) used in the calculations of the normal and shear stiffness is equal to 414400 KPa.

(a)   (b)
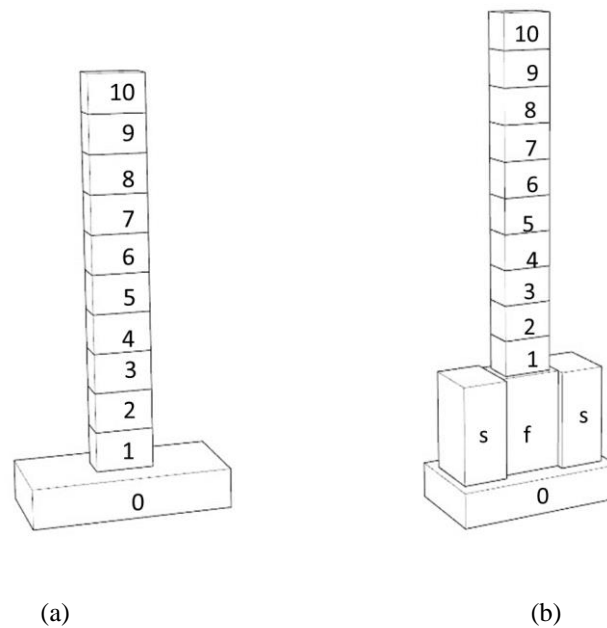
Figure 13-4: a) Column without the modelling of the foundation, b) Column and foundation

Modelling parameters

The parameters used in the analyses of the column without the modelling of the foundation are summarized in the Table 13-1 and Table 13-2.

Table 13-1- The properties of the blocks used in the analyses of the column without the modelling of the foundation

Element	Weight per unit volume [KN/m³]	Dimension of the blocks [m]	Density [10³Kg/m³]
Block$_{10}$	616 KN/m³	1,5·1·1m	62
Blocks$_1$	180 KN/m³	1,5·1·1m	18
Blocks$_{2-9}$	721 KN/m³	1,5·1·1m	72

Table 13-2- The properties of the interfaces used in the analyses of the column without the modelling of the foundation

Interface	Joint Kn [KPa/m]	Joint Ks [Kpa/m]	Damping
Block$_{2-10}$	4.2x10^7	1.8x10^7	242
Block$_0$.block$_1$	5.1x10^4	1.3x10^6	

The equivalent normal stiffness at the base of the column is:

$$k_{ntot} = k_n + \Delta k_n = 5.1 \cdot 10^4 + 3.8 \cdot 10^6 = 3.87 \cdot 10^6 \frac{kPa}{m}$$

(14.24)

The parameters used in the analyses of the column modelling of the foundation are summarized in the Table 13-3 and Table 13-4.

Table 13-3- The properties of the blocks used in the analyses of the column modelling of the foundation

Element	Weight per unit volume [KN/m³]	Dimension of the blocks [m]	Density [10³Kg/m³]
Block$_{10}$	616	1,5·1·1m	62
Blocks$_{1-9}$	180	1,5·1·1m	18
Foundation	121	1.9·2.8·1.4	12
Soil	84	1.4·2.8·1.9	8.4

Table 13-4- The properties of the interfaces used in the analyses of the column modelling of the foundation

Interface	Joint Kn [KPa/m]	Joint Ks [Kpa/m]	Damping
$Block_{1-10}$	$4.2x10^7$	$1.8x10^7$	271
$Block_1\_f$	$2.2x10^7$	$9.2x10^6$	
f-soil	$4.0x10^4$	$5.6x10^5$	
Lateral f-soil	$4.5x10^5$	$1.9x10^5$	

As expected, considering the stiffness at the base of the column as obtained from the geotechnical investigation without modelling the foundation, the system reaches the collapses. Figure 13-5 shows the displacement recorded at the top of the columns during the dynamic analysis for: (i) the model that consider the equivalent stiffness at the base (EQ) and (ii) the model that directly modelling the foundation (F). It seems that for this simple model the equivalent stiffness is able to take into account of the interaction soil-foundation-structure.
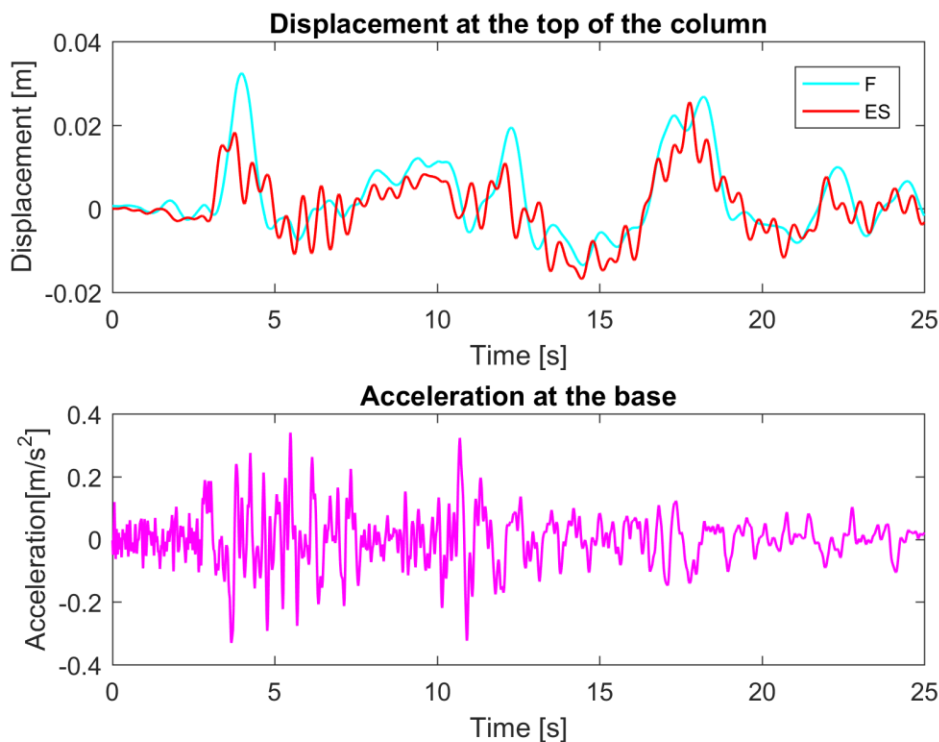
Figure 13-5: plot of the displacements at the top of the column as obtained for: (i) the model that consider the equivalent stiffness at the base (EQ) and (ii) the model that directly modelling the foundation (F) and the input acceleration used in the dynamic analysis.

13.3.3 Parametric study: buttressed vault

A sensitivity analysis has been conducted on a simple buttressed vault in order to evaluate the different influence on the structural response due to the modelling parameters. The 2D model analysed in 3DEC (Figure 13-6b) represents a portion of two longitudinal walls (10 meters) of the Cathedral and the two overhanging vaults (Figure 13-6a). The properties of the rigid blocks (density) and joints (normal stiffness, shear stiffness, friction angle) used in the 2D model are calculated in order to model the real portion of structure considered (the density of the blocks and the stiffness at the interfaces takes into account the depth of 10 meters of the walls and of the vaults and the weight of the overlying non-structural elements). Starting from the soil stiffness as obtained from geotechnical investigations for the Cathedral of Modena (§10.3.2), additional analyses have been carry out increasing the normal stiffness and shear stiffness at the base of the structure. The structural response considering different number of blocks to represent the arch has been also considered. The elastic modulus (E) used in the calculations of the normal and shear stiffness is equal to 414400 KPa.

(a)   (b)
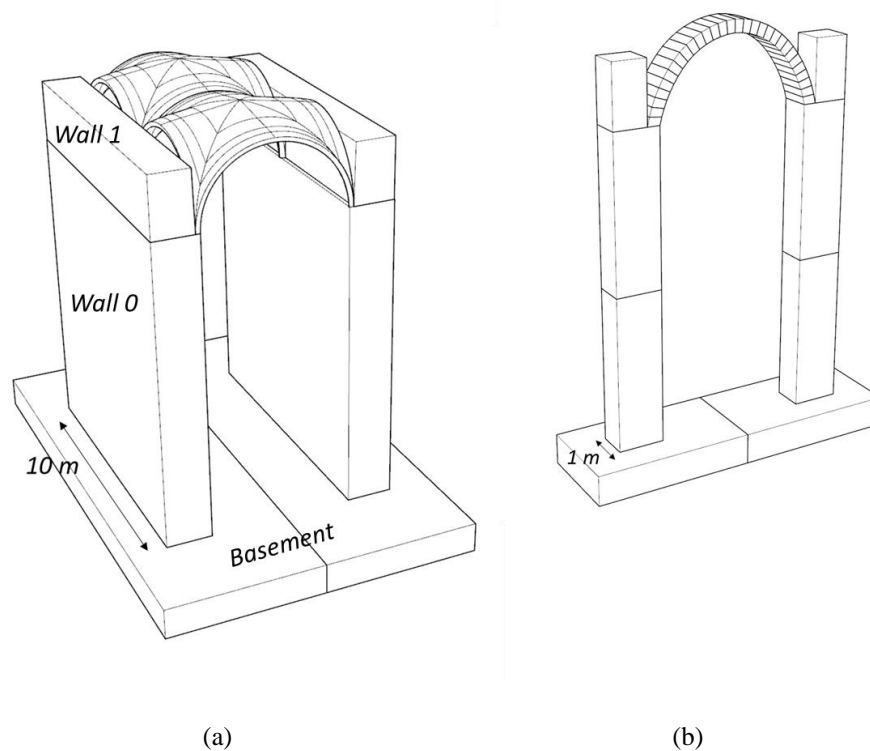
Figure 13-6: (a) Portion of the Cathedral of Modena, (b) 2D model

Modelling parameters

The calculation of the modelling parameters are reported on the Appendix D.1. Below the modelling parameters used are only synthetically shown in the Table 13-5 and Table 13-6.

Properties of the blocks:

Table 13-5- The properties of the blocks used in the analyses

Element	Weight per unit volume [KN/m³]	Dimension of the blocks [m]	Density [10^3Kg/m³]
$Wall_0$	125	1.5·1·5.05 m	12.5
$Wall_1$	213	1.1·1·1.9 m	21.3
Arch	141	0.4·1·0.27 m	14.1

Joint stiffness of the interfaces:

Table 13-6- The properties of the interfaces used in the analyses

Interface	Joint Kn [KPa/m]	Joint Ks [Kpa/m]
$Wall_0$	8.2 10^6	3.5 10^6
$Wall_0$-$Wall_1$	1.2 10^7	5.0 10^6
Arch	3.0 10^7	1.3 10^7
Arch-$wall_0$	1.3 10^7	5.5 10^6
$wall_0$-Soil	5.1 10^4	1.3 10^6

Damping

$$f_{crit} = \frac{\omega_e \sqrt{2}}{2\pi} = \frac{1270\sqrt{2}}{2\pi} = 202 cicles / \sec onds$$

13.3.3.1 Variation of the normal stiffness at the base of the walls

For the 2D model, the gravity load is first applied and then, when the structure reaches the equilibrium, the ground motion is applied to the blocks at base of the columns (considering as input the acceleration recorded by the MDN station during the 2012 earthquake §10.5). The values of the normal stiffness at the interface between the walls 0 and the soil are varied between the lower limit case (even though not realistic) of absence of foundation (e.g. normal stiffness equal to the stiffness of the soil, as obtained in the previous section) to the limiting case of fixed base condition (e.g. normal stiffness equal to the block-to-block normal stiffness without consider the influence of the soil). In addition, the value of the normal stiffness corresponding to absence of foundation was increased stepwise (approximately 5 times) in order to evaluate the influence on the structural response of these small increments of normal stiffness. The equivalent stiffness in order to take into account of the soil-foundation-structures was also considered. Table 13-7 displays the different values of normal stiffness used and the corresponding displacement, in the x direction (dx), recorded at the springers of the arch. The displacements recorded at the two springers of the arch for both the static and dynamic analyses are approximately the same. Therefore, the results plotted in Figure 13-7 for the dynamic analysis are concerning to the displacement of one of the two points monitored (right of the arch). For more detail, see Appendix D.1.1. Considering directly the soil stiffness under the Cathedral of Modena caused the collapse of the buttressed vault for static load (Figure 13-8). Therefore, the use of the normal stiffness of the soil without consider the soil-foundation-structure interaction misinterpret the structural response. The structural response, hence, is very sensitive to the variation of the normal stiffness at the base. Considering the static analysis, for values of the normal stiffness lower than around $7.0 \cdot 10^5$, the increase of 5 times the normal stiffness reduces the maximum displacements at the springers of the arch by around 50%. For values of the normal stiffness greater of around $7.0 \cdot 10^5$, the increase of 5 times the normal stiffness reduces the maximum displacements at the springers of the arch for static load of around 20-25%. Considering the dynamic analysis, for values of the normal stiffness lower of around $7.0 \cdot 10^5$ the maximum displacements recorded, for the different normal stiffness, are of the same order of magnitude. Increasing this normal stiffness by 5 times reduces the maximum displacements for dynamic loads by around 40%.

Table 13-7- The different normal stiffness used in the analyses and the corresponding maximum displacements

Default parameters	Kn at the base [Kpa/m]	Static Response "Local Damp" dx	Seismic Response Damp=202 dx
Ks=1.3·106 [KPa/m]	$Kn_{absence\_fondation} = 5.1 \cdot 10^4$	Static collapse	-
$\varphi = 35°$	$Kn_1 = 2.6 \cdot 10^5$	0.04 m	0.052 m
coh=0	$Kn_2 = 4.7 \cdot 10^5$	0.02 m	0.058
n blocks arch =6	$Kn_3 = 6.8 \cdot 10^5$	0.013 m	0.05m
	$Kn_4 = 8.9 \cdot 10^5$	0.010 m	0.034
	$Kn_5 = 1.1 \cdot 10^6$	0.008 m	0.033
	$Kn_{Equivalent} = K_n EQ = 2.7 \cdot 10^6$	0.004	0.029
	$Kn_{fixed\_base} = K_n FB = 8.2 \cdot 10^6$	0.002	0.023
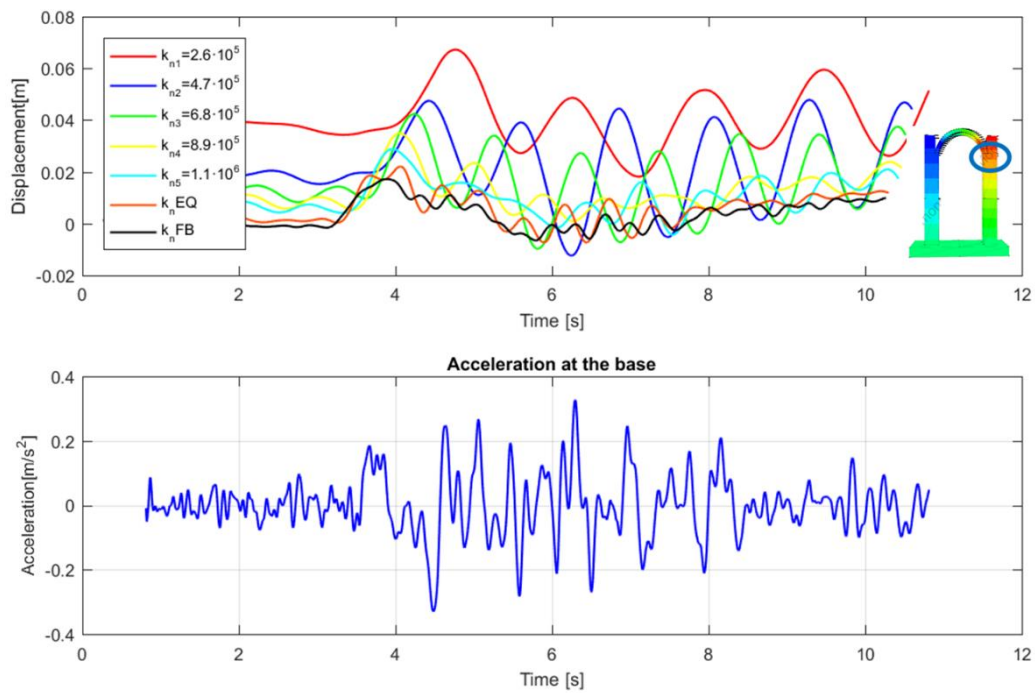
Figure 13-7: Plot of the maximum displacements recorded at the right springer of the arch during the dynamic analysis considering different normal stiffness at the base
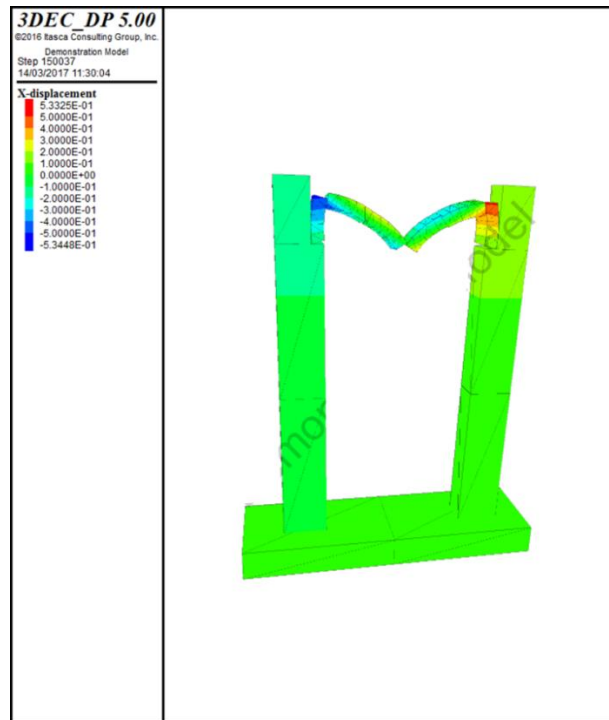
Figure 13-8: Collapse of the buttress vault considering directly the soil stiffness under the Cathedral of Modena

13.3.3.2 Variation of the shear stiffness at the base of the walls

The same analyses have been conducted considering the two limit cases for the shear stiffness (absence of foundation and fixed base condition) and gradually increasing (in increments of $2.0 \cdot 10^5$ times) the shear stiffness corresponding to the absence of foundation at the base of the walls. The normal stiffness used to perform these analyses is k_{n1}. Table 13-8 displays the different values of shear stiffness used and the respective maximum displacement (dx) recorded at the springers of the arch during the analyses. The results are plotted in Figure 13-9 for the dynamic analysis. For more detail, see Appendix D.1.2. The variation of the shear stiffness at the base of the walls appears not to affect the structural response of the buttress vault.

Table 13-8- The different shear stiffness used in the analyses and the corresponding maximum displacements

Default parameters	Ks at the base [Kpa/m]	Static Response "Local Damp" dx	Seismic Response Damp=202 dx
$K_{n1}=2.6\cdot10^5$ [Kpa/m]	$Ks_{absence\_fondation}=1.3\cdot10^6$	0.038m	0.05m
$\varphi=35°$	$K_{s1}=1.5\cdot10^6$	0.037m	0.05m
coh=0	$K_{s2}=1.7\cdot10^6$	0.037m	0.05m
n=6	$K_{s3}=1.9\cdot10^6$	0.037m	0.05m
	$K_{s4}=2.1\cdot10^6$	0.037m	0.05m
	$K_{s5}=2.3\cdot10^6$	0.037m	0.05m
	$Ks_{fixed\_base}=K_sFB=3.5\cdot10^6$	0.037	0.05
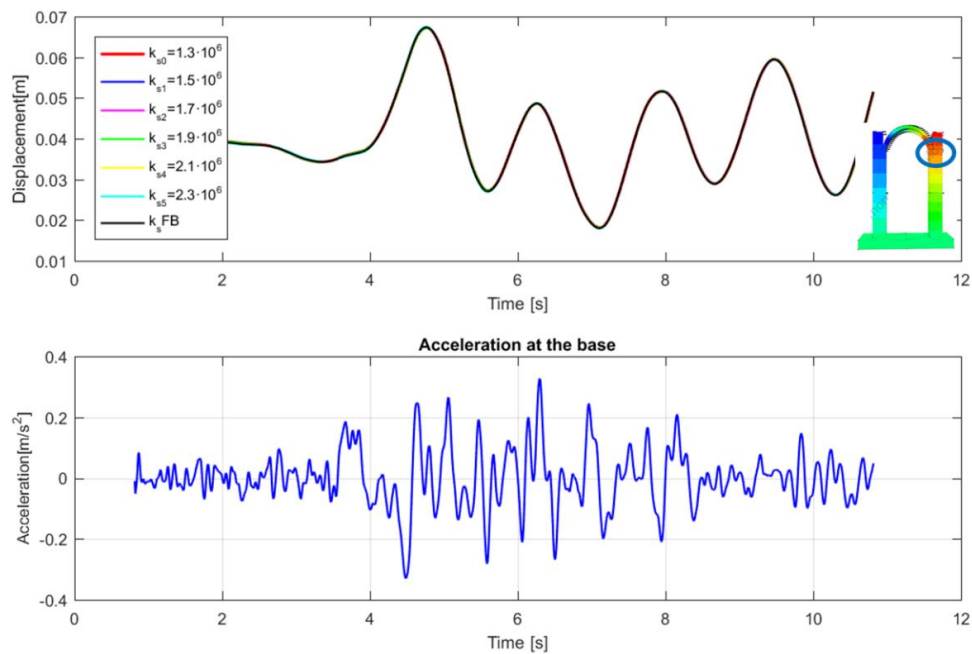
Figure 13-9: Plot of the maximum displacements recorded at the right springer of the arch during the dynamic analysis considering different shear stiffness at the base

13.3.3.3 Variation of numbers of blocks of the arch

The previous analyses have been also conducted considering the arch composed by different numbers of blocks.

13.3.3.3.1 Arch composed by three blocks

The joints stiffness of the interfaces between the three blocks of the arch are summarized in the Table 13-9- The properties of the interfaces considering the arch composed by three blocks (see Appendix

D.1.3 for more detail). Table 13-10Table 13-9 and Table 13-11 display the different values of normal stiffness and shear stiffness used and the respective maximum displacements (dx) recorded at the springers of the arch. The results are plotted in Figure 13-10 and Figure 13-11 for the dynamic analysis. For more detail, see Appendix D.1.3. Decreasing the number of blocks to model the arch the maximum displacements recorded during the analyses are approximately the same. As expected, for low normal stiffness at the base, the model with the arch composed by three blocks displays a lower maximum displacement compared with the same model with the arch composed by six blocks for the static analysis.

Table 13-9- The properties of the interfaces considering the arch composed by three blocks

Interface	Joint Kn [KPa/m]	Joint Ks [Kpa/m]
$Wall_0$	$8.2 \cdot 10^6$	$3.5 \cdot 10^6$
$Wall_0$-$Wall_1$	$1.2 \cdot 10^7$	$5.0 \cdot 10^6$
Arch	$\mathbf{1.5 \cdot 10^7}$	$\mathbf{6.5 \cdot 10^6}$
Arch-$wall_0$	$\mathbf{1.1 \cdot 10^7}$	$\mathbf{4.5 \cdot 10^6}$
$wall_0$-Soil	$5.1 \cdot 10^4$	$1.3 \cdot 10^6$

Variation of normal stiffness

Table 13-10- Arch composed by three blocks: the different normal stiffness used in the analyses and the corresponding maximum displacements

Default parameters	Kn at the base [Kpa/m]	Static Response "Local Damp" dx	Seismic Response Damp=101 dx
$Ks=1.3\cdot10^6$ [Kpa/m]	$Kn_{absence\_fondation}=5.1\cdot10^4$	Static collapse	-
$\varphi=35°$	$Kn1=2.6\cdot10^5$	0.03m	0.06m
coh=0	$Kn2=4.7\cdot10^5$	0.02	0.06m
n blocks arch =3	$Kn3=6.8\cdot10^5$	0.011	0.05m
	$Kn4=8.9\cdot10^5$	0.008	0.03m
	$Kn5=1.1\cdot10^6$	0.007	0.03m
	$Kn_{Equivalent}=K_nEQ=2.7\cdot10^6$	0.003	0.027
	$Kn_{fixed\_base}=K_nFB=8.2\cdot10^6$	0.001	0.023
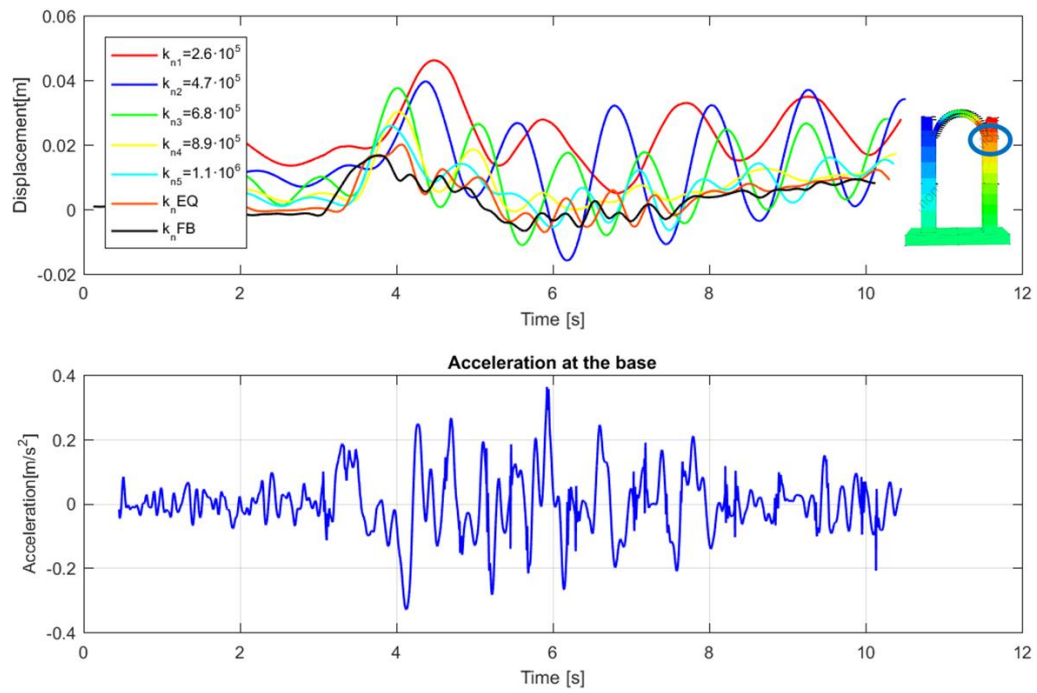
Figure 13-10: Plot of the maximum displacements recorded at the right springer of the arch during the dynamic analysis considering different normal stiffness at the base and the arch modelled by three blocks

Variation of shear stiffness

Table 13-11- Arch composed by three blocks: the different shear stiffness used in the analyses and the corresponding maximum displacements

Default parameters	Ks at the base [Kpa/m]	Static Response "Local Damp" dx	Seismic Response Damp=101 dx
Kn1=2.6·105 [Kpa/m]	$Ks_{absence\_fondation} = 1.3 \cdot 10^6$	0.038m	0.05m
φ =35°	$Ks_1 = 1.5 \cdot 10^6$	0.037m	0.05m
coh=0	$Ks_2 = 1.7 \cdot 10^6$	0.037m	0.05m
n blocks arch =3	$Ks_3 = 1.9 \cdot 10^6$	0.037m	0.05m
	$Ks_4 = 2.1 \cdot 10^6$	0.037m	0.05m
	$Ks_5 = 2.3 \cdot 10^6$	0.038m	0.05m
	$Ks_{fixed\_base} = K_s FB = 3.5 \cdot 10^6$	0.038	0.05
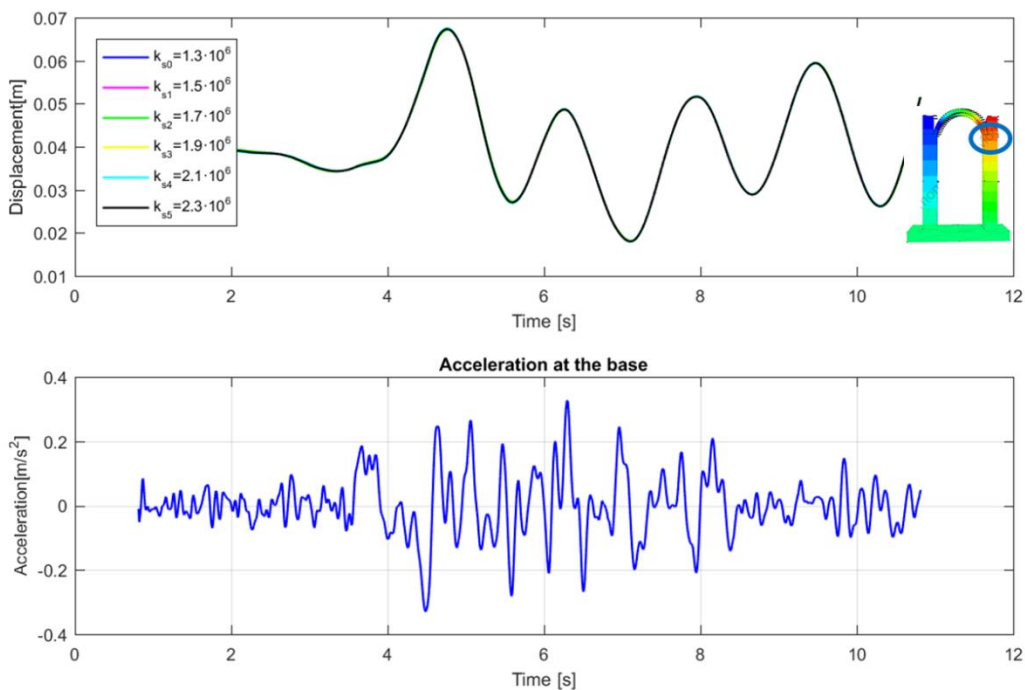
Figure 13-11: Plot of the maximum displacements recorded at the right springer of the arch during the dynamic analysis considering different shear stiffness at the base and the arch modelled by three blocks

13.3.3.3.2 Arch composed by two blocks

Similarly, the joints stiffness of the interfaces between the two blocks of the arch are summarized in the Table 13-12. Table 13-13 and Table 13-14 display the different values of normal stiffness and shear stiffness used and the respective maximum displacements (dx) recorded at the springers of the arch.

Table 13-12- The properties of the interfaces considering the arch composed by two blocks

Interface	Joint Kn [KPa/m]	Joint Ks [Kpa/m]
$Wall_0$	$8.2 \ 10^6$	$3.5 \ 10^6$
$Wall_0$-$Wall_1$	$1.2 \ 10^7$	$5.0 \ 10^6$
Arch	**$1.0 \ 10^7$**	**$4.3 \ 10^6$**
Arch-$wall_0$	**$9.1 \ 10^6$**	**$3.9 \ 10^6$**
$wall_0$-Soil	$5.1 \ 10^4$	$1.3 \ 10^6$

Variation of normal stiffness

Table 13-13-: Arch composed by two blocks: the different normal stiffness used in the analyses and the corresponding maximum displacements

Default parameters	Kn at the base [Kpa/m]	Static Response "Local Damp" dx	Seismic Response Damp=72 dx
Ks=1.3·106 [Kpa/m]	Kn0=5.1·10^4	collapse	-
φ =35°	Kn1=2.6·10^5	0.04m	0.06 m
coh=0	Kn2=4.7·10^5	0.02m	0.06m
n blocks arch =2	Kn3=6.8·10^5	0.01m	0.04m
	Kn4=8.9·10^5	0.01m	0.03 m
	Kn5=1.1·10^6	0.008 m	0.03
	Kn$_{Equivalent}$=K$_n$EQ=2.7·10^6	0.004	0.028
	Kn$_{fixed\_base}$=K$_n$FB=8.2·10^6	0.001	0.024

Figure 13-12 displays the results obtained from the dynamic analyses of the buttressed vaults considering the arch compose by two, three and six blocks respectively and for the normal stiffness Kn3=6.8·10^5 KPa/m, Kn$_{Equivalent}$=K$_n$EQ=2.7·10^6 and Kn$_{fixed\_base}$=K$_n$FB=8.2·10^6. Considering the arch composed by two blocks a slight difference in the structural response respect to the arch made up of three blocks has been identified.
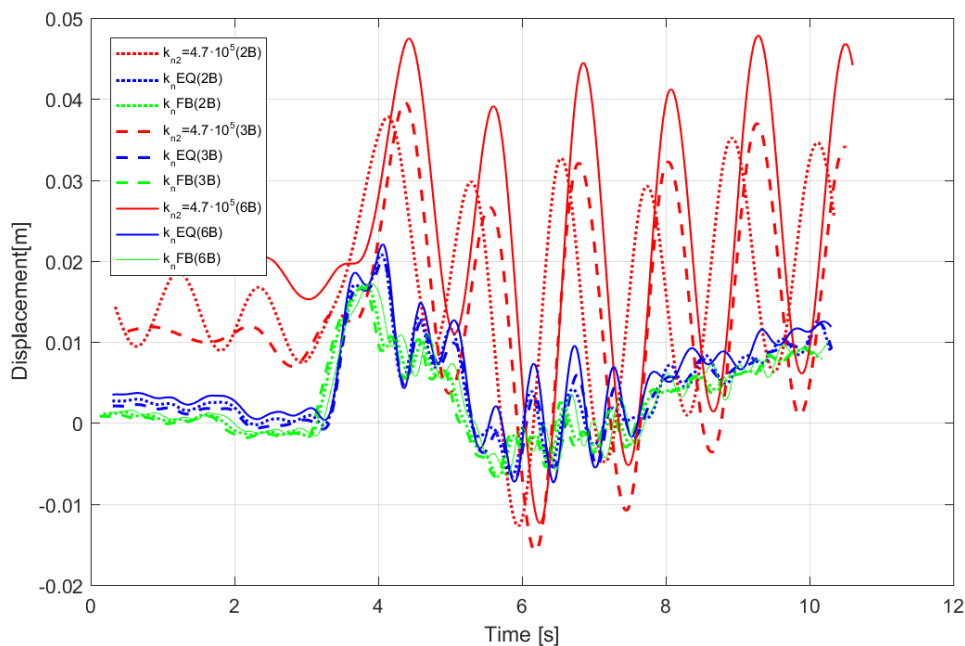
Figure 13-12: Plot of the maximum displacements recorded at the right springer of the arch during the dynamic analysis considering different normal stiffness at the base and the arch modelled by :two blocks (2B), three blocks (3B) and six blocks (6B).

Variation of shear stiffness

Table 13-14- Arch composed by two blocks: the different shear stiffness used in the analyses and the corresponding maximum displacements

Default parameters	Ks at the base [Kpa/m]	Static Response "Local Damp" dx	Seismic Response Damp=72 dx
$Kn1=2.6 \cdot 10^5$ [Kpa/m]	$Ks_{absence\_fondation}=1.3 \cdot 10^6$	0.037	0.64
$\varphi = 35°$	$Ks_1=1.5 \cdot 10^6$	0.037	0.64
coh=0	$Ks_2=1.7 \cdot 10^6$	0.037	0.64
n blocks arch =3	$Ks_3=1.9 \cdot 10^6$	0.037	0.64
	$Ks_4=2.1 \cdot 10^6$	0.037	0.64
	$Ks_5=2.3 \cdot 10^6$	0.037	0.64
	$Ks_{fixed\_base}=K_sFB=3.5 \cdot 10^6$		

Considering the arch composed by two blocks the variation of the shear stiffness at the base of the walls appears, also in this case, not to affect the structural response. Figure 13-13 shows the results obtained from the dynamic analyses of the buttressed vaults considering the arch compose by two, three and six blocks respectively and for the shear stiffness $Ks_2=1.7 \cdot 10^6$. It is interesting noticed that the structural response of the buttressed vault considering the arch composed by three and six blocks and the same normal and shear stiffness at the base does not present significant differences.
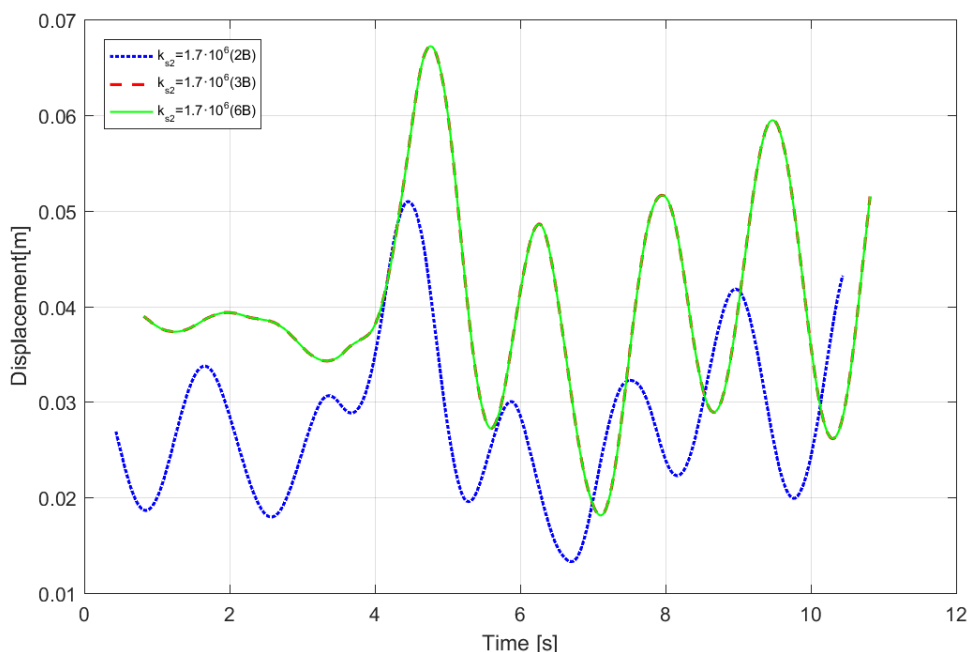
Figure 13-13: Plot of the maximum displacements recorded at the right springer of the arch during the dynamic analysis considering the shear stiffness k_{s2} at the base and the arch modelled by: two blocks (2B), three blocks (3B) and six blocks (6B).

13.4 3DEC analyses of transversal cross section

In the light of the results obtained in the previous chapters, the cross section located in the fourth span from the west and characterized by different soil stiffness and absence of tie-rods appears the most vulnerable portion of the cathedral (Figure 13-14). This cross section has been investigated in order to evaluate the interactions between the vaults and the longitudinal walls under seismic loads.
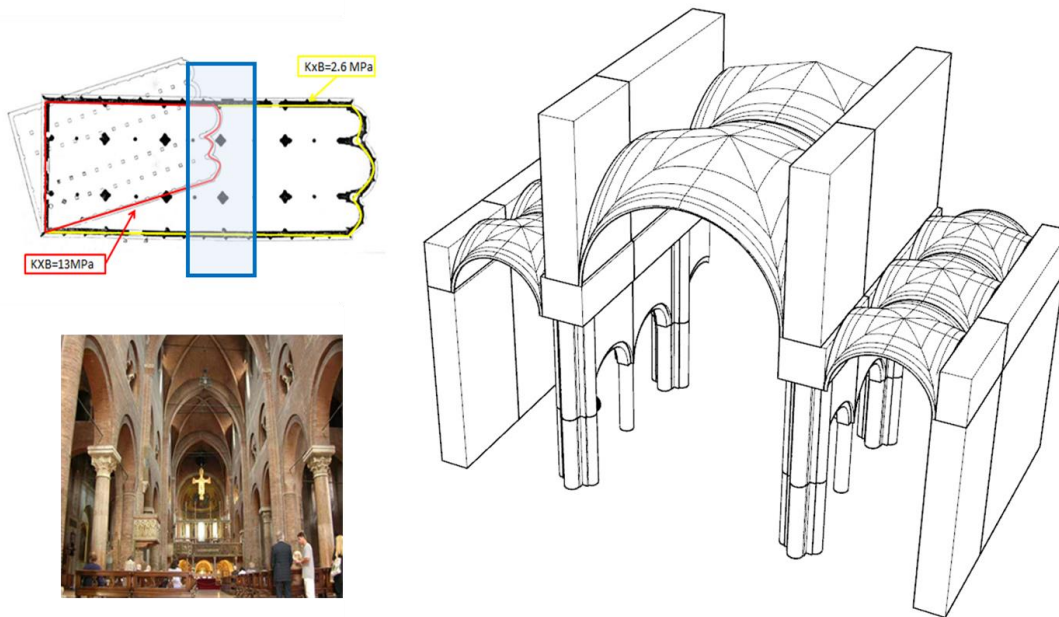
Figure 13-14: Position of the cross section studied

13.4.1 The model and the analyses

The cross section has been investigated trough 2D models (where the density of the blocks and the stiffness at the interfaces takes into account the depth of 10 meters of the walls and of the vaults and the weight of the overlying non-structural elements) in order to evaluate the dynamic response of this portion of the Cathedral and the interaction between the vaults and the longitudinal walls. Figure 13-15 schematizes the structural elements of the portion of the Cathedral investigated. Two-limit schematizations have been considered in the analyses:

(i)   2D cross section modelling the longitudinal walls, the vaults and also the transversal walls (hereinafter called "COMPLETE DEM" and represented in Figure 13-15b) and

(ii)   2D cross section schematizing only the longitudinal walls and the vaults (hereinafter called "SIMPLIFIED DEM" and represented in Figure 13-15c). The transversal walls are here considered only as weight applied.

The COMPLETE DEM model is analyzed under static loads only, given the onerous computational time required to develop an earthquake time-history analysis. The main issue is to evaluate the detachment

of the blocks (corresponding to the cracks openings) and compare them with the observed crack patterns. The SIMPLIFIED DEM model is analyzed under both static gravity loads and earthquake ground motion.

It has to be noted that the complete model is able to account for the lateral trust exerted by the lower arches, which is not considered in the simplified model. Such a discrepancy may affect the lateral displacement induced by both vertical and horizontal loads.

In the case of dynamic analyses, after the application of the gravity loads, the ground motion recorded in Modena during the 2012 Emilia's earthquake is applied to blocks 9,10,11. The earthquake response of the simplified DEM model has been also compared with the response of the corresponding FE models. The results obtained from the different structural analysis approaches have been compared in order to identify the limitation and reliability of these methods when applied to the structural assessment of masonry historical buildings. The analyses developed are summarized in Table 13-15.

(a)   (b)   (c)
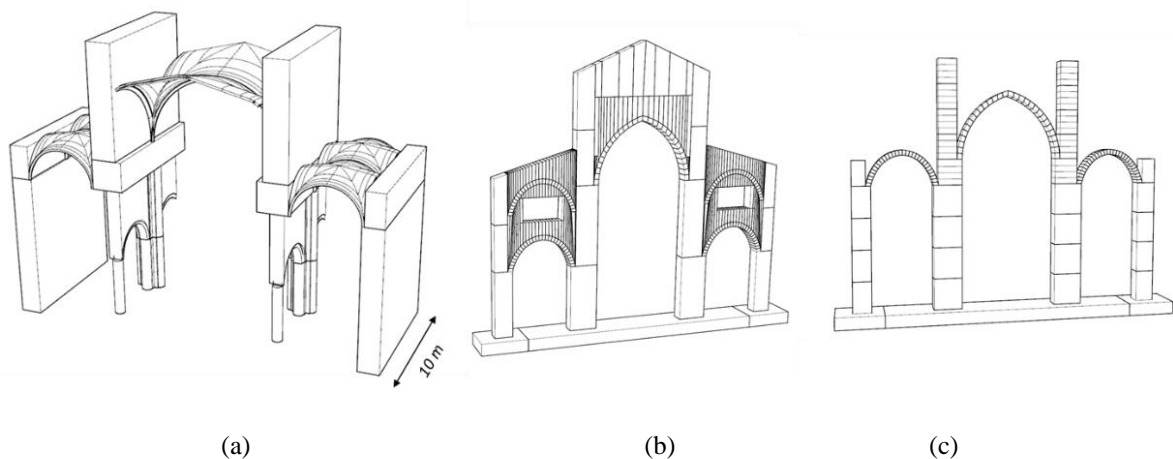
Figure 13-15: (a) The investigated cross-section of the Cathedral of Modena: representation of the structural elements, (b) the "COMPLETE DEM", (c) the "SIMPLIFIDE DEM"

Table 13-15- The different analyses developed

Model	Static analysis	Dynamic analysis (Acceleration recorded in Modena)
COMPLETE DEM	x	
SIMPLIFIED DEM	x	x
SIMPLIFIED FEM	x	x

13.4.2 The modelling parameters of the three numerical models

The calculation of the modelling parameters used in the models are reported on the Appendix D.2. In the next sections, the modelling parameters used in the analyses are only synthetically shown.

13.4.2.1 Complete DEM model

Figure 13-16a shows the "COMPLETE DEM" model analysed and the names of the elements used in the calculation of the properties of the blocks and interfaces. In particular, Figure 13-16a displays the rendering made with the software Rhinoceros 5 and imported in 3DEC. The specific number of blocks in which the elements have been subdivided is shown in Figure 13-16b (that represents the 3DEC model). It can be noticed that the arches were schematized with six blocks. The modelling parameters used are reported in the Table 13-16, Table 13-17 and Table 13-18.

(a)   (b)
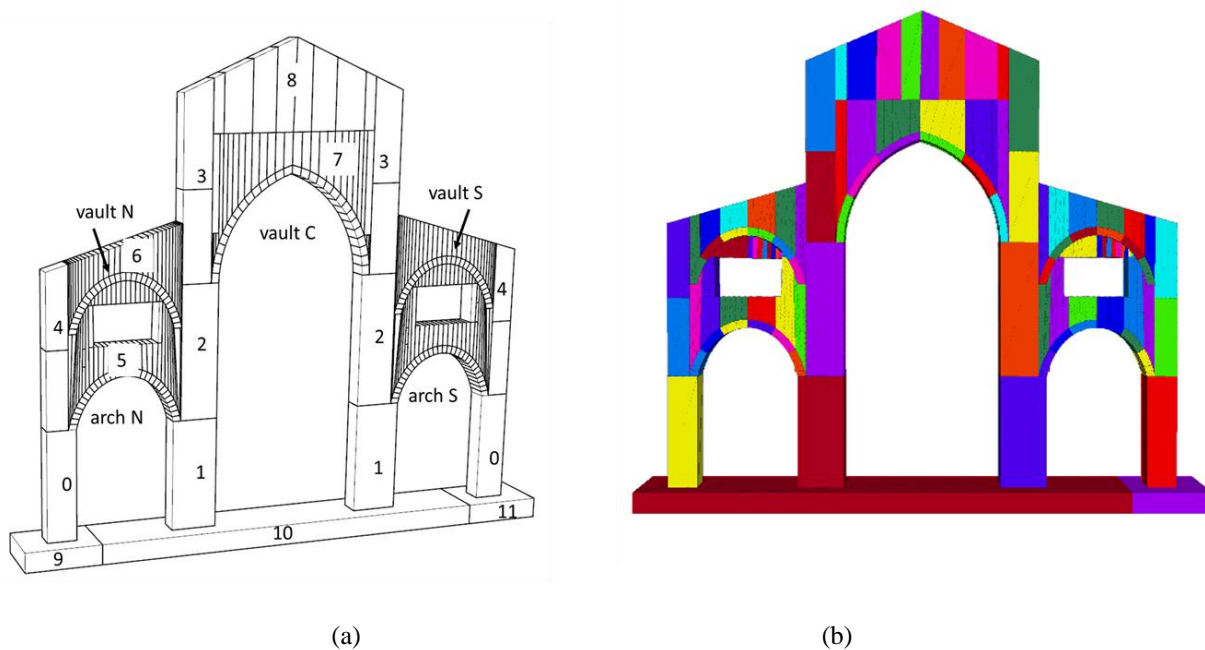
Figure 13-16: The "COMPLETE DEM" model analysed: (a) The Rhinoceros rendering and the name of the element used in the following calculation, and (b) the 3DEC model

Properties of the blocks:

Table 13-16- The properties of the blocks used in the analyses of the "complete cross-section"

Element	Weight per unit volume [KN/m^3]	*Elastic Modulus [KPa]	Dimension of the blocks [m]	Density [10^{3}Kg/m^3]
Wall$_0$	119	4144000	1.5·1·5.05 m	11.9
Wall$_1$	39	1727000	2.3·1·5.05 m	3.9
Wall$_2$	80	1727000	1.9·1·1.08	8.0
Wall$_3$	105	1727000	1.5·1·4.0	10.5
Wall$_4$	144	4144000	1.1·1·2	14.4
Wall$_5$	17	4144000		1.7
Wall$_6$	19	4144000		1.9
Wall$_7$	24	4144000		2.4
Wall$_8$	17	4144000		1.7
Vault N-S	141	4144000	0.4·1·0.27 m	2.44
Vault C	159	4144000	0.4·1·0.27	4.07
arch N-S	17	4144000		1.7

Elastic modulus used in the calculation of the interfaces stiffness (the blocks are here considered rigid)

Joint stiffness of the interfaces

Table 13-17- The properties of the interfaces in the vertical direction used in the analyses

Interface	Joint Kn [KPa/m]	Joint Ks [Kpa/m]
Wall$_0$ –Wall$_4$	4.4 10^6	1.9 10^6
Wall$_1$.Wall$_2$	6.5 10^5	2.8 10^5
Wall$_2$-Wall$_3$	2.7 10^6	1.9 10^6
Wall$_4$	9.7 10^6	4.1 10^6
Wall$_7$-Wall$_8$	9.98 10^5	4.2 10^5
Vault N-S	3.0 10^7	1.3 10^7
Vault C	1.8 10^7	7.5 10^6
Wall$_7$-Vault C	1.5 10^6	6.3 10^5
Wall$_6$-Vault N-S	1.8 10^6	7.6 10^5
Wall$_5$-Vault N_S	1.97 106	8.3 105
Arch N-S	1.99 10^7	8.4 10^6
Wall$_0$ –9	5.1 10^4	1.3 10^6
Wall$_1$ –10	1.1 10^4	3.0 10^6
Wall$_0$ –11	2.0 10^4	1.3 10^6

The equivalent normal stiffness at the base of walls of the cross-section have been used in the analysis and are calculated in the Equation 13-25-13-27:

$$k_{ntot\_wall_{0-9}} = k_n + \Delta k_n = 5.1 \cdot 10^4 + 2.6 \cdot 10^6 = 2.7 \cdot 10^6 \frac{kPa}{m} \tag{13-25}$$

$$k_{ntot\_wall_{1-10}} = k_n + \Delta k_n = 1.1 \cdot 10^4 + 6.0 \cdot 10^6 = 6.0 \cdot 10^6 \frac{kPa}{m} \tag{13-26}$$

$$k_{ntot\_wall_{0-11}} = k_n + \Delta k_n = 2.0 \cdot 10^4 + 2.6 \cdot 10^6 = 2.6 \cdot 10^6 \frac{kPa}{m} \tag{13-27}$$

Table 13-18- The properties of the interfaces in the horizontal direction used in the analyses

Interface	Joint Kn [KPa/m]	Joint Ks [Kpa/m]
$Wall_3 - Wall_7$	$4.2 \ 10^6$	$1.8 10^6$
$Wall_7$	$1.8 \ 10^6$	$8 \ 10^5$
$Wall_3-Wall_6$	$5.5 \ 10^6$	$2.3 10^6$
$Wall_6$	$3.2 \ 10^6$	$1.4 \ 10^6$
$Wall_4-Wall_5$	$5.5 \ 10^6$	$2.3 \ 10^6$
$Wall_2-Wall_5$	$5.5 \ 10^6$	$2.3 \ 10^6$
$Wall_5$	$3.2 \ 10^6$	$1.4 \ 10^6$
$Wall_3 - Wall_8$	$1.5 \ 10^6$	$6.2 \ 10^5$

13.4.2.2 Simplified DEM model

Figure 13-17 shows the "SIMPLIFID DEM" model analysed and the names of the elements used in the calculation of the properties of the blocks and interfaces. Also in this case the Figure 13-17 displays the 3DEC model with the respective subdivision in blocks of the elements used in the analyses. The modelling parameters used are reported in the Table 13-19 and Table 13-20.

(a)   (b)
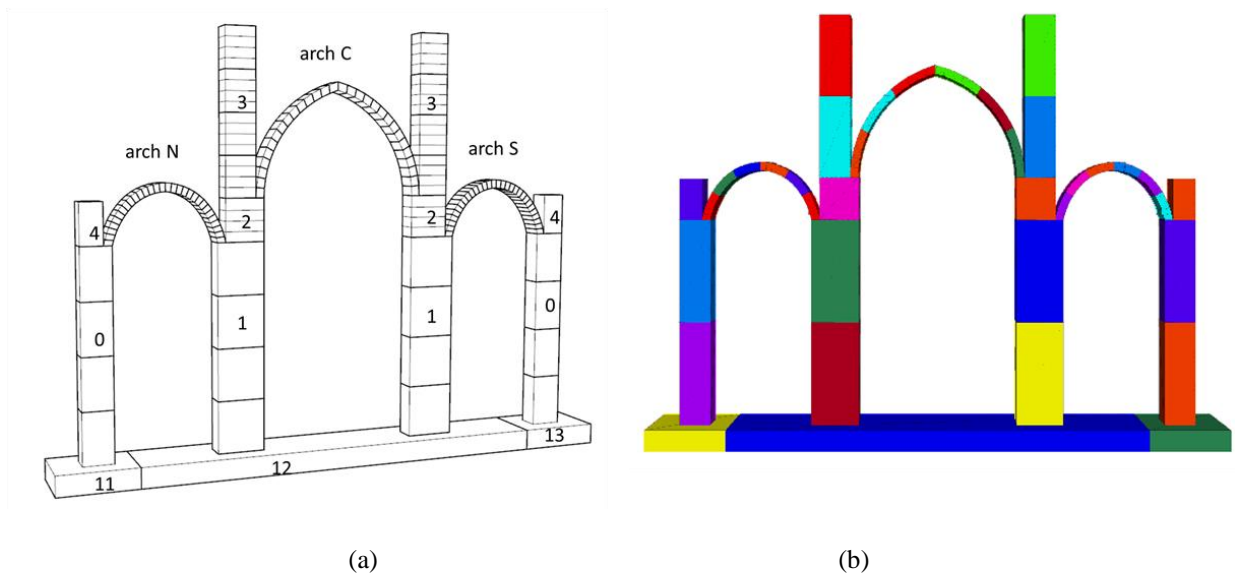
Figure 13-17: The "SIMPLIFIED DEM" model analysed: (a) The Rhinoceros rendering and the name of the element used in the following calculation, and (b) the 3DEC model

Properties of the blocks:

Table 13-19- The properties of the blocks used in the analyses of the "simple cross section"

Element	Weight per unit volume [KN/m^3]	*Elastic Modulus [KPa]	Dimension of the blocks [m]	Density [10^3Kg/m^3]
Wall$_0$	125	4144000	1.5·1·5.05 m	12.5
Wall$_1$	50	1727000	2.3·1·5.05 m	5.0
Wall$_2$	127	1727000	1.9·1·1.08	12.7
Wall$_3$	140	1727000	1.5·1·4.0	14.0
Wall$_4$	213	4144000	1.1·1·2	21.3
ArchN-S	141	4144000	0.4·1·0.27 m	14.1
Arch C	159	4144000	0.4·1·0.27	15.9

Elastic modulus used in the calculation of the interfaces stiffness (the blocks are here considered rigid)

Joint stiffness of the interfaces:

Table 13-20- The properties of the interfaces used in the analyses of the "simple cross-section"

Interface	Joint Kn [KPa/m]	Joint Ks [Kpa/m]
$Wall_0$	$8.2 \cdot 10^6$	$3.5 \cdot 10^6$
$Wall_0$-$Wall_4$	$1.2 \cdot 10^7$	$5.0 \cdot 10^6$
$Wall_1$	$7.8 \cdot 10^5$	$3.3 \cdot 10^5$
$Wall_1$-$Wall_2$	$1.1 \cdot 10^6$	$4.7 \cdot 10^5$
$Wall_2$-$Wall_3$	$1.3 \cdot 10^6$	$5.5 \cdot 10^5$
$Wall_3$	$1.2 \cdot 10^6$	$4.2 \cdot 10^5$
Arch N-S	$3.0 \cdot 10^7$	$1.3 \cdot 10^7$
ArchN-S-$Wall_0$	$1.3 \cdot 10^7$	$5.5 \cdot 10^7$
Arch C	$1.8 \cdot 10^7$	$7.5 \cdot 10^6$
Arch C-$Wall_1$	$1.9 \cdot 10^7$	$7.9 \cdot 10^6$
$Wall_0$-11	$\mathbf{2.7 \cdot 10^6}$	$\mathbf{1.3 \cdot 10^6}$
$Wall_1$-12	$\mathbf{6.0 \cdot 10^6}$	$\mathbf{3.0 \cdot 10^6}$
$Wall_0$-13	$\mathbf{2.6 \cdot 10^6}$	$\mathbf{1.3 \cdot 10^6}$

<u>*Damping*</u>

$$f_{crit} = \frac{\omega_e \sqrt{2}}{2\pi} = \frac{1391\sqrt{2}}{2\pi} = 222 cycles / \sec ond$$

13.4.2.3 The simplified FEM model

The dynamic response of the simplified DEM model is compared with that of a corresponding FEM model developed using the software Sap2000 (Figure 13-18). Each condensed portion of longitudinal wall is modelled with a unique elements, whereas the arches are modelled as a succession of beam elements. The density of the walls used in the FEM model are the same of the Table 13-19. The interaction between the soil and the structure has been explicitly taken into account by inserting vertical ($k_{m,n(Sap)}$), lateral ($k_{m,s(Sap)}$) and rotational (k_g) springs at the base. The stiffness of the springs are reported in the Table 13-21 (see Appendix D.2.1).

To account for the possible opening of hinges in the arches, two solutions have been considered:

-   Continuous arches (without hinges);
-   Arches with 3 hinges located at the mid span and at the supports (see Figure 13-18b).

(a) (b)
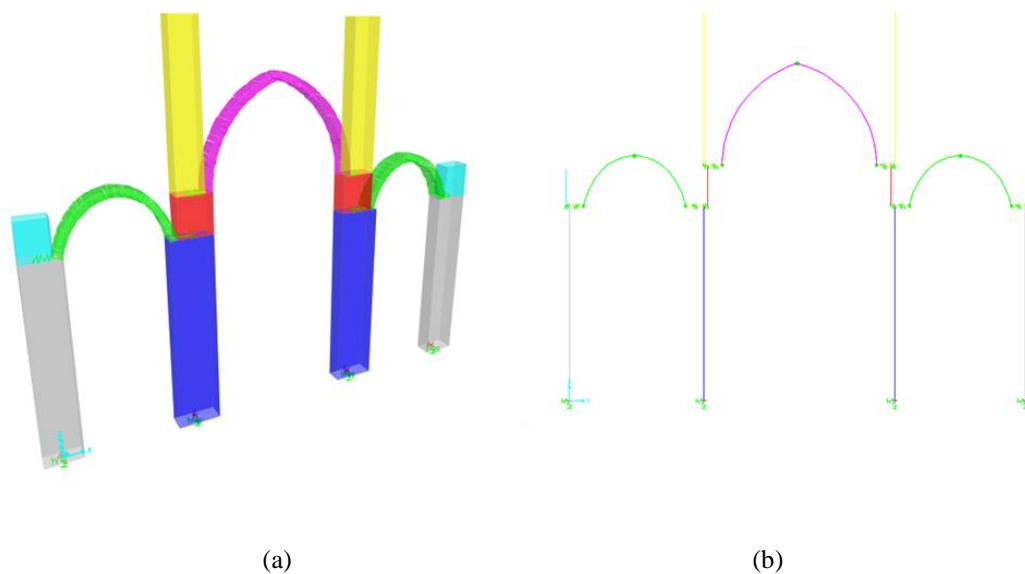
Figure 13-18: The "SIMPLIFIED FEM" model analysed: (a) model extruded considering continuous arches and (b) model not extruded considering 3 hinges in the arches

Table 13-21- The stiffness used at the base of the walls in the FE models

Interface	Vertical $k_{m,n(Sap)}$ [KN/m]	Lateral $k_{m,s(Sap)}$ [KN/m]	Rotational k_{ϑ} [KNm]
$Wall_0$-11	$4.1\ 10^6$	$1.9\ 10^6$	$2.3\ 10^6$
$Wall_1$-12	$1.4\ 10^7$	$7.0\ 10^6$	$3.5\ 10^6$
$Wall_0$-13	$3.9\ 10^6$	$1.9\ 10^6$	$2.2\ 10^6$

13.4.3 The results

13.4.3.1 Static analyses

Contour maps of the lateral displacements along x direction are reported in Figure 13-19. The maximum displacement in the x direction of the longitudinal walls obtained from the static analyses of the COMPLETE DEM model is around 0.012 m (Figure 13-19a). Instead, the SIMPLIFIED DEM model provides a maximum displacement by around 0.004m (Figure 13-19b). As expected, the COMPLETE DEM model gives larger lateral displacements probably due to the lateral trust exerted by the lower arches (not modelled in the SIMPLIFIED DEM model). Figure 13-20 display the contour maps of the lateral displacement along x direction as obtained from the SIMPLIFIED FEM model. In both cases of continuous arches (Figure 13-20a) and arches with three hinges (Figure 13-20b), the lateral displacements are much smaller than those obtained from DEM models (several order of magnitude less).

(a)   (b)
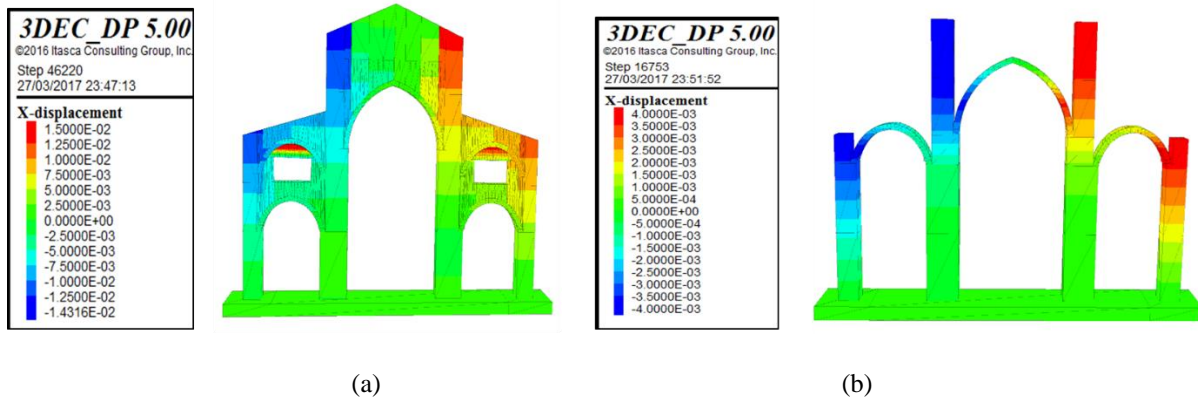
Figure 13-19: Contour maps of the lateral displacements along x direction obtained by : (a) COMPLETE DEM model and (b) SIMPLIFIED DEM model

(a)   (b)
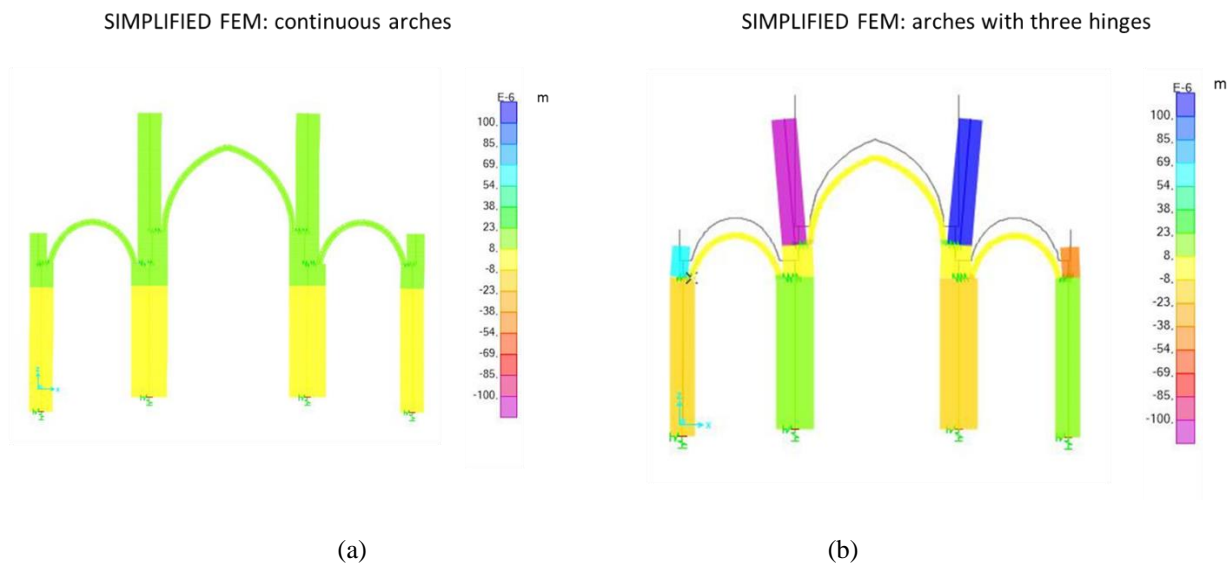
Figure 13-20:Countor maps of the lateral displacements along x direction obtained by : (a) SIMPLIFIED FEM model considering continuous arches and (b) SIMPLIFIED FEM model considering three hinges in the arches

Figure 13-21 displays the contour plot of the interfaces, relative block-to-block, displacement (blue indicate an opening between the blocks). The contour plot is qualitatively compared with the crack patterns as observed before the 2012 Emilia Earthquake (see §10.3.4). It can be noted that the block openings agrees with the location of the main cracks. It reminds that the model takes into account of the different soil stiffness at the base of the walls that are probably the first cause of the crack patterns detected before the 2012.
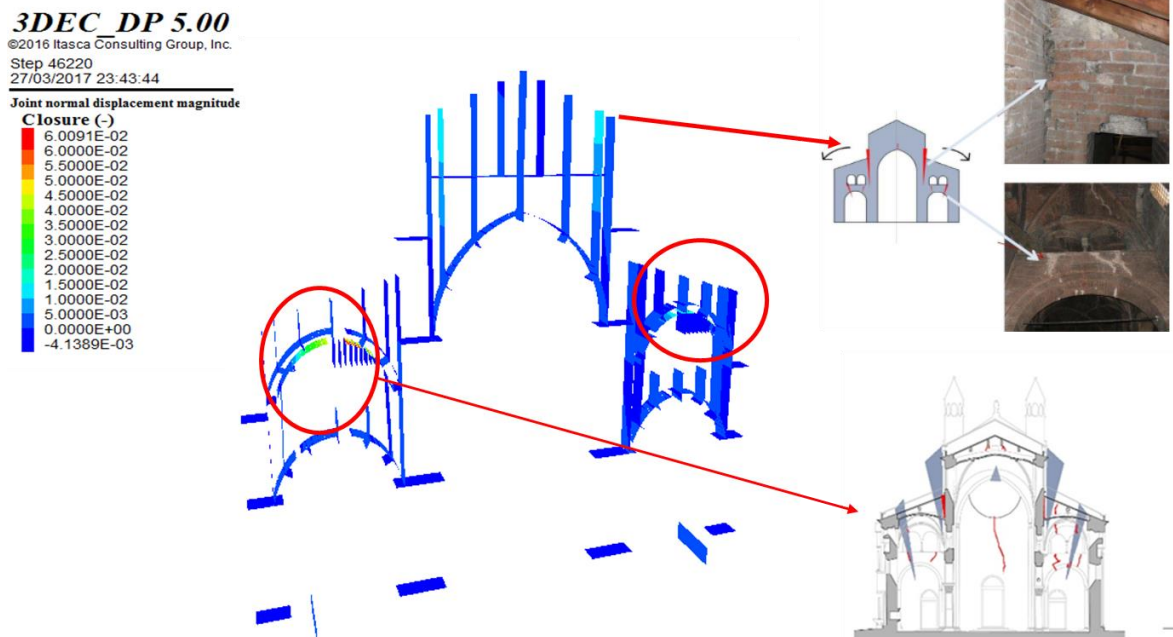
Figure 13-21: Contour plot of the interfaces of the COMPLETE DEM model and the crack pattern detected in the 2010

13.4.3.2 Dynamic analyses

As expected the dynamic analyses performed on the SIMPLIFED DEM model and on the SEMPLIFIED FEM models considering the ground motion recorded in Modena during the 2012 Emilia's earthquake (§10.5) do not lead to the collapse of the structure. Figure 13-22 displays the contour plot of the interfaces, relative block-to-block, displacement (orange and red colors indicate an opening between the blocks) obtained by the SIMPLIFED DEM model. It can be noticed that under the seismic loads several new openings appear mainly concentrated on the arches (that schematized the vaults). These openings are in good agreement with the cracks observed after the Emilia Earthquake (own concentrated predominantly in the vaults §10.3.4).

The results obtained by the three model are also compared in order to identify the limitation and reliability of these methods. For the SIMPLIFIED FEM models considering continuous arches (characterized by a fundamental period of T= 0.43 seconds) and the SIMPLIFIED FEM model considering three hinges in the arches (characterized by a fundamental period of T= 0.50 seconds) the dynamic analyses have been conducted considering two value of damping ratios (namely 5% and 30%).
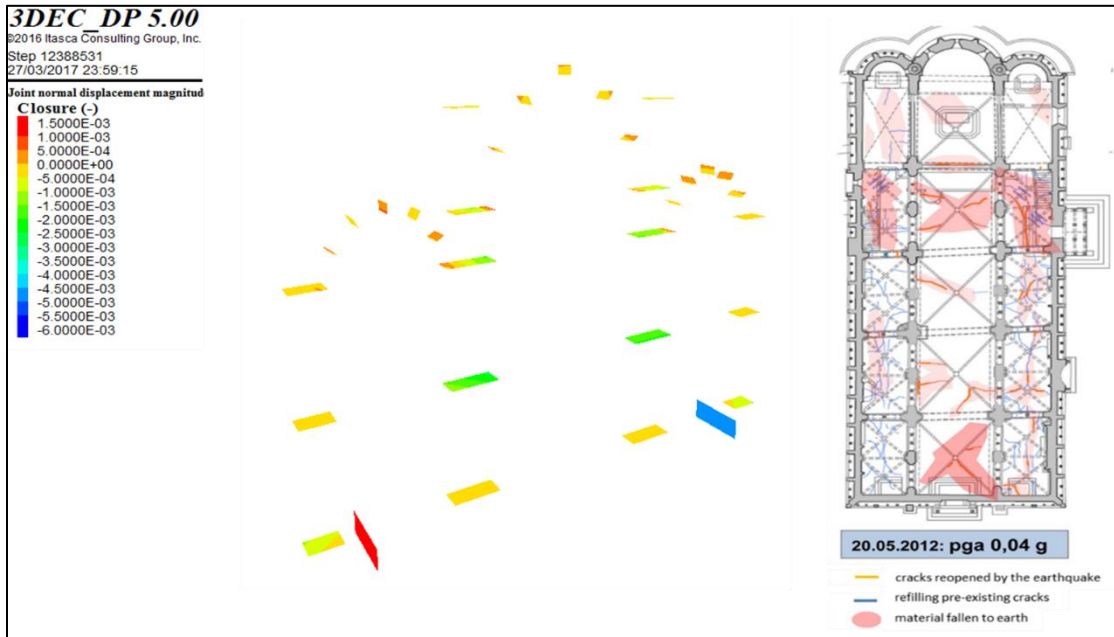
Figure 13-22: Contour plot of the interfaces of the SIMPLIFIED DEM model and the crack pattern detected in after the 2012 Emilia earthquake

Figure 13-24 compares the time-history of the lateral displacements as obtained from the SIMPLIFIED DEM and SIMPLIFIED FEM models recorded at:

- the springer of the arch N (top of the wall 0), (Figure 13-23);
- the springer of the arch C (top of the wall 2), (Figure 13-23);
- the springer of the arch S (top of the wall4), (Figure 13-23).
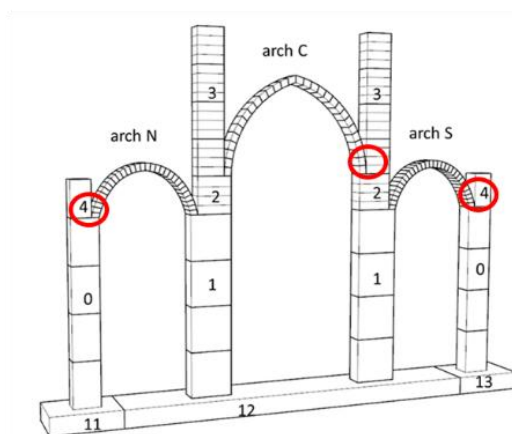
Figure 13-23: Control points used in the plots of the time history of the x-displacements recorded by the three different models
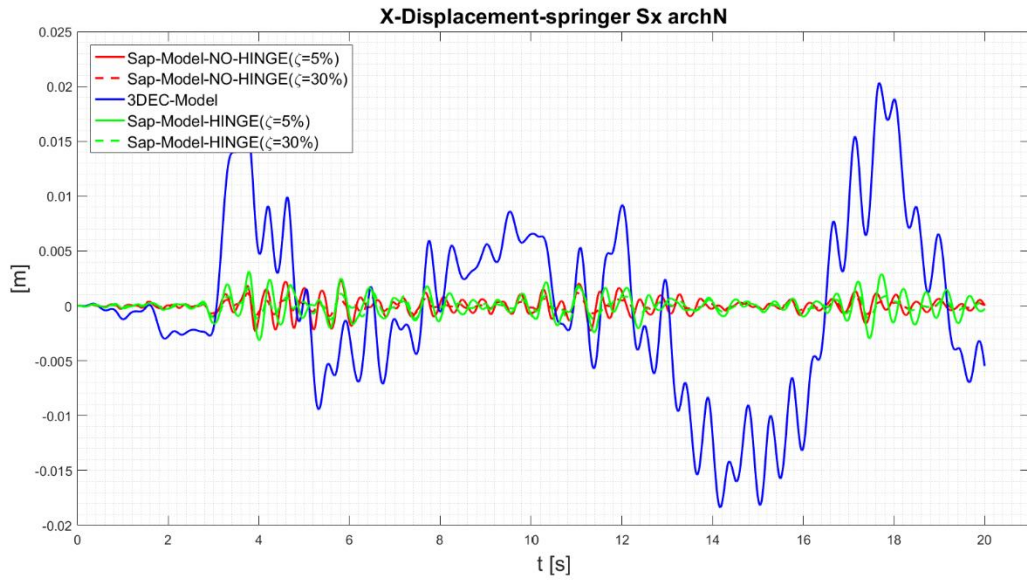
(a)
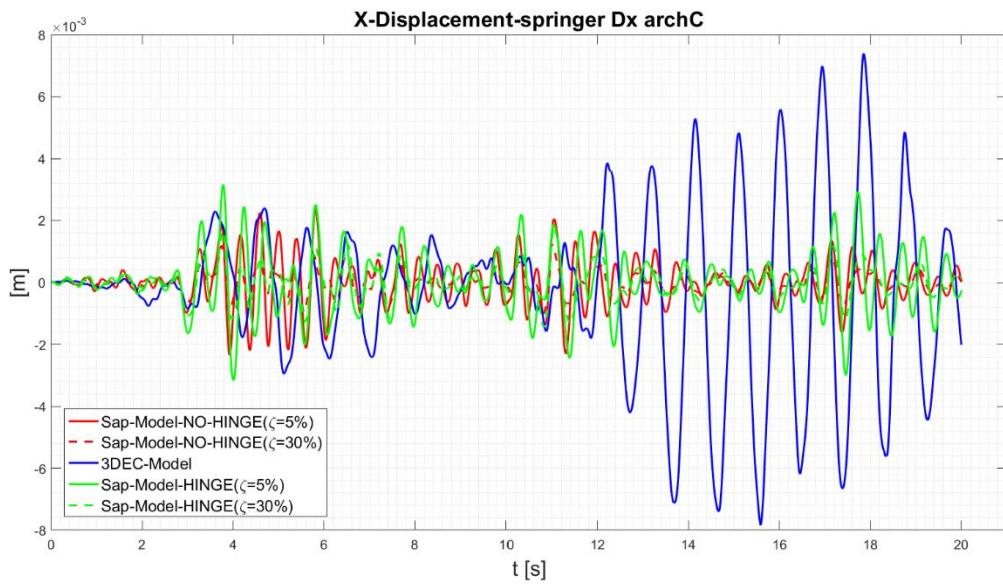
(b)
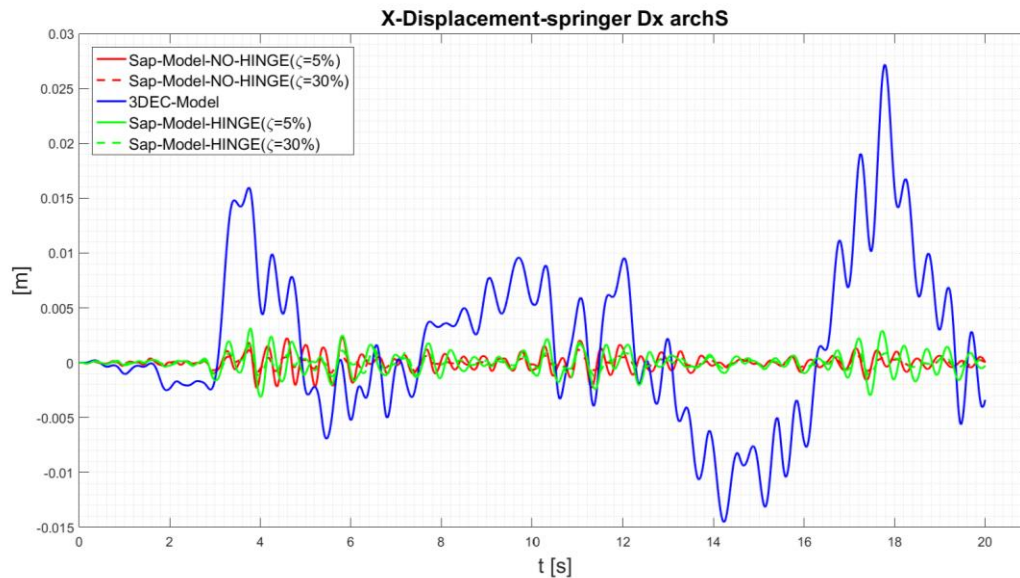
(c)

Figure 13-24:Plot of the time history of the displacements recorded during the dynamic analyses by the three different models: (a) springing of the arch N (Sx),(b) springing of the arch C(Dx) and (c) springing of the arch S(SX)

As expected the displacements recorded by the SIMPLIFIED DEM model are significant different to the respective FEM models. The FE modelling are not able to represent the natural discontinuity of the masonry because the material is supposed homogeneous and isotropic and the deformation is distributed along the elements. The elements are thus continuous and remain connected also during elasto-plastic failure, allowing thus to identify the stress level on the elements but not the stability. Instead the DEM modelling allows finite displacements and rotations of the rigid blocks including complete detachment through four interface springs defined in the contact, one at each corner, between the blocks. Different hypotheses could be considered in the Fem models (such as reduce the value of the elastic modulus in order to take into account of the presence of cracks in the elements) in order to have a structural response more similar to that obtained from the DEM modeling and probably more realistic of the masonry of historic buildings. However this is beyond the scope of this study which aims to a preliminary comparison of the limitations of the two different modelling due to their intrinsic characteristics.

The analysis of x-displacements recorded in the three control points from the models displays:

- the displacements recorded by the FEM models oscillate around a horizontal line: given the impossibility of these models to capture a non-linear behavior, the occurrence of damages and take into account the residual displacements.
- the displacements recorded by the DEM model oscillate around a non-horizontal line indicating the nonlinear behavior recorded.

- the frequency of the oscillation recorded by the three models is similar: the period of the Dem model seems close to those of the FEM models.
- The amplitude of the oscillation recoded by the FEM models appear smaller than those obtained from DEM model.

13.5 Conclusion

The sensitivity study presented in the previous section highlights the importance of a proper calibration of the model parameters in order to obtain realistic structural response through DE methods. These models seem to be particularly susceptible to the variation of the normal (axial) stiffness. Furthermore, it clearly appears that in some particular cases, such as the presence of soil with different properties, the interaction between the soil-foundation-structure cannot be neglected. In these cases, one possibility, alternative to the direct modelling of the soil-foundation blocks, is to calibrate equivalent springs (both normal and shear springs) so that they would be able to reproduce the axial, lateral and rotational flexibility of the soil-foundation blocks.

The DEM models of the cross section of the Cathedral of Modena allow to identify the cracks due to the gravity loads and the different stiffness of the soil at the base and those due to the seismic loads. The results obtained seem to be in agreement with the crack patterns detect (before and after the 2012 earthquake).

The preliminary comparison between the structural response detect by the DEM models and those of the corresponding FEM models point out the limitation of the FE modelling when applied to masonry structures.

Chapter 14

14 Conclusions

14.1 Introduction

This chapter recaps the researches carried out, pointing out the main results obtained and possible future developments for the research topic treated in this thesis.

The primary objective of the thesis resides in the identification of an approach for a standardized analysis of the data recorded by a static Structural Health Monitoring system installed in an historical building.

The second objective is to provide a summary of the studies conducted on a real monumental building, namely the Cathedral of Modena (UNESO world heritage) aimed at its reliable structural assessment based on a multi-disciplinary multi-analysis approach (MDMA), integrating the real field data obtained by the SHM.

14.2 Summary of researches carried out

The thesis has been divided into two main parts.

Part One is related to the Structural health monitoring of historical monuments.

The SHM has a very important role in the diagnostic process of cultural heritage buildings and can be considered a knowledge-based assessment tool.

Chapter 2 provides the state-of-the-art on the main strategies, methods and applications of the SHM strategy for the civil structures.

In the last years, several historical monuments have been equipped with static and dynamic monitoring systems. The literature review presented in §3.2 pointed out as several studies were focused on the

interpretation of the data acquired by dynamic monitoring and no standardized procedure for systematic and easy interpretation of data obtained by the static monitoring are yet available.

The primary objective of this research, as stated in Chapter 3, is to introduce an approach for a standardized analysis of the data recorded by a static Structural Health Monitoring system installed in an historical building.

The data recorded by the monitoring system often present irregularities due to malfunctioning of the sensor, which can lead to an interpretation of the signal not corresponding to the real behaviour of the phenomenon. The removal signal irregularities procedure has been illustrated in Chapter 4. Moreover, a preliminary overview of the signal analyses that could be used in the interpretation of the evolution of the state of the monument from the data acquired by static monitoring systems is treated in the same Chapter. The Fourier spectral analysis, despite its limitations, appears another possibility to estimate the evolution of the state, identifying and then removing the main periodicity of the signal. The Fourier spectral analyses has been used with the objective to compare the proposed approach.

Chapter 5, 6 and 7 present the application of the procedure proposed for the interpretation of the data obtained from the static monitoring system, on three monumental buildings: Asinelli tower, Garisenda tower and Cathedral of Modena. The evaluation of the reference quantities for the data recorded by each instruments installed on the monuments has allowed to identify if the phenomena under observation are in a stable condition or not.

Chapter 8 provided the reference values extrapolated to reference quantities which may be guidelines useful for the interpretation of data acquired by static monitoring system of other masonry monuments.

Part Two is related to the reliable structural assessment of the monumental buildings.

First, Chapters 9 provided an overview of the main methods applicable to the study of masonry historical buildings. Then, a possible approach for the reliable assessment of the structural "health" of historical monuments making use of a multi-disciplinary multi-analysis approach (MDMA) considering the building as model of itself is presented. The MDMA approach is grounded on the experience obtained during an almost decade of studies on the Cathedral of Modena, developed within of a Scientific Research Committee, with the purpose of identifying potential vulnerabilities and criticalities. A summary of the studies conducted on the Cathedral of Modena is reported in Chapter 10 to 13.

In more detail, the constructional phases, the geometrical configuration, the material properties, the actual state of degradation and the events that hit the Cathedral in the past have been investigated in Chapter 10.

Chapter 11 provides the main results of different structural analyses, based on the information obtained from the integrated knowledge, in order to identify the main static and seismic vulnerabilities of the Cathedral.

Chapter 12 presents the main results obtained from the study of the local collapse mechanisms of the main substructures of the Cathedral. In addition, the results, in terms of stress and deformation, of the most damaged vaults, after the 2012 Emilia Romagna earthquake, obtained through analyses on 3D Finite element models are provided.

Chapter 13 treated the most vulnerable cross section of the Cathedral of Modena through a Discrete Element (DE) modelling in order to evaluate the interactions between the vaults and the longitudinal walls and the influence of the different soil stiffness at the base.

14.3 Summary of findings

The fundamental findings of the thesis are summarised in the following.

The inherent complexity of historical buildings makes the assessment the "structural health" extremely challenging. The SHM has a very important role in the diagnostic process of cultural heritage buildings providing a prognosis of the actual state (evolution of damage, residual life, etc.). As discussed in Chapter 3, in the last years, several historical monuments have been equipped with static and dynamic monitoring systems. Despite the number of application, no standardized procedure for systematic and easy interpretation of data obtained by the static monitoring are yet available.

The primary contribution of this research is the definition of an approach for a standardized analysis of the data recorded by a static Structural Health Monitoring system installed in an historical building.. The evolution of the state of the building is evaluated through the identification of appropriate descriptors able to characterize the main features of the data acquired by the monitoring. This approach is intended as a contribution to move forward in the systematic use of the data acquired by the monitoring system within a policy for management of cultural buildings. Indeed the systematic collection of the specific values (along the time) of these reference quantities, referred to as reference values, in a database allow to make interesting comparisons among similar buildings in order to produce guidelines useful for the interpretation of data acquired by static monitoring system of masonry monuments. The study of the data obtained from the static monitoring of three monumental buildings (the Asinelli tower, the Garisenda tower and the Cathedral of Modena) through the proposed approach provides "reference values" which may be guidelines useful for the interpretation of data acquired by static monitoring system of other masonry monuments.

The second contribution aims to providing a possible operative procedure for the reliable assessment of the structural "health" of historical monuments based on a multi-disciplinary multi-analysis approach (MDMA), which integrates the real field data obtained by the SHM and considers the building as model of itself.

14.4 Future developments

In this thesis, I have stressed the importance of the implementation of SHM strategies to evaluate the "structural health" of the historical buildings and to obtain useful data to validate/calibrate the numerical models in order to develop reliable structural analyses. The work was focused mainly on the interpretation, through a standardized procedure, of the data acquired by static monitoring systems. However, the measure of phenomena such as the response to earthquake ground motion, or traffic induced vibrations, necessary to account for the dynamic nature of the structural response require the implementation of dynamic Structural Health Monitoring systems. Seismic monitoring experiments are under development on the two towers of Bologna and the analyses of these data will be investigated to improve the knowledge of these two monuments. The application of the proposed procedure for the analyses of the data obtained by static SHM system also to those obtained by the dynamic monitoring could provide interesting information on the influence of the temperature on the dynamic properties of masonry buildings.

Moreover, the damages observed after many Italian earthquakes pointed out that the most vulnerable elements on the historical buildings are generally the masonry cross vaults. The evaluation of seismic response of the masonry vaults is severely complex and depends on several factors, such as the three-dimensional geometry, the mechanical properties of the constituent materials and the behaviour of the underneath vertical elements (lateral walls and piers). Several studies were carried out on the analysis of the masonry vaults. Nonetheless, specific studies on the pseudo-static response of masonry cross vaults to imposed shear displacements at the springings are still not available in the scientific literature. Experimental research aimed at improving the pseudo-static response of the vaults therefore appear necessary.

References

Anastasi, G. et al., 2009. WSNs for Structural Health Monitoring of Historical Buildings. *Conference on Human System Interactions*.

Armandi, M., 1999. Copie e originali. Il repertorio di mensole figurate del Duomo di Modena. In C.FRUGONI, ed. *Il Duomo di Modena*. Franco Cosimo Panini.

ASCE7-98, 1998. Minimum Design Loads for Buildings and Other Structures. In American Society of Civil Engineers.

Azevedo, J., Sincraian, G. & Lemos, J. V., 2000. Seismic behavior of blocky masonry structures. *Earthquake Spectra*, 16(2), pp.337–365.

Baggio, C. & Trovalusci, P., 1998. Limit analysis for no-tension and frictional three-dimensional discrete systems. *Mech Struct Mach*, pp.287–304.

Balageas, D., Fritzen, C.-P. & Güemes, A., 2006. *Structural health monitoring*, Available at: http://onlinelibrary.wiley.com/doi/10.1002/9780470612071.ch1/summary.

Barnhart, B., 2011. The Hilbert-Huang Transform: theory, applications, development. *Theses and Dissertations*, p.101. Available at: http://ir.uiowa.edu/etd/2670%5Cnhttp://ir.uiowa.edu/etd/2670/.

Bergmeister, K. & U. Santa, 2001. Strumenti e precisione. *Structural Concrete*, 2, pp.29–39.

Berto, L. et al., 2002. An orthotropic damage model for masonry structures. *Numer Methods Eng*.

Bertoni, G., 1914. La cattedrale modenese preesistente all'attuale: Primo ragguaglio sugli scavi del Duomo, agosto-settembre 1913/Giulio Bertoni. In Orlandini, ed.

Beskhyroun, S., Wegner, L.D. & Sparling, B.F., 2011. New methodology for the application of vibration-based damage detection techniques. *Structural Control and Health Monitoring*, (May 2011), p.n/a-n/a. Available at: http://dx.doi.org/10.1002/stc.456.

Bićanić, N., Stirling, C. & Pearce, C.J., 2003. Discontinuous modelling of masonry bridges. *Computational Mechanics*, pp.60–68.

Blasi, C., and Coïsson, E., 2006. The importance of historical documents for the study of stability in ancient buildings: The french Panthéon case study. *Asian Journal of Civil Engineering (Building and Housing) 7*.

Block, P., 2005. *Equilibrium systems Studies in masonry structure,*.

Block, P., Ciblac, T. & Ochsendorf, J.A., 2006. Real-time limit analysis of vaulted masonry buildings.

Computers and Structures.

Brockwell, P.J. & Davis, R.A., 2009. Time series: theory and methods.

Brownjohn, J.M.W., 2007. Structural health monitoring of civil infrastructure. *Philosophical Transactions of the Royal Society a-Mathematical Physical and Engineering Sciences*, (December 2006), pp.589–622.

Cadigliani, R., 2009. La torre Ghirlandina. Un progetto per la Conservazione. In L. Sossella, ed. Taylor & Francis group,.

Carocci, C.. ., 2001. Guidelines for the safety and preservation of historical centres in seismic areas. *Historical constructions*.

Casapulla, C. & D'Ayala, D., 2001. Lower bound approach to the limit analysis of 3D vaulted block masonry structures. In *Proceedings of the 5th international symposium on computer methods in structural masonry*. pp. 28–36.

Castagnetti, C., E. Bertacchini, A. Capra, and M.D., 2011. Il laser scanning terrestre per l'analisi di edifici di interesse storico ed artistico. In *Geomatica - le radici del futuro*.

Cavani, F., 1912. Sulla pendenza e sulla stabilità della torre degli Asinelli di Bologna.

Ceccoli, C. et al., 2001. Indagini inerenti le strutture murarie e fondali e consolidamento delle parti in elevazione della Torre Garisenda".

Cornell C.A, 1968. Engineering seismic risk analysis. *Bulletin of the Seismological Society of America*.

Costa, T., 1984. *Il grande libro delle Torri Bolognesi* S. Costa, ed.,

Croci, G., 1996. THE COLOSSEUM : SAFETY EV ALUATION AND PRELIMINARY CRITERIA OF INTERVENTION.

DeJong, J.M. & Dimitrakopoulos, G.E., 2014. Dynamically equivalent rocking structures. *EARTHQUAKE ENGINEERING & STRUCTURAL DYNAMICS*, pp.1543–1563.

Dejong, M.J., 2009. *Seismic Assessment Strategies for Masonry Structures*.

Dimitri, R., De Lorenzis, L. & G., Z., 2011. Numerical study on the dynamic behaviour of masonry columns and arches on buttresses with the discrete element method. *Engineering Structures*, 33, pp.3172–3188.

Dolce, M. et al., 2012. The Emilia Thrust Earthquake of 20 May 2012 (Northern Italy): Strong Motion and Geological Observations - Report 1 -. , 2012, pp.1–12. Available at: http://www.protezionecivile.gov.it/resources/cms/documents/Report_DPC_1_Emilia_EQSd.pdf.

Dondi, A., 1896. Il Duomo di Modena, notizie storiche ed artistiche.

Fajfar, P., 1999. Capacity spectrum method based on inelastic demand spectra. *Earthquake Engineering & Structural Dynamics*.

De Felice, G. & Giannini, R., 2001. Out-of-plane seismic resistance of masonry walls. *Journal of Earthquake Engineering*, pp.53–271.

De Felice, G. & Mauro, A., 2010. On overturning of the façade in churches with single nave: some case studies from L'Aquila, Italy, 2009 earthquake. *Advanced material research*.

Ferris, M. & Tin-Loi, F., 2001. Limit analysis of frictional block assemblies as a mathematical program with complementarity constraints. *Int J Mech*, pp.209–224.

Frankl, P., 1927. Der Dom in Modena, in "Jahrbuch fur Kunstwissenschaft."

Gilbert, M. & Melbourne, C., 1994. Rigid-block analysis of masonry structures. *Struct Eng 72*, pp.356–361.

Giuffrè, A., 1990. Letture sulla meccanica delle murature storiche. In Kappa, Rome.

Giuffrè, A., 1995. Vulnerability of historical cities in seismic areas and conservation criteria. In *Congress "Terremoti e civiltà abitative."*

Giuffrè, A. & Carocci, C., 1993. Statica e dinamica delle costruzioni murarie storiche. In *Atti del Convegno internazionale CNR "Le pietre da costruzione: il tufo calcareo e la pietra leccese".*

Grosso, a Del, Inaudi, D. & Lanata, F., 2000. Strain and displacement monitoring of a quay wall in the Port of Genoa by means of fibre optic sensors. *2d European Conference on …*, (February), pp.3–6. Available at: http://www.roctest-group.com/~rtgroup/sites/default/files/bibliography/pdf/c46.pdf.

Guidelines for Evaluation and Mitigation of Seismic Risk to Cultural Heritage, 2011. Guidelines for Evaluation and Mitigation of Seismic Risk to Cultural Heritage. *Gazzetta Ufficiale*, 47.

Gutenberg, B. & Richter ,C. F., 1949. Seismicity of the Earth.

Harvey, B. & Maunder, E., 2001. Thrust line analysis of complex masonry structures using spreadsheets. *Historical Constructions,*.

Hendry, A.W., 1990. Structural masonry.

Heyman, J., 1969. The safety of masonry arches. *International Journal of Mechanical Sciences*.

Heyman, J., 1995. The stone skeleton: structural engineering of masonry architecture. In Cambridge University Press,.

Huang, N. et al., 1998. The empirical mode decomposition and the Hilbert spectrum for nonlinear and non-stationary time series analysis. *Proceedings of the Royal Society of London. Series A: Mathematical, Physical and Engineering Sciences*, 454(1971), pp.903–995. Available at:

http://dx.doi.org/10.1098/rspa.1998.0193%5Cnhttp://rspa.royalsocietypublishing.org/content/454/1971/903.

ISCARSAH, 2003. Recommendations for the analysis, conservation and structural restoration of Architectural Heritage. *Icomos*, (June), pp.3–6.

Istruzioni CNR-DT 206, 2007. Istruzioni CNR-DT 206/2007.Istruzioni per la Progettazione, l'Esecuzione ed il Controllo di Strutture di Legno, Cons. Nazionale delle Ricerch.

Ivorra, S. et al., 2010. An evaluation of the incidence of soil subsidence on the dynamic behaviour of a Gothic bell tower. *Engineering Structures*, 32(8), pp.2318–2325. Available at: http://dx.doi.org/10.1016/j.engstruct.2010.04.007.

Ivorra, S. & Pallarés, F.J., 2006. Dynamic investigations on a masonry bell tower. *Engineering Structures*, 28(5), pp.660–667.

Julius S. Benedat, A.G.P., 2000. *Random Data Analysis and Mesurement Proceedures* N. I. F. Vic Barnet, Noel A.C. Cressie, ed.,

Kooharian, A., 1952. Limit analysis of voussoir (segmental) and concrete arches. *Journal of the American Concrete Institute*.

Krinitzsky E.L., 1995. Deterministic versus probabilistic seismic hazard analysis for critical structures. *Engineering Geology*.

Labate, D., 2009. Il contributo dell'archeologia alla lettura di un monumento, in La torre Ghirlandina. Un progetto per la Conservazione. In L. Sossella, ed.

Lagomarsino, S., 2006. On the vulnerability assessment of monumental buildings. *Bulletin of Earthquake Engineering*.

Lanata, F. & Grosso, a Del, 2006. Damage detection and localization for continuous static monitoring of structures using a proper orthogonal decomposition of signals. *Smart Materials and Structures*, 15(6), pp.1811–1829.

Lancellotta, R., 2009a. Aspetti geotecnici nella salvaguardia della torre Ghirlandina. In *La Torre Ghirlandina. Un progetto per la conservazione*.

Lancellotta, R., 2009b. Geotechnical Engineering. In T. and Francis, ed.

Lancellotta, R., 2013. La torre Ghirlandina: Una storia di interazione strutturaterreno. *Rivista Italiana di Geotecnica*.

Lemos, J.V., 1995. Assesment of the ultimate load of a masonry arch using discrete elements. *omputer Methods in Structural Masonry*, p.294–302,.

Livesley, R.K., 1978. Limit analysis of structures formed from rigid blocks. *Numer Methods*.

Lomartire, S., 1989. Paramenti murari del Duomo di Modena. Materiali per un "edizione critica, in Wiligelmo e Lanfranco nell"Europa romanica.

Lourenço, P., 2002. Computations of historic masonry structures. *Structural Engineering and Materials*.

Lourenço, P.B., 1996. *Computational strategies for masonry structures*, Available at: http://www.narcis.nl/publication/RecordID/oai:tudelft.nl:uuid:4f5a2c6c-d5b7-4043-9d06-8c0b7b9f1f6f.

Lourenco, P.B. & Rots, J.., 1996. Multisurface Interface Model for Analysis of Masonry Structures Article. *Journal of Engineering Mechanics*, 230–238(123), pp.1–23.

De Luca, A., Giordano, A. & Mele, E., 2004. A simplified procedure for assessing the seismic capacity of masonry arches. *Engineering Structures,*.

Lugli, S., 2011. La Pietra Ringadora in Piazza Grande a Modena: Caratterizzazione geologica, provenienza, fenomeni di degrado e valorizzazione didattico-divulgativa.

Macchi, G., 2001. Diagnosis of the facade of St. Peter's Basilica in Rome. *Historical Constructions*, (Hibbard 1971), pp.309–318.

Macchi, G., Ruggeri, G. & Eusebio, M., 2017. Structural assessment of Leaning Tower of Pisa Structural Assessment of the Leaning Tower of Pisa.

Magalhães, F., Pacheco, J. & Cunha, Á., 2016. Illustrating the relevance of SHM in a case study : the Foz Tua centenary railway bridge. In pp. 5–8.

Masciotta, M.-G. et al., 2016. Development of Key Performance Indicators for the Structural Assessment of Heritage Buildings. In pp. 5–8.

McInerney, J. & DeJong, M., 2015. Discrete Element Modeling of Groin Vault Displacement Capacity. *International Journal of Architectural Heritage*, 9(8), pp.1037–1049. Available at: http://www.tandfonline.com/doi/full/10.1080/15583058.2014.923953.

Mola, F. & Vitaliani, R., 1996. ANAL YSIS , DIAGNOSIS AND PRESERVA TION OF ANCIENT MONUMENTS : THE ST . MARK â€™ S BASILICA IN VENICE.

Mukhopadhyay, S. & Betti, R., 2013. A new denoising procedure based on Empirical Mode Decomposition for SHM purpose. , pp.4547–4554.

Norme Tecniche per le Costruzioni, D.M., 2008. Italian Ministerial Decree of 14 January 2008. In Gazzetta Ufficale n. 29 of 04 Feb 2008.

Ochsendorf, J.A., 2002. *Collapse of masonry structures*.

Omenzetter, P., Brownjohn, J.M.W. & Moyo, P., 2004. Identification of unusual events in multi-channel bridge monitoring data. *Mechanical Systems and Signal Processing*, 18(2), pp.409–430.

Onate, E., Hanganu, A. & Miquel, J., 2000. Prediction of Damage and Failure in Civil Engineering Structures Using a Finite Element Model. In *European COST F3 Conference on System Identification and Structural Health Monitoring*.

Orduña, A. & Lourenço, P., 2003. Cap model for limit analysis and strengthening of masonry structures. *Struct Eng*.

Orduña, A. & Lourenço, P.B., 2005a. Three-dimensional limit analysis of rigid block assemblages. Part I: Torsion failure on frictional interfaces and limit analysis formulation. *Int J Solids Struct*.

Orduña, A. & Lourenço, P.B., 2005b. Three-dimensional limit analysis of rigid blocks assemblages. Part II: Load-path following solution procedure and validation. *Int J Solids Struct*.

Palermo, M. et al., 2015. An approach for the mechanical characterisation of the Asinelli Tower (Bologna) in presence of insufficient experimental data. *Journal of Cultural Heritage*, 16(4), pp.536–543. Available at: http://dx.doi.org/10.1016/j.culher.2014.05.002.

Palermo, M. et al., 2013. The structural health monitoring of the Garisenda Tower in Bologna , Italy. , 2013(314), pp.28–30.

Papa, E.A., 2000. Unilateral damage model for masonry based on a homogenization procedure.

Papantonopoulos, C. et al., 2002a. Numerical prediction of the earthquake response of classical columns using the distinct element method. *Earthquake Engineering & Structural Dynamics*, 31(9), pp.1699–1717.

Papantonopoulos, C. et al., 2002b. Numerical prediction of the earthquake response of classical columns using the distinct element method. *Earthquake Engineering and Structural Dynamics*, 31(9), pp.1699–1717.

Parisi, F. et al., 2012. *Field inspection after the May 20th and 29th 2012 Emilia-Romagna earthquakes*,

Pelà, L., Cervera, M. & Roca, P., 2013. An orthotropic damage model for the analysis of masonry structures. *Construction and Building Materials,*.

Pelà, L., Cervera, M. & Roca, P., Continuum model for inelastic behaviour of masonry. In *Congresso dell'Associazione Italiana di Meccanica Teorica e Applicata*.

Pena, F. et al., 2007. On the dynamics of rocking motions of single rigid-block structures. *Earthquake Engineering and Structural Dynamics*, p.2383–2399,.

Peroni, A., 1989. Architettura e scultura: Aggiornamenti, in Wiligelmo e Lanfranco nell'Europa romanica.

Peroni, A., 1999. Il Duomo di Modena. L'architettura, in Il Duomo di Modena,. In F. C. Panini, ed. Mirabilia Italiae 9.

Porter, A.K., 1917. Lombard Architecture. In H. & Milford, eds. Yale University Press.

Posenato, D. et al., 2008. Model-free data interpretation for continuous monitoring of complex structures. *Advanced Engineering Informatics*, 22(1), pp.135–144.

Robert-Nicoud, Y. et al., 2005. Model identification of bridges using measurement data. *Computer-Aided Civil and Infrastructure Engineering*, 20(2), pp.118–131.

Roca, P. et al., 2007. Limit analysis of reinforced masonry vaults,. *Engineering Structures*.

Roca, P. et al., 2010. Structural analysis of masonry historical constructions. Classical and advanced approaches. *Archives of Computational Methods in Engineering*, 17(3), pp.299–325.

Rossi, P.P. & Rossi, C., 1998. Surveillance and Monitoring of Ancient Structures : Recent Developments . *System*, pp.1–15.

Rots, J.G., 1997. Structural masonry: An experimental/numerical basis for practical design rules.

Sabetta, F. & Pugliese, A., 1987. Attenuation of Peak Horizontal Acceleration and Velocity from Italian Strong - motion Records. *Bulletin of the Seismological Society of America*.

De Santis, S. & de Felice, G., 2012. Seismic analysis of masonry arches. In *Proceedings of the fiftheenth world conference on earthquake engeneering*. Available at: http://www.iitk.ac.in/nicee/wcee/article/WCEE2012_0687.pdf.

Sassu, M., Andreini, M. & De Falco, A., 2012. *Damage mechanisms as seismic transducers in historic centres: the example of San Pio delle Camere after 2009 earthquake in Abruzzo (Italy)*,

Silvestri, E., 2013. Una rilettura delle fasi costruttive del Duomo di Modena. In *Atti E Memorie", Deputazione Di Storia Patria per Le Antiche Provincie Modenesi*.

Smoljanović, H., Živaljić, N. & Nikolić, Ž., 2013. Overview of the methods for the modelling of historical masonry structures. *Građevinar*, 65(December), pp.603–618. Available at: http://hrcak.srce.hr/index.php?show=clanak&id_clanak_jezik=156407.

Sohn, H. et al., 2003. A Review of Structural Health Monitoring Literature : 1996-2001. *Structural Health Monitoring*, LA-13976-M(LA-13976-MS), pp.1996–2001. Available at: http://library.lanl.gov/cgi-bin/getfile?00796820.pdf.

Sohn, H., 2007. Effects of environmental and operational variability on Structural Health Monitoring. *The Royal Society -- Philosophical Transactions: Mathematical, Physical and Engineering Sciences*, 365(1851), pp.539–560.

Tassios, T.P., 1988. Meccanica delle murature. In Liguori, ed.

Titchmarsh, E., 1948. Introduction to the theory of Fourier integrals. In O. U. Press, ed.

Tyagunov, S. & Petryna, Y., 2016. Structural Health Monitoring and Vulnerability Assessment of

Buildings in Earthquake Prone Areas. In pp. 5–8.

Figure Captions

Table Captions

APPENDIX A

Data analyses for the Asinelli tower

A.1 Reference quantities

The systematic identification of the reference quantities is here provided for each instrument installed on the Asinelli tower.

In more detail, for each instrument the following plots are reported:

- row-data recorded by the sensor over the entire monitoring period (2011-2016)
- the mean daily value
- the daily amplitude
- progressive daily residual on the mean value
- absolute daily residual on the mean value
- the annual amplitude
- progressive annual residual on the mean value
- absolute annual residual on the mean value

The table collects the mean values for each years of these reference quantities.

It is noted that the laser distance meters have recorded many spike and missing data throughout the monitoring period therefore are not considered in the analyses. Moreover, almost all the inclinometers recorded an anomalous behaviour in the first/second year of monitoring. In this case, the reference quantities have been calculated starting from the 2013.

Long Base Deformeters

Deformometer Invar 1-without Drops

Mean Daily Value

Daily Amplitude

Progressive Daily Residuals of the Mean Value

Absolute Daily Residuals of the Mean Value

Annual Amplitude

Progressive Annual Residuals of the Mean Value

Absolute Annual Residuals of the Mean Value
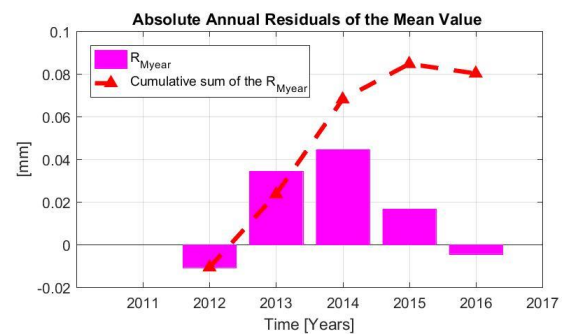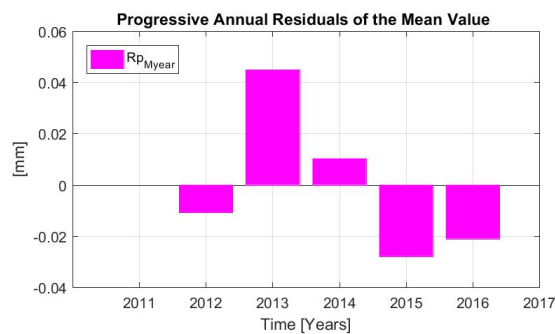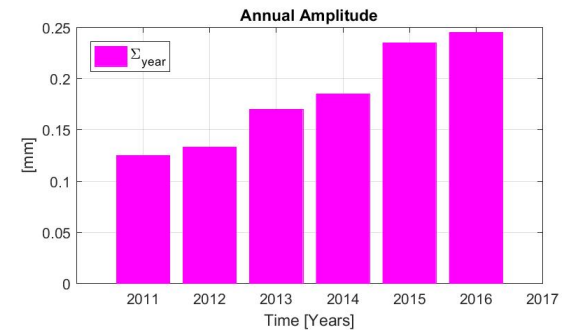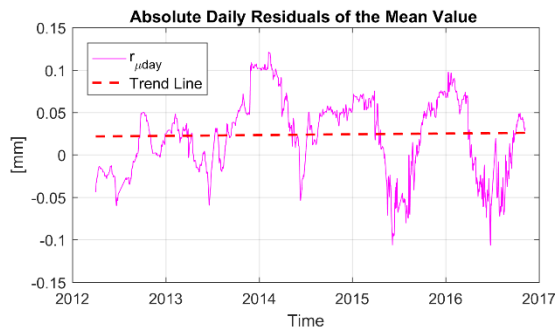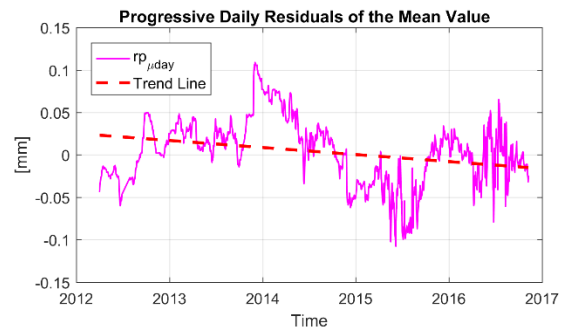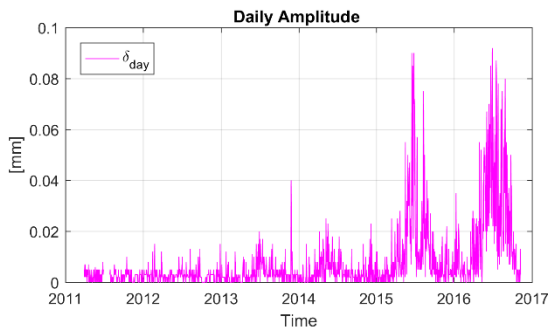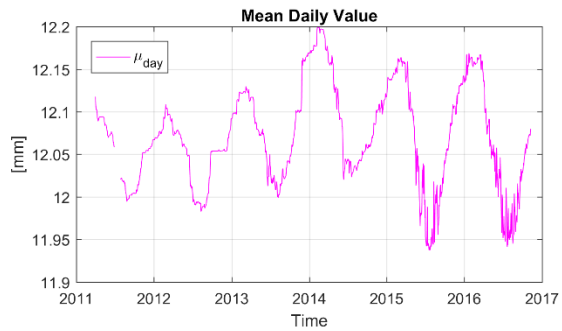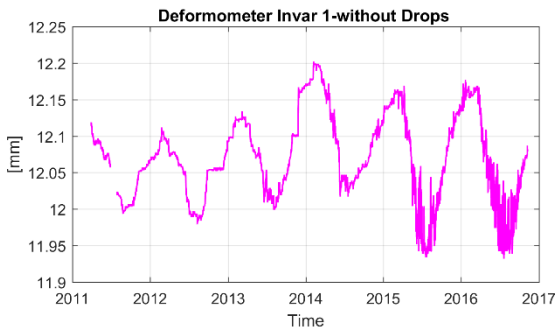
Sensor	Year	$\delta_{day,j}$	$\mathrm{rp}_{\mu day}$	$\mathrm{r}_{\mu day}$	M_{year}	Σ_{year}	Rp_{Myear}	R_{Myear}
	2011	0.002	-	-	12.053	0.1250	-	-
	2012	0.003	-0.004	-0.004	12.043	0.133	-0.011	-0.011
A-FO-F1	2013	0.004	0.030	0.028	12.088	0.170	0.045	0.034
[mm]	2014	0.004	0.024	0.052	12.098	0.185	0.010	0.044
	2015	0.012	-0.033	0.021	12.069	0.235	-0.028	0.016
	2016	0.021	-0.002	0.012	12.049	0.245	-0.021	-0.004
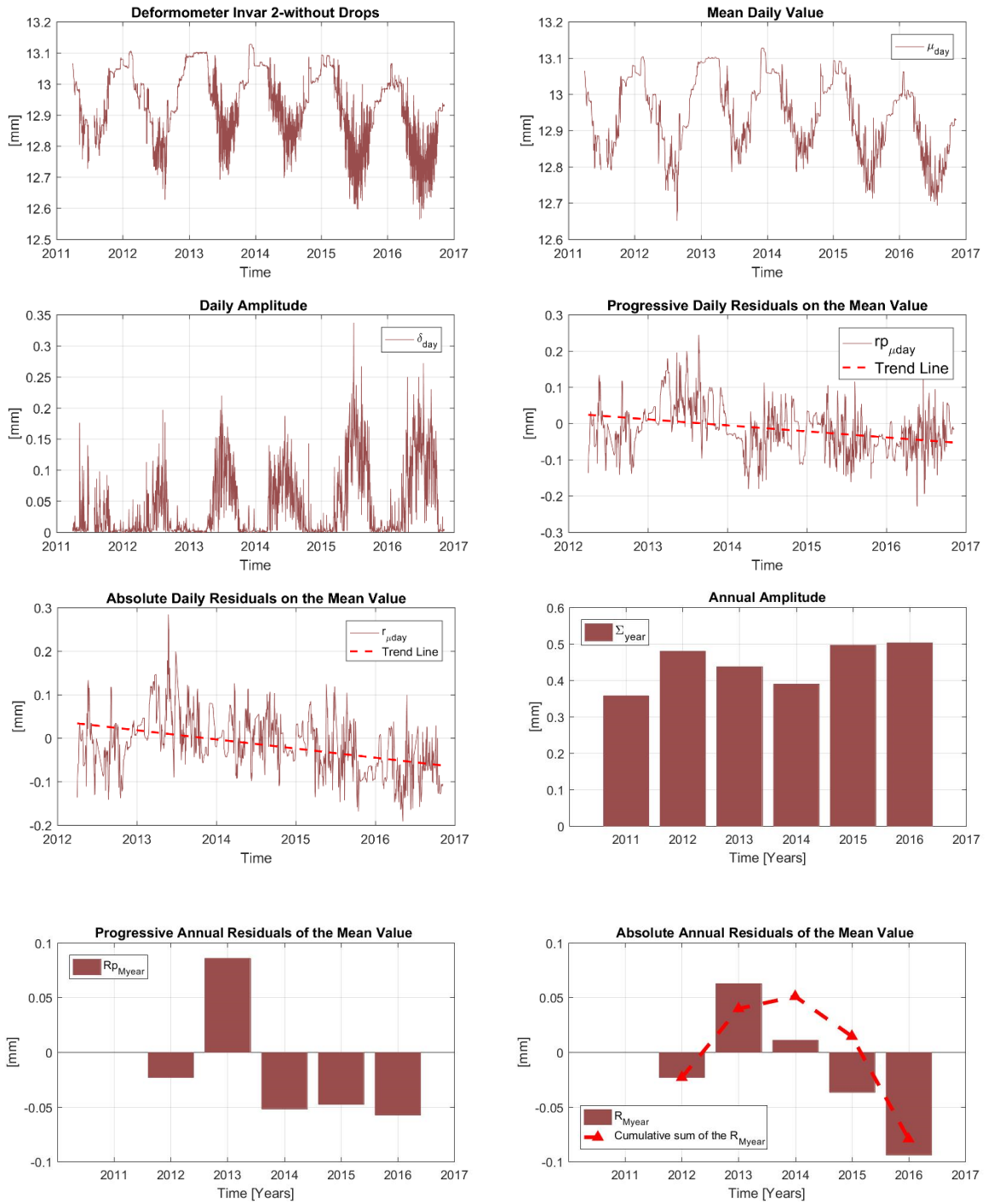
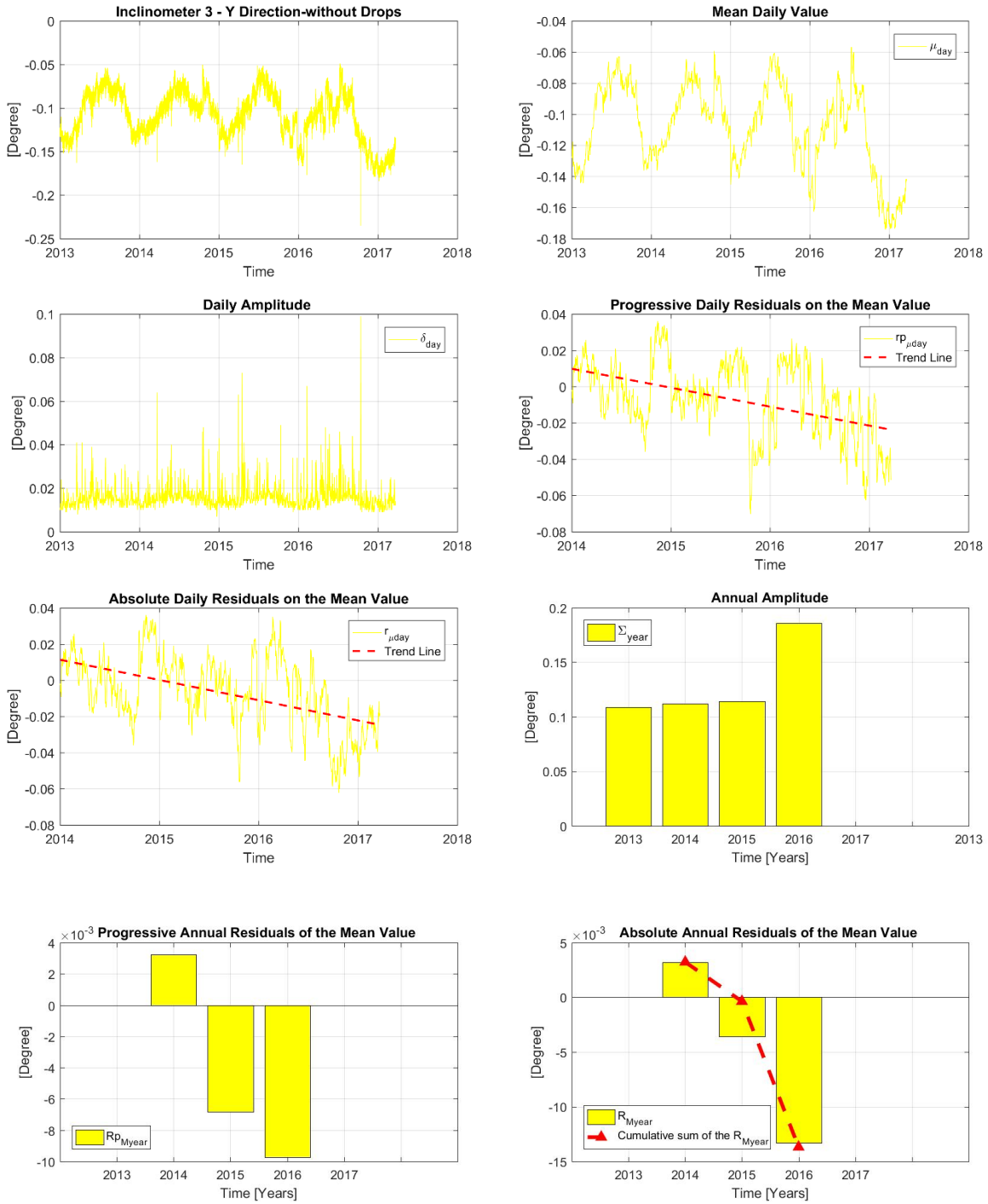| Sensor	Year	$\delta_{day,j}$	$\mathrm{rp}_{\mu day}$	$\mathrm{r}_{\mu day}$	M_{year}	Σ_{year}	Rp_{Myear}	R_{Myear}
	2011	0.016			12.957	0.358		0.000
	2012	0.019	-0.021	-0.021	12.933	0.480	-0.023	-0.023
A-FO-F2	2013	0.039	0.055	0.039	13.019	0.437	0.086	0.063
[mm]	2014	0.037	-0.038	-0.001	12.968	0.390	-0.052	0.011
	2015	0.059	-0.036	-0.034	12.920	0.497	-0.048	-0.036
	2016	0.074	-0.041	-0.067	12.863	0.503	-0.057	-0.094
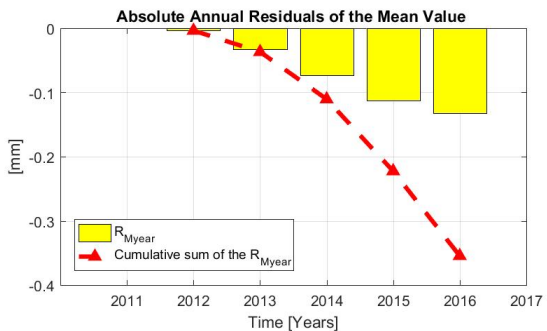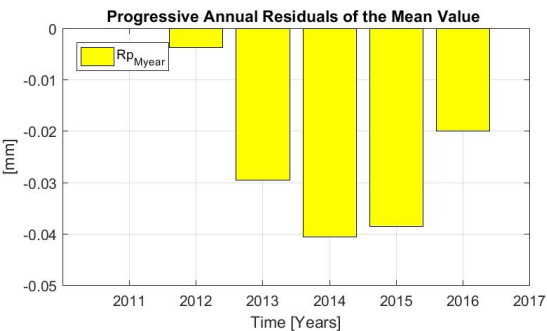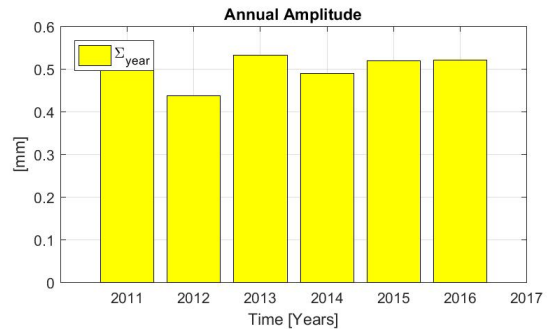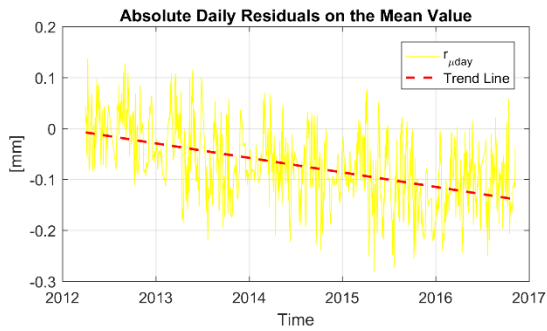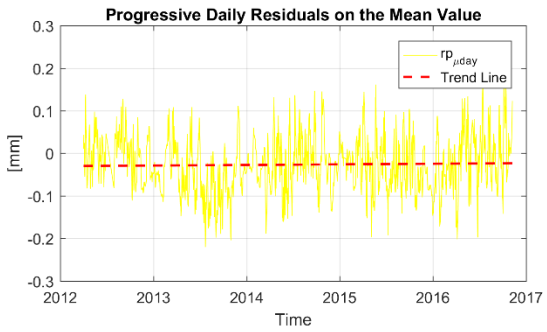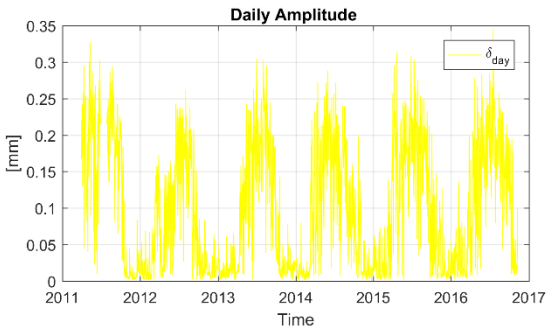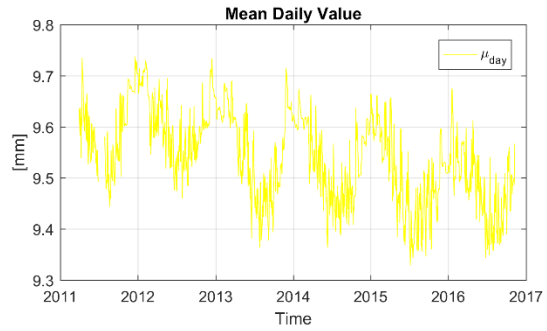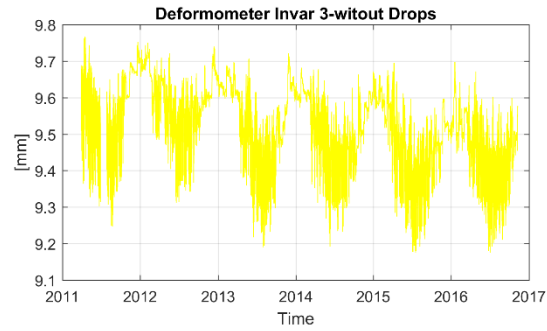
Sensor	Year	$\delta_{day,j}$	$rp_{\mu day}$	$r_{\mu day}$	M_{year}	Σ_{year}	Rp_{Myear}	R_{Myear}
	2011	0.135			9.604	0.520		
	2012	0.075	-0.002	-0.002	9.600	0.438	-0.004	-0.004
A-FO-F3	2013	0.086	-0.053	-0.055	9.571	0.533	-0.029	-0.033
[mm]	2014	0.091	-0.023	-0.079	9.530	0.490	-0.041	-0.074
	2015	0.101	-0.031	-0.108	9.492	0.520	-0.038	-0.112
	2016	0.118	-0.014	-0.111	9.472	0.522	-0.020	-0.132

Deformometer Invar 4-witout Drops

Mean Daily Value

Daily Amplitude

Progressive Daily Residuals on the Mean Value

Absolute Daily Residuals on the Mean Value

Annual Amplitude

Progressive Annual Residuals of the Mean Value

Absolute Annual Residuals of the Mean Value
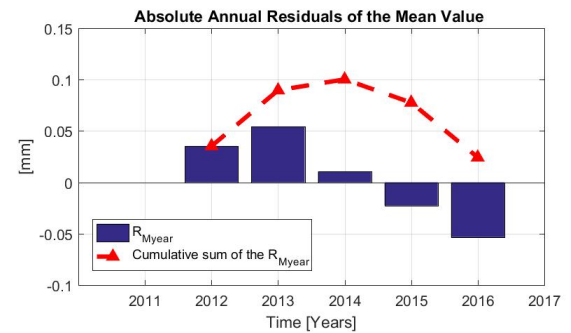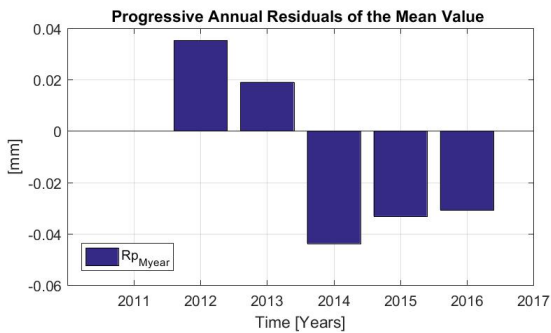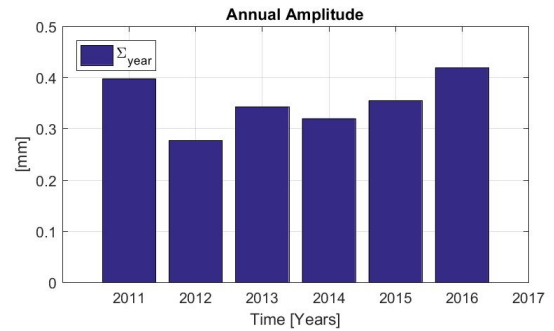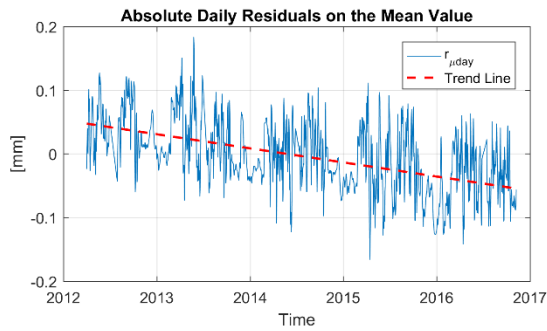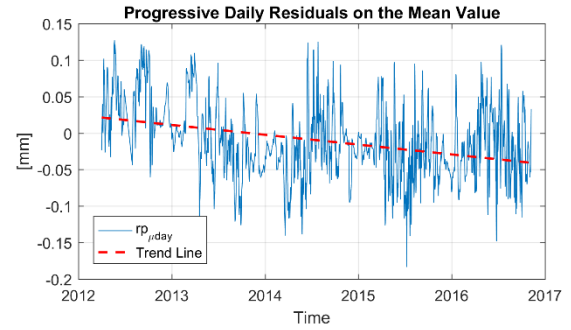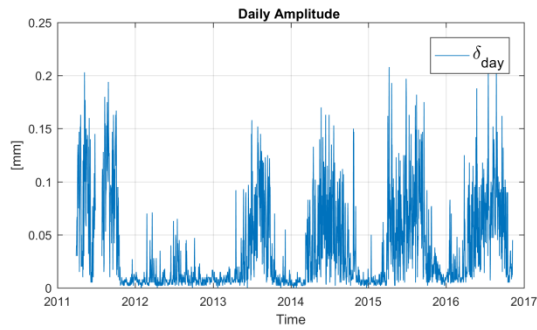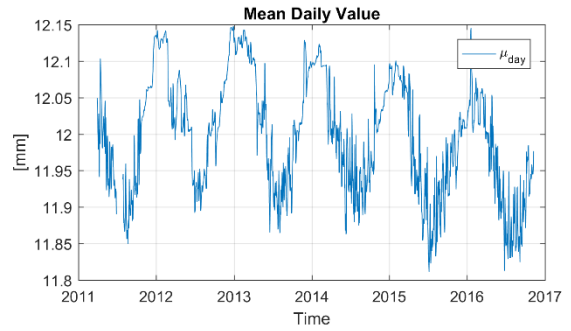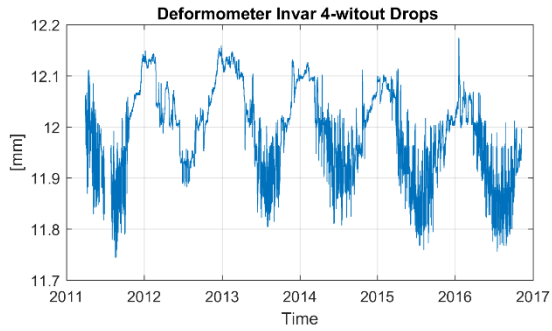
Sensor	Year	$\delta_{day,j}$	$rp_{\mu day}$	$r_{\mu day}$	M_{year}	Σ_{year}	Rp_{Myear}	R_{Myear}
A-FO-F4 [mm]	2011	0.061			11.993	0.398		
	2012	0.010	0.042	0.042	12.028	0.277	0.035	0.035
	2013	0.029	-0.009	0.020	12.047	3.046	0.019	0.055
	2014	0.033	-0.021	-0.004	12.003	0.320	-0.044	0.011
	2015	0.041	-0.029	-0.029	11.970	0.355	-0.033	-0.023
	2016	0.049	-0.018	-0.040	11.939	0.419	-0.031	-0.053

Deformometer Invar 5-witout Drops

Mean Daily Value

Daily Amplitude

Progressive Daily Residuals on the Mean Value

Absolute Daily Residuals on the Mean Value

Annual Amplitude

Progressive Annual Residuals of the Mean Value
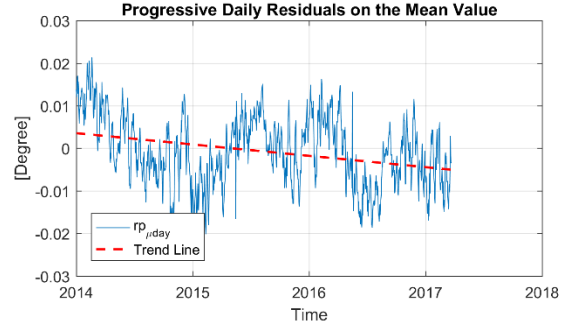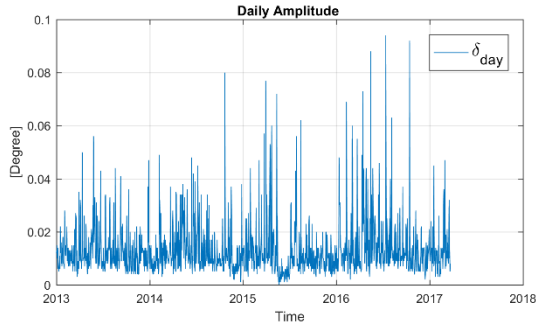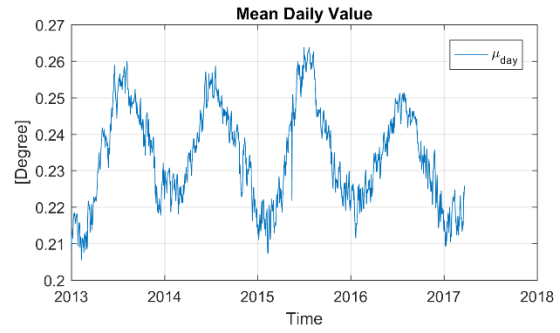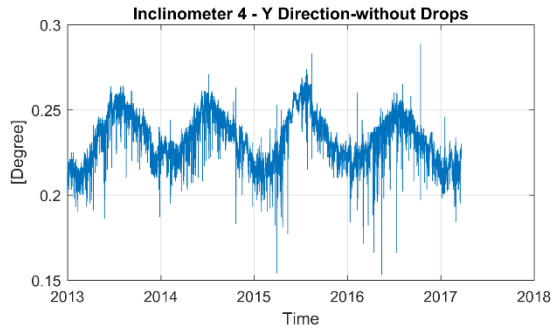

Absolute Annual Residuals of the Mean Value
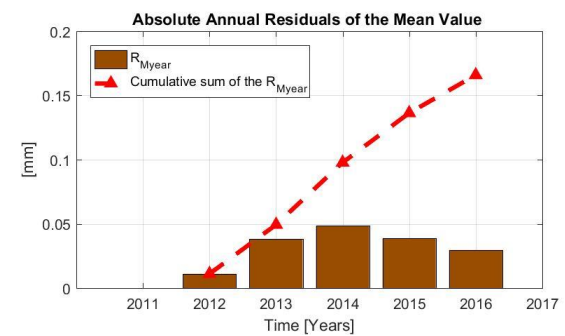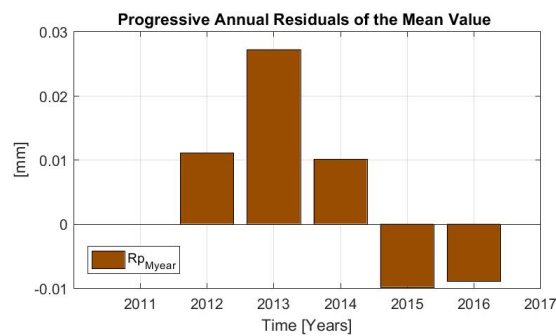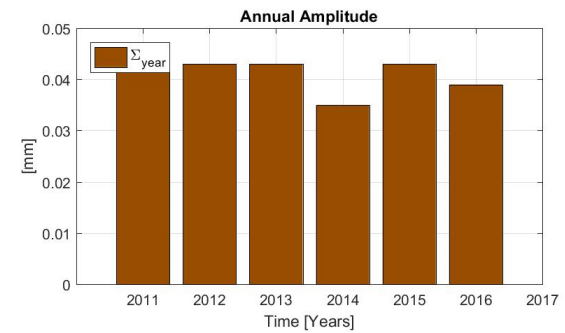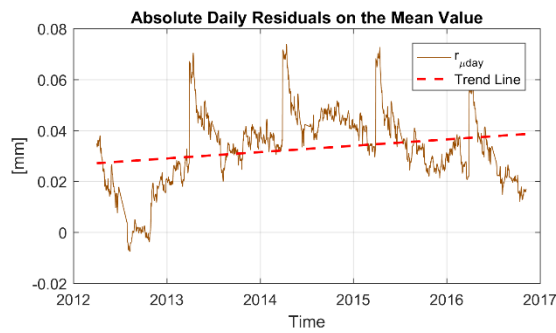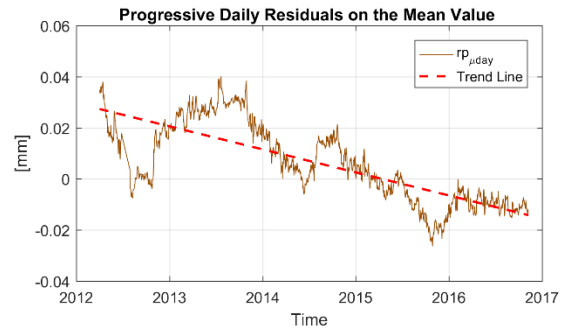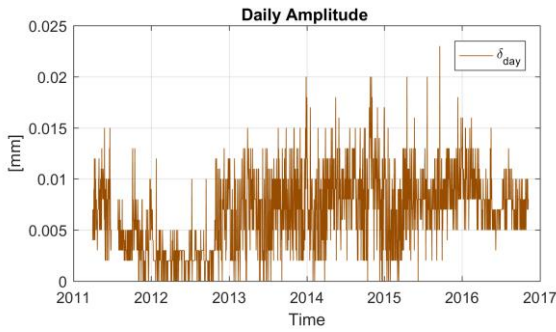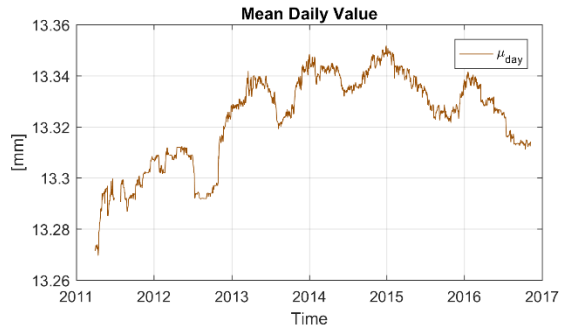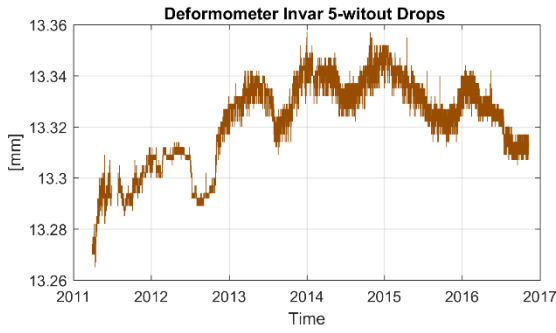
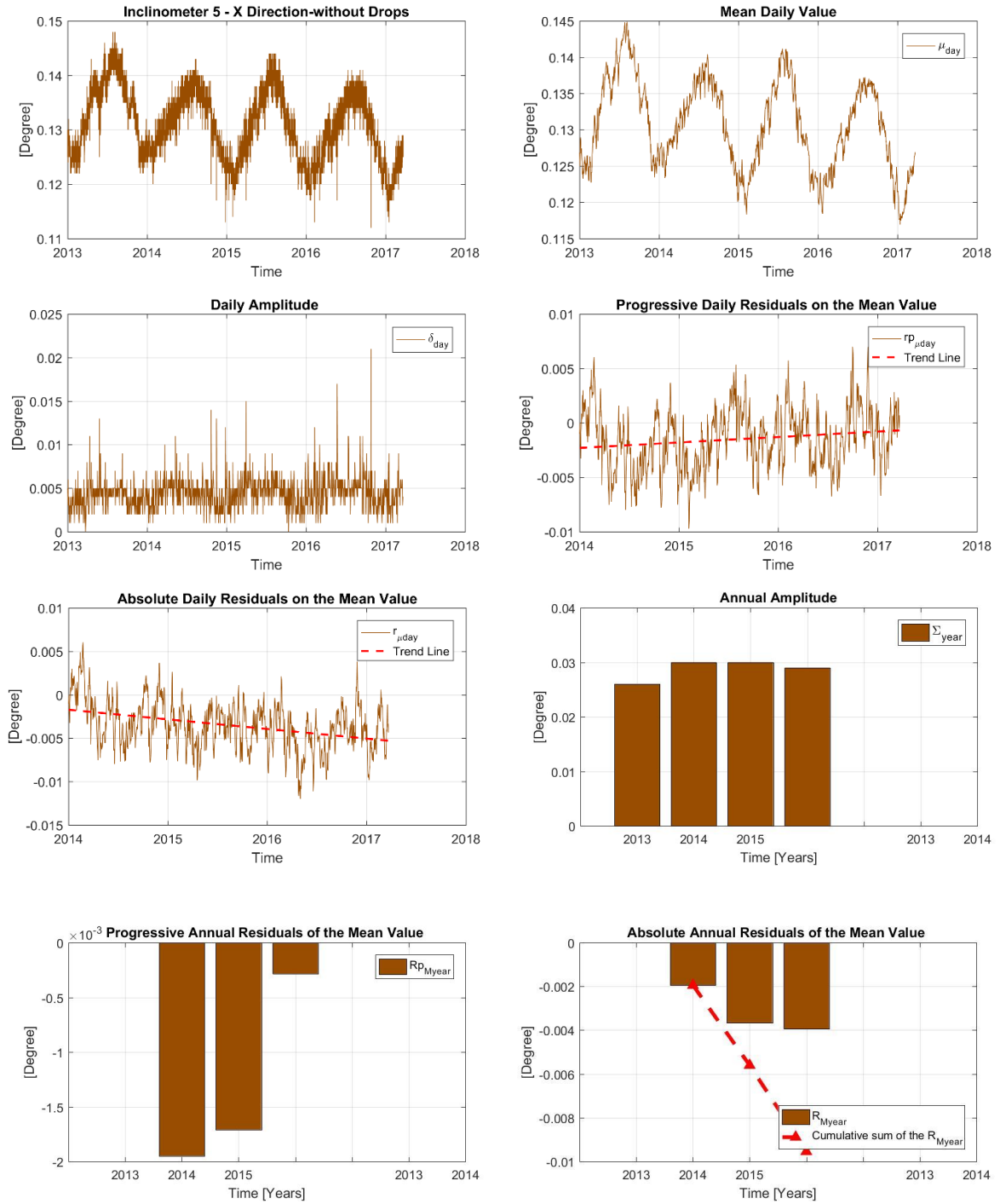| Sensor	Year	$\delta_{day,j}$	$rp_{\mu day}$	$r_{\mu day}$	M_{year}	Σ_{year}	Rp_{Myear}	R_{Myear}
A-FO-F5 [mm]	2011	0.005			13.294	0.047		
	2012	0.003	0.012	0.012	13.305	0.043	0.011	0.011
	2013	0.007	0.027	0.035	13.332	0.043	0.027	0.038
	2014	0.008	0.009	0.044	13.342	0.035	0.010	0.048
	2015	0.008	-0.007	0.037	13.332	0.043	-0.010	0.039
	2016	0.008	-0.010	0.029	13.324	0.038	-0.009	0.030

Sensor	Year	$\delta_{day,j}$	$rp_{\mu day}$	$r_{\mu day}$	M_{year}	Σ_{year}	Rp_{Myear}	R_{Myear}
	2011	0.002			13.935	0.123		0.000
	2012	0.004	-0.012	-0.012	13.922	0.383	-0.014	-0.014
A-FS-F6	2013	0.003	-0.076	-0.085	13.871	0.168	-0.050	-0.064
[mm]	2014	0.002	-0.052	-0.139	13.797	0.027	-0.074	-0.138
	2015	0.009	-0.017	-0.156	13.780	0.085	-0.018	-0.156
	2016	0.014	0.001	-0.154	13.782	0.082	0.002	-0.154

Deformometer Invar 7

Mean Daily Value

Daily Amplitude

Progressive Daily Residuals on the Mean Value

Absolute Daily Residuals on the Mean Value

Annual Amplitude

Progressive Annual Residuals of the Mean Value

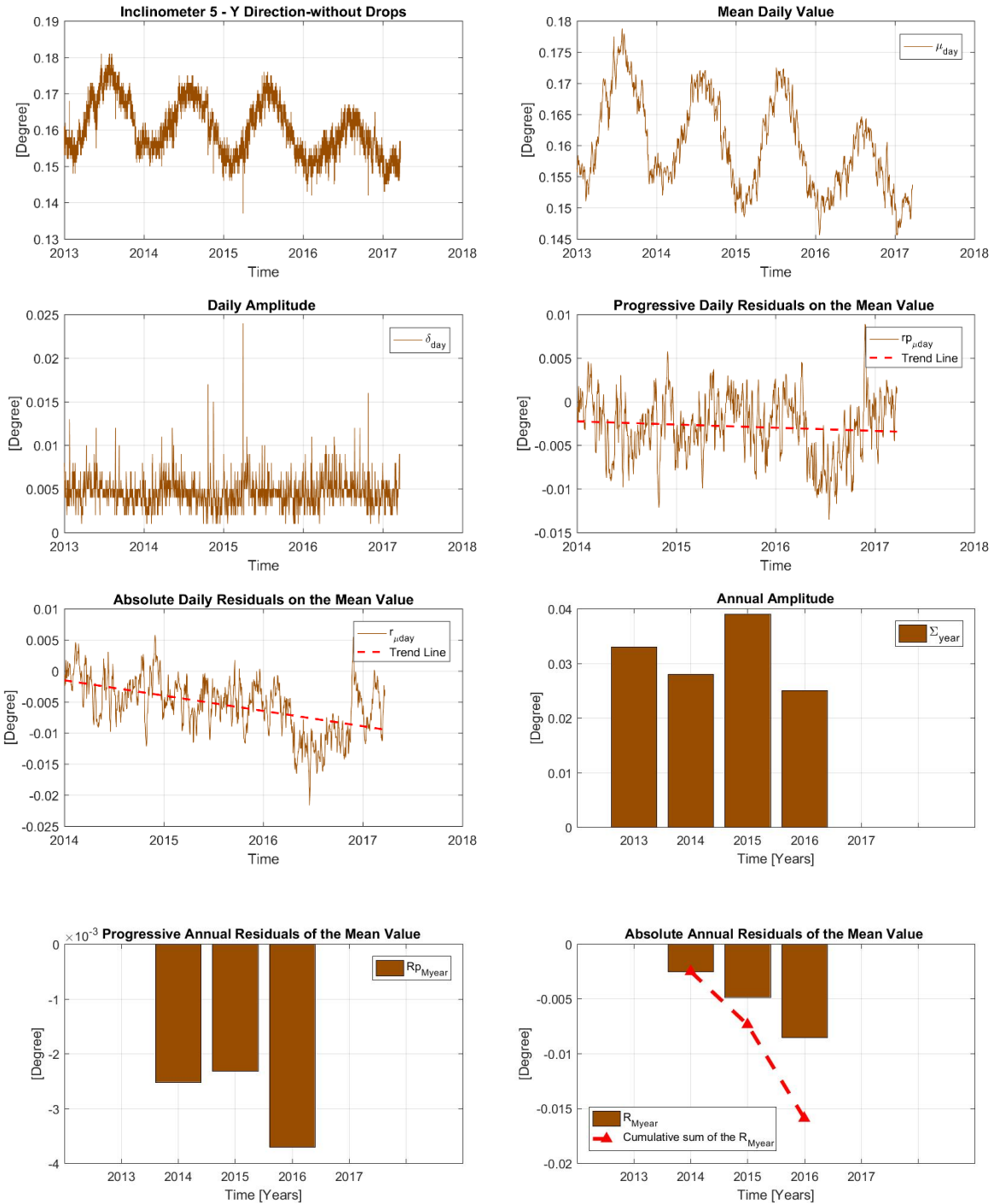Absolute Annual Residuals of the Mean Value
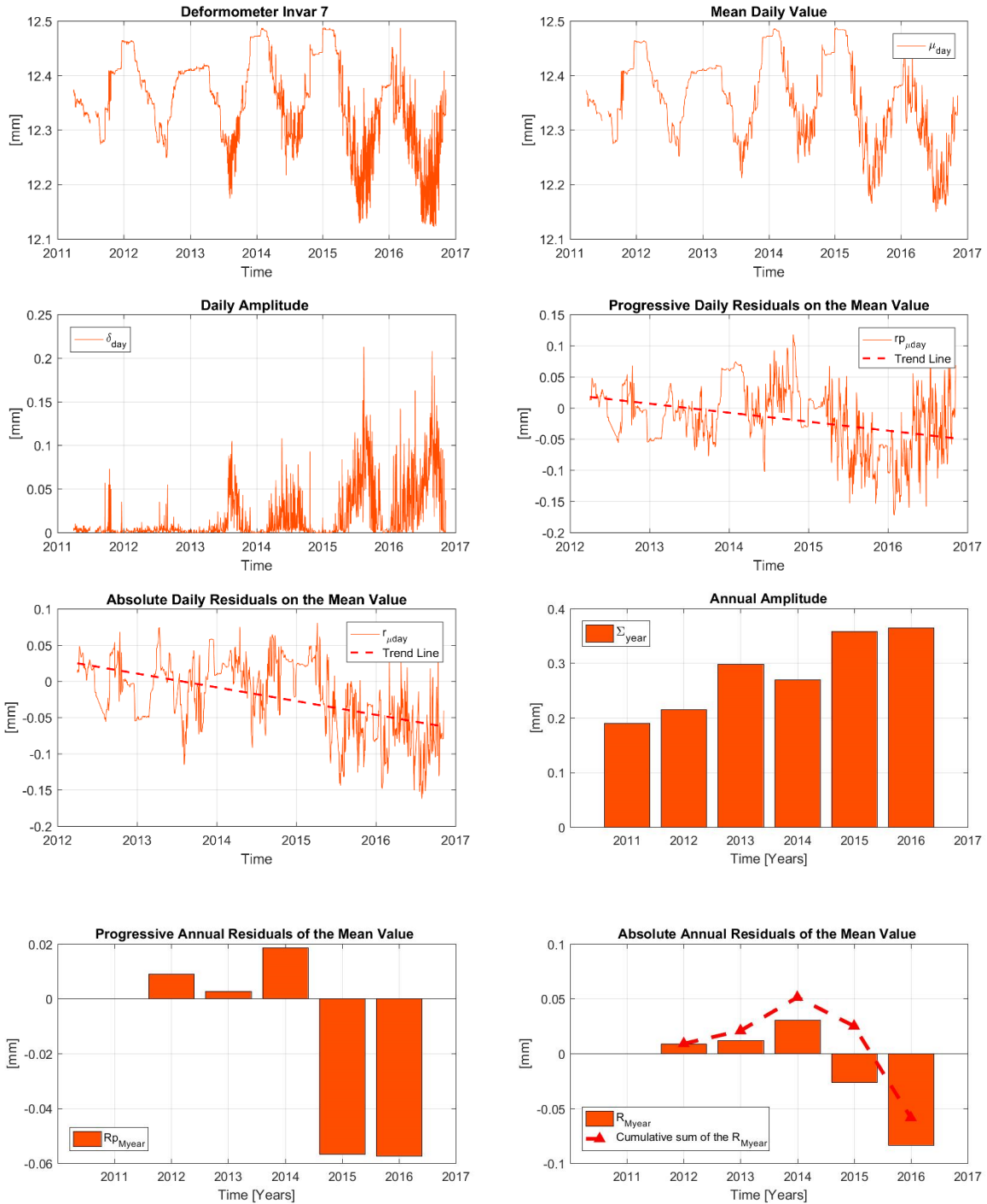
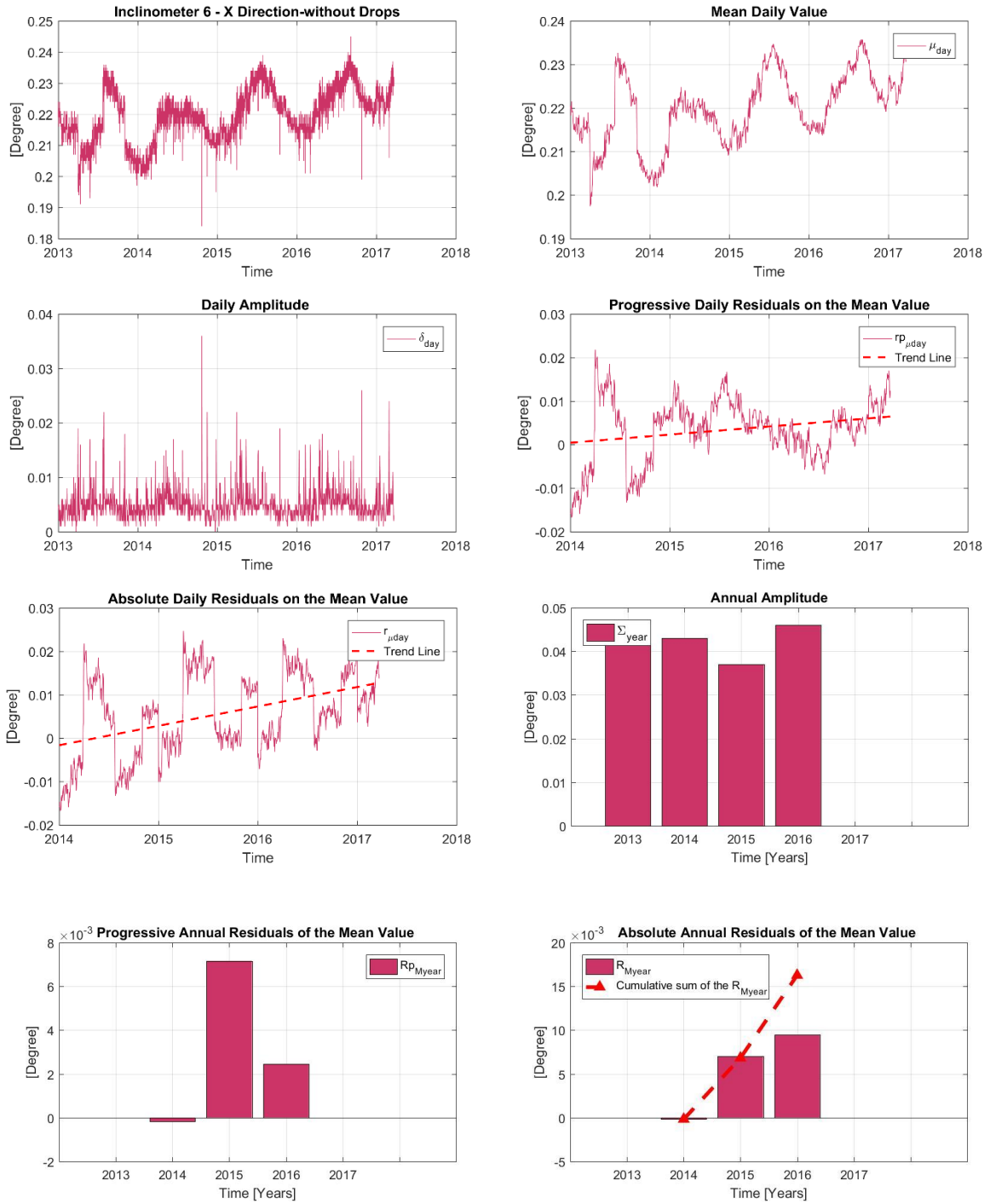| Sensor	Year	$\delta_{day,j}$	$rp_{\mu day}$	$r_{\mu day}$	M_{year}	Σ_{year}	Rp_{Myear}	R_{Myear}
	2011	0.004			12.362	0.190		
	2012	0.003	0.005	0.005	12.371	0.215	0.009	0.009
A-FS-F7	2013	0.011	-0.013	-0.010	12.374	0.298	0.003	0.012
[mm]	2014	0.010	0.021	0.011	12.392	0.270	0.019	0.030
	2015	0.029	-0.042	-0.028	12.336	0.358	-0.057	-0.026
	2016	0.047	-0.050	-0.075	12.278	0.365	-0.057	-0.084
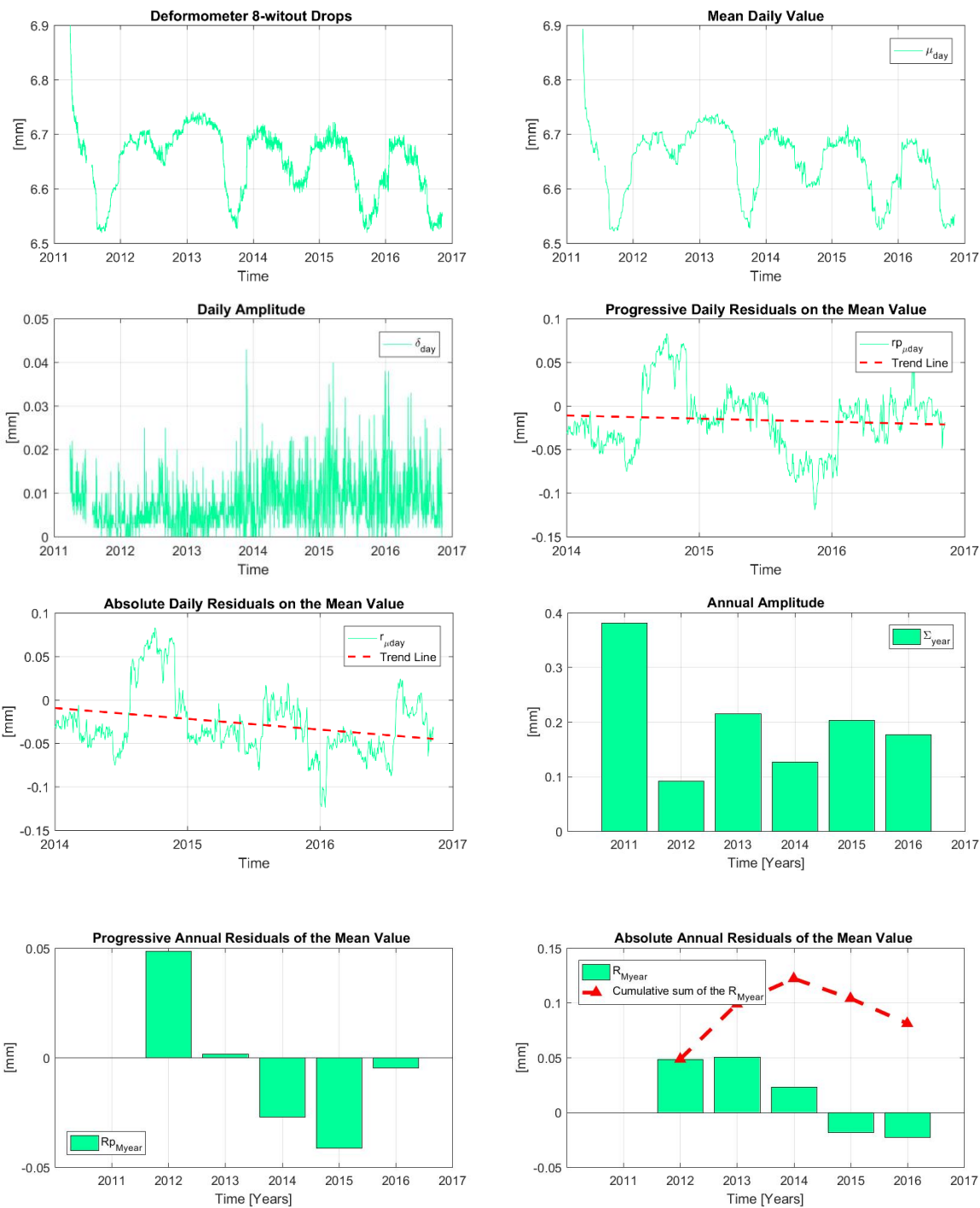
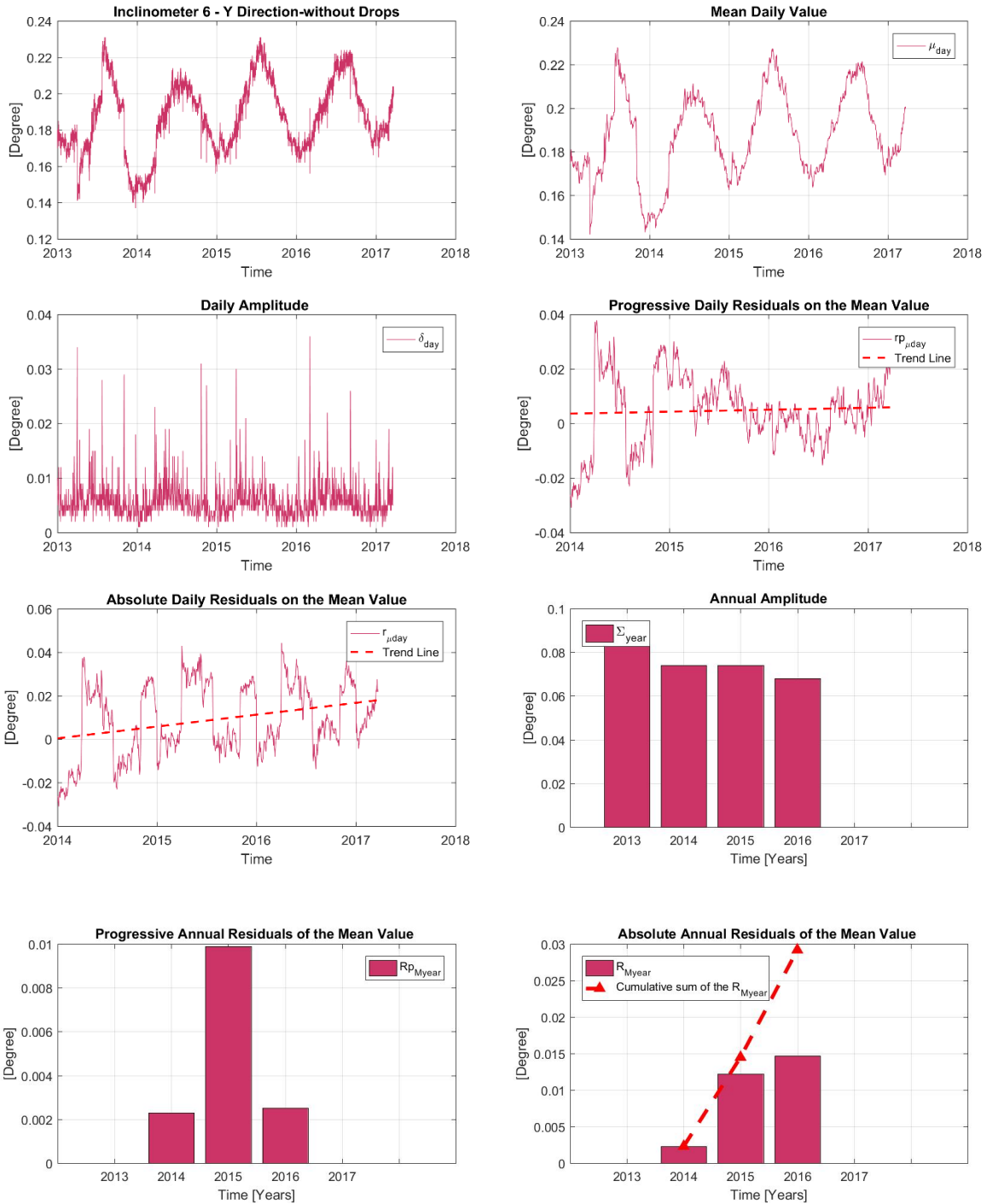| Sensor	Year	$\delta_{day,j}$	$rp_{\mu day}$	$r_{\mu day}$	M_{year}	Σ_{year}	Rp_{Myear}	R_{Myear}
A-FS-F8 [mm]	2011	0.006			6.635	0.381		
	2012	0.005			6.683	0.092	0.049	
	2013	0.006	-0.020	0.024	6.685	0.215	0.002	0.050
	2014	0.009	-0.004	0.022	6.658	0.127	-0.027	0.023
	2015	0.010	-0.031	-0.011	6.617	0.203	-0.041	-0.018
	2016	0.009	-0.012	-0.023	6.612	0.177	-0.005	-0.023

Deformeters
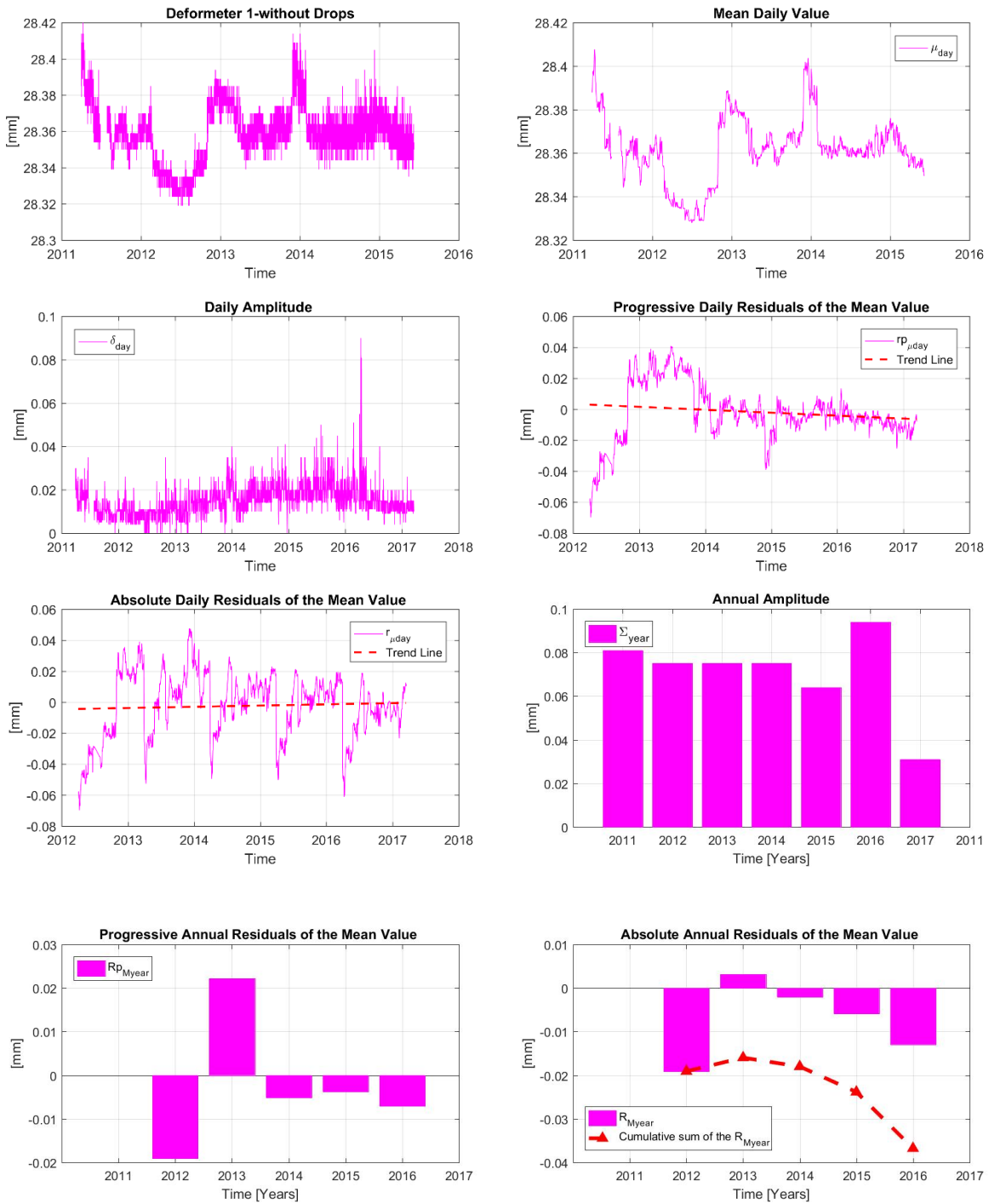
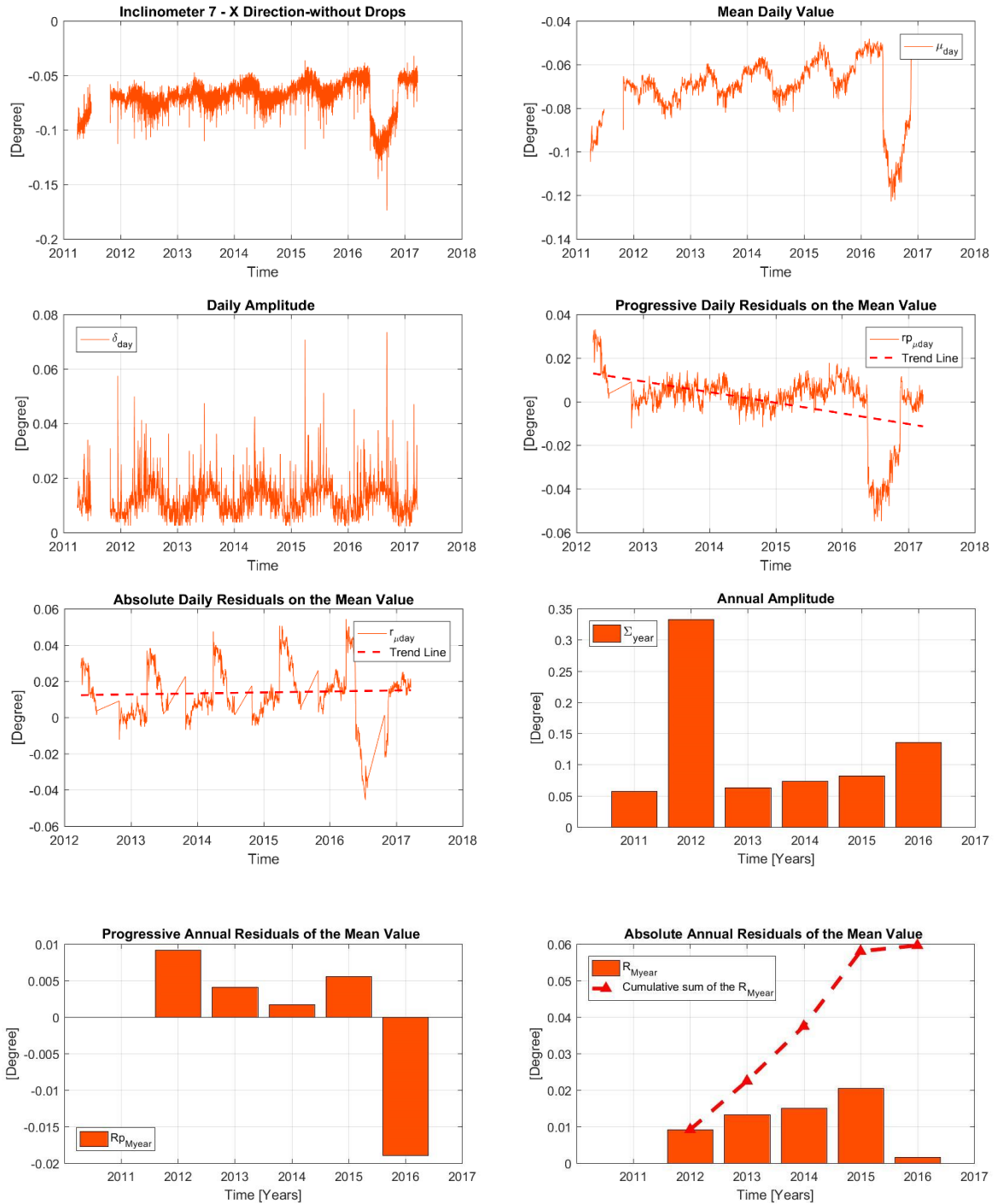| Sensor	Year	$\delta_{day,j}$	$rp_{\mu day}$	$r_{\mu day}$	M_{year}	Σ_{year}	Rp_{Myear}	R_{Myear}
A—FO-D1 [mm]	2011	0.013			28.366	0.081		
	2012	0.010	-0.019	-0.019	28.347	0.075	-0.019	-0.019
	2013	0.014	0.022	0.008	28.370	0.075	0.022	0.003
	2014	0.018	-0.005	0.003	28.365	0.176	-0.005	-0.002
	2015	0.019	-0.006	-0.006	28.361	0.050	-0.004	-0.006
	2016	0.017	-0.006	-0.008	28.354	0.094	-0.007	-0.013
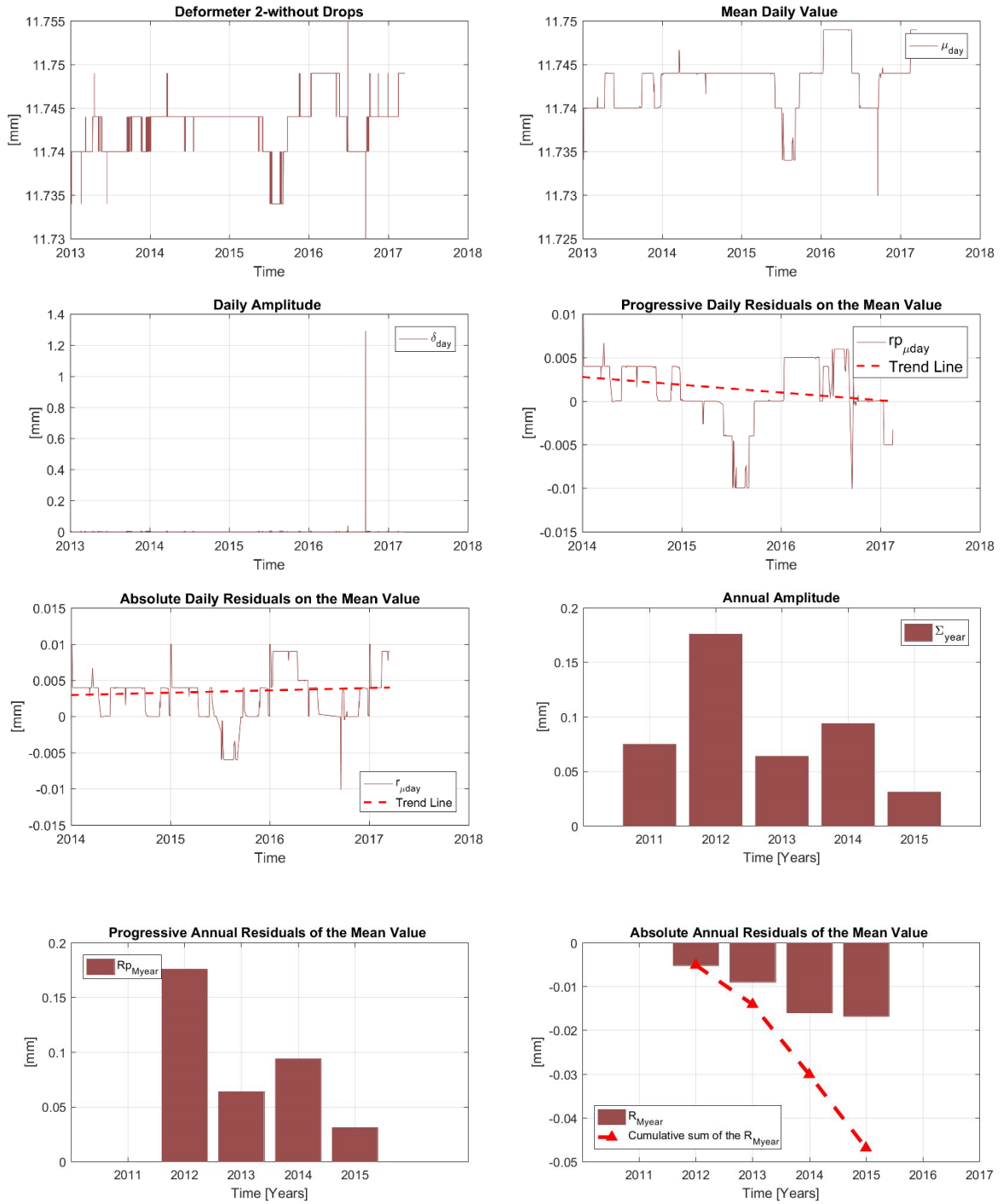
Sensor	Year	$\delta_{day,j}$	$rp_{\mu day}$	$r_{\mu day}$	M_{year}	Σ_{year}	Rp_{Myear}	R_{Myear}
A—FO-D2 [mm]	2013	0.003			28.370	0.075		0.000
	2014	0.002	-0.001	-0.001	28.365	0.176	-0.005	-0.005
	2015	0.004	0.004	0.003	28.361	0.064	-0.004	-0.009
	2016	0.004	0.003	0.006	28.354	0.094	-0.007	-0.016

Deformometer 5-without Drops

Mean Daily Value

Daily Amplitude

Progressive Daily Residuals on the Mean Value

Absolute Daily Residuals on the Mean Value

Annual Amplitude

Progressive Annual Residuals of the Mean Value

Absolute Annual Residuals of the Mean Value

Sensor	Year	$\delta_{day,j}$	$\mathrm{rp}_{\mu day}$	$\mathrm{r}_{\mu day}$	M_{year}	Σ_{year}	Rp_{Myear}	R_{Myear}
A—FE-D5 [mm]	2013	0.003			28.370	0.075		0.000
	2014	0.002	-0.001	-0.001	28.365	0.176	-0.005	-0.005
	2015	0.004	0.004	0.003	28.361	0.064	-0.004	-0.009
	2016	0.004	0.003	0.006	28.354	0.094	-0.007	-0.016

Extensometers
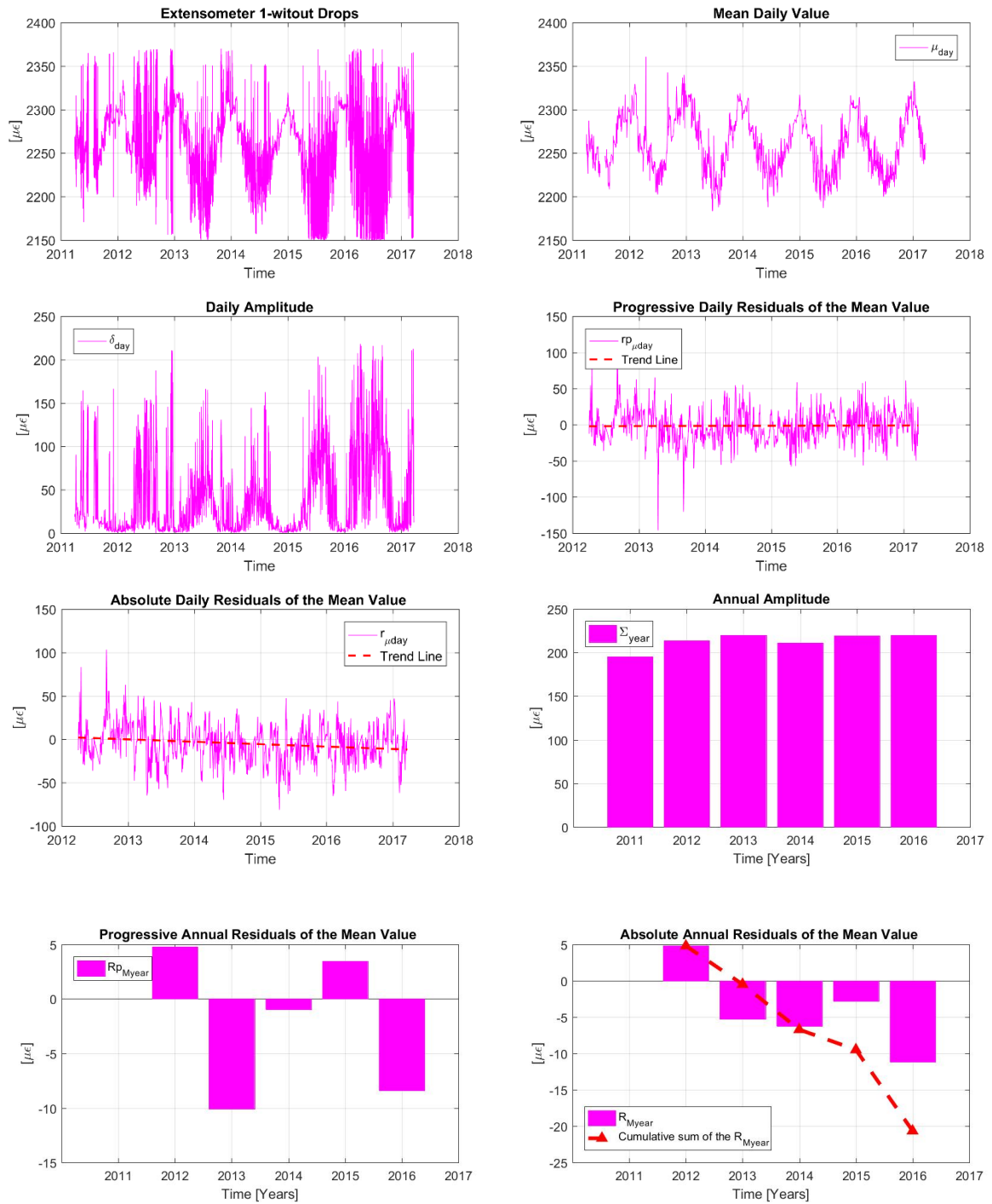
Sensor	Year	$\delta_{day,j}$	$\mathrm{rp}_{\mu day}$	$\mathrm{r}_{\mu day}$	M_{year}	Σ_{year}	Rp_{Myear}	R_{Myear}
	2011	30.27			2260.33	195.32		
	2012	36.46	8.03	8.03	2265.12	213.84	4.80	4.80
A—FO-E1	2013	31.58	-8.14	-2.85	2255.05	219.70	-10.08	-5.28
[µε]	2014	24.36	-3.75	-7.67	2254.10	211.13	-0.95	-6.23
	2015	42.41	-2.60	-9.60	2257.55	219.35	3.45	-2.78
	2016	68.51	1.64	-7.73	2249.16	219.70	-8.39	-11.17

Extensometer 2-witout Drops

Mean Daily Value

Daily Amplitude

Progressive Daily Residuals of the Mean Value

Absolute Daily Residuals of the Mean Value

Annual Amplitude

Progressive Annual Residuals of the Mean Value

Absolute Annual Residuals of the Mean Value
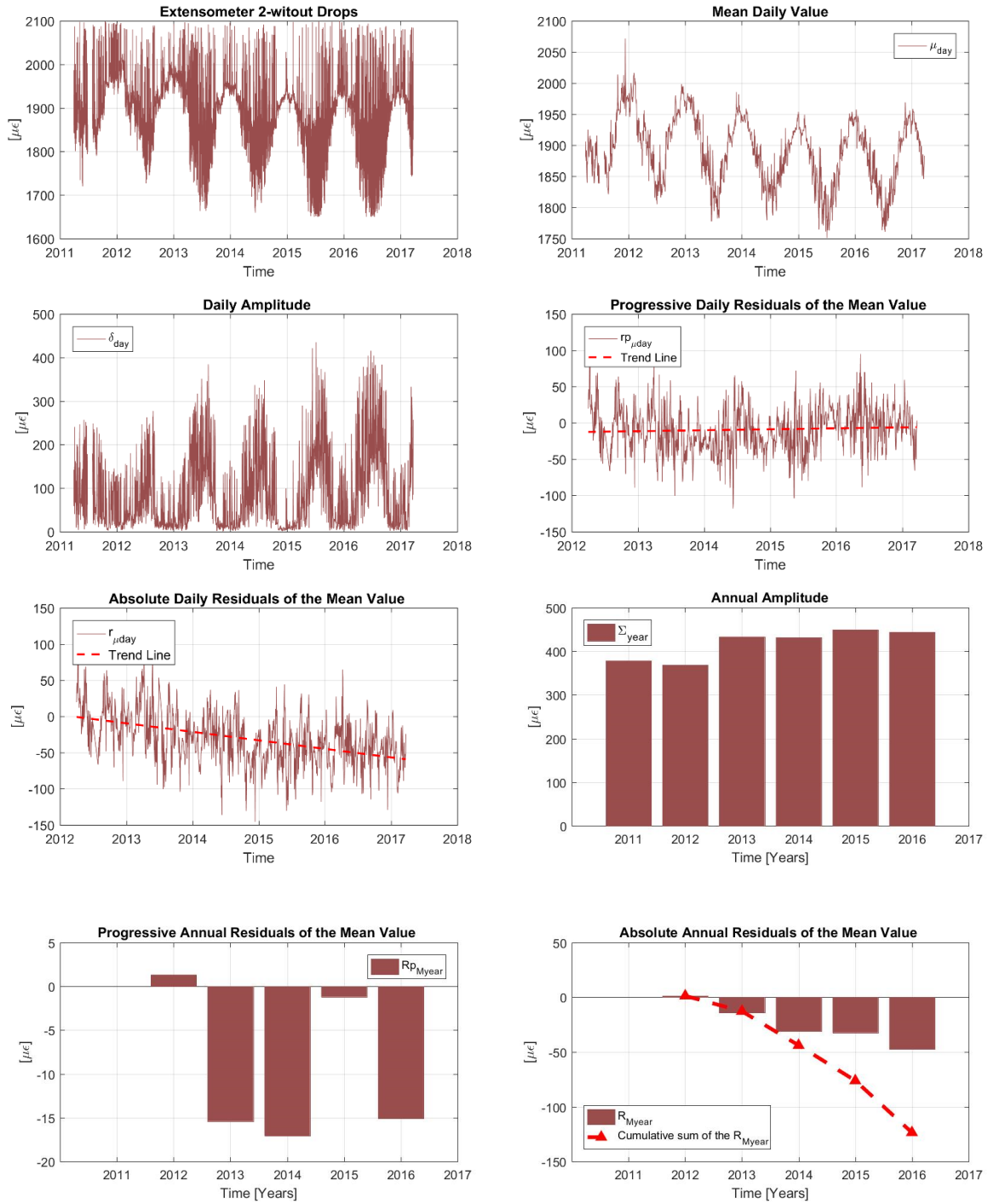
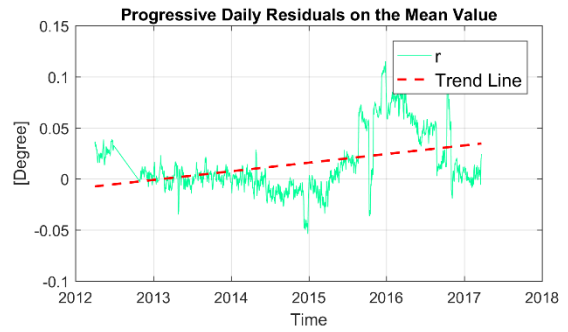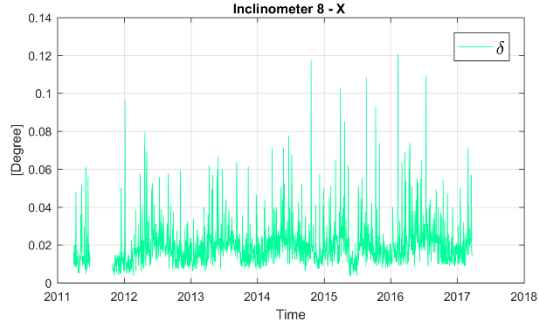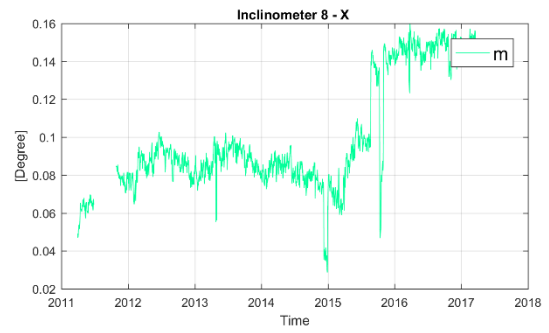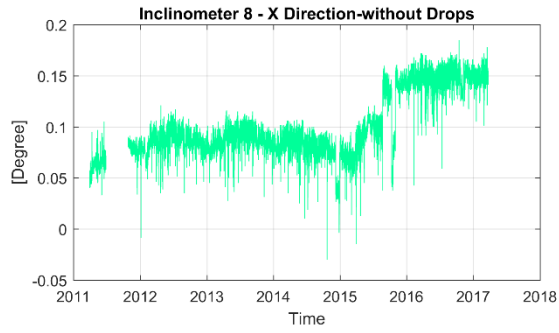| Sensor	Year	$\delta_{day,j}$	$rp_{\mu day}$	$r_{\mu day}$	M_{year}	Σ_{year}	Rp_{Myear}	R_{Myear}
A—FO-E2 [μɛ]	2011	78.10			1905.80	378.58		0.00
	2012	54.84	2.76	2.76	1907.14	368.32	1.34	1.34
	2013	94.39	-16.68	-15.47	1891.73	433.45	-15.41	-14.07
	2014	79.20	-18.56	-35.58	1874.66	431.89	-17.07	-31.14
	2015	96.19	-10.53	-44.23	1873.47	449.63	-1.19	-32.33
	2016	126.58	0.73	-43.28	1858.37	444.20	-15.09	-47.43

Sensor	Year	$\delta_{day,j}$	rp$_{\mu day}$	r$_{\mu day}$	M_{year}	Σ_{year}	Rp$_{Myear}$	R_{Myear}
	2011	50.48			2325.25	346.82		0.00
	2012	26.29	3.31	2.52	2326.32	314.87	1.07	1.07
A—FO_E3	2013	57.98	-3.62	-3.47	2324.02	305.05	-2.30	-1.22
[με]	2014	81.75	-11.51	-15.15	2313.66	441.51	-10.37	-11.59
	2015	59.83	4.25	-8.27	2322.92	364.77	9.26	-2.33
	2016	80.57	9.57	-2.6	2321.23	391.58	-1.69	-4.02
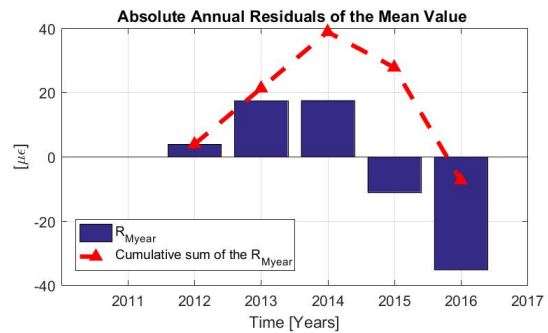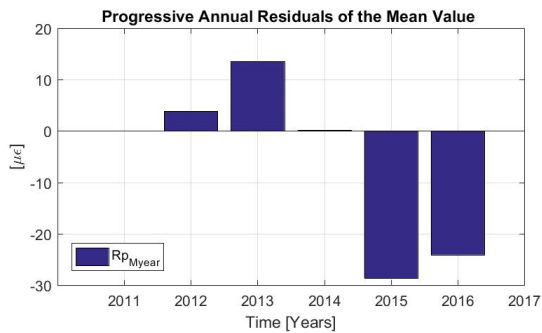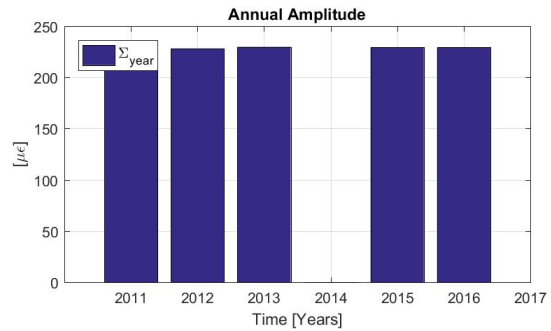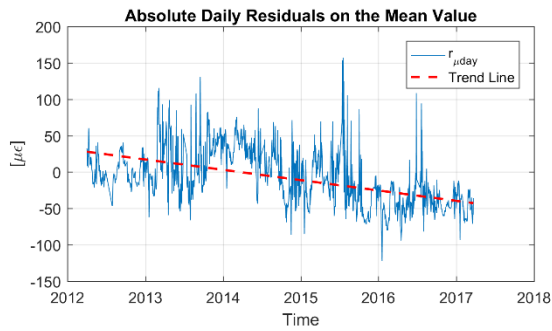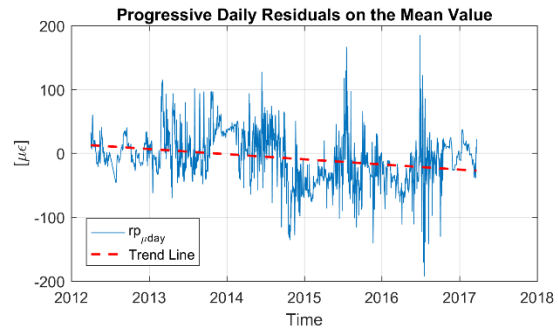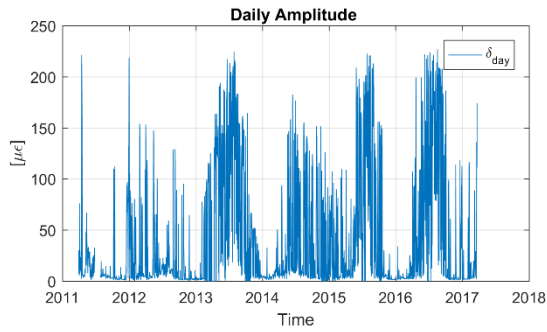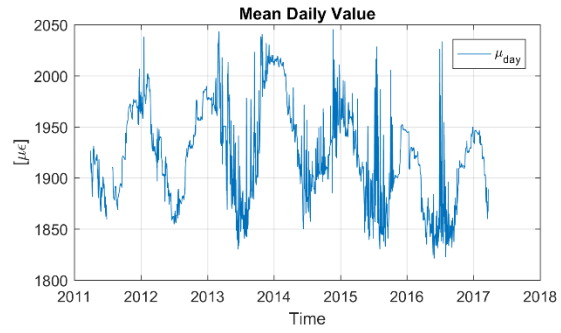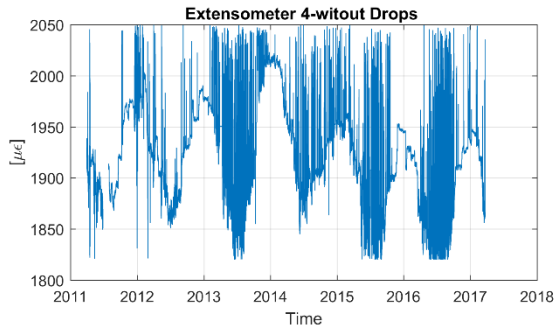
Sensor	Year	$\delta_{day,j}$	$rp_{\mu day}$	$r_{\mu day}$	M_{year}	Σ_{year}	Rp_{Myear}	R_{Myear}
	2011	16.85			1917.70	228.20		0.00
	2012	17.58	2.89	2.89	1921.57	19679.07	3.87	3.87
A—FS_E4	2013	62.92	12.54	14.90	1935.12	229.78	13.55	17.42
[με]	2014	30.60	0.04	13.79	1935.27	20090.26	0.15	17.57
	2015	49.19	-28.54	-16.34	1906.64	229.21	-28.63	-11.06
	2016	55.24	-23.10	-41.94	1882.55	3272.18	-24.09	-35.15

Extensometer 5-without Drops

Mean Daily Value

Daily Amplitude

Progressive Daily Residuals on the Mean Value

Absolute Daily Residuals on the Mean Value

Annual Amplitude

Progressive Annual Residuals of the Mean Value
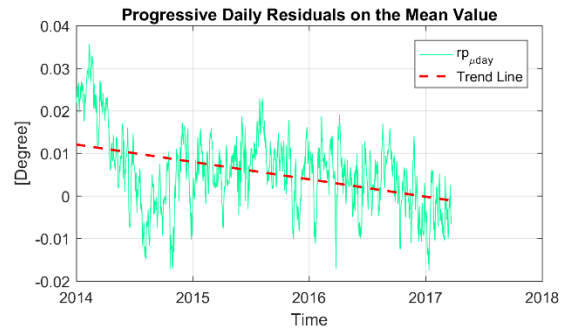
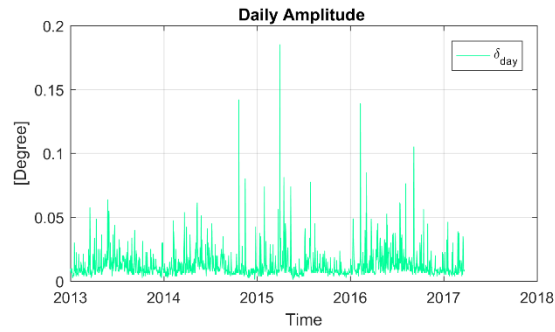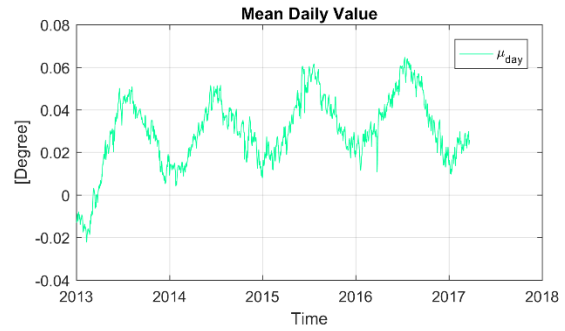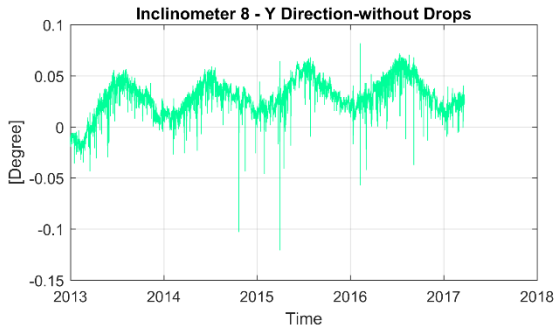**Absolute Annual Residuals of the Mean Value**
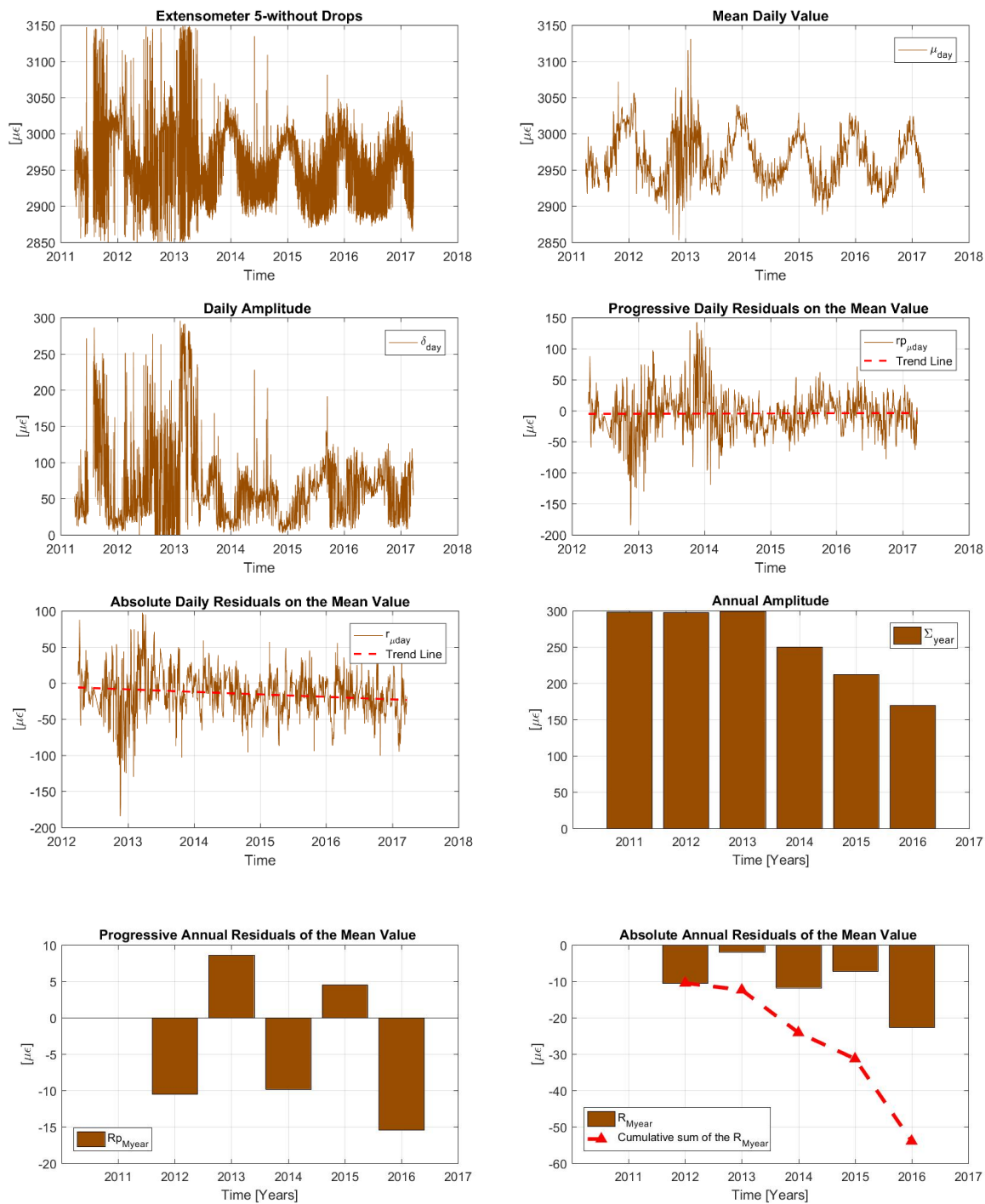
Sensor	Year	$\delta_{day,j}$	$rp_{\mu day}$	$r_{\mu day}$	M_{year}	Σ_{year}	Rp_{Myear}	R_{Myear}
	2011	78.25			2971.68	298.36		0.00
	2012	62.46	-18.37	-18.37	2961.19	297.81	-10.50	-10.50
A-FS-E5	2013	91.14	11.51	-1.92	2969.79	299.45	8.60	-1.90
[με]	2014	45.34	-11.41	-14.17	2959.96	250.14	-9.83	-11.73
	2015	58.51	-3.29	-16.43	2964.50	211.93	4.54	-7.19
	2016	64.40	-3.59	-19.93	2949.07	169.78	-15.43	-22.62

Extensometer 6-without Drops

Mean Daily Value

Daily Amplitude

Progressive Daily Residuals on the Mean Value

Absolute Daily Residuals on the Mean Value

Annual Amplitude

Progressive Annual Residuals of the Mean Value

Absolute Annual Residuals of the Mean Value

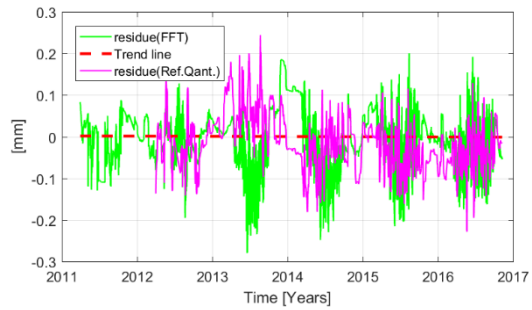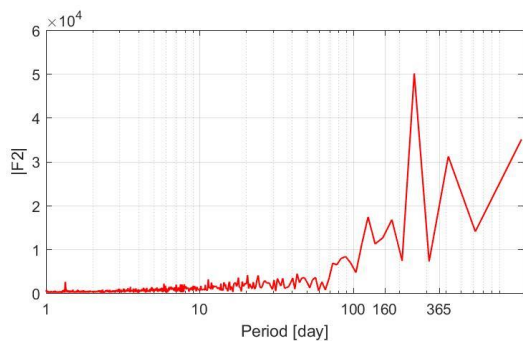| Sensor	Year	$\delta_{day,j}$	$rp_{\mu day}$	$r_{\mu day}$	M_{year}	Σ_{year}	Rp_{Myear}	R_{Myear}
A-FS-E6 [μɛ]	2011	33.47			2432.90	134.28		0.00
	2012	22.21	-0.70	-1.00	2430.22	145.78	-2.68	-2.68
	2013	33.58	-1.30	-2.93	2428.94	132.02	-1.28	-3.96
	2014	27.49	-11.99	-15.69	2418.73	139.33	-10.21	-14.17
	2015	29.85	-7.62	-22.69	2413.47	138.50	-5.25	-19.43
	2016	29.17	-4.31	-27.01	2404.94	134.97	-8.53	-27.96

Inclinometers

Sensor	Year	$\delta_{day,j}$	$rp_{\mu day}$	$r_{\mu day}$	M_{year}	Σ_{year}	Rp_{Myear}	R_{Myear}
	2011	0.0104			-0.1626	0.0460		
	2012	0.0068	0.0021	0.0021	-0.1609	0.0410	0.0017	0.0017
A-FO-I1X	2013	0.0057	-0.0146	-0.0115	-0.1750	0.0840	-0.0141	-0.0124
[°]	2014	0.0057	-0.0042	-0.0140	-0.1796	0.0220	-0.0046	-0.0170
	2015	0.0056	0.0048	-0.0130	-0.1748	0.0380	0.0048	-0.0122
	2016	0.0057	0.0009	-0.0090	-0.1739	0.0310	0.0009	-0.0112

Inclinometer 1 - Y Direction-without Drops

Mean Daily Value

Daily Amplitude

Progressive Daily Residuals of the Mean Value

Absolute Daily Residuals of the Mean Value

Annual Amplitude

Progressive Annual Residuals of the Mean Value
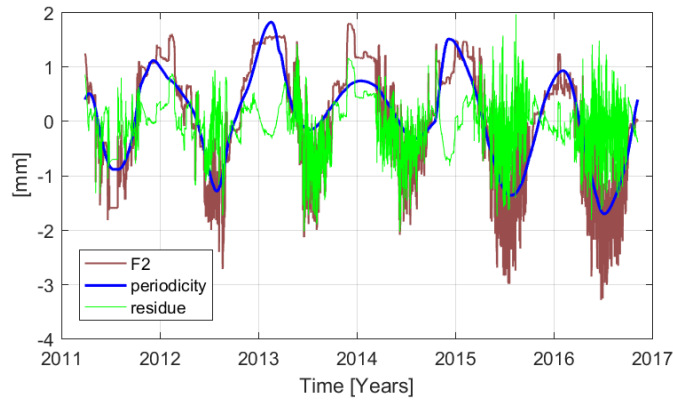

Absolute Annual Residuals of the Mean Value
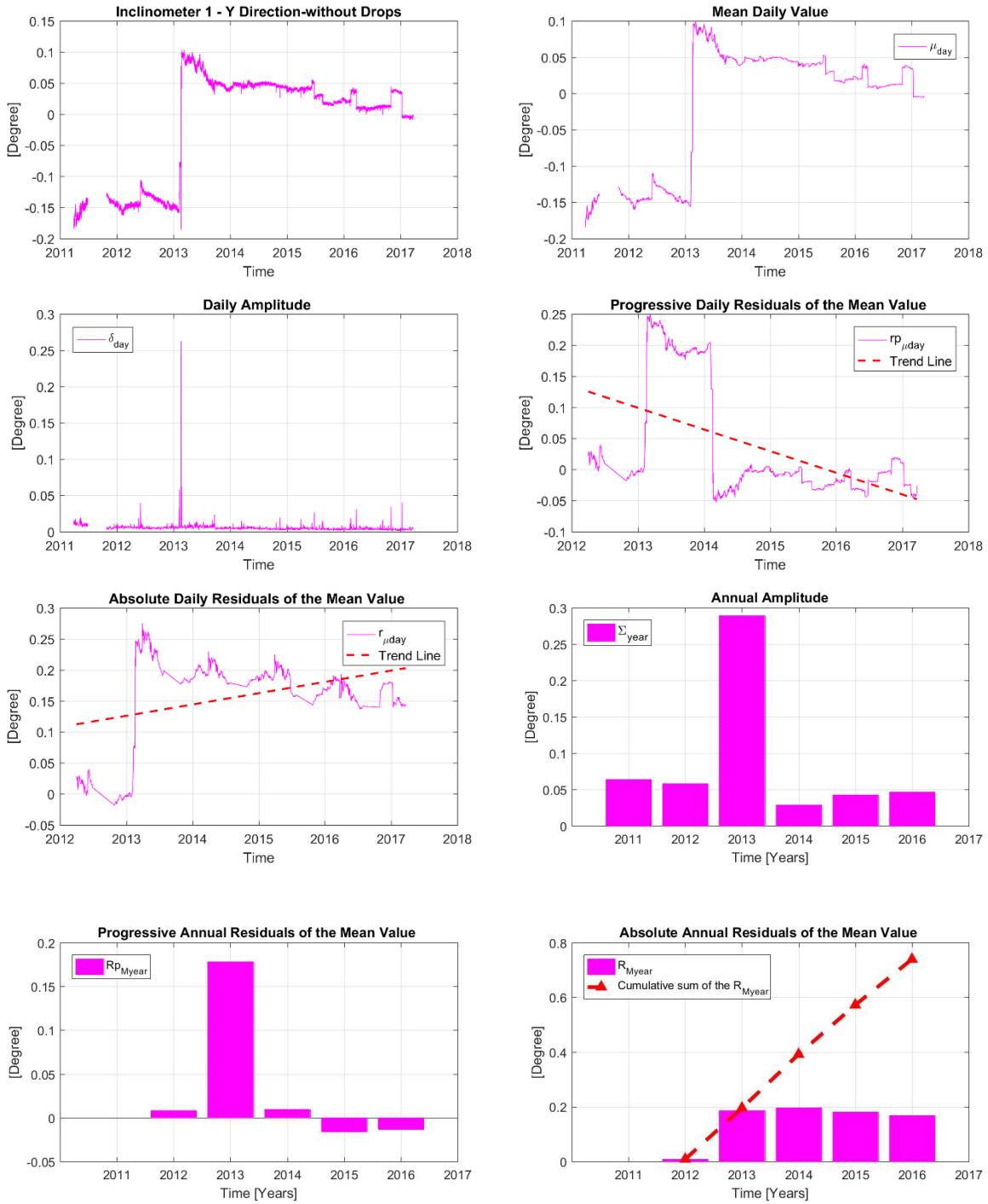
Sensor	Year	$\delta_{day,j}$	$rp_{\mu day}$	$r_{\mu day}$	M_{year}	Σ_{year}	Rp_{Myear}	R_{Myear}
A-FO-I1Y [°]	2011	0.0083			-0.1494	0.0640		
	2012	0.0059	0.0071	0.0071	-0.1411	0.0580	0.0083	0.0083
	2013	0.0076	0.1797	0.1801	0.0373	0.2890	0.1784	0.1867
	2014	0.0046	0.0084	0.1946	0.0470	0.0289	0.0097	0.1964
	2015	0.0042	-0.0159	0.1836	0.0311	0.0427	-0.0160	0.1805
	2016	0.0040	-0.0125	0.1698	0.0178	0.0465	-0.0132	0.1672
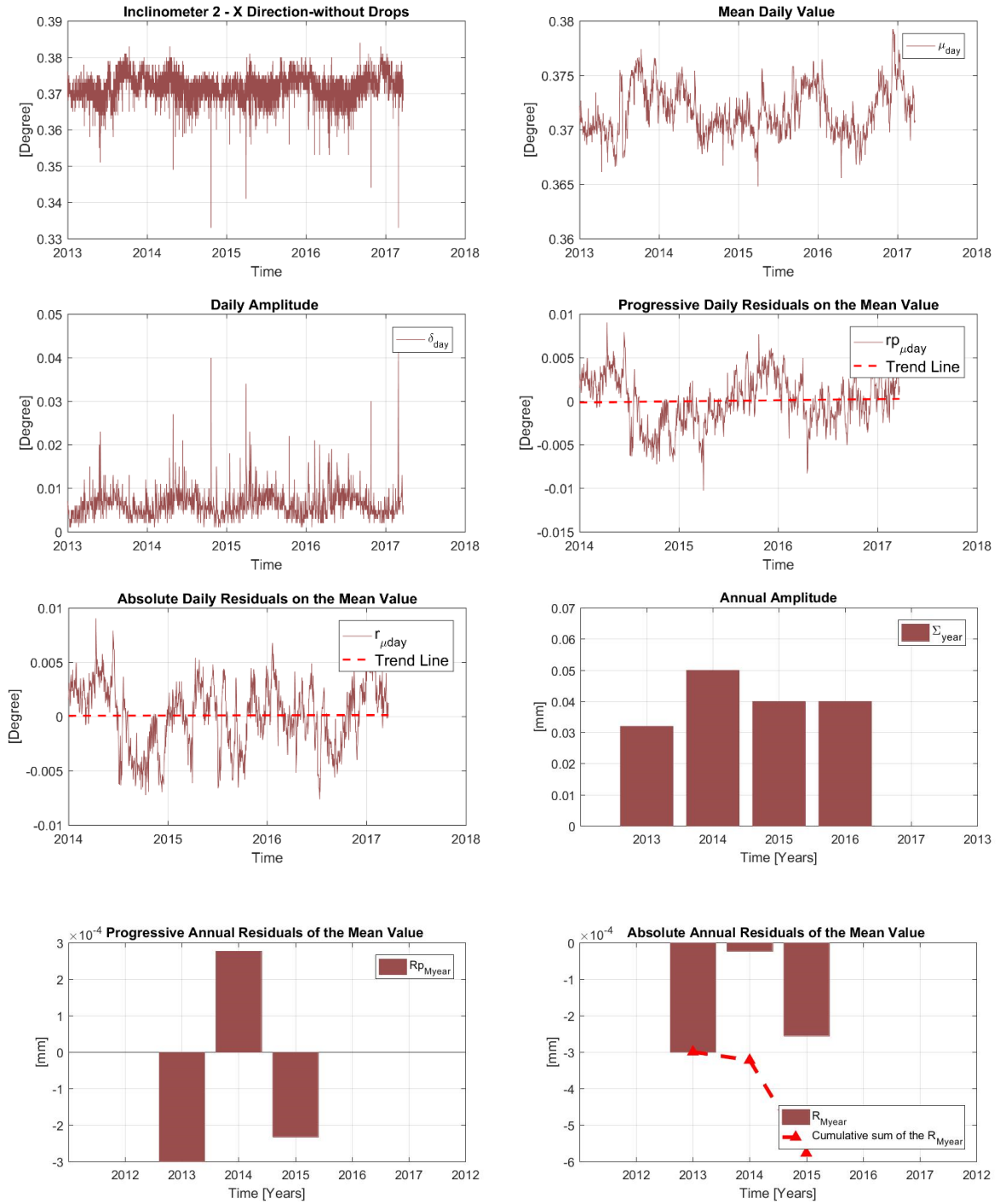
Sensor	Year	$\delta_{day,j}$	$rp_{\mu day}$	$r_{\mu day}$	M_{year}	Σ_{year}	Rp_{Myear}	R_{Myear}
A-FO-I2X	2013	0.0059			0.3717	0.0320		
	2014	0.0063	-0.0002	-0.0002	0.3714	0.0500	-0.0003	-0.0003
[°]	2015	0.0066	0.0003	0.0000	0.3717	0.0400	0.0003	0.0000
	2016	0.0067	-0.0002	-0.0001	0.3715	0.0400	-0.0002	-0.0003
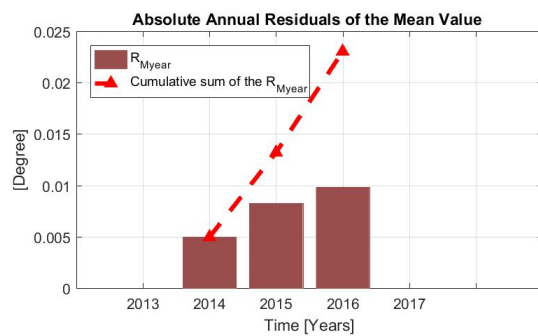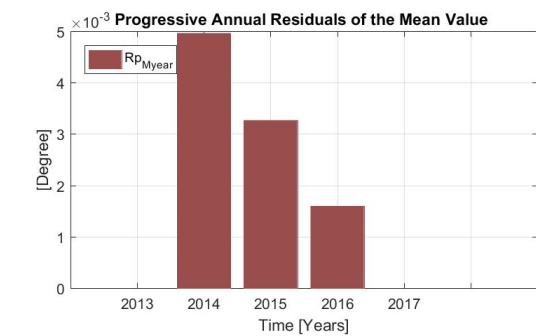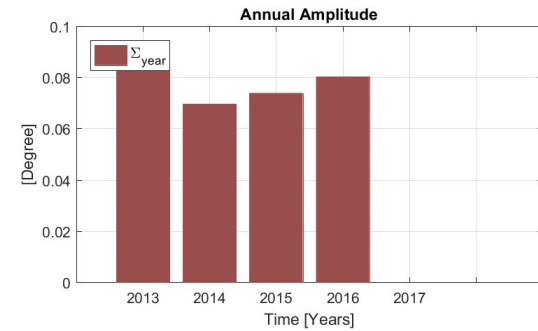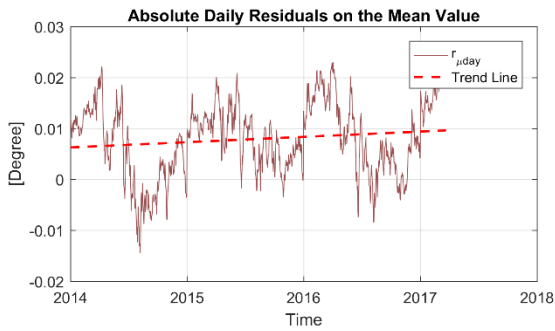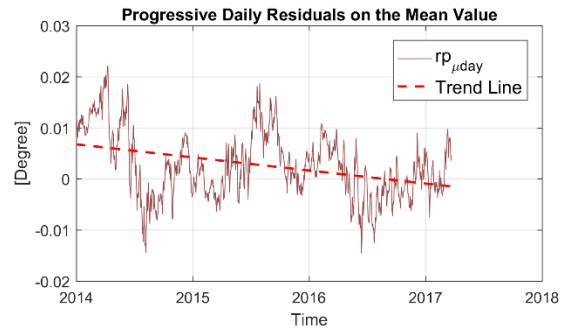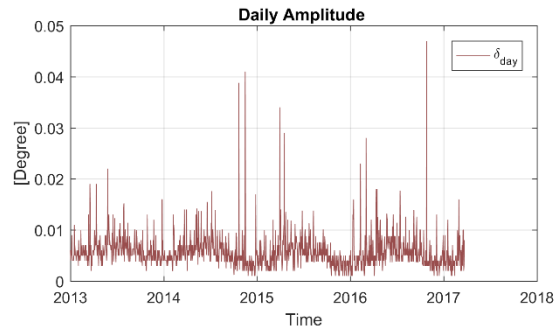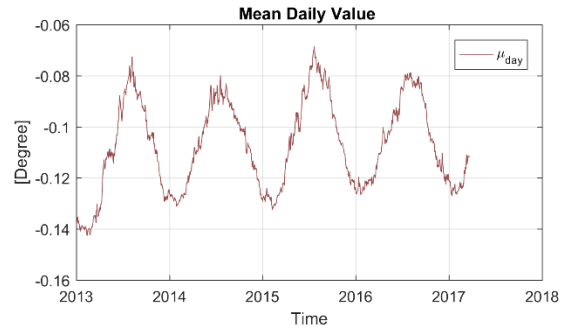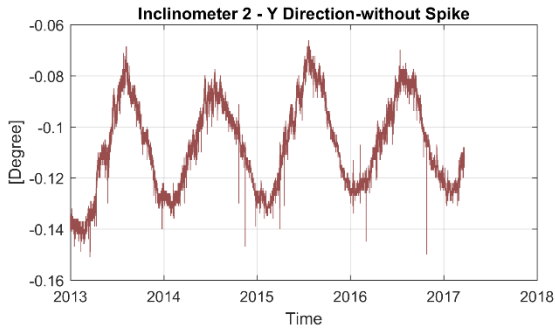
Sensor	Year	$\delta_{day,j}$	$rp_{\mu day}$	$r_{\mu day}$	M_{year}	Σ_{year}	Rp_{Myear}	R_{Myear}
A-FO-I2Y [°]	2013	0.0062			-0.1118	0.0824		
	2014	0.0058	0.0051	0.0051	-0.1068	0.0696	0.0050	0.0050
	2015	0.0053	0.0033	0.0084	-0.1036	0.0739	0.0033	0.0082
	2016	0.0057	-0.0001	0.0083	-0.1020	0.0802	0.0016	0.0098
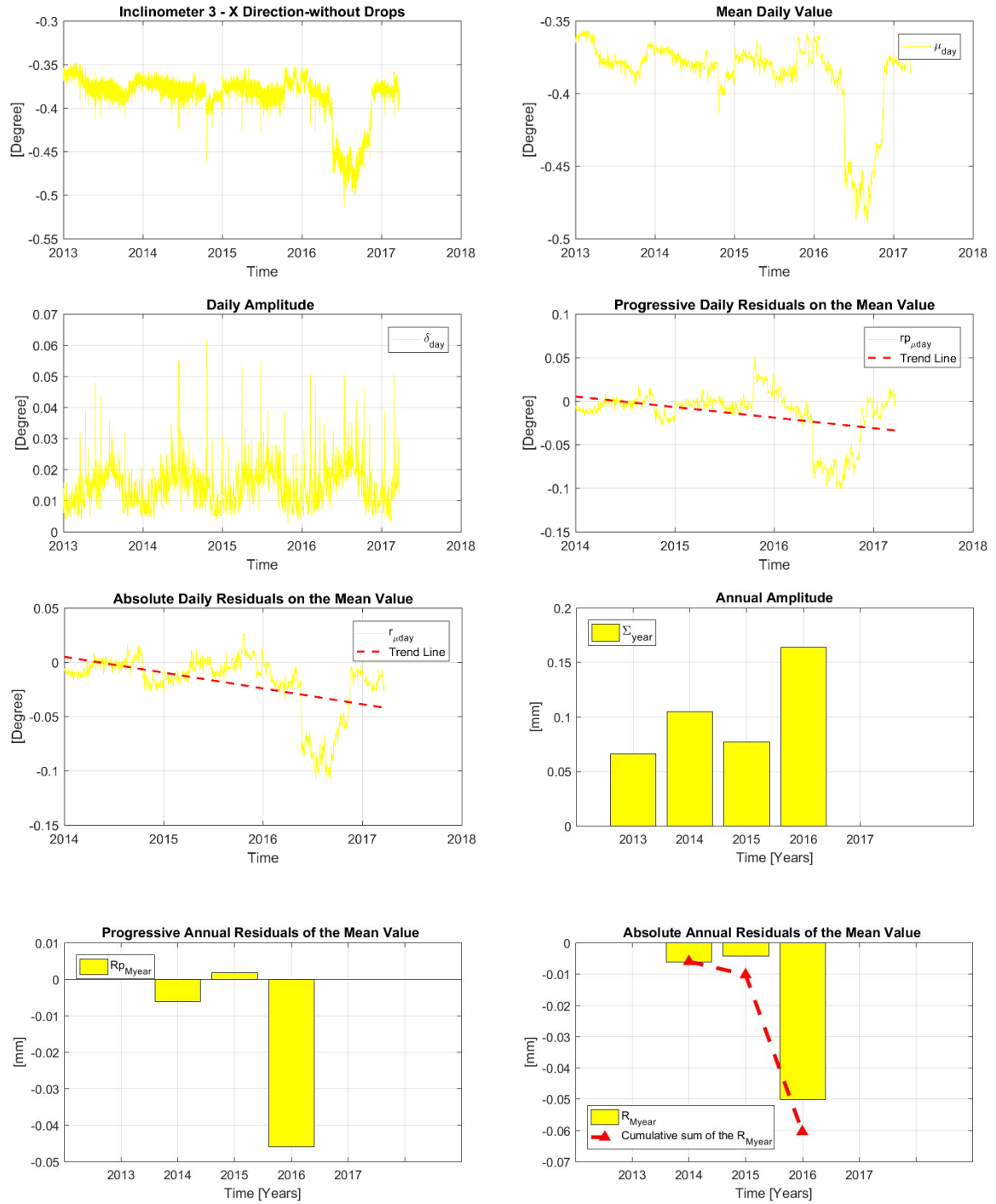
Sensor	Year	$\delta_{day,j}$	$rp_{\mu day}$	$r_{\mu day}$	M_{year}	Σ_{year}	Rp_{Myear}	R_{Myear}
A-FO-I3X [°]	2013	0.0139			-0.3738	0.0660		
	2014	0.0147	-0.0061	-0.0061	-0.3799	0.1048	-0.0060	-0.0060
	2015	0.0154	0.0019	-0.0043	-0.3781	0.0770	0.0018	-0.0042
	2016	0.0163	-0.0406	-0.0449	-0.4240	0.1639	-0.0460	-0.0502

Inclinometer 3 - Y Direction-without Drops

Mean Daily Value

Daily Amplitude

Progressive Daily Residuals on the Mean Value

Absolute Daily Residuals on the Mean Value

Annual Amplitude

Progressive Annual Residuals of the Mean Value

Absolute Annual Residuals of the Mean Value

Sensor	Year	$\delta_{day,j}$	$rp_{\mu day}$	$r_{\mu day}$	M_{year}	Σ_{year}	Rp_{Myear}	R_{Myear}
A-FO-I3Y [°]	2013	0.0154			-0.1010	0.1090		
	2014	0.0163	0.0033	0.0033	-0.0977	0.1120	0.0032	0.0032
	2015	0.0167	-0.0068	-0.0035	-0.1046	0.1140	-0.0068	-0.0036
	2016	0.0168	-0.0112	-0.0148	-0.1143	0.1860	-0.0097	-0.0133
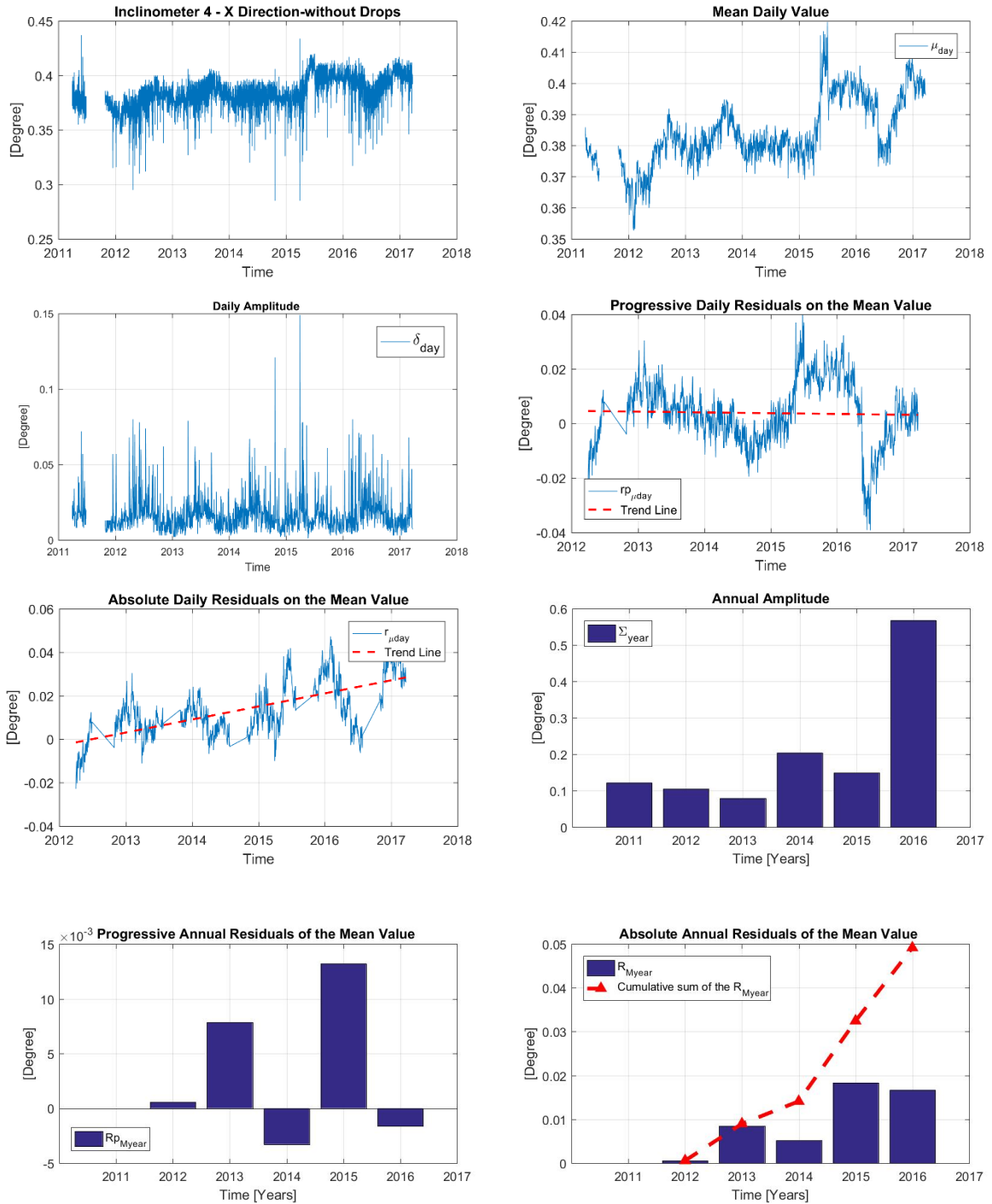
Sensor	Year	$\delta_{day,j}$	$rp_{\mu day}$	$r_{\mu day}$	M_{year}	Σ_{year}	Rp_{Myear}	R_{Myear}
A-FO-I4X [°]	2011	0.0160			0.3746	0.1220		
	2012	0.0178	0.0006	0.0006	0.3751	0.1050	0.0006	0.0006
	2013	0.0155	0.0077	0.0087	0.3830	0.0790	0.0079	0.0084
	2014	0.0167	-0.0031	0.0075	0.3797	0.2040	-0.0033	0.0051
	2015	0.0162	0.0132	0.0187	0.3929	0.1490	0.0132	0.0183
	2016	0.0186	-0.0008	0.0218	0.3913	0.5680	-0.0016	0.0167

Inclinometer 4 - Y Direction-without Drops

Mean Daily Value

Daily Amplitude

Progressive Daily Residuals on the Mean Value

Absolute Daily Residuals on the Mean Value

Annual Amplitude

Progressive Annual Residuals of the Mean Value

Absolute Annual Residuals of the Mean Value
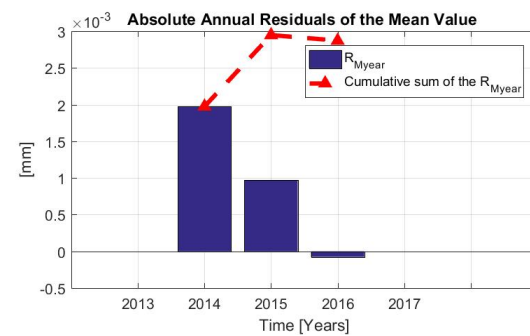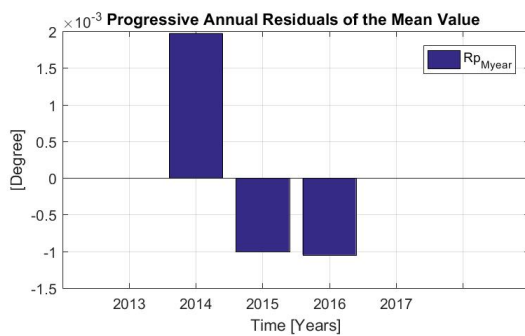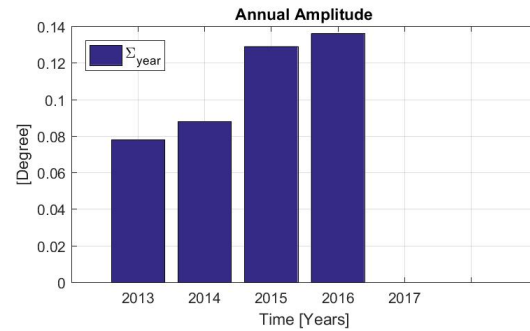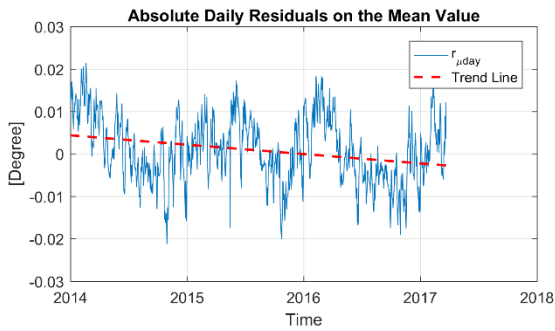
Sensor	Year	$\delta_{day,j}$	$rp_{\mu day}$	$r_{\mu day}$	M_{year}	Σ_{year}	Rp_{Myear}	R_{Myear}
A-FO-I4Y [°]	2013	0.0132			0.2344	0.0780		
	2014	0.0130	0.0020	0.0020	0.2363	0.0880	0.0020	0.0020
	2015	0.0121	-0.0010	0.0010	0.2353	0.1290	-0.0010	0.0010
	2016	0.0149	-0.0021	-0.0010	0.2343	0.1360	-0.0010	-0.0001

Sensor	Year	$\delta_{day,j}$	$rp_{\mu day}$	$r_{\mu day}$	M_{year}	Σ_{year}	Rp_{Myear}	R_{Myear}
A-FS-I5X [°]	2013	0.0040			0.1337	0.0260		
	2014	0.0044	-0.0020	-0.0020	0.1318	0.0300	-0.0019	-0.0019
	2015	0.0045	-0.0017	-0.0037	0.1301	0.0300	-0.0017	-0.0037
	2016	0.0048	-0.0009	-0.0046	0.1298	0.0290	-0.0003	-0.0039

Inclinometer 5 - Y Direction-without Drops

Mean Daily Value

Daily Amplitude

Progressive Daily Residuals on the Mean Value

Absolute Daily Residuals on the Mean Value

Annual Amplitude

Progressive Annual Residuals of the Mean Value

**Absolute Annual Residuals of the Mean Value**

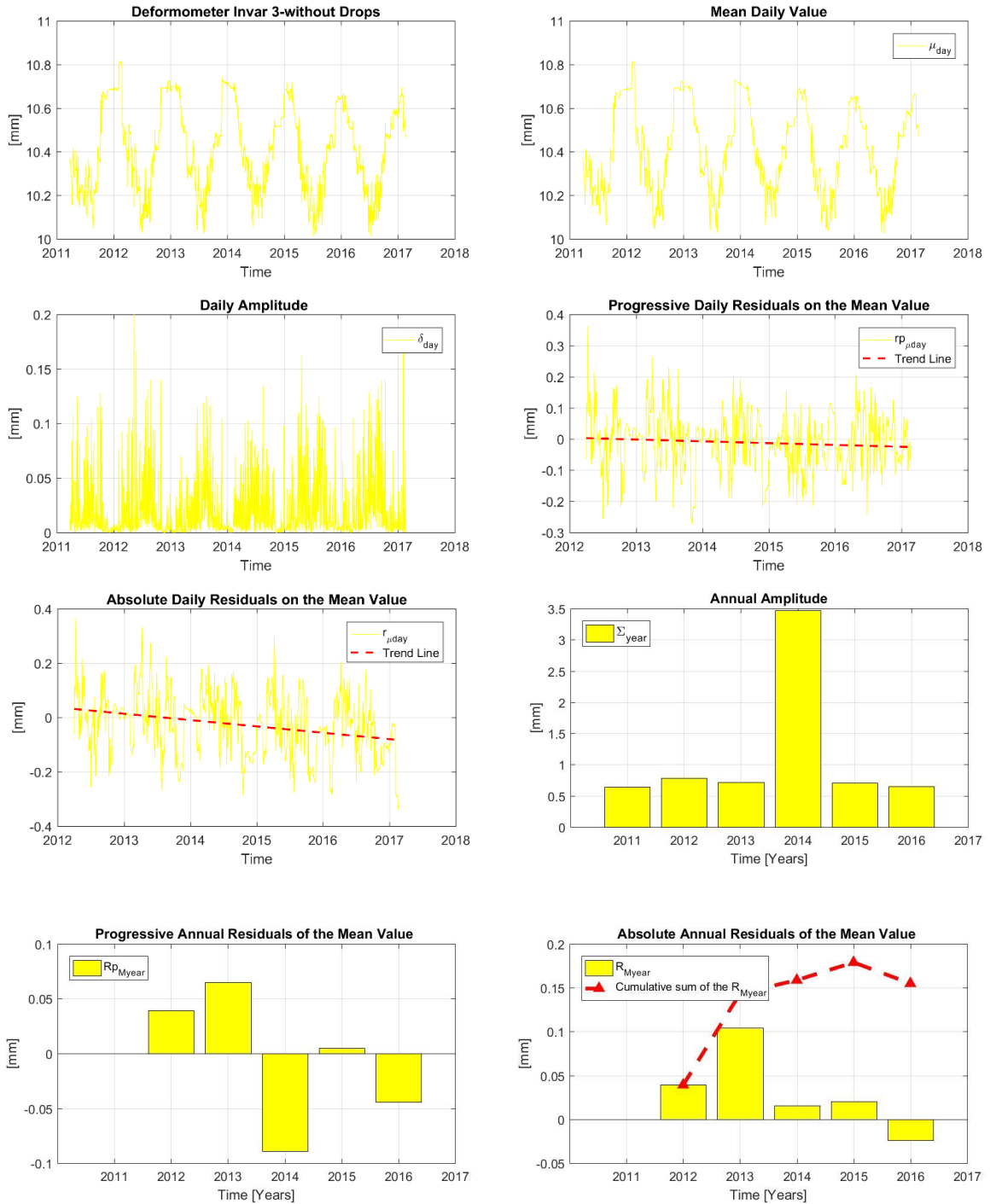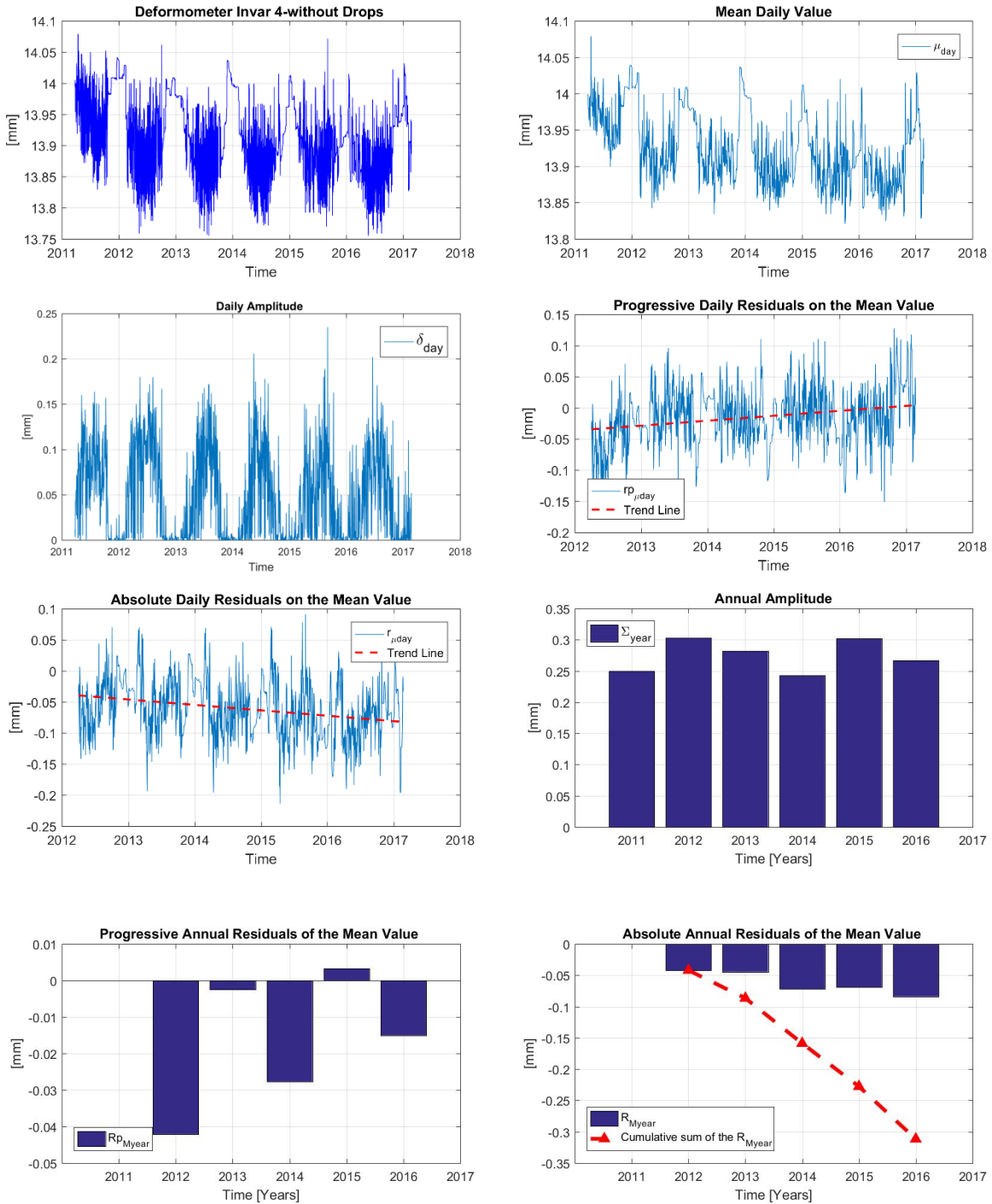| Sensor	Year	$\delta_{day,j}$	$rp_{\mu day}$	$r_{\mu day}$	M_{year}	Σ_{year}	Rp_{Myear}	R_{Myear}
A-FS-I5Y [°]	2013	0.0047			0.1648	0.0330		
	2014	0.0044	-0.0025	-0.0025	0.1622	0.0280	-0.0025	-0.0025
	2015	0.0046	-0.0023	-0.0048	0.1599	0.0390	-0.0023	-0.0048
	2016	0.0048	-0.0041	-0.0089	0.1562	0.0250	-0.0037	-0.0085

Sensor	Year	$\delta_{day,j}$	$rp_{\mu day}$	$r_{\mu day}$	M_{year}	Σ_{year}	Rp_{Myear}	R_{Myear}
	2013	0.0048			0.2155	0.0450		0.0000
A-FS-I6x	2014	0.0050	-0.0001	-0.0001	0.2153	0.0430	-0.0002	-0.0002
[°]	2015	0.0050	0.0072	0.0070	0.2224	0.0370	0.0072	0.0070
	2016	0.0053	0.0018	0.0089	0.2249	0.0460	0.0025	0.0095

Inclinometer 6 - Y Direction-without Drops

Mean Daily Value

Daily Amplitude

Progressive Daily Residuals on the Mean Value

Absolute Daily Residuals on the Mean Value

Annual Amplitude

Progressive Annual Residuals of the Mean Value

Absolute Annual Residuals of the Mean Value

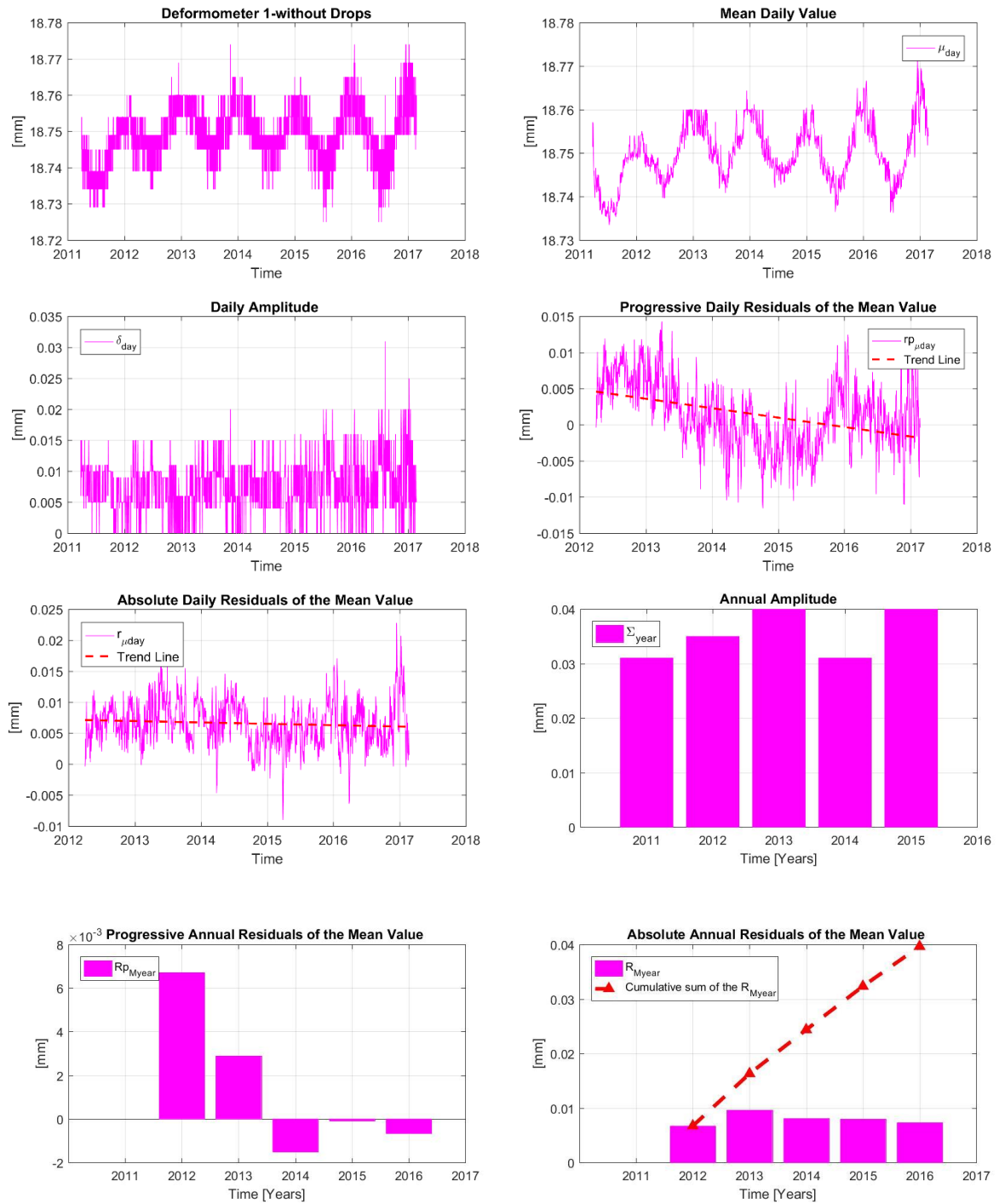| Sensor	Year	$\delta_{day,j}$	$rp_{\mu day}$	$r_{\mu day}$	M_{year}	Σ_{year}	Rp_{Myear}	R_{Myear}
A-FS-I6Y [°]	2013	0.0059			0.1807	0.0940		
	2014	0.0058	0.0023	0.0023	0.1829	0.0740	0.0023	0.0023
	2015	0.0056	0.0099	0.0122	0.1928	0.0740	0.0099	0.0122
	2016	0.0058	0.0005	0.0128	0.1954	0.0680	0.0025	0.0147

Sensor	Year	$\delta_{day,j}$	$rp_{\mu day}$	$r_{\mu day}$	M_{year}	Σ_{year}	Rp_{Myear}	R_{Myear}
	2011	0.0109			-0.0822	0.0575		0.0000
	2012	0.0127	0.0111	0.0111	-0.0730	0.3329	0.0092	0.0092
A-FS-I7X	2013	0.0118	0.0041	0.0106	-0.0689	0.0633	0.0041	0.0133
[°]	2014	0.0124	0.0017	0.0133	-0.0672	0.1545	0.0017	0.0150
	2015	0.0131	0.0055	0.0190	-0.0616	0.0818	0.0055	0.0205
	2016	0.0130	-0.0155	0.0124	-0.0806	0.1359	-0.0189	0.0016
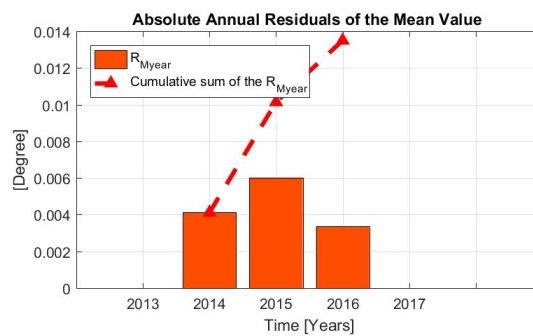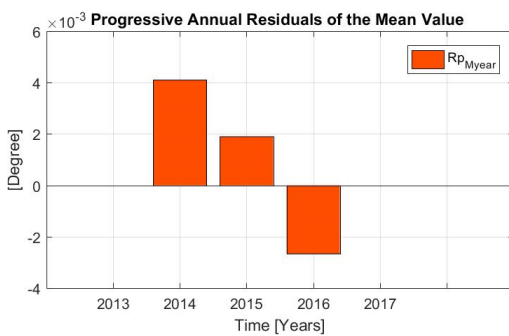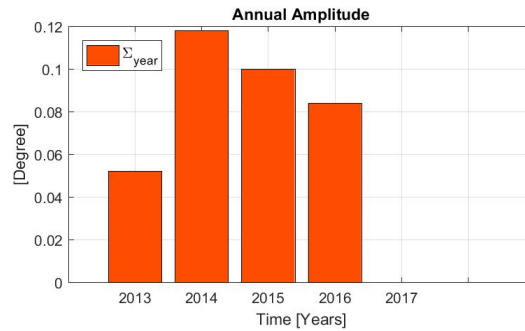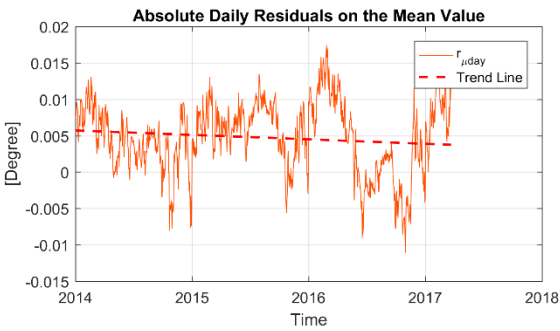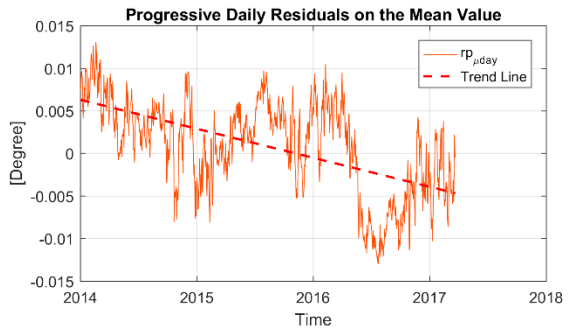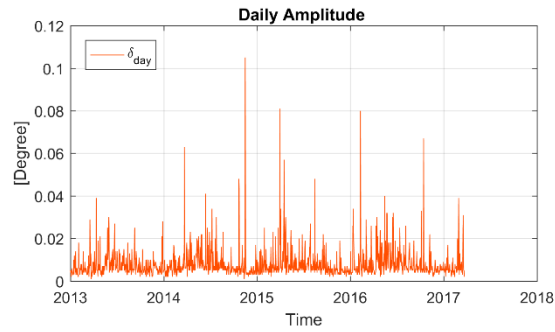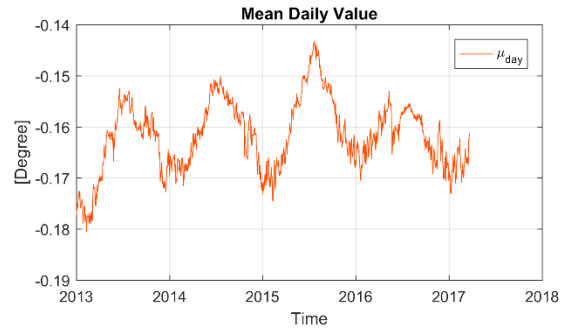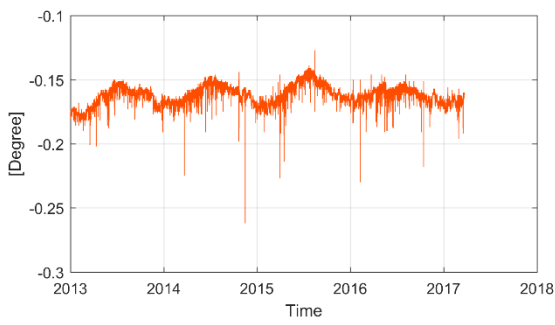
Sensor	Year	$\delta_{day,j}$	$rp_{\mu day}$	$r_{\mu day}$	M_{year}	Σ_{year}	Rp_{Myear}	R_{Myear}
A-FS-I7Y [°]	2013	0.0072			-0.1648	0.0520		
	2014	0.0082	0.0041	0.0041	-0.1607	0.1180	0.0041	0.0041
	2015	0.0080	0.0019	0.0060	-0.1588	0.1000	0.0019	0.0060
	2016	0.0087	-0.0028	0.0032	-0.1614	0.0840	-0.0027	0.0034

Inclinometer 8 - X Direction-without Drops

Inclinometer 8 - X

Inclinometer 8 - X

Progressive Daily Residuals on the Mean Value

Absolute Daily Residuals on the Mean Value

Annual Amplitude

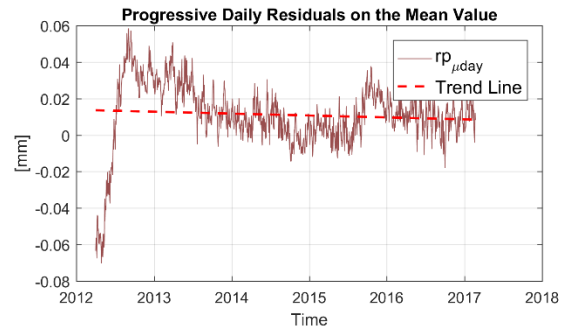Progressive Annual Residuals of the Mean Value

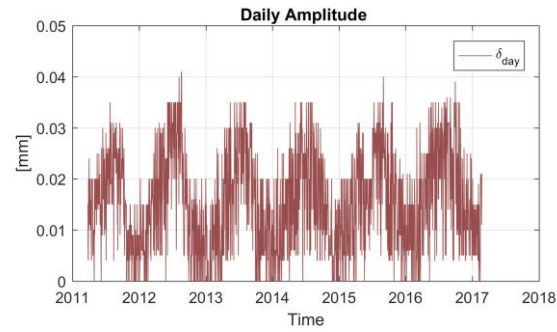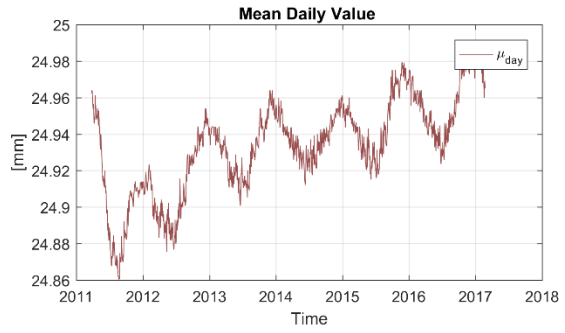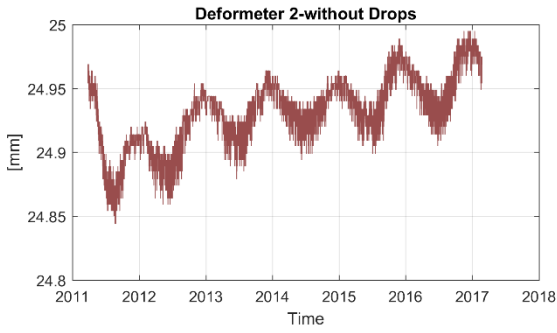Absolute Annual Residuals of the Mean Value
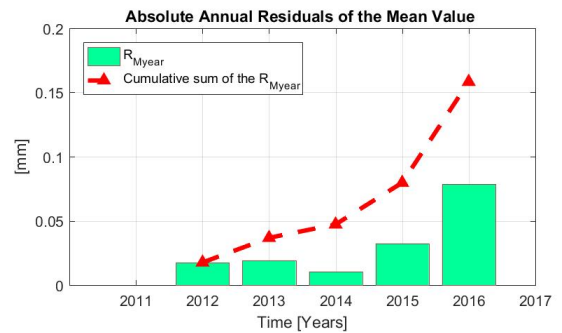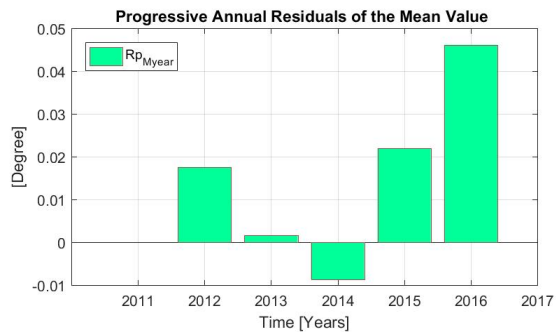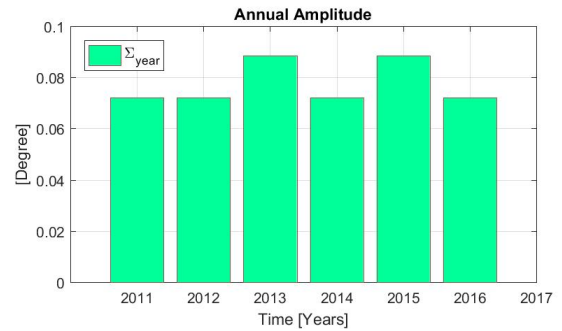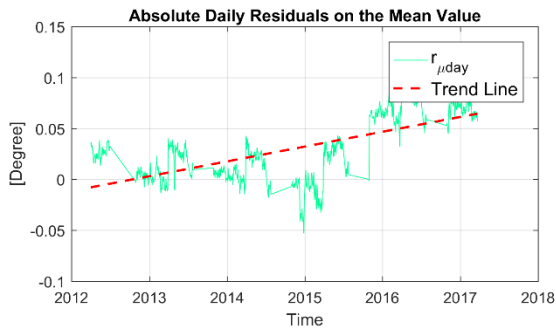
Sensor	Year	$\delta_{day,j}$	$rp_{\mu day}$	$r_{\mu day}$	M_{year}	Σ_{year}	Rp_{Myear}	R_{Myear}
A-FS-I8X [°]	2011	0.0135			0.0686	0.0721		
	2012	0.0192	0.0171	0.0171	0.0862	1.8930	0.0176	0.0176
	2013	0.0192	0.0015	0.0116	0.0878	0.0885	0.0016	0.0192
	2014	0.0208	-0.0088	0.0044	0.0791	0.1370	-0.0087	0.0105
	2015	0.0200	0.0221	0.0226	0.1011	0.1760	0.0220	0.0325
	2016	0.0225	0.0463	0.0721	0.1472	1.8940	0.0461	0.0786

Inclinometer 8 - Y Direction-without Drops

Mean Daily Value

Daily Amplitude

Progressive Daily Residuals on the Mean Value

Absolute Daily Residuals on the Mean Value

Annual Amplitude

Progressive Annual Residuals of the Mean Value

Absolute Annual Residuals of the Mean Value
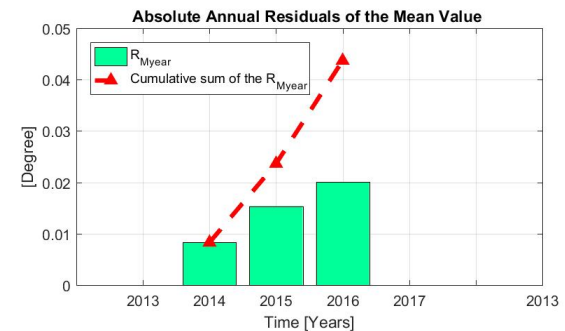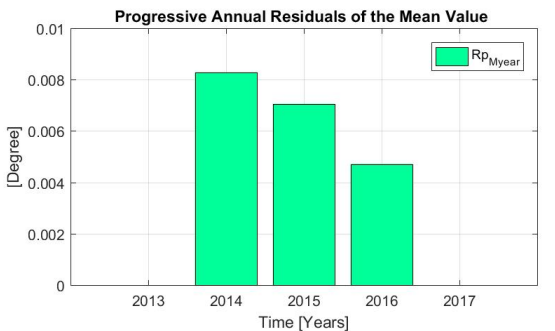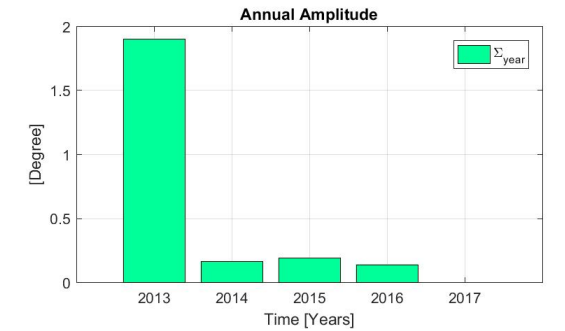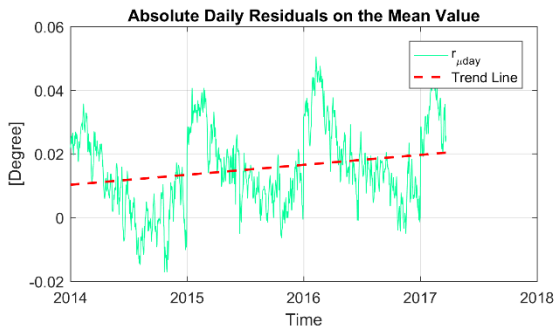
Sensor	Year	$\delta_{day,j}$	$rp_{\mu day}$	$r_{\mu day}$	M_{year}	Σ_{year}	Rp_{Myear}	R_{Myear}
	2013	0.0124			0.0200	1.9007		
A-FS-I8Y	2014	0.0128	0.0083	0.0083	0.0283	0.1622	0.0083	0.0083
[°]	2015	0.0118	0.0071	0.0153	0.0353	0.1890	0.0071	0.0153
	2016	0.0148	0.0033	0.0186	0.0400	0.1392	0.0047	0.0201

A.2 Signal frequency analyses

The main periodicity of the data recorded has been obtained through a frequency analysis of the signal using a Fourier analysis. The frequency analysis has been applied to data obtained by the instruments which have not presented malfunction, interruptions and / or many drops. In this case, some of the Long base deformeters, the extensimeter and the inclinometers. In more detail, for each of these typologies of instruments the following plots are reported:

- recorded signal by the sensor and its main components (the periodical component and the residual)
- the Fourier Transform
- the residue as obtained from the FFT and from the mathematical considerations (reference quantities)

Long Base Deformeter F2

Long Base Deformeter F3
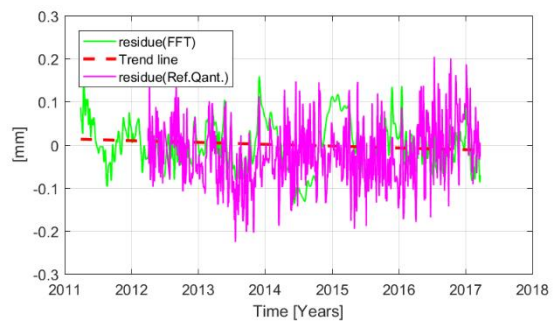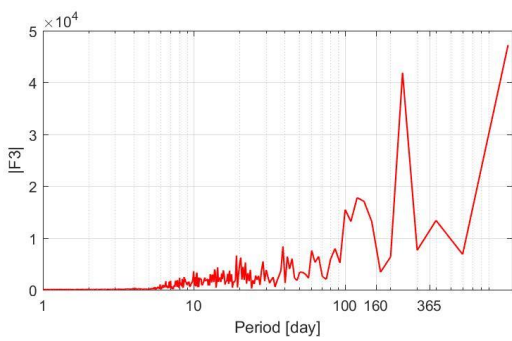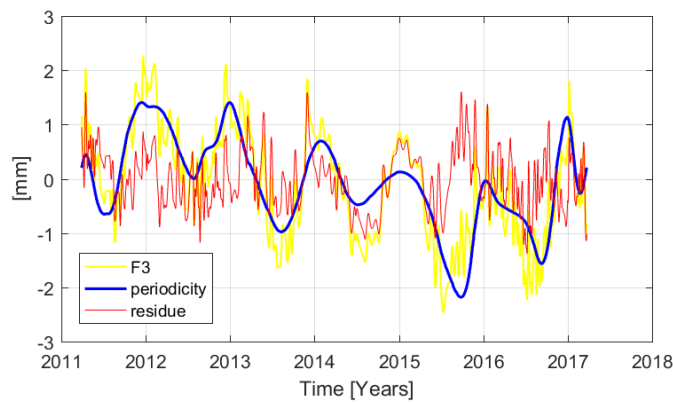
Long Base Deformeter F4
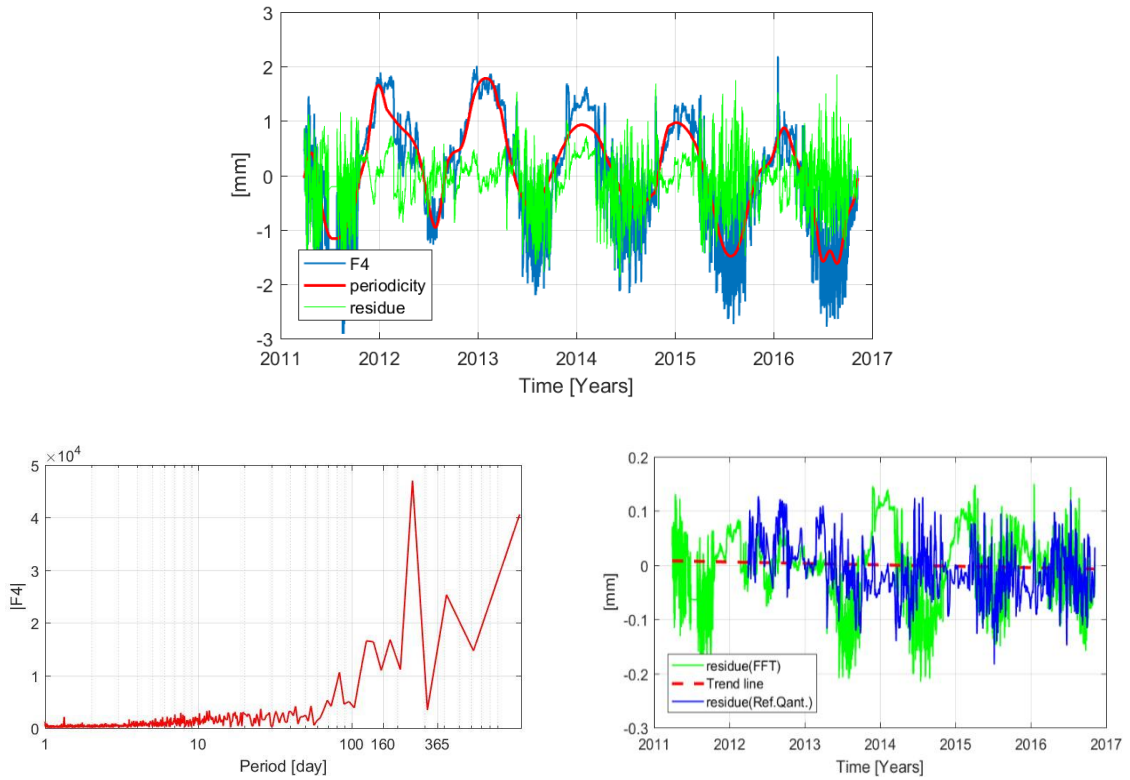
Long Base Deformeter F7
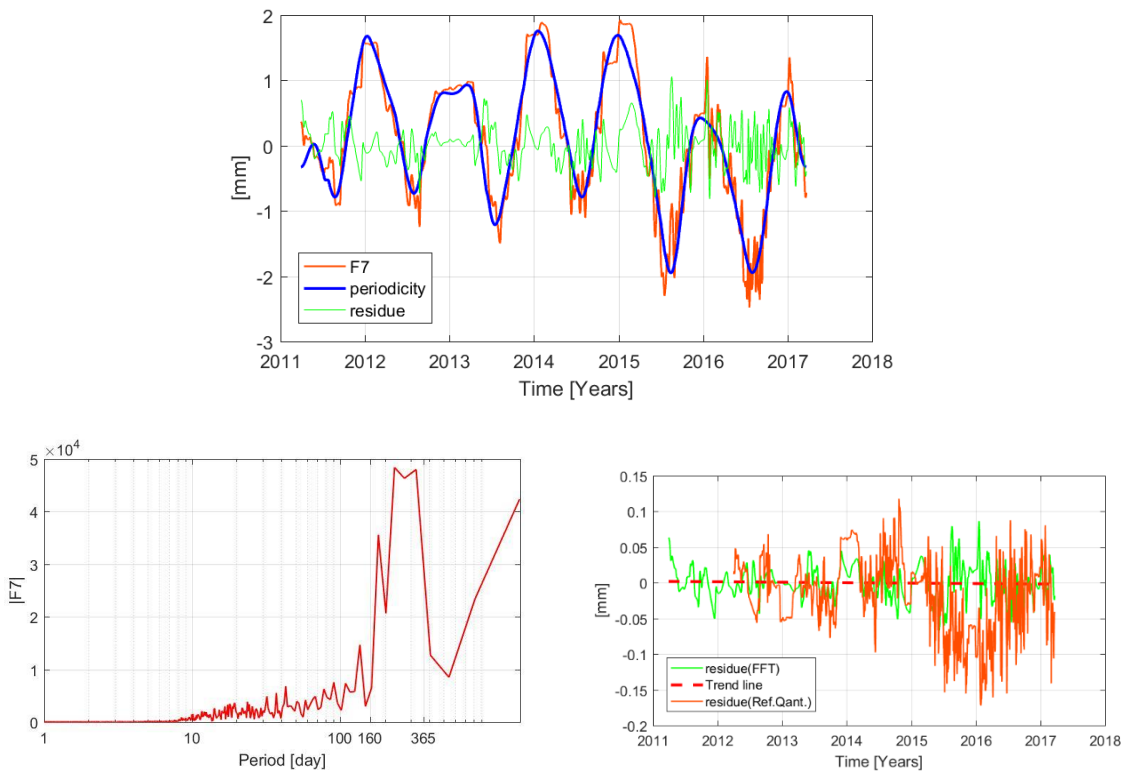
Long Base Deformeter F8
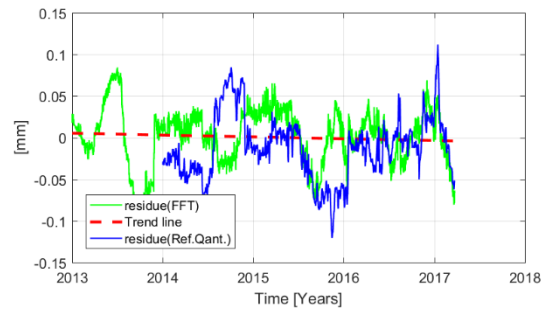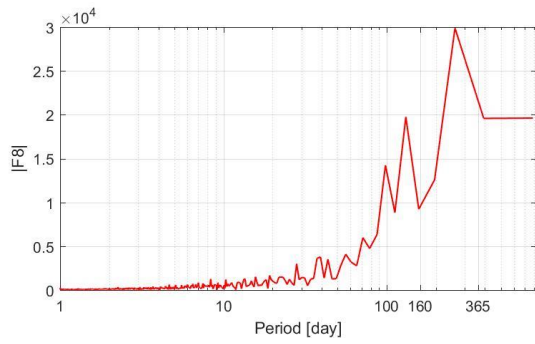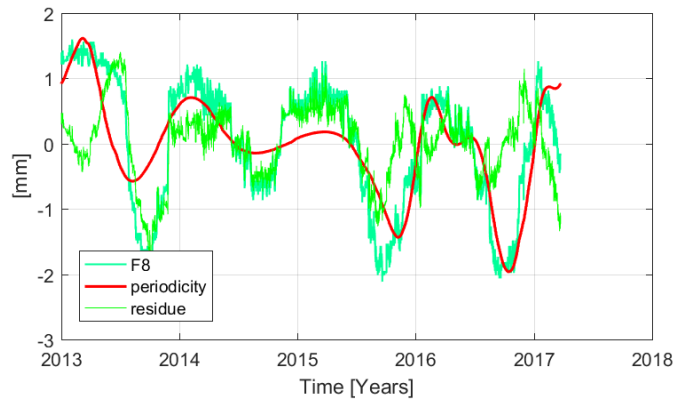
Extensometers E2
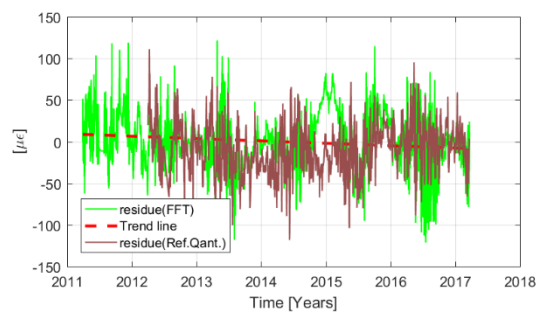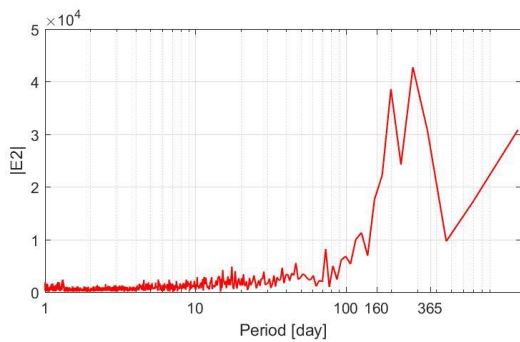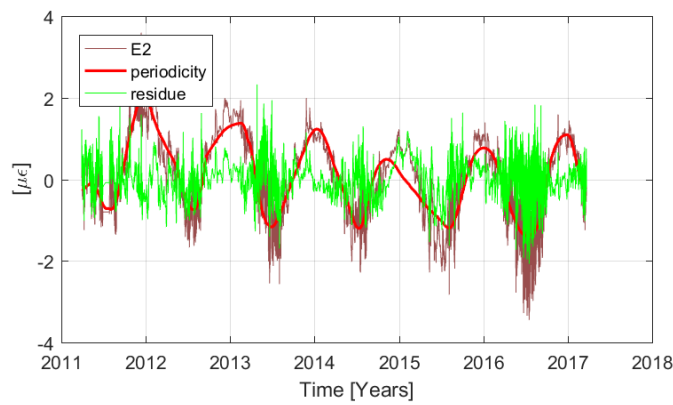
Extensometers E3
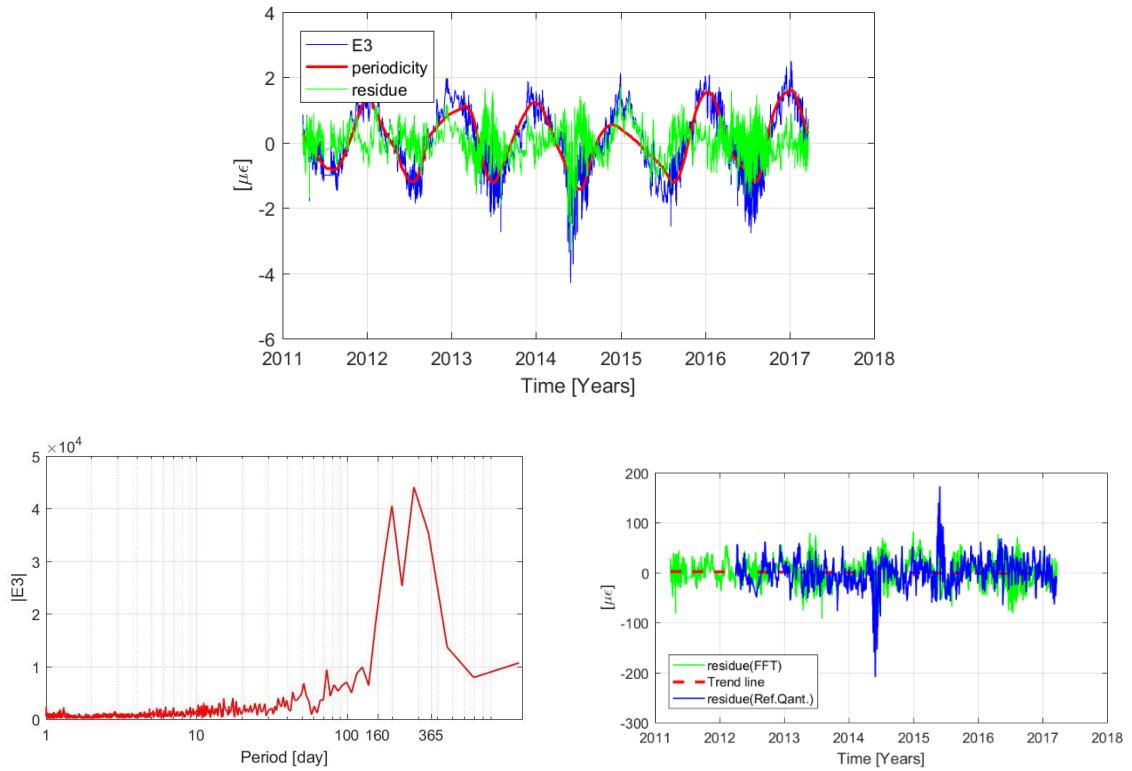
Extensometers E4
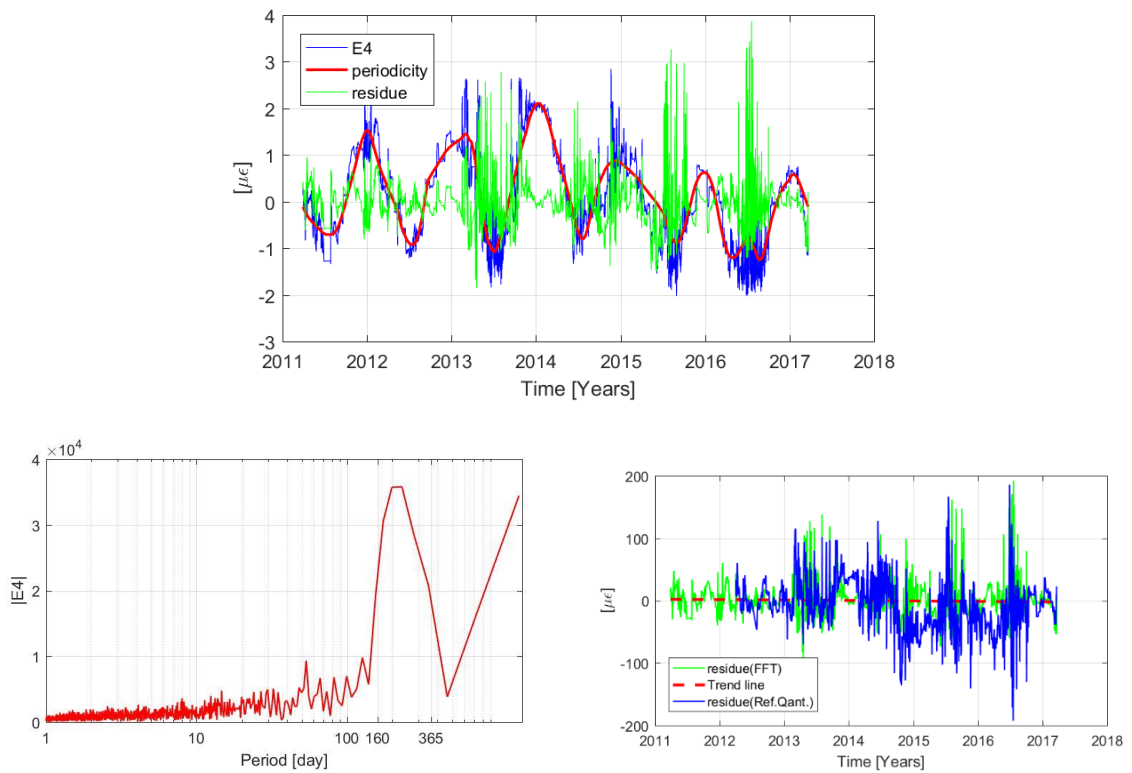
Inclinometers I4-X
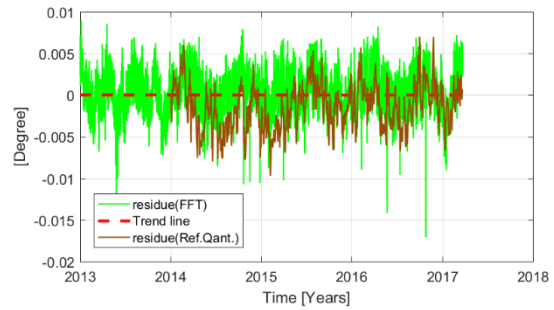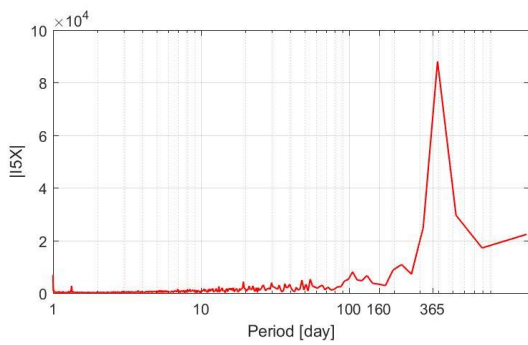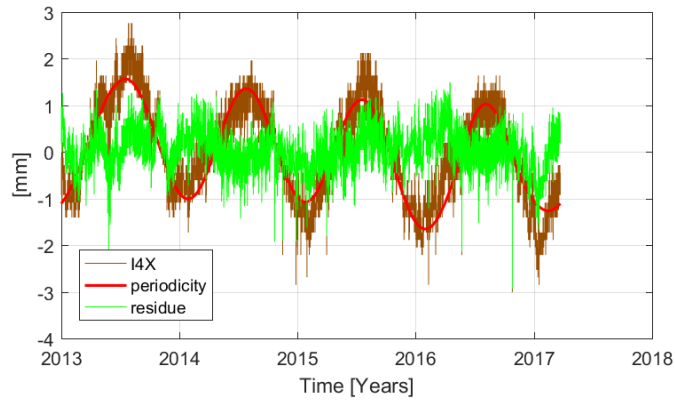
Inclinometers I4-Y
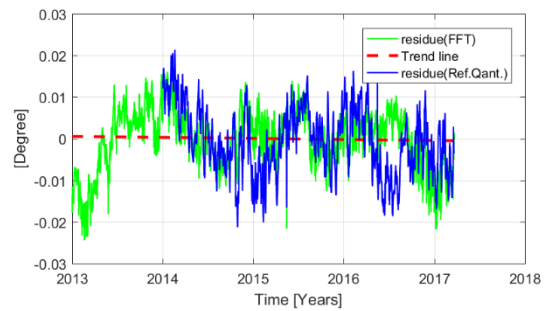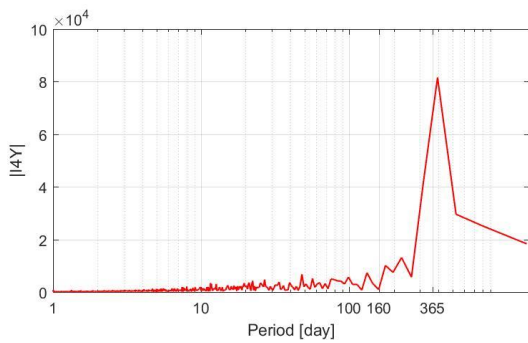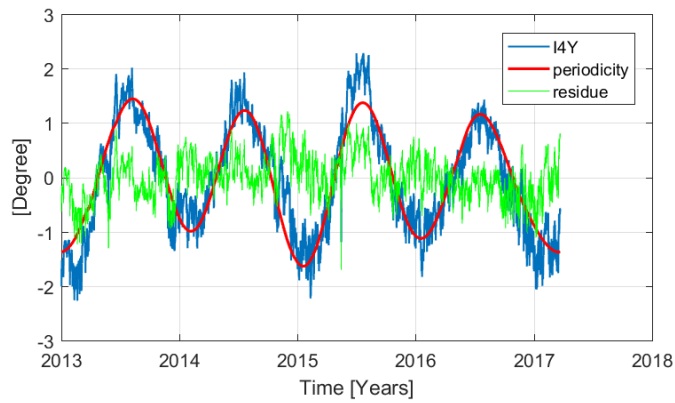
Inclinometers I5-Y
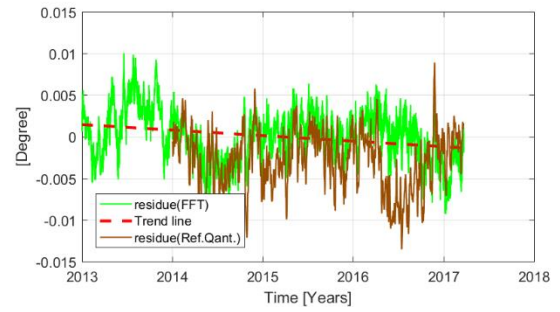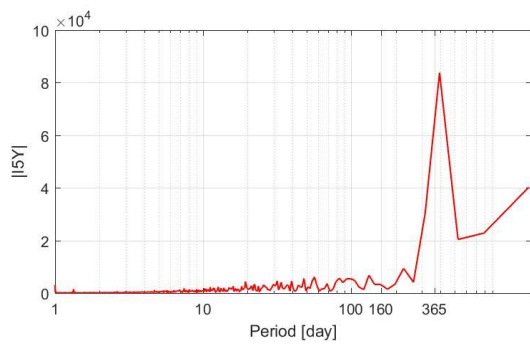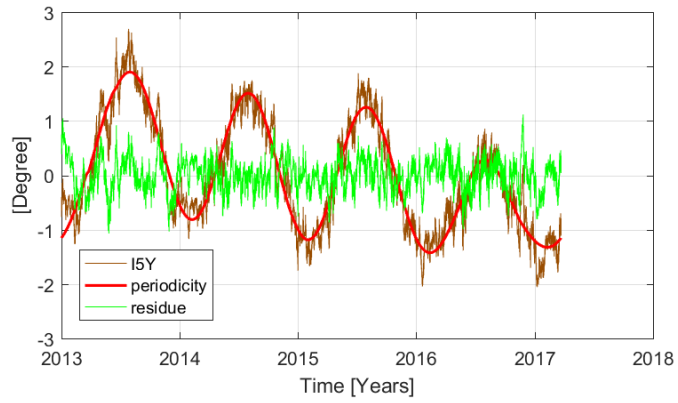
APPENDIX B

Data analyses for the Garisenda tower

B.1 Reference quantities

The systematic identification of the reference quantities is here provided for each instrument installed on the Garisenda tower.

In more detail, for each instrument the following plots are reported:

- row-data recorded by the sensor over the entire monitoring period (2011-2016)
- the mean daily value
- the daily amplitude
- progressive daily residual on the mean value
- absolute daily residual on the mean value
- the annual amplitude
- progressive annual residual on the mean value
- absolute annual residual on the mean value

The table collects the mean values for each years of these reference quantities.

It is noted that the laser distance meters have recorded many spike and missing data throughout the monitoring period therefore are not considered in the analyses.

Long Base Deformeters

Deformometer Invar 1-without Drops

Mean Daily Value

Daily Amplitude

Progressive Daily Residuals of the Mean Value

Absolute Daily Residuals of the Mean Value

Annual Amplitude

Progressive Annual Residuals of the Mean Value

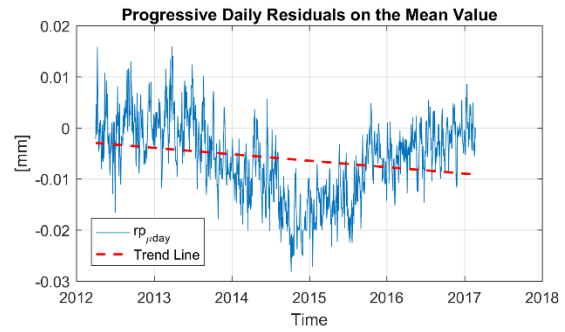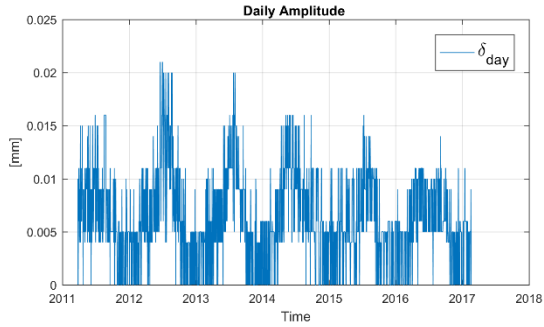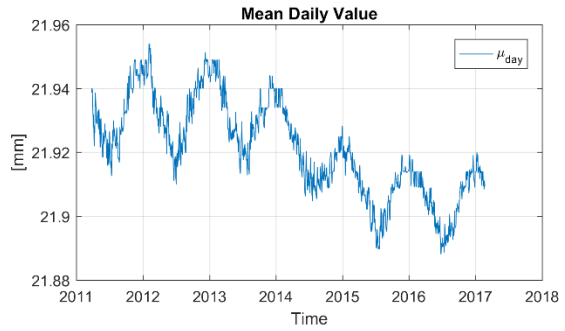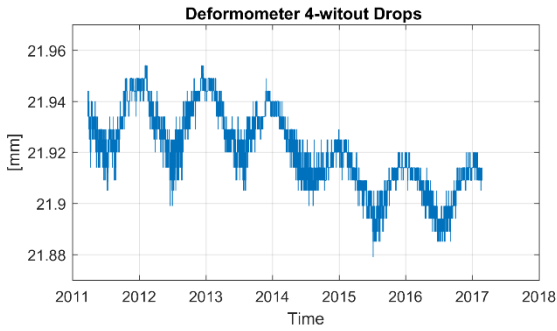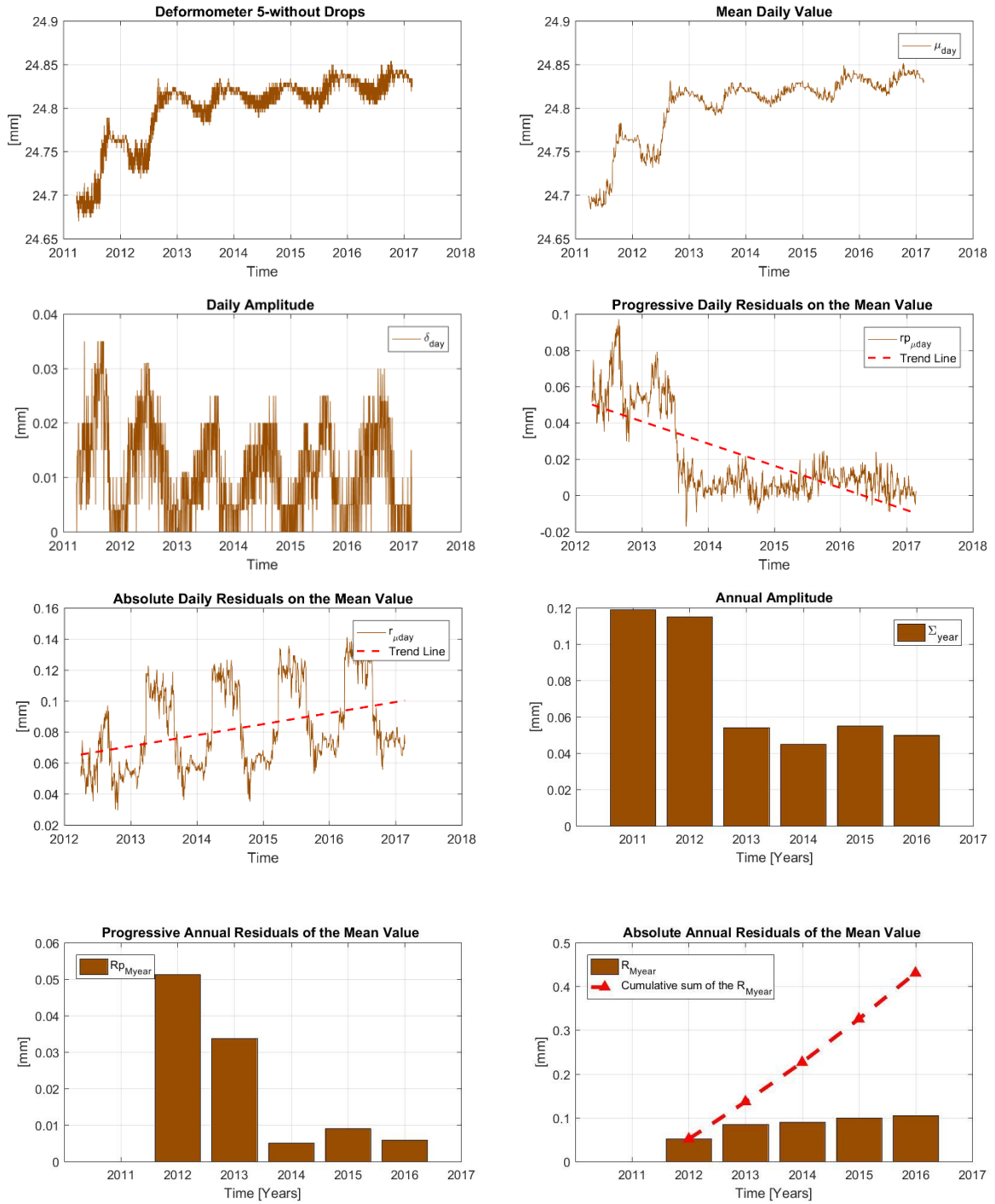Absolute Annual Residuals of the Mean Value
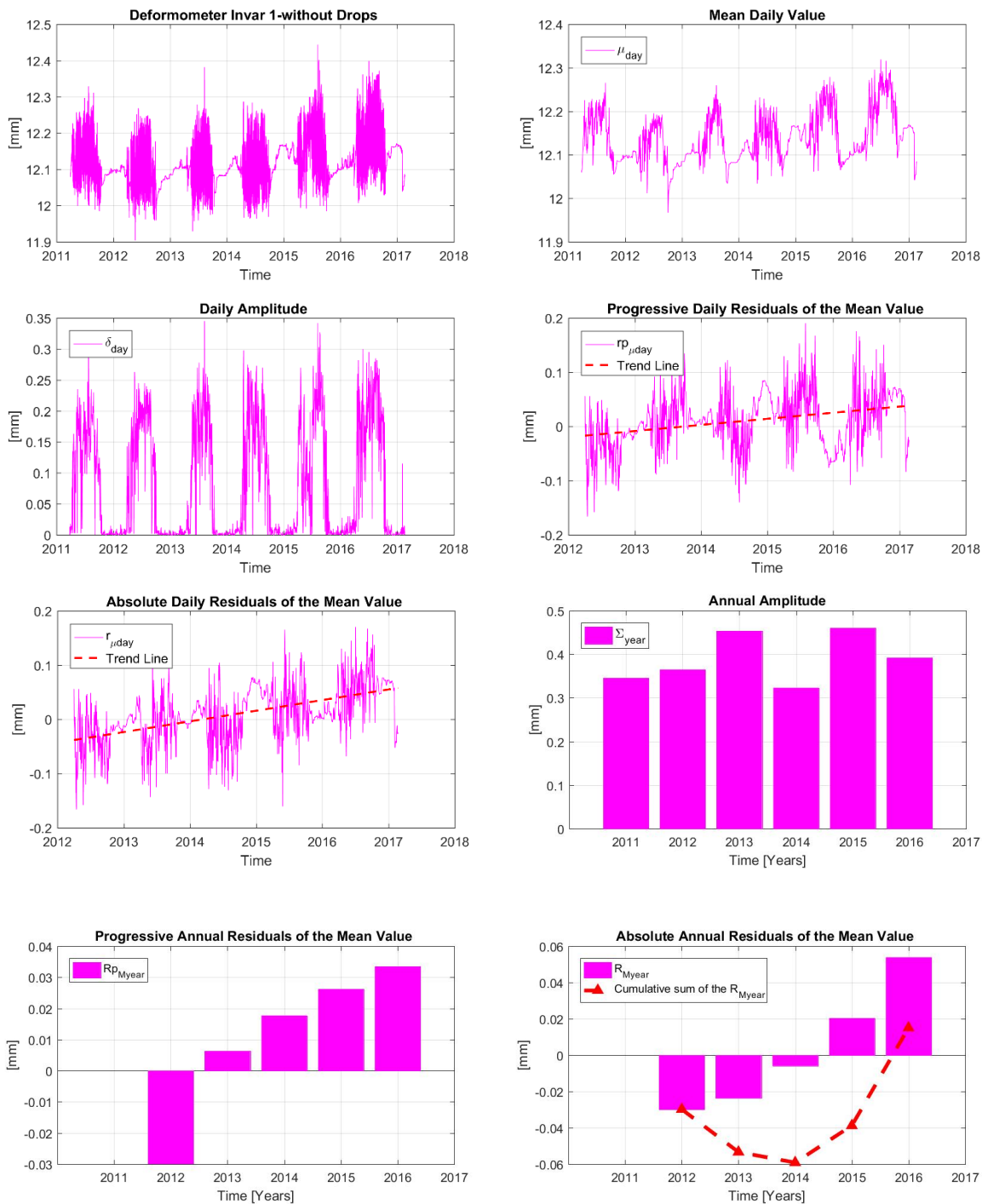
Sensor	Year	$\delta_{day,j}$	$rp_{\mu day}$	$r_{\mu day}$	M_{year}	Σ_{year}	Rp_{Myear}	R_{Myear}
	2011	0.095			12.140	0.345		
	2012	0.076	-0.034	-0.034	12.110	0.365	-0.030	-0.030
G-FS-F1	2013	0.071	0.017	-0.008	12.117	0.453	0.006	-0.024
[mm]	2014	0.079	0.009	0.001	12.134	0.323	0.018	-0.006
	2015	0.080	0.025	0.027	12.160	0.460	0.026	0.020
	2016	0.099	0.024	0.051	12.194	0.392	0.033	0.054
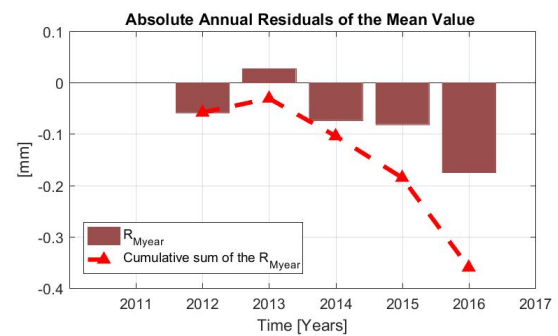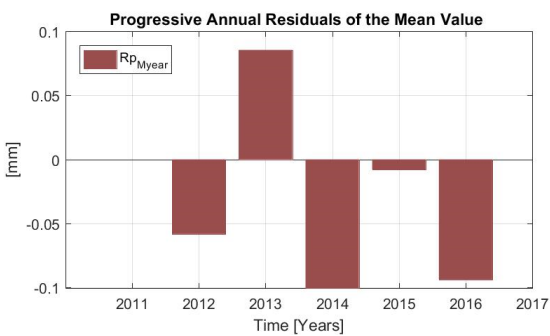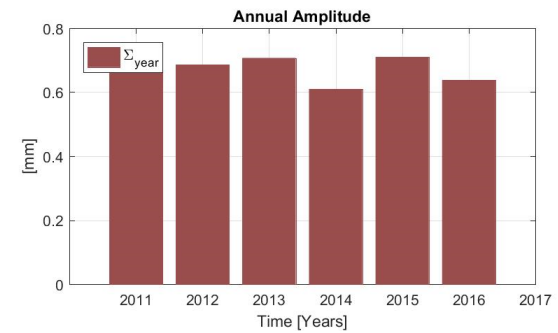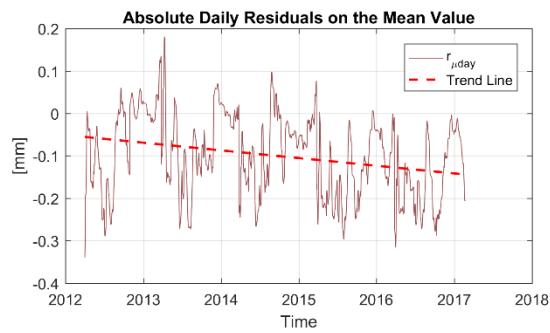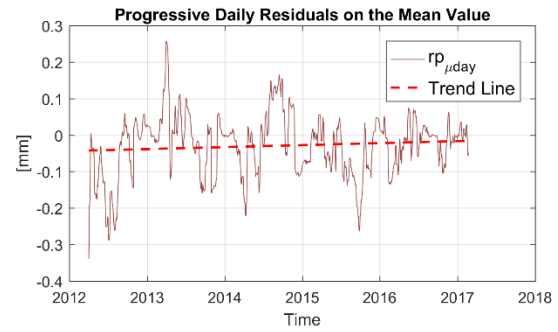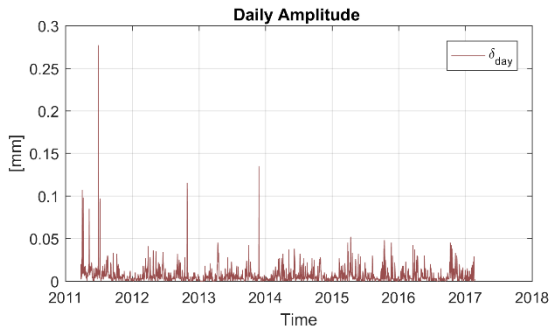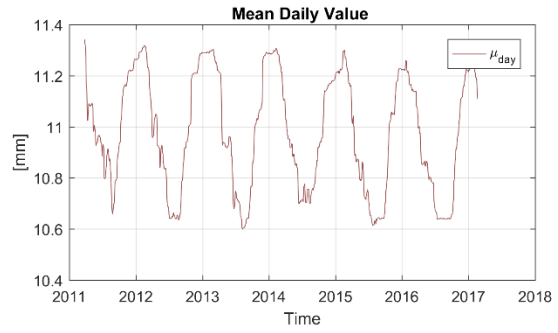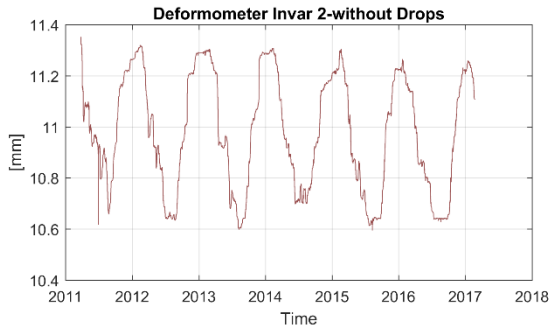
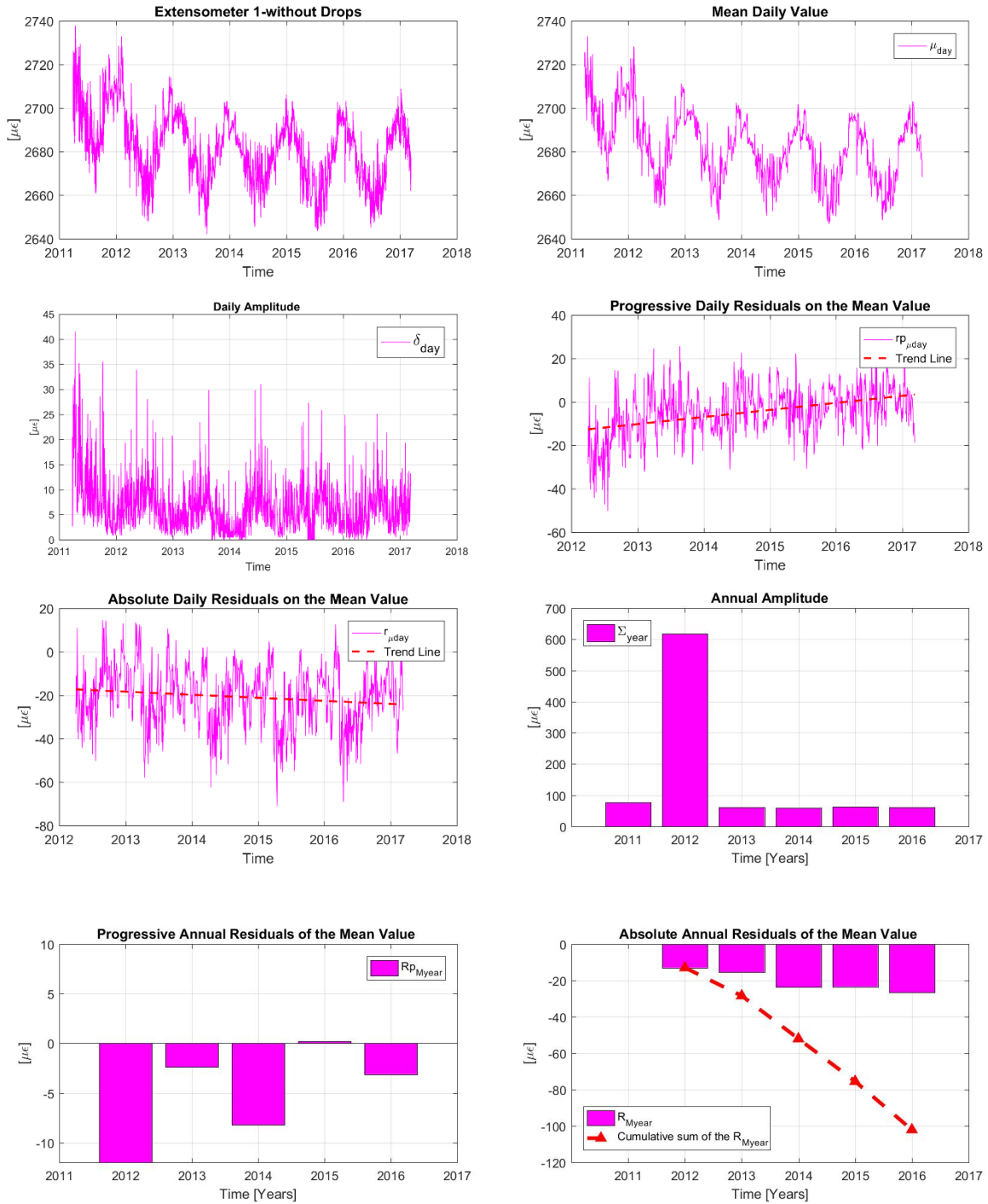| Sensor	Year	$\delta_{day,j}$	$rp_{\mu day}$	$r_{\mu day}$	M_{year}	Σ_{year}	Rp_{Myear}	R_{Myear}
	2011	0.010			11.023	0.735		0.000
	2012	0.006	-0.084	-0.084	10.965	0.686	-0.058	-0.058
G-FS-F2	2013	0.005	0.001	-0.067	11.050	0.707	0.085	0.027
[mm]	2014	0.006	-0.005	-0.071	10.950	0.610	-0.100	-0.073
	2015	0.006	-0.057	-0.128	10.942	0.710	-0.008	-0.081
	2016	0.006	-0.020	-0.148	10.848	0.638	-0.094	-0.175

Sensor	Year	$\delta_{day,j}$	$rp_{\mu day}$	$r_{\mu day}$	M_{year}	Σ_{year}	Rp_{Myear}	R_{Myear}
	2011	0.019			10.372	0.642		0.000
	2012	0.022	0.008	0.008	10.411	0.788	0.039	0.039
G-FE-F3	2013	0.018	-0.008	-0.003	10.476	0.719	0.065	0.104
[mm]	2014	0.019	-0.012	-0.015	10.387	3.474	-0.089	0.015
	2015	0.024	-0.026	-0.041	10.392	0.708	0.005	0.020
	2016	0.025	-0.012	-0.053	10.348	0.655	-0.044	-0.024

Deformometer Invar 4-without Drops

Mean Daily Value

Daily Amplitude

Progressive Daily Residuals on the Mean Value

Absolute Daily Residuals on the Mean Value

Annual Amplitude

Progressive Annual Residuals of the Mean Value
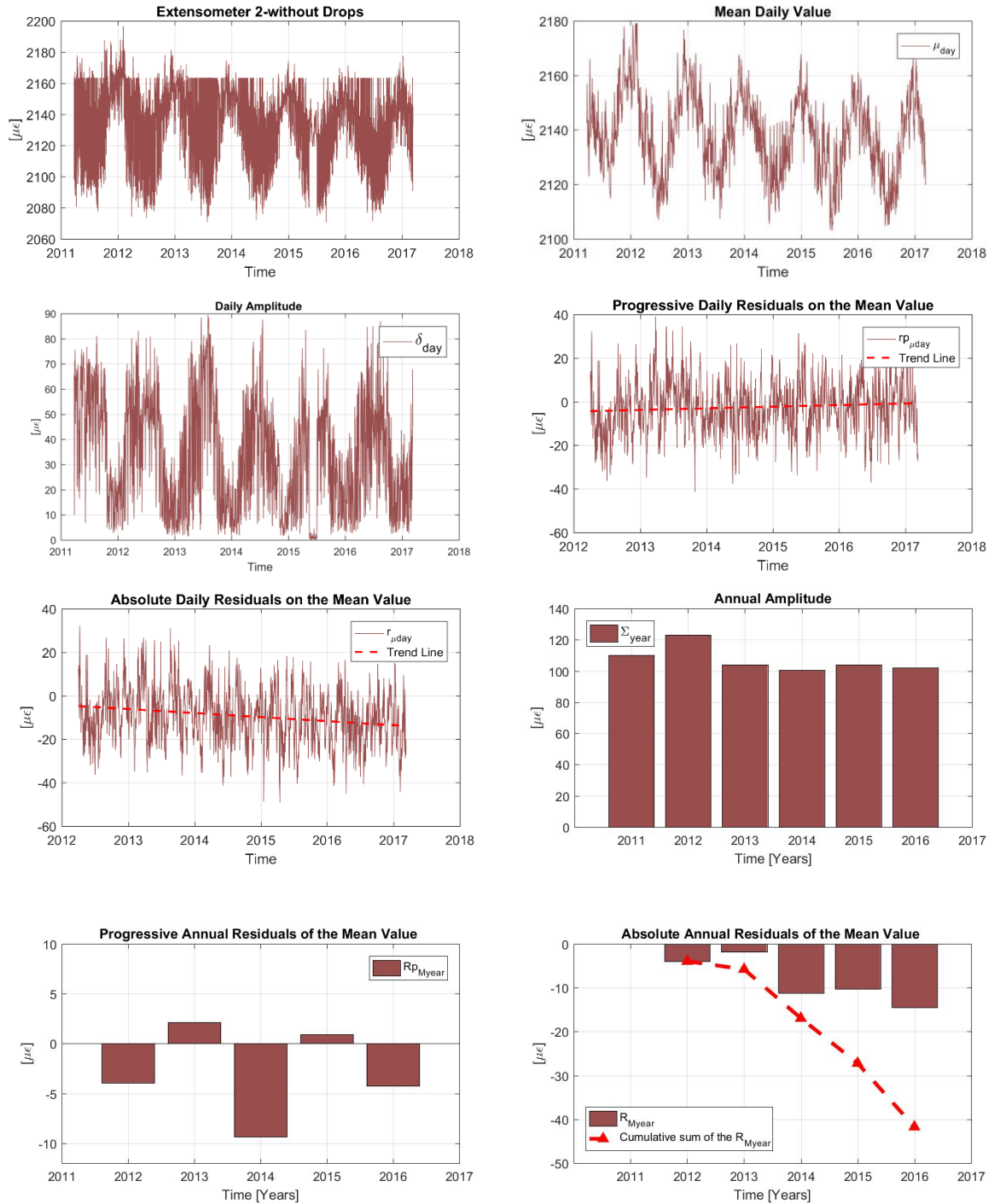

Absolute Annual Residuals of the Mean Value

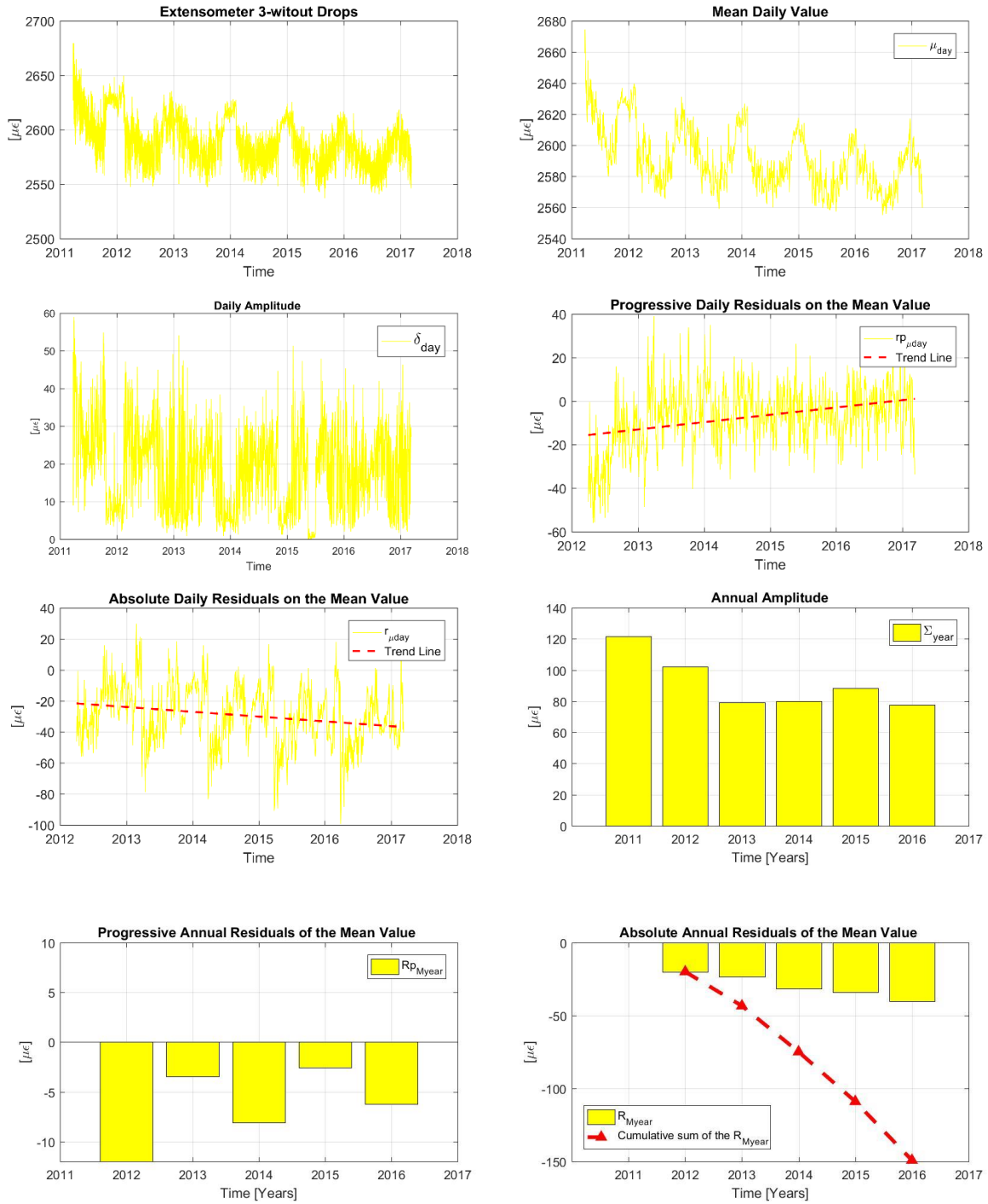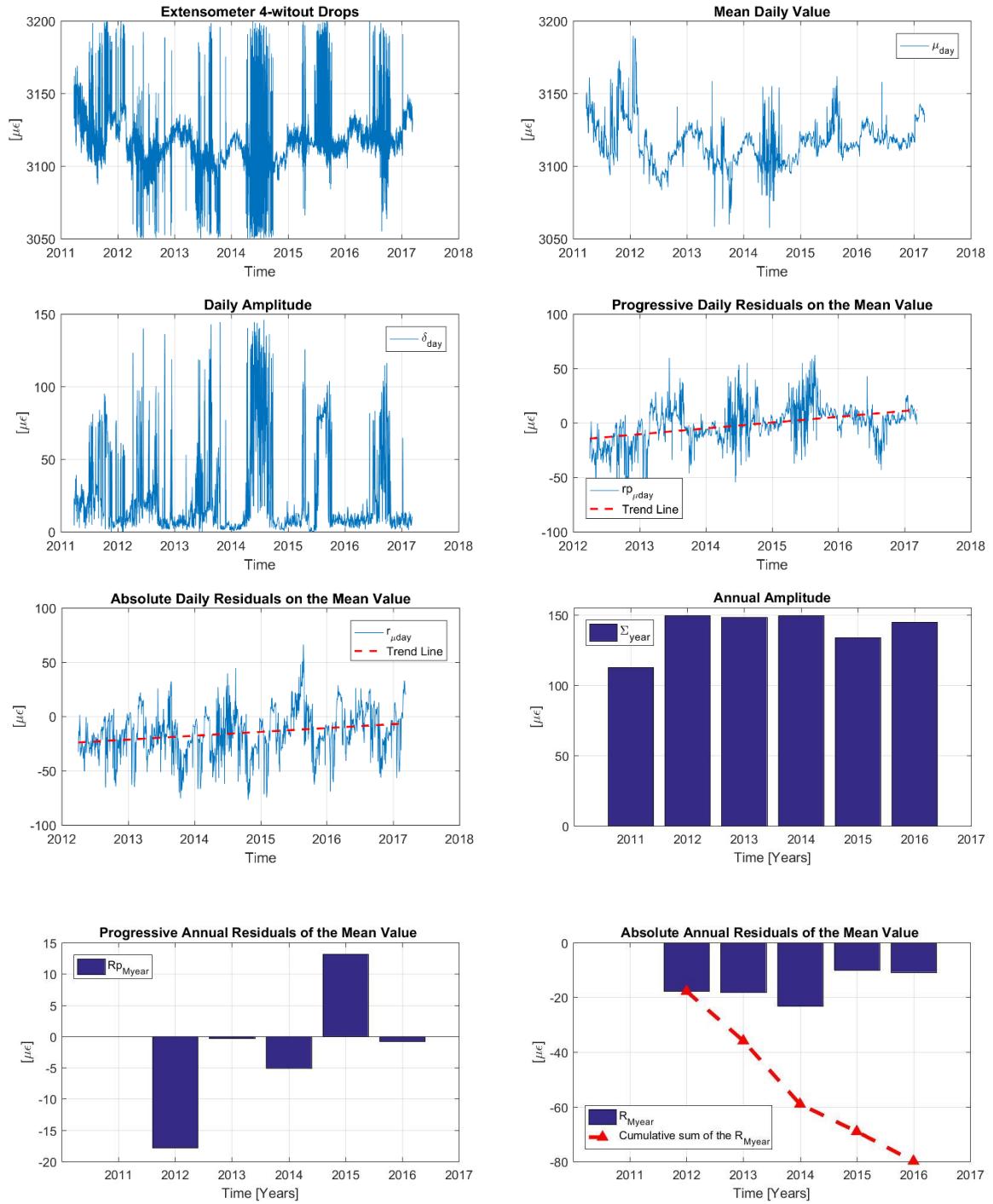| Sensor	Year	$\delta_{day,j}$	$rp_{\mu day}$	$r_{\mu day}$	M_{year}	Σ_{year}	Rp_{Myear}	R_{Myear}
G-FE-F4 [mm]	2011	0.060			13.979	0.250		0.000
	2012	0.055	-0.045	-0.045	13.937	0.303	-0.042	-0.042
	2013	0.044	-0.011	-0.046	13.934	0.282	-0.002	-0.045
	2014	0.041	-0.017	-0.063	13.907	0.243	-0.028	-0.072
	2015	0.040	-0.004	-0.067	13.910	0.302	0.003	-0.069
	2016	0.046	-0.012	-0.079	13.895	0.267	-0.015	-0.084

Deformeters

Sensor	Year	$\delta_{day,j}$	$rp_{\mu day}$	$r_{\mu day}$	M_{year}	Σ_{year}	Rp_{Myear}	R_{Myear}
	2011	0.007			18.743	0.031		0.000
	2012	0.007	0.007	0.007	18.750	0.035	0.007	0.007
G—FE-D1	2013	0.007	0.003	0.003	18.752	0.040	0.003	0.010
[mm]	2014	0.007	-0.002	-0.002	18.751	0.031	-0.002	0.008
	2015	0.008	-0.001	-0.001	18.751	0.040	0.000	0.008
	2016	0.009	0.001	0.001	18.750	0.049	-0.001	0.007

Deformeter 2-without Drops

Mean Daily Value

Daily Amplitude

Progressive Daily Residuals on the Mean Value

Absolute Daily Residuals on the Mean Value

Annual Amplitude

Progressive Annual Residuals of the Mean Value

Absolute Annual Residuals of the Mean Value
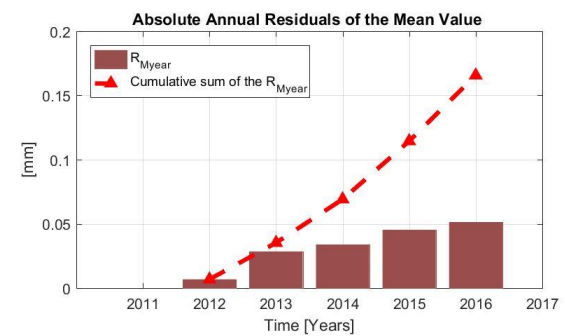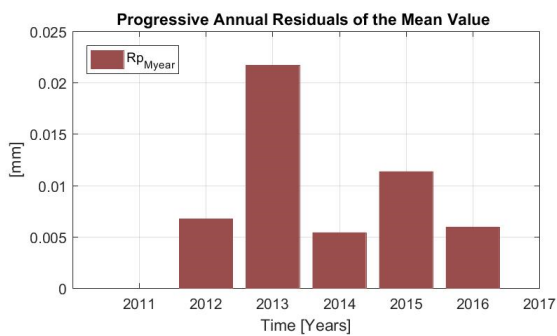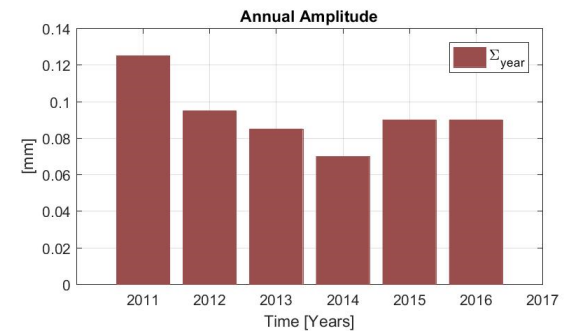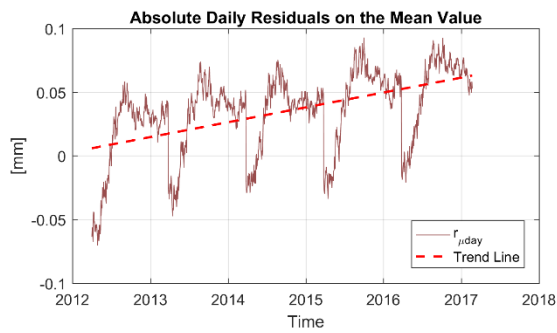
Sensor	Year	$\delta_{day,j}$	$rp_{\mu day}$	$r_{\mu day}$	M_{year}	Σ_{year}	Rp_{Myear}	R_{Myear}
	2011	0.015			24.904	0.125		0.000
	2012	0.016	0.009	0.009	24.911	0.095	0.007	0.007
G—FE-D2	2013	0.015	0.021	0.027	24.932	0.085	0.022	0.028
[mm]	2014	0.015	0.006	0.033	24.938	0.070	0.005	0.034
	2015	0.016	0.009	0.042	24.949	0.090	0.011	0.045
	2016	0.018	0.010	0.051	24.955	0.090	0.006	0.051
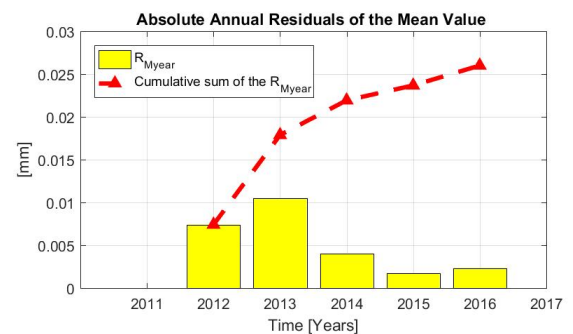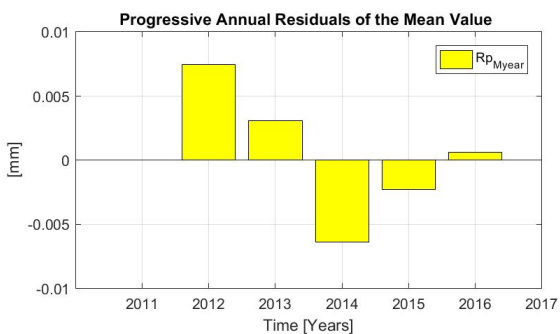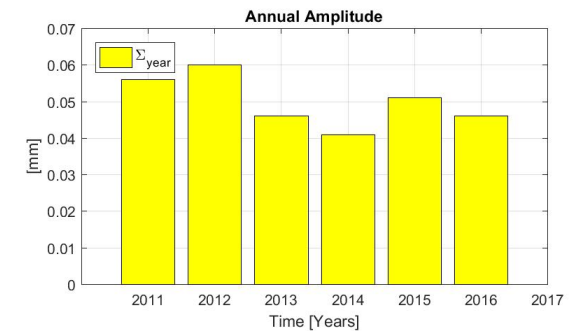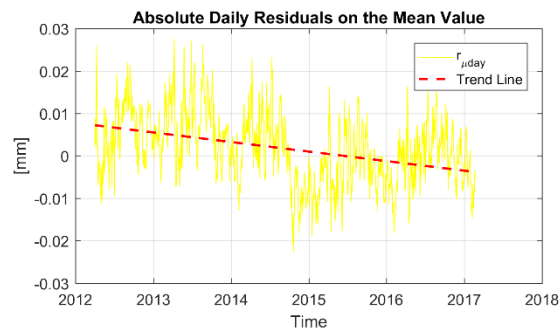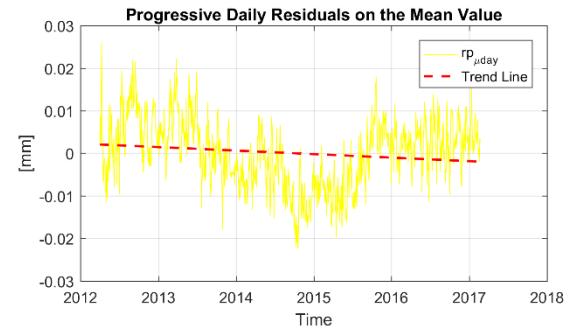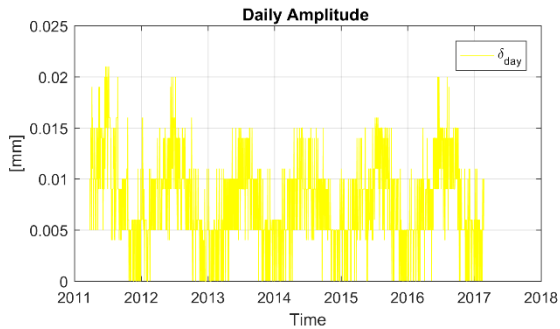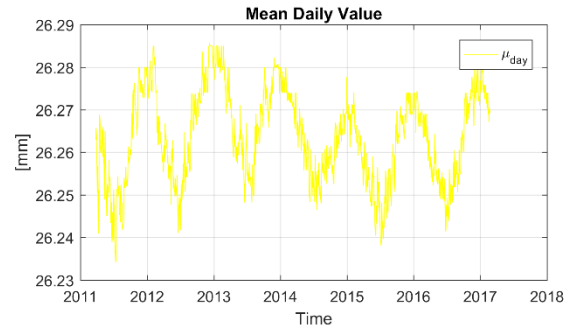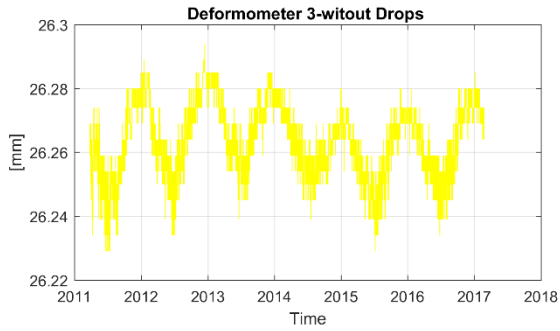
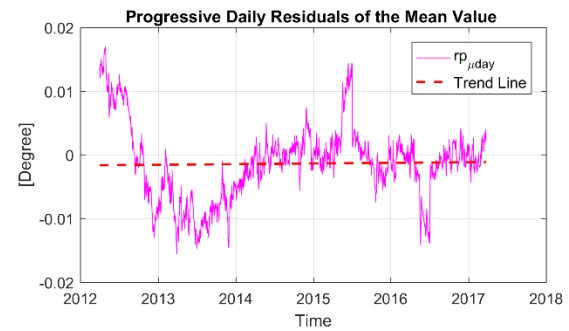| Sensor	Year	$\delta_{day,j}$	$\mathrm{rp}_{\mu day}$	$\mathrm{r}_{\mu day}$	M_{year}	Σ_{year}	Rp_{Myear}	R_{Myear}
	2011	0.009			26.259	0.056		0.000
	2012	0.008	0.006	0.006	26.266	0.060	0.007	0.007
G—FN-D3	2013	0.007	0.003	0.007	26.269	0.046	0.003	0.010
[mm]	2014	0.007	-0.006	0.001	26.263	0.041	-0.006	0.004
	2015	0.007	-0.004	-0.003	26.261	0.051	-0.002	0.002
	2016	0.008	0.003	-0.0003	26.261	0.046	0.001	0.002

Deformometer 4-witout Drops

Mean Daily Value

Daily Amplitude

Progressive Daily Residuals on the Mean Value

Absolute Daily Residuals on the Mean Value

Annual Amplitude

Progressive Annual Residuals of the Mean Value

Absolute Annual Residuals of the Mean Value
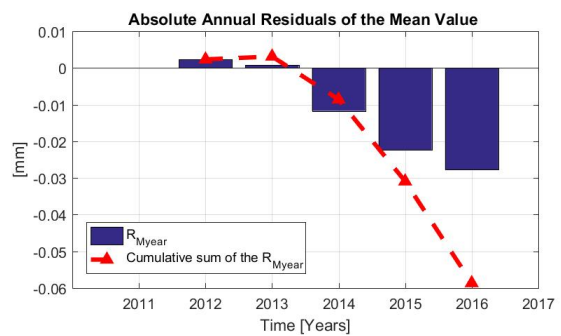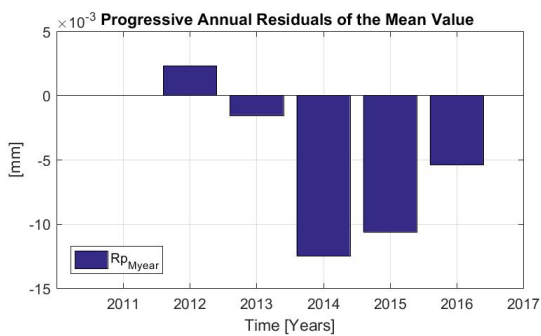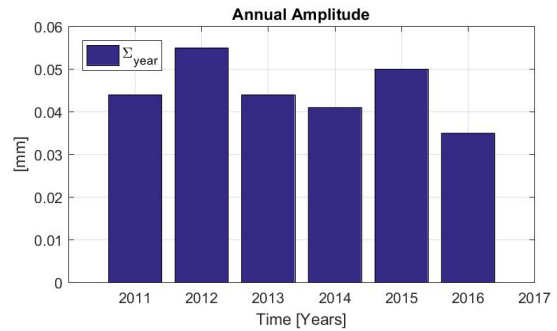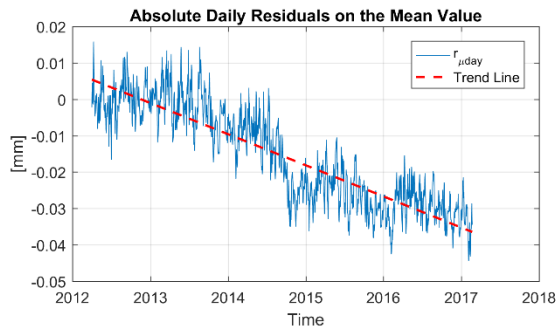
Sensor	Year	$\delta_{day,j}$	$\text{rp}_{\mu day}$	$\text{r}_{\mu day}$	M_{year}	Σ_{year}	Rp_{Myear}	R_{Myear}
	2011	0.007			21.932	0.044		0.000
	2012	0.007	0.000	0.000	21.934	0.055	0.002	0.002
G—FN-D4	2013	0.006	-0.002	-0.002	21.932	0.044	-0.002	0.001
[mm]	2014	0.007	-0.012	-0.014	21.920	0.041	-0.012	-0.012
	2015	0.006	-0.012	-0.026	21.909	0.050	-0.011	-0.022
	2016	0.006	-0.004	-0.029	21.904	0.035	-0.005	-0.028

Deformometer 5-without Drops

Mean Daily Value

Daily Amplitude

Progressive Daily Residuals on the Mean Value

Absolute Daily Residuals on the Mean Value

Annual Amplitude

Progressive Annual Residuals of the Mean Value

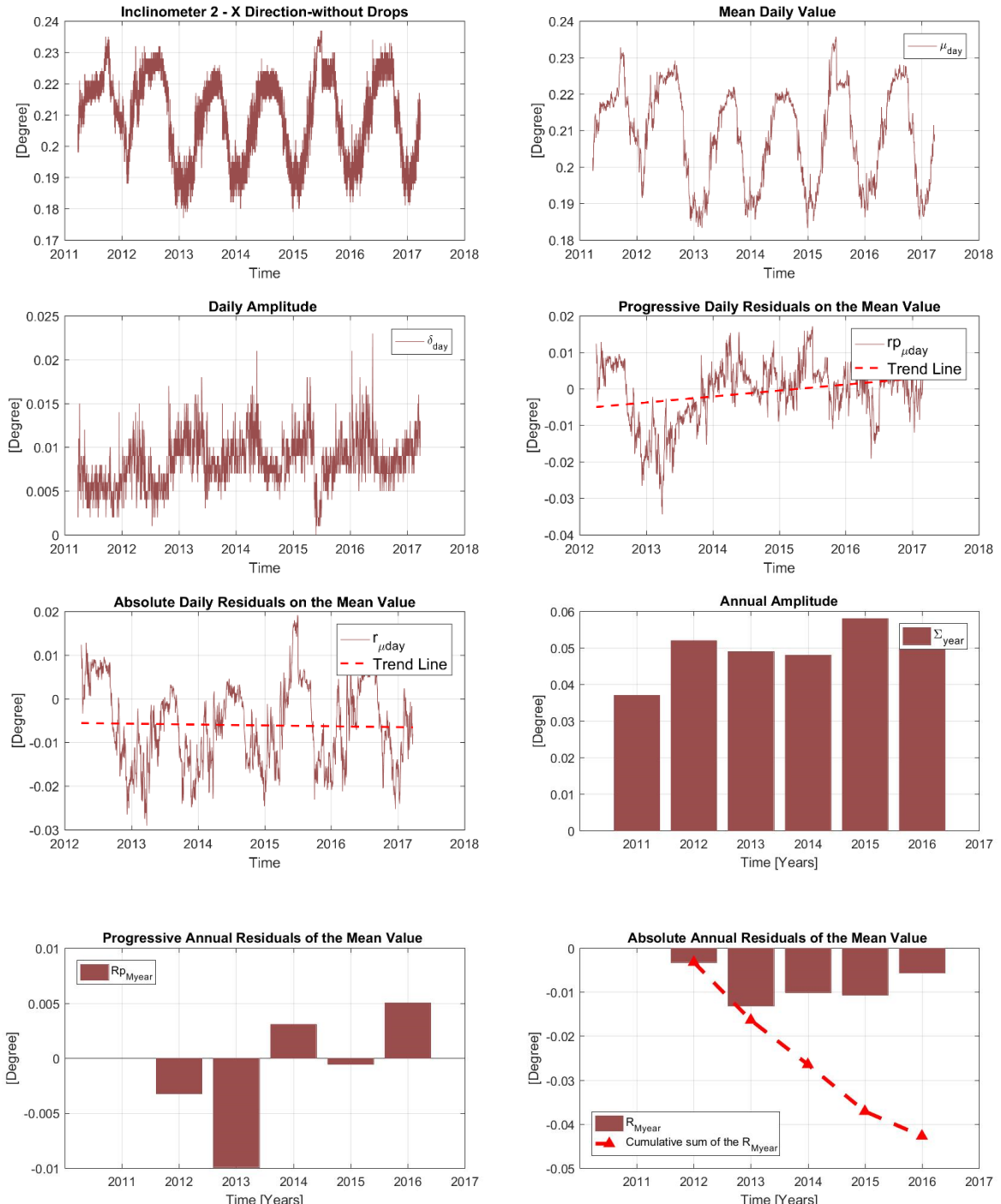Absolute Annual Residuals of the Mean Value

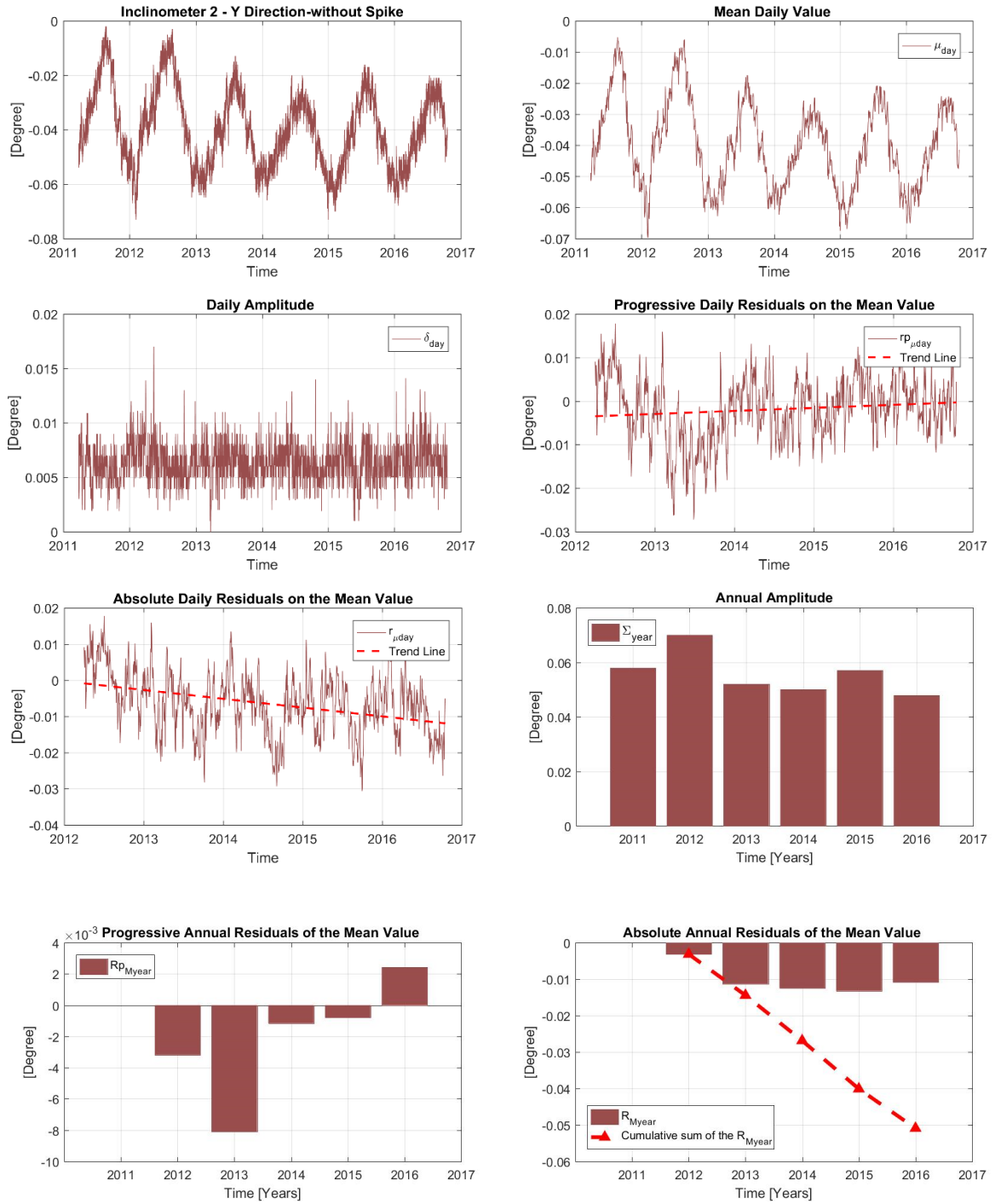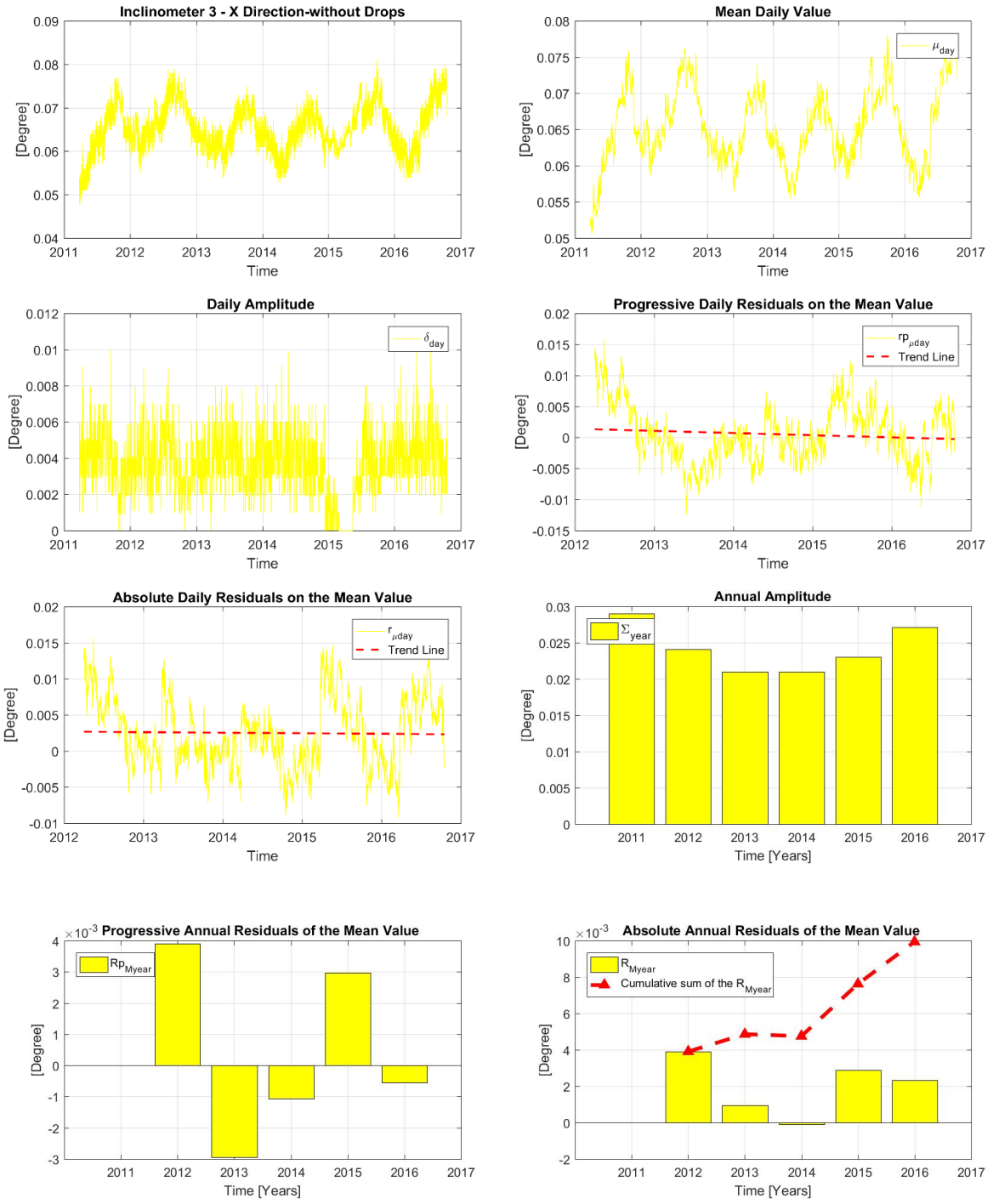| Sensor	Year	$\delta_{day,j}$	$rp_{\mu day}$	$r_{\mu day}$	M_{year}	Σ_{year}	Rp_{Myear}	R_{Myear}
G—FO-D5 [mm]	2011	0.015			24.727	0.119		0.000
	2012	0.013	0.059	0.059	24.778	0.115	0.051	0.051
	2013	0.009	0.034	0.078	24.812	0.054	0.034	0.085
	2014	0.010	0.005	0.083	24.817	0.045	0.005	0.090
	2015	0.010	0.008	0.091	24.826	0.055	0.009	0.099
	2016	0.011	0.007	0.098	24.832	0.050	0.006	0.105

Extensometers

Sensor	Year	$\delta_{day,j}$	rp$_{\mu day}$	r$_{\mu day}$	M_{year}	Σ_{year}	Rp$_{Myear}$	R_{Myear}
	2011	10.503			2699.308	77.096		
	2012	10.600	−16.148	−16.148	2686.297	618.068	−13.012	−13.012
G—FN-E1	2013	5.354	−4.830	−17.743	2683.892	61.025	−2.405	−15.416
[με]	2014	5.482	−3.704	−21.447	2675.673	58.969	−8.219	−23.635
	2015	6.362	−2.179	−23.625	2675.858	62.808	0.185	−23.450
	2016	5.889	0.349	−23.218	2672.722	60.259	−3.136	−26.586

Extensometer 2-without Drops

Mean Daily Value

Daily Amplitude

Progressive Daily Residuals on the Mean Value

Absolute Daily Residuals on the Mean Value

Annual Amplitude

Progressive Annual Residuals of the Mean Value

**Absolute Annual Residuals of the Mean Value**

Sensor	Year	$\delta_{day,j}$	$rp_{\mu day}$	$r_{\mu day}$	M_{year}	Σ_{year}	Rp_{Myear}	R_{Myear}
	2011	44.781			2144.712	110.073		0.000
	2012	36.974	-6.783	-6.783	2140.753	123.037	-3.959	-3.959
G—FE-E2	2013	35.651	0.654	-4.826	2142.893	103.883	2.140	-1.819
[με]	2014	29.834	-4.928	-9.754	2133.535	100.527	-9.358	-11.177
	2015	27.225	-1.280	-11.035	2134.438	103.859	0.903	-10.274
	2016	32.208	-1.261	-12.270	2130.188	102.048	-4.250	-14.524

Extensometer 3-witout Drops

Mean Daily Value

Daily Amplitude

Progressive Daily Residuals on the Mean Value

Absolute Daily Residuals on the Mean Value

Annual Amplitude

Progressive Annual Residuals of the Mean Value

Absolute Annual Residuals of the Mean Value

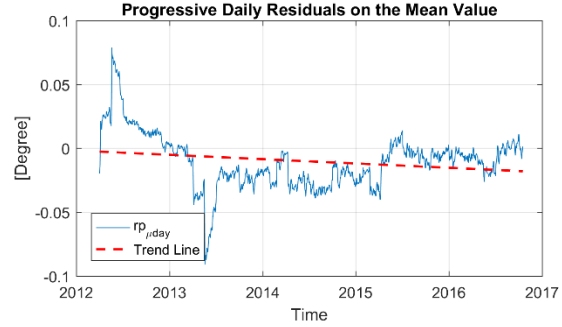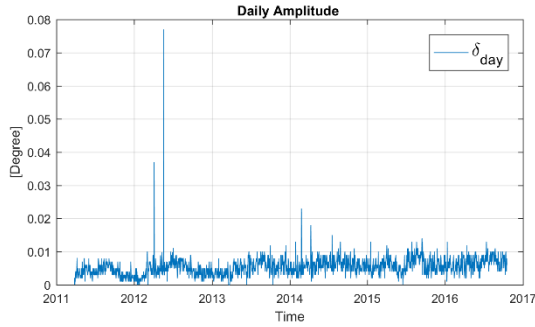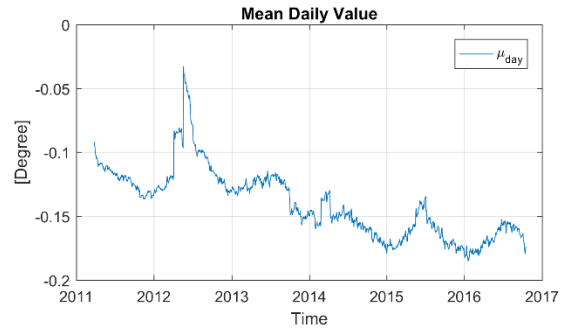| Sensor	Year	$\delta_{day,j}$	$rp_{\mu day}$	$r_{\mu day}$	M_{year}	Σ_{year}	Rp_{Myear}	R_{Myear}
G—FS-E3 [με]	2011	24.289			2617.581	121.648		0.000
	2012	20.778	-22.988	-22.988	2597.610	102.267	-19.971	-19.971
	2013	16.325	-5.128	-23.840	2594.169	79.227	-3.441	-23.411
	2014	16.703	-3.696	-27.536	2586.081	80.117	-8.089	-31.500
	2015	17.428	-5.449	-32.984	2583.523	88.295	-2.558	-34.057
	2016	18.011	-3.362	-36.250	2577.300	77.689	-6.223	-40.280

Sensor	Year	$\delta_{day,j}$	$\mathrm{rp}_{\mu day}$	$\mathrm{r}_{\mu day}$	M_{year}	Σ_{year}	Rp_{Myear}	R_{Myear}
	2011	29.073			3129.279	112.659		0.000
	2012	21.398	-21.825	-21.825	3111.473	149.412	-17.806	-17.806
G—FO-E4	2013	18.458	-2.093	-19.263	3111.172	148.296	-0.302	-18.107
[με]	2014	36.252	-1.223	-20.486	3106.117	149.412	-5.055	-23.162
	2015	26.809	10.806	-9.680	3119.265	133.741	13.148	-10.014
	2016	19.824	0.840	-8.765	3118.447	144.724	-0.817	-10.832

Inclinometers
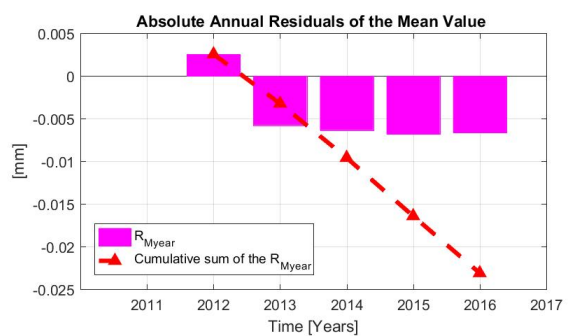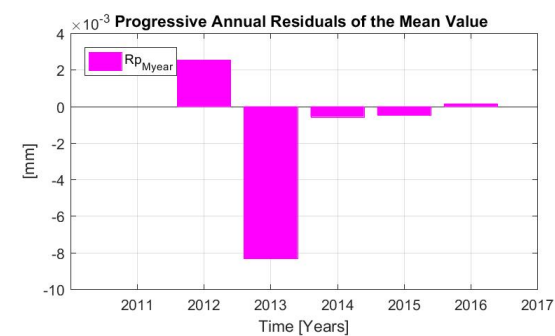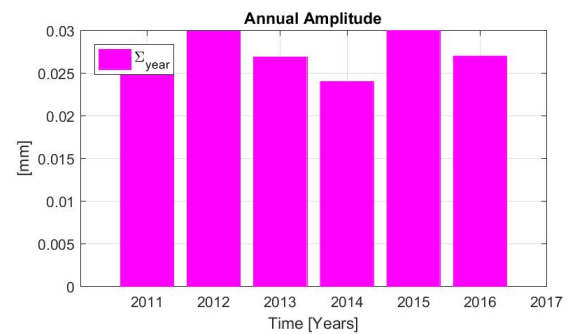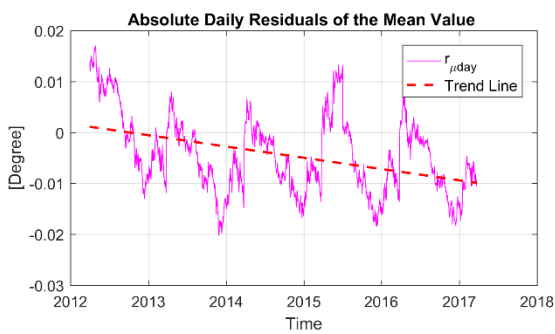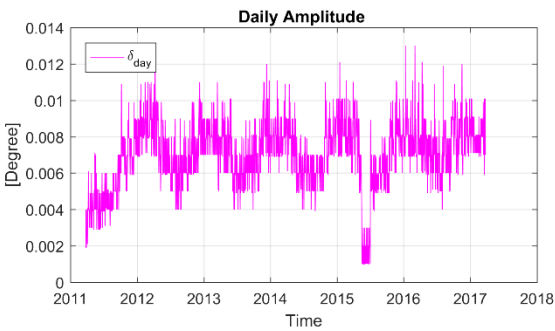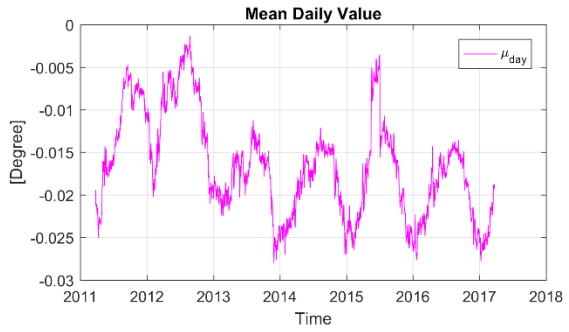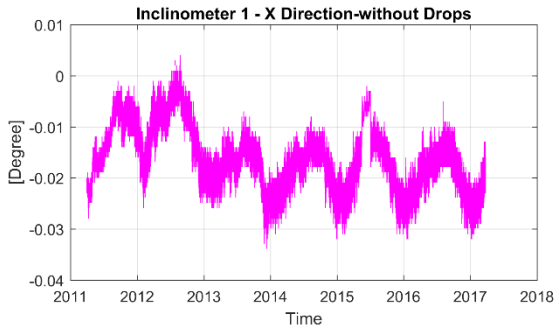
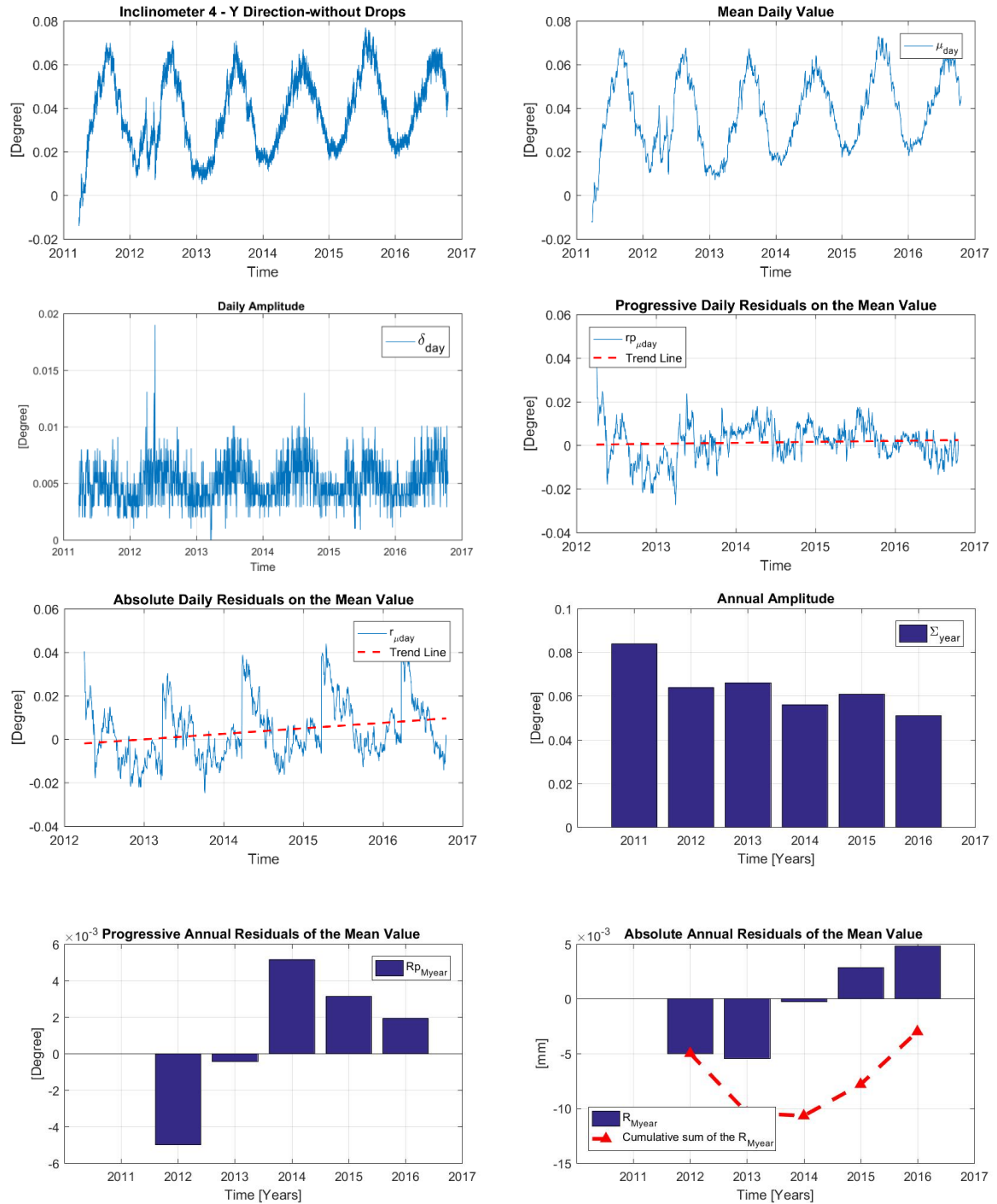| Sensor	Year	$\delta_{day,j}$	$\mathrm{rp}_{\mu day}$	$\mathrm{r}_{\mu day}$	M_{year}	Σ_{year}	Rp_{Myear}	R_{Myear}
	2011	0.0054			-0.0125	0.0270		0.0000
	2012	0.0075	0.0038	0.0038	-0.0100	0.0299	0.0025	0.0025
G-FS-I1X	2013	0.0073	-0.0084	-0.0053	-0.0183	0.0269	-0.0083	-0.0058
[°]	2014	0.0072	-0.0006	-0.0059	-0.0188	0.0240	-0.0006	-0.0064
	2015	0.0066	0.0012	-0.0047	-0.0193	0.0300	-0.0005	-0.0068
	2016	0.0077	-0.0019	-0.0066	-0.0192	0.0270	0.0002	-0.0067
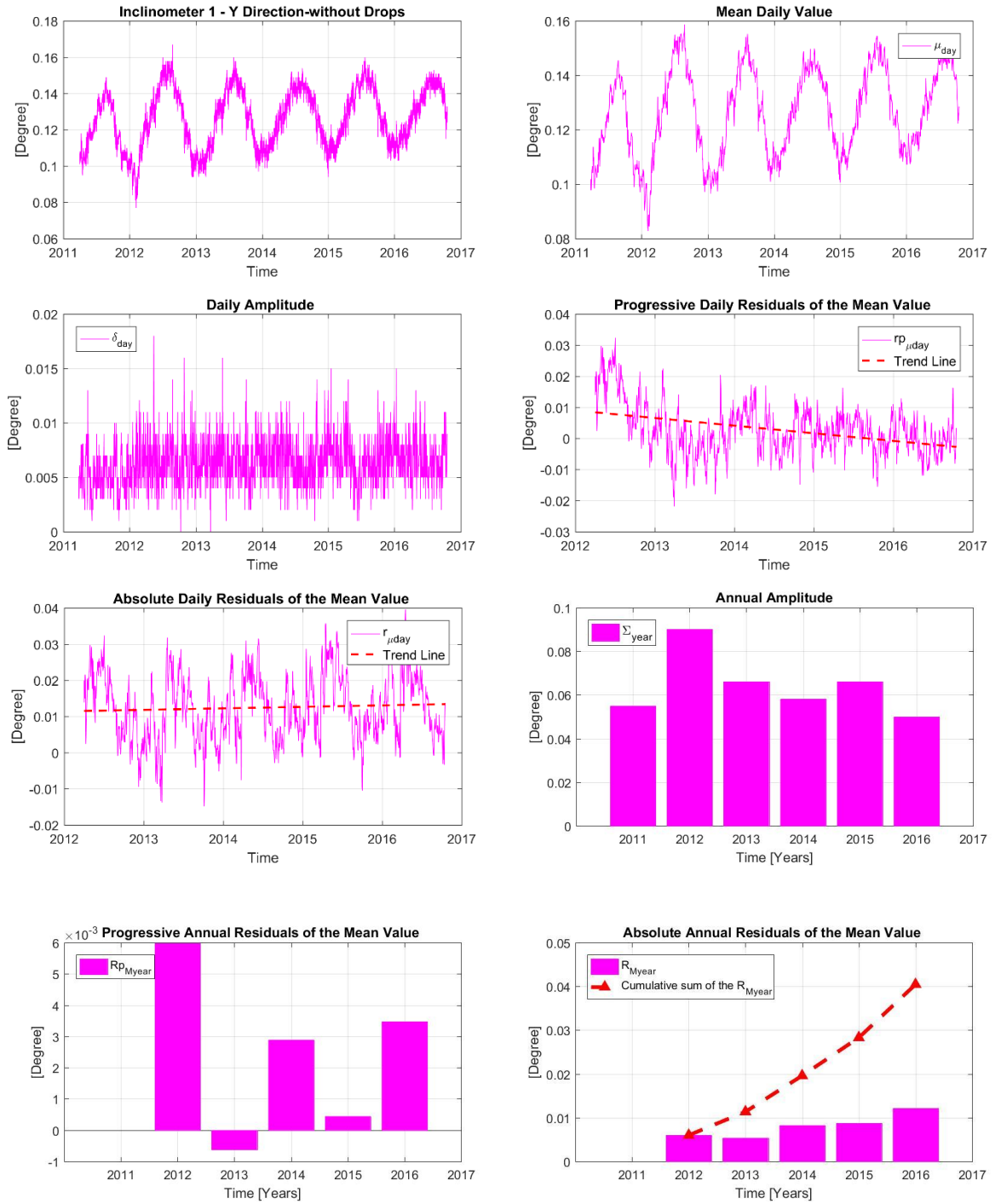
Sensor	Year	$\delta_{day,j}$	$rp_{\mu day}$	$r_{\mu day}$	M_{year}	Σ_{year}	Rp_{Myear}	R_{Myear}
	2011	0.0067			0.1195	0.0560		0.0000
	2012	0.0085	0.0129	0.0129	0.1255	0.0911	0.0059	0.0059
G—FS-I1Y	2013	0.0088	-0.0008	0.0093	0.1248	0.0690	-0.0007	0.0053
[°]	2014	0.0087	0.0031	0.0124	0.1278	0.0591	0.0030	0.0083
	2015	0.0087	0.0014	0.0138	0.1273	0.0660	-0.0005	0.0077
	2016	0.0091	-0.0004	0.0133	0.1301	0.0571	0.0028	0.0106

Inclinometer 2 - X Direction-without Drops

Mean Daily Value

Daily Amplitude

Progressive Daily Residuals on the Mean Value

Absolute Daily Residuals on the Mean Value

Annual Amplitude

Progressive Annual Residuals of the Mean Value

Absolute Annual Residuals of the Mean Value

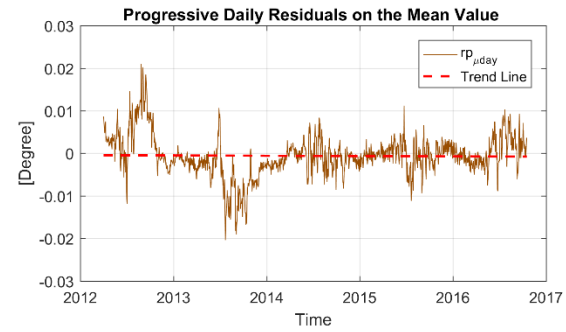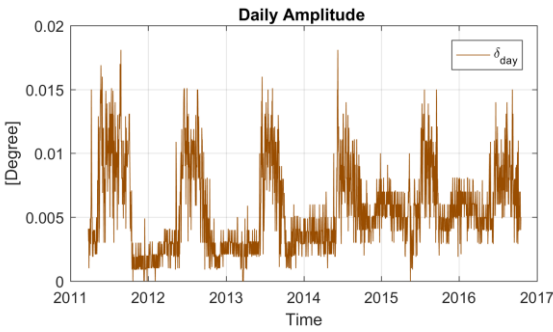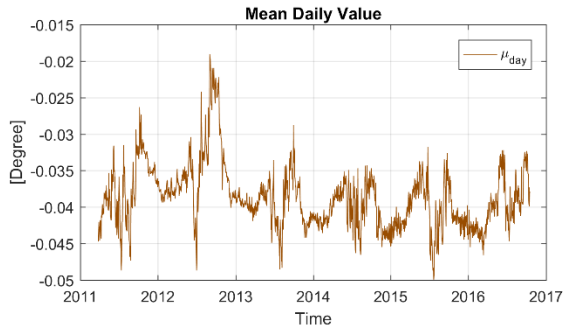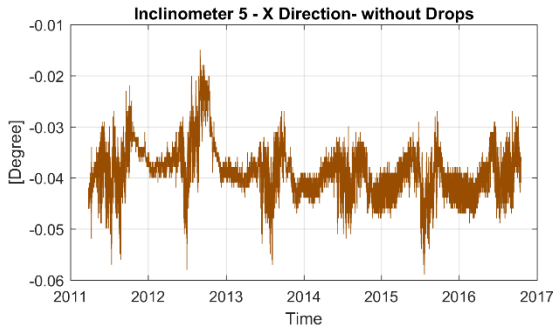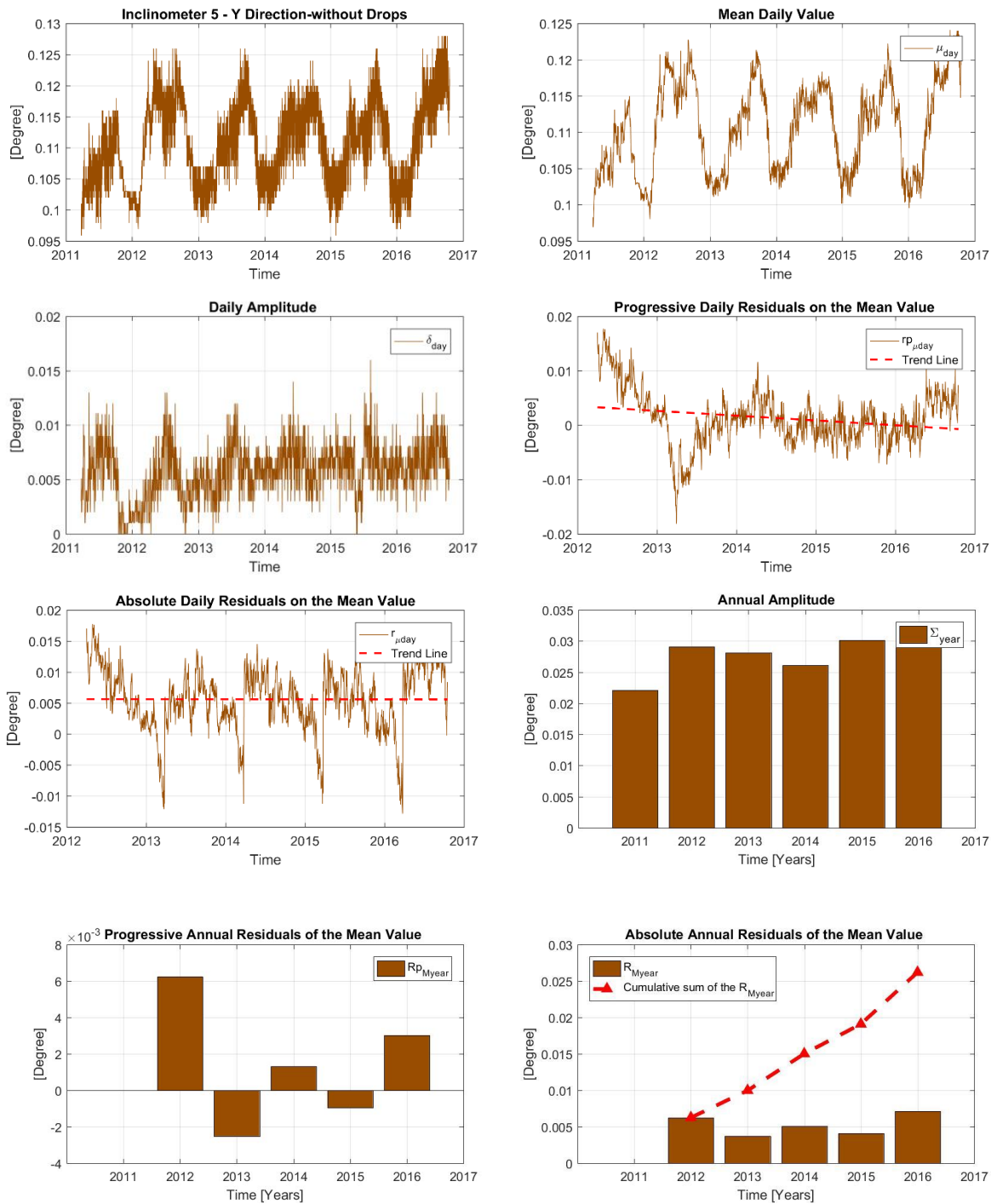| Sensor	Year	$\delta_{day,j}$	$\mathrm{rp}_{\mu day}$	$\mathrm{r}_{\mu day}$	M_{year}	Σ_{year}	Rp_{Myear}	R_{Myear}
	2011	0.0057			0.2166	0.0370		0.0000
	2012	0.0073	-0.0011	-0.0011	0.2134	0.0520	-0.0032	-0.0032
G-FS-I2X	2013	0.0092	-0.0101	-0.0106	0.2034	0.0490	-0.0099	-0.0132
[°]	2014	0.0091	0.0032	-0.0074	0.2065	0.0480	0.0031	-0.0101
	2015	0.0086	0.0025	-0.0049	0.2059	0.0580	-0.0006	-0.0106
	2016	0.0092	0.0004	-0.0045	0.2110	0.0530	0.0050	-0.0056

Sensor	Year	$\delta_{day,j}$	$rp_{\mu day}$	$r_{\mu day}$	M_{year}	Σ_{year}	Rp_{Myear}	R_{Myear}
	2011	0.0076			0.0382	0.0859		0.0000
	2012	0.0090	0.0013	0.0013	0.0332	0.0650	-0.0050	-0.0050
G—FS-I2Y	2013	0.0084	-0.0083	-0.0070	0.0328	0.0660	-0.0004	-0.0054
[°]	2014	0.0082	-0.0010	-0.0080	0.0379	0.0570	0.0051	-0.0003
	2015	0.0078	-0.0002	-0.0082	0.0404	0.0609	0.0025	0.0022
	2016	0.0085	-0.0005	-0.0087	0.0420	0.0570	0.0015	0.0038

Inclinometer 3 - X Direction-without Drops

Mean Daily Value

Daily Amplitude

Progressive Daily Residuals on the Mean Value

Absolute Daily Residuals on the Mean Value

Annual Amplitude

Progressive Annual Residuals of the Mean Value

Absolute Annual Residuals of the Mean Value

Sensor	Year	$\delta_{day,j}$	$\text{rp}_{\mu day}$	$r_{\mu day}$	M_{year}	Σ_{year}	Rp_{Myear}	R_{Myear}
	2011	0.0062			0.0636	0.0310		0.0000
	2012	0.0060	0.0052	0.0052	0.0675	0.0310	0.0039	0.0039
G-FS-I3X	2013	0.0063	-0.0031	0.0011	0.0646	0.0240	-0.0029	0.0010
[°]	2014	0.0061	-0.0010	0.0001	0.0635	0.0310	-0.0011	-0.0001
	2015	0.0042	0.0032	0.0033	0.0663	0.0240	0.0028	0.0027
	2016	0.0069	-0.0009	0.0025	0.0666	0.0319	0.0004	0.0030
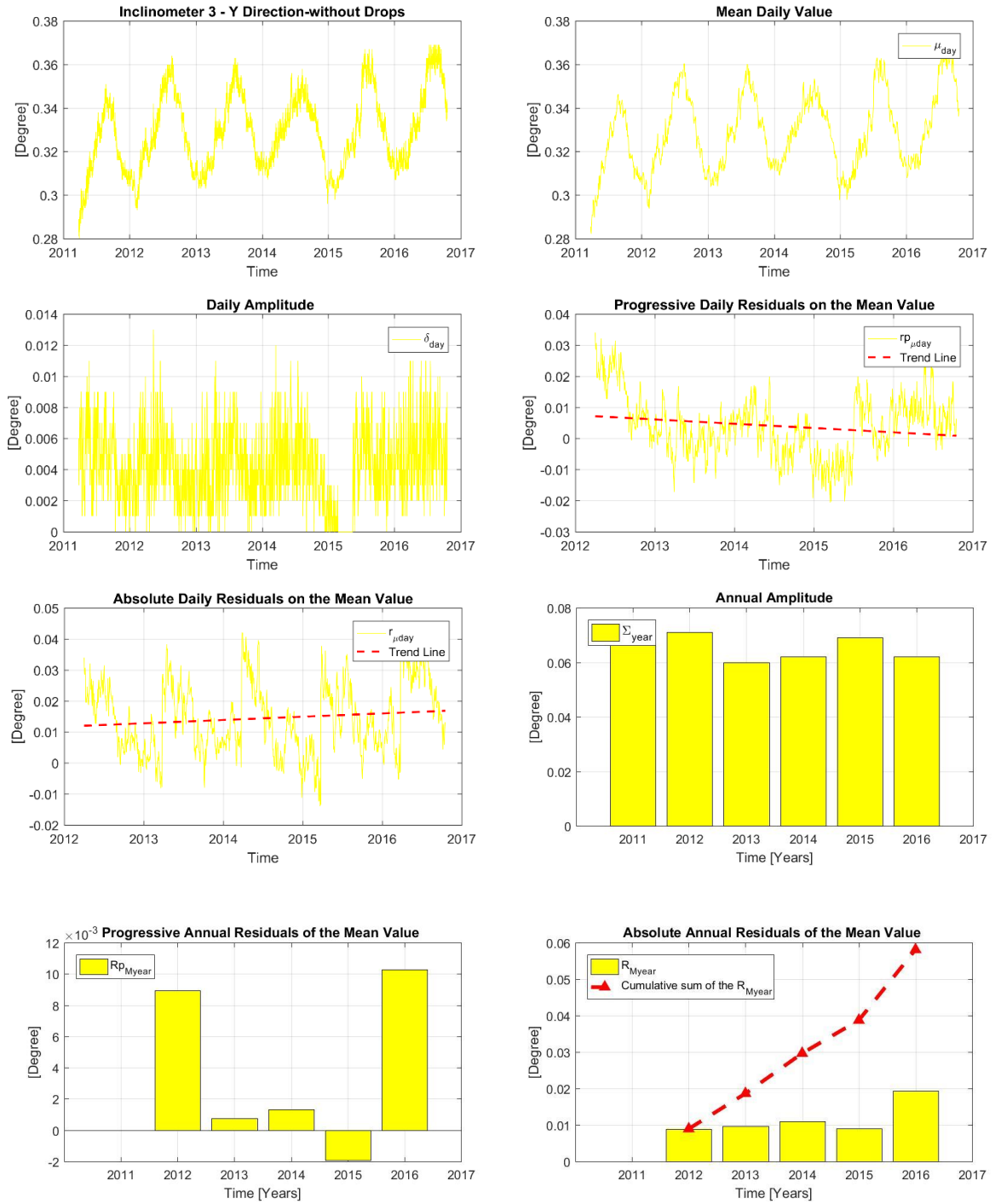
Sensor	Year	$\delta_{day,j}$	$\mathrm{rp}_{\mu day}$	$\mathrm{r}_{\mu day}$	M_{year}	Σ_{year}	Rp_{Myear}	R_{Myear}
	2011	0.005			0.319	0.071		0.000
	2012	0.004	0.015	0.015	0.328	0.071	0.009	0.009
G—FS-I3Y	2013	0.004	0.000	0.012	0.329	0.060	0.001	0.010
[°]	2014	0.004	0.002	0.014	0.330	0.062	0.001	0.011
	2015	0.003	-0.002	0.012	0.328	0.069	-0.002	0.009
	2016	0.005	0.009	0.021	0.338	0.062	0.010	0.019

Inclinometer 4 - X Direction-without Drops

Mean Daily Value

Daily Amplitude

Progressive Daily Residuals on the Mean Value

Absolute Daily Residuals on the Mean Value

Annual Amplitude

Progressive Annual Residuals of the Mean Value

Absolute Annual Residuals of the Mean Value
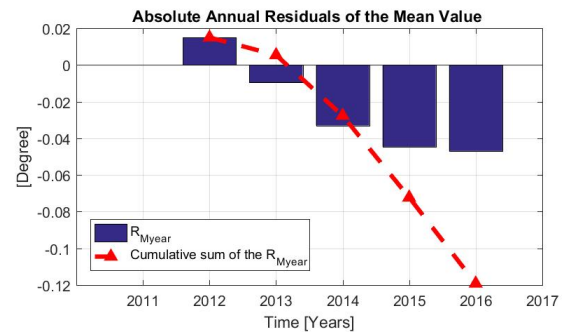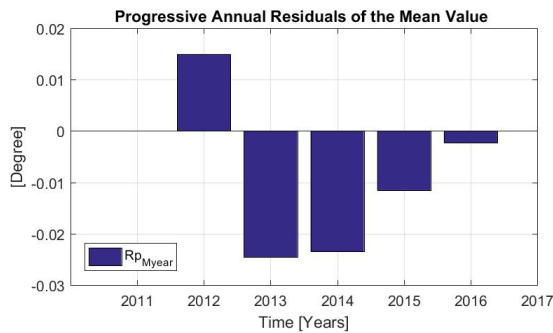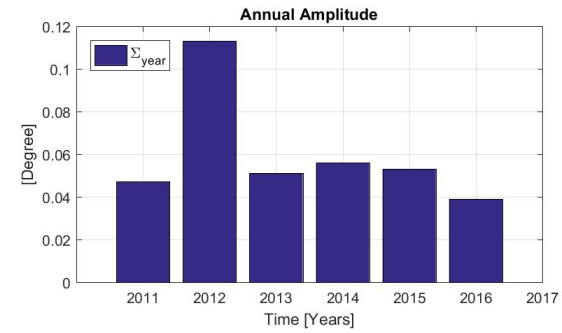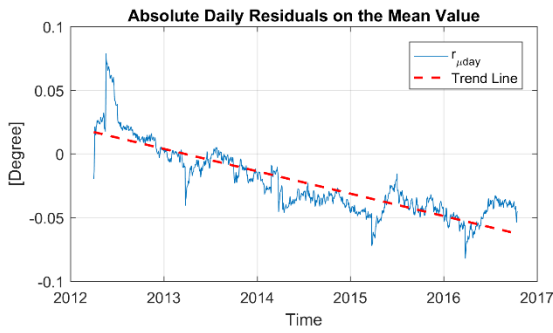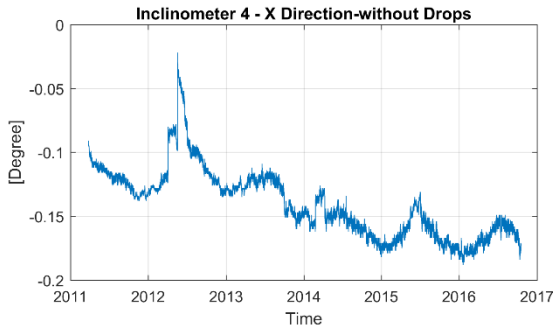
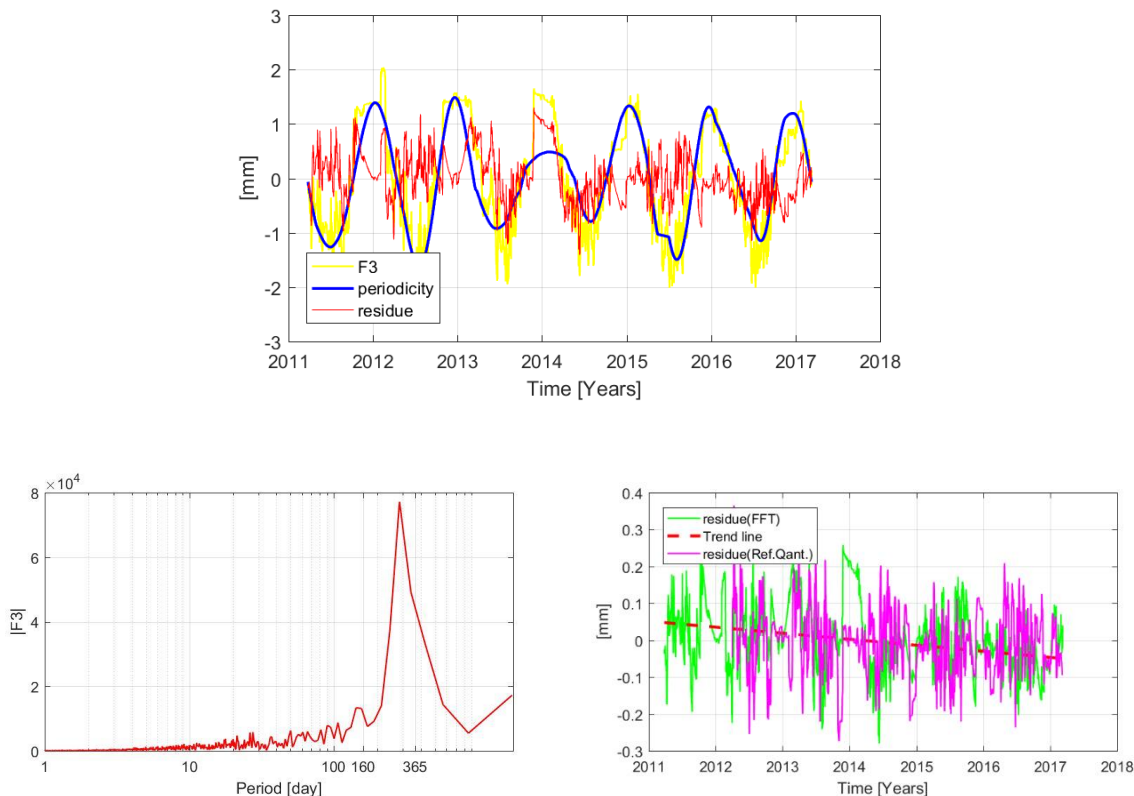| Sensor	Year	$\delta_{day,j}$	$\mathrm{rp}_{\mu day}$	$\mathrm{r}_{\mu day}$	M_{year}	Σ_{year}	Rp_{Myear}	R_{Myear}
	2011	0.0049			-0.1208	0.0480		0.0000
	2012	0.0061	0.0221	0.0221	-0.1058	0.1151	0.0150	0.0150
G—FE-I4X	2013	0.0063	-0.0245	-0.0082	-0.1305	0.0530	-0.0246	-0.0096
[°]	2014	0.0079	-0.0236	-0.0318	-0.1538	0.0560	-0.0234	-0.0330
	2015	0.0076	-0.0100	-0.0418	-0.1670	0.0540	-0.0131	-0.0461
	2016	0.0084	-0.0068	-0.0486	-0.1698	0.0510	-0.0028	-0.0489

Sensor	Year	$\delta_{day,j}$	$rp_{\mu day}$	$r_{\mu day}$	M_{year}	Σ_{year}	Rp_{Myear}	R_{Myear}
	2011	0.005			0.038	0.084		0.000
	2012	0.005	-0.002	-0.002	0.033	0.064	-0.005	-0.005
G—FS-I4Y	2013	0.005	-0.001	-0.001	0.033	0.066	0.000	-0.005
[°]	2014	0.005	0.005	0.004	0.038	0.056	0.005	0.000
	2015	0.005	0.004	0.008	0.041	0.061	0.003	0.003
	2016	0.006	-0.001	0.010	0.043	0.051	0.002	0.005

Inclinometer 5 - X Direction- without Drops

Mean Daily Value

Daily Amplitude

Progressive Daily Residuals on the Mean Value

Absolute Daily Residuals on the Mean Value

Annual Amplitude

Progressive Annual Residuals of the Mean Value

Absolute Annual Residuals of the Mean Value
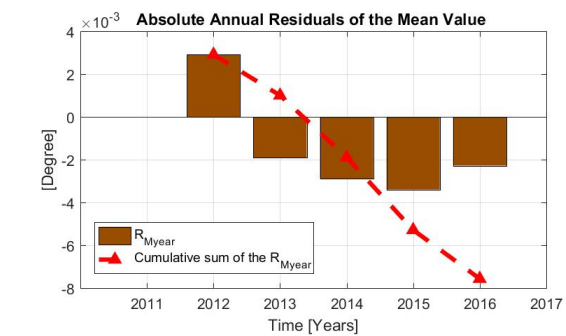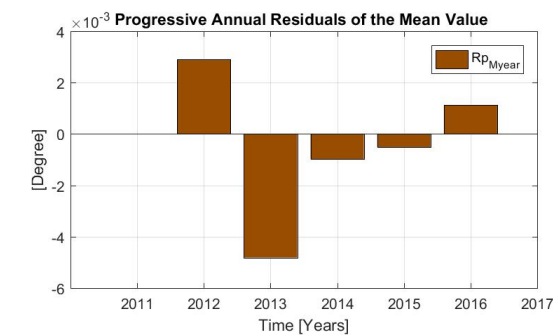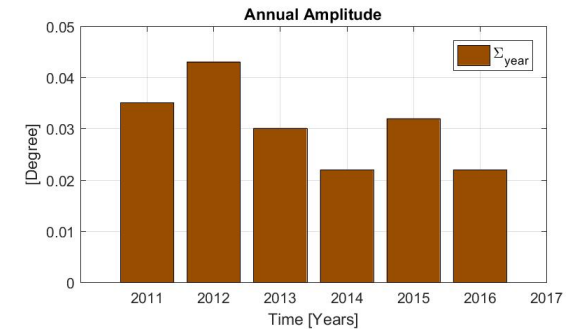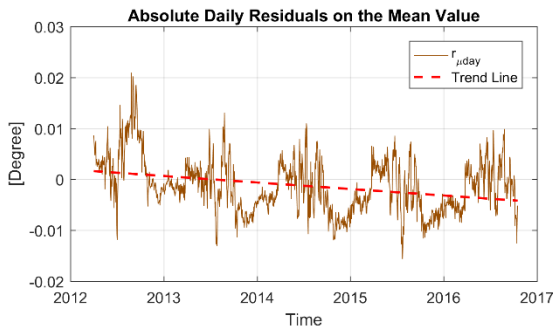
Sensor	Year	$\delta_{day,j}$	$\mathrm{rp}_{\mu day}$	$\mathrm{r}_{\mu day}$	M_{year}	Σ_{year}	Rp_{Myear}	R_{Myear}
	2011	0.0076			-0.0375	0.0401		0.0000
	2012	0.0060	0.0038	0.0038	-0.0346	0.0440	0.0029	0.0029
G—FE-I5X	2013	0.0061	-0.0048	-0.0018	-0.0394	0.0311	-0.0048	-0.0019
[°]	2014	0.0070	-0.0011	-0.0028	-0.0404	0.0239	-0.0010	-0.0029
	2015	0.0077	-0.0002	-0.0030	-0.0412	0.0340	-0.0008	-0.0037
	2016	0.0085	0.0004	-0.0027	-0.0400	0.0240	0.0012	-0.0025

Sensor	Year	$\delta_{day,j}$	rp$_{\mu day}$	r$_{\mu day}$	M_{year}	Σ_{year}	Rp$_{Myear}$	R_{Myear}
G—FS-I5Y [°]	2011	0.005			0.106	0.022		0.000
	2012	0.005	0.008	0.008	0.112	0.029	0.006	0.006
	2013	0.006	-0.003	0.004	0.110	0.028	-0.003	0.004
	2014	0.006	0.001	0.005	0.111	0.026	0.001	0.005
	2015	0.006	-0.001	0.005	0.110	0.030	-0.001	0.004
	2016	0.007	0.002	0.007	0.113	0.031	0.003	0.007

Inclinometer 6 - X Direction-without Drops

Mean Daily Value

Daily Amplitude

Progressive Daily Residuals on the Mean Value

Absolute Daily Residuals on the Mean Value

Annual Amplitude

Progressive Annual Residuals of the Mean Value

Absolute Annual Residuals of the Mean Value
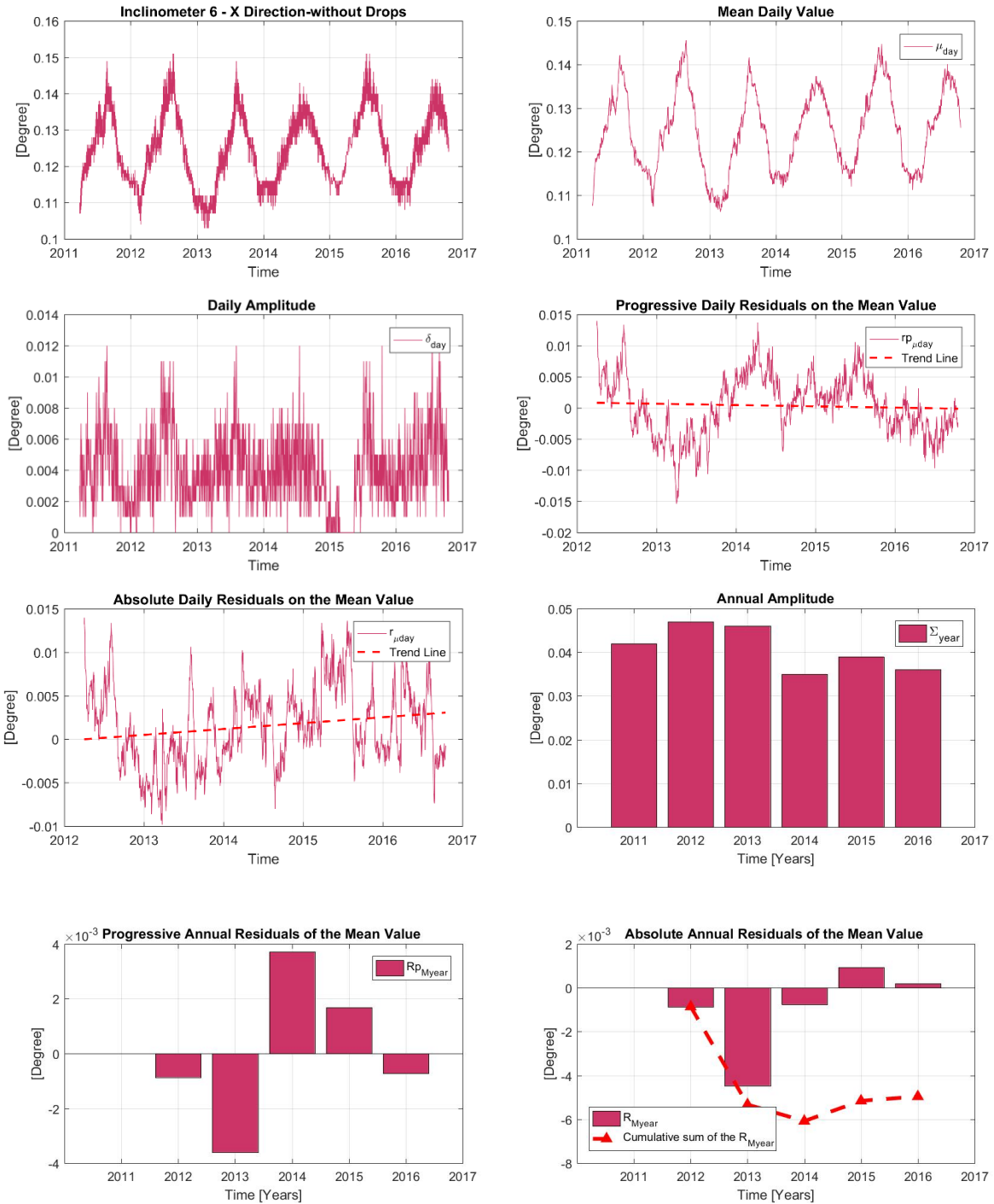
Sensor	Year	$\delta_{day,j}$	$\text{rp}_{\mu day}$	$\text{r}_{\mu day}$	M_{year}	Σ_{year}	Rp_{Myear}	R_{Myear}
G—FE-I6X [°]	2011	0.0057			0.1257	0.0440		0.0000
	2012	0.0058	0.0021	0.0021	0.1248	0.0490	-0.0009	-0.0009
	2013	0.0057	-0.0038	-0.0021	0.1212	0.0470	-0.0036	-0.0045
	2014	0.0056	0.0039	0.0018	0.1249	0.0360	0.0037	-0.0008
	2015	0.0045	0.0022	0.0040	0.1261	0.0390	0.0012	0.0004
	2016	0.0066	-0.0025	0.0015	0.1255	0.0380	-0.0006	-0.0002
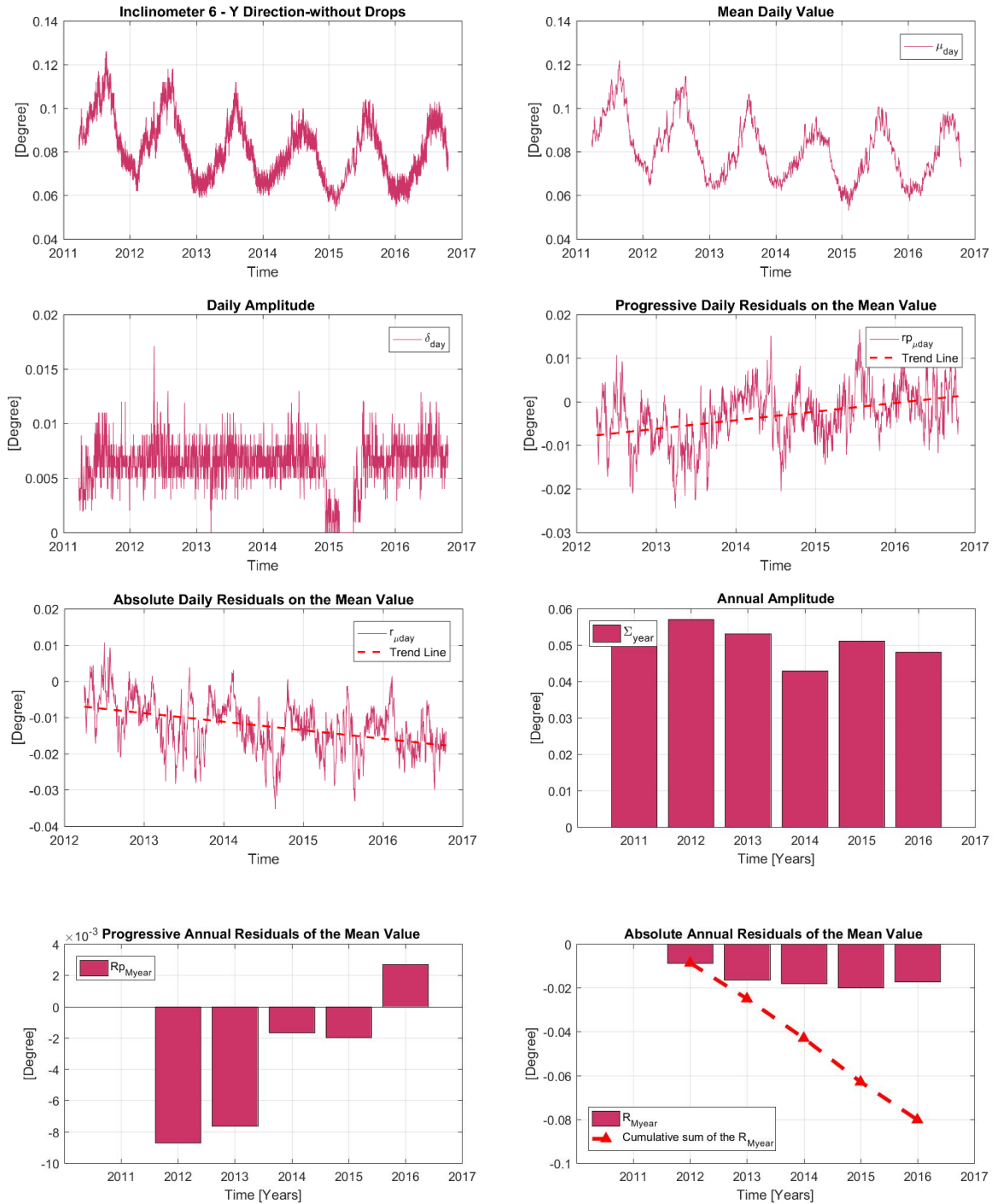
Sensor	Year	$\delta_{day,j}$	$rp_{\mu day}$	$r_{\mu day}$	M_{year}	Σ_{year}	Rp_{Myear}	R_{Myear}
	2011	0.006			0.095	0.055		0.000
	2012	0.007	-0.005	-0.005	0.086	0.057	-0.009	-0.009
G—FE-I6Y	2013	0.007	-0.008	-0.012	0.079	0.053	-0.008	-0.016
[°]	2014	0.006	-0.002	-0.013	0.077	0.043	-0.002	-0.018
	2015	0.004	-0.002	-0.015	0.075	0.051	-0.002	-0.020
	2016	0.007	0.001	-0.015	0.078	0.048	0.003	-0.017

B.2 Signal frequency analyses

The main periodicity of the data recorded has been obtained through a frequency analysis of the signal using a Fourier analysis. The frequency analysis has been applied to data obtained by the instruments, which have not presented malfunction, interruptions and / or many drops. In this case, some of the Long base deformeters, the extensimeter and the inclinometers. In more detail, for each of these typologies of instruments the following plots are reported:

- recorded signal by the sensor and its main components (the periodical component and the residual)
- the Fourier Transform
- the residue as obtained from the FFT and from the mathematical considerations (reference quantities)

Long Base Deformeter F3

ExtensimeterE2
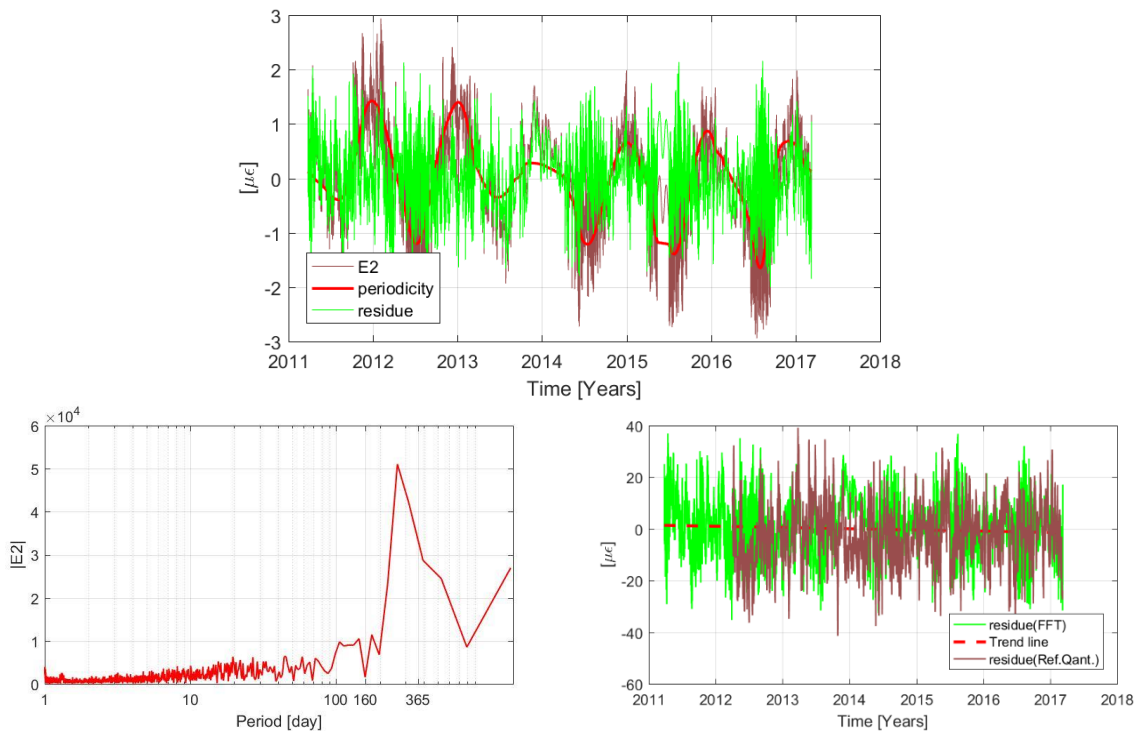
Inclinometer I2-Y
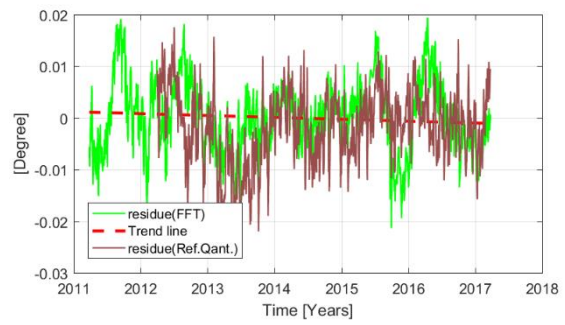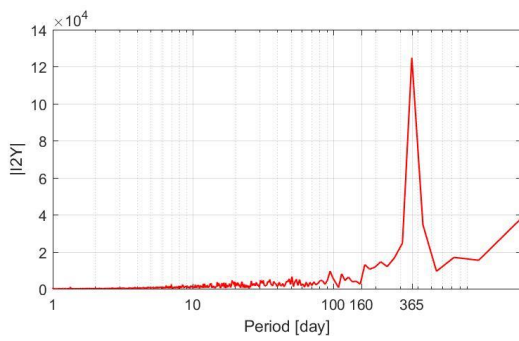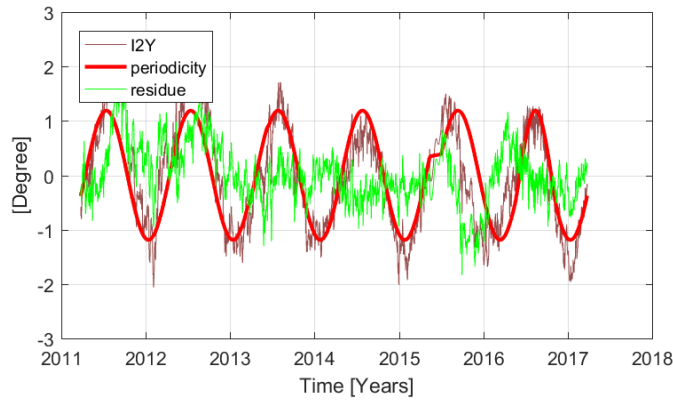
Inclinometer I5-Y
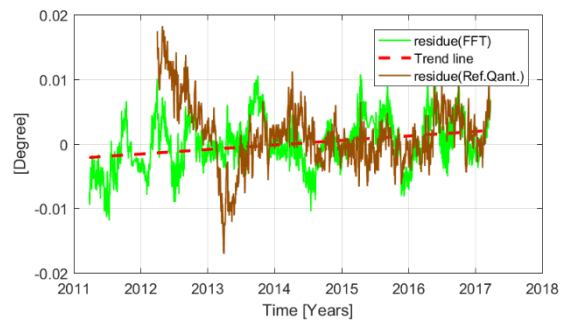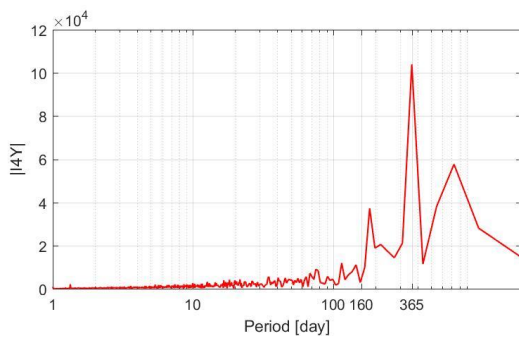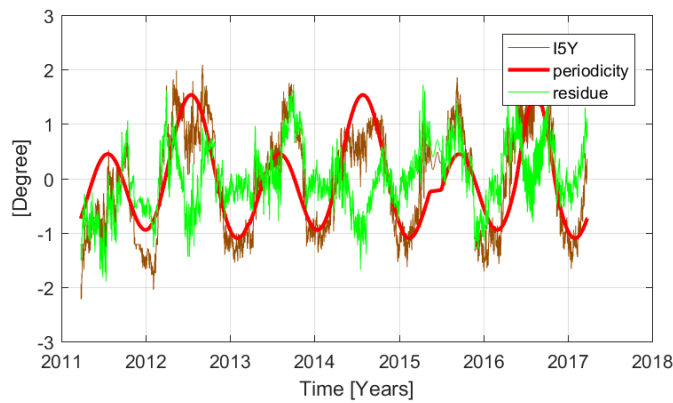
Inclinometer I6-X
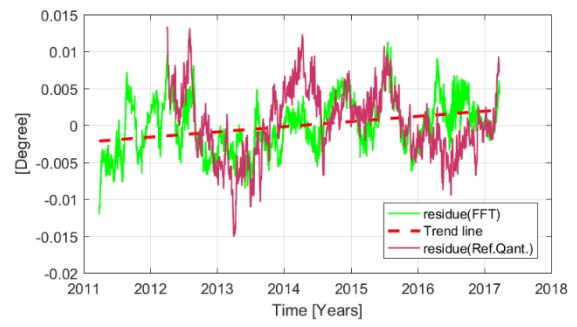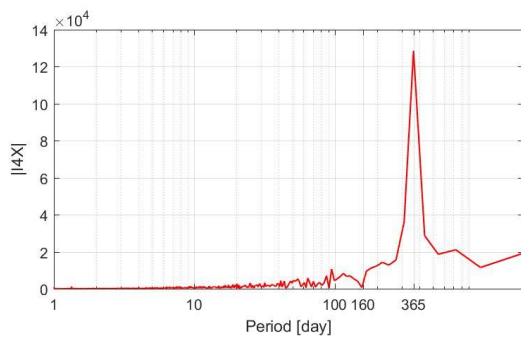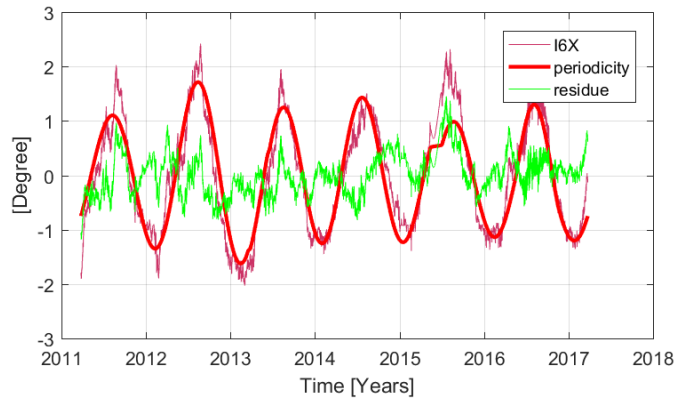
APPENDIX C

Data analyses for the Cathedral of Modena

C.1 Reference quantities

The systematic identification of the reference quantities is here provided for each instrument installed on the Cathedral of Modena .

In more detail, for each instrument the following plots are reported:

- row-data recorded by the sensor over the entire monitoring period (2011-2016)
- the mean daily value
- the daily amplitude
- progressive daily residual on the mean value
- absolute daily residual on the mean value
- the annual amplitude
- progressive annual residual on the mean value
- absolute annual residual on the mean value

The table collects the mean values for each years of these reference quantities.

It is noted that the deformeters and the inclinometers have recorded many spike and missing data throughout the monitoring period therefore are not considered in the analyses.

Biaxial joint meter MGB1-X component
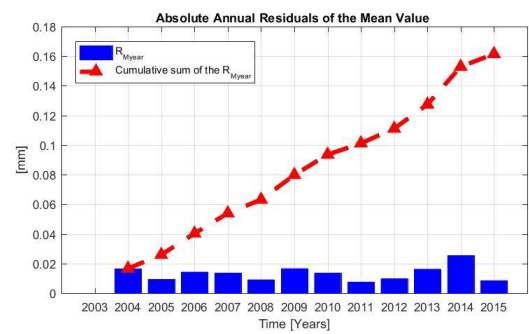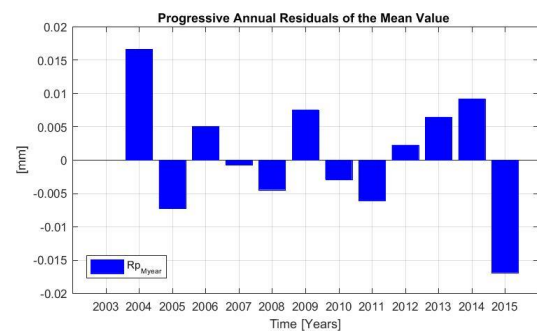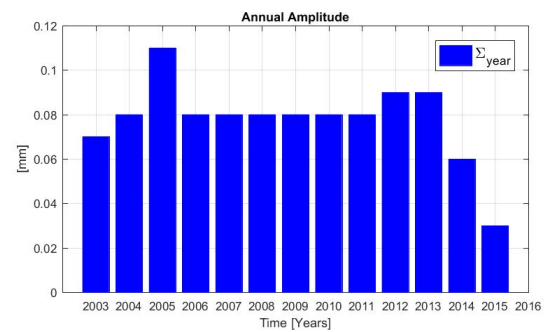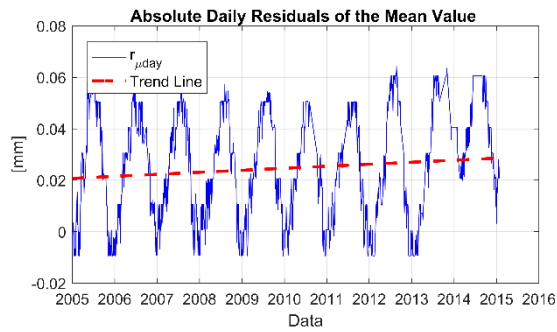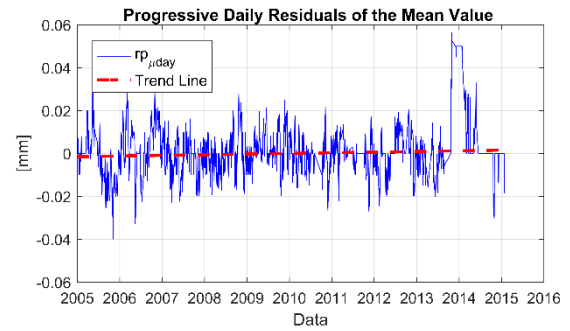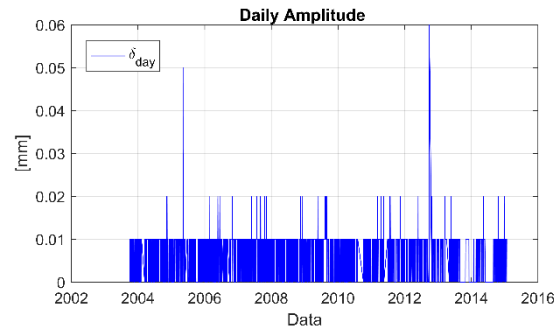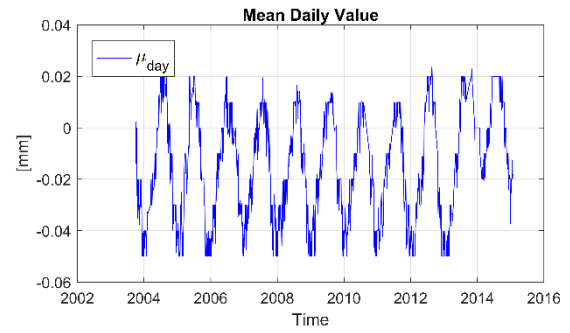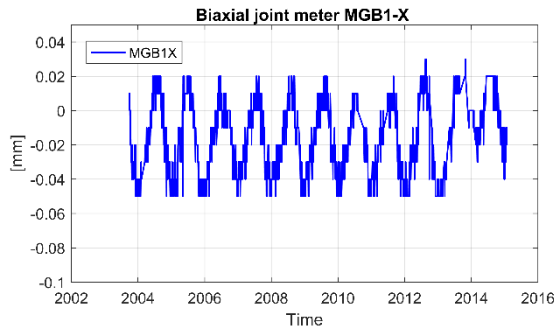
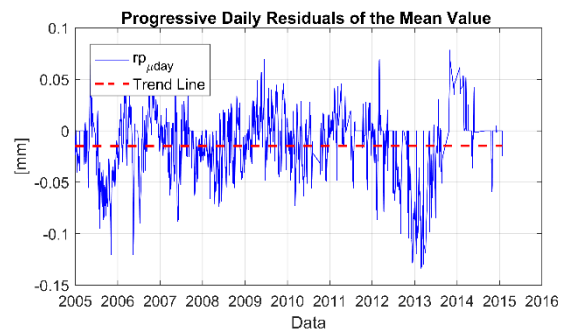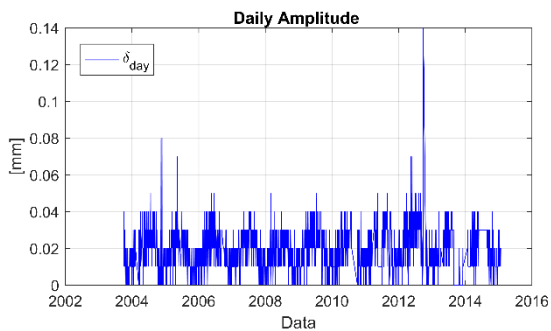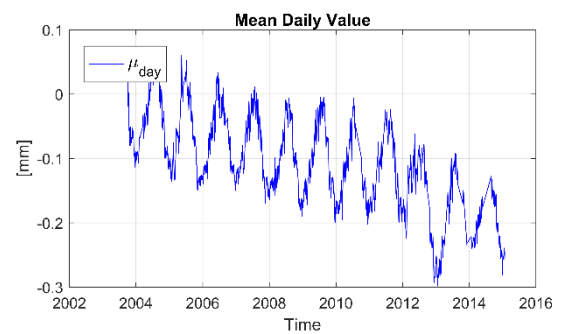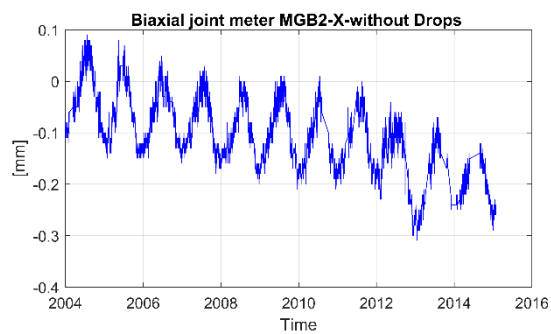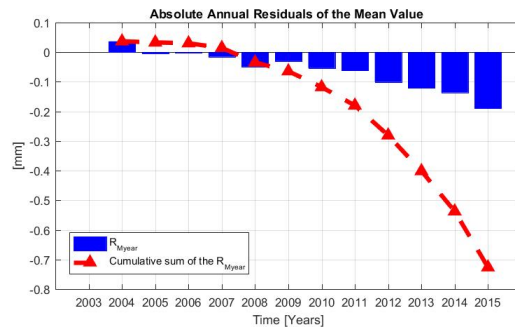| Sensor	Year	$\delta_{day,j}$	$rp_{\mu day}$	$r_{\mu day}$	M_{year}	Σ_{year}	Rp_{Myear}	R_{Myear}
MGB1-X [mm]	2004	0.006			-0.013	0.080	0.017	0.017
	2005	0.006	-0.004	0.020	-0.020	0.110	-0.007	0.009
	2006	0.006	0.004	0.025	-0.015	0.080	0.005	0.014
	2007	0.007	-0.002	0.024	-0.016	0.080	-0.001	0.014
	2008	0.005	-0.001	0.023	-0.021	0.080	-0.004	0.009
	2009	0.007	0.003	0.026	-0.013	0.080	0.008	0.017
	2010	0.005	-0.002	0.020	-0.016	0.080	-0.003	0.014
	2011	0.007	0.000	0.021	-0.022	0.080	-0.006	0.008
	2012	0.006	0.000	0.023	-0.020	0.080	0.002	0.010
	2013	0.006	-0.001	0.027	-0.013	0.090	0.006	0.016
	2014	0.006	0.005	0.036	-0.004	0.060	0.009	0.026
	2015	0.008	-0.001	0.019	-0.021	0.030	-0.017	0.009

*Biaxial joint meter MGB1-Y component*
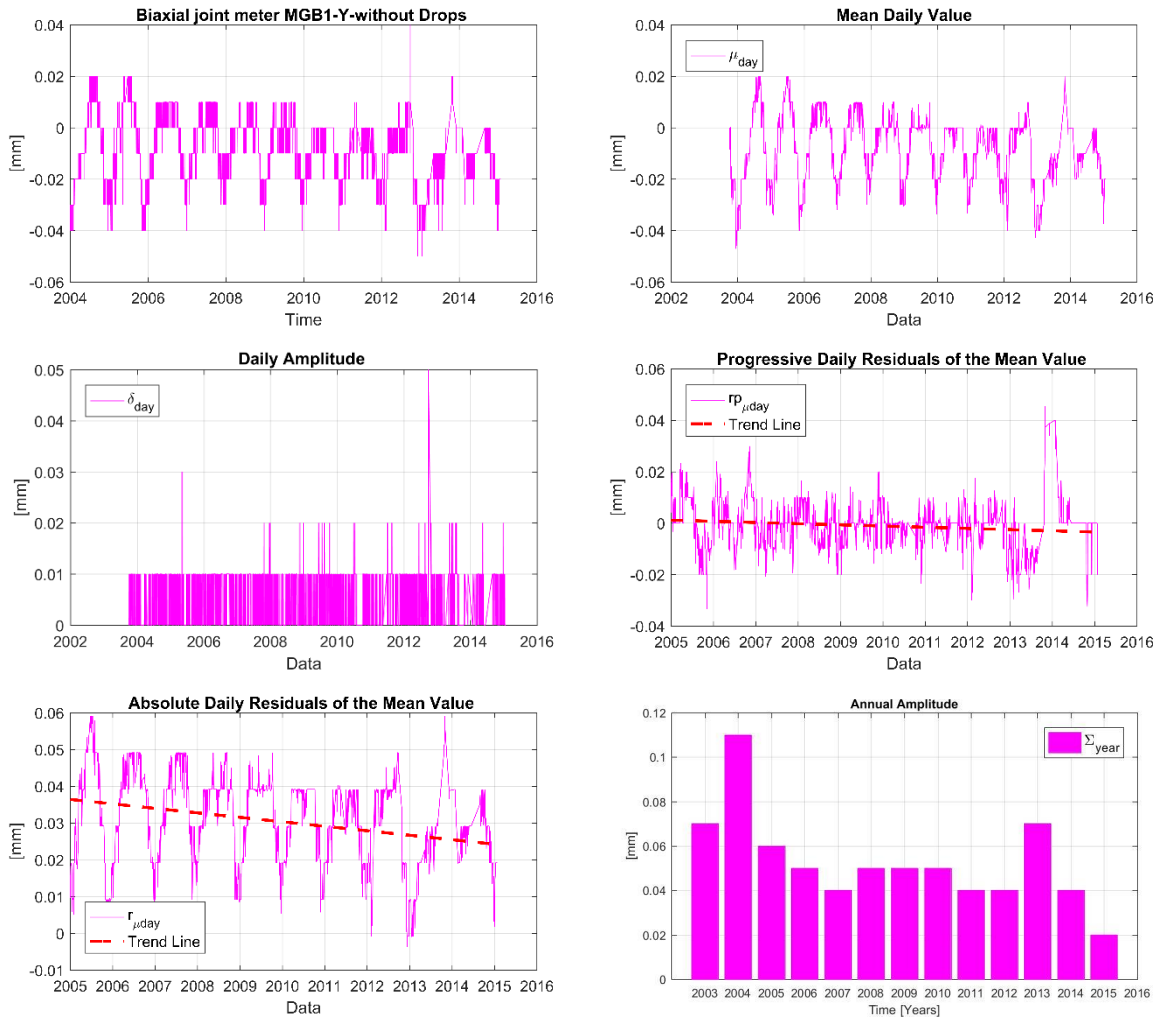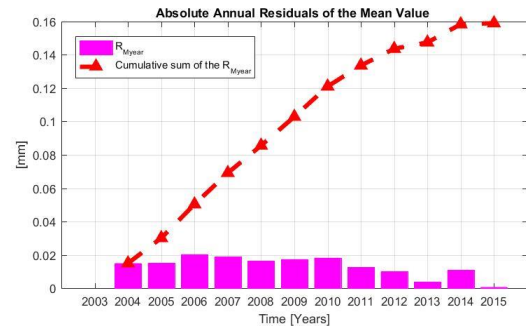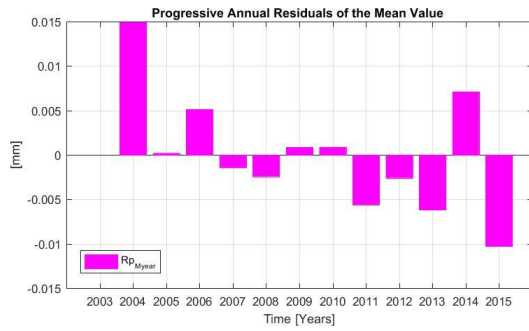
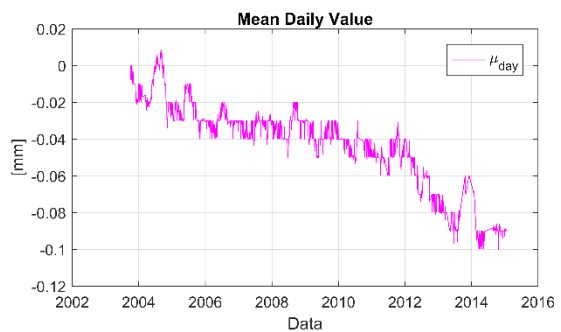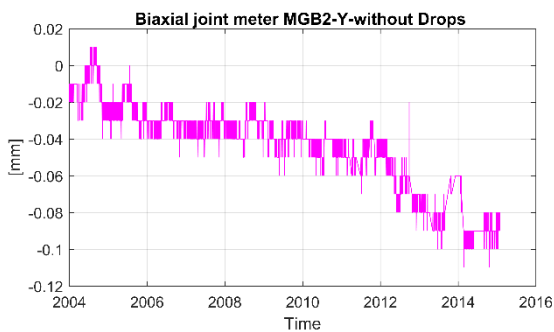| Sensor	Year	$\delta_{day,j}$	$rp_{\mu day}$	$r_{\mu day}$	M_{year}	Σ_{year}	Rp_{Myear}	R_{Myear}
	2004	0.004			-0.008	0.110	0.015	0.015
	2005	0.004	0.000	0.031	-0.008	0.060	0.000	0.015
	2006	0.005	0.005	0.036	-0.003	0.050	0.005	0.020
	2007	0.005	-0.002	0.035	-0.004	0.040	-0.001	0.019
	2008	0.004	-0.001	0.034	-0.007	0.050	-0.002	0.016
MGB1-Y	2009	0.004	-0.001	0.033	-0.006	0.050	0.001	0.017
[mm]	2010	0.004	-0.002	0.029	-0.005	0.050	0.001	0.018
	2011	0.006	0.000	0.029	-0.011	0.040	-0.006	0.013
	2012	0.005	-0.002	0.028	-0.013	0.050	-0.003	0.010
	2013	0.007	-0.010	0.020	-0.019	0.070	-0.006	0.004
	2014	0.006	0.002	0.027	-0.012	0.040	0.007	0.011
	2015	0.003	-0.001	0.017	-0.023	0.020	-0.010	0.001

*Biaxial joint meter MGB2-X component*
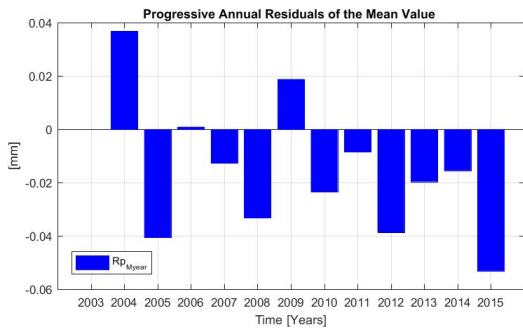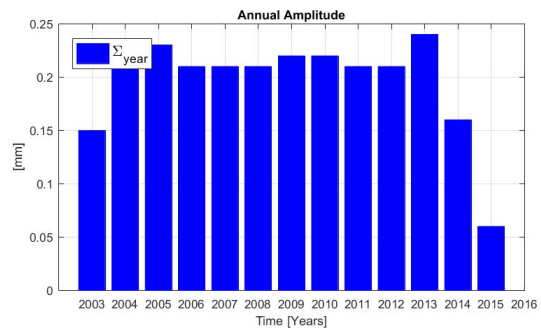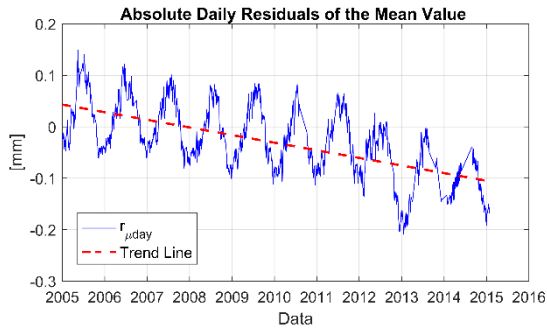
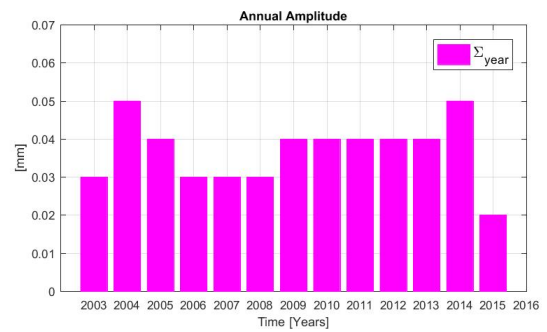| Sensor	Year	$\delta_{day,j}$	$\text{rp}_{\mu day}$	$\text{r}_{\mu day}$	M_{year}	Σ_{year}	Rp_{Myear}	R_{Myear}
	2004	0.020			-0.027	0.210	0.037	0.037
	2005	0.017	-0.030	0.021	-0.068	0.230	-0.041	-0.004
	2006	0.019	-0.002	0.022	-0.067	0.210	0.001	-0.003
	2007	0.019	-0.015	0.009	-0.079	0.210	-0.013	-0.016
	2008	0.017	-0.022	-0.013	-0.113	0.210	-0.033	-0.049
MGB2-X	2009	0.021	0.005	-0.007	-0.094	0.220	0.019	-0.030
[mm]	2010	0.019	-0.016	-0.035	-0.118	0.220	-0.024	-0.054
	2011	0.022	0.000	-0.032	-0.126	0.210	-0.008	-0.062
	2012	0.024	-0.030	-0.067	-0.165	0.220	-0.039	-0.101
	2013	0.021	-0.046	-0.097	-0.184	0.240	-0.020	-0.120
	2014	0.019	0.003	-0.112	-0.200	0.160	-0.015	-0.136
	2015	0.017	-0.001	-0.164	-0.253	0.060	-0.053	-0.189

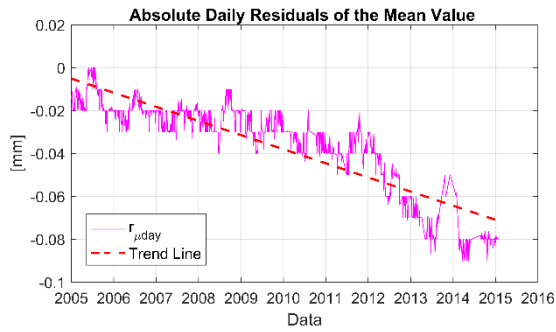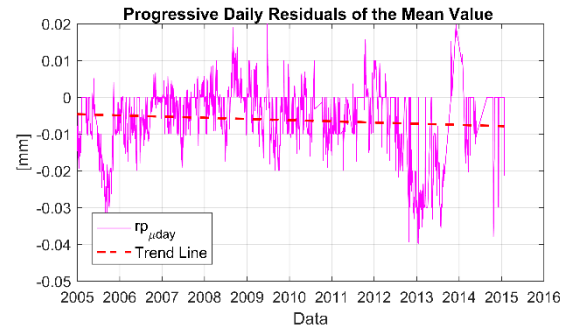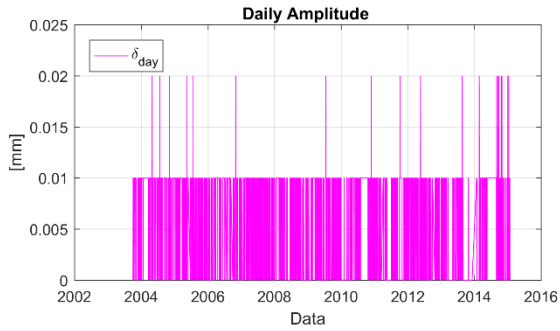*Biaxial joint meter MGB2-Y component*
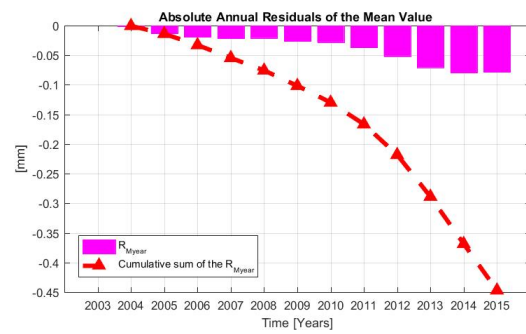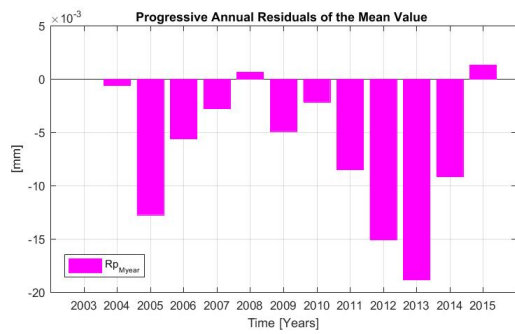
Sensor	Year	$\delta_{day,j}$	$rp_{\mu day}$	$r_{\mu day}$	M_{year}	Σ_{year}	Rp_{Myear}	R_{Myear}
MGB2-Y [mm]	2004	0.007			-0.012	0.050	-0.001	-0.001
	2005	0.006	-0.011	-0.015	-0.025	0.040	-0.013	-0.013
	2006	0.006	-0.005	-0.020	-0.030	0.030	-0.006	-0.019
	2007	0.005	-0.003	-0.023	-0.033	0.030	-0.003	-0.022
	2008	0.005	0.000	-0.023	-0.032	0.030	0.001	-0.021
	2009	0.005	-0.004	-0.027	-0.037	0.040	-0.005	-0.026
	2010	0.005	-0.006	-0.034	-0.040	0.040	-0.002	-0.028
	2011	0.005	-0.004	-0.038	-0.048	0.040	-0.008	-0.037
	2012	0.005	-0.008	-0.051	-0.063	0.040	-0.015	-0.052
	2013	0.005	-0.022	-0.072	-0.082	0.040	-0.019	-0.071
	2014	0.006	-0.004	-0.081	-0.091	0.050	-0.009	-0.080
	2015	0.005	-0.001	-0.080	-0.090	0.020	0.001	-0.078

Biaxial joint meter MGB3-X component
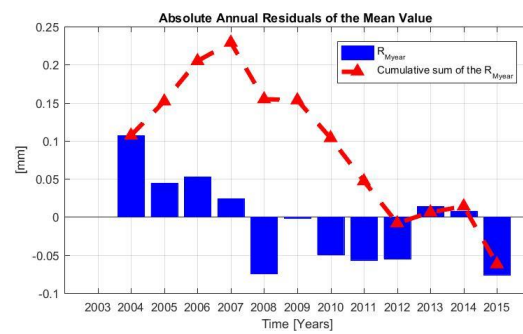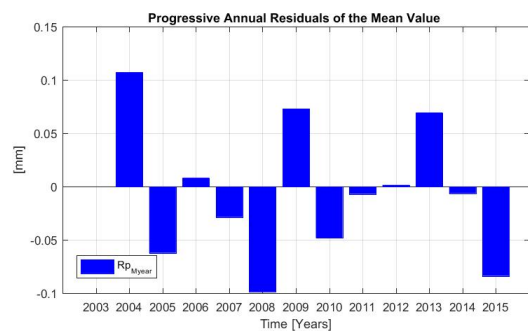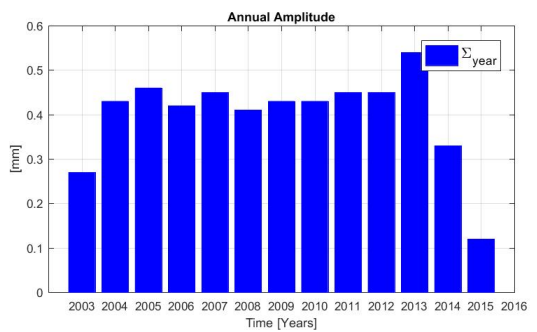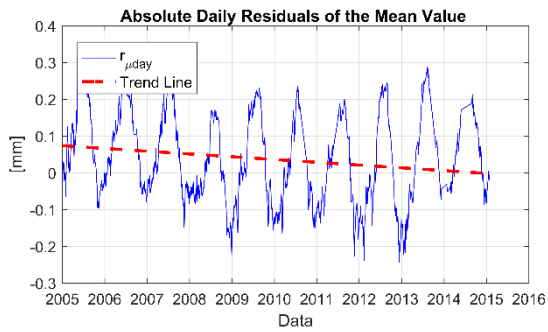
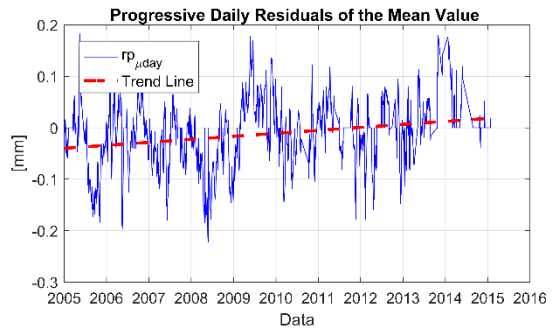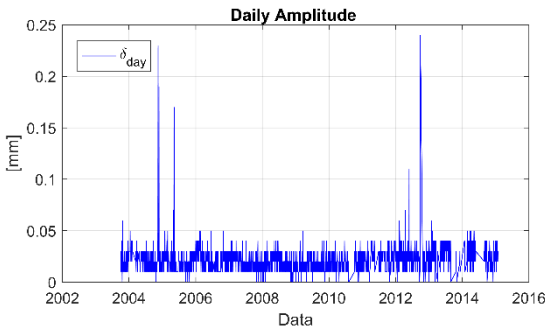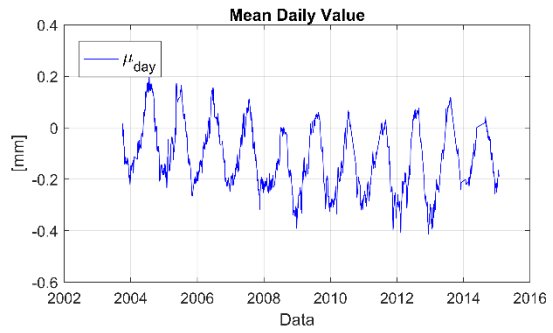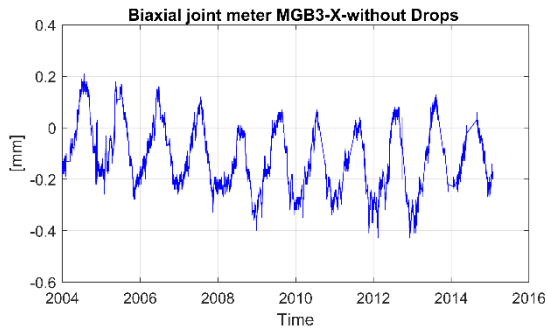| Sensor	Year	$\delta_{day,j}$	$rp_{\mu day}$	$r_{\mu day}$	M_{year}	Σ_{year}	Rp_{Myear}	R_{Myear}
MGB3-X [mm]	2004	0.022			-0.017	0.430	0.107	0.107
	2005	0.022	-0.045	0.091	-0.079	0.460	-0.062	0.045
	2006	0.022	-0.001	0.099	-0.071	0.420	0.008	0.053
	2007	0.019	-0.033	0.070	-0.100	0.450	-0.029	0.024
	2008	0.019	-0.075	-0.006	-0.198	0.410	-0.099	-0.074
	2009	0.017	0.041	0.038	-0.125	0.430	0.073	-0.001
	2010	0.019	-0.022	-0.013	-0.174	0.430	-0.048	-0.050
	2011	0.023	0.004	0.000	-0.181	0.450	-0.007	-0.057
	2012	0.025	-0.008	0.001	-0.179	0.430	0.001	-0.055
	2013	0.029	0.017	0.056	-0.110	0.540	0.069	0.014
	2014	0.026	0.018	0.051	-0.116	0.330	-0.006	0.008
	2015	0.027	0.001	-0.030	-0.200	0.120	-0.084	-0.076

Biaxial joint meter MGB3-Y component
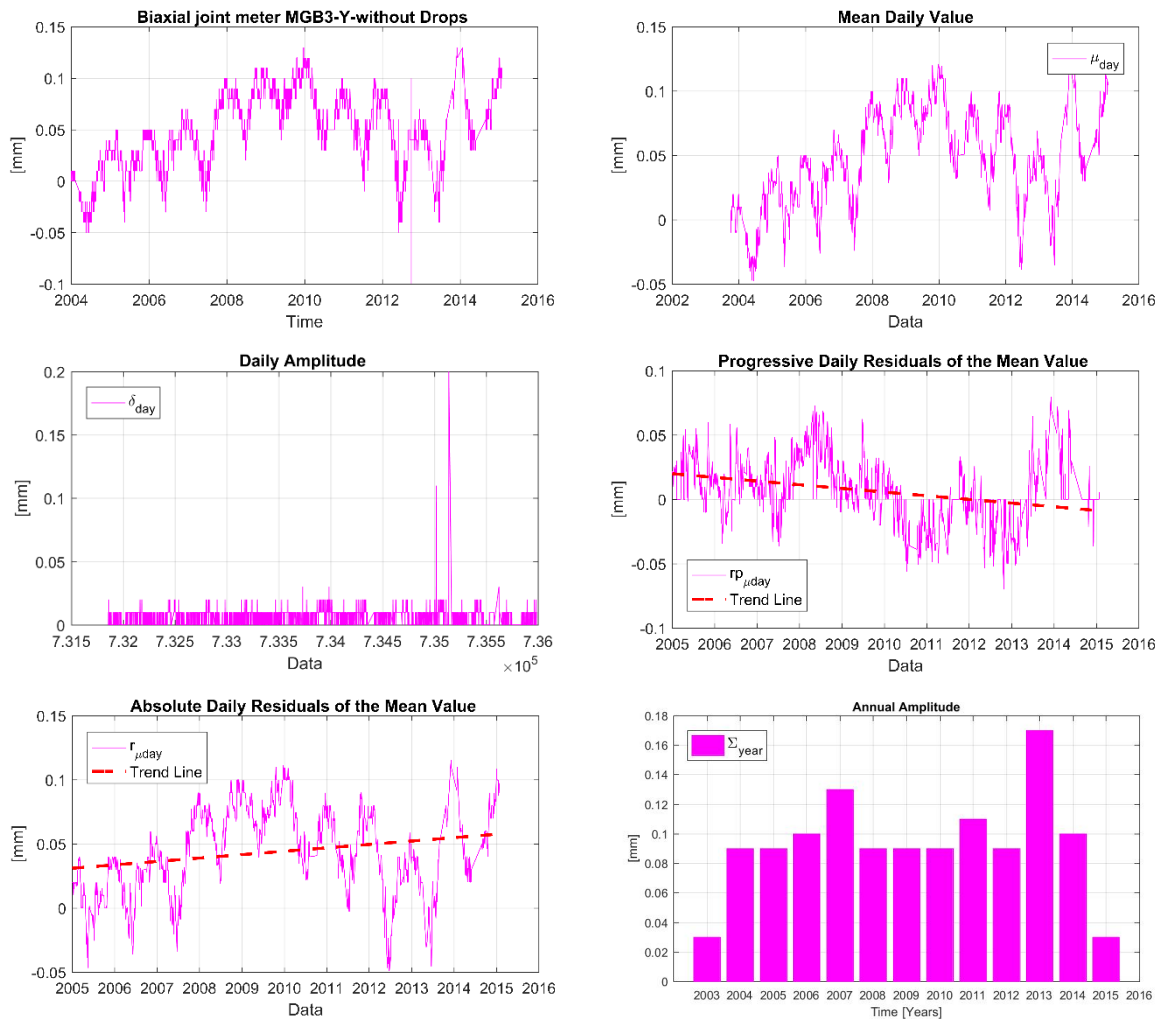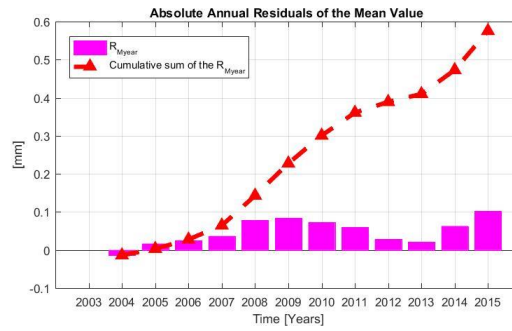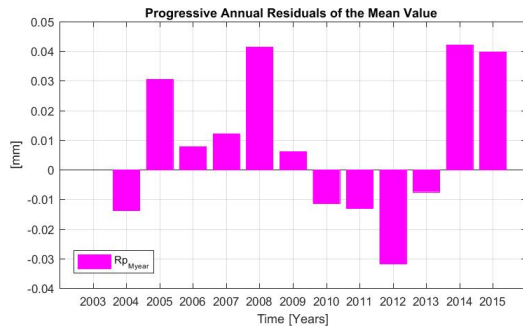
Sensor	Year	$\delta_{day,j}$	$\mathrm{rp}_{\mu day}$	$\mathrm{r}_{\mu day}$	M_{year}	Σ_{year}	Rp_{Myear}	R_{Myear}
	2004	0.006			-0.009	0.090	-0.014	-0.014
	2005	0.006	0.018	0.012	0.022	0.090	0.031	0.017
	2006	0.006	0.010	0.020	0.030	0.100	0.008	0.025
	2007	0.006	0.010	0.032	0.042	0.130	0.012	0.037
	2008	0.006	0.037	0.068	0.083	0.090	0.041	0.078
MGB3-Y	2009	0.008	0.009	0.078	0.090	0.090	0.006	0.084
[mm]	2010	0.008	-0.013	0.065	0.078	0.090	-0.011	0.073
	2011	0.007	-0.010	0.053	0.065	0.110	-0.013	0.060
	2012	0.008	-0.014	0.023	0.033	0.090	-0.032	0.028
	2013	0.008	-0.001	0.017	0.026	0.170	-0.007	0.021
	2014	0.007	0.011	0.057	0.068	0.100	0.042	0.063
	2015	0.008	0.000	0.098	0.108	0.030	0.040	0.103

*Biaxial joint meter MGB4-X component*
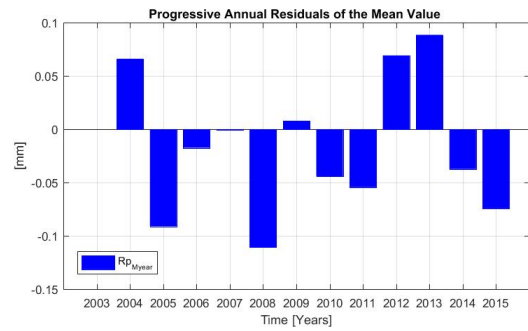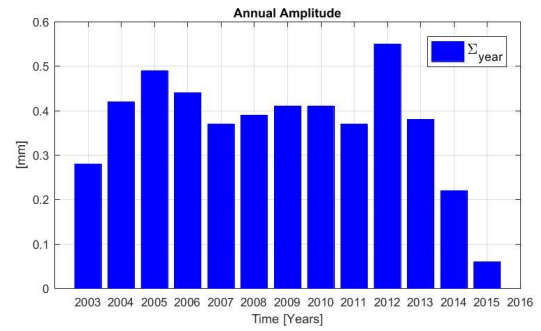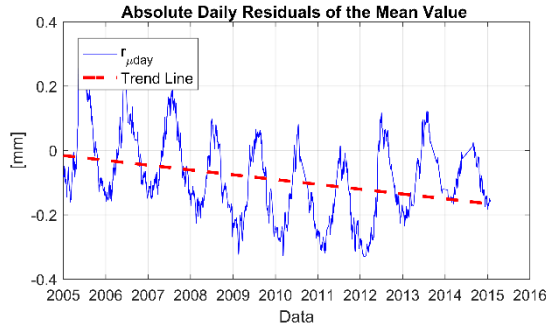
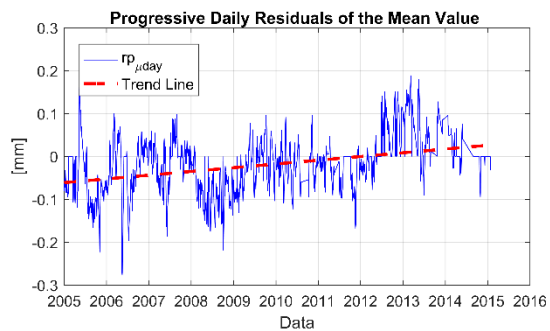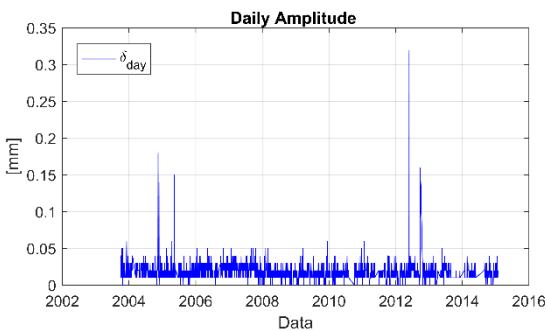| Sensor	Year	$\delta_{day,j}$	$rp_{\mu day}$	$r_{\mu day}$	M_{year}	Σ_{year}	Rp_{Myear}	R_{Myear}
	2004	0.021			-0.070	0.420	0.066	0.066
	2005	0.018	-0.063	0.010	-0.162	0.490	-0.091	-0.025
	2006	0.021	-0.023	-0.008	-0.179	0.440	-0.017	-0.043
	2007	0.022	-0.009	-0.009	-0.180	0.370	-0.001	-0.043
	2008	0.016	-0.088	-0.098	-0.290	0.390	-0.111	-0.154
MGB4-X	2009	0.016	-0.022	-0.121	-0.283	0.410	0.008	-0.146
[mm]	2010	0.016	-0.020	-0.166	-0.327	0.410	-0.044	-0.190
	2011	0.018	-0.031	-0.197	-0.381	0.370	-0.054	-0.245
	2012	0.019	0.028	-0.141	-0.312	0.550	0.069	-0.175
	2013	0.018	0.063	-0.056	-0.223	0.380	0.088	-0.087
	2014	0.017	0.003	-0.091	-0.261	0.220	-0.037	-0.124
	2015	0.018	-0.001	-0.164	-0.335	0.060	-0.074	-0.199

Biaxial joint meter MGB4-Y component
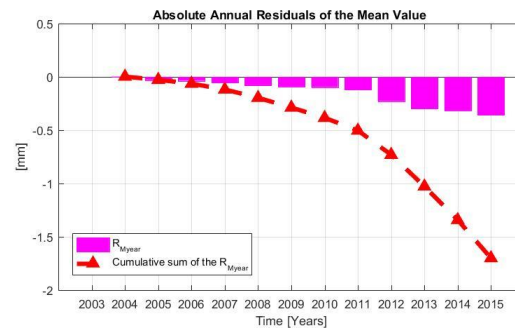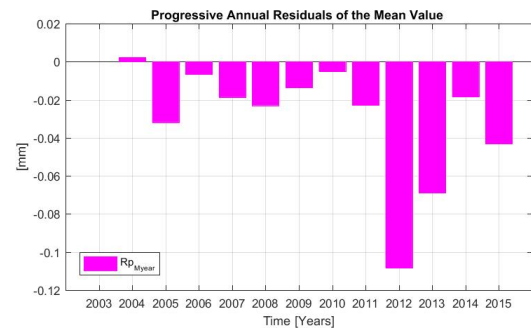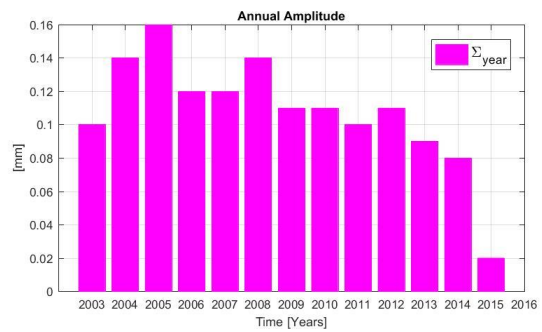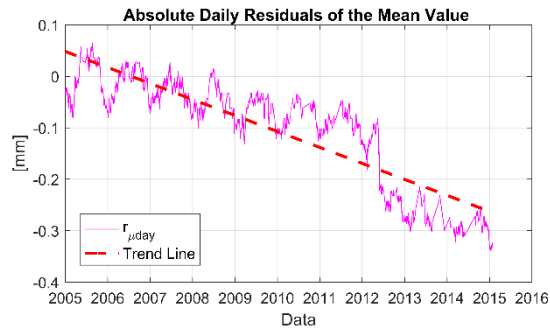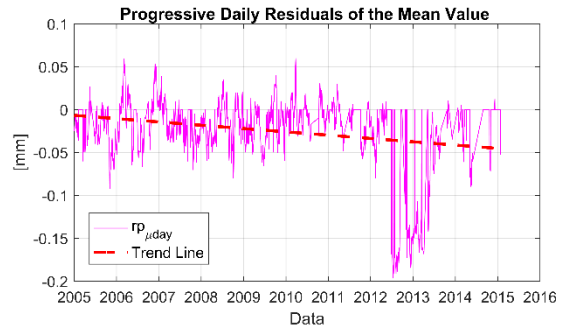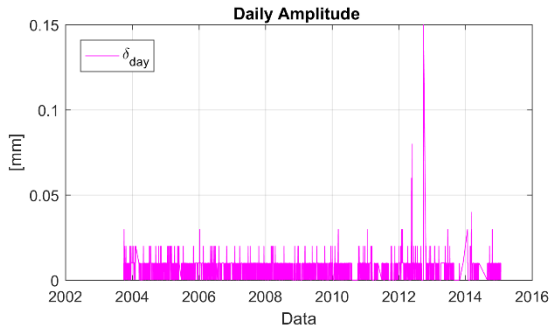
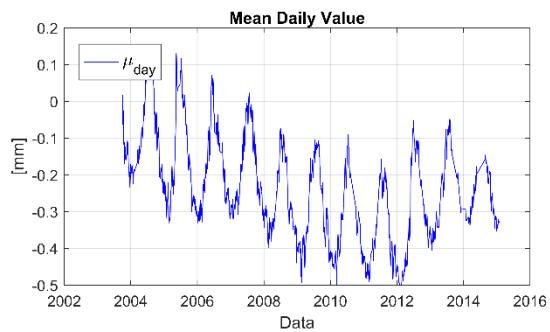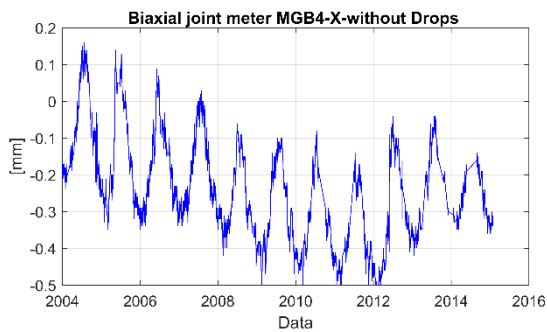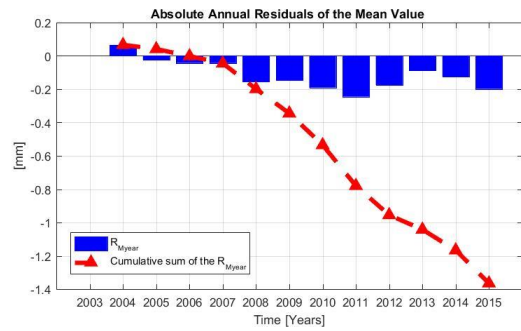| Sensor	Year	$\delta_{day,j}$	$\mathrm{rp}_{\mu day}$	$\mathrm{r}_{\mu day}$	M_{year}	Σ_{year}	Rp_{Myear}	R_{Myear}
	2004	0.007			-0.030	0.140	0.002	0.002
	2005	0.007	-0.023	-0.004	-0.062	0.160	-0.032	-0.030
	2006	0.007	-0.005	-0.011	-0.069	0.120	-0.007	-0.036
	2007	0.007	-0.017	-0.030	-0.087	0.120	-0.019	-0.055
	2008	0.006	-0.017	-0.047	-0.110	0.140	-0.023	-0.078
MGB4-Y	2009	0.006	-0.020	-0.068	-0.124	0.110	-0.014	-0.091
[mm]	2010	0.007	-0.004	-0.076	-0.129	0.110	-0.005	-0.096
	2011	0.006	-0.011	-0.092	-0.152	0.100	-0.023	-0.119
	2012	0.009	-0.075	-0.194	-0.260	0.110	-0.108	-0.228
	2013	0.007	-0.080	-0.271	-0.329	0.090	-0.069	-0.296
	2014	0.007	-0.013	-0.290	-0.347	0.080	-0.018	-0.315
	2015	0.008	-0.002	-0.333	-0.390	0.020	-0.043	-0.358

Biaxial joint meter MGB5-X component

Sensor	Year	$\delta_{day,j}$	$\mathrm{rp}_{\mu day}$	$\mathfrak{r}_{\mu day}$	M_{year}	Σ_{year}	Rp_{Myear}	R_{Myear}
	2010	0.023			0.176	3.390		0.000
	2011	0.081			0.091	0.500	-0.085	-0.085
MGB5-X	2012	0.078	-0.020	0.000	0.043	0.500	-0.048	-0.133
[mm]	2013	0.070	-0.159	-0.156	-0.097	0.360	-0.140	-0.273
	2014	0.063	0.019	-0.123	-0.069	0.340	0.028	-0.245
	2015	0.040	-0.002	-0.139	-0.080	0.130	-0.011	-0.256

Biaxial joint meter MGB5-Y component
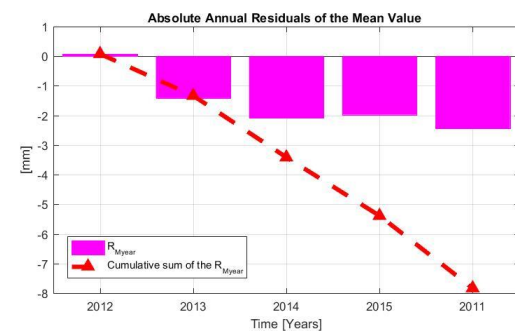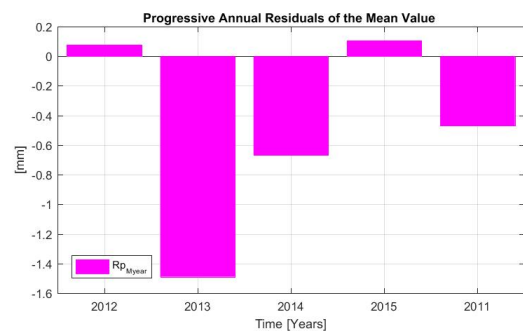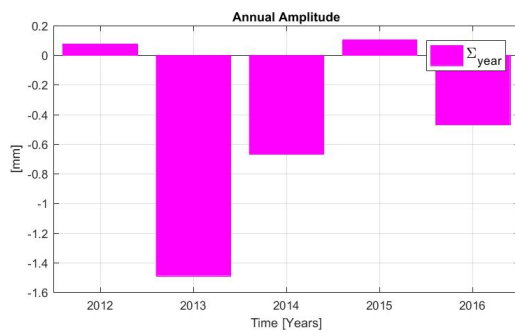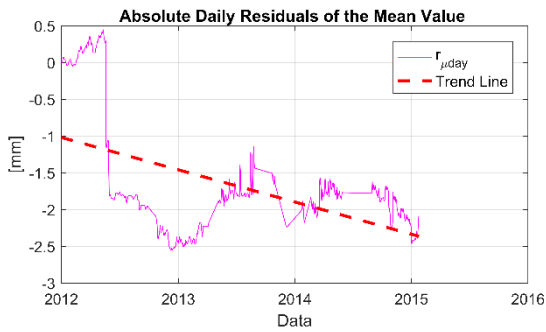
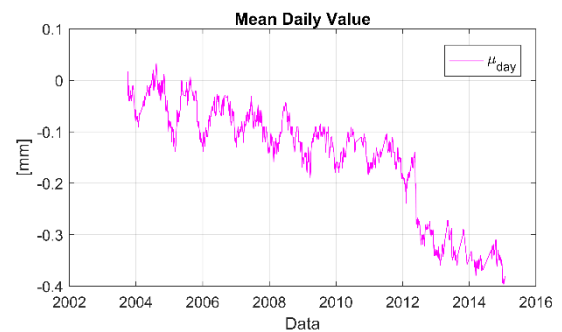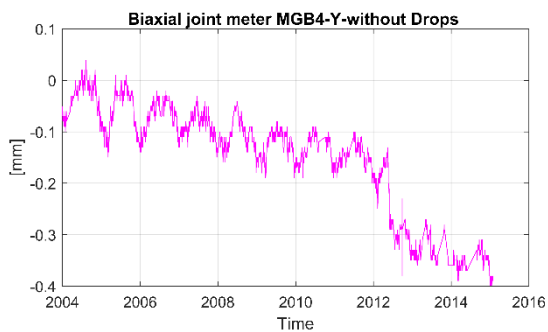| Sensor	Year	$\delta_{day,j}$	$\mathrm{rp}_{\mu day}$	$\mathrm{r}_{\mu day}$	M_{year}	Σ_{year}	Rp_{Myear}	R_{Myear}
MGB5-Y [mm]	2010	0.060			0.352			0.000
	2011	0.080			0.429	0.940	0.077	0.077
	2012	0.064	-0.929	-1.171	-1.060	1.4	-1.489	-1.412
	2013	0.091	-0.941	-1.997	-1.728	0.61	-0.668	-2.080
	2014	0.134	0.048	-1.886	-1.622	0.940	0.106	-1.974
	2015	0.083	-0.004	-2.369	-2.092	0.480	-0.470	-2.444

Triaxial joint meter MGT1-X component
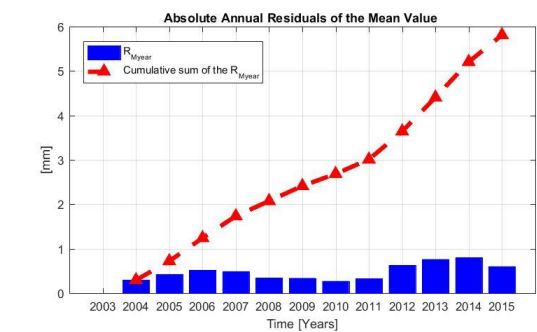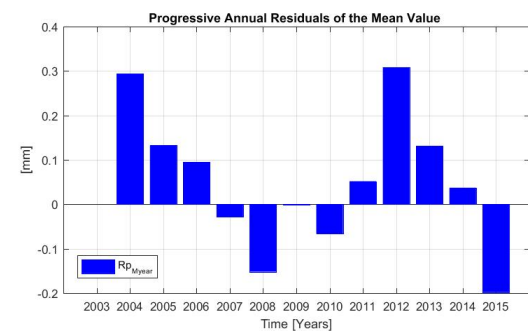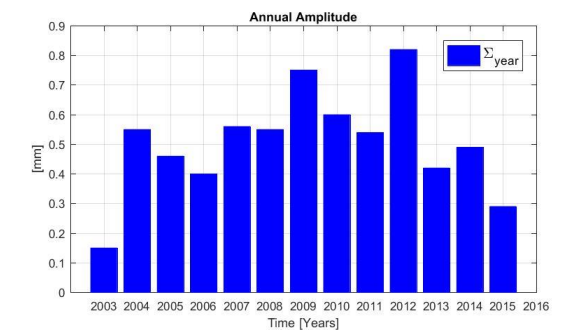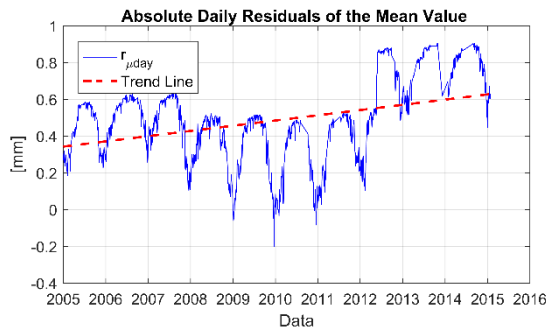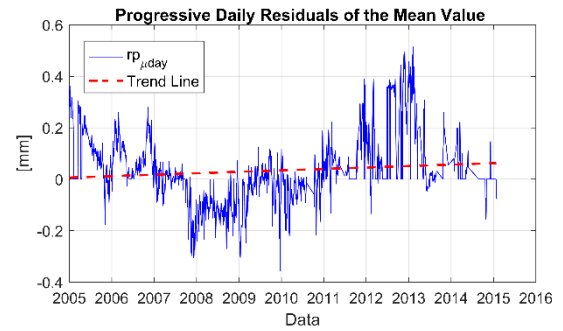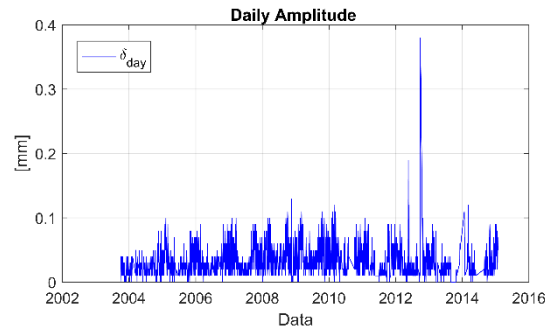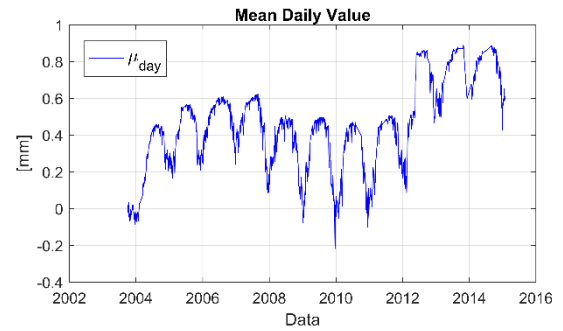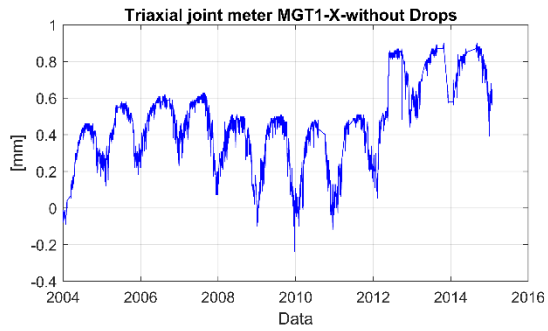
Sensor	Year	$\delta_{day,j}$	$\mathrm{rp}_{\mu day}$	$\mathrm{r}_{\mu day}$	M_{year}	Σ_{year}	Rp_{Myear}	R_{Myear}
MGT1-X [mm]	2004	0.024			0.272	0.550	0.294	0.294
	2005	0.030	0.107	0.423	0.404	0.460	0.133	0.426
	2006	0.030	0.095	0.518	0.499	0.400	0.095	0.521
	2007	0.035	-0.033	0.489	0.470	0.560	-0.029	0.492
	2008	0.038	-0.117	0.369	0.319	0.550	-0.152	0.340
	2009	0.041	-0.038	0.334	0.317	0.750	-0.002	0.339
	2010	0.038	-0.039	0.261	0.250	0.600	-0.066	0.272
	2011	0.034	0.077	0.346	0.302	0.540	0.052	0.324
	2012	0.031	0.176	0.621	0.611	0.820	0.308	0.633
	2013	0.026	0.141	0.758	0.742	0.420	0.131	0.764
	2014	0.032	0.021	0.795	0.779	0.490	0.037	0.801
	2015	0.058	-0.003	0.600	0.581	0.290	-0.198	0.603

*Triaxial joint meter MGT1-Y component*
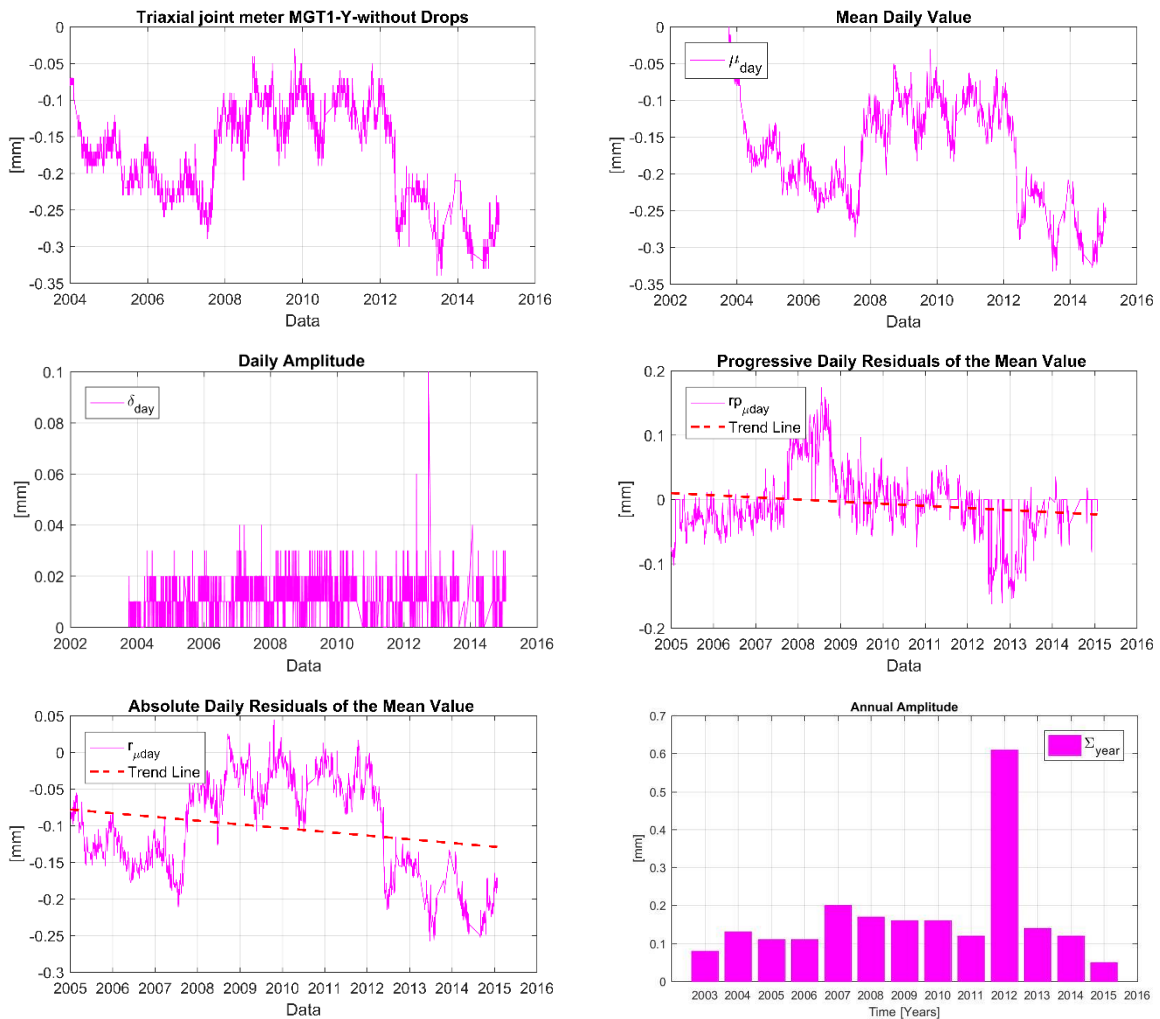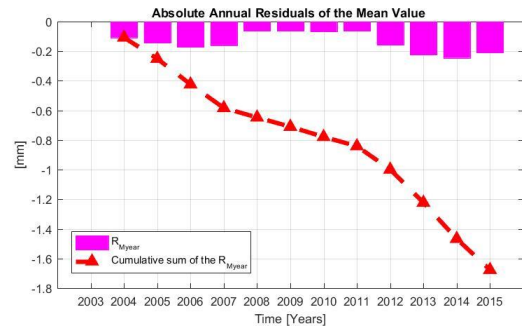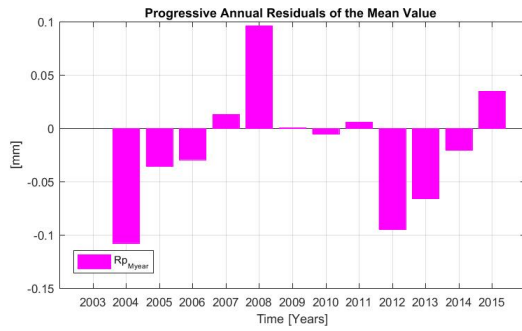
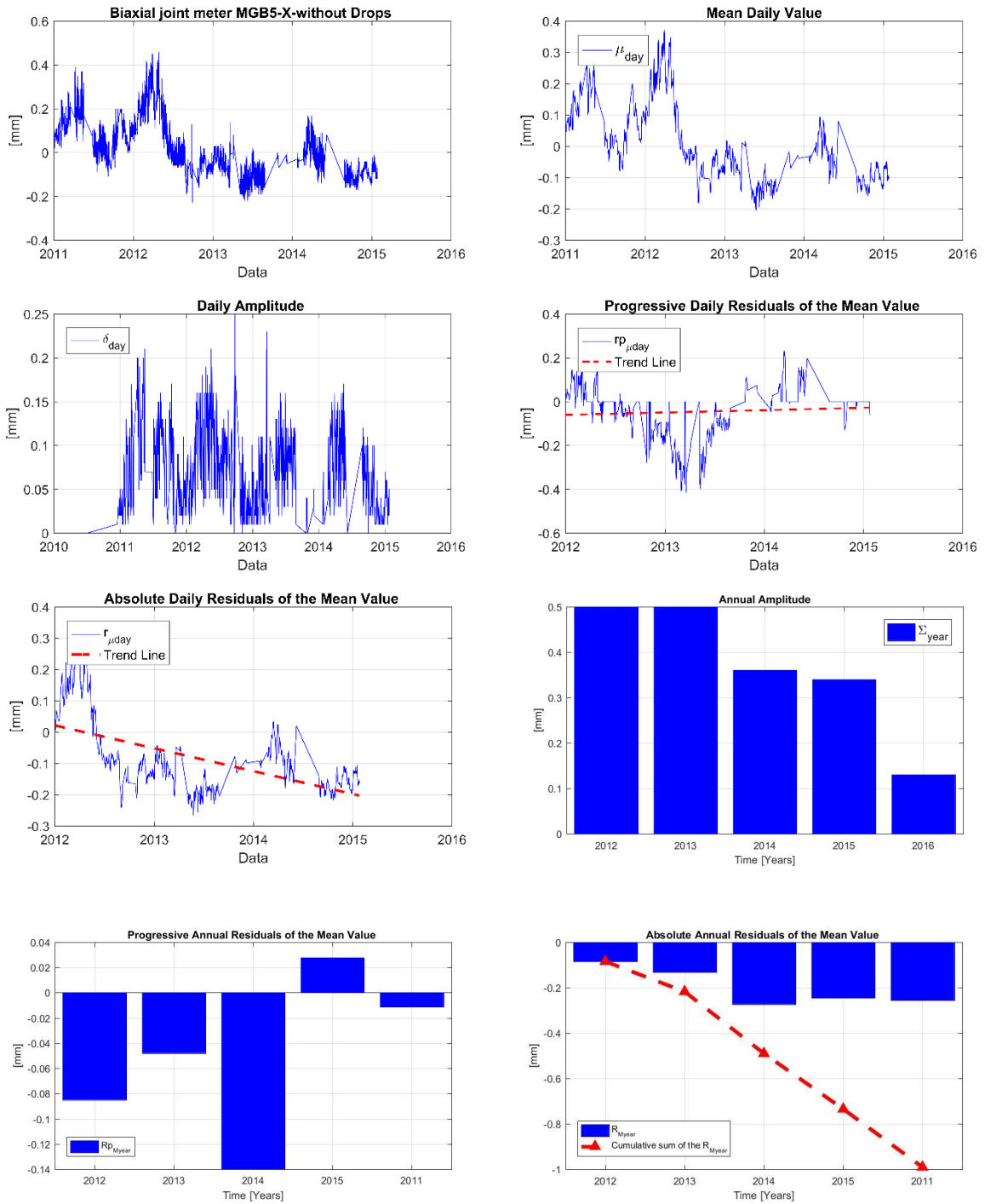| Sensor	Year	$\delta_{day,j}$	$rp_{\mu day}$	$r_{\mu day}$	M_{year}	Σ_{year}	Rp_{Myear}	R_{Myear}
	2004	0.009			-0.152	0.130	-0.108	-0.108
	2005	0.009	-0.032	-0.112	-0.187	0.110	-0.036	-0.143
	2006	0.010	-0.027	-0.142	-0.217	0.110	-0.029	-0.173
	2007	0.013	0.012	-0.129	-0.204	0.200	0.013	-0.160
	2008	0.013	0.084	-0.045	-0.108	0.170	0.096	-0.064
MGT1-Y	2009	0.014	0.010	-0.034	-0.107	0.160	0.001	-0.063
[mm]	2010	0.012	-0.007	-0.041	-0.112	2.850	-0.005	-0.068
	2011	0.010	0.002	-0.035	-0.107	0.120	0.006	-0.063
	2012	0.012	-0.054	-0.122	-0.202	0.610	-0.095	-0.158
	2013	0.012	-0.068	-0.191	-0.268	0.140	-0.066	-0.224
	2014	0.011	-0.009	-0.213	-0.288	0.120	-0.021	-0.244
	2015	0.018	-0.001	-0.178	-0.254	0.050	0.035	-0.210

Triaxial joint meter MGT1-Z component

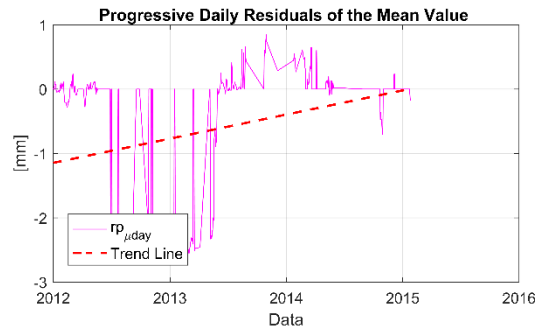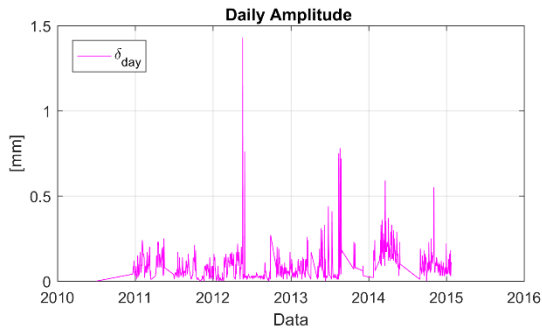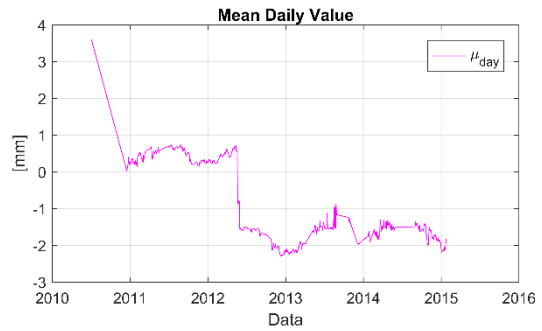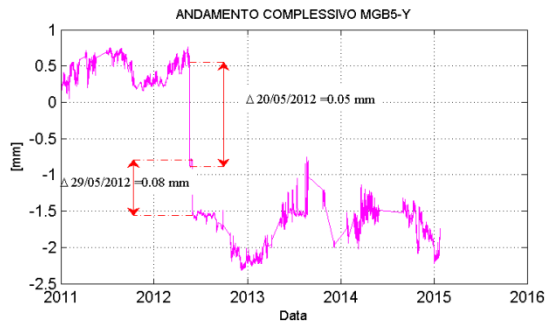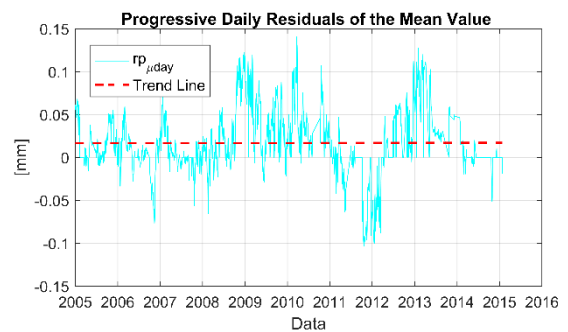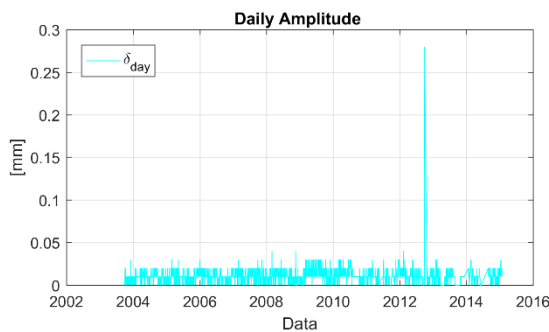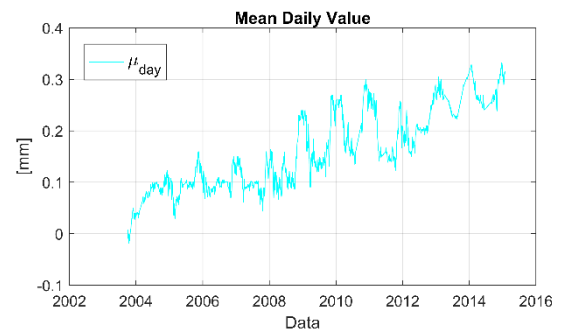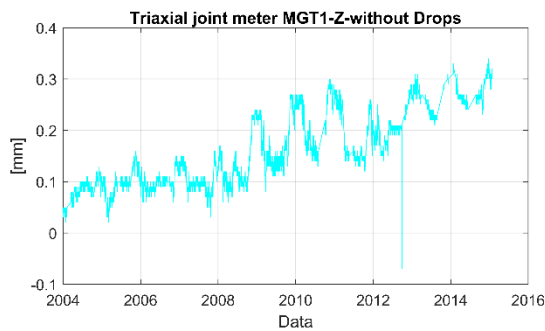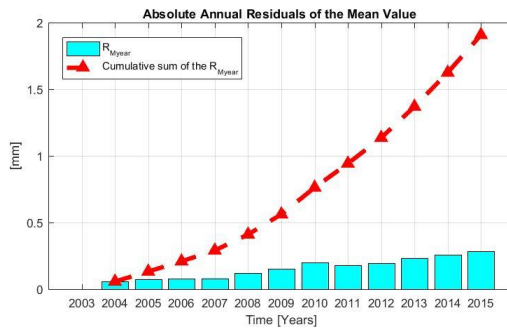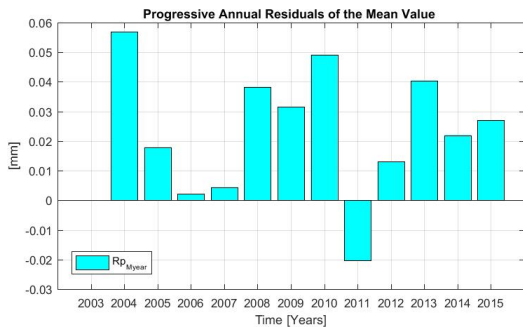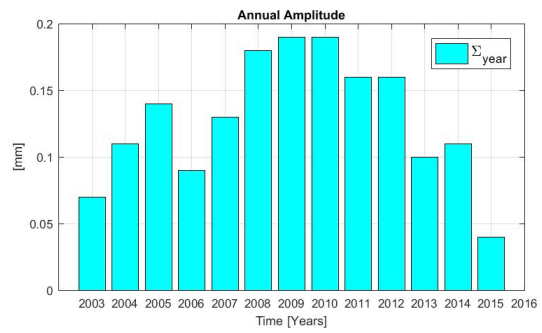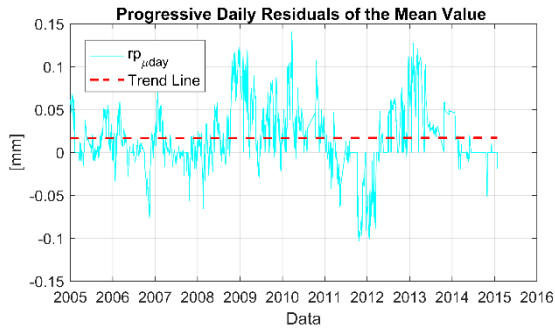| Sensor	Year	$\delta_{day,j}$	$rp_{\mu day}$	$r_{\mu day}$	M_{year}	Σ_{year}	Rp_{Myear}	R_{Myear}
MGT1-Z [mm]	2004	0.009			0.077	0.110	0.057	0.057
	2005	0.010	0.017	0.055	0.095	0.140	0.018	0.075
	2006	0.010	0.002	0.058	0.098	0.090	0.002	0.077
	2007	0.011	0.006	0.062	0.102	0.130	0.004	0.081
	2008	0.010	0.027	0.090	0.140	0.180	0.038	0.120
	2009	0.014	0.040	0.130	0.172	0.190	0.032	0.151
	2010	0.013	0.041	0.178	0.221	2.910	0.049	0.201
	2011	0.011	-0.020	0.154	0.201	0.160	-0.020	0.180
	2012	0.012	0.007	0.167	0.214	25.300	0.013	0.193
	2013	0.010	0.054	0.215	0.254	0.100	0.040	0.234
	2014	0.010	-0.001	0.236	0.276	0.110	0.022	0.256
	2015	0.017	-0.001	0.263	0.303	0.040	0.027	0.283

C.2 Signal frequency analyses

The main periodicity of the data recorded has been obtained through a frequency analysis of the signal using a Fourier analysis. The frequency analysis has been applied to data obtained by the instruments, which have not presented malfunction, interruptions and / or many drops. In this case, some of the biaxial joint meters. In more detail, for these instruments the following plots are reported:

- recorded signal by the sensor and its main components (the periodical component and the residual)
- the Fourier Transform
- the residue as obtained from the FFT and from the mathematical considerations (reference quantities)

Biaxial joint meter MGB1-Y
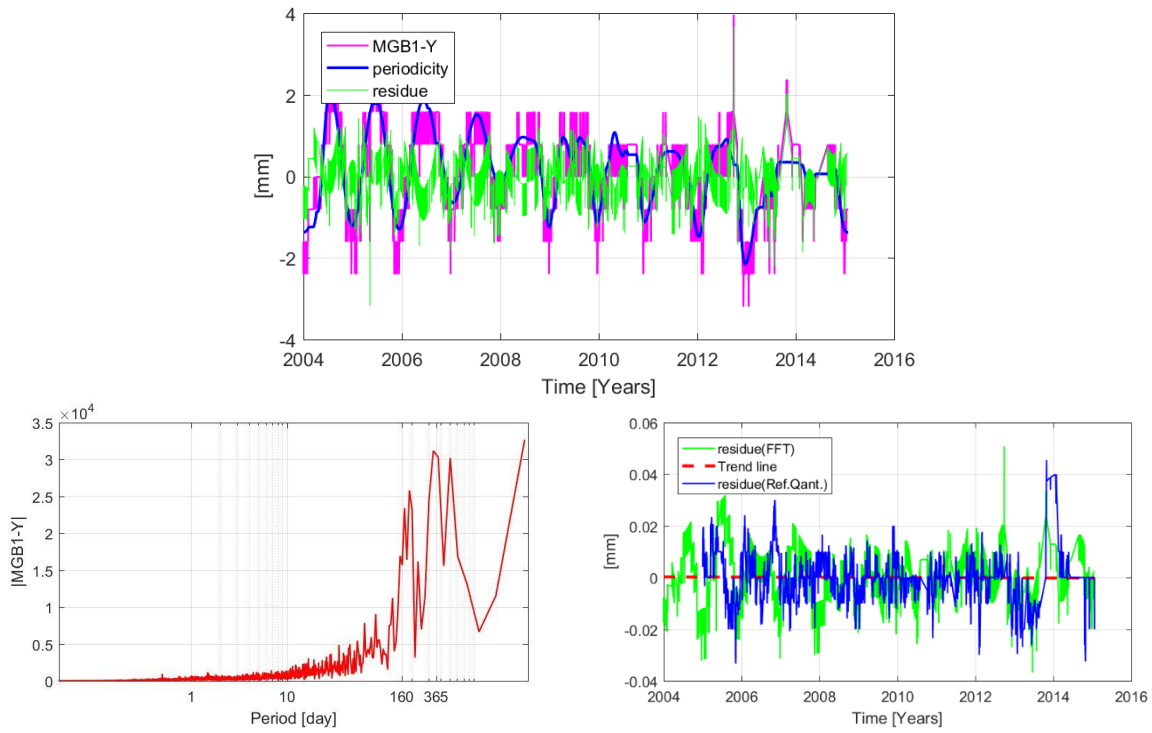
Biaxial joint meter MGB3-X
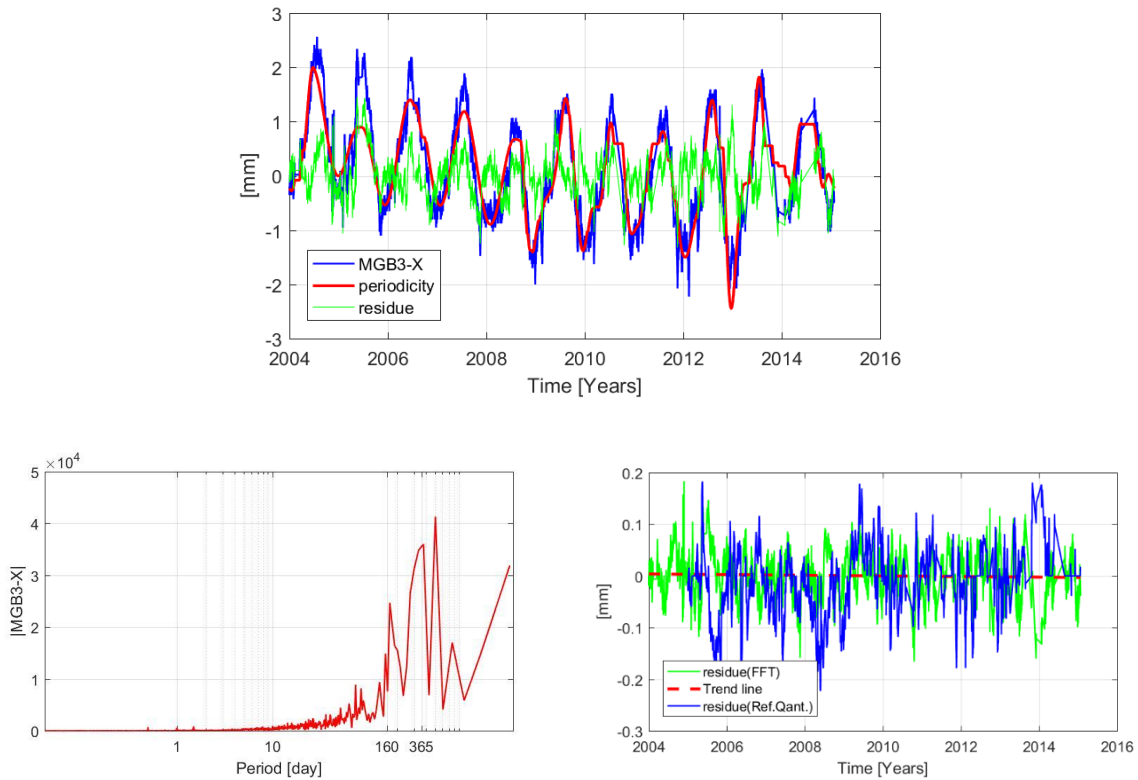
APPENDIX D

Parametric study: buttressed vault

D.1 The modelling parameters of the buttressed vault

The density of the blocks considers also the weight of the elements that rest on the longitudinal walls and on the vaults (as evaluated from the static analysis (§11.3), and summarized below:

Arch:

Weight on the arch due to:

- the self-weight of the portion of the two vaults: $W_{vaults} = \dfrac{149}{4} + \dfrac{162}{4} = 78 KN$

- the roof : $W_{roof} = 28 KN$

- the portion of wall $W_{wall} = (5.78 \cdot 1 \cdot 3.5) \cdot 17 = 344 KN$

Dimension of the blocks: $0.4 \cdot 1 \cdot 0.27$ m

Volume of the arch: $3.2 m^3$

Weight per unit volume of the arch: $\dfrac{W}{V} = \dfrac{78 + 28 + 344}{3.2} = 141 \dfrac{KN}{m^3}$

Wall$_0$:

- Self-weight of the wall$_0$: $W_{wall} = (10.1 \cdot 1.5 \cdot 1) \cdot 17 + (10.1 \cdot 1 \cdot 9) \cdot 17 = 1800 KN$

Weight on the wall$_0$ due to:

- the self-weight of the portion of the two vaults: $W_{vaults} = \dfrac{149}{4} + \dfrac{162}{4} = 78KN$

Dimension of the blocks: 1.5·1·5.05 m

Volume of the arch: 15 m^3

Weight per unit volume of the wall$_0$: $\dfrac{W}{V} = \dfrac{1800 + 78}{15} = 125\dfrac{KN}{m^3}$

Wall$_1$:

Self-weight of the wall$_1$: $W_{wall1} = (1.1 \cdot 1.9 \cdot 10) \cdot 17 = 355KN$

Weight on the wall 1 due to:

- Weight of the slab: $W_{slab} = 39KN$

- Weight of the roof: $W_{roof} = 52KN$

Dimension of the blocks: 1.1·1·1.9 m

Volume of the arch: 2.09 m3

Weight per unit volume wall$_1$: $\dfrac{W}{V} = \dfrac{39 + 52 + 355}{2.09} = 213\dfrac{KN}{m^3}$

The joint stiffness for the 2D model have been calculated considering the equivalence between the real section (*r*) and the modelled section (*m*)

Joint stiffness between the blocks of the arch (the arch is subdivide in 6 blocks):

$$k_{r,n} = \frac{E}{L}A = \frac{4144000}{1.35} \cdot 0.4 \cdot 10 = 1.2 \cdot 10^7 \, KPa \cdot m$$

$$k_{m,n} = \frac{1.2 \cdot 10^7}{0.4 \cdot 1} = 3.0 \cdot 10^7 \, \frac{KPa}{m}$$

$$k_{r,s} = \frac{G}{L}A = \frac{E}{2(1+v)L}A = \frac{4144000}{2(1+0.18)1.35} \cdot (0.4 \cdot 10) = 5.2 \cdot 10^6 \, KPa \cdot m$$

$$k_{m,s} = \frac{5.2 \cdot 10^6}{0.4 \cdot 1} = 1.3 \cdot 10^7 \, \frac{KPa}{m}$$

Joint stiffness between the blocks of the arch and wall$_0$

$$k_{r,n} = \frac{E}{L} A = \frac{4144000}{3.2} \cdot 0.4 \cdot 10 = 5.2 \cdot 10^6 \, KPa \cdot m$$

$$k_{m,n} = \frac{5.2 \cdot 10^6}{0.4 \cdot 1} = 1.3 \cdot 10^7 \, \frac{KPa}{m}$$

$$k_{r,s} = \frac{G}{L} A = \frac{E}{2(1+v)L} A = \frac{4144000}{2(1+0.18)3.2} \cdot (0.4 \cdot 10) = 2.2 \cdot 10^6 \, KPa \cdot m$$

$$k_{m,s} = \frac{2.2 \cdot 10^6}{0.4 \cdot 1} = 5.5 \cdot 10^6 \, \frac{KPa}{m}$$

Joint stiffness between the blocks of the wall$_0$:

$$K_{r,n} = \frac{E}{L} = \frac{4144000}{5.05} \cdot 1.5 \cdot 10 = 1.23 \cdot 10^7 \, KPa \cdot m$$

$$K_{m,n} = \frac{K_j}{A_{sect}} = \frac{1.23 \cdot 10^7}{1.5 \cdot 1} = 8.2 \cdot 10^6 \, \frac{KPa}{m}$$

$$k_{r,s} = \frac{G}{L} A = \frac{E}{2(1+v)L} A = \frac{4144000}{2(1+0.18)5.05} \cdot (1.5 \cdot 10) = 5.2 \cdot 10^6 \, KPa \cdot m$$

$$k_{m,s} = \frac{5.2 \cdot 10^6}{1.5 \cdot 1} = 3.5 \cdot 10^6 \, \frac{KPa}{m}$$

Joint stiffness between the block of the wall$_1$ ant top of the wall$_0$

$$K_{r,n} = \frac{E}{L} = \frac{4144000}{3.525} \cdot 1.1 \cdot 10 = 1.3 \cdot 10^7 \, KPa \cdot m$$

$$K_{m,n} = \frac{K_j}{A_{sect}} = \frac{1.3 \cdot 10^7}{1.1 \cdot 1} = 1.2 \cdot 10^7 \, \frac{KPa}{m}$$

$$k_{r,s} = \frac{G}{L} A = \frac{E}{2(1+v)L} A = \frac{4144000}{2(1+0.18)3.525} \cdot (1.1 \cdot 10) = 5.5 \cdot 10^6 \, KPa \cdot m$$

$$k_{m,s} = \frac{5.5 \cdot 10^6}{1.1 \cdot 1} = 5.0 \cdot 10^6 \, \frac{KPa}{m}$$

Joint stiffness between wall 0 and soil

From the geotechnical investigation the stiffness of the soil are:
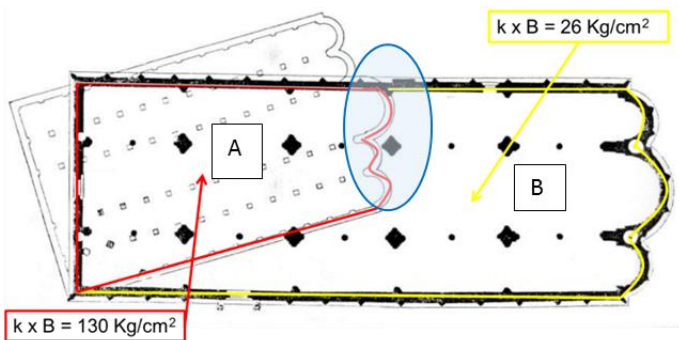
$U_{3B}(z)$=1342 KN/m³

$U_{3A}(z)$=6710 KN/m³

To the horizontal constraint, from the geotechnical study :

$U_2(x)= U_1(y)$=0.65xN(KN)/0,004=162.5 KN/m

The soil stiffness under the wall at left is characterized for the first 5 meters for a stiffness $U_A(z)$, then for $U_B(z)$. So in the following calculation it has been considered the mean value of the two.

$$k_{m,n} = \frac{B_r}{B_m} \cdot \frac{H_r}{H_m} \cdot U_3(z) = \frac{1.9}{1.5} \cdot \frac{10}{1} \cdot 4026 = 5.1 \cdot 10^4 \frac{KPa}{m}$$

N=3305 KN

$$U1(x) = U2(y) = 537063\, KN/m$$

$$k_{r,s} = \frac{B_r}{B_m} \cdot \frac{H_r}{H_m} \cdot U_1(x) = \frac{1.9}{1.5} \cdot \frac{2.8}{1} \cdot 537063 = 1.9 \cdot 10^6\, KN / m$$

$$k_{m,s} = \frac{1.9 \cdot 10^6}{1.5 \cdot 1} = 1.3 \cdot 10^6 \frac{KPa}{m}$$

Modelling of the damping

Identification of the frequency at which the structures should be critically damped:

-Joint Stiffness:

$$K_j = \frac{E}{H}$$

-Spring Stiffness:

$$K_s = K_j \cdot \frac{B \cdot D}{4}$$

-Natural frequency associated with rocking impact:

$$\omega_r = \sqrt{\frac{K_s \cdot B^2}{J}}$$

Natural frequency associated with edge impact:

$$\omega_e = \sqrt{\frac{2 \cdot K_s}{m}}$$

If only mass or stiffness damping is used, then the damping must be doubled (since each contributes 1/2 to the Rayleigh damping) to obtain critical damping.

$$f_{crit} = \frac{\omega_e \sqrt{2}}{2\pi} = 202$$

Block: wall 0			Single block		Multi block			Damping	
			we=	254.9462	we,m= 360.5483	βwe= 0.005547	ξwe 100		ξwr 34.87272
H=	5.05	m	wr=	88.90667	wr,m= 125.733	βwr= 0.015907	ξwe 286.7571		ξwr 100
D=	1	m							
B=	1.5	m							
density=	12.5	10^3Kg/m^3							
V=	7.575	m3			fcrit= 57.41215				
m=	94.6875	10^3kg							
J=	875.9383	10^3kgm^2							
E=	4144000	KN/m^2							
Kj=	8205941	KN/m^3							
Ks=	3077228	KN/m							

Block: arch			Single block		Multi block			Damping	
			we=	897.9488	we,m= 1269.891	βwe= 0.001575	ξwe 100		ξwr 34.79357
H=	1.35	m	wr=	312.4284	wr,m= 441.8406	βwr= 0.004527	ξwe 287.4094		ξwr 100
D=	1	m							
B=	0.4	m							
density=	14.1	10^3Kg/m^3							
V=	0.54	m3			fcrit= 202.212				
m=	7.614	10^3kg							
J=	5.031585	10^3kgm^2							
E=	4144000	KN/m^2							
Kj=	30696296	KN/m^3							
Ks=	3069630	KN/m							

Block: wall 1			Single block		Multi block			Damping	
			we=	279.7989	we,m= 395.6954	βwe= 0.005054	ξwe 100		ξwr 36.48386
H=	3.525	m	wr=	102.0814	wr,m= 144.3649	βwr= 0.013854	ξwe 274.0938		ξwr 100
D=	1	m							
B=	1.1	m							
density=	21.3	10^3Kg/m^3							
V=	3.8775	m3			fcrit= 63.00881				
m=	82.59075	10^3kg							
J=	375.3922	10^3kgm^2							
E=	4144000	KN/m^2							
Kj=	11756028	KN/m^3							
Ks=	3232908	KN/m							

D.1.1 Variation of the normal stiffness at the base of the walls

Figures display the displacement in the x direction of the point monitored at the left of the arch obtained from the static and dynamic analysis for the different normal stiffness considered.

(a)

(b)
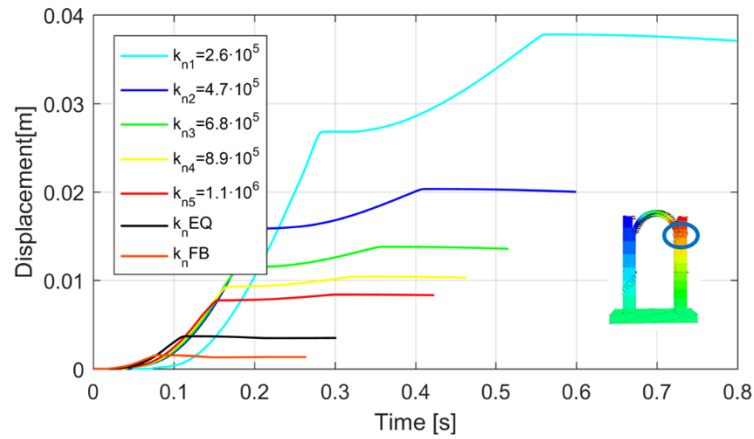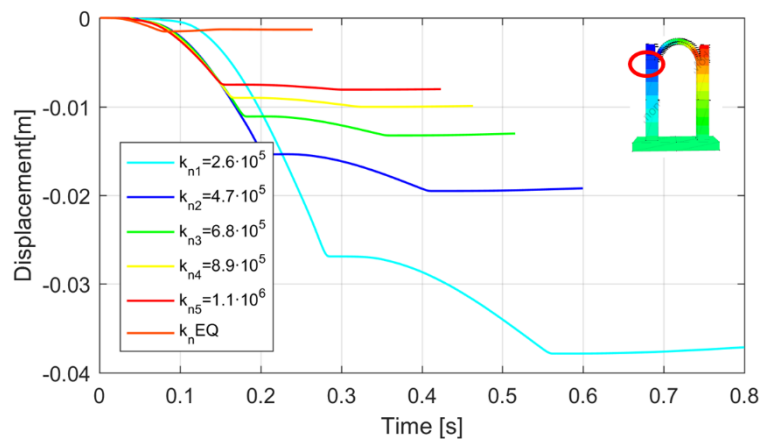
Plot of the maximum displacements recorded during the static analysis considering different shear stiffness at the base: (a) at the right springer of the arch, (b) at the left springer of the arch

Plot of the maximum displacements recorded at the left springer of the arch during the dynamic analysis considering different normal stiffness at the base

D.1.2Variation of the shear stiffness at the base of the walls

Figures display the displacement in the x direction of the point monitored at the left of the arch obtained from the static and dynamic analysis for the different shear stiffness considered.

(a)

(b)

Plot of the maximum displacements recorded during the static analysis considering different shear stiffness at the base: (a) at the right springer of the arch, (b) at the left springer of the arch

Plot of the maximum displacements recorded at the left springer of the arch during the dynamic analysis considering different shear stiffness at the base

D.1.3 Variation of numbers of blocks of the arch

Arch composed by three blocks

The calculation of the stiffness at the interfaces between the three blocks which composed the arch are here reported.

Joint stiffness between the blocks of the arch:

$$K_j = \frac{E}{L}A = \frac{4144000}{2.7}0.4 \cdot 10 = 6.1 \cdot 10^6 \, KPa \cdot m$$

$$K_n = \frac{K_j}{A_{sect}} = \frac{6.1 \cdot 10^6}{0.4 \cdot 1} = 1.5 \cdot 10^7 \, \frac{KPa}{m}$$

$$K_{sj} = \frac{G}{L}A = \frac{E}{3(1+\upsilon)L}A = \frac{4144000}{2(1+0.18)2.7} \cdot (0.4 \cdot 10) = 2.6 \cdot 10^6 \, KPa \cdot m$$

$$K_s = \frac{K_{sj}}{A_{sect}} = \frac{2.6 \cdot 10^6}{0.4 \cdot 1} = 6.5 \cdot 10^6 \, \frac{KPa}{m}$$

Joint stiffness Arch- wall 0

$$K_j = \frac{E}{L}A = \frac{4144000}{3.87}0.4 \cdot 10 = 4.3 \cdot 10^6 \, KPa \cdot m$$

$$K_n = \frac{K_j}{A_{sect}} = \frac{4.3 \cdot 10^6}{0.4 \cdot 1} = 1.1 \cdot 10^7 \, \frac{KPa}{m}$$

$$K_{sj} = \frac{G}{L}A = \frac{E}{3(1+\upsilon)L}A = \frac{4144000}{2(1+0.18)3.87} \cdot (0.4 \cdot 10) = 1.8 \cdot 10^6 \, KPa \cdot m$$

$$K_s = \frac{K_{sj}}{A_{sect}} = \frac{1.8 \cdot 10^6}{0.4 \cdot 1} = 4.5 \cdot 10^6 \, \frac{KPa}{m}$$

Damping

Block: wall 0

Property	Value	Unit
H=	5.05	m
D=	1	m
B=	1.5	m
density=	12.5	10^3Kg/m^3
V=	7.575	m3
m=	94.6875	10^3kg
J=	875.9383	10^3kgm^2
E=	4144000	KN/m^2
Kj=	8205941	KN/m^3
Ks=	3077228	KN/m

Single block		Multi block			Damping			
we=	254.9462	we,m= 360.5483	βwe=	0.005547	ξwe	100	ξwr	34.87272
wr=	88.90667	wr,m= 125.733	βwr=	0.015907	ξwe	286.7571	ξwr	100

fcrit= 57.41215

Block: arch

Property	Value	Unit
H=	2.7	m
D=	1	m
B=	0.4	m
density=	14.1	10^3Kg/m^3
V=	1.08	m3
m=	15.228	10^3kg
J=	37.8162	10^3kgm^2
E=	4144000	KN/m^2
Kj=	15348148	KN/m^3
Ks=	1534815	KN/m

Single block		Multi block			Damping			
we=	448.9744	we,m= 634.9457	βwe=	0.00315	ξwe	100	ξwr	17.94847
wr=	80.58404	wr,m= 113.963	βwr=	0.01755	ξwe	557.1505	ξwr	100

fcrit= 101.106

Block: wall 1

Property	Value	Unit
H=	3.525	m
D=	1	m
B=	1.1	m
density=	21.3	10^3Kg/m^3
V=	3.8775	m3
m=	82.59075	10^3kg
J=	375.3922	10^3kgm^2
E=	4144000	KN/m^2
Kj=	11756028	KN/m^3
Ks=	3232908	KN/m

Single block		Multi block			Damping			
we=	279.7989	we,m= 395.6954	βwe=	0.005054	ξwe	100	ξwr	36.48386
wr=	102.0814	wr,m= 144.3649	βwr=	0.013854	ξwe	274.0938	ξwr	100

fcrit= 63.00881

Variation of normal stiffness

Figures display the displacement in the x direction of the point monitored at the left of the arch obtained from the static and dynamic analysis for the different normal stiffness considered.

(a)

(b)

Plot of the maximum displacements recorded during the static analysis considering different normal stiffness at the base and the arch modelled by three blocks: (a) at the right springer of the arch, (b) at the left springer of the arch

Plot of the maximum displacements recorded at the left springer of the arch during the dynamic analysis considering different normal stiffness at the base and the arch modelled by three blocks

Variation of shear stiffness

Figures display the displacement in the x direction of the point monitored at the left of the arch obtained from the static and dynamic analysis for the different shear stiffness considered.

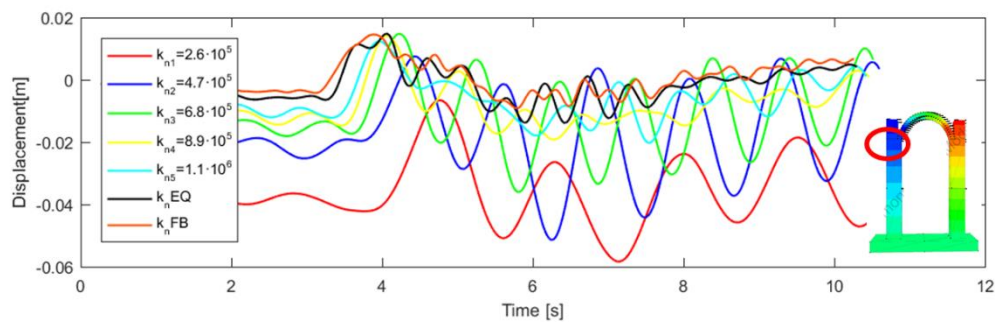
(a)

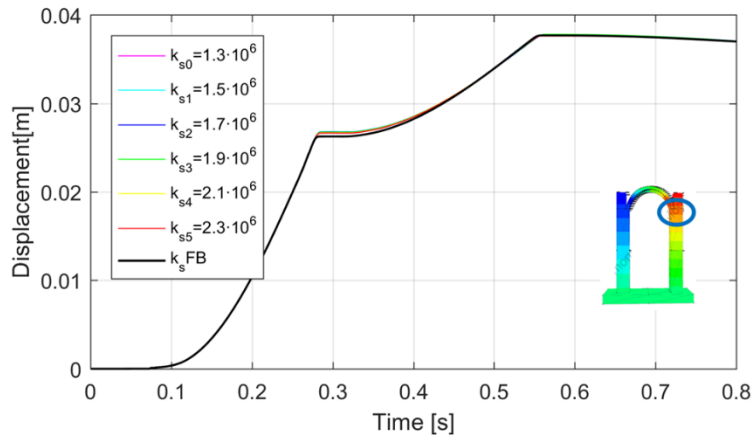
(b)

Plot of the maximum displacements recorded during the static analysis considering different shear stiffness at the base and the arch modelled by three blocks: (a) at the right springer of the arch, (b) at the left springer of the arch

Plot of the maximum displacements recorded at the left springer of the arch during the dynamic analysis considering different shear stiffness at the base and the arch modelled by three blocks

D.1.3.2 Arch composed by two blocks

The calculation of the stiffness at the interfaces between the two blocks which composed the arch are here reported.

Joint stiffness between the blocks of the arch:

$$K_j = \frac{E}{L} A = \frac{4144000}{4.05} 0.4 \cdot 10 = 4.1 \cdot 10^6 \, KPa \cdot m$$

$$K_n = \frac{K_j}{A_{sect}} = \frac{4.1 \cdot 10^6}{0.4 \cdot 1} = 1.0 \cdot 10^7 \, \frac{KPa}{m}$$

$$K_{sj} = \frac{G}{L} A = \frac{E}{3(1+\upsilon)L} A = \frac{4144000}{2(1+0.18)4.05} \cdot (0.4 \cdot 10) = 1.7 \cdot 10^6 \, KPa \cdot m$$

$$K_s = \frac{K_{sj}}{A_{sect}} = \frac{1.7 \cdot 10^6}{0.4 \cdot 1} = 4.3 \cdot 10^6 \, \frac{KPa}{m}$$

Joint stiffness Arch N- wall 0

$$K_j = \frac{E}{L} A = \frac{4144000}{4.55} 0.4 \cdot 10 = 3.6 \cdot 10^6 \, KPa \cdot m$$

$$K_n = \frac{K_j}{A_{sect}} = \frac{3.6 \cdot 10^6}{0.4 \cdot 1} = 9.1 \cdot 10^6 \, \frac{KPa}{m}$$

$$K_{sj} = \frac{G}{L} A = \frac{E}{3(1+\upsilon)L} A = \frac{4144000}{2(1+0.18)4.55} \cdot (0.4 \cdot 10) = 1.5 \cdot 10^6 \, KPa \cdot m$$

$$K_s = \frac{K_{sj}}{A_{sect}} = \frac{1.5 \cdot 10^6}{0.4 \cdot 1} = 3.9 \cdot 10^6 \, \frac{KPa}{m}$$

Damping

Block: wall 0			Single block		Multi block			Damping	
			we=	254.9462	**we,m= 360.5483**	βwe= 0.005547	ξwe 100		ξwr 34.87272
H=	5.05	m	wr=	88.90667	**wr,m= 125.733**	βwr= 0.015907	ξwe 286.7571		ξwr 100
D=	1	m							
B=	1.5	m							
density=	12.5	10^3Kg/m^3							
V=	7.575	m3			fcrit= 57.41215				
m=	94.6875	10^3kg							
J=	875.9383	10^3kgm^2							
E=	4144000	KN/m^2							
Kj=	8205941	KN/m^3							
Ks=	3077228	KN/m							

Block: arch			Single block		Multi block			Damping	
			we=	299.3163	**we,m= 423.2971**	βwe= 0.004725	ξwe 100		ξwr 12.03768
H=	4.05	m	wr=	36.03072	**wr,m= 50.95514**	βwr= 0.03925	ξwe 830.7251		ξwr 100
D=	1	m							
B=	0.4	m							
density=	14.1	10^3Kg/m^3							
V=	1.62	m3			fcrit= 67.404				
m=	22.842	10^3kg							
J=	126.1069	10^3kgm^2							
E=	4144000	KN/m^2							
Kj=	10232099	KN/m^3							
Ks=	1023210	KN/m							

Block: wall 1			Single block		Multi block			Damping	
			we=	279.7989	**we,m= 395.6954**	βwe= 0.005054	ξwe 100		ξwr 36.48386
H=	3.525	m	wr=	102.0814	**wr,m= 144.3649**	βwr= 0.013854	ξwe 274.0938		ξwr 100
D=	1	m							
B=	1.1	m							
density=	21.3	10^3Kg/m^3							
V=	3.8775	m3			fcrit= 63.00881				
m=	82.59075	10^3kg							
J=	375.3922	10^3kgm^2							
E=	4144000	KN/m^2							
Kj=	11756028	KN/m^3							
Ks=	3232908	KN/m							

Variation of normal stiffness

Figures display the displacement in the x direction of the point monitored at the left of the arch obtained from the static and dynamic analysis for the different normal stiffness considered.
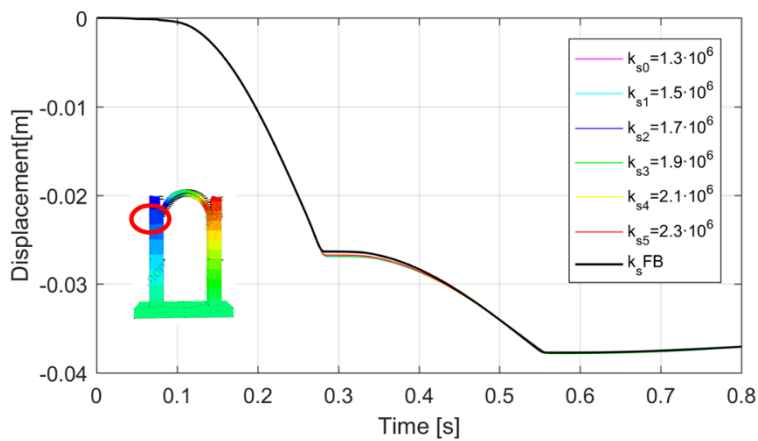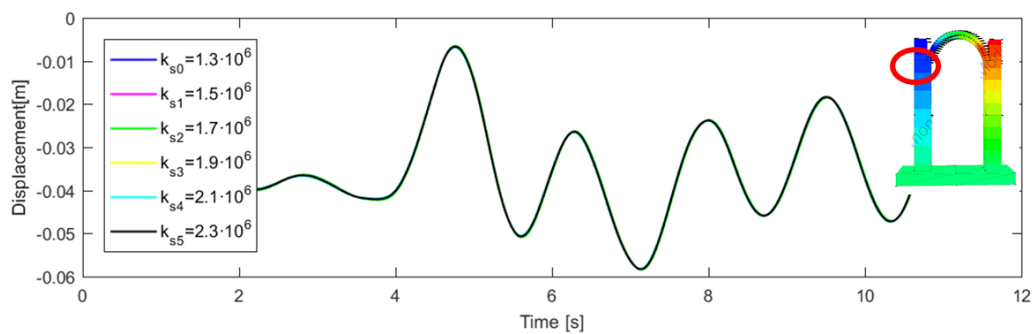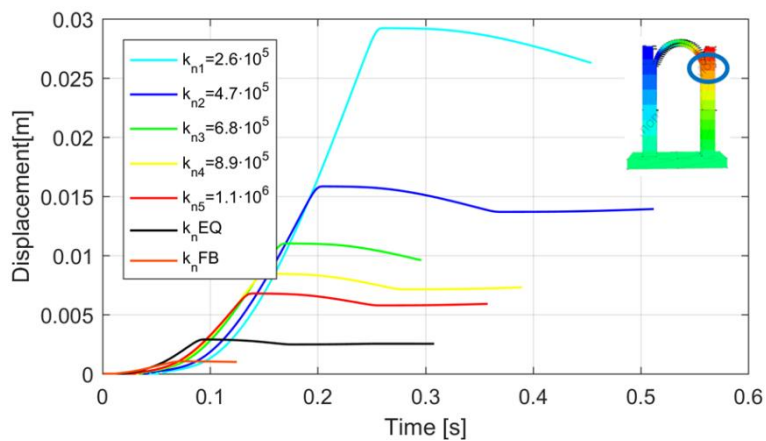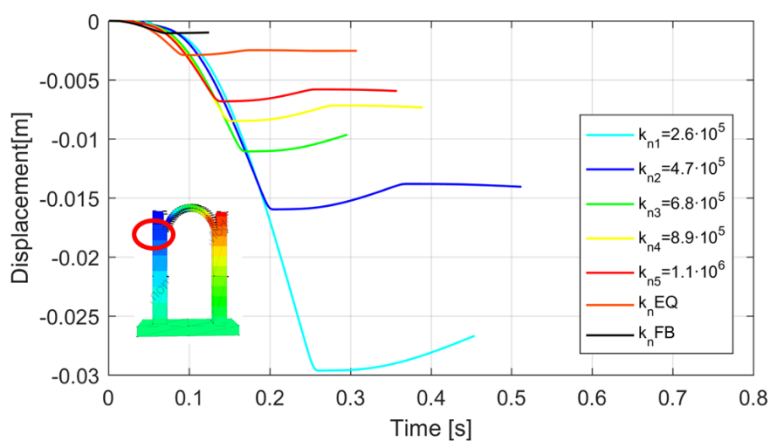

(a)

(b)

Figure 14-11: Plot of the maximum displacements recorded at the right springer of the arch during the static analysis considering different normal stiffness at the base and the arch modelled by two blocks
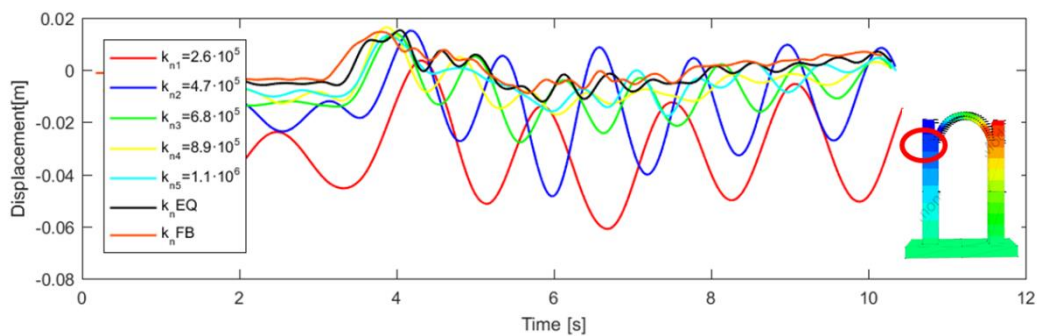
Plot of the maximum displacements recorded at the left springer of the arch during the dynamic analysis considering different normal stiffness at the base and the arch modelled by two blocks

Variation of shear stiffness

Figures display the displacement in the x direction of the point monitored at the left of the arch obtained from the static and dynamic analysis for the different shear stiffness considered.
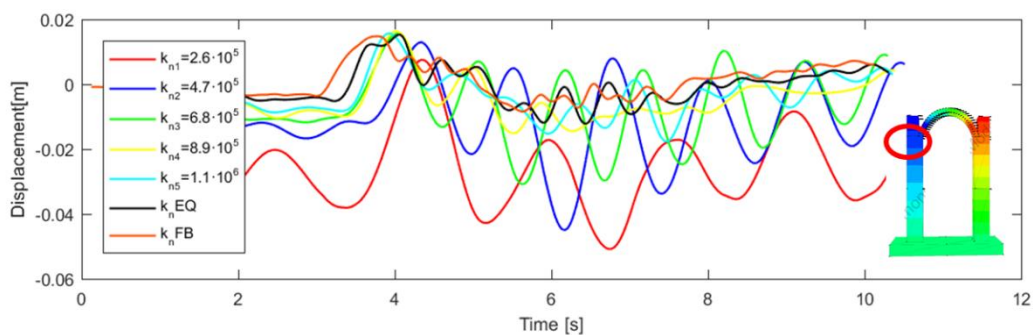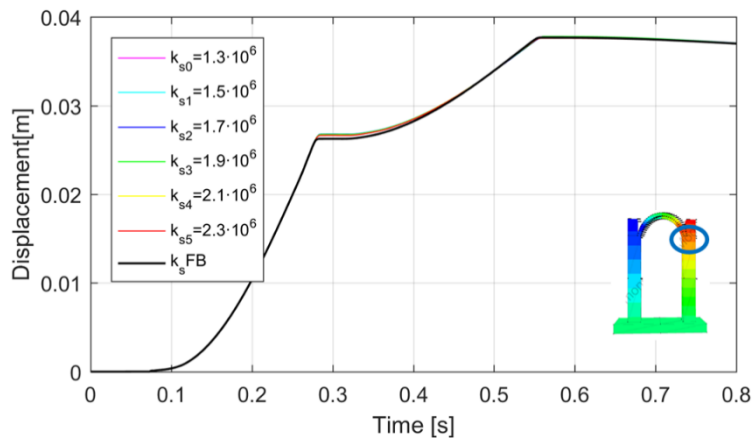

(a)

(b)

Plot of the maximum displacements recorded at the right springer of the arch during the static analysis considering different shear stiffness at the base and the arch modelled by two blocks
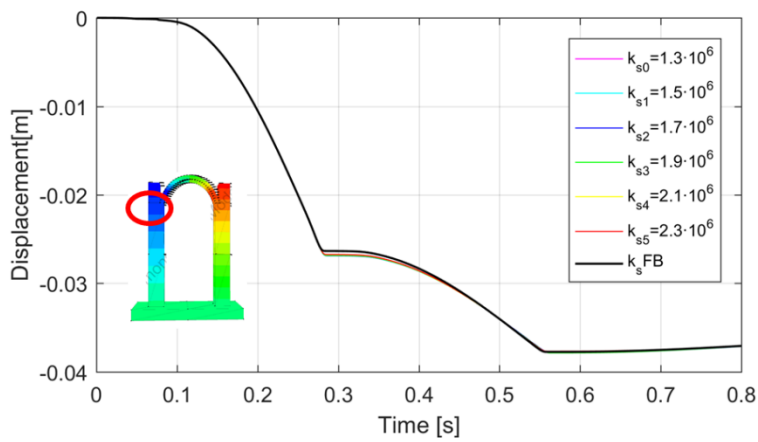

Plot of the maximum displacements recorded at the left springer of the arch during the dynamic analysis considering different shear stiffness at the base and the arch modelled by two blocks

3DEC analyses of transversal cross section

D.2 The modelling parameters of the simple cross section used in the DEM models

The density of the blocks considers also the weight of the elements that rest on the longitudinal walls and on the vaults (as evaluated from the static analysis (§11)), and summarized below:

Arch C:

Weight on the arch due to:

- the self-weight of the portion of the two vaults: $W_{vaults} = \frac{223}{4} + \frac{234}{4} = 114 KN$

- the roof : $W_{roof} = 181 KN$

- the portion of wall : $W_{wall} = (8.6 \cdot 1 \cdot 4) \cdot 17 = 585 KN$

Dimension of the blocks: $0.4 \cdot 1 \cdot 0.27$ m

Volume of the arch C: 5.53 m^3

Weight per unit volume of the arch: $\frac{W}{V} = \frac{114 + 181 + 585}{5,53} = 159 \frac{KN}{m^3}$

Arch N, arch S:

Weight on the arch due to:

- the self-weight of the portion of the two vaults: $W_{vaults} = \frac{149}{4} + \frac{162}{4} = 78 KN$

- the roof : $W_{roof} = 28 KN$

- the portion of wall : $W_{wall} = (5.78 \cdot 1 \cdot 3.5) \cdot 17 = 344 KN$

Dimension of the blocks: $0.4 \cdot 1 \cdot 0.27$ m

Volume of the arch: 3.2m^3

Weight per unit volume of the arch: $\frac{W}{V} = \frac{78 + 28 + 344}{3.2} = 141 \frac{KN}{m^3}$

Wall$_0$:

- Self-weight of the wall$_0$: $W_{wall} = (10.1 \cdot 1.5 \cdot 1) \cdot 17 + (10.1 \cdot 1 \cdot 9) \cdot 17 = 1800 KN$

Weight on the wall$_0$ due to:

- the self-weight of the portion of the two vaults: $W_{vaults} = \dfrac{149}{4} + \dfrac{162}{4} = 78 KN$

Dimension of the blocks: $1.5 \cdot 1 \cdot 5.05$ m

Volume: 15 m^3

Weight per unit volume of the wall$_0$: $\dfrac{W}{V} = \dfrac{1800 + 78}{15} = 125 \dfrac{KN}{m^3}$

Wall$_1$:

- Self-weight of the wall$_1$: $W_{wall} = (2.3 \cdot 2.3 \cdot 8) \cdot 17 + (1 \cdot 10 \cdot 2) \cdot 17 = 1060 KN$

Weight on the wall$_0$ due to:

- the self-weight of the portion of the two vaults: $W_{vaults} = \dfrac{149}{4} + \dfrac{162}{4} = 78 KN$

Dimension of the blocks: $2.3 \cdot 1 \cdot 5.05$ m

Volume: 23 m^3

Weight per unit volume of the wall$_1$: $\dfrac{W}{V} = \dfrac{1060 + 78}{23} = 50 KN \dfrac{kN}{m^3}$

Wall$_2$:

- Self-weight of the wall$_2$: $W_{wall} = (1.9 \cdot 1 \cdot 2) \cdot 17 + (1 \cdot 9 \cdot 2) \cdot 17 = 370 KN$

Weight on the wall$_0$ due to:

- the self-weight of the portion of the central vaults: $W_{vaults} = \dfrac{223}{4} + \dfrac{234}{4} = 114 KN$

Dimension of the blocks: $1.9 \cdot 1 \cdot 1.08$ m

Volume: 3.8 m^3

Weight per unit volume of the wall$_2$: $\dfrac{W}{V} = \dfrac{370 + 114}{3.8} = 127 KN \dfrac{kN}{m^3}$

Wall$_3$:

- Self-weight of the wall$_3$: $W_{wall} = (1.5 \cdot 1 \cdot 8) \cdot 17 + (1 \cdot 9 \cdot 8) \cdot 17 = 1428 KN$

Weight on the wall$_0$ due to:

- Weight of the slab: $W_{slab} = 152 KN$

- Weight of the roof: $W_{roof} = 106 KN$

Dimension of the blocks: 1.5·1·2.0 m

Volume: 12 m³

Weight per unit volume of the wall₃: $\dfrac{W}{V} = \dfrac{1428 + 152 + 106}{12} = 140 KN \dfrac{kN}{m^3}$

Wall₄:

Self-weight of the wall₄: $W_{wall1} = (1.1 \cdot 1.9 \cdot 10) \cdot 17 = 355 KN$

Weight on the wall 1 due to:

- Weight of the slab: $W_{slab} = 39 KN$

- Weight of the roof: $W_{roof} = 52 KN$

Dimension of the block: 1.1·1·2 m

Volume: 2.09 m3

Weight per unit volume wall₄: $\dfrac{W}{V} = \dfrac{39 + 52 + 355}{2.09} = 213 KN \dfrac{kN}{m^3}$

The joint stiffness for the 2D model have been calculated considering the equivalence between the real section (*r*) and the modelled section (*m*)

Joint stiffness between the blocks of the arch N-S (the arch is subdivide in 6 blocks):

$$k_{r,n} = \frac{E}{L} A = \frac{4144000}{1.35} \cdot 0.4 \cdot 10 = 1.2 \cdot 10^7 \, KPa \cdot m$$

$$k_{m,n} = \frac{1.2 \cdot 10^7}{0.4 \cdot 1} = 3.0 \cdot 10^7 \, \frac{KPa}{m}$$

$$k_{r,s} = \frac{G}{L} A = \frac{E}{2(1+v)L} A = \frac{4144000}{2(1+0.18)1.35} \cdot (0.4 \cdot 10) = 5.2 \cdot 10^6 \, KPa \cdot m$$

$$k_{m,s} = \frac{5.2 \cdot 10^6}{0.4 \cdot 1} = 1.3 \cdot 10^7 \, \frac{KPa}{m}$$

Joint stiffness between the blocks of the arch C (the arch is subdivide in 6 blocks):

$$k_{r,n} = \frac{E}{L}A = \frac{4144000}{2.35} \cdot 0.4 \cdot 10 = 7.0 \cdot 10^6 \, KPa \cdot m$$

$$k_{m,n} = \frac{7.0 \cdot 10^6}{0.4 \cdot 1} = 1.8 \cdot 10^7 \, \frac{KPa}{m}$$

$$k_{r,s} = \frac{G}{L}A = \frac{E}{2(1+\nu)L}A = \frac{4144000}{2(1+0.18)2.35} \cdot (0.4 \cdot 10) = 3.0 \cdot 10^6 \, KPa \cdot m$$

$$k_{m,s} = \frac{3.0 \cdot 10^6}{0.4 \cdot 1} = 7.5 \cdot 10^6 \, \frac{KPa}{m}$$

Joint stiffness between the blocks of the arch N-S and wall$_0$

$$k_{r,n} = \frac{E}{L}A = \frac{4144000}{3.2} \cdot 0.4 \cdot 10 = 5.2 \cdot 10^6 \, KPa \cdot m$$

$$k_{m,n} = \frac{5.2 \cdot 10^6}{0.4 \cdot 1} = 1.3 \cdot 10^7 \, \frac{KPa}{m}$$

$$k_{r,s} = \frac{G}{L}A = \frac{E}{2(1+\nu)L}A = \frac{4144000}{2(1+0.18)3.2} \cdot (0.4 \cdot 10) = 2.2 \cdot 10^6 \, KPa \cdot m$$

$$k_{m,s} = \frac{2.2 \cdot 10^6}{0.4 \cdot 1} = 5.5 \cdot 10^6 \, \frac{KPa}{m}$$

Joint stiffness between the blocks of the arch C and wall$_1$

$$k_{r,n} = \frac{E}{L}A = \frac{4144000}{2.215} \cdot 0.4 \cdot 10 = 7.5 \cdot 10^6 \, KPa \cdot m$$

$$k_{m,n} = \frac{7.5 \cdot 10^6}{0.4 \cdot 1} = 1.9 \cdot 10^7 \, \frac{KPa}{m}$$

$$k_{r,s} = \frac{G}{L}A = \frac{E}{2(1+\nu)L}A = \frac{4144000}{2(1+0.18)2.215} \cdot (0.4 \cdot 10) = 3.2 \cdot 10^6 \, KPa \cdot m$$

$$k_{m,s} = \frac{3.2 \cdot 10^6}{0.4 \cdot 1} = 7.9 \cdot 10^6 \, \frac{KPa}{m}$$

Joint stiffness between the blocks of the wall$_0$:

$$K_{r,n} = \frac{E}{L} = \frac{4144000}{5.05} \cdot 1.5 \cdot 10 = 1.23 \cdot 10^7 \, KPa \cdot m$$

$$K_{m,n} = \frac{K_j}{A_{sect}} = \frac{1.23 \cdot 10^7}{1.5 \cdot 1} = 8.2 \cdot 10^6 \, \frac{KPa}{m}$$

$$k_{r,s} = \frac{G}{L}A = \frac{E}{2(1+v)L}A = \frac{4144000}{2(1+0.18)5.05} \cdot (1.5 \cdot 10) = 5.2 \cdot 10^6 \, KPa \cdot m$$

$$k_{m,s} = \frac{5.2 \cdot 10^6}{1.5 \cdot 1} = 3.5 \cdot 10^6 \, \frac{KPa}{m}$$

Joint stiffness between the block of the wall$_4$ ant top of the wall$_0$

$$K_{r,n} = \frac{E}{L} = \frac{4144000}{3.525} \cdot 1.1 \cdot 10 = 1.3 \cdot 10^7 \, KPa \cdot m$$

$$K_{m,n} = \frac{K_j}{A_{sect}} = \frac{1.3 \cdot 10^7}{1.1 \cdot 1} = 1.2 \cdot 10^7 \, \frac{KPa}{m}$$

$$k_{r,s} = \frac{G}{L}A = \frac{E}{2(1+v)L}A = \frac{4144000}{2(1+0.18)3.525} \cdot (1.1 \cdot 10) = 5.5 \cdot 10^6 \, KPa \cdot m$$

$$k_{m,s} = \frac{5.5 \cdot 10^6}{1.1 \cdot 1} = 5.0 \cdot 10^6 \, \frac{KPa}{m}$$

Joint stiffness between the block of the wall$_1$

$$K_j = \frac{E}{L} = \frac{1727000}{5.05} \cdot 2.3 \cdot 2.3 = 1.8 \cdot 10^6 \, KPa \cdot m$$

$$K_n = \frac{K_j}{A_{sect}} = \frac{1.8 \cdot 10^6}{2.3 \cdot 1} = 7.8 \cdot 10^5 \, \frac{KPa}{m}$$

$$K_{sj} = \frac{G}{L}A = \frac{E}{2(1+v)L}A = \frac{1727000}{2(1+0.18)5.05} \cdot (2.3 \cdot 2.3) = 7.6 \cdot 10^5 \, KPa \cdot m$$

$$K_s = \frac{K_{sj}}{A_{sect}} = \frac{7.6 \cdot 10^5}{2.3 \cdot 1} = 3.3 \cdot 10^5 \, \frac{KPa}{m}$$

Joint stiffness between the block of the wall$_1$ and the wall$_2$

$$K_j = \frac{E}{L} = \frac{1727000}{3.565} \cdot 1.9 \cdot 2.3 = 2.1 \cdot 10^6 \, KPa \cdot m$$

$$K_n = \frac{K_j}{A_{sect}} = \frac{2.5 \cdot 10^6}{1.9 \cdot 1} = 1.1 \cdot 10^6 \, \frac{KPa}{m}$$

$$K_{sj} = \frac{G}{L}A = \frac{E}{2(1+v)L}A = \frac{1727000}{2(1+0.18)3.565} \cdot (1.9 \cdot 2.3) = 9 \cdot 10^5 \, KPa \cdot m$$

$$K_s = \frac{K_{sj}}{A_{\sec t}} = \frac{9.0 \cdot 10^5}{1.9 \cdot 1} = 4.7 \cdot 10^5 \frac{KPa}{m}$$

Joint stiffness between the block of the wall₂ ant base of the wall₃

$$K_j = \frac{E}{L} = \frac{1727000}{3.04} \cdot 1.5 \cdot 2.3 = 1.95 \cdot 10^6 \, KPa \cdot m$$

$$K_n = \frac{K_j}{A_{\sec t}} = \frac{1.8 \cdot 10^6}{1.5 \cdot 1} = 1.3 \cdot 10^6 \frac{KPa}{m}$$

$$K_{sj} = \frac{G}{L} A = \frac{E}{3(1+\upsilon)L} A = \frac{1727000}{2(1+0.18)3.04} \cdot (1.5 \cdot 2.3) = 8.3 \cdot 10^5 \, KPa \cdot m$$

$$K_s = \frac{K_{sj}}{A_{\sec t}} = \frac{8.3 \cdot 10^5}{1.5 \cdot 1} = 5.5 \cdot 10^5 \frac{KPa}{m}$$

Joint stiffness between the block of the wall₃

$$K_j = \frac{E}{L} = \frac{1727000}{4.0} \cdot 1.5 \cdot 2.3 = 1.8 \cdot 10^6 \, KPa \cdot m$$

$$K_n = \frac{K_j}{A_{\sec t}} = \frac{1.8 \cdot 10^6}{1.5 \cdot 1} = 1.2 \cdot 10^6 \frac{KPa}{m}$$

$$K_{sj} = \frac{G}{L} A = \frac{E}{3(1+\upsilon)L} A = \frac{1727000}{2(1+0.18)4.0} \cdot (1.5 \cdot 2.3) = 6.3 \cdot 10^5 \, KPa \cdot m$$

$$K_s = \frac{K_{sj}}{A_{\sec t}} = \frac{6.3 \cdot 10^5}{1.5 \cdot 1} = 4.2 \cdot 10^5 \frac{KPa}{m}$$

Joint stiffness between wall 0 and soil 11

$$k_{m,n} = \frac{B_r}{B_m} \cdot \frac{H_r}{H_m} \cdot U_3(z) = \frac{1.9}{1.5} \cdot \frac{10}{1} \cdot 4026 = 5.1 \cdot 10^4 \frac{KPa}{m}$$

N=3305 KN

$$U1(x) = U2(y) = 537063 \, KN/m$$

$$k_{r,s} = \frac{B_r}{B_m} \cdot \frac{H_r}{H_m} \cdot U_1(x) = \frac{1.9}{1.5} \cdot \frac{2.8}{1} \cdot 537063 = 1.9 \cdot 10^6 \frac{KPa}{m}$$

$$k_{m,s} = \frac{1.9 \cdot 10^6}{1.5 \cdot 1} = 1.3 \cdot 10^6 \frac{KPa}{m}$$

Joint stiffness between wall 1 and soil 12

$$k_{m,n} = \frac{B_r}{B_m} \cdot \frac{H_r}{H_m} \cdot U_3(z) = \frac{1.9}{2.3} \cdot \frac{10}{1} \cdot 1342 = 11086 \, KN/m^3$$

N=15318 KN

$$U1(x) = U2(y) = 2489175 \, KN/m$$

$$K_{r,s} = \frac{B_r}{B_m} \cdot \frac{S_r}{S_m} \cdot U_{1,2}(x) = \frac{2.3}{2.3} \cdot \frac{2.8}{1} 2489175 = 7.0 \cdot 10^6 \, KN/m$$

$$K_{m,s} = \frac{7.0 \cdot 10^6}{2.3 \cdot 1} = 3.0 \cdot 10^6 \, KN/m^3$$

Joint stiffness between wall 0 and soil 13

$$k_{m,n} = \frac{B_r}{B_m} \cdot \frac{H_r}{H_m} \cdot U_3(z) = \frac{1.9}{1.5} \cdot \frac{12}{1} \cdot 1342 = 20398 \, KN/m^3$$

N=3304 KN

$$U1(x) = U2(y) = 536900 \, KN/m$$

$$k_{r,s} = \frac{B_r}{B_m} \cdot \frac{S_r}{S_m} \cdot U_1(x) = \frac{1.9}{1.5} \cdot \frac{2.8}{1} \cdot 536900 = 1.9 \cdot 10^6 \, KN/m$$

$$k_{m,s} = \frac{1.9 \cdot 10^6}{1.5 \cdot 1} = 1.3 \cdot 10^6 \, KN/m^3$$

Damping

Block: wall 0

Parameter	Value	Unit	Single block	Multi block		Damping	
			we= 254.9462	**we,m= 360.5483**	βwe= 0.005547	ξwe 100	ξwr 34.87272
H=	5.05	m	wr= 88.90667	**wr,m= 125.733**	βwr= 0.015907	ξwe 286.7571	ξwr 100
D=	1	m					
B=	1.5	m					
density=	12.5	10^3Kg/m^3					
V=	7.575	m3		fcrit= 57.41215			
m=	94.6875	10^3kg					
J=	875.938281	10^3kgm^2					
E=	4144000	KN/m^2					
Kj=	8205940.59	KN/m^3					
Ks=	3077227.72	KN/m					

Block: arch N-S

Parameter	Value	Unit	Single block	Multi block		Damping	
			we= 897.9488	**we,m= 1269.891**	βwe= 0.001575	ξwe 100	ξwr 34.79357
H=	1.35	m	wr= 312.4284	**wr,m= 441.8406**	βwr= 0.004527	ξwe 287.4094	ξwr 100
D=	1	m					
B=	0.4	m					
density=	14.1	10^3Kg/m^3					
V=	0.54	m3		fcrit= 202.212			
m=	7.614	10^3kg					
J=	5.031585	10^3kgm^2					
E=	4144000	KN/m^2					
Kj=	30696296.3	KN/m^3					
Ks=	3069629.63	KN/m					

Block: wall 1

Parameter	Value	Unit	Single block	Multi block		Damping	
			we= 124.8012	**we,m= 176.4955**	βwe= 0.011332	ξwe 100	ξwr 50.76343
H=	5.05	m	wr= 63.35337	**wr,m= 89.59519**	βwr= 0.022323	ξwe 196.9922	ξwr 100
D=	1	m					
B=	2.3	m					
density=	5	10^3Kg/m^3					
V=	11.615	m3		fcrit= 28.10438			
m=	58.075	10^3kg					
J=	596.091479	10^3kgm^2					
E=	1727000	KN/m^2					
Kj=	786554.455	KN/m^3					
Ks=	452268.812	KN/m					

Block: arch C

Parameter	Value	Unit	Single block	Multi block		Damping	
			we= 485.7675	**we,m= 686.979**	βwe= 0.002911	ξwe 100	ξwr 20.55114
H=	2.35	m	wr= 99.83075	**wr,m= 141.182**	βwr= 0.014166	ξwe 486.591	ξwr 100
D=	1	m					
B=	0.4	m					
density=	15.9	10^3Kg/m^3					
V=	0.94	m3		fcrit= 109.3916			
m=	14.946	10^3kg					
J=	28.310215	10^3kgm^2					
E=	4144000	KN/m^2					
Kj=	17634042.6	KN/m^3					
Ks=	1763404.26	KN/m					

Block: wall 2

Parameter	Value	Unit	Single block	Multi block		Damping	
			we= 190.1209	**we,m= 268.8716**	βwe= 0.007438	ξwe 100	ξwr 82.60141
H=	2.08	m	wr= 157.0426	**wr,m= 222.0917**	βwr= 0.009005	ξwe 121.0633	ξwr 100
D=	1	m					
B=	1.9	m					
density=	12.7	10^3Kg/m^3					
V=	3.952	m3		fcrit= 42.81395			
m=	50.1904	10^3kg					
J=	132.77703	10^3kgm^2					
E=	1727000	KN/m^2					
Kj=	1909663.46	KN/m^3					
Ks=	907090.144	KN/m					

Block: wall 3			Single block		Multi block				Damping		
			we=	94.161	**we,m= 133.1638**		βwe= 0.015019		ξwe 100		ξwr 43.00366
H=	4	m	wr=	40.49268	**wr,m= 57.2653**		βwr= 0.034925		ξwe 232.5383		ξwr 100
D=	1	m									
B=	1.5	m									
density=	14	10^3Kg/m^3									
V=	6	m3				fcrit= 21.20442					
m=	84	10^3kg									
J=	511	10^3kgm^2									
E=	1727000	KN/m^2									
Kj=	993025	KN/m^3									
Ks=	372384.375	KN/m									
Block: wall 4			Single block		Multi block				Damping		
			we=	282.982	**we,m= 400.197**		βwe= 0.004998		ξwe 100		ξwr 53.79204
H=	2.25	m	wr=	152.2218	**wr,m= 215.2741**		βwr= 0.00929		ξwe 185.9011		ξwr 100
D=	1	m									
B=	1.1	m									
density=	21.3	10^3Kg/m^3									
V=	2.475	m3				fcrit= 63.72564					
m=	52.7175	10^3kg									
J=	110.223506	10^3kgm^2									
E=	1727000	KN/m^2									
Kj=	7675555.56	KN/m^3									
Ks=	2110777.78	KN/m									

D.2.1 The modelling parameters of the simple cross section used in the FEM models

Joint stiffness between wall 0 and soil 11

$$k_{m,n(Sap)} = B_m \cdot H_m \cdot k_{m,ntot} = 1.5 \cdot 1 \cdot 2.7 \cdot 10^6 = 4.1 \cdot 10^6 \, KN/m$$

$$k_{m,s(Sap)} = \frac{B_r}{B_m} \cdot \frac{H_r}{H_m} \cdot U_1(x) = \frac{1.9}{1.5} \cdot \frac{2.8}{1} \cdot 537063 = 1.9 \cdot 10^6 \, KN/m$$

$$k_9 = \frac{k_{m,ntot} \cdot B^3 \cdot D}{4} = \frac{2.7 \cdot 10^6 \cdot 1.5^3 \cdot 1}{4} = 2.3 \cdot 10^6 \, KNm$$

Joint stiffness between wall 1 and soil 12

$$k_{m,n(Sap)} = B_m \cdot H_m \cdot k_{m,n} = 2.3 \cdot 1 \cdot 6.0 \cdot 10^6 = 1.4 \cdot 10^7 \, KN/m$$

$$K_{m,s(Sap)} = \frac{B_r}{B_m} \cdot \frac{S_r}{S_m} \cdot U_{1,2}(x) = \frac{2.3}{2.3} \cdot \frac{2.8}{1} \cdot 2489175 = 7.0 \cdot 10^6 \, KN/m$$

$$k_9 = \frac{k_{m,ntot} \cdot B^3 \cdot D}{4} = \frac{6.0 \cdot 10^6 \cdot 2.3^3 \cdot 1}{4} = 3.5 \cdot 10^6 \, KNm$$

Joint stiffness between wall 0 and soil 13

$$k_{m,n(Sap)} = B_m \cdot H_m \cdot k_{m,ntot} = 1.5 \cdot 1 \cdot 2.6 \cdot 10^6 = 3.9 \cdot 10^6 \, KN/m$$

$$k_{m,s(Sap)} = \frac{B_r}{B_m} \cdot \frac{S_r}{S_m} \cdot U_1(x) = \frac{1.9}{1.5} \cdot \frac{2.8}{1} \cdot 536900 = 1.9 \cdot 10^6 \, KN/m$$

$$k_9 = \frac{k_{m,ntot} \cdot B^3 \cdot D}{4} = \frac{2.6 \cdot 10^6 \cdot 1.5^3 \cdot 1}{4} = 2.2 \cdot 10^6 \, KNm$$